AD-A071 709 ADVISORY GROUP FOR AEROSPACE RESEARCH AND DEVELOPMENT--ETC F/G 1/3
STABILITY AND CONTROL.(U)
MAY 79

UNCLASSIFIED AGARD-CP-260 NL

1 OF 4
AD A071709

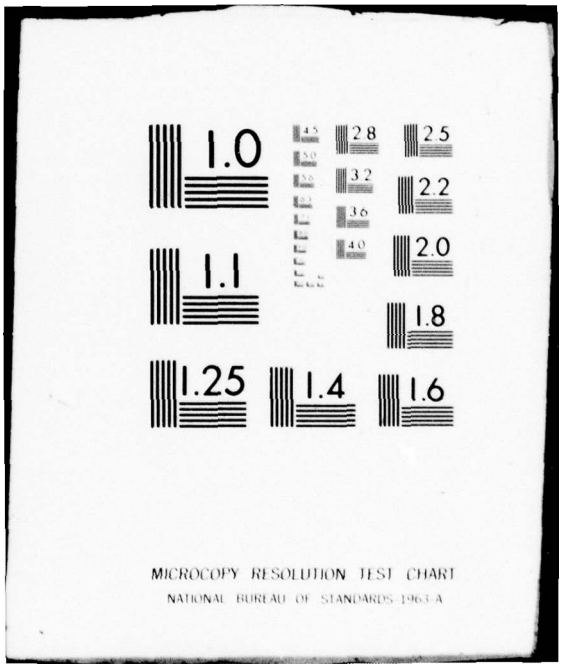
1.0
1.1
1.25
1.4
1.6
1.8
2.0
2.2
2.5
2.8
3.2
3.6
4.0
4.5
5.0
MICROCOPY RESOLUTION TEST CHART
NATIONAL BUREAU OF STANDARDS 1963-A

LEVEL II — (2) B.S.

AGARD-CP-260

AGARD-CP-260

AGARD

ADVISORY GROUP FOR AEROSPACE RESEARCH & DEVELOPMENT

7 RUE ANCELLE 92200 NEUILLY SUR SEINE FRANCE

AD A071709

DDC FILE COPY

This document has been approved for public release and sale; its distribution is unlimited.

AGARD CONFERENCE PROCEEDINGS No. 260

Stability and Control

DDC RECEIVED JUL 26 1979 C

NORTH ATLANTIC TREATY ORGANIZATION

DISTRIBUTION AND AVAILABILITY
ON BACK COVER

79 07 24 100

(14) AGARD-CP-260

(2)

NORTH ATLANTIC TREATY ORGANIZATION

ADVISORY GROUP FOR AEROSPACE RESEARCH AND DEVELOPMENT

(ORGANISATION DU TRAITE DE L'ATLANTIQUE NORD)

(11) May 79

(9) ~~AGARD~~ Conference Proceedings ~~No.260~~

(6) STABILITY AND CONTROL

(12) 359 p.

DDC
RECEIVED
JUL 26 1979
C

This document has been approved for public release and sale; its distribution is unlimited.

Papers presented at the Flight Mechanics Panel Symposium on
Stability and Control held in Ottawa, Canada, 25–28 September 1978.

400 043 79 07 24 100 slb

THE MISSION OF AGARD

The mission of AGARD is to bring together the leading personalities of the NATO nations in the fields of science and technology relating to aerospace for the following purposes:

- Exchanging of scientific and technical information;
- Continuously stimulating advances in the aerospace sciences relevant to strengthening the common defence posture;
- Improving the co-operation among member nations in aerospace research and development;
- Providing scientific and technical advice and assistance to the North Atlantic Military Committee in the field of aerospace research and development;
- Rendering scientific and technical assistance, as requested, to other NATO bodies and to member nations in connection with research and development problems in the aerospace field;
- Providing assistance to member nations for the purpose of increasing their scientific and technical potential;
- Recommending effective ways for the member nations to use their research and development capabilities for the common benefit of the NATO community.

The highest authority within AGARD is the National Delegates Board consisting of officially appointed senior representatives from each member nation. The mission of AGARD is carried out through the Panels which are composed of experts appointed by the National Delegates, the Consultant and Exchange Programme and the Aerospace Applications Studies Programme. The results of AGARD work are reported to the member nations and the NATO Authorities through the AGARD series of publications of which this is one.

Participation in AGARD activities is by invitation only and is normally limited to citizens of the NATO nations.

The content of this publication has been reproduced
directly from material supplied by AGARD or the authors.

Published May 1979

Copyright © AGARD 1979
All Rights Reserved

ISBN 92-835-0239-6

Printed by Technical Editing and Reproduction Ltd
Harford House, 7–9 Charlotte St, London, W1P 1HD

PREFACE

The Flight Mechanics Panel sponsored a symposium on Stability and Control in Ottawa, Canada, September 25th to 28th, 1978. In view of the rapid development of automatic control systems incorporating artificial stability, this symposium sought to examine the possibilities of matching control system characteristics to aircraft mission requirements and the resultant effects on aircraft design. The emphasis was placed not on control system design but on the more fundamental relationship between the use of advanced control concepts and appropriate aircraft design.

The meeting consisted of six sessions:

I. Summary of Recent Experiences in Stability and Control.

II. Application of Active Controls to Specific Aircraft and Aircraft Configurations.

III. General Problems Concerning Stability and Control and Associated Mathematical Models.

IV. Results Obtained with CCV's.

V. Criteria for Satisfactory Behaviour of Aircraft with Advanced Stability and Control Systems.

VI. The Participation of the Pilot.

The symposium was well attended and the active discussion during the closing round table session indicated the high degree of interest by the participants.

Since a Technical Evaluation Report, AGARD Advisory Report No.134 has been prepared for this symposium no lengthy summary is required here. The table of contents serves to give an overview of the type of material presented. Perhaps one overall result worthy of special mention is that the technical capability of developing and applying automatic stability and control systems has progressed faster than the ability to evaluate the costs and benefits of such systems. The major unanswered question was not whether active control systems could be properly and reliably designed and built but whether the benefits were worth the costs of acquisition and maintenance when all flight and redundancy requirements were taken into account. Obviously, the answer may be different for each possible active control function on each type of aircraft. Even the methodology of evaluation is difficult, however, because of lack of a data base on costs.

Drs J.BUHRMAN
National Aerospace Laboratory
Amsterdam
Netherlands

Prof. D.SHEVELL
Stanford University
California
USA

Accession For
NTIS GRA&I
DDC TAB
Unannounced
Justification
By
Distribution/
Availability Codes
Dist | Avail and/or special

CONTENTS

	Page
PREFACE	iii

	Reference
SESSION I – SUMMARY OF RECENT EXPERIENCES IN STABILITY AND CONTROL	
SYSTEMS IMPLICATIONS OF ACTIVE CONTROLS by P.R.Kurzhals	1
A SUMMARY OF AGARD F.D.P. MEETING ON DYNAMIC STABILITY PARAMETERS by L.E.Ericsson	2
ASPECTS STRUCTURAUX DU CONTROLE ACTIF par R.Destuynder	3
CONTROL OF MISSILE AIRFRAMES by D.J.Frary	4
SESSION II – APPLICATION OF ACTIVE CONTROLS TO SPECIFIC AIRCRAFT AND AIRCRAFT CONFIGURATIONS	
ENHANCED FIGHTER MISSION EFFECTIVENESS BY USE OF INTEGRATED FLIGHT SYSTEMS by J.H.Watson and W.S.Bennett II	5
RESULTATS RELATIFS A L'EXPERIMENTATION SUR SIMULATEUR ET EN VOL D'UN SYSTEME DE COMMANDES DE VOL ELECTRIQUES GENERALISABLES par A.Cazenave et J.Irvoas	6
IMPROVEMENT OF FIGHTER AIRCRAFT MANEUVERABILITY THROUGH EMPLOYMENT OF CONTROL CONFIGURED VECHICLE TECHNOLOGY by J.Stalony-Dobrzanski and N.Shah	7
Paper 8 cancelled	8
Paper 9 cancelled	9
SESSION III – GENERAL PROBLEMS CONCERNING STABILITY AND CONTROL AND ASSOCIATED MATHEMATICAL MODELS	
LATERAL STABILITY AT HIGH ANGLES OF ATTACK, PARTICULARLY WING ROCK by A.J.Ross	10
STALL BEHAVIOUR EVALUATION FROM FLIGHT TEST RESULTS by G.Sachs and H.Wünnenberg	11
HYBRID COMPUTER INVESTIGATION OF DISCRETE GUST AND WINDSHEAR EFFECTS ON AUTOMATIC LANDING SYSTEM PERFORMANCE by K.W.Rosenberg	12
AIRCRAFT RESPONSE TO WINDSHEARS AND DOWNDRAUGHTS by J.C. van der Vaart	13
GUST ALLEVIATOR FEASIBILITY STUDY FOR G91Y by R.Carabelli	14
DESIGN CONSIDERATIONS FOR RELIABLE FBW FLIGHT CONTROL by J.K.Ramage and J.W.Morris	15

Reference

OPEN/CLOSED LOOP INDENTIFICATION OF STABILITY AND CONTROL CHARACTERISTICS OF COMBAT AIRCRAFT
by R.Koehler and M.Marchand 16

DYNAMIC WIND TUNNEL SIMULATION OF ACTIVE CONTROL SYSTEMS
by P.G.Hamel and B.Krag 16A

SESSION IV – RESULTS OBTAINED WITH CCVs

STABILITY AND CONTROL ASPECTS OF THE CCV F104G
by G.Löbert, H.Beh and U.Korte 17

DESIGN GUIDANCE FROM FIGHTER CCV FLIGHT EVALUATIONS
by F.R.Swortzel and J.D.McAllister 18

USE OF DIRECT FORCES – PREDICTIONS AND FLIGHT TESTS ON A LIGHT 6 AXES VARIABLE STABILITY AIRCRAFT OF PRINCETON UNIVERSITY*
by C. la Burthe, J.P.Petit and A.Guillard 19

L-1011 ACTIVE CONTROLS, DESIGN PHILOSOPHY AND EXPERIENCE
by D.M.Urie 20

IN-FLIGHT HANDLING QUALITIES INVESTIGATION OF VARIOUS LONGITUDINAL SHORT TERM DYNAMICS AND DIRECT LIFT CONTROL COMBINATIONS FOR FLIGHT PATH TRACKING USING DFVLR HFB 320 VARIABLE STABILITY AIRCRAFT
by D.Hanke and H.-H.Lange 21

SESSION V – CRITERIA FOR SATISFACTORY BEHAVIOUR OF AIRCRAFT WITH ADVANCED STABILITY AND CONTROL SYSTEMS

FLYING QUALITIES AND THE FLY-BY-WIRE AEROPLANE
by J.C.Gibson 22

ARE TODAY'S SPECIFICATIONS APPROPRIATE FOR TOMORROW'S AEROPLANES?
by R.C.A'Harrah, J.Hodgkinson and W.J.Lamanna 23

A SIMULATOR INVESTIGATION OF HANDLING QUALITY CRITERIA FOR CCV TRANSPORT AIRCRAFT
by H.A.Mooij, W.P. de Boer and M.F.C. van Gool 24

SESSION VI – THE PARTICIPATION OF THE PILOT

MATHEMATICAL MODELS OF MANNED AEROSPACE SYSTEMS
by P.H.Wewerinke 25

LE MODELE DE PILOTE EN TEMPS DISCRET DE L'ONERA
by D.Cavalli 26

FLIGHT EXPERIENCE WITH ADVANCED CONTROLS AND DISPLAYS DURING PILOTED CURVED DECELERATING APPROACHES IN A POWERED-LIFT STOL AIRCRAFT
by W.S.Hindson 27

*Not available at time of printing

SYSTEMS IMPLICATIONS OF ACTIVE CONTROLS

by

Dr. Peter R. Kurzhals, Director
Electronics Division
NASA Headquarters
Washington, D.C.

ABSTRACT

Active controls offer the promise of significantly increased aircraft performance and operational capability. However, realization of these gains will require major changes in both the aircraft design approach and in the implementation of the flight control system. This paper outlines attendant control-configured vehicle design and system considerations and summarizes representative applications of active control for fighter and transport aircraft. Specific examples include relaxed static stability and angle of attack limiting on the F-16, envelope limiting and ride smoothing on the F-8, maneuver load control and relaxed static stability on the L-1011, load alleviation for the C-5, and B-1 ride control. Principal features, problem areas, and mechanization trends for these and projected future active control applications are outlined.

INTRODUCTION

The revolution in solid-state electronics, illustrated in Figure 1 for a representative autopilot subassembly, has permitted a hundred-fold decrease in control computer size, power and cost over the past two decades.[1] Thus, a typical 1958 subsystem with about 950 cubic centimeters of circuit cards could, by 1968, be produced as two microelectronics modules taking up less than 50 cubic centimeters. During the mid-70's, hybrid design concepts further reduced the volume of these modules to less than 10 cubic centimeters. Designers have capitalized on these gains primarily by adding new flight control system functions aimed at improving aircraft performance.

As a result, flight control applications are now evolving from simple pilot-relief autopilots to flight-critical and redundant fly-by-wire and active control systems. To assure the integrity of these systems, more hardware had to be added to achieve the reliability for flight safety. The related growth in complexity has led to a twenty-fold increase in the number of system elements and an exponential growth in control reliability requirements, depicted in Figure 2 in terms of computer systems failure probability for a 10 hour flight period.[1] This reliability increase spans some six orders of magnitude over the past 20 years, with failure probabilities of less than 10^{-9} per flight hour needed for flight-critical control systems of the next generation of aircraft. Highly sophisticated reconfigurable and fault-tolerant computers are now beginning to emerge to meet these stringent reliability requirements and to pave the way for the cost-effective operational application of active controls.[2]

Concurrent with these control system hardware developments, individual active control functions are being incorporated into both fighter- and transport-class aircraft.[3] This paper summarizes associated design and application experiences, based largely on recent AGARDographs generated by the Guidance and Control Panel.

DESIGN CONSIDERATIONS

The basic active-control or control-configured-vehicle (CCV) concept[4] aims at optimizing aircraft geometry for each flight condition by considering flight control in the preliminary design process, as indicated in Figure 3. This approach extends the traditional tradeoffs between aerodynamics, structures and propulsion to include the capabilities of a full-time, full-authority fly-by-wire control system. For example, aerodynamic stability could be reduced to neutral or negative and overall aircraft performance improved by relying on the control system to provide artificial stability. Similarly, active redistribution of dynamic wing loads can significantly reduce wing root bending moment and permit reductions in wing structural weight. Clearly, these and other active control tasks involve an unprecedented understanding of the anticipated external disturbances, aerodynamic characteristics, control system responses and compatibility problems, requiring considerable advances in our ability to describe and model such phenomena.

Nevertheless, both individual and combined active control concepts are now being demonstrated on experimental, commercial and military aircraft.[5] Figure 4 illustrates this application experience for the principal active control technology (ACT) functions currently under consideration. While most ACT functions have been explored in some detail, there remains a significant disparity between the application status of the various functions. Relaxed longitudinal stability has been implemented on the F-16 and flight tested for transport application. Control of the aircraft center of gravity through wing fuel management is in operational service on the Concorde, and ride improvement systems have been certified for the Boeing B-747 and incorporated in the Rockwell B-1. Directional stability augmentation has seen extensive transport application and the yaw damper currently flying on large transport aircraft has progressed from a system designed to increase passenger comfort to a system which must be operating before the aircraft is

cleared for flight. Maneuver load and gust load alleviation have been flight tested on a Boeing B-52 CCV and an active lift distribution control system was retrofitted into the Lockheed C-5A force. Elastic mode stabilization or flutter control, flight tested on the B-52 CCV and investigated in wind tunnel and remotely-piloted vehicle tests, has made considerable progress in the last few years but the technology for a good structural dynamics and unsteady aerodynamics model, required for design of an effective flutter mode control system, still needs to be developed. Envelope limiting, such as the angle-of-attack and normal acceleration limiter used on the F-16 to allow use of the full maneuver envelope without danger of stall-spin departure or structural damage, is now being applied to fighter aircraft and some form of envelope warning and limiting is built into most modern aircraft. Although not shown in the figure, direct lift and side force control to improve maneuverability and weapon delivery have also been evaluated on several research aircraft, most recently on a modified YF-16 as discussed later in this symposium.

Key factors in bringing these ACT functions to operational application will be their potential to achieve significant cost and performance benefits for future aircraft and the emergence of proven design criteria and practices. Some of the major drivers in this process include adequate reliability from both a safety and economic viewpoint, expanded flying quality criteria to cover normal ACT operation and failure modes, and better airframe and control system analyses.

Reliability

The extent to which inherent aircraft characteristics are augmented depends strongly on the level of ACT system degradation considered in the design. If a complete loss of ACT functions is viewed as acceptable, then sufficient inherent characteristics must be provided and the benefits obtainable from ACT can be severely restricted.

Since safety of flight cannot be compromised by ACT, early active control applications do not generally reduce structural capability under normal flight conditions and provide only limited performance gains. In comparison, future active control functions will, in effect, replace primary structure and the reliability for those functions upon which safe completion of the flight depends will have to approach that of the primary structure. However, as shown in Figure 5 which assesses the severity of situations resulting from ACT function degradation, not all resultant ACT systems are truly flight-critical. Complementary means of controlling the risk presented by failures in ACT functions are provided by control system redundancy, actuation and/or surface authority distribution and a reduced operating envelope. Ultimate levels of functional reliability with short-term failure probabilities of less than 10^{-9} are basically required only for applications such as flutter control and inherently unstable aircraft, and the control systems designer should take advantage of these reliability considerations to minimize ACT mechanization costs and simplify verification of the resultant failure modes.

Maintenance cost and dispatch reliability for CCV aircraft represent a major related concern. As an example, a typical design goal for commercial dispatch reliability is that, mechanically, an aircraft shall be capable of departure within 15 minutes of schedule 99 percent of the time. The ACT system redundancies dictated by safety requirements may severely penalize such dispatch rates unless further redundancy is added as dispatch-inoperative allowance. This would in turn increase total system acquisition and maintenance costs, already high because of the projected complexity of ACT systems. Reliable, maintainable and cost-effective control systems are thus an essential prerequisite to full use of ACT.

Flying Qualities

Although design criteria for flight characteristics appear to be well developed and in most cases can be applied to CCV aircraft, these criteria were derived over 10 years ago and should be updated to reflect the increased freedom in specifying modes of control and response for ACT functions. This break from traditional relations between control effectors and functions will obviously cause difficulties in the use of many of the conventional criteria based on these relations. Flying qualities criteria associated with failure modes also need to be addressed. The three allowable levels of flying qualities specified in MIL-F-8785B as a function of likelihood of occurrence represent a good approach to this problem, but more stringent encounter probabilities will be needed for civil or flight-critical ACT applications.

Analysis

The methodology required for external loads and flutter analyses will be directly impacted by active controls. Not only will ACT change the magnitude, distribution and frequency of occurrence of the loads for which the structure is designed but more exact techniques which account for the complete dynamic transient response of distributed loads as well as the total airframe will have to be developed. Such properties as nonlinear structural characteristics and unsteady transonic aerodynamics now need to be accounted for in the determination of acceptable design loads.

Aircraft structural fatigue life predictions will similarly be impacted by ACT. For example, because the application of ACT provides a more efficient distribution of external loads at the aircraft design conditions but does not change the total load in steady 1g flight, new relationships between structural design stresses and 1g stresses will result. Inflight fatigue damage cycles and peak-to-peak stress relationships may also be altered, and future fatigue investigations will involve increased use of mission analysis to

determine ACT effects on the fatigue spectrum.

Control design techniques also will become much more important for ACT applications. Because of the higher gains required for active control, system components will have to meet and maintain tighter specifications over the life of the control system. This may require new design criteria for components such as hydraulic actuators whose phase and gain are affected by wear, and the control system must be able to compensate for out-of-tolerance conditions. Variations in airframe parameters associated with modeling inaccuracies or inflight changes must also be accomodated by the control system. An insensitive control system approach may be the best solution to such parameter variations.

Progress in these design areas will directly contribute to the cost-effective implementation of ACT for fighter and transport aircraft, addressed in the following sections.

FIGHTER APPLICATIONS

Active control effects for combat and strike aircraft can perhaps best be described in terms of weight reduction achieved, aerodynamic efficiency (i.e. maximum lift and lift/drag ratio), performance (i.e. sustained maneuverability, fuel economy, take-off and landing distances), and combat score.[6] Related intangible gains which lead to carefree maneuvering are improved handling qualities, reduced pilot workload, and removal of flight restrictions. These benefits, derived from British Aircraft Corporation (BAC) studies, are due to artificial longitudinal stability, automatic configuration management, stall/spin prevention, and overstress prevention. Maneuver load control, active flutter control and gust alleviation were also considered but were found to have relatively small gains.

Typical benefits for artificial longitudinal stability included a 35% reduction in tailplane area and a rearward c.g. shift of 17%c for a low-low strike mission at 0.7M, with attendant planform comparisons shown in Figure 6. The rearward location of the c.g. range results in a favorable variation of tail load to trim. Associated increased lift permits a 12% reduction in wing area because of reduced drag which in turn reduces fuel area requirements and engine size. Savings of 9% in drag and weight were obtained.[6] This weight saving is, of course, strongly dependent on the fixed weight fraction and design mission. The smaller the weight fraction, the larger are the structural, fuel and power plant contributions which are susceptible to scaling down with ACT. The addition of combat high lift devices, such as maneuver flaps and strakes, can further augment lift and reduce drag at subsonic speed and help to provide the control flexibility required for stall/spin and overstress prevention and effective configuration management.

The most commonly used parameters for evaluation of the effects of aircraft performance on combat success are sustained turn rate (STR), attained turn rate (ATR) and specific excess power (SEP). Various combinations of these performance parameters have evolved into combat scoring criteria. For this discussion, consider a Combat Correlation Parameter (CCP), defined as $STR \times \sqrt{ATR}$, and Panic Time, defined as the time during which an aircraft is in imminent danger of being shot down. Since sustained turn rate at a given speed is roughly proportional to sustained normal acceleration (which equals the product of the thrust/weight and the lift/drag ratios) and attained turn rate is proportional to maximum lift divided by wing loading, the effects of CCP at constant thrust/weight ratio and wing loading can be directly deduced from the changes in L/D and maximum lift due to drag. For the example mission considered earlier, ACT increased maximum L/D and lift by 10% and 15%, respectively, leading to an 18% increase in CCP. Based on BAC combat simulations between equally matched aircraft for a number of one-on-one 3-minute combats at low altitude, such an 18% improvement would put the aircraft not equipped with ACT into a panic situation for 60 seconds, or 1/3 of the time. Even larger gains result if the speed unwinds to 0.6M or lower during the maneuver, yielding clear superiority for the ACT-equipped aircraft.

Benefits in maximum L/D also produce proportional decrements in thrust and fuel requirements during loiter or sustained maneuvers, with some 8% in fuel or about 2% of the mission gross takeoff weight saved through ACT. This could be used to increase performance, providing a 20% improvement in combat endurance or a 40% improvement in radius of action. Additional benefits identified by the BAC are an 8% reduction in take-off distance, a 2% reduction in landing distance and a 3% increase in SEP.[6]

A quadruplex full-time digital fly-by-wire system compatible with these and other ACT functions is being developed through a national U.K. research program for flight test on a Jaguar airframe. The objectives are to demonstrate confidence in the airworthiness of full-time digital fly-by-wire, control of longitudinal instability and stall departure and spin prevention. It is anticipated that such application of ACT to combat aircraft will provide future pilots with greatly enhanced combat effectiveness, such as 10% improvement in sustained maneuverability, 15% improvement in attained maneuverability, and 25% improvement in radius of action - combined with maneuvering free from the possibility of spinning or overstressing.

F-16

Other key developments in ACT include the F-16 multinational fighter, shown in Figure 7, the first production aircraft to incorporate an active control system from its inception.[7] Principal F-16 flight control features, illustrated in Figure 8, are a quadruplex analog fly-by-wire system with fail-operative/fail-operative redundancy, three-axis stability and command augmentation, built-in self-testing capability, relaxed static stability (RSS) and

automatic angle-of-attack and normal-acceleration limiting. Flight path control is achieved by actuating the all-movable horizontal tails for pitch and roll control, the partial-span, wing-mounted flaperons for roll control, and the conventional rudder for yaw control. Maneuver capability at high angles of attack is enhanced by a full-span leading-edge flap, automatically programmed as a function of Mach number and angle of attack. The result is a variable, near-optimum camber that maintains effective lift coefficients at high angles of attack, thereby providing a higher maximum lift capability, improved buffet characteristics and improved directional stability. Symmetrical downward deflection of the flaperons and fixed deflection of the leading-edge flap provide increased lift for takeoff and landing.

System mechanization of the F-16 flight control system is accomplished by applying the basic system elements depicted in Figure 8. Pilot control of the primary control surfaces is accomplished without mechanical linkage by using displacement-type, force-sensing control stick and rudder pedals, and through pilot-initiated trim commands in each of the three axes. Four independent electronic branches with quadruple redundant pilot sidestick controller sensors accept pilot command inputs. Feedback of quadruplex airplane motion sensors (rate gyros and accelerometers) provides static and/or dynamic stabilization. The quadruplex system is protected through automatic failure detection and correction which provides fail-operative performance following two like electronic failures. The prime electronic assembly is the flight control computer, which processes, gain-adjusts, filters, and amplifies signals to command the five integrated servoactuators used to power the primary control surfaces. Gain scheduling of commands in the various control axes, as required for a particular command, is performed as a function of static pressure, impact pressure, or the ratio of impact pressure to static pressure. These functions are supplied by the air data system, which senses triple sources of total pressure, static pressure and angle of attack.

Performance benefits for the F-16 RSS configuration with its c.g. in the range of 35-40%c, in comparison with a conventionally balanced airplane having a c.g. at 25%c, included some 200kg fuel savings and significant improvements in acceleration time and turn rate for typical combat missions. Angle of attack limitation to 25^{O} and incorporation of an automatic "g" limiter further allows the pilot to consistently find his maximum-turn performance condition and to use it without fear of losing control of the aircraft.

F-8

Limited investigations of ACT functions have also been conducted on an F-8C aircraft, illustrated in Figure 9 and equipped with a full-authority triplex digital fly-by-wire (DFBW) control system.[8] The purpose of these investigations was to examine the design, mechanization, and performance of an integrated set of control laws which would be typical of those for projected aircraft employing full-time active controls. The selected control laws emphasized CCV benefits for fighter aircraft. Specific pitch axis objectives were improved handling qualities, angle-of-attack limiting, gust alleviation, drag reduction in steady and maneuvering flight, and a capability to fly with reduced static stability. Lateral-directional design objectives were improved Dutch roll damping and turn coordination over a wide range in angle-of-attack. Modern control design methodology was used to derive control laws focusing on these specific CCV benefits.

The control laws were constrained to be compatible with the existing airframe without structural modification and employed only available DFBW hardware, schematically indicated in Figure 10. Control effectors included elevators, rudder and aileron, powered by electrohydraulic actuators; control laws were mechanized on IBM AP-101 computers and associated interfaces; and sensing elements included pitch, roll and yaw rate gyros, vertical and directional gyros, normal and lateral accelerometers, and angle-of-attack, Mach number and pressure altitude air-data measurements.

Major steps in the design process involved linear modeling at some 25 flight conditions, control law synthesis with modern linear quadratic optimization techniques to satisfy conventional design requirements at each flight condition, derivation of approximate gains as functions of air data measurements, and validation of the resultant control laws on a nonlinear six-degree-of-freedom simulation. Flight tests of selected command augmentation, boundary control, ride smoothing and maneuver flap functions were also conducted on the F-8C. While the F-8C performance benefits were relatively modest, excellent agreement was obtained between flight test results and design/analysis/simulation predictions - suggesting that the development of digital CCV control can proceed with confidence.

HIMAT

Another interesting approach for obtaining fighter ACT design data involves flight tests of remotely piloted research vehicles (RPRV's) with active controls to validate highly maneuverable aircraft technologies (HIMAT).[9] The HIMAT RPRV, illustrated in Figure 11, is a subscale closely coupled canard-wing vehicle which includes relaxed static stability, direct force control, and a digital active control system. The maneuverability goal for the full-scale fighter aircraft was the ability to sustain an 8g turn at Mach 0.9 at an altitude of 9140 meters; equivalent performance will be demonstrated by the RPRV at an altitude of 7620 meters to match the wing loading of the full-scale aircraft.

This goal and nonlinearities in the HIMAT aerodynamics placed unusual demands on the active control system. While a maximum of 10% negative static margin was used as a guideline for relaxed longitudinal stability and was increased to 15% later, nonlinear aerodynamics led to more than 30% static margin for some high angle-of-attack flight conditions and low Mach

numbers. As a result, an angle of attack limiter was required to assure adequate excess control authority to stabilize the aircraft. Similarly, although neutral directional stability was selected as a limit for the rigid airplane, flexibility effects caused negative stability for small angles of sideslip and special provisions to prevent trimming to nonzero angles of sideslip had to be added to the relaxed directional static stability system. Some penalties were also incurred because of the active control function. Actuators and hydraulic systems were larger than those required for conventional aircraft, and the addition of wingtip ventrals was necessary to compensate for destabilizing canard dihedral effects.

Figure 12 is a three-view drawing of the HIMAT RPRV with control surfaces indicated. The canard flaps are used either symmetrically, for longitudinal control, or antisymmetrically, for direct side force control. The ailerons and elevators are used for roll and pitch control, respectively. The elevons may be commanded antisymmetrically for roll control or symmetrically for pitching moment control. The rudders may be commanded collectively for yawing moment control or differentially as a speed brake.

PROFIT

The extension of ACT to propulsion/flight-control integration technology (PROFIT) is a next logical step in the designer's quest for increased performance.[10] This controls evolution is outlined in Figure 13. Early jet-powered aircraft of the 1940's had simple mechanical flight control systems and simple turbojet engines with hydromechanical fuel controls. The next generation of aircraft, introduced in the 1950's, had afterburning turbojet engines to provide greater thrust, and analog electronic stability augmentation systems to provide acceptable handling qualities at supersonic speeds. Aircraft introduced during the 1960's typically had variable-geometry inlets, autopilots and air data computers. The turbofan engine was introduced but there was little or no propulsion/flight control integration. The first step towards integration, the autothrottle, was used on some aircraft introduced in the 1970's which also saw the application of digital computers for fly-by-wire and integrated propulsion control systems (IPCS). The YF-12 cooperative control program subsequently digitally implemented the autopilot, autothrottle, air and inlet control functions. The PROFIT program will extend this integration to all propulsion and flight control functions using the F-15 research aircraft shown in Figure 14. Controlled elements will include the inlet, gas generator, afterburner and nozzle on both engines for the propulsion system as well as pitch, roll, yaw control and autopilot and stability augmentation functions for the flight control system. Appropriate pilot displays and interfaces will also be developed and evaluated. Remote computation capability to extend the onboard computer capability will be provided via telemetry links. Particular concepts to be investigated include engine-inlet-nozzle integration, trajectory optimization (i.e. minimum-noise takeoff, terrain following, energy management), multivariable engine control and engine-problem detection and correction. Results of this work should provide design data for future integrated controls which optimize aircraft performance and permit reduced system costs.

TRANSPORT APPLICATIONS

While active control applications for fighters are clearly driven by military requirements, much of the current motivation for transport applications comes from the civil arena where designers have turned to ACT to reduce fuel consumption and direct operating costs (DOC). Principal ACT concepts now being considered for transport applications are relaxed static stability and wing load alleviation. Analysis of a typical transport at constant aspect ratio indicates that a 50% design-wing bending-moment reduction can be obtained with existing types of controls (ailerons, spoilers, flaps). This yields some 15% reduction in wing weight and 2-3% reduction in DOC. Similarly, by relaxing longitudinal stability to just above neutral, tail size and load can be reduced with DOC gains of about 2%. These gains are roughly doubled if the aircraft is stretched with a given engine size and performance standard. For a medium-range (2000 n.m.), 200 seat aircraft, combination of these functions can provide 4-5% DOC gains with a constant payload or 7-9% if the aircraft is stretched. Since a 1% DOC reduction on a DC9, BAC 1-11, or B-737 amounts to a saving of about $50K per aircraft per year for a typical 3000 hour utilization, or about $1M for the 20 year life of an aircraft, such gains are highly significant.[11]

The spectrum of ACT functions that have been investigated for transports includes maneuver load alleviation, gust load alleviation, relaxed stability, flutter suppression, fatigue life improvement and ride-quality control. An indication of the systems impact of such functions can be derived from the following examples.

L-1011

In the United States, NASA and industry have begun a program to define means for reducing the energy demands for air transportation. As part of this program, promising near-term technologies are being evaluated on current transports. One of these efforts, described in detail by a paper in this Symposium, involves development of an active control system for commercial application in the Lockheed L-1011 airplane,[12] shown in Figure 15. Both relaxed static stability and load relief were investigated. The combined impact of these two functions yields a 6½ percent fuel saving for the L-1011; for a fleet of thirty L-1011 airplanes operating for 10 years, that savings translates into about $45M.

Based on these promising results, a load relief system providing maneuver load control and elastic mode suppression was selected for flight test. As illustrated in Figure 16, this

load redistribution permits a wing tip extension of about 1½ meters per side. Associated reductions in induced drag allow a 3% fuel saving with minimal structural modifications. The load relief system, which uses integrated movements of the ailerons and horizontal tail, has been mechanized and evaluated with an L-1011 aircraft. Measured flight responses closely agreed with design predictions.

C-5

A second load alleviation system,[13] aimed at fatigue life improvement, has been in operational service with the entire C-5 fleet since 1975. This system, designated the Active Lift Distribution Control System (ALDCS), is depicted in Figure 17. The ALDCS systems mechanization consists of an array of sensors, gains, and filters used with existing control effectors. The maneuver load relief function is accomplished by commanding the right and left ailerons symmetrically. Feedback sensors used are two vertical accelerometers per wing, both at an outer wing location. The signals from these accelerometers are averaged and compensated by smoothing filters that attenuate sensor noise and aid in the elimination of higher frequency wing vibration modes. Resulting control signals are gain scheduled by aircraft dynamic pressure from the Central Air Data Computer (CADC) to provide proper stability and load-relief schedules and to minimize handling qualities degrations throughout the aircraft speed envelope. Airplane pitch rate, obtained from the pitch Stability Augmentation System (SAS) rate gyro, is utilized to augment the airplane short period damping and thereby alleviate the excitation of short-period induced-gust loads and restore handling qualities degraded by aileron pitching moment effects. An existing C-5 autopilot subsystem vertical accelerometer mounted in the forward fuselage provides additional gust loads control and compensates the airplane pitch response characteristics.

Flight data, obtained by instrumenting 13 of the modified aircraft, closely followed the system analysis/design predictions. Maneuver and gust load incremental wing stresses were reduced by approximately 30% during normal operation and by some 20% during aerial refueling. Significant improvements in fatigue endurance are projected as a result of the ALDCS, with a conservative 1.25 life improvement factor now being used to track individual C-5 aircraft. System reliability initially predicted to be 3,000 operational hours, actually resulted in a mean time between unscheduled removals of about 1000 hours.

B-1

This last example of ACT for transports, the B-1 ride control system, involves one of the first aircraft to include CCV concepts in the early design phases.[14] The Rockwell B-1 has a requirement to provide a specified level of ride quality for the crew. To meet this requirement, the B-1 incorporates a Structural Mode Control System (SMCS) whose main external feature is a set of vanes near the crew station which are canted down 30° from the horizontal as shown in Figure 18. Since the B-1 has full structural integrity with or without the SMCS operating, a fail-safe approach using dual redundancy in the sensors, electronics and actuators was employed to permit centering of the vanes in case of system failure. Sensor inputs are derived from vertical and lateral accelerometers, with gains again scheduled by dynamic pressure, and relatively simple control algorithms are used to generate commands for forward and aft vane actuators.

Tradeoff studies indicated that 4,482 kg would have been added to the fuselage to meet ride quality requirements without SMCS. Since the SMCS weighs about 182 kg, active control permits a weight saving of some 4300 kg, a substantial active control benefit. Evaluation of the system performance in flight showed that the SMCS reduced both lateral and vertical load factors to the specified levels without degrading basic handling qualities.

CONCLUDING REMARKS

Based on this brief overview of recent experiences in the application of ACT to fighter and transport aircraft, several general observations can be made. First, in the design area, although major advances in ACT design practices have been realized, considerable work remains to be done before structural dynamic and aerodynamic models can be used with confidence in the initial CCV configuration selection. Alternate control approaches, such as parameter-insensitive systems which can deal with errors in predicted aircraft parameters, should also be pursued to permit the increased application of CCV designs. Second, in the ACT system mechanization area, cost-effective reliability and maintainability will be the principal factor in determing the extent of ACT applications. Recent trends towards distributed, fault-tolerant systems and increased integration of aircraft control functions, which permit greater commonality in control processor modules and reductions in overall control system cost, should significantly aid this process. Third, although more and more ACT concepts are now being introduced into flight systems, the implementation of true flight-critical integrated CCV configurations clearly is still a long-term goal and must be viewed as the culmination of a continuing growth in the technology of aircraft design. Active controls are now approaching the relative state of readiness of jet engines when they were first introduced into commercial service; while their near-term potential is high, the best is yet to come.

REFERENCES

1. Osder, S. S.: "Chronological Overview of Past Avionic Flight Control System Reliability in Military and Commercial System Operations". AGARDOGRAPH AG-224, May 1977.

2. Kurzhals, P. R.: "Integrity in Flight Control Systems". Paper presented at JAAC Conference, San Francisco, California, June 1977.

3. Rediess, H. A. and Szalai, K. J.: "Status and Trends in Active Control Technology". Paper presented at NASA/University Conference on Aeronautics, Lawrence, Kansas, October 1974.

4. Duc, J. M.: "Control Configured Vehicle Design Philosophy". AGARDOGRAPH GCP-514, October 1978.

5. Harris, R. H. and Rickard, W. W.: "Active Control Transport Design Criteria". AGARDOGRAPH GCP-514, October 1978.

6. Burns, B. R. A.: "Control-Configured Combat Aircraft". AGARDOGRAPH GCP-514, October 1978.

7. Anderson, C. A.: "F-16 Multi-National Fighter". AGARDOGRAPH GCP-514, October 1978.

8. Hartman, Gary L. et al.: "Design and Flight Experience with F-8C Active Controls". AGARDOGRAPH GCP-514, October 1978.

9. Deets, D. A. and Crother, C. A.: "Active Controls in HIMAT Design". AGARDOGRAPH GCP-514, October 1978.

10. Burcham, F. W.: "The Concept for Profit". AGARDOGRAPH GCP-514, October 1978.

11. Hitch, H.: "Active Controls for Civil Transports". AGARDOGRAPH GCP-514, October 1978.

12. Stauffer, W. A. et al.: "Fuel-Conservative Subsonic Transport". AGARDOGRAPH GCP-514, October 1978.

13. Disney, T. E.: "C-5A Load Alleviation". AGARDOGRAPH GCP-514, October 1978.

14. Wykes, J. H. and Borland, C. J.: "B-1 Ride Control". AGARDOGRAPH GCP-514, October 1978.

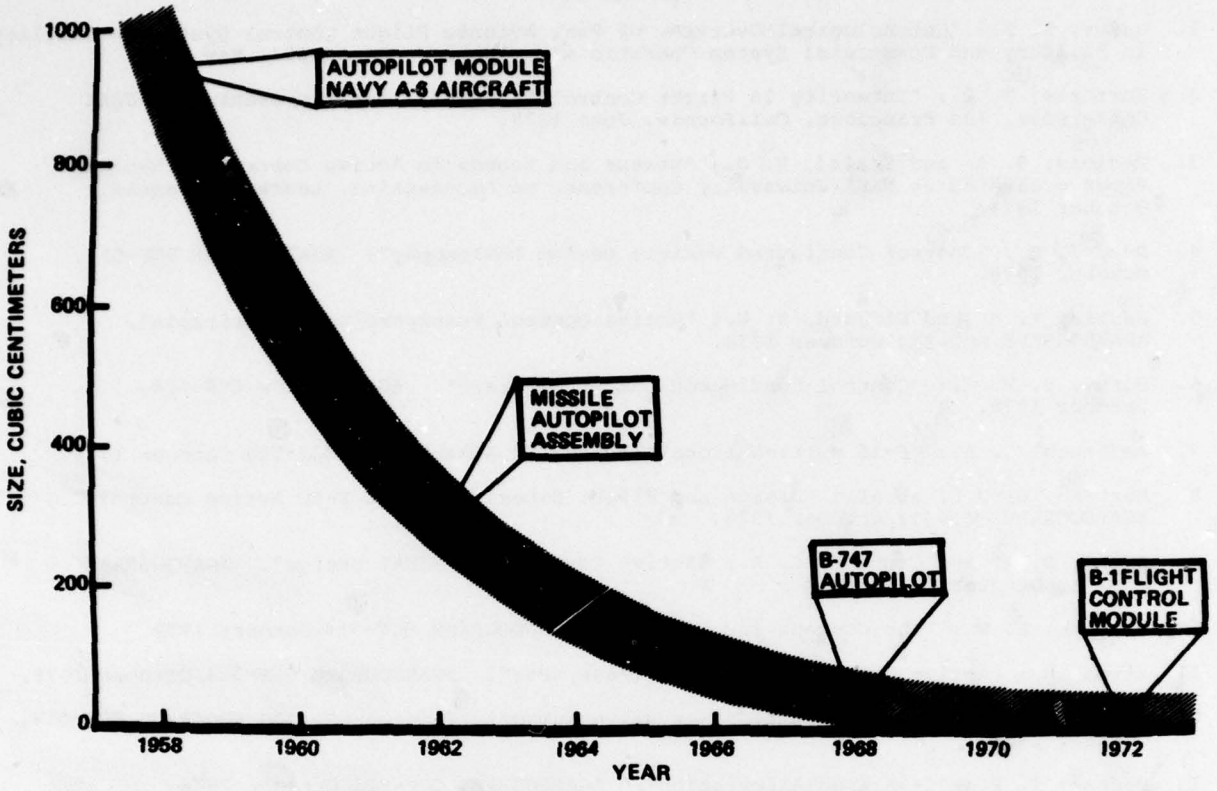

Fig.1 Miniaturization of representative flight control hardware

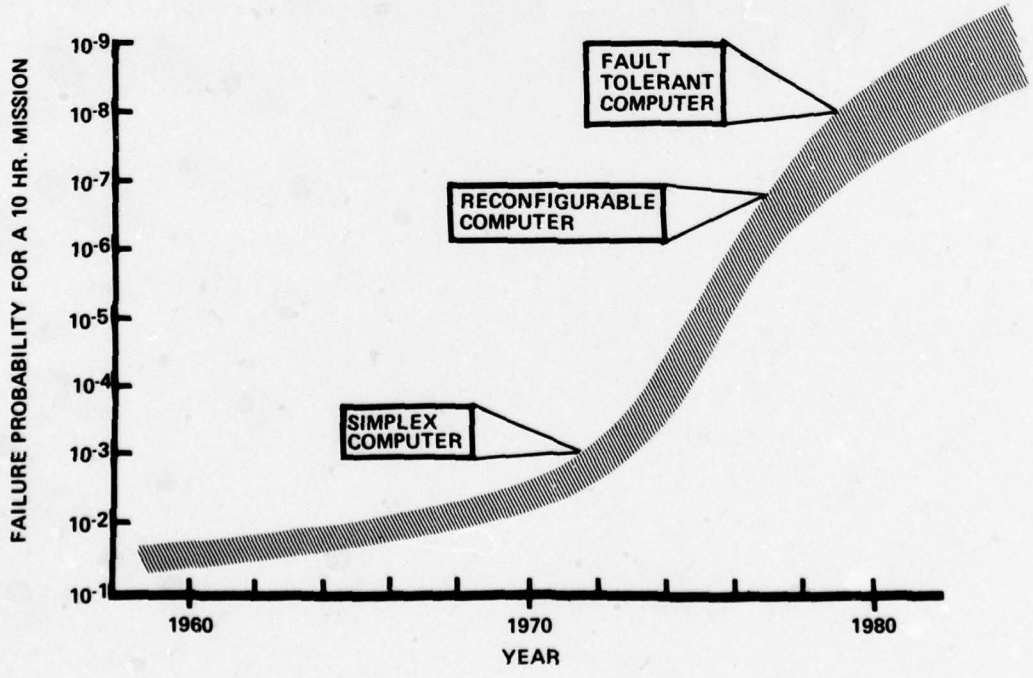

Fig.2 Computer system reliability

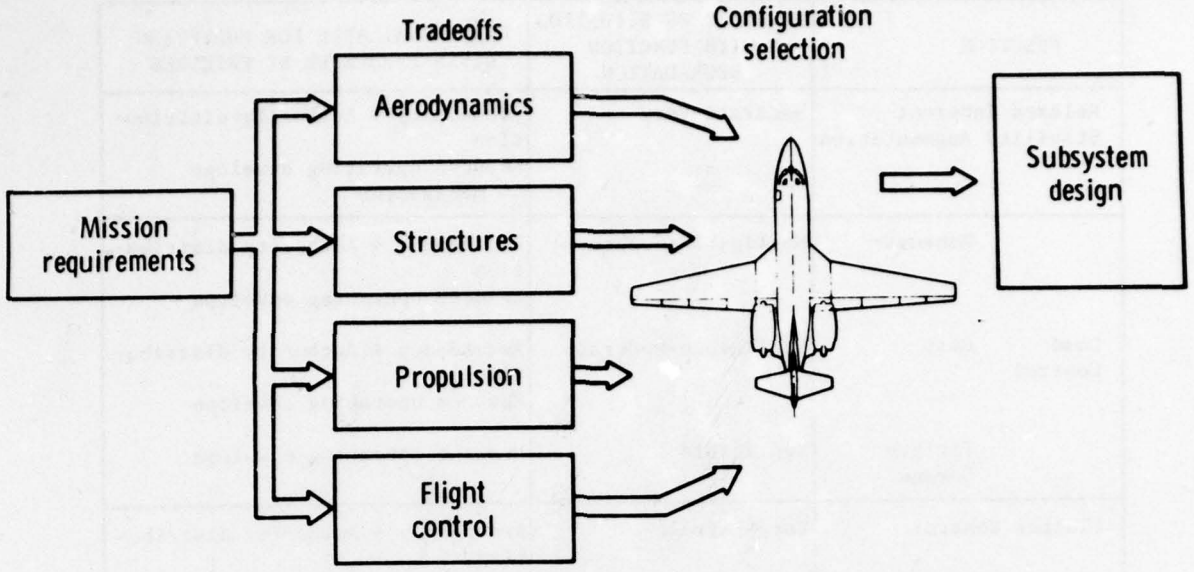

Fig.3 Active control technology design approach

ACT FUNCTION	AIRCRAFT	STATE OF READINESS	PAYOFF & TRADE DATA	SYSTEM MECHANIZED	FLIGHT TESTED	OPERATIONAL EXPERIENCE
Relaxed Inherent Stability *Augmentation*	Military Experimental					
Center of Gravity Control	Military Commercial					
Ride Quality Control	Military					
Yaw Damper	Military Commercial Transport					
Maneuver Load Control	Military					
Gust Load Control	Military Commercial Transport					
Fatigue Damage Control	Military					
Flutter Control	Military					
Envelope Limiting	Military Commercial Transport					

Fig.4 ACT function application experience

FUNCTION		SEVERITY OF SITUATION WITH FUNCTION DEGRADATION	MEANS AVAILABLE FOR MODIFYING RISKS PRESENTED BY FAILURES
Relaxed Inherent Stability Augmentation		Moderate-Very	Redundancy + Authority distribution Reduced operating envelope CG management
Load Control	Maneuver	Negligible-Moderate	Redundancy + Authority distribution Reduced operating envelope
	Gust	Negligible-Moderate	Redundancy + Authority distribution Reduced operating envelope
	Fatigue Damage	Negligible	Reduced operating envelope
Flutter Control		Very-Extreme	Redundancy + Authority distribution Reduced operating envelope
Ride Quality Control		Negligible-Moderate	Redundancy + Authority distribution Reduced operating envelope
Envelope Limiting		Negligible-Moderate	Redundancy Reduced operating envelope
CG Control		Negligible	Reduced operating envelope

Fig.5 Degraded situation impact

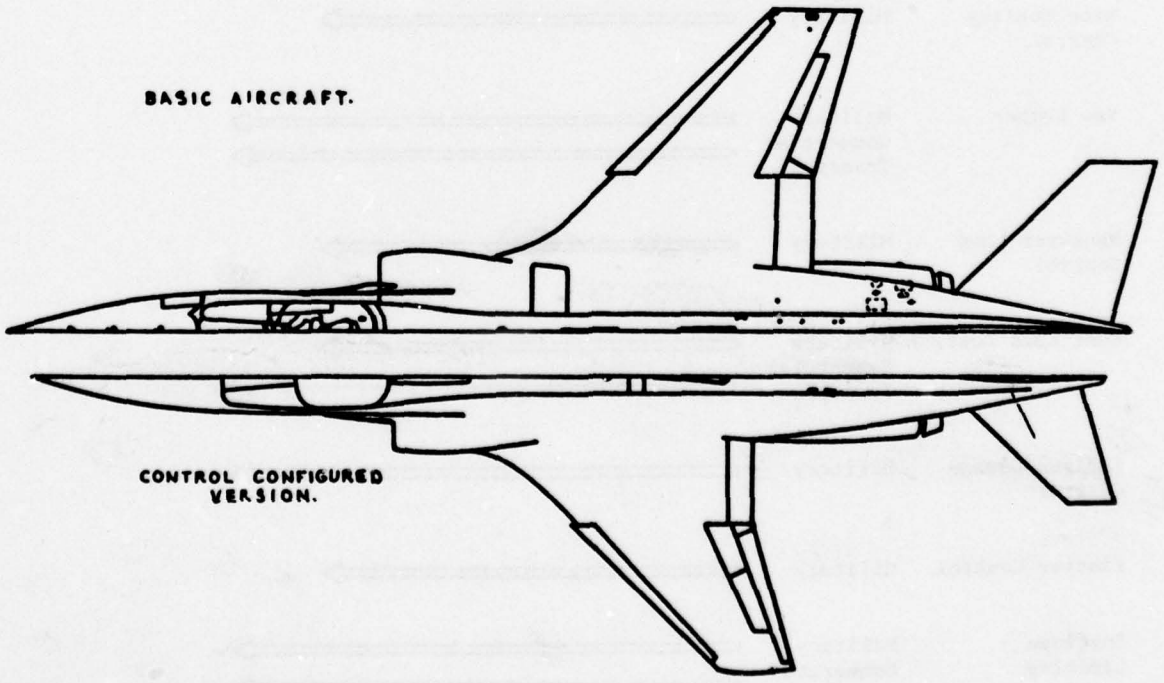

Fig.6 Effect of artificial stability on aircraft size

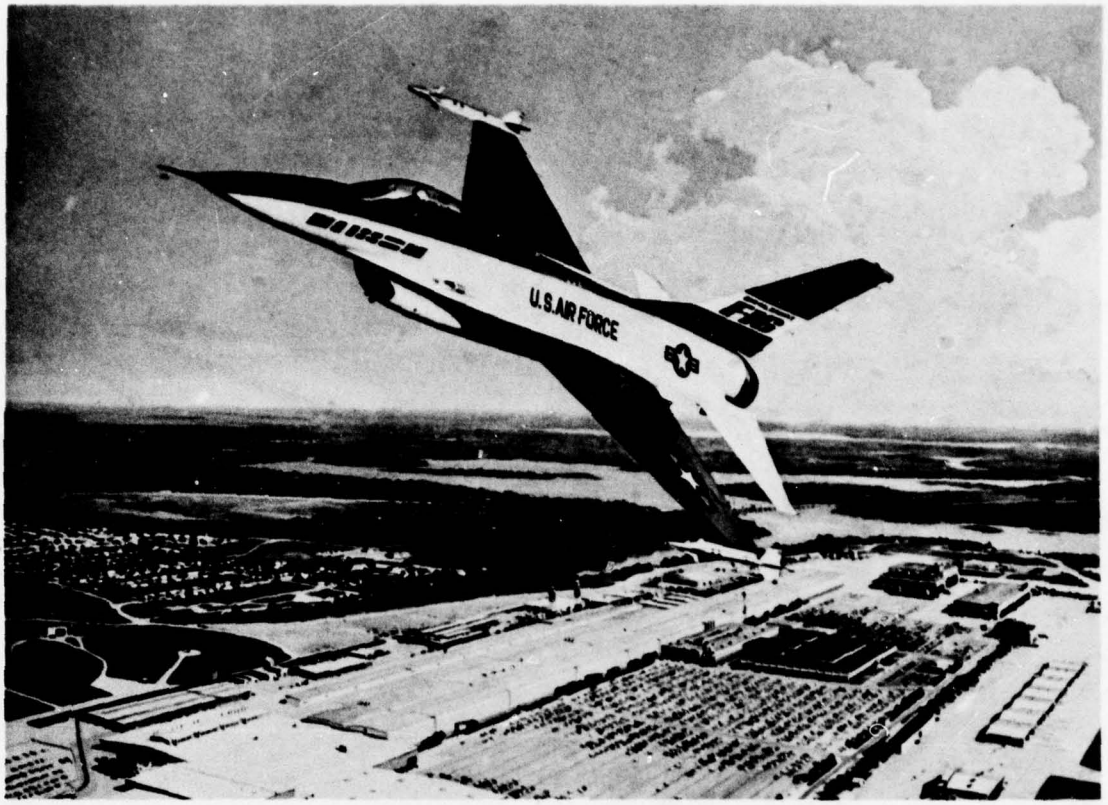

Fig.7 The multi-national F-16 fighter

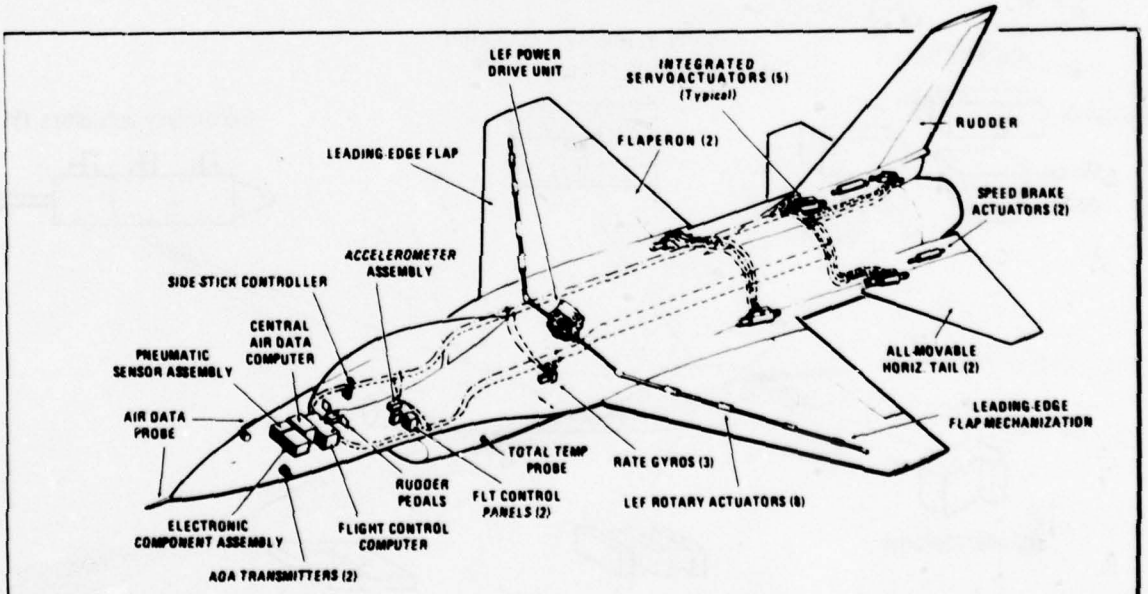

Fig.8 F-16 flight control features

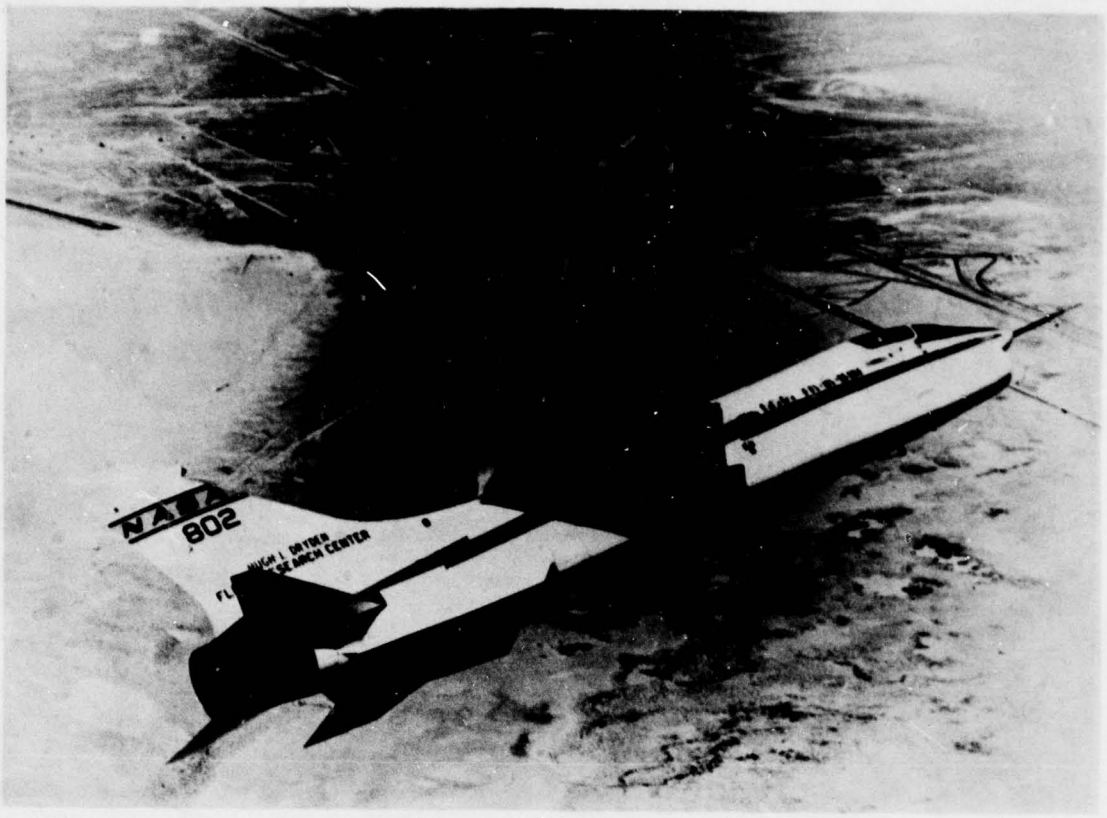

Fig.9 F-8 DFBW aircraft

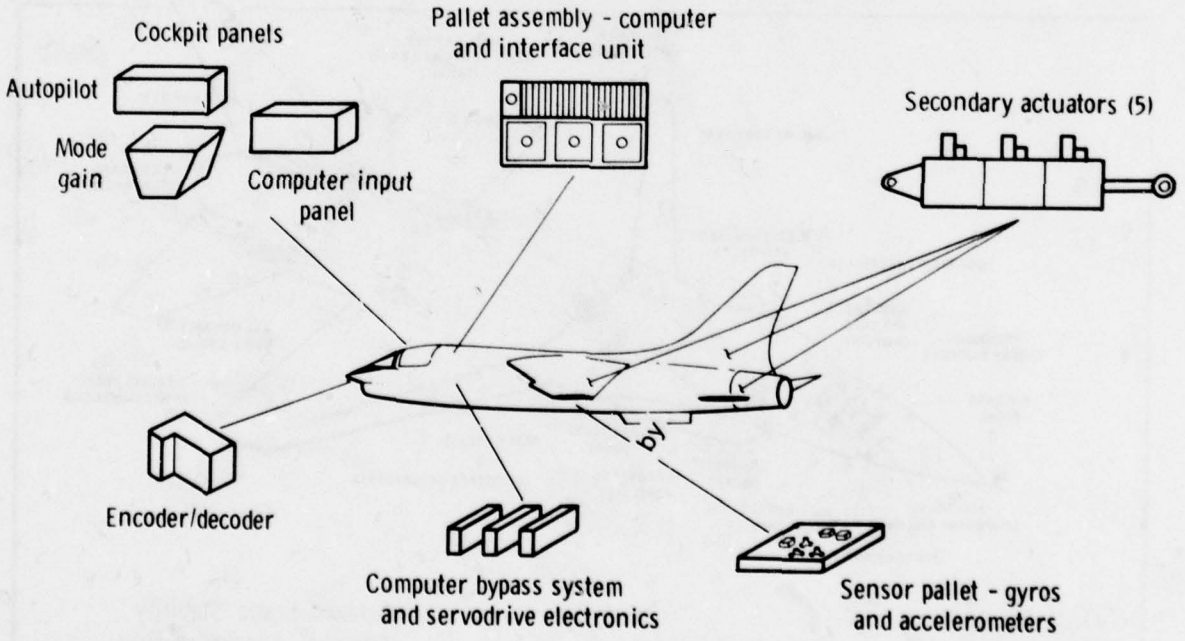

Fig.10 F-8 DFBW hardware elements

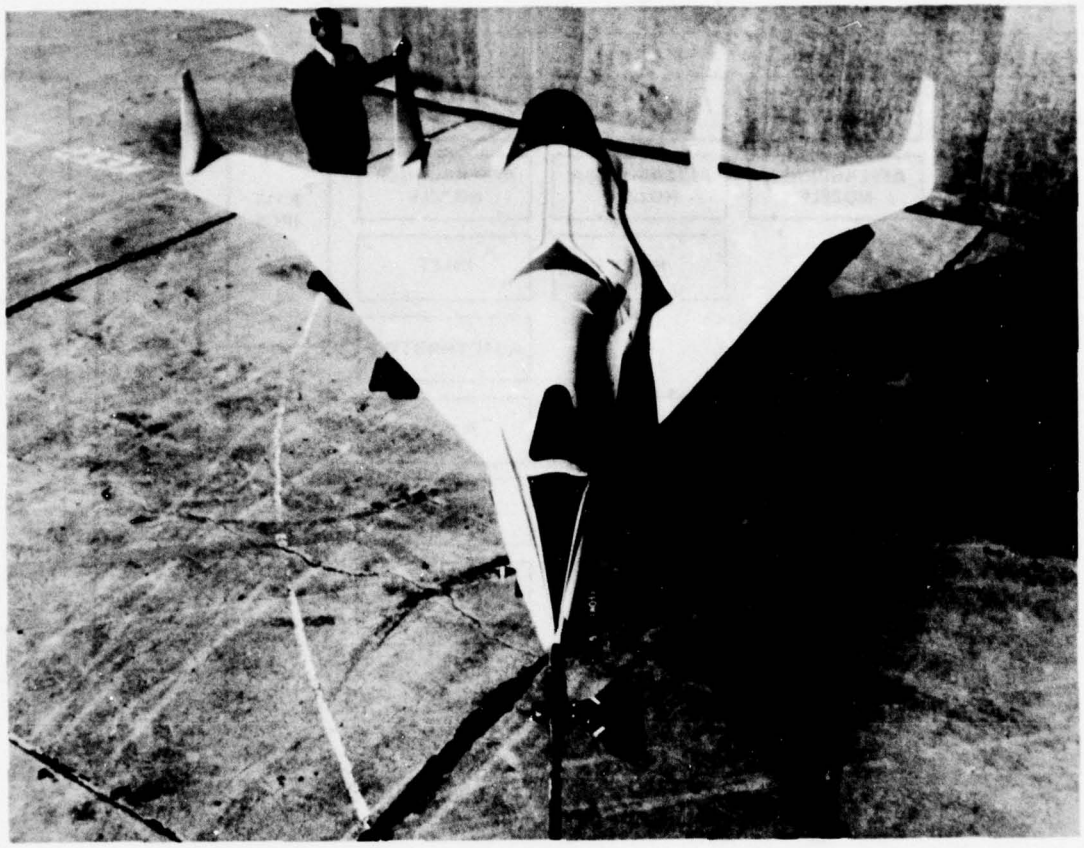

Fig.11 HIMAT prototype

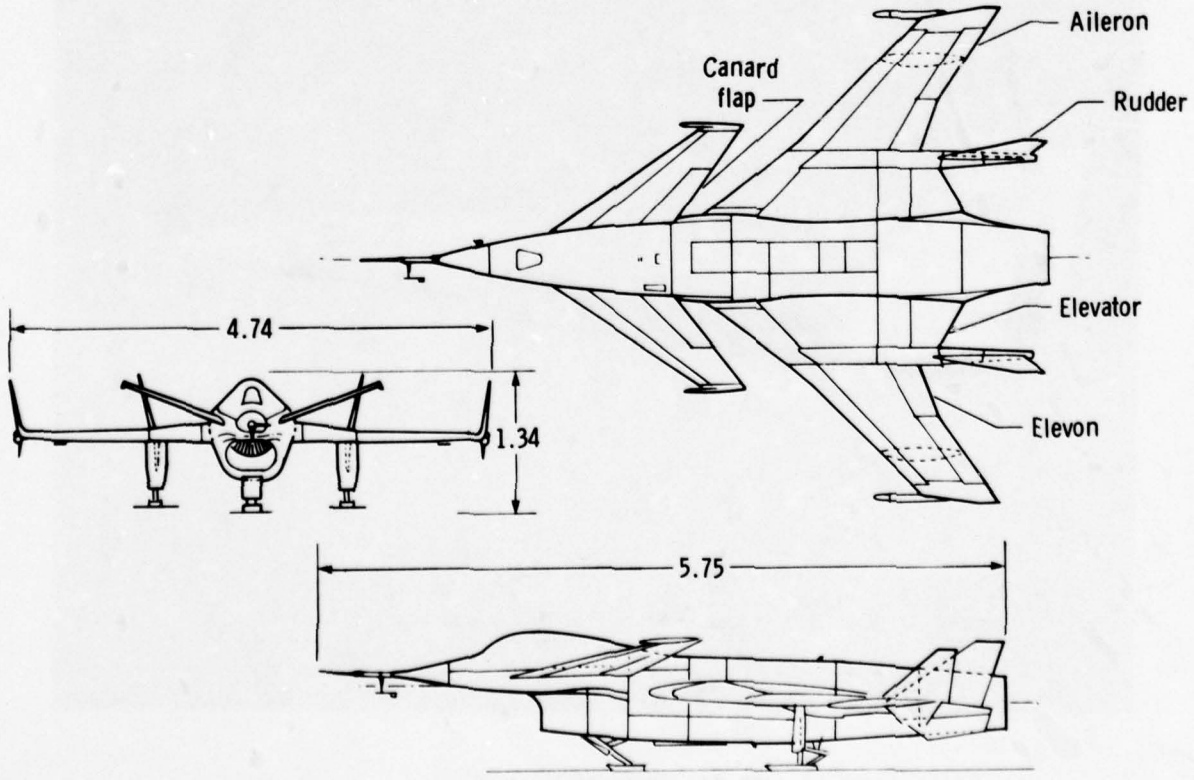

Fig.12 Three-view drawing of HIMAT RPRV. dimensions in meters

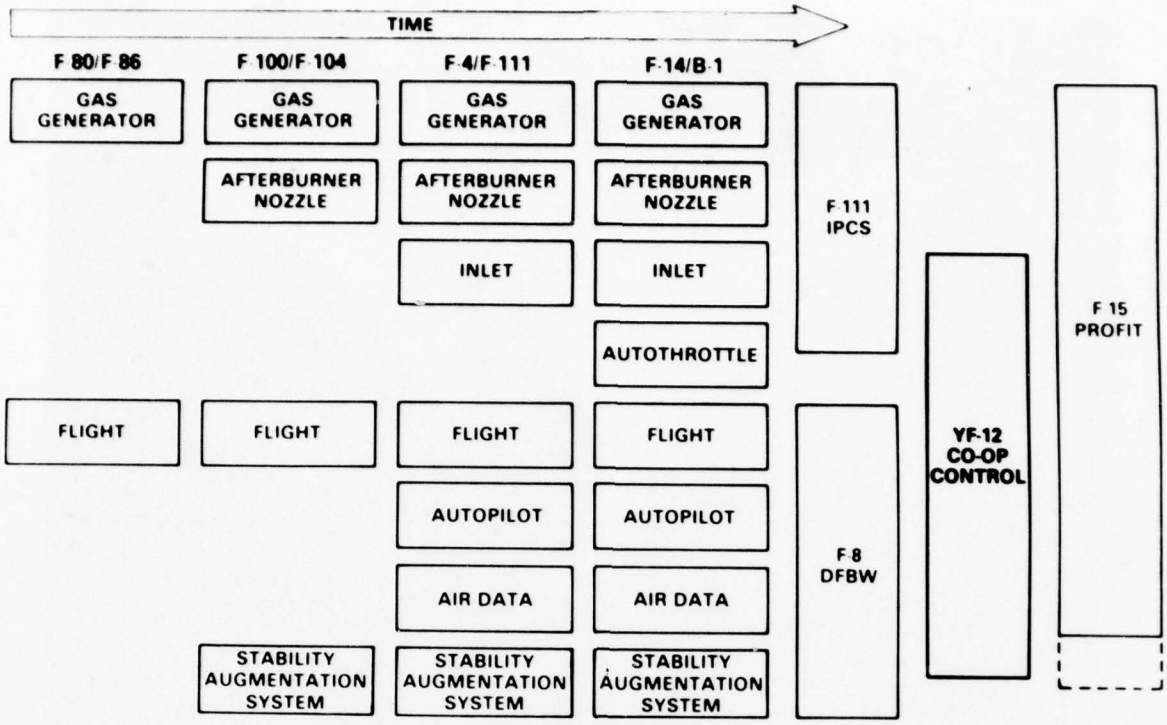

Fig.13 Propulsion/flight control evolution

Fig.14 PROFIT research aircraft

Fig.15 Lockheed L-1011 Tristar

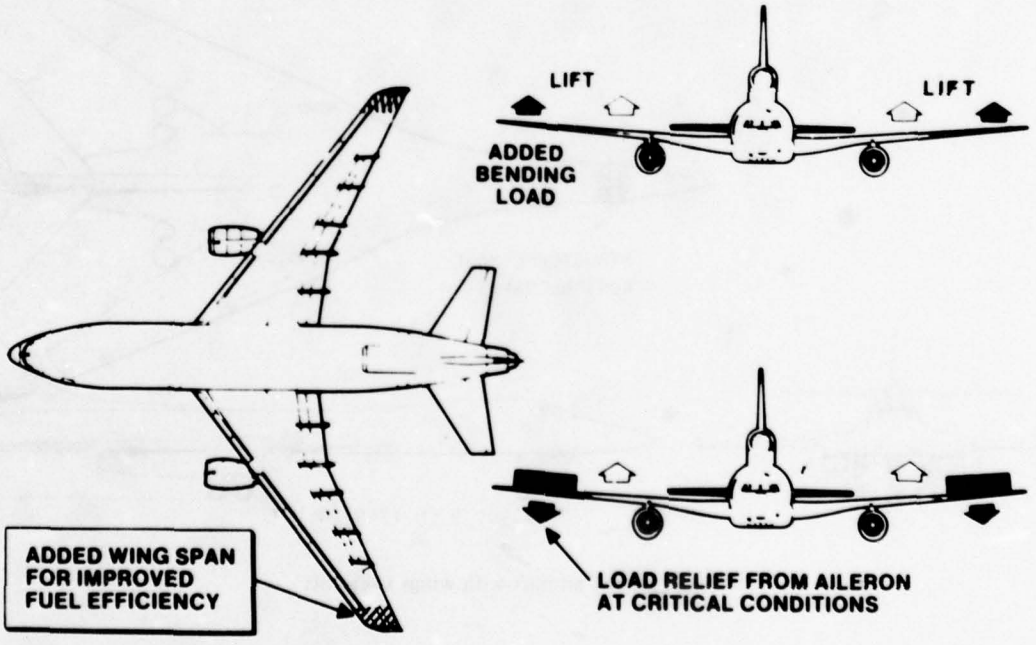

Fig.16 L-1011 active controls

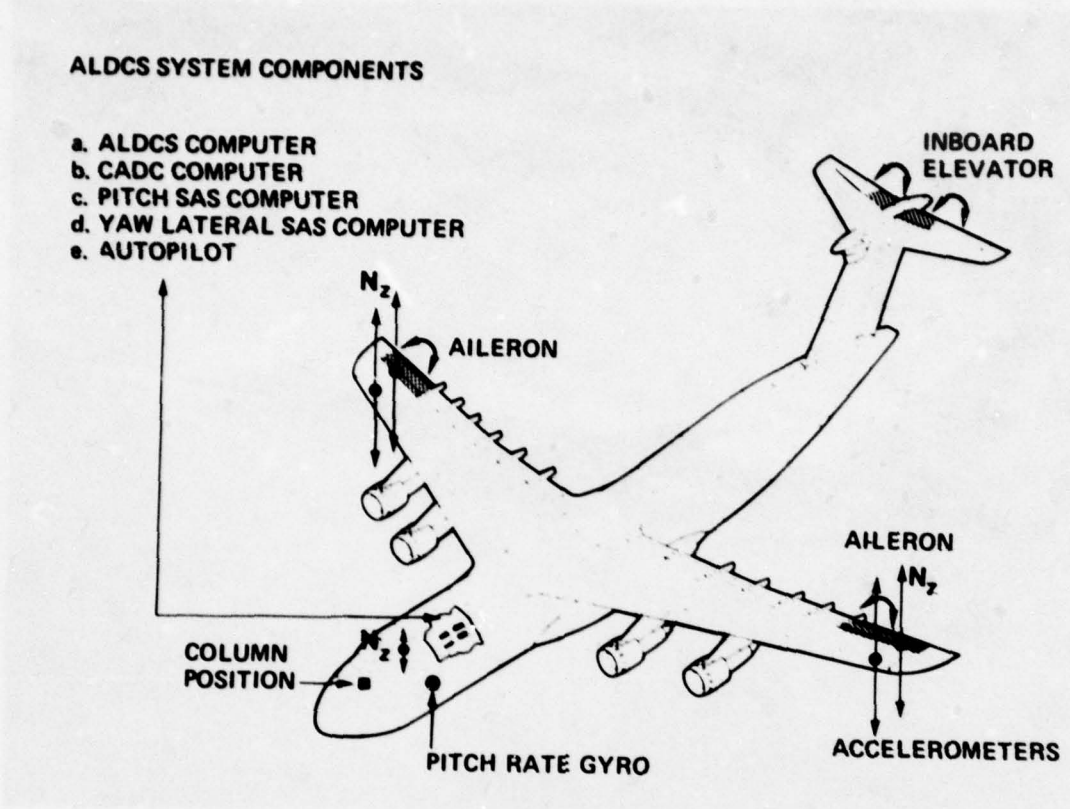

Fig.17 ALDCS system components

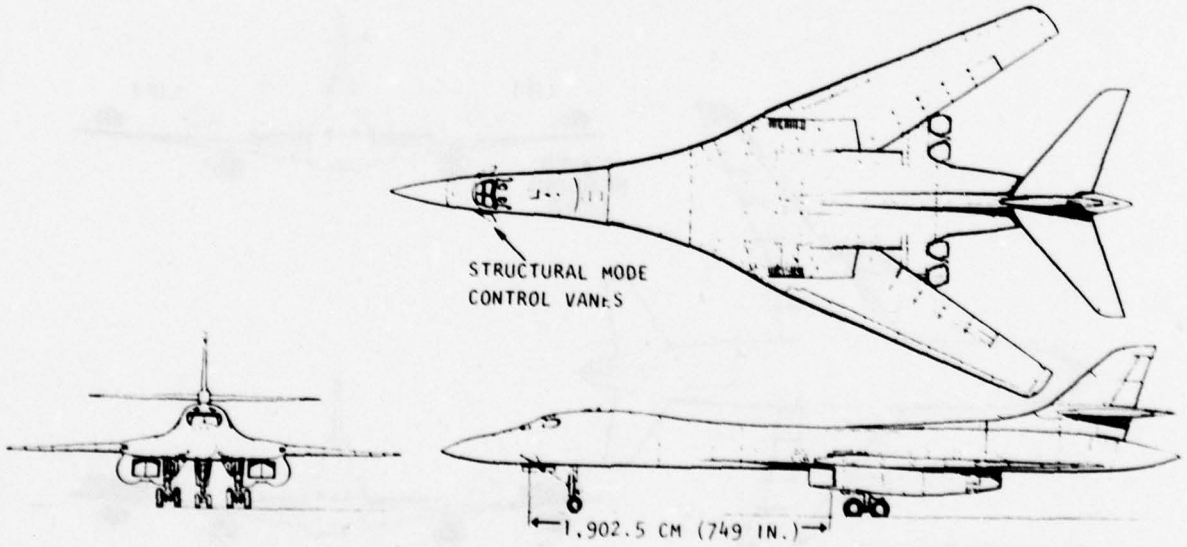

Fig.18 B-1 aircraft with wings swept aft

A SUMMARY OF AGARD FDP MEETING ON DYNAMIC STABILITY PARAMETERS

L. E. Ericsson
Lockheed Missiles and Space Company, Inc.
Sunnyvale, California, USA

SUMMARY

The AGARD Symposium on Dynamic Stability Parameters, held in Athens, Greece, May 22-24, 1978, covered wind tunnel and flight testing techniques, analytical techniques, including motion analysis and nonlinear formulations, and contained a session on sensitivity and simulator studies to assess the importance of the various dynamic stability parameters, including cross-coupling effects between lateral and longitudinal degrees of freedom. One important question to be answered by the meeting was the following: To what extent do we have to abandon past practice of decoupling lateral and longitudinal degrees of freedom? The answer that evolved was that when describing the vehicle dynamics of present day advanced aircraft and aerospace vehicles, which perform sustained operations at high angles of attack, the cross-coupling effects are usually significant and one has to consider lateral and longitudinal degrees of freedom together. The meeting revealed that large communication gaps still exist between the various groups responsible for the design of present and future advanced performance aircraft that must be able to carry out sustained operations at high angles of attack. The meeting filled a void, and the NATO technical community owes a debt of thanks to the AGARD Fluid Dynamics Panel and the meeting program committee chaired by Orlik-Rückemann, Canada, for organizing this rather unique meeting.

1. INTRODUCTION

The aim of the symposium was to determine the needs for dynamic stability information, the form in which it should be presented, and the best means for obtaining such information. A review of the 36 papers presented at the meeting is contained in AGARD Advisory Report No. , "Technical Evaluation Report of the AGARD Fluid Dynamics Panel Symposium on Dynamic Stability Parameters." The present paper is a further condensation and summary to coordinate the mutual interests between the Flight Mechanics Panel and the Fluid Dynamics Panel.

The program consisted of six sessions: Wind Tunnel Techniques I and II, Flight Testing Techniques, Analytical Techniques, Motion Analysis and Nonlinear Formulations, and Sensitivity and Simulator Studies. A Workshop Session, a novel feature for an AGARD meeting, preceded the customary Round Table Discussion, which concluded the meeting.

2. DISCUSSION

Because of the great number of papers presented, it is impossible to present summaries of each paper in the space allowed here. The approach will instead be to highlight the main technical questions raised at the meeting and to illustrate them with the material presented at the meeting and also with additional data when appropriate.

2.1 Wind Tunnel Techniques

A thorough review of the techniques for dynamic stability testing in wind tunnels used within NATO[1#] showed a great diversity in the approach used. However, it was very apparent that little or no attention had been given to the problem of support interference. At high angles of attack the used strut mounting (A1)[##] (Fig. 1a) or sting-strut support (A2) (Fig. 1b) will obviously interfere with the separated flow vortices and base flow wake from the model. The new rotary balances discussed at this meeting[3,4,5] have for structural and mechanical reasons even bulkier support systems (see Figs. 2, 3 and 4).

2.1.1 Support Interference

It is by now well known in the missile industry that asymmetric support systems can cause strong dynamic interference effects (A3, A4), generating nonlinear departure from the expected linear characteristics of slender cones both at hypersonic (A5) and transonic (A6) speeds (Fig. 5). The sting-strut juncture is a typical source of such asymmetric sting interference (A7) (Fig. 6). Although moving the strut downstream eliminated the dynamic support interference for 1 degree amplitude oscillations around $\alpha = 4^\circ$ (Fig. 6a), the support interference still persisted at some angles of attack until the sting-strut juncture was supplied with a splitter-plate fairing (Fig. 6b). Though the splitter-plate solution in Fig. 6b is of little direct help for solving the rotary rig support problem (Figs. 1-4), it illustrates what can be accomplished through simple means. The results (A6) in Fig. 7 illustrate the effect of "wake-flipping." Oscillations around $\alpha = 0$ experience the full effect of the support-induced moment-discontinuity $\Delta^i C_m$, with the result that the measured damping derivative[###] contains one component that varies inversely with amplitude

$$\Delta^i \overline{Cm}_{\dot{\theta}_d} = -\frac{2}{\pi} \frac{\Delta^i C_m}{\Delta\theta} \frac{U_\infty \Delta t}{c} \tag{1}$$

and another, due to associated static α-hysteresis, that is inversely proportional to the amplitude squared and to the reduced frequency

$$\Delta^i \overline{Cm}_{\dot{\theta}_h} = -\frac{2}{\pi} \frac{\Delta^i C_m}{\Delta\theta} \frac{1}{\bar{\omega}} \frac{\Delta\alpha_h}{\Delta\theta} \tag{2}$$

where Δt and $\Delta\alpha_h$ are the lumped representations of time lag and hysteresis effects (A3).

\# Superscript n designates paper number in the AGARD meeting.
\## Parenthesis (An) designates additional references.
\### The derivative concept is no longer valid in this case. However, the mean integrated measure of the energy dissipation, indicated by the bar in the derivative symbol, is still a descriptive measure.

The "wake-flipping" in Fig. 7 gives an indication of the problem one can anticipate for the wake and vortex interactions with the high α support systems shown in Figs. 1-4. Support-induced hysteresis effects on side force $C_Y(\alpha)$ and side moment $C_n(\alpha)$ have been reported (A8).

One way to avoid sting and sting-strut support problems is to use the half-model technique[1] (Fig. 9). However, in this case one has instead to deal with the effects of model-induced separation of the boundary layer on the side plate or side wall. How this side wall interference can distort a two-dimensional separated flow region has been demonstrated for static and dynamic airfoil stall (A9, A10) (Fig. 9). That an oscillating three-dimensional body will interact with the side wall boundary layer equally strongly is indicated by static (A11) and dynamic (A12, A13) measurements.

It should be emphasized that even if the static support interference is small, the dynamic effect may still be large. This is the result of the convective flow time lag involved, which also causes the support interference to have opposite effects on static and dynamic stability, as is illustrated in Fig. 10. Both support systems cause interference (A4). However, the difference between the two sets of data in Fig. 10 illustrates the fact that the dynamic interference effect is much larger than the static.

How dramatic the support interference effect could be for an advanced performance aircraft at high angles of attack is illustrated by the experimental results (A14) shown in Fig. 11. An obstacle placed one (center) chord length downstream of the trailing edge on one half of a 76° swept delta wing causes the vortex breakdown to move from 80% to 40% chord, thereby changing the wing loading extensively. In the Workshop at the meeting , selected data were shown from a forthcoming publication (A15) which demonstrated that dynamic sting support interference is aggravated greatly if boundary layer transition occurs on the aft body. This is often the case in transonic wind tunnel tests at close to maximum Reynolds number, a test condition usually sought for subscale tests in most existing facilities.

The side moment derivatives measured by the rotary rigs shown in Fig. 3 and Fig. 4 are compared with flight data in Fig. 12a and Fig. 12b, respectively. It can be seen that significant differences exist already at low angles of attack. The most likely reason for the deviations is support interference (A8), although poor Reynolds number simulation also could cause significant errors (A16). Tunnel wall interference is a much less likely source of error (A17).

2.1.2 Nonlinear Aerodynamics

At high angles of attack the aerodynamic characteristics usually become highly nonlinear. This is the result of various types of separated flow effects. One very common characteristic generated by separated flow is the aerodynamic discontinuity, often associated with hysteresis effects. A mathematical model of how such nonlinear characteristics can affect one degree-of-freedom dynamic behavior was presented in Ref. 10, together with experimental data at $M = 4.5$ for an ogive-cylinder-flare body describing free oscillations in pitch (Fig. 13). The smooth model had retarded, flare-induced, laminar separation with a discontinuous change in the aerodynamic loading taking place when the separation jumps to the nose. The nonlinear behavior results in limit cycle oscillations. Similar flow separations with associated limit cycle oscillations occur at transonic speeds, and have been studied extensively in connection with the first generation of ballistic reentry bodies of heat-sink design (A18). Fig. 14a and Fig. 14b show the two types of nonlinear characteristics occurring, both leading to limit cycle oscillations. Note that the flow separation increases static but decreases dynamic stability, and that the separation-induced effect on the damping increases with decreasing amplitude. This is seen directly in Figs. 14a and 14b, and indirectly through frequency and amplitude characteristics in Fig. 13.

Also shown in Fig. 13 is the effect of applying roughness to the nose of the model. It eliminated the extensive flow separation with associated limit cycle characteristics. This illustrates the problem of scaling dynamic wind tunnel data (A16). Without roughness, flow separation may occur only in the wind tunnel test and not in full scale. On the other hand, applying boundary layer tripping devices destroys the coupling between transition and vehicle motion existing in full scale flight (A19). The trip wire completely eliminates the coupling while distributed roughness may reverse it as it promotes earlier transition on the windward side (A20). The effects of transition on vehicle dynamics can be large even for attached flow (A19), and will, of course, be much greater in presence of separated flow (A16).

The dynamic rolling moment due to pitching measured on a 7° ogive-cone with truncated 45° delta wing and fin[8] shows a narrow peak at $\alpha = 18°$ (Fig. 15), reminiscent of the effect observed (A18) when oscillating at small amplitude around the discontinuity in Fig. 14b (see Fig. 16). One would expect that doubling the 1.5° oscillation amplitude would greatly reduce the magnitude of this peak, as was the case for the flared body shown in Figs. 13 and 14 (see Fig. 17). In order to interpret the nonlinear characteristics in Fig. 15, one would also need the static characteristics, rolling moment due to roll angle (analogous to the data shown in Figs. 13 and 14). The damping-in-yaw derivative shows a corresponding nonlinear peak at $\alpha = 18°$ (Fig. 18).

The roll damping of current fighter aircraft has according to Ref. 33 the amplitude and frequency characteristics shown in Figs. 19a and b. It would appear that a discontinuous rolling moment component ΔC_ℓ due to a change in separated flow pattern, similar to the moment discontinuity $\Delta^i C_m$ used in Eqs. (1) and (2), could be found which together with a suitable roll angle hysteresis $\Delta\varphi_h$ could explain the characteristics shown in Figs. 19a and b. Again, one needs the static characteristics, obtained for increasing and decreasing roll angle in order to define the hysteresis, $\Delta\varphi_h$, before one can identify the type of nonlinear dynamic characteristics described by results such as those shown in Figs. 19a and b.

2.2 Flight Testing Techniques

In flight tests one avoids the difficult problem of support interference but has instead the equally difficult one of identifying stability and control parameters from a multi-degree-of-freedom analysis of dynamic flight test maneuvers. The experience with military aircraft shows a less than satisfactory state of the art[14] (Fig. 20). Most of the results obtained to date are based on linear aircraft modelling[15]. For a few special cases of cross-coupling at moderate angles of attack, such as for the oblique wing aircraft, the aerodynamic cross-coupling can be obtained with a linear model (Fig. 21). Linear equations

of motion can also be used for small perturbations around a nominal condition to describe a continuous, nonlinear aerodynamic characteristic (Fig. 22). However, for the general case of an aircraft flying at high angles of attack, one needs a realistic, nonlinear mathematical model, including cross-coupling effects, before good parameter identification is possible. Until such a model with sound phenomenological basis becomes available, all flight test data analysis should meet the following criteria according to Iliff (see Round Table discussion in CP-235). 1) Higher order error statistics must indicate that the estimates are valid. 2) The quality of the fit must be very good, and even small discrepancies must be explained. 3) The simplest mathematical model that fits the data must be used. 4) A consistent trend must result for each estimated coefficient as each independent variable is changed. 5) A plausible physical explanation for each resulting model should be found. 6) The resulting mathematical model must be evaluated on a completely independent set of data.

Flight test data for a YF-16 fighter, modified to provide the control capabilities required by a Control Configured Vehicle (CCV), revealed the existence of significant aerodynamic interactions.[16] When using Direct Lift Control (DLC) in the pitch-pointing mode at high angles of attack the required trailing-edge-up flap deflection caused a severe loss in tail power, limiting the application of DLC to $\alpha < 18^{\circ}$ (Fig. 23). Negative flap deflections also caused buffet problems (Fig. 24). Direct Side Force Control (DSFC) had been accomplished by means of coordinated deflections of vertical, ventral canards and the rudder. The addition of the canards reduced the static directional stability by 50% (Fig. 25a), but did not significantly degrade the dynamic directional stability (Fig. 25b). The Relaxed Static Stability (RSS) limits for safe operation had also been investigated, revealing the difficulties existing in realizing the full RSS-benefits (Fig. 26). It was concluded that the CCV-concept rather than reducing was increasing the demands on an accurate determination of the aerodynamic characteristics.

2.3 Analytical Techniques

A review of available theoretical methods for prediction of the unsteady missile aerodynamics[20] revealed that the state of the art has matured in regard to predicting the stability derivatives at $\alpha = 0$, using linear aerodynamic methods. However, the state of the art is still in a state of rapid development in regard to predicting the nonlinear aerodynamics at high angles of attack. Fig. 27 shows the predictions of delta wing pitch damping as given by various theories. In Fig. 28 the bandwidth of the theoretical predictions from Fig. 27 is indicated and compared with available experimental data. The agreement is rather good. In Fig. 29 the effect of angle of attack on a unit aspect ratio delta wing is shown. These nearly linear data are realized only for the mid-chord oscillation center. The experimental data (A21) for the three quarter chord oscillation center shows a very strong nonlinear effect of angle of attack, a trend that is well predicted by the theory of Ref. 24 (see Fig. 30). Notice how the leading edge vortex has opposite effects on static and dynamic stability. Using static experimental data as an input, the method of Ref. 24 can also predict the highly nonlinear stability characteristics of the Space Shuttle Orbiter (Fig. 31).

A review of analytical and experimental techniques to predict aerodynamic characteristics at high angles of attack of a fighter aircraft[19] showed numerous examples of how such high-α flow phenomena as vortex burst, asymmetric body vortices, and wing stall could cause various vehicle dynamics problems such as spin entry, wing rock and buffet, roll reversal and departure, yaw and pitch departures, as well as strong aerodynamic pitch-yaw cross-coupling. That vortex breakdown is associated with yaw-hysteresis (Fig. 32) is no surprise in view of the observed α-hysteresis (A22) (Fig. 33). Fig. 34a shows how a geometric modification greatly improved the directional stability in the stall region. It was, therefore, a disappointment that the wing-rock behavior was not improved in the flight tests. This was ascribed to lack of any beneficial effects on the roll-damping from the modification, as roll damping has a dominant influence on wing rock (Fig. 34b). It was not indicated what the geometric change consisted of. However, in the stall region one can be certain that it affected the separated flow behavior (vortices, shock-boundary layer interaction, etc.). Consequently, one can expect the modification to have an adverse effect on the yaw damping (C_{n_β}) (according to the previous discussion). The C_ℓ-data in Fig. 34a indicate that also the roll damping would be affected adversely. Thus, the flight test results simply demonstrated that separated flow affects static and dynamic stability in opposite ways.

Fig. 35 shows how the asymmetric vortex shedding effects observed in a wind tunnel test can be representative of full scale flight. In this case the reason must be that the Reynolds number in both cases was well on the supercritical side, and the difference in actual magnitude had an insignificant effect. However, considering the non-repeatability of these asymmetric vortex effects in wind tunnel tests at subcritical Reynolds numbers (A23) (Fig. 36), the agreement in Fig. 35 is nothing short of remarkable. At critical Reynolds numbers, where the side load induced by the asymmetric vortices reaches its maximum, the tunnel data scatter makes it very difficult to obtain a prediction of the maximum possible side force. However, a conservative estimate can be obtained using unsteady two-dimensional cylinder data (A24). An effective fix for elimination of the asymmetric vortex effects is the use of a forebody strake (Fig. 37a). However, it has the adverse effect of reducing the directional stability (Fig. 37b). If one instead of using forebody strakes changes the nose geometry as is shown in Fig. 38, the so-called Shark Nose modification, one not only gets rid of the asymmetric vortex effects (Fig. 39a)# but also obtains improved directional stability characteristics (Fig. 39b). Adding a Wing Leading Edge Extension (LEX) (Fig. 40a) further improves $C_{n_{\beta DYN}}$ (Fig. 40b). This Shark Nose/W6LEX fix[19] is a beautiful example of what can be accomplished by subtle geometric configuration changes when the flow phenomenon causing the problem is well understood.

Another type of leading edge extension, the conventional wing-body strake (Fig. 41), had also been investigated[11], showing highly beneficial effects on buffet characteristics (Fig. 42) and on the damping in pitch, yaw, and roll (Fig. 43). It was emphasized in Ref. 19 that vast amounts of tunnel and flight test data are available which have not been fully analyzed and correlated, not even for individual aircraft, much less across the board. Across the board correlation efforts are made very difficult by the extreme configuration sensitivity of these high-α flow phenomena. However, this also makes the achievable gains in future military aircraft designs that much greater.

#The W_6 LEX modification does not affect C_n at $\alpha > 30^{\circ}$.

2.4 Motion Analysis and Nonlinear Formulations

By inclusion of time-history effects a formulation of the aerodynamics of aircraft dynamics had been obtained that is general enough to allow for the discontinuous, hysteretic aerodynamic characteristics usually experienced at high angles of attack.[26] That one cannot substitute the basic, steady-state coning motion of Ref. 26 with a simplified formulation independent of side slip was amply demonstrated in Ref. 27 by comparison with free-flight test data for a quarter scale aircraft model (Figs. 44-46). The difficulty presently is that there are no aerodynamic test data available that make it possible to use the correct, more general formulation of Ref. 26. Hopefully, such data will become available in the near future using the appropriate testing procedures (A25).

A nonlinear analysis of aircraft stability characteristics at high angles of attack[29] had provided stability critieria for the fully coupled six-degrees-of-freedom case. The criteria had been validated by a complete six-degrees-of-freedom perturbation analysis and by flight test results. Even the non-linear, non-zero aerodynamic characteristics generated at zero sideslip, e.g., by asymmetric forebody vortices, could be accounted for (Fig. 47). The formulation does in its present form not account for any unsteady aerodynamic effects, but is being modified to remove this deficiency.

2.5 Sensitivity and Simulator Studies

In a review of results of piloted simulator studies of fighter aircraft at high angles of attack[33] various examples were given showing how nonlinear aerodynamic characteristics could explain nose slice, wing rock, adverse yaw, and other problems encountered by an advanced fighter maneuvering at high angles of attack. While airframe modifications and use of control interconnects sometimes provided solutions, more often than not the only recourse had been maneuver limiting. Fig. 48a shows the extremely nonlinear characteristics caused by asymmetric vortex shedding off a pointed slender nose (note the non-zero C_n-value at $\beta = 0$). At yaw angles above 10° magnitude the original asymmetric vortex shedding is changed and the directional stability changes from highly favorable to highly adverse. The rapid change of directional stability changes from highly favorable to highly adverse. The rapid change of directional stability with angle of attack is illustrated in Fig. 48b, and Fig. 48c demonstrates the coupling existing between the deflection of an all movable tail and the directional stability. The corresponding dynamic stability derivatives are also highly nonlinear (Fig. 49). How important the dynamic stability parameters are is demonstrated in Fig. 50. A small change of the roll damping in the stall region caused a large change in vehicle motion[19]. If one adds to these results the amplitude and frequency effects illustrated in Fig. 19, one can appreciate fully the difficulty involved when simulating something like wing rock. That one sometimes beats these odds, provided that the needed forced oscillation test results are available, is demonstrated by Fig. 51. The high-α aerodynamics are extremely configuration sensitive, and as a consequence the relative importance of static and dynamic stability parameters had varied considerably, the simulator studies showing the dynamic stability parameters to be of little importance for some configurations and very important for others. It is extremely important to identify the true nature of the aerodynamic high-α characteristics, especially in regard to existing discontinuities and aerodynamic hysteresis effects. In addition to the α-, β-, and φ-hystereses discussed so far one has also to recognize the possibility of spin-rate-hysteresis[3](Fig. 52).

In a hybrid computer study of the sensitivity of aircraft motion to aerodynamic cross-coupling[34] linear and locally linearized representation of the aerodynamic characteristics had been used. A representative military aircraft had been chosen for the physical characteristics and the traditional aerodynamic derivatives were based on experiment for such an aircraft. However, because they were the only experimental results available the cross-coupling derivatives for the generalized configuration of Ref. 8 had been used (Figs. 15 and 53). When judging the results of the study, one has to keep this in mind. The study showed that the most important aerodynamic cross-coupling was the effect of pitch rate on lateral characteristics, whereas the effects of yaw and roll rates on longitudinal characteristics were insignificant. It was found that the rolling and yawing moments due to pitch rate were larger than those due to roll and yaw rates, respectively. Use of locally linearized derivative values greatly increased the effect of cross-coupling on vehicle motion. The study showed the dynamic cross-coupling terms to have a larger effect on the vehicle motion than the static terms. Although the results may be distorted due to the lack of matched aerodynamic cross-coupling derivatives, the authors felt that the results should be quite representative of a present-day fighter flying at high angles of attack.

The same mismatched cross-coupling derivatives had been used in another study of aircraft motion sensitivity to variations in dynamic stability parameters[35], and the results were, therefore, similar in many respects. For the aircraft characteristics chosen, the results of the study showed that when the cross-coupling derivatives $C_{\ell q}$ and C_{nq} were of a magnitude four (4) times as large as the lateral cross derivatives $C_{\ell r}$ and C_{np}, they become of equal importance to the vehicle motion. Using hypothetical separate values for acceleration and rotation derivatives the authors had found the acceleration derivatives $C_{n\dot{\beta}}$ and $C_{\ell\dot{\beta}}$ to have a strong effect by themselves on the aircraft lateral/directional motion characteristics. Consequently, they should be separated from their rate counterparts, C_{nr} and $C_{\ell r}$, in motion analyses. They had analyzed two different aircraft, a Fighter/Bomber type and an Attack Type, and had found the general results of their sensitivity study to be independent of the aircraft considered. This was contrary to results presented earlier in this meeting[28], a fact that may be explained if one looks closer at the two aircraft studied (Fig. 54). The similar geometric features would imply that the aerodynamic high-α characteristics are not very different, contrary to the low sweep versus high sweep geometries in the other transport versus fighter aircraft study[28]. In a paper about the identification of key maneuver-limiting factors in high angles of attack flight[36], the cross-coupling effect of angle of attack on rolling moment was one identified important factor. It caused a decrease of roll damping for the F-4 aircraft and led to wing rock. The limit-cycle characteristic of the F-4 wing rock was determined by the effect of yaw on the pitching moment derivative, $C_{m\beta}$, a cross-coupling effect found to be insignificant in the preceding two papers. An interesting feature of $C_{m\beta}$ is that it is insensitive to the sign of β and, therefore, responds at twice the β-frequency. It was pointed out in the discussion that the inertia coupling also gives this double frequency response. However, according to the author the rates were so small that the kinetic cross-coupling was negligible. That this often is not the case had been shown earlier[15] (Fig. 55).

3. CONCLUSIONS

The greatest service this AGARD meeting on Dynamic Stability Parameters performed for the NATO technical community may well be that it revealed that large communication gaps still exist between the various groups responsible for the design of present and future advanced performance aircraft, which must be able to carry on sustained operations at high angles of attack. Because of the magnitude and complexity of the tasks involved, the various specialists tend to be absorbed by their own problems and have little time over for inter-disciplinary dialogue. It was apparent that this meeting filled a void. As so often is the case, the very difficulties that make communication so hard also make it essential that communication does take place. What follows is a list of the problems I became aware of during the meeting - not only through the many excellent, official presentations and discussions but also to a large extent through private conversations with many meeting participants.

- o Cross-Coupling. There was convincing evidence presented in this meeting that, when analyzing the aircraft characteristics at high angles of attack, one can no longer decouple lateral and longitudinal degrees of freedom. Although the results of the various linearized analyses have to be viewed with a certain degree of caution because of the highly nonlinear nature of the high-α characteristics, this does not change the fact that for the amplitudes and reduced frequencies for which the used aerodynamic parameters apply, the cross-coupling effects were found to be very significant. The largest effect was that of pitch on lateral characteristics, whereas in general the effect of yaw and roll on longitudinal characteristics were found to be modest. It should be emphasized that this applies only to the particular types of configurations investigated. In view of the extreme configuration sensitivity no general statements can be made.

- o Configuration Sensitivity. The new unusual aerodynamic characteristics encountered at high angles of attack are generated by various forms of flow separation. Consequently, the high-α aerodynamics are extremely configuration sensitive. Even a boundary layer trip can in many cases qualify as a geometric configuration change. Thus, apparently similar configurations can exhibit widely different high-α characteristics.

- o Reynolds Number Effects. As the high-α characteristics are dominated by separated flow effects, they are very dependent upon Reynolds number. This makes the use of subscale test data very difficult, especially in regard to dynamic characteristics. It is well documented that there is a strong coupling between the boundary layer transition process and the vehicle motion. This coupling affects the unsteady aerodynamics significantly even for attached flow and has a much stronger effect in presence of separated flow. Thus, one cannot use boundary layer tripping devices if one wants to simulate full-scale unsteady aerodynamics in a subscale model test.

- o Dynamic Test Techniques. Because of the nonlinear character of the high-α characteristics it is important to have a direct, single-parameter relationship between the quantity measured and the stability parameter to be determined. Even though the standard type derivative measure obtained in such a dynamic test may vary with both amplitude and frequency, thus strictly speaking invalidating the derivative concept, the measure obtained is descriptive and will together with appropriate static data make it possible to define uniquely the mathematical model that correctly describes the nonlinear high-α dynamic characteristics. Theoretical models established in this fashion may be applied as building blocks in the mathematical modelling of multi-degrees-of-freedom vehicle motion. The unknown character of the aerodynamic high-α characteristics, including cross-coupling effects, necessitates using a dynamic calibrator of some type, e.g., as is described in paper 9.

- o Support Interference. In captive testing model support interference presents a problem even at low angles of attack. At high-α, with associated separated flow vortices and wakes, the downtream support system is an even larger source of interference. It has already been shown that a strut support provides a formidable static support interference. The problem is compounded when one considers that based upon past experience the dynamic support interference can be large even when the static interference is negligible. All the high-α dynamic test rigs discussed at this meeting could cause significant support interference. Although the interference characteristics are different for sting, strut and side plate supports, they can all be significant.

- o Nonlinear Aerodynamics. The nonlinear characteristics at high angles of attack are generated by separated flow. When the dominating effect comes from leading edge or trailing vortices there is an α-range in which series expansion methods are valid, because the aerodynamics are continuous. However, when the vortices burst, or a sudden change of separated flow pattern or extent occurs, the aerodynamic characteristics become discontinuous, and are often associated with hysteresis effects, which all are characteristics that cannot be modelled by the popular series expansion approach. Thus, it is essential that one understands the physical background for the nonlinear characteristics. For the discontinuous characteristic the dynamic stability parameter (the damping derivative) measured in a wind tunnel test will have a major component that is inversely proportional to the oscillation amplitude. If static (rate-independent) hysteresis is present, another component will be inversely proportional to the reduced frequency and the amplitude squared. In this case locally linearized methods will not suffice. The correct treatment is not mathematically difficult, but one must know when to apply it.

- o Mathematical Modelling. There is no doubt that when one wants to model the high-α aerodynamics of an advanced aircraft one needs a formulation as general as that presented by Tobak and Schiff, which can handle discontinuities and hysteresis effects. However, the practical application of such a formulation hinges strongly on the availability of the mathematical building blocks discussed earlier. The problem is to obtain the aerodynamic parameters in the form needed to verify the mathematical modelling through comparison with multi-degrees-of-freedom test results. The mathematical modelling is the pacing factor in present simulation and flight data analysis for aircraft maneuvers at high angles of attack.

- o Dynamic Stability Parameters. Throughout the meeting questions were raised in regard to the relative importance of static and dynamic stability parameters, including cross-coupling terms. Invariably the answer seemed to be that this depended entirely upon the configuration, a seemingly unimportant change swinging the importance from dynamic to static and vice versa. This may be understood if one considers the fact that the high-α aerodynamics are dominated by separated flow effects. It is by now well established that for rigid body dynamics (and elastic vehicle dynamics of modest reduced frequency) the separation-induced aerodynamic forces affect static and dynamic stability in opposite ways, i.e., the effect can be statically stabilizing and dynamically destabilizing, or the other way around, as was demonstrated in paper 24. Which it is depends on such configuration details as the location of separation source and responding aircraft surface in relation to the center of gravity. If one makes the rather safe assumption that it is the adverse effect that receives the main attention, one can see why it depends so much on configuration details whether dynamic or static stability parameters are important. However, because of the amplification through convective time lag effects, the dynamic effects of separated flow are generally much greater than the static effects. Consequently, one should be most concerned about the dynamic stability parameters of an aircraft operating at high angles of attack. Hence, the topic of this meeting could not have been more appropriate.

- o Credibility/Communication. Because of all the problems listed above it is quite possible, even likely that flight test engineers and vehicle designers can have experimental results that in their eyes cast doubt upon the validity of results published by wind tunnel test engineers and analysts, which show large cross-coupling effects and adverse vehicle dynamics. Thus, it is vitally important that communication channels are kept open and that every effort is made to improve the interdisciplinary dialogue, as was emphasized by Iliff and others throughout the meeting.

4. RECOMMENDATIONS

The present meeting took the first step towards establishing a mechanism through which the various groups involved in the aerodynamic design of aircraft and missiles can exchange information that will lead to a more efficient use of available resources. This should only be the beginning, the first meeting in a regular series. The many problem areas uncovered in this meeting should be investigated and reported on next time. The following recommendations are made:

a) Initiate a cooperative research program to investigate the difficult problem of support interference. Because of the complete dependence on wind tunnel test data of motion simulations, flight test data reduction and sensitivity studies, this problem of support interference must be resolved before meaningful progress can be made.

b) Stress the importance of obtaining the following complementary data in all high-α testing.

   1. Flow visualization data
   2. Static data for increasing and decreasing parameter values (α,β, η, etc.) in order to define aerodynamic hysteresis
   3. Static and dynamic stability data for the same test conditions, in the same wind tunnel, and with the same support geometry
   4. Test data for the widest possible Reynolds number range including effects of boundary layer tripping devices.

c) Investigate the scaling problem for high-α dynamic (and static) data.

d) Promote more extensive analysis of available high-α experimental data.

e) Continue work on formulation and verification of mathematical modelling of high-α unsteady aerodynamics, including the effects of cross-coupling and the effect of discontinuous and hysteretic static aerodynamic characteristics.

f) Establish a consistent set of aerodynamic data to determine the importance of cross-coupling for a few basic configurations.

g) Measure the effects of small geometric perturbations from these basic configurations to establish in a systematic manner the configuration sensitivity of high-α aerodynamics, including cross-coupling effects.

h) Attempt to generate design guidelines for aircraft operating at high angles of attack.

The ultimate goal is, of course, to obtain the detailed understanding of the steady and unsteady fluid dynamics needed for successful design of future advanced aircraft and aerospace vehicles.

5. REFERENCES

Papers in AGARD CP-235

1. K. J. ORLIK-RÜCKEMANN, NAE, Canada - Dynamic Stability Testing in Wind Tunnels.

2. W. CHARON et R. VERBRUGGE, IMFL, France - Nouvelle Technique d-Essais sur Maquettes Libres en Laboratoire pour la Détermination de Caractéristiques Aérodynamiques Instationnaires.

3. G. N. MALCOLM and S. S. DAVIS, NASA-Ames, USA - New NASA-Ames Wind Tunnel Techniques for Studying Airplane Spin and Two-Dimensional Unsteady Aerodynamics.

4. A. W. MATTHEWS, B.A.C., UK - Experimental Determination of Dynamic Derivatives due to Roll at B.A.C. Warton.

5. X.HAFER, T. H. Darmstadt, W. Germany - Wind Tunnel Testing of Dynamic Derivatives in W. Germany.

6. J. v.d. DECKEN, Dornier, E. Schmidt, DFVLR and B. SCHULZE, MBB, W. Germany - On the Test Procedures of the Derivative Balances Used in W. Germany.

7. Paper withdrawn

8. K. J. ORLIK-RUCKEMANN, NAE, Canada - Experiments on Cross-Coupling and Translational Acceleration Derivatives

9. E. S. HANFF and K. J. ORLIK-RUCKEMANN, NAE, Canada - A Generalized Technique for Measuring Cross-Coupling Derivatives in Wind Tunnels.

10. X. VAUCHERET, ONERA, France - Détermination de Non-Linéarités de Stabilité Dynamique.

11. P. POISSON- QUINTON and M. CANU, ONERA, France; B. LASCHKA, B. SCHULZE and W. STAUDACHER, MBB, W. Germany - Some Factors Affecting the Dynamic Stability Derivatives of a Fighter-Type Model.

12. R. A. EAST, A.M.S. QASRAWI and M. KHALID, U. of Southampton, UK - An Experimental Study of the Hypersonic Dynamic Stability of Pitching Blunt Conical and Hyperballistic Shapes in a Short Running Time Facility.

13. A. SIMPSON and J. W. FLOWER, U. of Bristol, UK - Unsteady Aerodynamics of Oscillating Containers and Application to the Problem of Dynamic Stability of Helicopter Underslung Loads.

14. P. M. JEGLUM, AFFTC, USA - AFFTC Experience in the Identification of Stability and Control Parameters (Stability Derivatives) from Dynamic Flight Test Maneuvers.

15. K. W. ILIFF, NASA-Dryden, USA - Estimation of Aerodynamic Characteristics from Dynamic Flight Test Data.

16. R. A. WHITMOYER, AFFDL, USA - Aerodynamic Interactions on the Fighter CCV Test Aircraft.

17. E. G. RYNASKI, D. ANDRISANI, II, and N. C. WEINGARTEN, Calspan, USA - Identification of the Stability Parameters of an Aeroelastic Aircraft.

18. T. J. GALBRAITH and T. J. PETERSEN, Boeing, USA - Nonlinear Parameter Identification and its Application to Transport Aircraft.

19. A. TITIRIGA and A. M. SKOW, Northrop, USA - Analytical and Experimental Techniques to Predict Aircraft Dynamic Characteristics at High Angle of Attack.

20. C. P. SCHNEIDER, MBB, W. Germany - Presentation of Stability Derivatives in Missile Aerodynamics and Theoretical Methods for their Prediction.

21. R. ROSS, NLR, Netherlands - The Use of Panel Methods for Stability Derivatives.

22. W. H. HUI, U. of Waterloo, Canada - An Analytic Theory for Supersonic/Hypersonic Stability at High Angles of Attack.

23. R. HIRSCH, P. MEREAU, G. COULON and A. RAULT, ADERSA/GERBIOS, France - Identification of Unsteady Effects in Lift Build Up.

24. L. E. ERICSSON and J. P. REDING, LMSC, USA - Effect of Flow Separation Vortices on Aircraft Unsteady Aerodynamics.

25. R. BERNIER, CIT, USA and G. V. PARKINSON, UBC, Canada - Oscillatory Aerodynamics and Stability Derivatives for Airfoil Spoiler Motions.

26. M. TOBAK and L. B. SCHIFF, NASA-Ames, USA - The Role of Time-History Effects in the Formulation of the Aerodynamics of Aircraft Dynamics.

27. H.H.B.M. Thomas and G. Edwards, RAE, UK - Mathematical Models of an Aircraft for Extreme Flight Conditions (Theory and Experiment)

28. J. ROSKAM, U. of Kansas, USA - Linear or Nonlinear Methods - When and How?

29. J. KALVISTE, Northrop, USA - Aircraft Stability Characteristics at High Angles of Attack.

30. M. SCHERER, ONERA, France - Expressions des Forces Aérodynamiques Non-Linéaires en Vue des Etudes de Dynamique du Vol.

31. G. D. PADFIELD, RAE, UK - Nonlinear Oscillations at High Incidence.

32. P. C. PARKS, RMCS, UK - The Dynamic Stability in Flight of Spinning Blunt Body Projectiles.

33. J. R. CHAMBERS, W. P. GILBERT and L. T. NGUYEN, NASA-Langley, USA - Results of Piloted Simulator Studies of Fighter Aircraft at High Angles of Attack.

34. W. H. CURRY, Sandia, USA and K. J. ORLIK-RÜCKEMANN, NAE, Canada - Sensitivity of Aircraft Motion to Aerodynamic Cross-Coupling at High Angles of Attack.

35. R. W. BUTLER and T. F. LANGHAM, ARO, USA - Aircraft Motion Sensitivity to Variations in Dynamic Stability Parameters.

36. D. E. JOHNSTON, Systems Technology, USA - Identification of Key Maneuver-Limiting Factors in High Angle-of-Attack Flight.

Additional References

A1. Uselton, B. L. and Jenke, L. M., "Test Mechanisms for Obtaining Dynamic Stability Characteristics of High Fineness Ratio Bodies at Angles of Attack up to 90 Deg.," AIAA Paper No. 76-90, June 1976.

A2. Henderson, W. P., Phillips, W. P., and Gainer, T. G., "Rolling Stability Derivatives of a Variable-Sweep Tactical Fighter Model at Subsonic and Transonic Speeds," NASA TN D-3845, 1976.

A3. Ericsson, L. E. and Reding, J. P., "Viscous Interaction or Support Interference - The Dynamicist's Dilemma," AIAA Journal, Vol. 16, No. 4, April 1978, pp. 363-368.

A4. Reding, J. P. and Ericsson, L. E., "Dynamic Support Interference," Journal of Spacecraft and Rockets, Vol. 9, No. 7, July 1972, pp. 547-553.

A5. Hobbs, R. B., Jr., "Hypersonic Dynamic Stability, Part II, Conical Body Experimental Program," FDL-TDR-64-149, Part II, Jan. 1967.

A6. Adcock, J. B., "Some Experimental Relations Between the Static and Dynamic Stability Characteristics of Sting-Mounted Cones with Bulbous Bases," Transactions of the 3rd Technical Workshop on Dynamic Stability Problems," Vol. II, NASA-Ames RC, Moffett Field, Calif. Nov.1968, Paper 5.

A7. Walchner, O. and Clay, J. T., "Nose Bluntness Effects on the Stability Derivatives of Cones in Hypersonic Flow," Transactions of the Second Technical Workshop on Dynamic Stability Testing, Vol. 1, Arnold Engineering Development Center, Tullahoma, Tenn., April 1965, Paper 8.

A8. Uselton, J. C., "Aerodynamic Characteristics of a High Fineness Ratio Model with Various Spin Rates at M_∞ = 3.0 and 5.0," AEDC-TR-66-171, Sept. 1966.

A9. Moss, G. F. and Murdin, P. M., "Two-Dimensional Low-Speed Tunnel Tests on the NACA 0012 Section Including Measurements Made During Pitch Oscillation at the Stall,"CP No. 1145, 1971, Aeronautical Research Council, Great Britain.

A10. Ericsson, L. E. and Reding, J. P., "Dynamic Stall Simulation Problems," J. Aircraft, Vol. 8, No. 7, July 1971, pp. 579-583.

A11. Peake, D. J. and Rainbird, W. J., "The Three-Dimensional Separation of a Turbulent Boundary Layer by a Skewed Shock Wave; and its Control by the Use of Tangential Air Injection," Paper 40, AGARD-CP-168, 1975.

A12. Ericsson, L. E., "Supersonic Interference Flow Effects on Finned Bodies," AIAA Journal, Vol. 14, No. 9, Sept. 1976, pp. 1342-1343.

A13. East, R. A., "A Theoretical and Experimental Study of Oscillating Wedge Shaped Airfoils in Hypersonic Flow," AASU Report 228, Nov. 1962, University of Southampton, Hampshire, England.

A14. Hummel, D., "Untersuchungen über das Aufplatzen der Wirbel an schlanken Delta Flügeln," Z. Flugwiss. 13 (1965), pp. 158-168.

A15. Ericsson, L. E. and Reding, J. P, "Transonic Sting Interference," AIAA Paper No. 79-0109, The AIAA 17th Aerospace Sciences Meeting, New Orleans, Jan. 15-17, 1979.

A16. Ericsson, L. E. and Reding, J. P., "Scaling Problems in Dynamic Tests of Aircraft-Like Configurations, Paper 25, AGARD-CP-227, 1977.

A17. Starr, R. F., Jr., "Experimental Observation of Wall Interference at Transonic Speeds, AIAA Paper No. 78-164, Jan. 1978.

A18. Ericsson, L. E., "Unsteady Aerodynamics of Separating and Reattaching Flow on Bodies of Revolution," Recent Research on Unsteady Boundary Layers, Vol. 1, IUTAM Symposium, Laval University, Quebec, 1971, pp. 481-512.

A19. Ericsson, L. E., "Effect of Boundary-Layer Transition on Vehicle Dynamics," J. Spacecraft and Rockets, Vol. 6, No. 12, Dec. 1969, pp. 1404-1409.

A20. Ericsson, L. E., "Correlation of Attitude Effects on Slender Vehicle Transition," AIAA Journal, Vol. 12, No. 4, April 1974, pp. 523-529.

A21. Woodgate, L., "Measurements of the Oscillatory Pitching Moment Derivatives on a Slender Sharp-Edged Delta Wing in Incompressible Flow," R&M No. 3628, Part 2., Aer. Res. Council, Great Britain, 1963.

A22. Lawson, M. V., "Some Experiments with Vortex Breakdown," J. Royal Aer. Soc., Vol. 68, May 1964, pp. 343-346.

A23. Chambers, J. R., Anglin, E. L., and Bowman, J. B., Jr., "Effects of Pointed Nose on Spin Characteristics of a Fighter Airplane Model Including Correlation with Theoretical Calculations," NASA TN-D-5921, 1970.

A24. Reding, J. P. and Ericsson, L. E., "Maximum Vortex-Induced Side Force," J. Spacecraft and Rockets, Vol. 15, No. 4, July-Aug., 1978, pp. 201-207.

A25. Tobak, M. and Schiff, L. B., "Generalized Formulation of Nonlinear Pitch-Yaw-Roll Coupling: Part I-Non-Axisymmetric Bodies. Part II, Nonlinear Coning-Rate Dependence," AIAA Journal, Vol. 13, No. 3, March 1975, pp. 323-332.

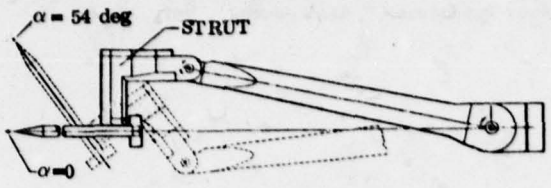

a. High Alpha Free-Oscillation Pitch Apparatus, AEDC-VKF

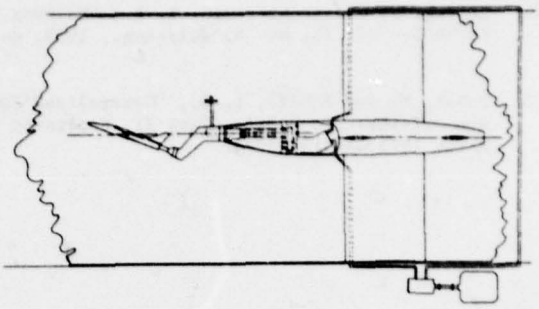

b. Steady-Roll Apparatus, NASA-Langley

Figure 1 High-α Model Support Systems (Ref 1)

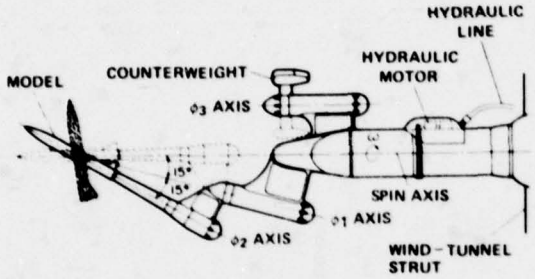

Figure 2 Rotary Rig of NASA-Ames RC (Ref 3)

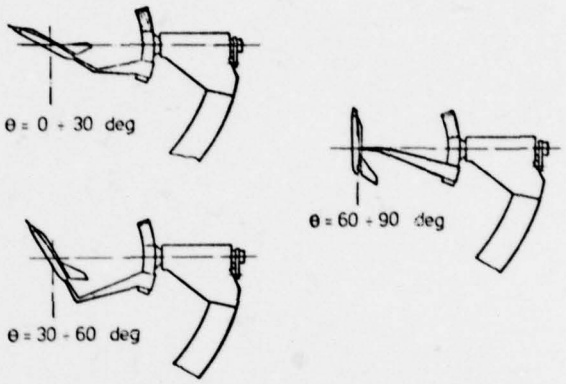

Figure 4 Rotary Rig of DFVLR (Ref 5)

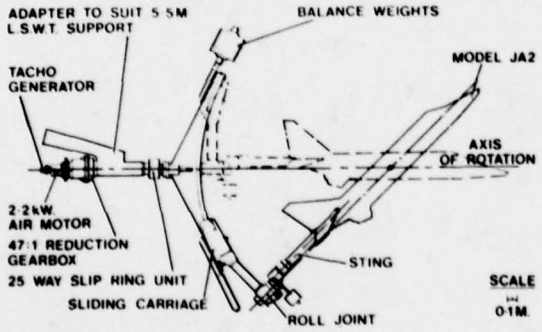

a. 5·5 LSWT Rotary Derivative Rig

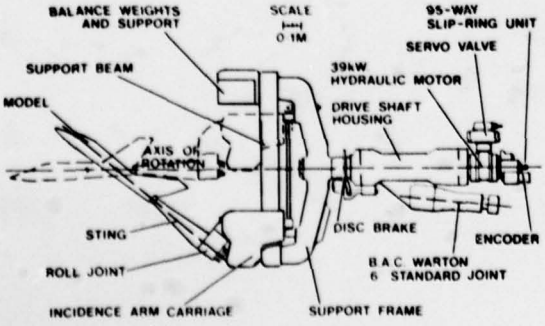

b. Multifacility Rotary Derivative Rig

Figure 3 Rotary Derivative Rigs, BAC, Warton Div (Ref 4)

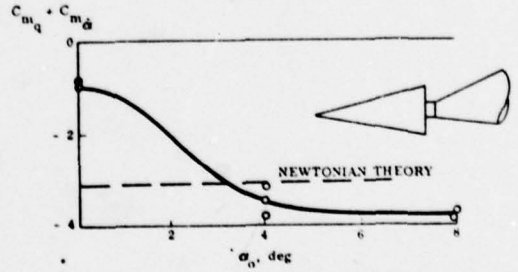

a. $M_\infty = 20.2$, $\Delta\theta = 3$ deg, $\theta_c = 10$ deg

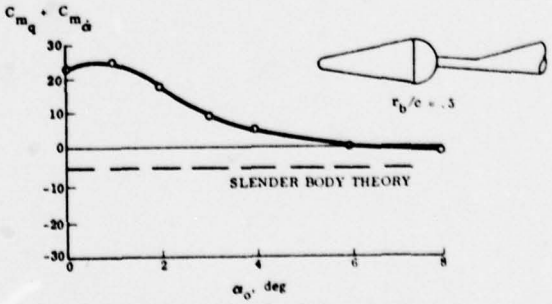

b. $M_\infty = 0.9$, $\Delta\theta = 1$ deg, $\theta_c = 6$ deg

Figure 5 Sting Interference Effects (Ref A4)

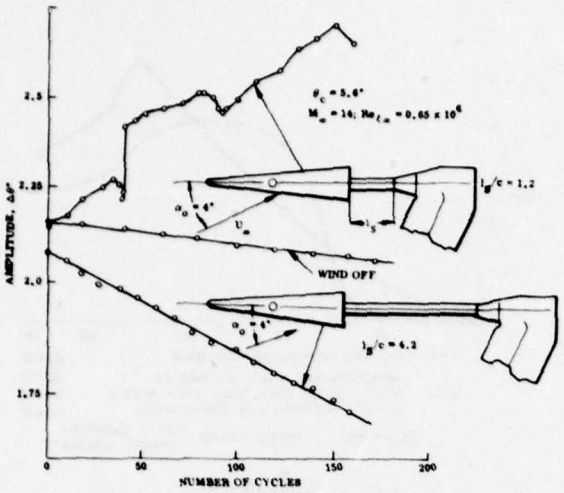

a. Strut Interference Effect on Pitch Damping

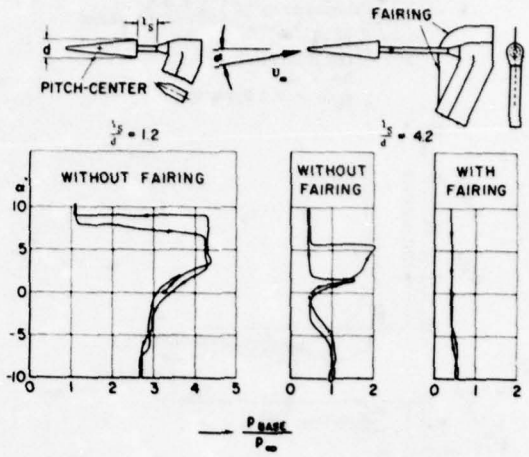

b. Support Effect on Base Pressure

Figure 6 Sting-Strut Support Interference (Ref A7)

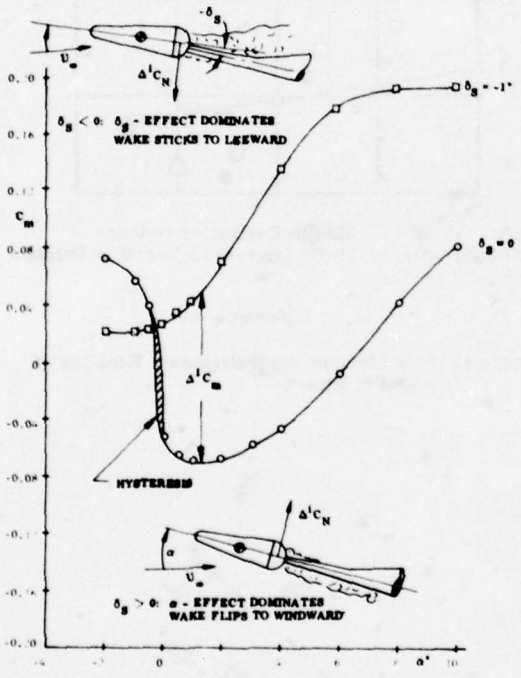

Figure 7 Nonlinear Sting Interference With Hysteresis (Ref. A6)

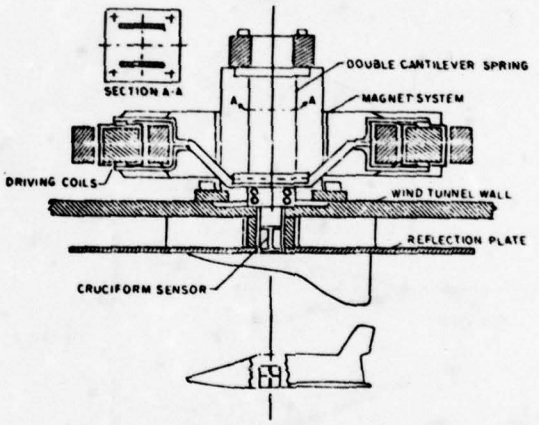

Figure 8 Half-Model Support (Ref 1)

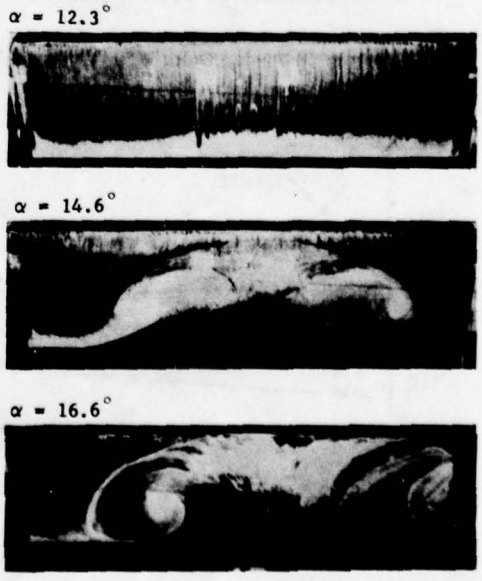

Figure 9 Side Wall Effects on Wing Stall Pattern (Ref A9)

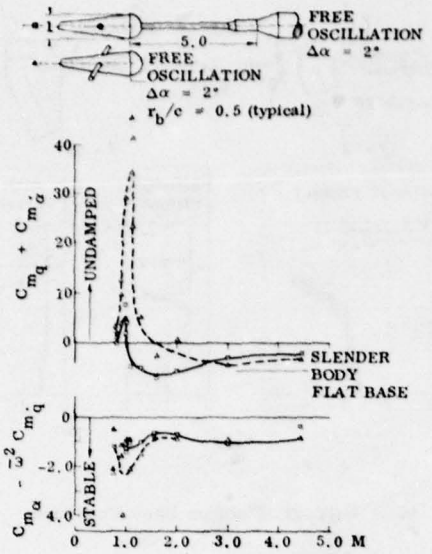

Figure 10 Dynamic Support Interference on a Slender Cone with Hemispherical Base (Ref A4)

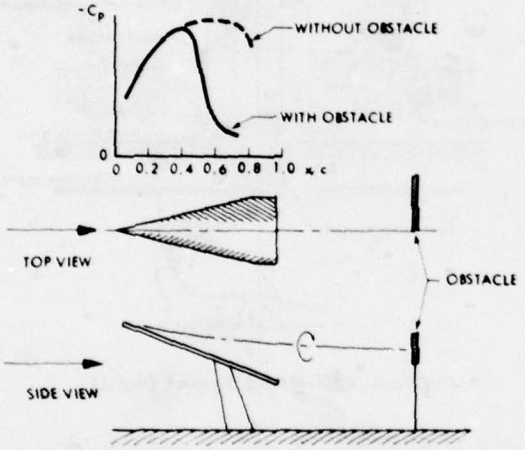

Figure 11 Vortex Burst Caused by Downstream Obstacle on 76-deg Delta Wing at α = 20 deg (Ref A15)

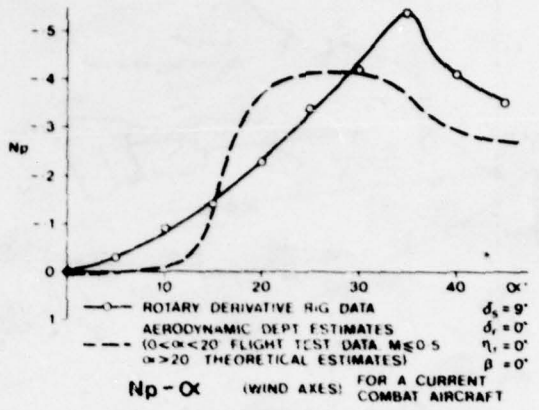

a. Reference 4

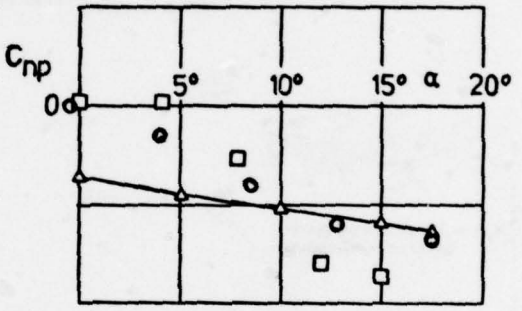

b. Reference 5

Figure 12 Side Moment Derivative as a Function of Angle of Attack

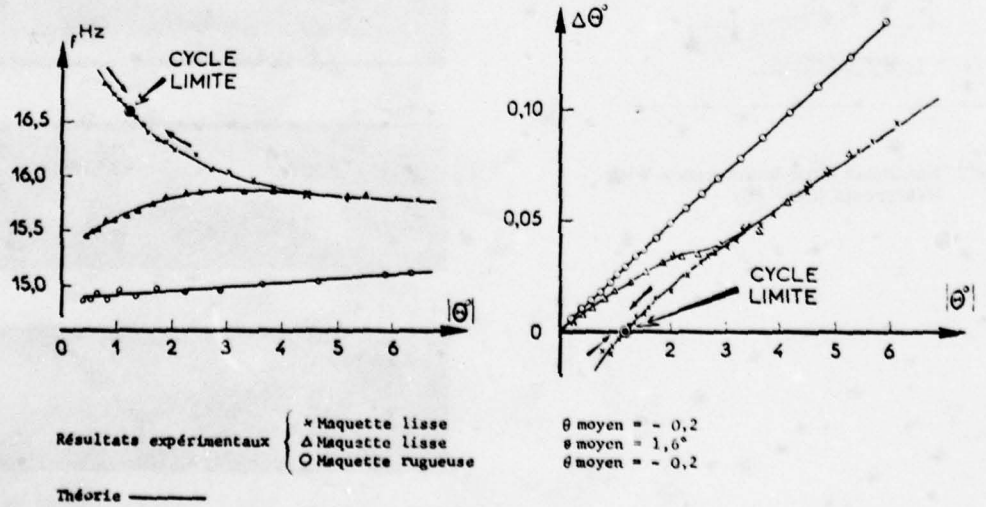

Figure 13 Limit Cycle Oscillations of Ogive - Cylinder - Flare Body (Ref 10)

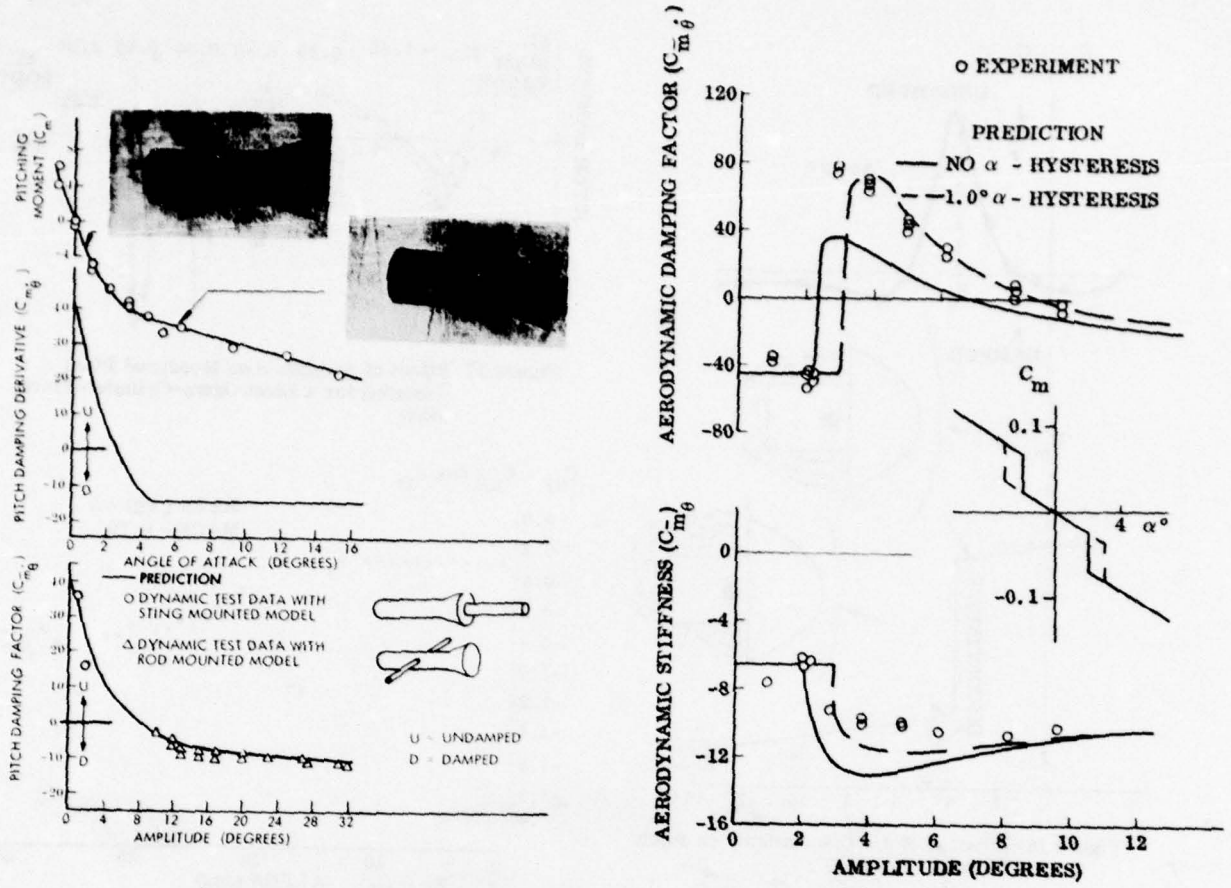

Figure 14 Predicted and Measured Nonlinear Pitch Damping (Ref A18)

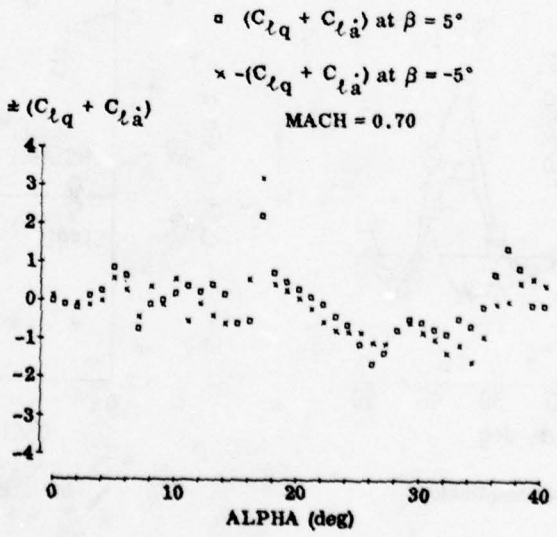

Figure 15 Rolling Moment Derivative Due to Pitch Rate (Ref 8)

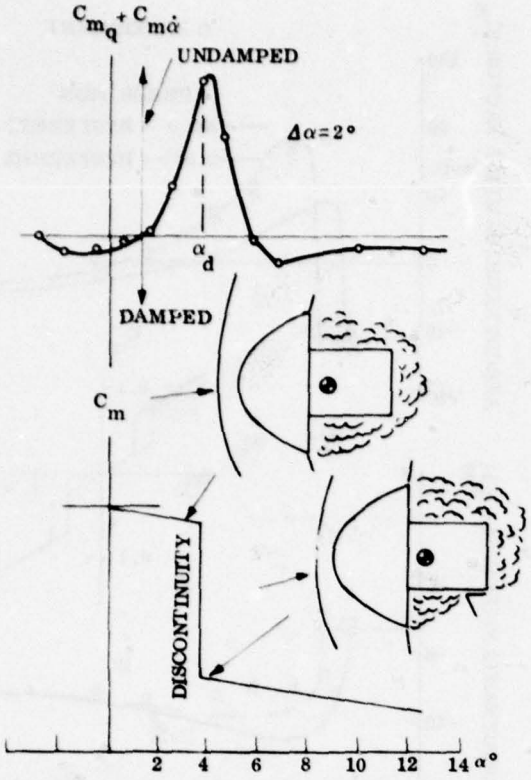

Figure 16 Effect of Static Discontinuity on Pitch Damping (Ref A18)

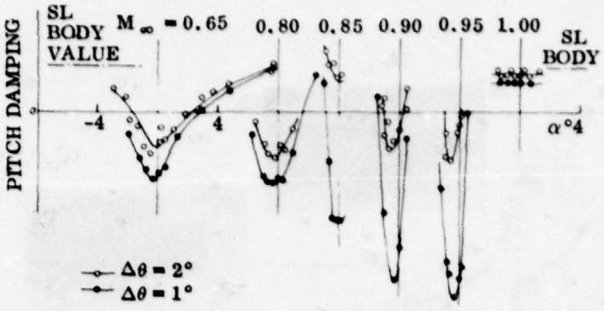

Figure 17 Effect of Amplitude on Measured Pitch Damping for a Blunt Ogive-Cylinder-Flare Body

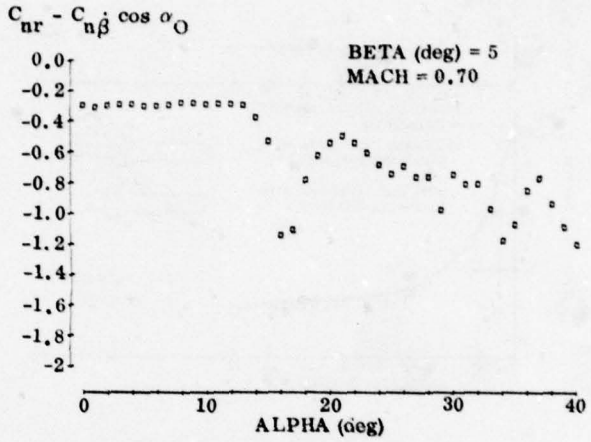

Figure 18 Yaw Damping Derivative at High Angles of Attack (Ref 8)

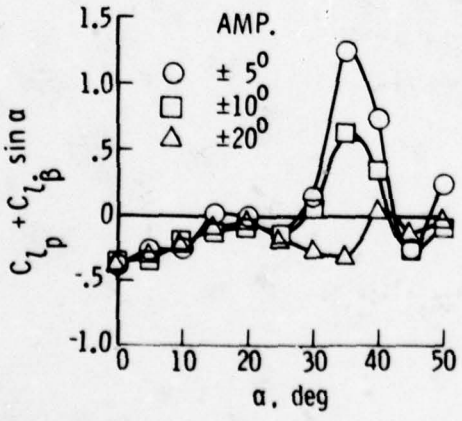

a. Effect of Amplitude

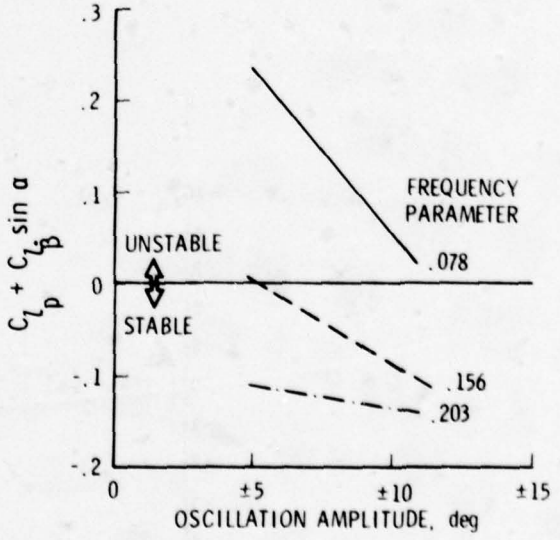

b. Effect of Reduced Frequency

Figure 19 Nonlinear Roll Damping Characteristics (Ref 33)

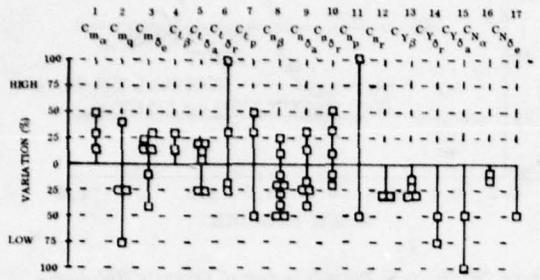

Figure 20 Variation of Derivative Prediction From Flight Test Results (Ref 14)

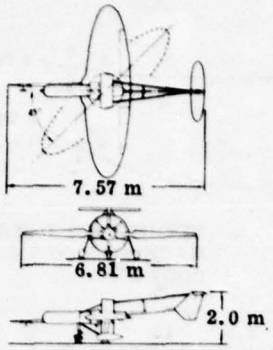

a. Three-view drawing of remotely piloted oblique wing aircraft.

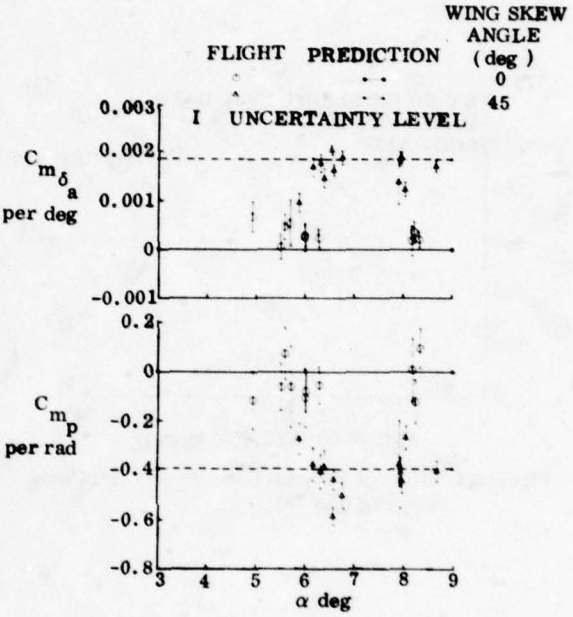

b. Maximum likelihood estimates of aerodynamic cross-coupling derivatives obtained for the oblique wing aircraft at two wing skew angles.

Figure 21 Oblique Wing Cross-Coupling (Ref 15)

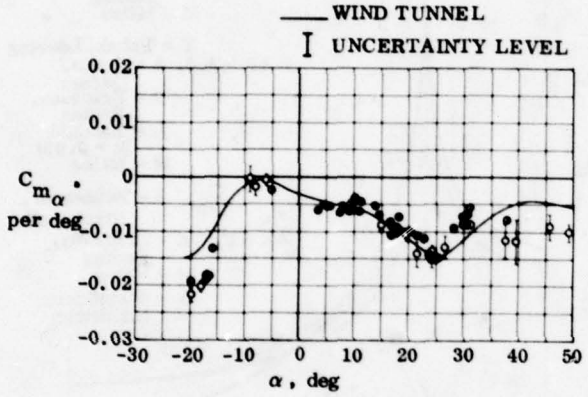

Figure 22 Comparison of Flight and Wind Tunnel Results for the Static Stability Parameter $C_{m\alpha}$ for a Large Angle-of-Attack Range (Ref 15)

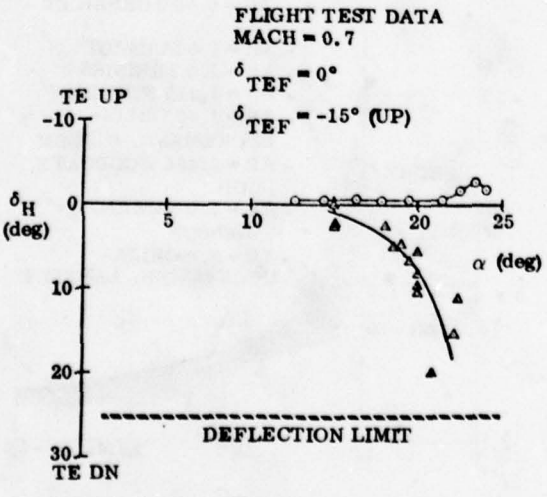

Figure 23 Trim Tail Deflection for CCV YF-16 (Ref 16)

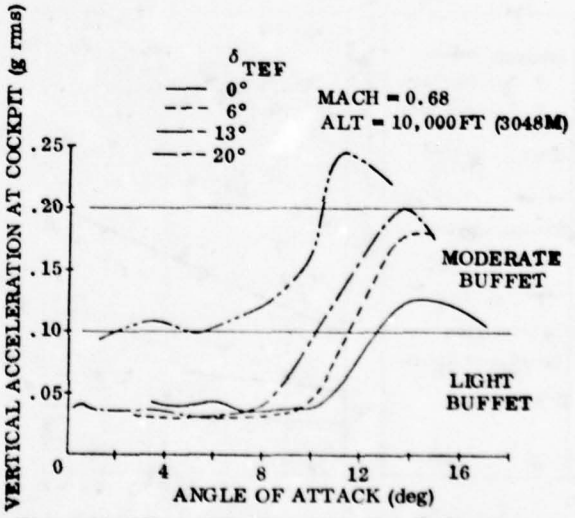

Figure 24 Effect of Trailing Edge Flap Deflections on YF-16 Buffet Level (Ref 16)

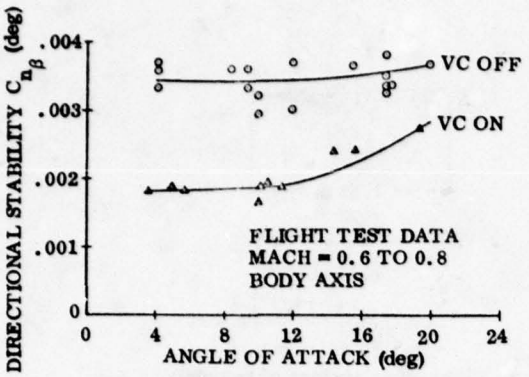

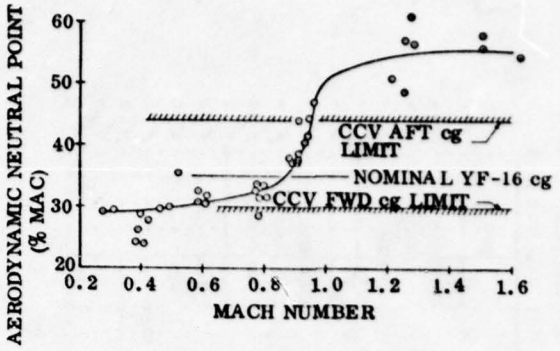

Figure 26 Neutral Point/Center of Gravity Relationships for RSS Testing (Ref 16)

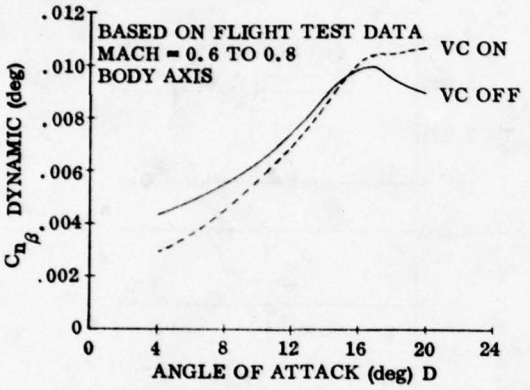

Figure 25 Effect of Vertical Canards on Directional Stability (Ref 16)

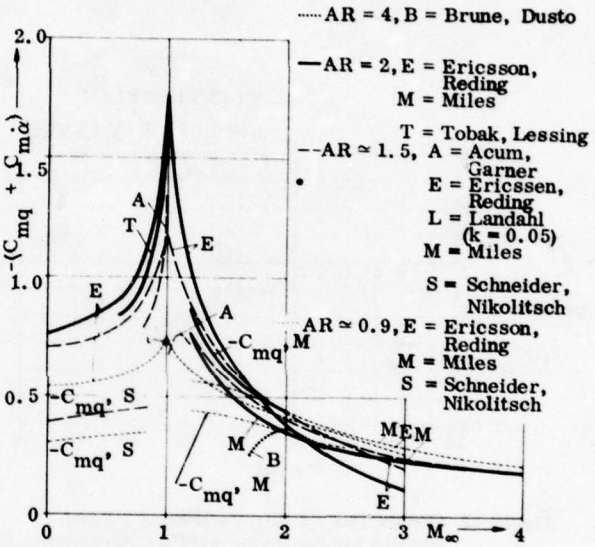

Figure 27 Theoretical Pitch Damping Data for Slender Delta Wings Oscillating Around Midchord (Ref 20)

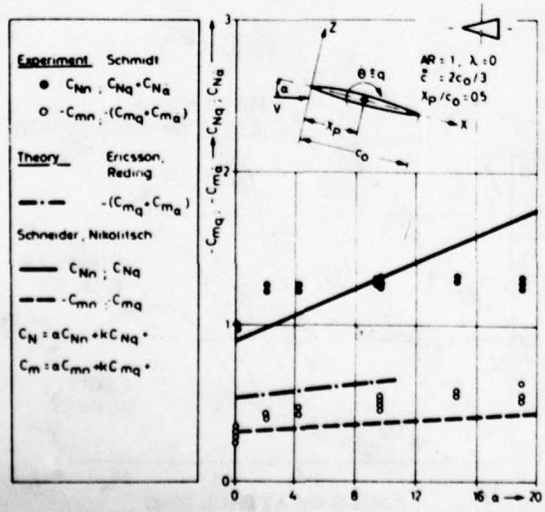

Figure 29 Normal Force and Pitching Moment Damping Derivatives for an AR = 1 Delta Wing at M = 0.2 (Ref 20)

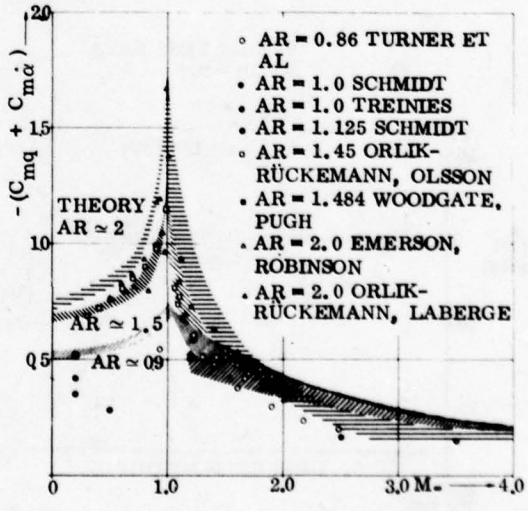

Figure 28 Experimental Pitch Damping of Slender Delta Wings Oscillating Around Midchord Compared with Theoretical Estimates (Ref 20)

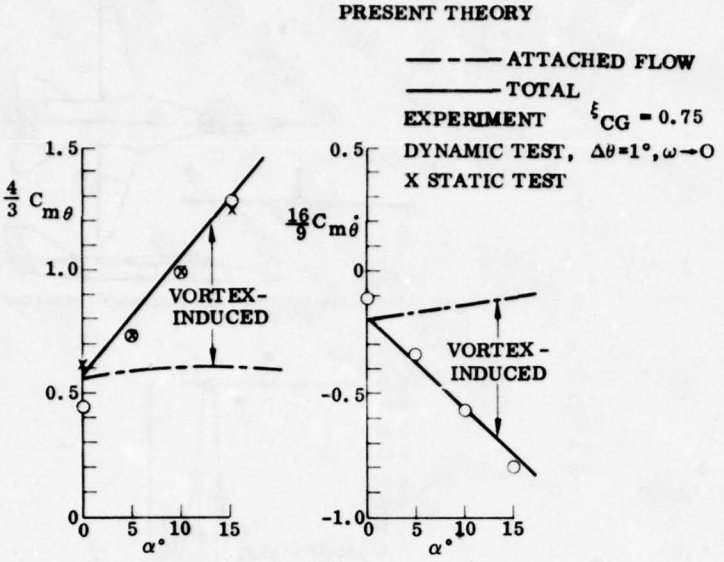

Figure 30 Nonlinear Effects of Angle of Attack on an AR = 1.5 Delta Wing Oscillating Around 75 Percent Chord (Ref 24)

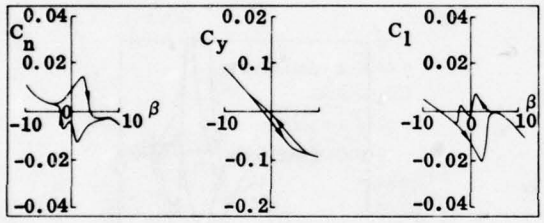

Figure 32 Aerodynamic Hysteresis in a Region of Vortex Breakdown (Ref 19)

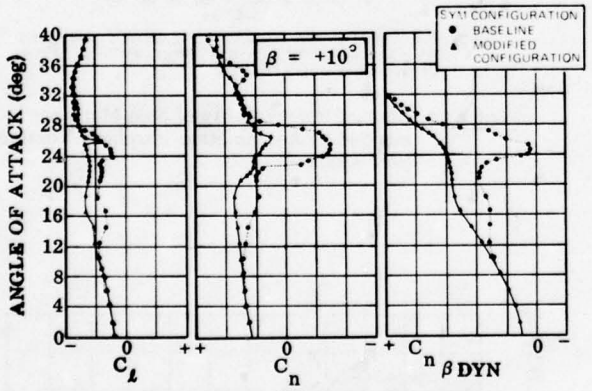

a. STABILITY CHARACTERISTICS

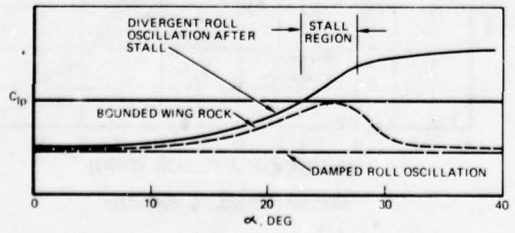

b. EFFECT OF ROLL DAMPING FOR THREE CONFIGURATIONS

Figure 34 Sensitivity of Lateral Aerodynamics to Configuration Changes (Ref 19)

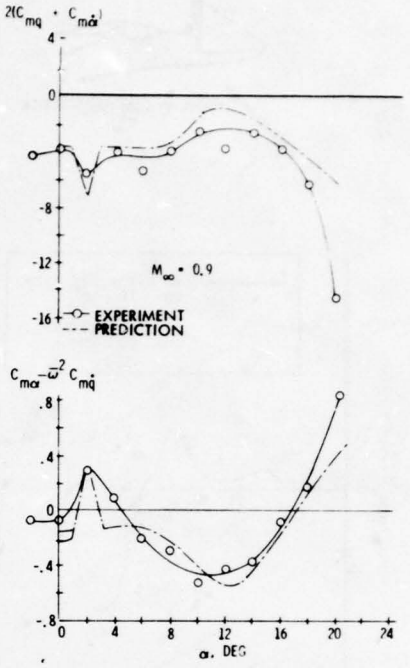

Figure 31 Predicted and Measured Orbiter Dynamics at M = 0.9 (Ref 24)

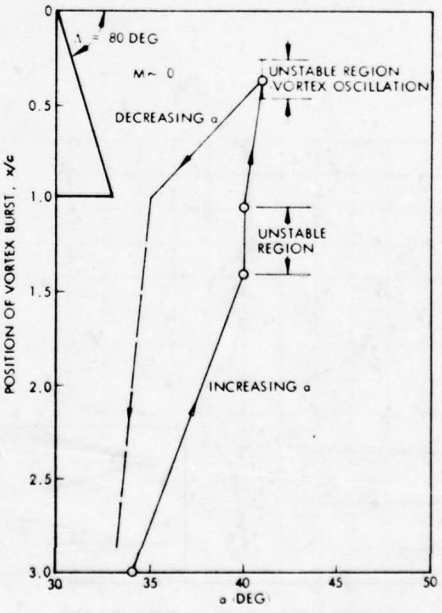

Figure 33 Hysteresis and Unstable Vortex Burst Locations (Ref A22)

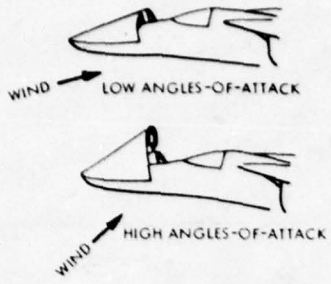

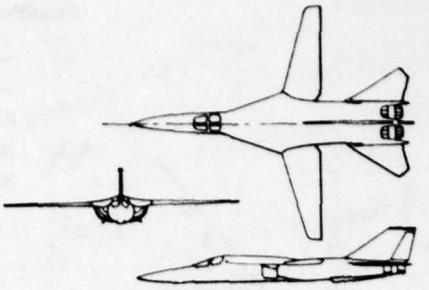

THREE-VIEW SKETCH OF CONFIGURATION WITH LONG POINTED NOSE

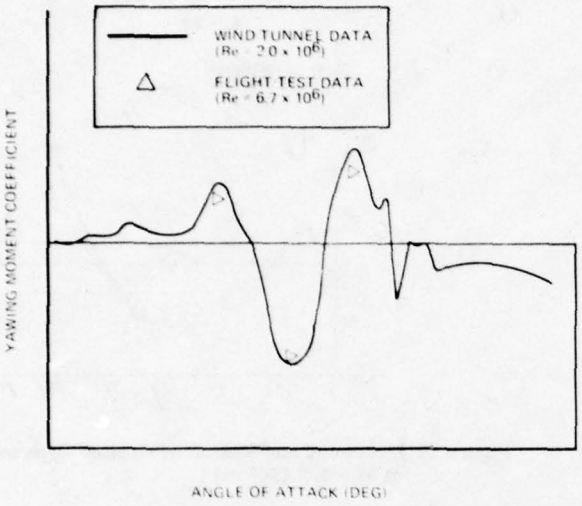

Figure 35 Wind Tunnel/Flight Test Correlation for the Effects of Asymmetric Forebody Vortices (Ref 19)

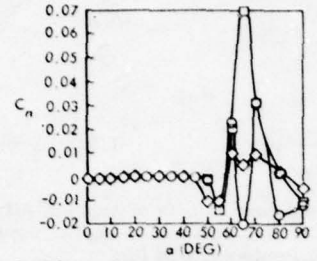

a. VARIATION OF YAWING-MOMENT COEFFICIENT WITH ANGLE-OF-ATTACK, SYMBOLS INDICATE VALUES OBTAINED IN SEVERAL REPEAT TESTS

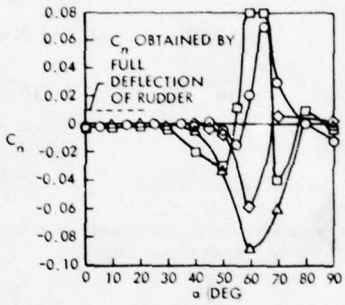

b. VARIATION OF STATIC YAWING-MOMENT COEFFICIENT WITH ANGLE-OF-ATTACK FOR SEVERAL MODELS OF THE CONFIGURATION; β = 0 DEG

Figure 36 Lack of Repeatability of Side Moments Induced by Asymmetric Forebody Vortices (Ref A23)

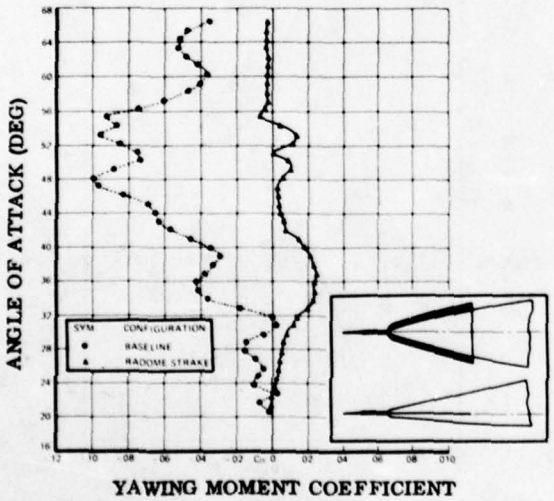

a. **Strake Effect on Aerodynamic Asymmetries**

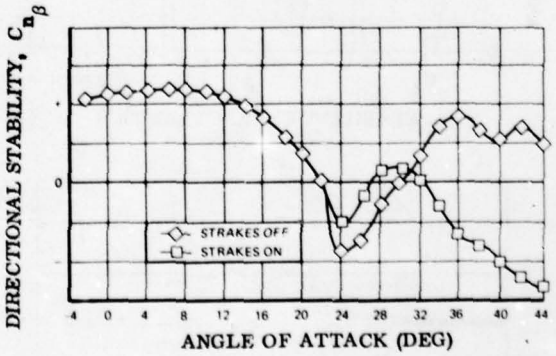

b. **Strake Effect on Stability**

Figure 37 Effect of Nose Strake on Aerodynamic Asymmetries (Ref 19)

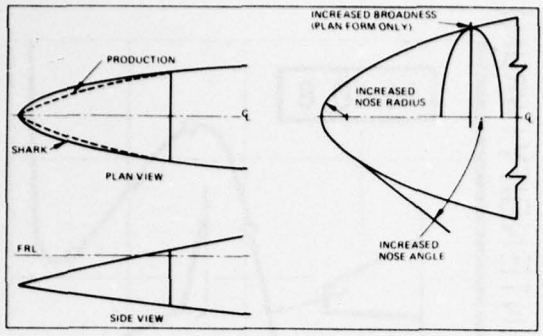

Figure 38 Shark Nose Geometry (Ref 19)

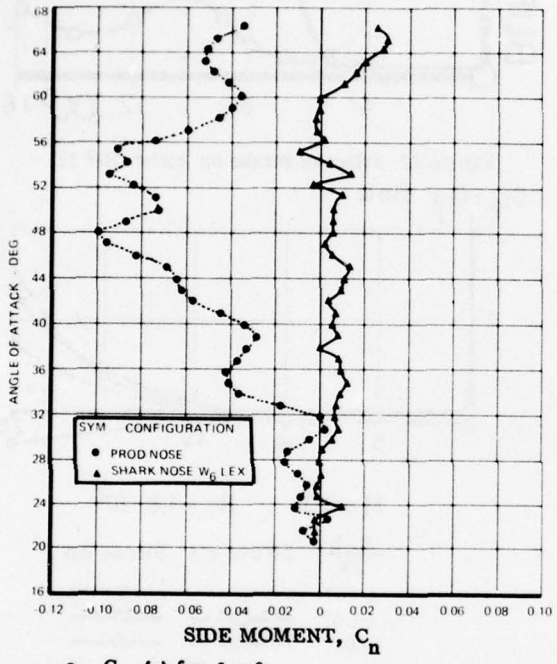

a. C_n (α) for $\beta = 0$

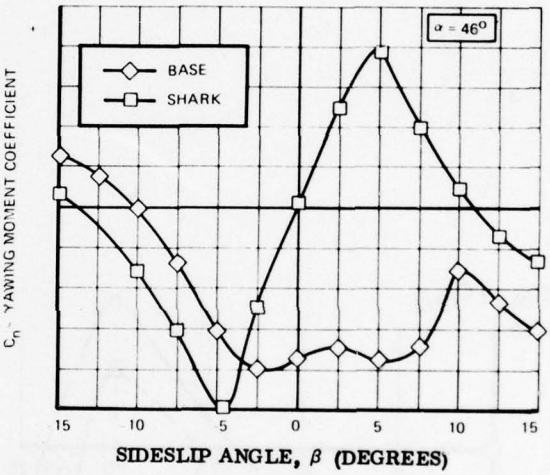

b. C_n (β) for $\alpha = 46^\circ$

Figure 39 Effect of Shark Nose Modification on Lateral Aerodynamic Characteristics (Ref 19)

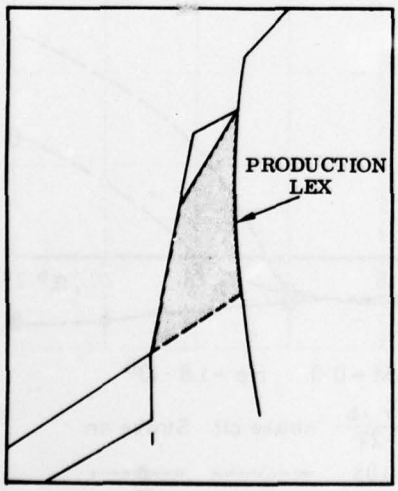

a. W_6 Lex Geometry

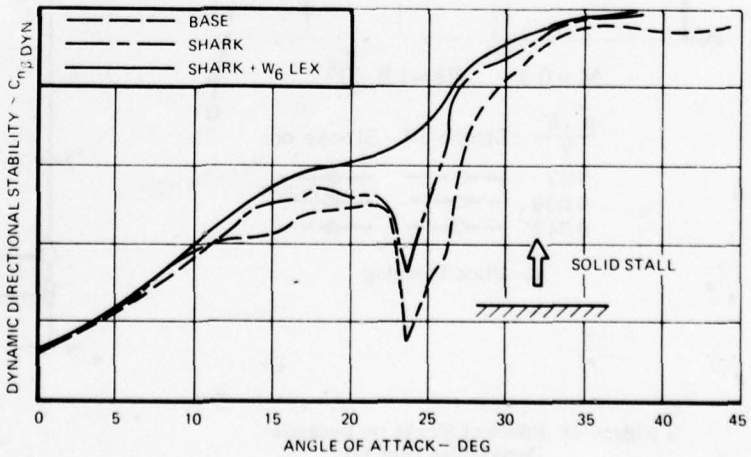

b. $C_{n_\beta\ DYN} = f(\alpha)$

Figure 40 Dynamic Stability Comparison (Ref 19)

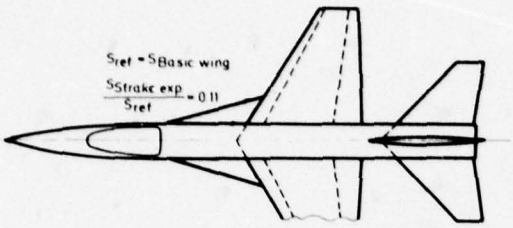

Figure 41 Wing-Body-Strake Geometry (Ref 11)

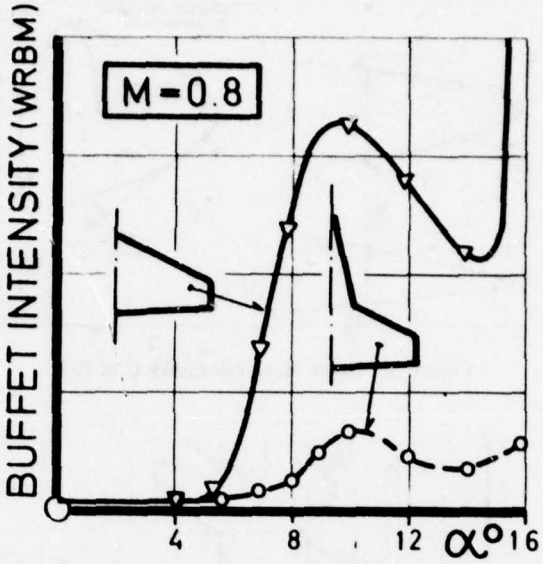

Figure 42 Effect of Strake on Buffet (Ref 11)

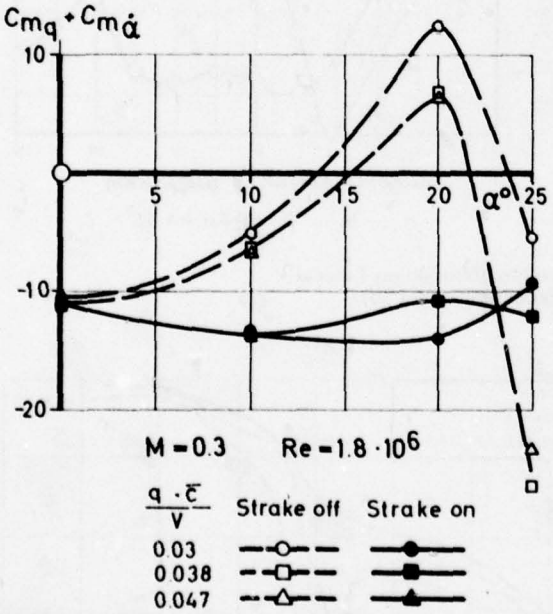

a. Pitch Damping

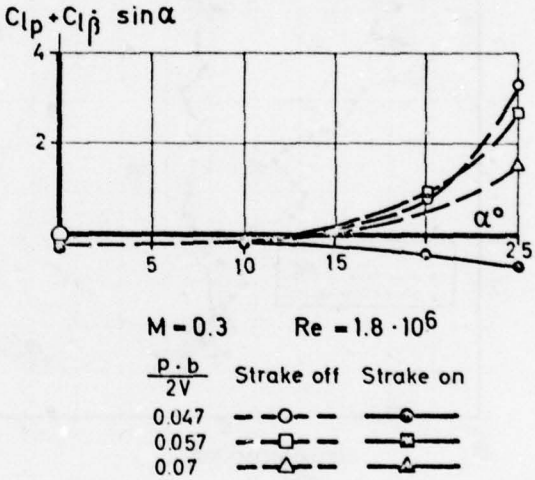

b. Roll Damping

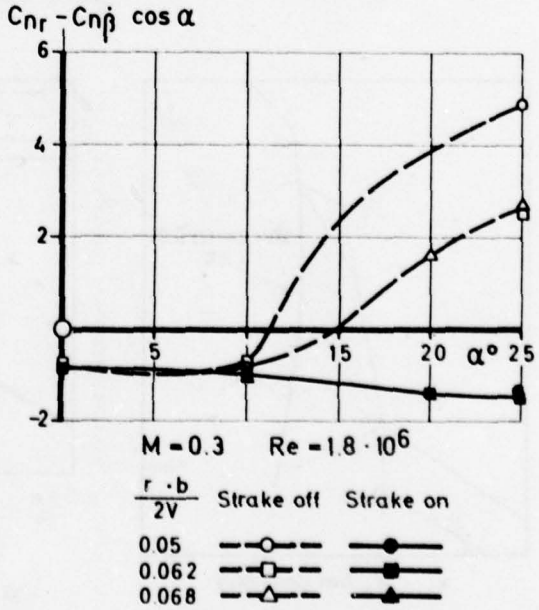

c. Yaw Damping

Figure 43 Effect of Strake on Dynamic Derivatives (Ref 11)

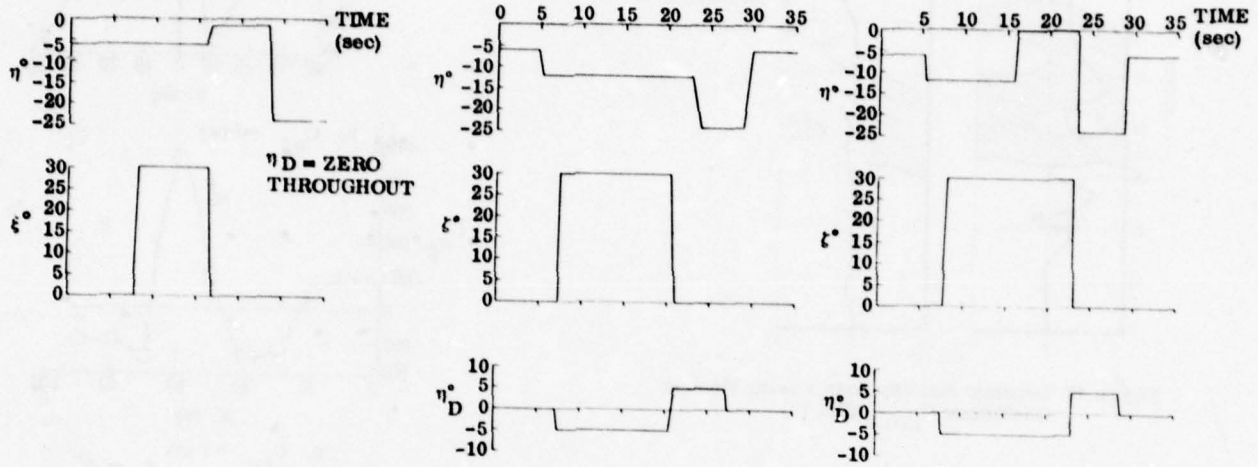

Figure 44 Histories of Certain Motion Variables During Drop 6 (Post-Stall Gyration) (Ref 27)

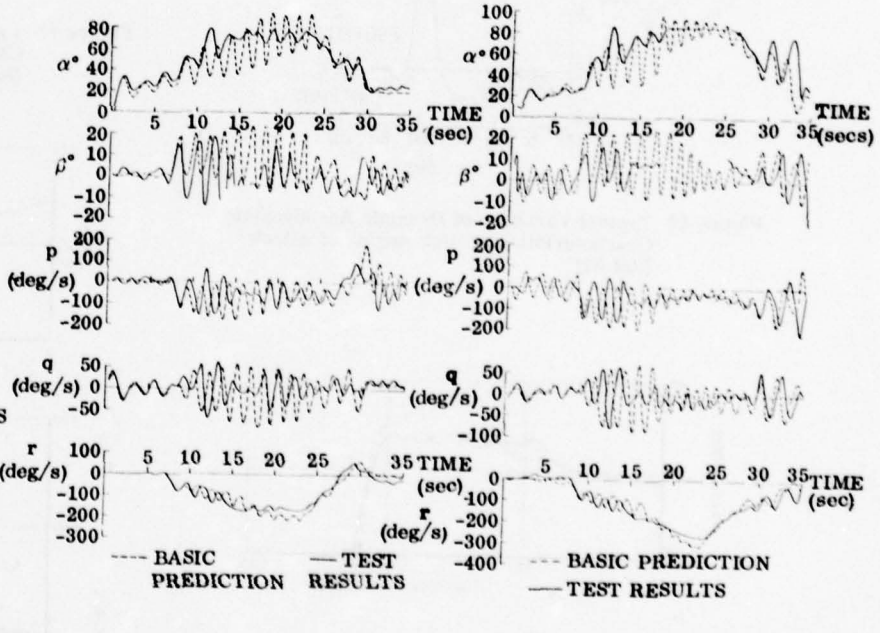

Figure 45 Histories of Certain Motion Variables During Drop 4 (Entry Into and Recovery From Moderately Steep Spin) (Ref 27)

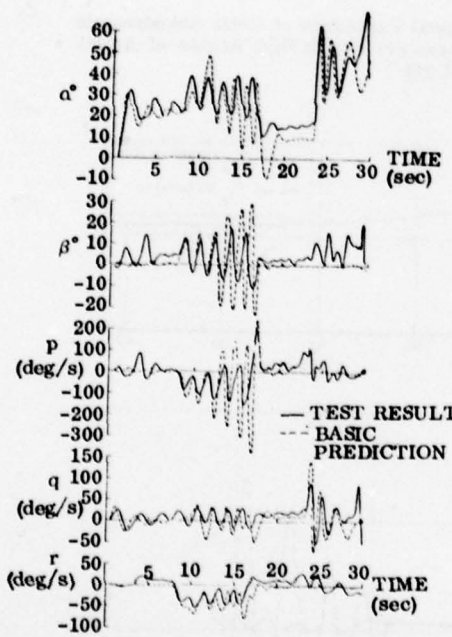

Figure 46 Histories of Certain Motion Variables During Drop 7 (Entry Into and Recovery From a Fast, Flat Spin) (Ref 27)

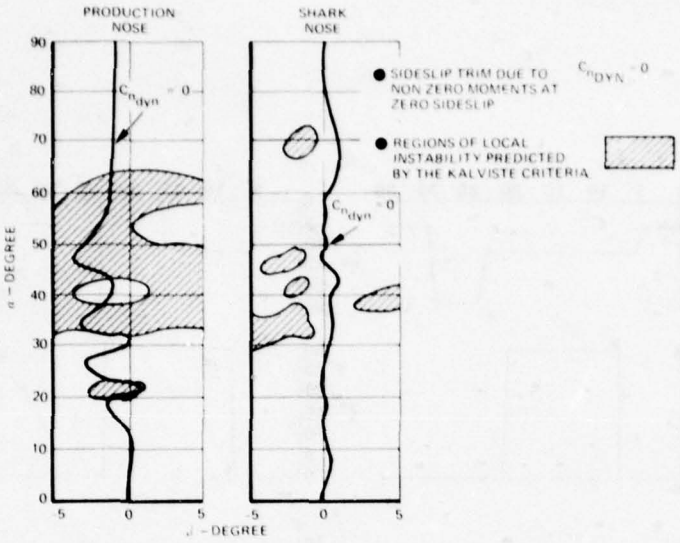

Figure 47 Dynamic Stability Axis Yawing Moment Coefficient C_{nDYN} (Ref 19)

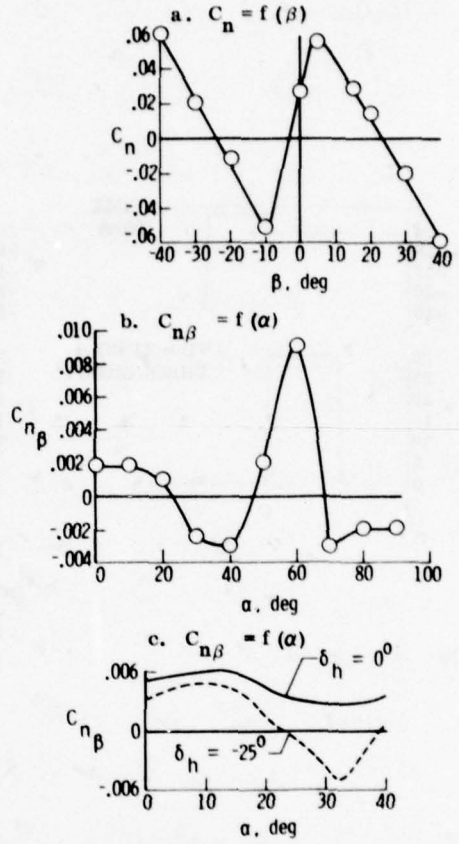

Figure 48 Typical Variations of Static Aerodynamic Characteristics at High Angles-of-Attack (Ref 33)

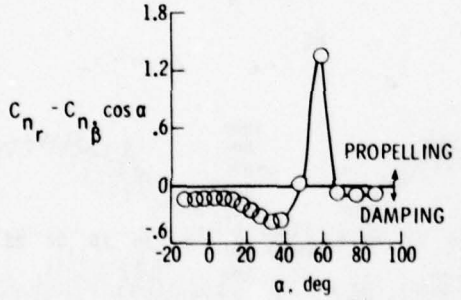

Figure 49 Typical Variation of Dynamic Aerodynamic Characteristics at High Angles of Attack (Ref 33)

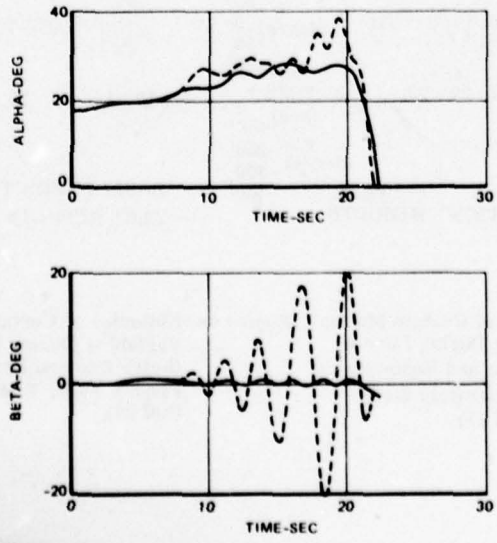

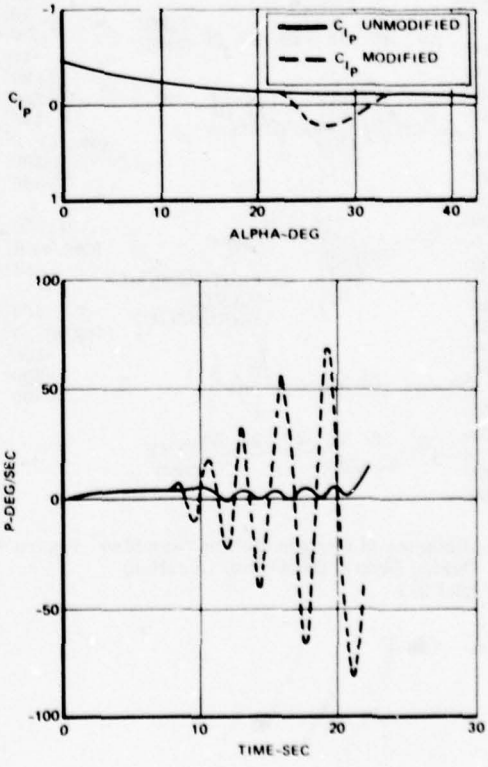

Figure 50 Effect of Roll Damping on Predicted Static Characteristics (Ref 19)

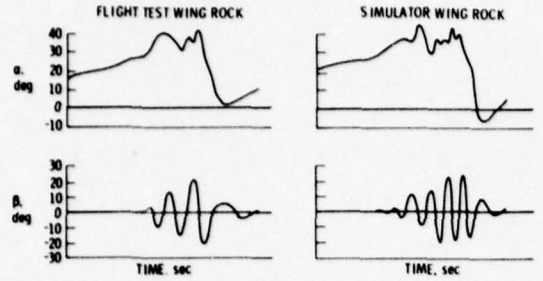

Figure 51 Correlation of Wing-Rock Motions Experienced in Flight and Simulation (Ref 33)

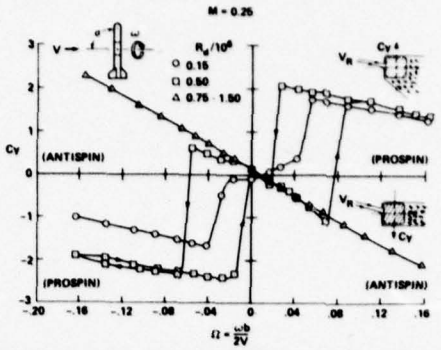

Figure 52 Rate-Hysteresis Effects on Nose Side Force Coefficients (Ref 3)

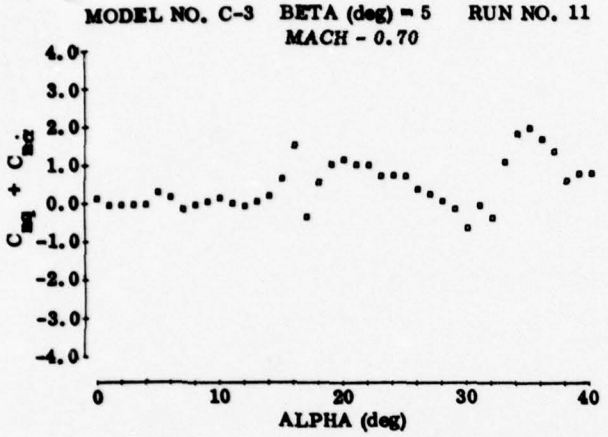

Figure 53 Dynamic Yawing Moment Derivative Due to Pitching (Ref 8)

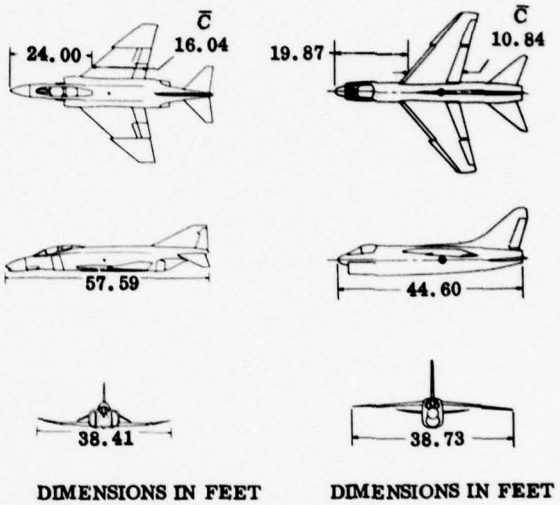

Figure 54 Geometries of Aircraft Studied (Ref 35)

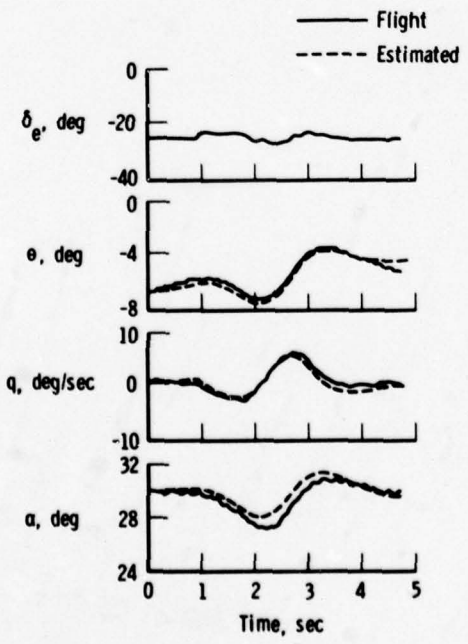

a. Lateral-directional kinematic coupling terms ignored.

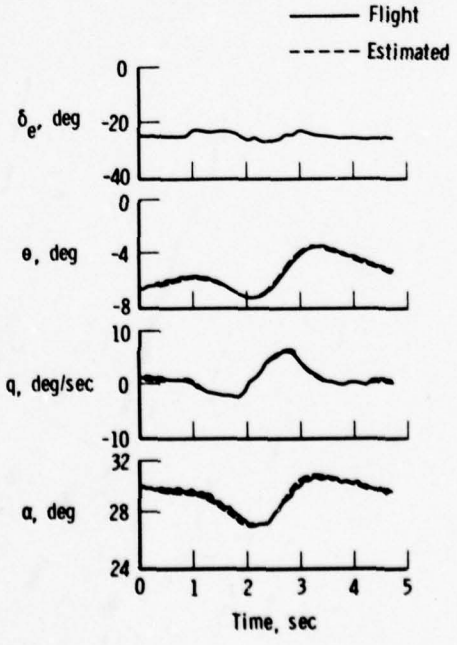

b. Lateral-directional kinematic coupling terms included.

Figure 55 Effect of Lateral-Directional Kinematic Coupling Terms (Ref 15)

ASPECTS STRUCTURAUX DU CONTROLE ACTIF

(Revue des mémoires présentés à la Réunion de Spécialistes tenue à Lisbonne, 21 avril 1977)

par Roger DESTUYNDER

Office National d'Etudes et de Recherches Aérospatiales (ONERA)
92320 Châtillon (France)

SUMMARY

STRUCTURAL ASPECTS OF ACTIVE CONTROLS

Survey of the papers presented at the Specialists Meeting on "Structural Aspects of Active Controls", held in Lisbon, 21 April 1977, under the sponsorship of the Structures and Materials Panel.

Emphasis is put on three main points :
- use of preliminary simple calculations to cover the different configurations and the possible control law,
- improvement with the help of corrections obtained by wind tunnel tests,
- proof, through flight test or wind tunnel test, of the validity of the solution.

Lastly, the paper presents the latest progress in flutter suppression obtained at ONERA.

INTRODUCTION -

Ce papier tentera de faire la synthèse des différents articles relatifs aux "Aspects Structuraux du Contrôle Actif" du 44ème meeting de l'Agard tenu à Lisbonne en Avril 1977.

D'autre part, dans une deuxième partie, le point sera fait sur les développements récents du problème de contrôle de flottement par gouvernes actives à l'ONERA.

Le problème du contrôle d'une structure à partir d'une excitation due soit à une rafale, à des manoeuvres, à un impact à l'atterrissage, soit encore à un phénomène de flottement, est incroyablement compliqué et onéreux à traiter dans sa généralité. Le nombre de paramètres susceptibles d'intervenir est très grand. Citons les modes propres de la structure, les modes d'ensemble de l'avion, l'aérodynamique stationnaire et instationnaire relative à plusieurs surfaces portantes couplées, ces forces dépendant elles-mêmes de plusieurs paramètres (Mach, fréquence réduite, etc...).

Tous les auteurs s'accordent à déplorer les sommes importantes de temps et d'argent qu'il faut mettre en oeuvre pour traiter le problème, encore que les solutions obtenues correspondent souvent à des cas d'espèce dans des versions le plus souvent linéaires. Mais en même temps, tous sont d'accord pour montrer l'importance du problème du contrôle actif pour les avions d'un avenir proche.

Si on tente de faire une classification par bande de fréquences, on peut dire que les problèmes de contrôle actif, sauf quelques cas. d'exception pour des appareils de très grandes dimensions se divisent en 3 groupes :

A savoir :

a) La bande des fréquences "basses" qui intéresse la mécanique du vol avec, par exemple, les problèmes de contrôle de portance, de stabilité dynamique ou de charges en manoeuvre sans déformations dynamiques de la structure.

b) La bande des fréquences "moyennes" qui comprend la réduction des phénomènes de rafales, d'impact à l'atterrissage et peut-être de buffeting.

c) La bande des fréquences "Hautes" qui implique les phénomènes de contrôle du flottement et presque par définition concerne les modes propres de la structure.

Bien entendu, cette classification sommaire peut impliquer des recoupements entre groupes, mais c'est justement l'un des problèmes fondamentaux qui se posent pour les véhicules à contrôle automatique généralisé que d'étudier les interactions entre ces différents systèmes.

Par exemple, un système supresseur de flottement ne doit pas interférer par sa loi de contrôle avec les modes d'ensemble de la mécanique du vol.

Différentes approches ont été proposées pour résoudre ces problèmes. Elles peuvent se classer en 3 grandes catégories :

a) Simplification théorique du problème au stade du projet afin de sélectionner les cas susceptibles d'un développement ultérieur, puis traitement plus élaboré par le calcul de configurations réputées critiques.

b) Comparaison entre essais et théories pour faire apparaître les termes qui jouent un rôle important dans le problème et pour ajuster la théorie à des valeurs d'essais plus réalistes.

c) Une voie purement expérimentale dans la première étape qui permet en soufflerie ou en vol de résoudre, sur des cas particuliers, les problèmes qui peuvent se poser. Les calculs sont ensuite ajustés a posteriori pour être transposés sur des cas de vol. Ce sont ces trois aspects qui seront analysés dans ce texte.

Dans une première phase le côté prévisionnel est envisagé par deux auteurs en ce qui

concerne, entre autres, le contrôle du flottement :

a) Voie d'approche théorique simplifiée

M.R. Turner et C.G. Lodge font des calculs simplifiés selon une méthode de tranches corrigées. Ces calculs permettent la recherche d'une optimisation dans la position du capteur et de la gouverne de contrôle, l'optimisation portant sur l'usage des mêmes éléments de contrôle pour différents cas de flottement.

L'autre aspect, présenté par K.L. Roger est une tentative de schématisation d'une méthode mathématique de doublets avec comme objectif la simplification des calculs. La matrice d'influence aérodynamique est calculée à partir d'une méthode de distribution limitée de doublets.

On peut voir dans ces 2 approches, qui restent simples, un prolongement naturel l'une de l'autre.

Turner et Lodge prennent comme exemple l'aile d'un avion à géométrie variable équipée de 2 engins sous voilure.

Ils en extraient 4 configurations (figure 1) pour lesquelles ils recherchent si il existe une solution commune de contrôle, c'est-à-dire si un capteur et une gouverne donnés peuvent contrôler les différents cas de flottements choisis. Bien entendu les flottements réalisés sont fictifs et obtenus par un ballastage judicieux des engins. Plusieurs dizaines de positions de capteurs et de gouvernes ont été essayées par le calcul.

Cette recherche s'accompagne de nombreux calculs très simples. La difficulté de trouver une solution provient en grande partie de la marge de stabilité que les auteurs se sont imposée (à savoir $\pm$ 60° sur la phase et $\pm$ 6 dB sur le gain à toutes les fréquences et toutes les vitesses dans le domaine de vol). (Ces normes de marge sont celles utilisées par les ingénieurs travaillant avec des systèmes hydrauliques bouclés).

Il ressort de ces calculs qu'une loi de contrôle du type $P = K f(s) \dot{W}$ appliquée en un point P sur l'aile au droit de l'aileron fournit une première série de renseignements qui permet d'envisager ensuite un calcul plus compliqué (figure 2).

Dans cette équation, on a :

P = Point d'application de la force de contrôle

K = Gain de la boucle (scalaire réel)

f(s) = filtre du premier ordre

$\dot{W}$ = vecteur vitesse au point d'application du capteur.

Les auteurs admettent toutefois que la non représentation de la fonction de transfert de la servo-commande, fonction prise égale à l'unité en module et à zéro en phase dans les calculs, peut modifier de façon sensible les résultats.

Le système I.L.A.F. (Identical Location Accelerometer and Force) est envisagé et donne une solution simple lorsqu'il est appliqué directement sur les engins. Ce système consiste à injecter de l'amortissement positif, par l'intermédiaire d'une palette, sur le mode de tangage de l'engin. (Cette solution est d'ailleurs partiellement reprise dans une autre conférence).

De même, l'idée de prendre des forces aérodynamiques instationnaires induites par la gouverne agissant sur la seule tranche concernée par cette gouverne est exploitée dans un autre papier (Destuynder).

Une méthode de modélisation mathématique des forces aérodynamiques est proposée ensuite par K.L. Roger. Cette méthode approxime la dépendance avec la fréquence des forces aérodynamiques de la méthode des doublets par une fonction polynomiale de la variable de Laplace ce qui simplifie les calculs en fonction du nombre de Mach de façon sensible.

L'auteur insiste sur l'intérêt de traiter le problème du contrôle dans son ensemble (particulièrement pour des avions de grandes dimensions pour lesquels des effets d'interaction peuvent exister entre les différents systèmes de contrôle si leurs fréquences d'action sont voisines).

Par ailleurs, l'auteur rejoint les idées de Collman et Sensburg lorsqu'ils proposent d'ajuster les calculs à partir d'essais en vol ou en soufflerie, donnant par exemple, l'interaction aérodynamique entre 2 surfaces portantes ou l'action en instationnaire d'une gouverne sur une aile.

Comme d'autres auteurs, K.L. Roger souligne l'importance d'une représentation correcte de la fonction de transfert d'un système aéroélastique d'abord en boucle ouverte, puis avec contrôle, en boucle fermée, en incluant les non linéarités de la servo-commande.

Dans le domaine de la turbulence, l'auteur recommande une méthode tridimensionnelle développée à partir d'un travail de Sawdy. Cette méthode permet de tenir compte d'une décroissance très rapide de la fonction de cohérence avec l'envergure pour des fréquences croissantes. La figure 3 illustre l'intérêt de cette méthode pour un appareil de grandes dimensions.

Dans un autre papier R. Schwarz montre que le fait de ne pas traiter du point de vue du contrôle généralisé un avion dans son ensemble c'est-à-dire au sens de la stabilité dynamique, de la mécanique du vol, de la réduction des charges, de la turbulence ou du flottement, conduit à de graves difficultés dans l'application des spécifications militaires (MILSPECS). Ces difficultés peuvent aller jusqu'à l'incompatibilité entre des disciplines aussi différentes que celles qui traitent des problèmes de structures, de contrôle en vol ou du flottement.

L'auteur propose une généralisation des équations des systèmes qui permettrait de modifier les (MILSPECS) pour leur donner une portée plus générale.

b) Approche mixte calculs/expériences

L'article de K.D. Collman et O. Sensburg aborde le 2ème type d'approche, à savoir : utilisation de méthodes mixtes basées sur les calculs corrigés par l'expérience.

Les auteurs mettent en évidence d'une part les gains substantiels que l'on peut attendre de la technologie du contrôle actif et d'autre part les difficultés théoriques qui existent. En particulier l'interaction entre voilure et empennage ou empennage et dérive apparaît comme fondamentale (figure 4).

Les valeurs de ces paramètres d'interaction mesurées en soufflerie permettent de corriger de façon sensible, les valeurs théoriques. D'autre part, les auteurs montrent que pour obte-

nir des résultats raisonnables dans les calculs de réponse d'un avion à la rafale, il est nécessaire d'introduire son comportement élastique ainsi que les lois des systèmes de contrôle (CSAS) dans le modèle mathématique.

Les fonctions de transfert des boucles de contrôle sont fortement non linéaires et très difficiles à déterminer, il semble intéressant de les déterminer expérimentalement, particulièrement pour les servo-commandes hydrauliques, et de les introduire dans les équations déterminant l'élasticité de l'avion.

La réponse de l'avion à la rafale est successivement étudiée en boucle ouverte puis en boucle fermée, d'où la mesure de l'augmentation de stabilité (Control System Augmented Stability) (Figure 5).

La généralisation est ensuite réalisée avec plusieurs systèmes de contrôle travaillant simultanément afin de contrôler les non-interactions entre les différentes boucles de contrôle.

W. Hamilton, avec l'avion YC 14, illustre de façon saisissante ce que peuvent apporter les systèmes de contrôle multiredondants appliqués à un avion moderne.

Indépendamment des nouvelles qualités de vol apportées à l'avion par l'utilisation de l'effet "Coranda" sur les volets, cet appareil rassemble un grand nombre de possibilités nouvelles de systèmes de contrôle.

Sur le plan technologique, l'usage d'ordinateurs redondants embarqués à bord de l'avion, l'utilisation abondante de la transmission des informations par fibres de verre, les commandes électriques de certaines surfaces de contrôle, apportent des solutions qui montrent nettement les progrès énormes qui peuvent être faits dans un futur proche.

Une illustration des surfaces de contrôle est donnée sur la figure 6. Enfin sur la figure 7, on a la représentation de deux cas d'actions de contrôle automatique, l'un affecte un ordre de variation de vitesse en configuration d'atterrissage, l'autre la réponse de l'avion, sans intervention du pilote, à une panne d'un réacteur.

c) Approche expérimentale

Pour terminer cette revue des articles concernant les contrôles actifs, nous abordons la 3ème méthode d'approche qui est basée sur l'expérience, puis comparaison avec la théorie.

Deux papiers sont relatifs à des problèmes très précis de contrôle de flottement l'un en vol sur l'avion Fiat G 90, par H.Hönlinger, l'autre en soufflerie à basses vitesses, par R. Destuynder.

Dans l'article de Hönlinger, il s'agit d'un système de contrôle de flottement agissant sur un mode de tangage d'un bidon sous voilure couplé avec un mode de flexion aile (Figure 8, figure 9).

Le contrôle consiste à annuler l'instabilité par réinjection d'une force proportionnelle et en phase avec la vitesse de tangage du bidon. Cette force d'amortissement est créée par le mouvement de deux petits ailerons placés au nez de chaque bidon. L'efficacité du contrôle est très grande puisqu'on agit directement sur le mode instable ; de très faibles angles de contrôle suffisent pour amortir le mode (conclusion identique aux résultats de Lodge dans son calcul de prévision).

Une autre possibilité offerte par la méthode proposée consiste à créer à l'aide des petits ailerons, un système d'excitation automatique en retournant la phase de 180° dans la boucle de contrôle. Ainsi, le système est rendu instable, puis pour une amplitude donnée, l'excitation est coupée et le régime transitoire qui s'ensuit permet de déterminer le facteur d'amortissement et la fréquence du mode critique sans contrôle.

Ces essais en vol, qui ont suivi des essais préliminaires en soufflerie ont démontré l'efficacité du principe de supresseur de flottement adopté. A la limite, si un seul capteur, situé au droit de l'ailette du bidon, était utilisé, on aurait affaire à un système ILAF (même position du capteur de détection de la vitesse et de la force d'amortissement introduite).

Un autre type de contrôle a été développé par Destuynder. Il agit par un principe de réinjection de rigidité.

Des essais de base ont été effectués à basses vitesses en soufflerie qui ont permis d'obtenir un gain sur la vitesse critique de 30 %. L'idée consiste à réinjecter sur l'aile des forces aérodynamiques de raideur (positive ou négative) par l'intermédiaire du mouvement d'une gouverne, (figure 10).

Cette idée s'appuie sur un certain nombre d'hypothèses, à savoir que la partie imaginaire des forces instationnaires induites par la gouverne sur l'aile reste suffisamment faible pour ne pas apporter de déphasage entre le mouvement de la gouverne de contrôle et la force induite.

D'autre part, seule la tranche d'aile au droit de la gouverne est intéressée par les forces de contrôle (hypothèse bidimensionnelle) et enfin les forces aérodynamiques dépendent peu de la fréquence réduite pour la gamme qui contrôle le flottement.

(Ces hypothèses se retrouvent en partie dans les calculs de Lodge).

Développements nouveaux

Pour achever ce tour d'horizon des différents papiers publiés sur le contrôle actif, nous voudrions donner quelques résultats récents relatifs à des calculs et des essais de flottement avec et sans contrôle dans le domaine transsonique.

Il s'agit de travaux effectués en soufflerie sur une aile en flèche, équipée de charges sous voilure (figure 11).

La méthode de contrôle utilisée dans les calculs et dans les essais est la même que celle décrite en subsonique, à savoir réinjection d'une force sur l'aile en phase ou en contre phase avec le mouvement de l'aile, ce qui a pour effet d'écarter ou de rapprocher les fréquences des modes du flottement.

La loi de contrôle se présente sous la forme d'un filtre passe bande, une première intégration suivie d'un gain variable et en parallèle une deuxième intégration suivie d'un gain variable. On utilise un seul capteur dans l'aile placé dans la tranche d'aileron entre les lignes de

noeuds, (figure 12). La loi de contrôle consiste à doser relativement les 2 vecteurs de vitesse et de déplacement ainsi créés de façon à annuler par une avance de phase, le déphasage en retard introduit par le filtre de bande et la servo-commande.

A partir de ce schéma, selon la position de l'accéléromètre le long de la corde médiane de l'aileron, plusieurs possibilités de contrôle sont offertes en agissant par les raideurs (figure 13).

Dans un premier cas, nous avons supprimé le flottement en écartant les fréquences couplées (ceci était possible parce qu'il n'y avait pas de fréquences en-dessous de la flexion fondamentale, l'aile étant encastrée). Très loin du flottement, on empêche ainsi les termes de couplage de la matrice aérodynamique de jouer leur rôle.

Dans ce cas de flottement doux, parceque, dû à des modes de grandes masses généralisées, calcul et essais donnent une bonne concordance jusqu'à M = 0,92. La figure 14 donne un exemple de comparaison entre le calcul avec contrôle et les essais.

Dans un deuxième cas réalisé sur la même maquette (figure 15), mais équipée d'engins différents, on a créé un flottement antisymétrique en incorporant à l'emplanture un mode d'ensemble de roulis. Ceci afin de voir si on pouvait, sans inconvénient, superposer sur la même servo-commande, une loi de contrôle dynamique pour contrer le flottement et une loi de pilotage de la maquette en roulis qui maintienne celle-ci à une position fixe.

Bien que la maquette soit à la paroi, ce qui donne une distribution des forces aérodynamiques du type symétrique (effet miroir), on a fait les calculs de flottement avec des modes antisymétriques.

L'introduction de forces antisymétriques n'aurait apporté qu'une très faible différence sur les termes des matrices des forces aérodynamiques généralisées. En effet dans les modes considérés dans le flottement, les déplacements, relatifs à une norme unitaire en bout d'aile, sont nuls ou très faibles sur une partie de l'envergure à partir de l'emplanture de l'aile.

L'engin du bout d'aile, qui intervient avec un mode de tangage, entraîne seulement l'extrémité de l'aile (c'est-à-dire la tranche qui comporte la gouverne de contrôle). Le couplage se fait dans ce cas, sans contrôle, entre la flexion antisymétrique à 20 Hz et le tangage engin à 25 Hz.

Le contrôle est réalisé par un rapprochement et un croisement très rapide des fréquences dans des conditions subcritiques loin du flottement (figure 16 + figure 17).

Calcul et essais avec et sans contrôle donnent une bonne représentation du phénomène qui valide les hypothèses faites sur les forces induites par l'aileron sur l'aile.

En ce qui concerne les forces aérodynamiques sur engins (soit les termes directs, soit les termes de couplage), elles ont été déterminées par des essais préliminaires et ce sont ces valeurs expérimentales qui ont été introduites dans les calculs.

De la même façon que précédemment, avec la même loi de contrôle, on a atteint M = 0,92 pour des valeurs de pressions dynamiques supérieures de 50 % à la valeur critique sans contrôle.

Sur la figure 18, on trouve un exemple de l'efficacité de la loi de contrôle. Le contrôle a été coupé au delà du flottement. La maquette part en instabilité et pour une amplitude donnée, 12 g au nez de l'engin, le contrôle est réintroduit d'où restabilisation du système.

Conclusion

L'ensemble des textes examinés dans cet exposé montre le grand intérêt qui existe dans de nombreux pays pour la technologie des contrôles actifs. Ces articles, qui mettent en lumière les difficultés de calcul que l'on rencontre pour faire des prévisions valables, insistent sur 2 points :

- le premier est qu'il faut traiter le problème du contrôle automatique généralisé dans son ensemble par suite des interférences qui peuvent exister entre les différents systèmes.

- le second point est que devant la complexité du problème, il y a intérêt à faire ressortir, dans une première étape, les paramètres importants par des calculs simplifiés et à s'appuyer ensuite sur des résultats expérimentaux dans les cas précis où le modèle mathématique se révèle impuissant à cerner la réalité avec suffisamment de précision (cas des non linéarités prononcées, des servo-commandes, interaction entre surfaces portantes ou entre engins et surfaces portantes).

Bibliographie

Agard Conference Proceedings n° 228
Structural Aspects of Active Controls
Lisbonne, 21 avril 1977

R. Destuynder
Suppresseur de flottement en transsonique
Recherche Aérospatiale n° 1978-3

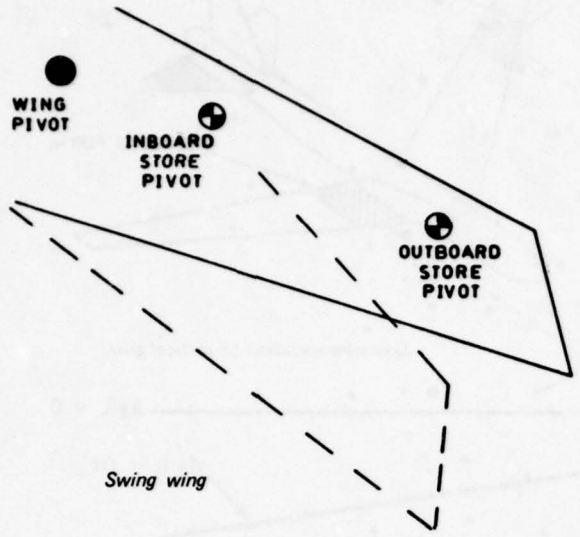

CASE	STORE AND POSITION	MACH No.	WING SWEEP
1	STORE A INBOARD	0·8	25°
2	STORE B INBOARD	0·8	25°
3	STORE C OUTBOARD	0·9	45°
4	STORE C OUTBOARD	1·35	45°

Design cases

Fig. 1 (M.R. Turner - C.G. Lodge).

CASE	FORCE POSITION	TRANSDUCER POSITION	FILTER ON VELOCITY	GAIN K
1	P90	∝ 110	$\frac{1}{S(S+79{\cdot}4)}$	$-1{\cdot}45\times10^{8}\left(\frac{V}{0{\cdot}575VR}\right)^{2}$
	P100	∝ 110	$\frac{1}{S(S+62)}$	$-1{\cdot}14\times10^{8}\left(\frac{V}{0{\cdot}575VR}\right)^{2}$
2	P12	W85	$\frac{1}{S}$	$3{\cdot}8\times10^{5}\left(\frac{V}{0{\cdot}575VR}\right)^{2}$
	P90	∝ 110	$\frac{1}{S+22{\cdot}5}$	$-2{\cdot}2\times10^{6}\left(\frac{V}{0{\cdot}575VR}\right)^{2}$
	P100	W43	$\frac{1}{S}$	$7{\cdot}8\times10^{5}\left(\frac{V}{0{\cdot}575VR}\right)^{2}$
3	P90	W1	$\frac{1}{S}$	$1{\cdot}64\times10^{7}\left(\frac{V}{0{\cdot}757VR}\right)^{2}$
	P100	W85	$\frac{1}{S}$	$9{\cdot}37\times10^{5}\left(\frac{V}{0{\cdot}757VR}\right)^{2}$
4	P90	∝ 114	$\frac{1}{(S+6)^{2}}$	$5{\cdot}11\times10^{6}\left(\frac{V}{0{\cdot}805VR}\right)^{2}$
	P90	W1	$\frac{1}{(S+6)^{2}}$	$-1{\cdot}06\times10^{8}\left(\frac{V}{0{\cdot}805VR}\right)^{2}$

FEEDBACK LAW: $P = K f(s) \dot{W}$

P = POINT FORCE
K = FEEDBACK GAIN
f(s) = FEEDBACK FILTER
$\dot{W}$ = STRUCTURAL VELOCITY

Fig. 2 — Chosen best flutter control systems with control surface on the wing. (M.R. Turner - C.G. Lodge).

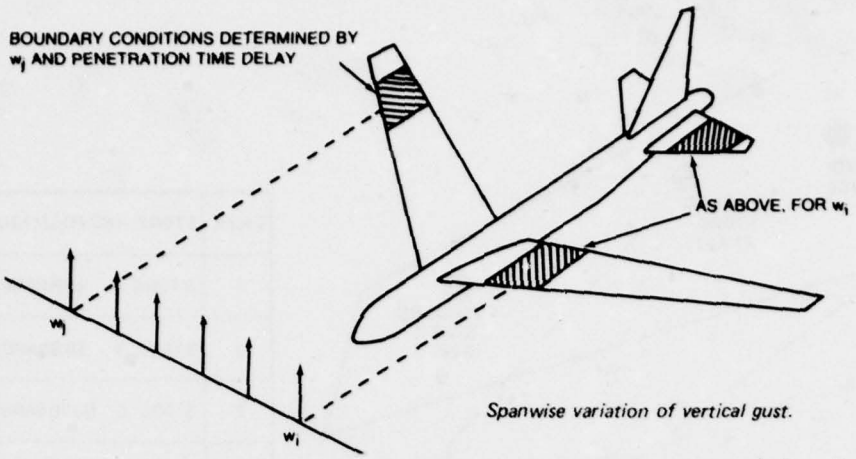

Spanwise variation of vertical gust.

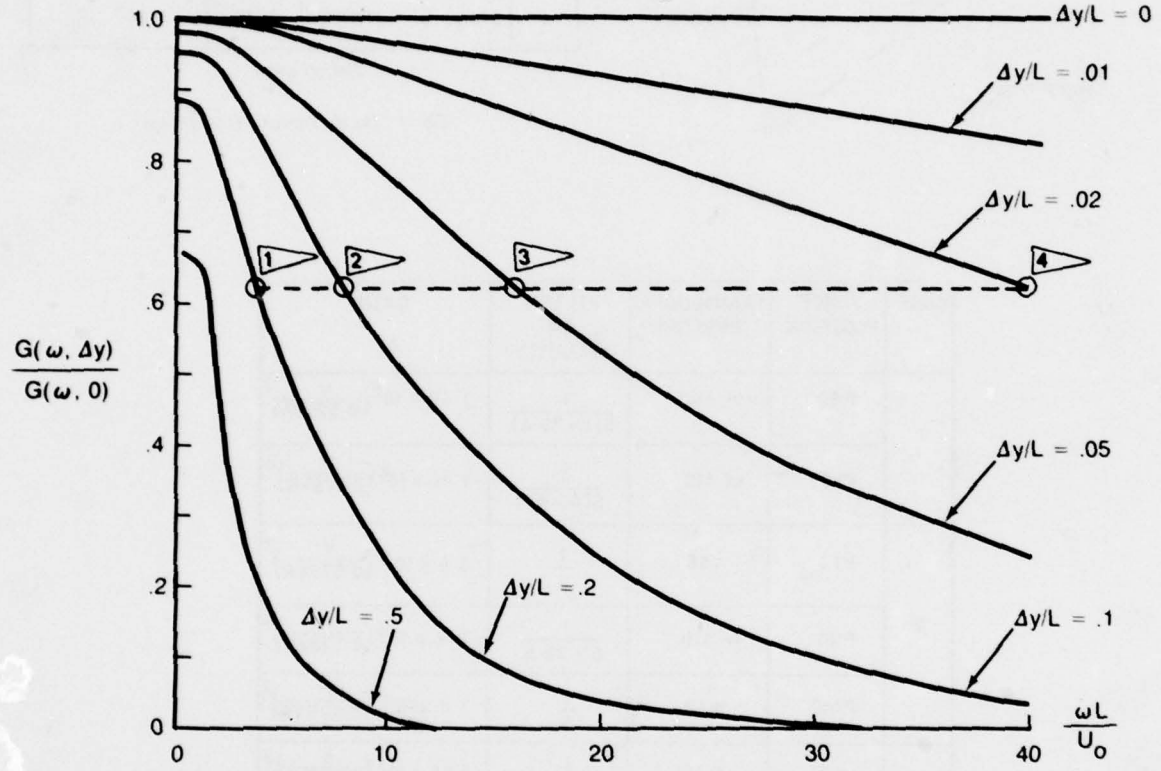

Fig. 3 – Effect of spanwise separation on vertical gust cross spectral density. (K.L. Roger).

Δy = spanwise separation distance
L = scale of turbulence ≃ 150 m

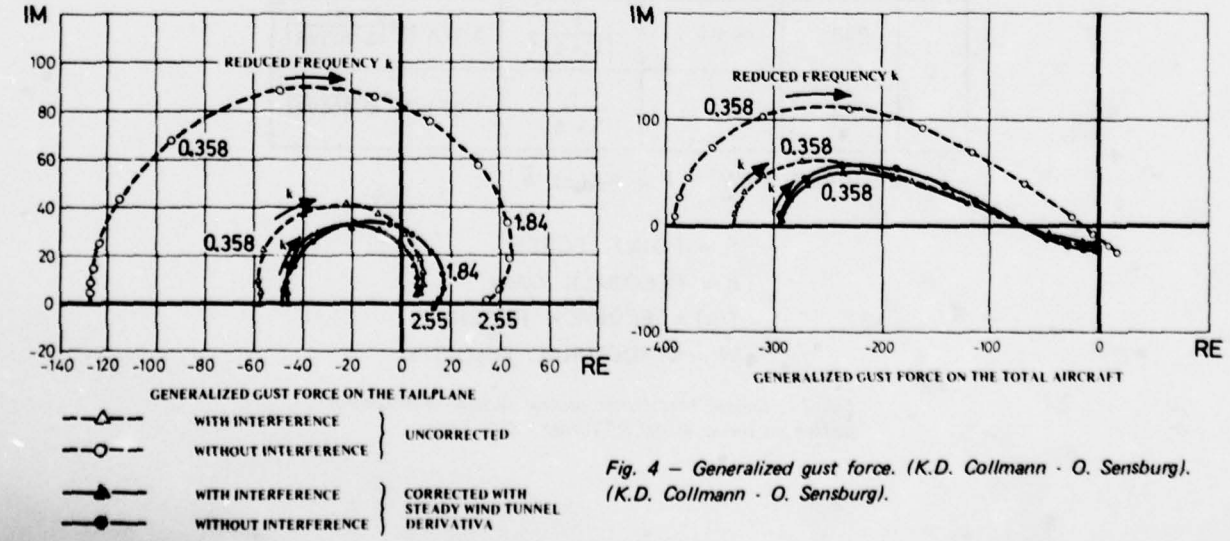

Fig. 4 – Generalized gust force. (K.D. Collmann · O. Sensburg).
(K.D. Collmann · O. Sensburg).

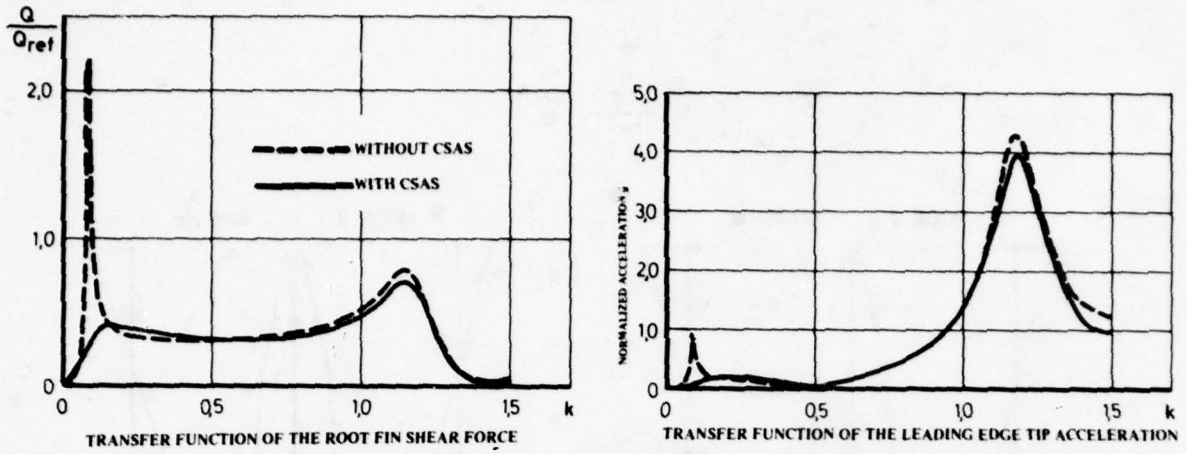

Fig. 5 – Fin transfer functions for lateral gust. (K.D. Collmann - O. Sensburg).

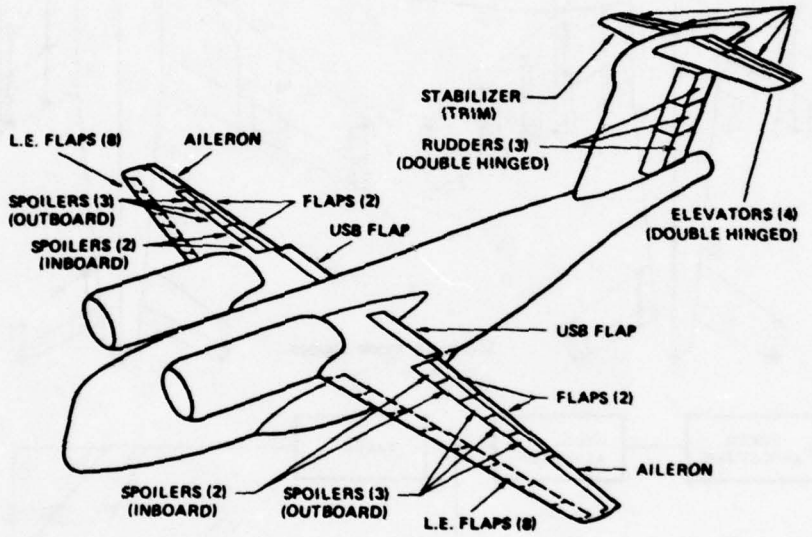

Fig. 6 – Flight control surfaces. (W.T. Hamilton).

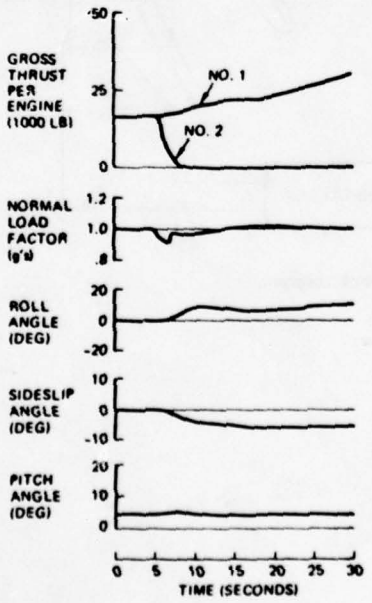

Normal response to speed command, STOL landing configuration.

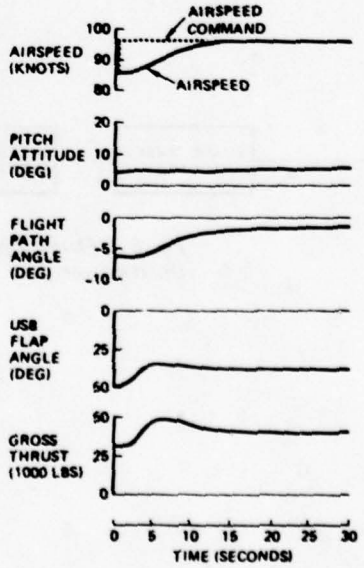

Fig. 7 – Response to engine failure with pilot "Hands off" of control. (W. Hamilton).

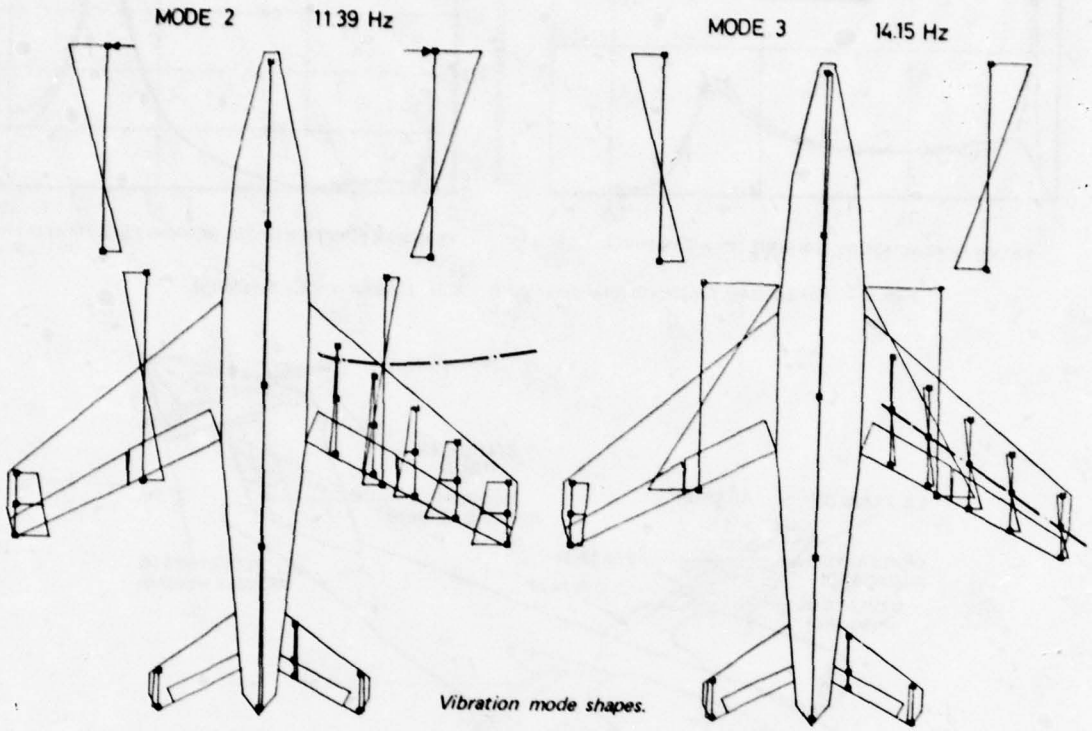

Vibration mode shapes.

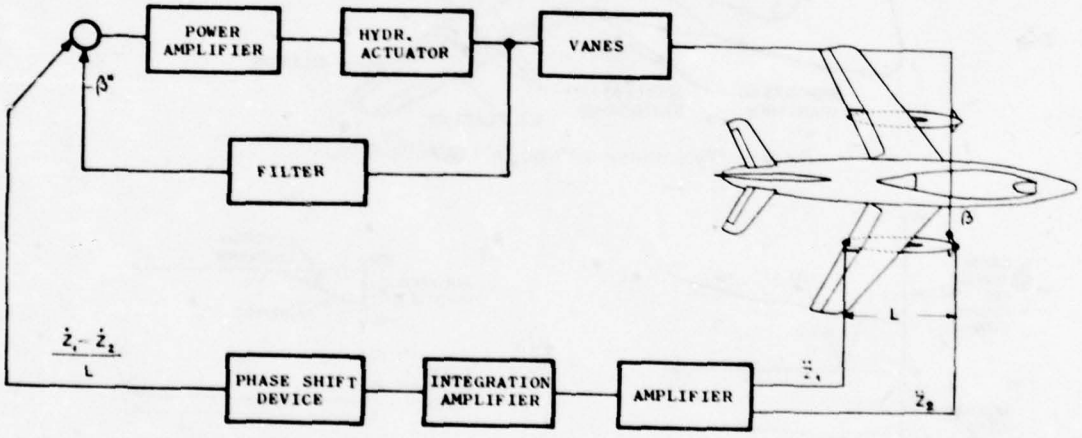

Fig. 8 – Flutter suppression system block diagram. (H. Hönlinger).

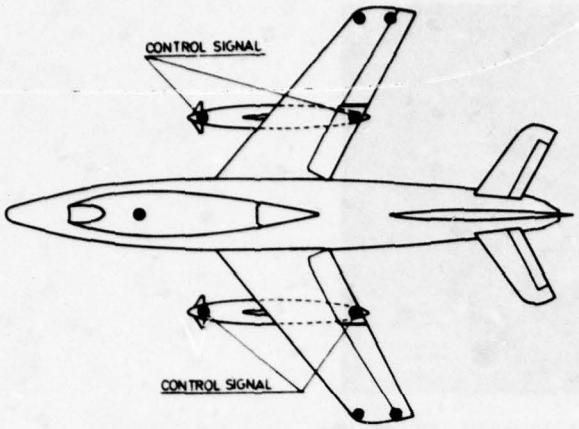

Accelerometer locations

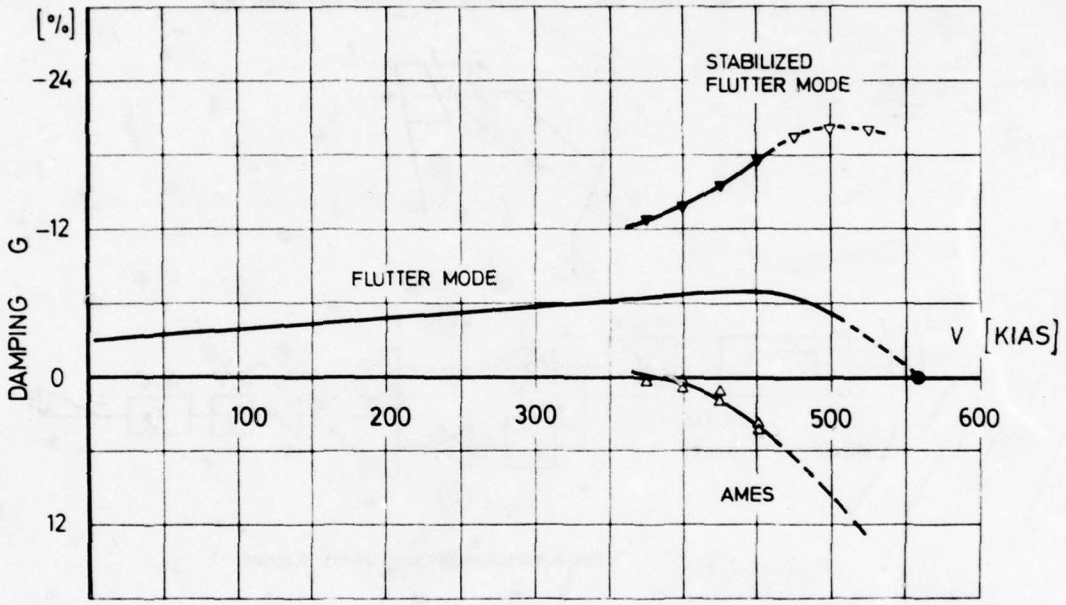

Fig. 9 – Efficiency of FSS. (H. Hönlinger).

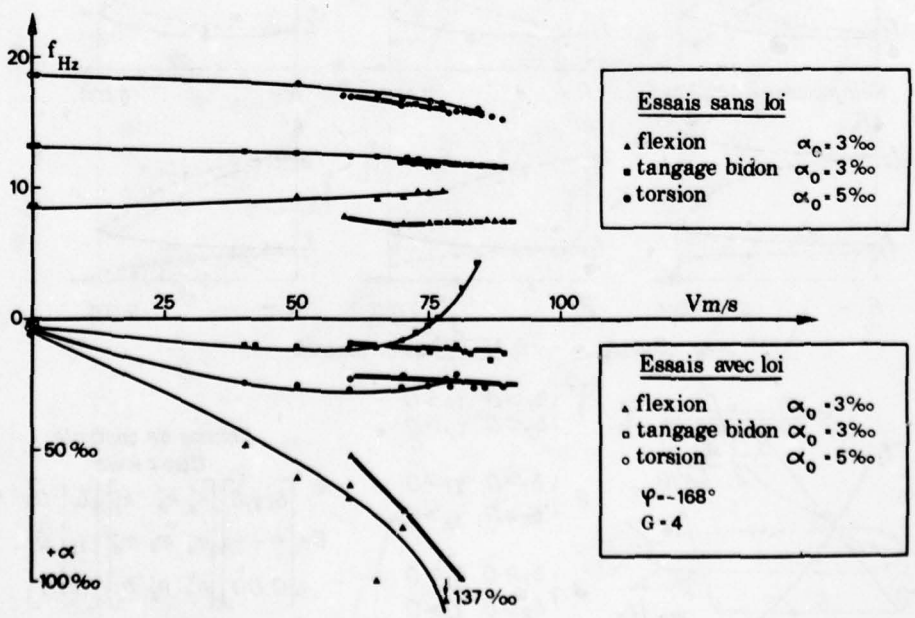

Fig. 10 (R. Destyunder).

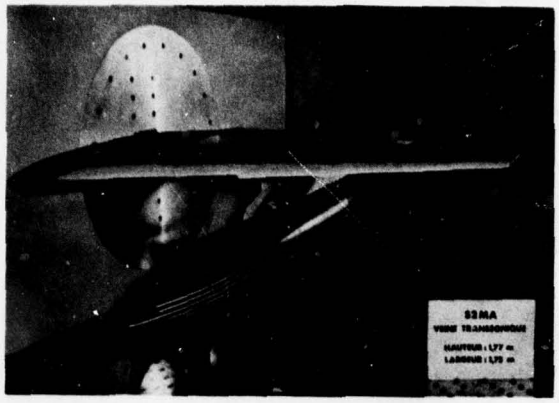

Fig. 11 – Aeroelastic model clamped at the tunnel wall with tank.

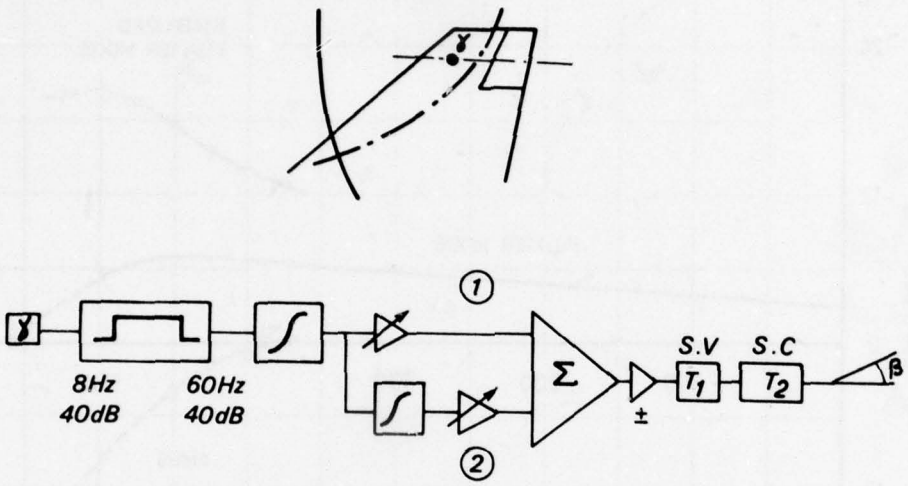

Fig. 12 – Flutter suppression system - Block diagram.

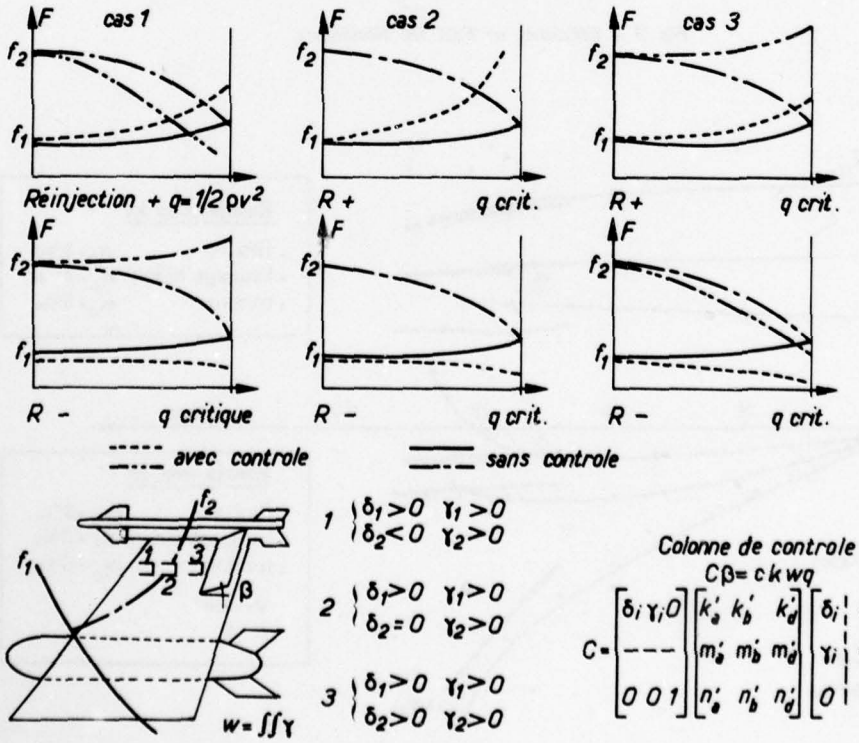

Fig. 13 – Contrôle par des termes de rigidité induits.

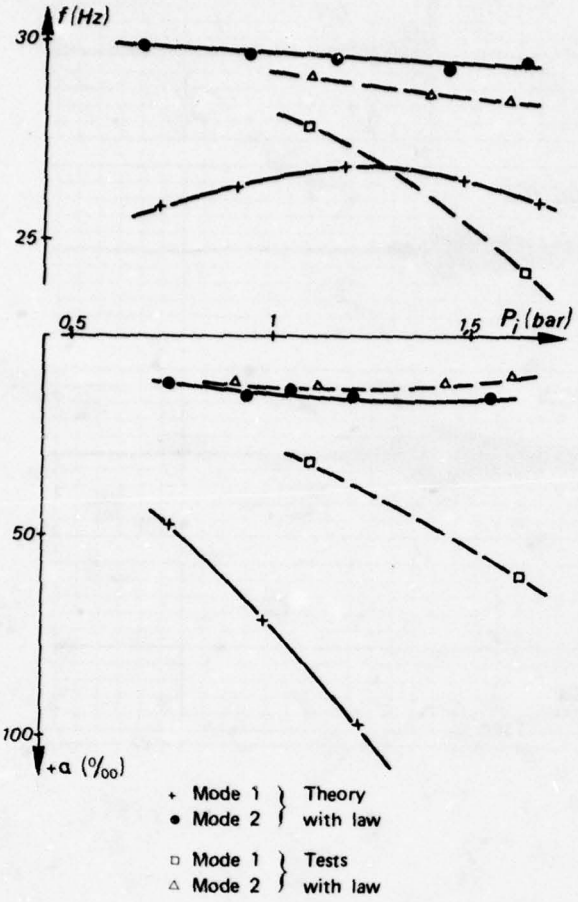

Fig. 14 – Comparison theory-tests with control law. Mach = 0,80 (Destuynder).

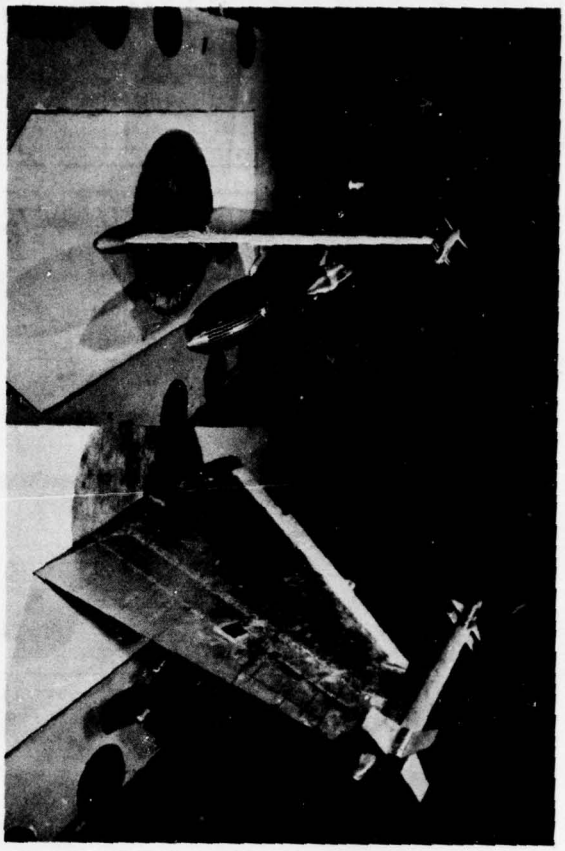

Fig. 15 – Aeroelastic model free, in roll, with stores.

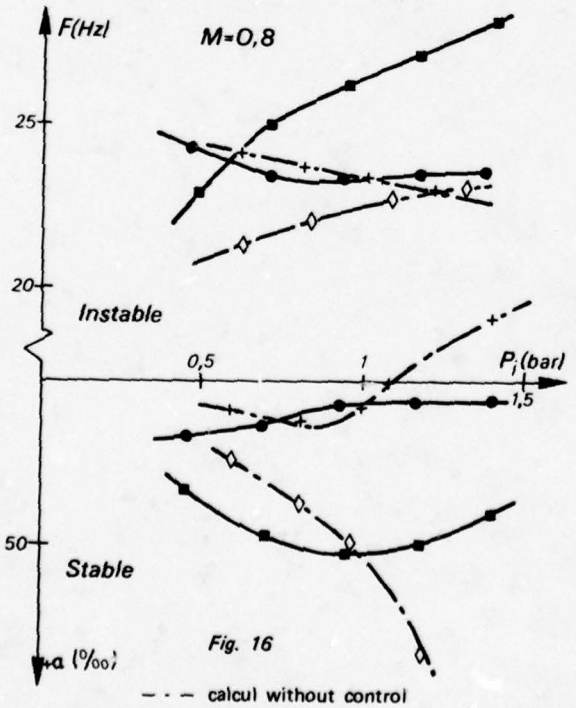

Fig. 16

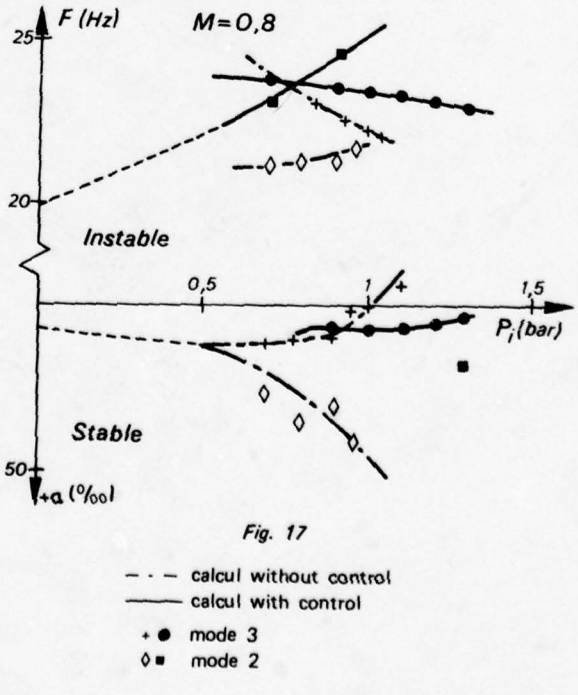

Fig. 17

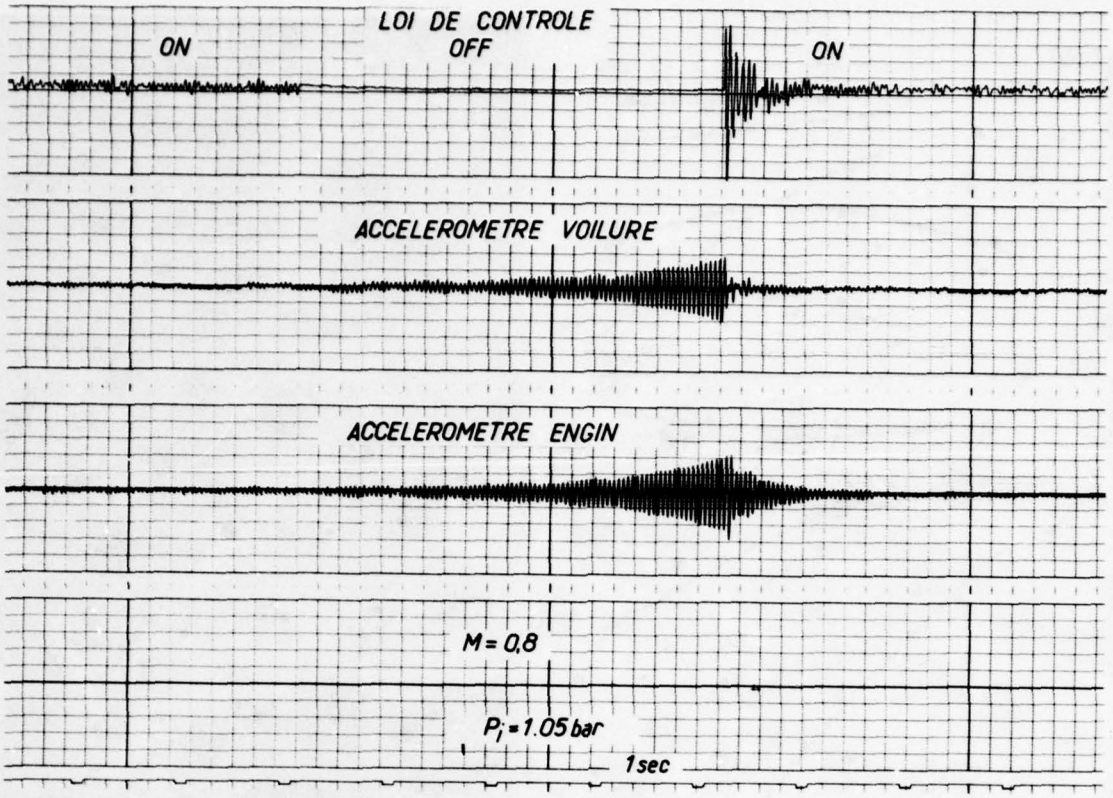
LOI DE CONTROLE
ON
OFF
ON
ACCELEROMETRE VOILURE
ACCELEROMETRE ENGIN
M = 0,8
P_i = 1.05 bar
1 sec

Fig. 18

CONTROL OF MISSILE AIRFRAMES

by
Derek J. Frary
Group Leader, Theoretical Studies Dept.
British Aerospace Dynamics Group
Filton House
Bristol
BS99 7AR
England

SUMMARY

The main differences between manned aircraft and missiles and the approach to the design of missile airframe control systems is presented in a general manner. The requirements placed on airframe control loops by guidance systems are described which illustrate the advantages of using a neutrally stable airframe.

Various airframe control systems in current use are reviewed, thus showing how active control technology is applied to missile systems. Detailed design factors such as body flexure and non-linearities are discussed. Also included is a brief description of some typical airframe control systems and avionics loops which are used for unmanned aircraft.

1. INTRODUCTION

The performance of manned aircraft for modern high speed military and civil applications is steadily increasing. At the same time missile technology is diversifying into the realms of unmanned aircraft, remotely piloted vehicles and cruise missiles. Stability and control problems in the spheres of manned aircraft and missile design are now more closely allied than ever previously, and this trend may well continue whilst each field remains as a separate entity.

The object of this paper is to outline the techniques used in missile airframe control systems in simple terms without placing undue emphasis on theoretical control giving a few examples. In this way it is intended to narrow the gap between those engaged in missile and aircraft technology and perhaps highlight areas of commonality where improved collaboration may provide some mutual benefit.

The paper reviews the differences between missile and manned aircraft systems. The range of speeds and accelerations encountered in missiles are considered in order to illustrate the differences in the design problem. A brief outline is given of the missile performance requirements illustrating the factors which dominate control system and airframe design. There follows a review of the type of airframe control systems in common usage. Some of the more important detailed aspects involved in the design are also considered and the paper concludes with a summary of techniques which apply to unmanned aircraft and remotely piloted vehicles.

2. CHARACTERISTICS OF MISSILES COMPARED TO MANNED AIRCRAFT

A missile can be classified as a projectile carrying a payload (usually a warhead) which is guided onto a target by manual or automatic means. Missiles usually employ a cruciform wing configuration but sometimes a monowing layout is used. Generally missiles are capable of relatively large levels of lateral acceleration (normal to the wings), e.g. 200 m/s^2 or greater. Recently, the term Remotely Piloted Vehicle (RPV) has emerged which is used to describe vehicles controlled by a ground station or pilot in order to carry out a particular role, e.g. reconnaissance, target designation, crop spraying. The manually guided anti-tank weapon could be considered as a type of RPV but it would usually be referred to as a missile. A further term sometimes used is Unmanned Aircraft (UMA) which describes any aircraft-like vehicle which is either remotely piloted or autonomous.

This paper mainly considers missiles with some references to RPVs and UMAs in Section 6.

Modern high performance manned aircraft are generally much larger and necessarily more complex than missiles. Furthermore, aircraft costs are generally much higher. This is as might be expected since a fighter aircraft for example would normally have a capability of attacking many targets in its useful life. Missiles on the other hand often only attack a single target and must be relatively inexpensive to remain cost effective.

The obvious difference between aircraft and missiles is the pilot. In the case of aircraft, the airframe designer must always bear in mind the requirements of the pilot in terms of airframe characteristics. Missiles are often autonomous and effects of variations in airframe aerodynamic behaviour must not degrade the system performance. This means the automatic control systems must be tolerant of variations or these must be minimised in the airframe design. In the case of manually guided missiles, the effect of changing airframe behaviour must be kept within the capabilities of the operator, who is generally less tolerant than a compensated automatic system, as is the aircraft pilot.

A further implication of a pilot and perhaps passengers on board the vehicle is safety and reliability. Very high levels of aircraft safety and reliability are necessary which often lead to equipment duplication; this is rarely used for missiles except to ensure safe handling of the warhead and motor during deployment of the weapon. Safety and Arming units are an important part of missile design and subject to rigid tests in order to give confidence that any failure will result in a safe situation for the launch vehicle and personnel. Once a missile is safely launched, safety is limited to consideration of one's own troops; the missile is expendable and any faults which lead to its destruction need not be catastrophic. Reliability is important in order that the missile completes its mission, but this is generally a cost-effective decision

in that the most efficient means of destroying a target is what really matters. For example, if it is cheaper to use two simple missiles rather than one expensive, sophisticated weapon then, provided there are no serious deployment or logistical constraints, the cheaper missiles would be preferred.

Missiles generally operate over a wider range of speeds and accelerations than aircraft. For example, a typical medium range missile (30 km) could accelerate up to Mach 2.5 with a longitudinal acceleration of 300 m/s^2 ($\sim$30 g). Accelerations may sometimes be much higher than this, and the design of components such as homing heads or gyroscopes in order to withstand the forces experienced can be quite critical. Similarly, lateral accelerations can also be very high (300 m/s^2 typically for high performance anti-aircraft roles) which again poses problems in the structural design as well as the behaviour of the missile control system.

Operational factors arising from the use of an automatic guidance and control system generally give large levels of electronic noise. This characterises missile systems which are often constrained in terms of performance by the effects of noise. This is particularly true in modern-day jamming environments where electronic CMs tend to produce results similar to the effects of noise, thus further constraining performance.

3. CONTROL SYSTEM PERFORMANCE REQUIREMENT

In this paper, the techniques used for controlling missile airframes are reviewed. In order to understand the reasoning behind these techniques, some of the fundamental requirements of the airframe control system must be considered. This will be done for two basic guidance systems:

(a) Command to line-of-sight (CLOS)

(b) Homing

The guidance system is most important for a missile since this enables the weapon to fulfil its function of hitting the target. The critical aspects are miss distance, the closest approach of the missile to the target and the geometrical relationship of the missile and target at that point since these factors determine the lethality of the warhead.

An airframe control system (ACS) is illustrated in general form in Fig.1. It is often referred to as a missile autopilot, although it is perhaps better described as an autostabiliser. The instrumentation or sensors measure the airframe motion, generally providing an electrical output signal. These electrical signals are used as feedback providing an error voltage to drive the control surface servos. The simple schematic of Fig.1 shows no electronic gains or shaping networks which may in practice exist within the forward path or feedback channel.

Fig.2 shows the geometry of a missile engagement. In CLOS guidance, the missile is controlled from the base, i.e. near the launch point. The motion of the target and missile are observed by some means (e.g. radar, infra-red, television or optically) using a tracker. These measurements are then fed into the missile control system via a command link to ensure that the missile flies down the line-of-sight from the tracker to the target. In this way the missile hits the target, provided it always lies on the line-of-sight. This process can be

(a) manual, where an operator guides the missile along the line-of-sight, or

(b) semi-automatic, where an operator tracks the target manually but the missile guidance is automatic, or

(c) fully automatic where both target and missile tracking are automatic as well as the guidance.

Other types of CLOS guidance exist such as beam riding (Ref.1) but, for simplicity, these are not considered here.

A simplified block diagram of a non-manual CLOS guidance loop is shown in Fig.3. This is illustrated for an airframe control system (ACS) which controls missile lateral acceleration, i.e. a steady electrical input demand results in an approximately constant acceleration turn. In practice the guidance system operates in three dimensions and therefore there may be two such guidance loops as shown in Fig.3, one in the horizontal and one in the vertical plane. The important control system element in the CLOS guidance loop is the double integration between acceleration and displacement. This gives 180^o phase lag which makes the guidance loop inherently unstable unless some phase advance is added, as shown in the forward path of Fig.3. Unfortunately the degree of phase advance must be restricted or the guidance system tends to amplify the noise from the tracker, particularly in the case of automatic target tracking. Tracker noise levels increase with missile and target range and therefore a poor guidance loop noise response can seriously degrade the miss distance, particularly if any system elements experience signal saturation by noise.

For high performance missile systems such as anti-aircraft missiles, the high target angular crossing rates encountered by the tracker ($\dot{\psi}_t$) require the guidance loop speed of response or bandwidth to be as high as possible. Thus the guidance loop gain must be maximised. In order to achieve this without using large amounts of phase advance, the missile ACS must have minimum phase lag at low frequency and hence maximum bandwidth whilst keeping the noise response within bounds.

In fact, the loop in Fig.3 shows that in the steady state, a fixed gain results in steady error for constant missile lateral acceleration. Therefore, ignoring the feed-forward term in Fig.3 initially, if a particular target engagement requires an acceleration of say 200 m/s^2 from the missile, for a gain of 10 s^{-2} the miss would be 20 m in the steady state. The miss could be reduced if the gain could be increased but stability and noise considerations in the automatic guidance loop do not normally allow gains much above this value. However, the feed-forward term in Fig.3 is introduced to overcome this problem. This block derives a signal which is equivalent to the missile lateral acceleration needed to remain on the line-of-sight. This acceleration is not known exactly but it can be estimated from prior knowledge of the missile speed and range together with measured target tracker rates. In this way the bulk of the missile

acceleration is generated by the feed-forward block and the guidance system control loop signals are kept low, perhaps only one-tenth of the total missile acceleration. Thus the steady state miss distances are reduced by the same factor.

Using this principle, CLOS guidance errors of less than a few metres can be achieved. In fact the practical limitations of tracking targets tend to make CLOS guidance systems useful at only short range (<10 km). Missiles for this type of application can be kept relatively small in size provided miss distance and hence warhead weight are not large.

The implication of using feed-forward acceleration in Fig.3 is that the missile ACS must have a well controlled, low-frequency or steady state gain, normally unity. In fact the acceleration demanded must be actually achieved to within a tolerance of about $\pm$ 10%, which implies an ACS steady state gain of within $\pm$ 10% of a known value.

Therefore, the missile ACS requirements for CLOS guidance can be summarised by maximum bandwidth for acceptable noise performance coupled with a closely controlled steady state gain over the flight envelope.

Homing missiles employ measurements of the missile-target sightline which is illustrated in Fig.2. On board the missile is a target tracking device known as a homing head or seeker head. The homing head makes use of radiation reflected from the target (e.g. radar) or emitted by it (e.g. infra-red). With radar the target may be illuminated by a source in the missile (known as active homing) or by a separate transmitter (semi-active homing). Use of emissions generated by the target itself for guidance is called passive homing.

The missile homing head usually generates a measure of sightline rate which is used to guide the missile according to a particular law. As an example, a common guidance strategy known as proportional navigation (PN) may be used, Ref.2. This takes the form of:

$$\dot{\psi}_f = \lambda \dot{\psi}_s$$

where ψ_f is the missile flight path angle

λ is the navigation constant

ψ_s is the sightline angle (see Fig.2)

For a missile ACS which controls missile lateral acceleration, the guidance system takes the form shown in Fig.4 and the PN law is modified to:

$$a_d = \lambda^* \dot{\psi}_s$$

where a_d is the demanded missile lateral acceleration

λ^* is the modified navigation constant

For PN homing guidance the miss distance is determined by the overall system bandwidth and high bandwidth generally means improved guidance accuracy. It is therefore necessary to make the missile ACS bandwidth as high as possible. At long missile-target ranges the homing head may experience high noise levels which generally impose a limit on system bandwidth and gain in order to avoid saturation of the guidance system by noise.

A further requirement to maintain system accuracy is to keep the navigation gain relatively constant which implies a closely controlled missile ACS steady state gain. In this case the variation of steady state gain is less critical than in the case of CLOS; $\pm$ 20% is normally adequate.

In summary, missile ACS requirements are:

(1) Maximum bandwidth commensurate with acceptable response to noise disturbances.

(2) Constant steady state gain of unity or a gain which varies in a predetermined manner in the presence of noise and aerodynamic variations.

In addition, other more general factors emerge:

(3) Capacity to operate in the presence of noise disturbances without:

  (a) becoming unstable
  (b) giving excessive induced drag
  (c) causing damage to the airframe
  (d) inducing extra biases arising from saturation effects

(4) The effect of biases must be minimised.

(5) The closed loop performance (i.e. speed of response) must not change excessively with operational changes, e.g. with varying missile speed.

(6) The effects of body flexure must be small

(7) The effects of roll motion must be small.

The above factors are typical of those considered in the design of a missile ACS. In practice some are more important than others and the more obvious factors must also be taken into account, such as design, development and production costs, complexity, mass, size, installation constraints, etc.

4. AIRFRAME STABILITY

As seen from the discussion in Section 3, the airframe control system performance requirements can be adequately defined. In turn, these requirements place constraints on the control system elements, i.e. control surface servos, feedback sensors, electronic package and airframe. In the design of the ACS, the designer is responsible for specifying the required performance of the system elements (including the aerodynamic performance of the airframe). The ACS designer therefore works in close collaboration with the aerodynamic engineer during the definition phases of a missile system study.

The control surface servos must have a high bandwidth in order to ensure adequate ACS stability; in practice this implies a servo bandwidth of at least three times the ACS. Also there are advantages in providing adequate servo torque in order to avoid rate limiting. The effect of servo rate limiting is to reduce the ACS stability which places further constraints on the design.

Control feedback sensors must similarly have high bandwidth but this does not normally raise any design difficulties. The ACS design is aimed at ensuring that the system is tolerant of variations in sensor biases and scale factor errors, therefore ensuring that the sensor accuracy requirements are not too demanding. Electronic circuits also introduce errors into the missile ACS which are not always insignificant. In practice, a cost-effective solution may well emerge with electronic errors being similar to the sensor package in terms of contributions to overall system errors. Modern electronic techniques, e.g. by the use of digital processing, can alleviate this problem.

Missile aerodynamic design is often dominated by the need to achieve high lateral acceleration, particularly in the case of high performance missiles. This leads to a design which in the case of fixed-wing missiles must have high lift without excessive incidence and a high aerodynamic gain, i.e. large lateral acceleration can be achieved for reasonable control surface deflection angles. This can be achieved quite readily by using an airframe with near to neutral stability which therefore gives the necessary wide trim capability. For tail-controlled airframes, the fins must be small with a relatively long tail arm in order to give high control moments whilst reducing the effect of fin forces, which give acceleration in the wrong direction. If forward controls (Canards) are used the trim capability is limited since the canards stall at lower deflection angles. This arises from the canard angle with respect to the airstream being the arithmetic sum of canard deflection and incidence. In the case of a tail-controlled missile, the airstream passing over the fin is almost parallel to the body.

Moving-wing configurations, i.e. an airframe where the aerodynamic control surfaces are larger than the fixed surfaces, generate lateral acceleration largely from the lift on the moving wings. Therefore, as the body rotation is not needed to produce manoeuvre and since neutral stability is not necessary, the airframe is best made relatively stable. The acceleration capability of moving-wing missiles is often restricted by the control torques required and hence the servo performance limitations.

A further consideration is the control of airframe roll motion which is frequently necessary in the case of homing missiles and can cause ACS instability (Ref.3). Roll control can readily be achieved by the use of tail controls but is more difficult using moving wings as a result of control reversals from downwash effects on the rear surfaces. It is not normally possible to control roll motion using canards.

Another airframe control technique is thrust vector control (TVC). This is particularly useful where low speed manoeuvre is necessary, e.g. turnover following vertical launch. It also can be used to give guidance with very low levels of lateral acceleration normal to the missile body; the TVC system simply rotates the body sufficient to give a component of the longitudinal body acceleration. However, this means of control is inefficient compared with aerodynamic control since the motor must burn all the time control is needed. Therefore, TVC missiles often turn out much heavier than equivalent aerodynamically controlled designs. Combinations of TVC and aerodynamic controls sometimes exist, but the use of two sets of aerodynamic controls, for example moving wing and tail controls, is comparatively rare.

The requirements of the ACS which influence aerodynamic design are well defined steady state gain, high bandwidth and minimum noise saturation effects.

In order to maintain good steady state gain, the control loop must not be influenced at low frequencies by aerodynamic variations. This implies high gain in the control loop and in the case of fixed-wing airframes is also improved by a near neutrally stable solution. In the case of moving-wing configurations, which are normally made stable, it is often necessary to use a special ACS design which is not susceptible to aerodynamic variations during flight.

If the ACS is to have high bandwidth, it would appear logical to make the airframe weathercock frequency high. However, since the control system gains must be kept high, it is far better to use a very low bandwidth airframe. This again points to the use of an airframe with near to neutral stability.

In the presence of noise, a difficult problem is ensuring the elements in the missile ACS are not saturated by noise. Normally if, for example, the missile acceleration in response to noise is unacceptable, then this can only be overcome by reduced ACS bandwidth and hence reduced performance in terms of guidance accuracy. However, in many cases the most difficult problem arises with levels of control servo angles and rates in the presence of noise. In this case, a reduction of servo noise can be achieved by increasing the airframe aerodynamic gain, which is evident from Fig.1, provided the overall ACS bandwidth is kept the same. This further emphasises the need for neutral stability of the missile airframe.

Although neutral stability is generally desirable from the point of view of performance, in practice it cannot always be achieved. The missile centre of gravity frequently shifts forward during flight as a result of fuel burning within the rear motor. Therefore, if one aims to choose neutral stability for the middle of the motor burn period, this would result in an unstable airframe at launch which becomes more stable as the flight proceeds. In many cases this could turn out to be the best compromise. However, problems may exist in launch and the early part of flight when automatic control is limited in effectiveness as a result of the low speed and poor aerodynamic manoeuvrability. The ACS design is then limited by

the restrictions of an airframe which is clearly too stable during the later flight period, i.e. when missile impact is most likely to occur. Other factors such as cost, manufacture, etc. influence aerodynamic design of the missile apart from guidance and ACS performance. The eventual design is inevitably a cost-effective compromise.

In summary, the aerodynamic control configuration is normally selected on the basis of required lateral acceleration capability and the degree of roll control needed. To give high lateral acceleration levels as well as roll control capability a tail-controlled airframe is necessary. In order to ensure that high lateral accelerations can be achieved with such an airframe at low levels of incidence and control deflection, high lift coupled with nearly neutral stability is needed. The ACS requirements enforce the need for neutral stability and high lift coefficient and furthermore airframe stability is not required except in relatively few cases where special considerations exist at launch or low speed, e.g. ensuring launch aircraft safety.

5. AIRFRAME CONTROL SYSTEMS

The requirements of the airframe control system and its components have been discussed in Sections 3 and 4. This section illustrates typical missile ACS which are in common usage.

The main ACS components are control surface servo, airframe, sensors and electronic package. The airframe characteristics have been outlined in Section 4. Control surface servos used are electrical, hydraulic and pneumatic. Hydraulic actuators are most useful for high torque applications such as moving wing missiles or large, long range weapons. The electrical and pneumatic (hot or cold gas) devices are generally limited in torque capability, i.e. generally for smaller missiles using canard or tail controls. The gas servos have good power to weight ratio, although most systems are bang-bang rather than linear and can introduce difficulties into the ACS design. The servos used are normally proportional devices, i.e. a steady input voltage gives rise to a steady control surface angle. However, in some cases, rate servos are used (i.e. a steady input gives a fixed angular rate) although this is comparatively rare. Thrust vector control actuation techniques are very specialised and often require expensive development programmes. Techniques include spoilers, vanes, jetavators and fluid injection (Ref.1) employing all forms of actuation techniques.

Airframe sensors consist of accelerometers, rate gyroscopes, attitude gyroscopes and pitot tubes. These are normally body-fixed or strapdown instruments but sometimes stable platforms or homing head instruments also serve for the ACS.

Electronic circuits of current weapons are varied in nature ranging from vacuum tube or valve devices to modern solid state integrated circuits. Systems using microprocessors are now being designed, employing digital techniques. To take advantage of a digital ACS, the use of sensors giving a digital output and also a control actuation system with a digital input drive would provide the neatest solution. However, the most cost-effective solution is usually a standard analogue device plus the appropriate analogue to digital convertor or vice versa.

Fig.5 shows a schematic diagram of a missile lateral ACS using rate gyro and accelerometer feedback sensors. The ACS is designed to control missile lateral acceleration and the accelerometer is therefore used to provide the dominant steady state feedback component. The rate gyro feedback is mainly a stabilising signal, analogous to the use of tachometer feedback in a position servo. It can also play a very important part in providing more sensitive feedback than acceleration at low speeds, e.g. following launch to reduce the effect of dispersions as a result of misalignments. This particular type of ACS is commonly used for high performance applications. The use of two sensors in each plane gives considerable design flexibility and relative freedom from the disturbing effects of aerodynamic variations. However, the cost of the instrumentation constitutes a significant proportion of the overall cost and cannot be justified for low-cost weapons, e.g. anti-tank.

In the design of the ACS, the various gains shown in Fig.5 are established as well as the shaping network. These may well be fixed throughout the flight envelope for some applications provided the performance at the extreme cases remains acceptable. Other cases require some variation in gain which can be carried out either by switching or in a continuously variable fashion. Switched gains provide a fairly cheap option but can give a performance penalty in the form of large disturbances at switching points which may result in considerable transient errors in the missile trajectory. The gains would generally be switched three or four times in flight and probably be switched on the basis of time. In this case the flight profile is assumed to be sufficiently invariant between missiles, e.g. as in the case of low-level short range missiles. To vary gains continuously is complex electronically unless digital techniques are to be used. The process can be carried out as time functions, if the flight profile is sufficiently consistent, or in conjunction with measurements of dynamic pressure using a pitot tube.

Thus the electronic pack of the ACS in Fig.5 can consist of simple gains and shaping networks as well as servo drive amplifiers and sensor demodulators if necessary. Alternatively it may include complicated gain variations. The instrument package is normally situated in such a position that the sensors are able to measure the desired variable in the most favourable fashion. For example, the accelerometer will only sense lateral acceleration if placed very close to the missile centre of gravity. For a fixed-wing-tail-controlled missile, this could turn out to be a disadvantage since it would measure the non-minimum phase acceleration which arises from the fin force giving the missile an initial acceleration in the direction opposite to the demanded direction. It is generally better to site the accelerometer close to the centre of percussion which is the point in the missile body, ahead of the centre of gravity, about which fin control forces cause the body to rotate. If this is done, the non-minimum phase terms are therefore eliminated from the accelerometer feedback signal which gives attendant advantages in stability and performance of the ACS. Other considerations also affect the positioning of the instrumentation such as body flexure; this is mentioned briefly in Section 6.

Fig.6 shows a typical fixed-wing tail-controlled missile layout illustrating how the various ACS components may be positioned within the body. The items are spread out in this type of airframe as can be seen

which makes assembly difficult and can have reliability penalties unless careful checking and quality control is maintained. A similar canard-controlled layout would have the entire ACS package concentrated at the front of the vehicle with attractive advantages in terms of modular construction, potential reliability and cost. This perhaps indicates why there are a good deal of canard-controlled missiles when performance factors might indicate otherwise.

Fig.7 illustrates a missile ACS with a single rate gyro feedback sensor. This configuration gives a system which apparently controls missile body rate but normally the ACS is given a response which is dominantly a phase advance equal to the missile incidence lag. In this way, a step input to the ACS gives rise to an approximate step change in missile flight path rate. The rate gyro ACS is therefore most useful in conventional PN guidance systems as described in Section 3. The feedback shaping network shown in Fig.7 is a lag-lead and the lag term is designed to match the missile incidence lag as closely as possible throughout the flight. Because the transfer function between body rate and lateral acceleration (Ref.5) is dominated by the incidence lag, the feedback signal can be made to give a body rate component plus a measure of the missile acceleration. This technique is very effective for applications where the missile behaviour is well known during the engagement. However, one invariably is left with some mismatch and the ACS then suffers from a low frequency lag-lead or phase advance response accompanied by a loss in guidance accuracy.

Rate gyros are generally more costly and less reliable than accelerometers of equivalent performance. Gyros also require a certain period of time to reach working speed which can impose limitations on the missile reaction time. This can be overcome by running the gyros at an early state of missile readiness, provided the missile is maintained frequently to ensure adequate reliability. Alternatively, gas-blown gyros can be used. These devices used either a pressurised gas bottle or cordite charge energy supply. This is capable of giving rotor spin-up times of only one or two seconds although generally with a limited operational time of up to one minute. A further disadvantage of gas-blown gyros is that the effect of decaying rotor speed is to alter the instrument scale factor which must be taken into account in the ACS design. Fig.8 shows a missile ACS which avoids the use of a gyro. As in the case of the single rate gyro ACS, the shaping network is designed to reconstitute the missing feedback signal. This is done with the use of a phase advance network for the ACS in Fig.8. This type of ACS is simple and cheap but not often used; problems exist in maintaining control at launch and also the effects of noise amplified by the phase advance shaping and the destabilising effects of roll motion for freely-rolling applications.

An extension of the single accelerometer configuration is the twin accelerometer system (Fig.9). This uses one accelerometer at the front of the missile and one at the rear. The system operates by using different gains in each feedback path and a lag network in the rear accelerometer channel. This produces an overall phase advance feedback making the ACS similar in principle to the single accelerometer system. This ACS is much better than the single accelerometer system and is used more often. The system appears simple and cheap but unfortunately suffers from the effects of missile body flexure and can involve complicated compensation filters; also the configuration can be slightly susceptible to the effects of roll motion.

The Lateral ACS using a position gyro is not normally associated with high performance missile systems. However, many anti-ship, anti-tank and air-to-surface missiles employ this type of system. Attitude control is particularly suited to manually guided anti-tank weapons. The effect is one of producing an operating function equivalent to velocity control which is very convenient to use. This has advantages in ease of training as well as improved accuracy.

Attitude control is not really suitable for automatic guidance systems except for a modified form of proportional navigation which is an integrated version of the conventional law and is therefore known as integrated PN. Attitude gyros are generally more costly than equivalent rate sensors which is why they are only used in special cases, e.g. if roll attitude stabilisation is needed. An example of this type of ACS is given in Fig.10. The system uses phase advance shaping which gives the system the necessary stability. An alternative but probably more costly approach is to use rate feedback in addition to attitude in order to provide the desired stability.

Lateral ACS are used in practically all missiles but far fewer employ roll control systems. This is simply a cost factor since it is generally cheaper to design a system which will tolerate the effect of roll motion rather than include roll control. The effect of roll motion on a missile is basically destabilising (Ref.4). Increased roll rates result in reduced stability of the lateral ACS until eventually it becomes unstable, although for a well designed system this will not occur until the rates are very high, typically four or five times greater than the ACS bandwidth. Roll motion also destabilises the guidance system and gimballed homing heads are often not capable of operation above roll rates of a few radians per second.

These are a few reasons why roll motion may not be acceptable in a particular situation. The technique used to control roll depends on the type of control needed. If the roll rates are simply to be reduced, a roll rate control system using rate feedback similar to the lateral autopilot of Fig.7 could be used. In this case the feedback shaping may not be necessary and there would be no input demand. Another method is to use rollerons which are gyroscopic devices attached to the ailerons (see Fig.11). The rollerons are spun up by the airstream and mounted on the spring-loaded ailerons in such a way that the gyroscopic torque resulting from a roll rate produces an aileron deflection in the direction required to counteract the roll rate. These devices are simple and robust but are limited in their effectiveness.

If roll attitude stabilisation is necessary, e.g. as a special homing head requirement, in order to ensure correct warhead orientation or if a strapdown radar altimeter is in use, then a position gyro is necessary. The ACS system used for roll attitude control is similar to the lateral system illustrated in Fig.10.

6. DETAILED DESIGN FACTORS

Missile ACS design is made by carrying out a preliminary design process and then a more detailed design using real data from wind tunnel or flight trial results. The more detailed study is normally heavily weighted towards simulation techniques using both digital and hybrid computing methods. Factors which can introduce problems at this stage are body flexure, roll motion (see Section 4), non-linearities and various three-dimensional problems.

6.1 Flight Phases

The implications of other aspects of the missile flight also have to be considered. The flight phases can be expressed generally as launch, gathering (capturing or gaining control of the missile following launch), mid-course (interim phase of flight prior to guidance) and the terminal guidance phase. The mid-course phase only exists in the case of relatively long range weapons. The ACS must be capable of giving adequate performance throughout all flight phases. The discussion in this paper is mainly concerned with terminal guidance which is generally the most critical phase. However, some systems may experience severe performance limitations in other flight phases, for example gathering, which can severely constrain the ACS design. In such cases, the guidance performance is often degraded as a result of the restrictions in the design. As an example, the shaping network in the rate gyro plus accelerometer ACS, as illustrated in Fig.5, is best confined to very low frequencies (10% of the ACS bandwidth) on the basis of stability and guidance accuracy. However, in a particular CLOS application, it was found that the effect of gathering with such a shaping network gave large transients with unacceptable short range capability. The solution involved using higher frequency shaping networks which impaired the stability and therefore reduced the performance at higher speed. In addition, the ACS was made more susceptible to roll motion but the short range capability was improved, therefore giving a better overall compromise.

6.2 Body Flexure

The effect of an elastic airframe is almost always only significant in terms of body flexure. Normally missile wings and control surfaces are relatively small and can be considered rigid. Body bending is sensed by the strapdown instruments. Therefore the dynamic response from control surface force to sensor output has two components, one aerodynamic and the other structural. Problems arise because the structure has a lightly damped oscillatory response at high frequency, i.e. a typical mechanical resonance characteristic. In actual fact, the body resonance has many modes but usually only the fundamental mode of oscillation is important. The effect of the structural resonance is to feed back a large component at high frequency. This results in instability if the gain at the body bending frequency is too high. Similarly if the instrument is situated in the wrong side of a node, the oscillation is 180° out of phase which constitutes positive feedback, also giving rise to instability. Therefore body flexure places strict constraints on the sensor positioning. For example, in the ACS of Fig.5 which uses rate and acceleration feedback, a typical body flexure mode may be of the form shown in Fig.12. If the fin is displaced as shown in Fig.12, the airframe pitches downwards and accelerates upwards initially then downwards as the body rotates. Also the fin force bends the body in the form of the graph shown in Fig.12. To give negative feedback from the accelerometer, the acceleration must be instantaneously downwards, i.e. of opposite sense to the instantaneous missile acceleration. It can be seen that this occurs if the accelerometer is placed between the two nodes. The ideal position would be forward of the centre of gravity, at the centre of percussion, in order to satisfy stability and performance requirements alone. Thus, to satisfy body flexure considerations also, the accelerometer should be forward of the centre of gravity, aft of the forward node and as close to the centre of percussion as possible. The body flexure characteristic varies with motor fuel mass; in fact the node positions and the frequency are likely to change considerably. Therefore the accelerometer must be positioned to allow for this variation. The variation of body bending frequencies also limits the effectiveness of notch filters which are sometimes added to filter out the body flexure modes.

Similarly the rate gyro must be positioned to sense body rates opposite to the instantaneous rates generated by fin forces. In Fig.12, the rate measured must be a pitch upward motion. This is achieved by any gyro position forward of the antinode which conveniently coincides with the acceptable accelerometer position, therefore allowing the instruments to be situated together.

This illustrates the care which must be taken when positioning instrumentation to avoid problems with body flexure. The positions depend on the type of instrument, ACS and the airframe control configuration used, i.e. tail, canard or moving wing control. Also the effect of higher order modes must be allowed for if necessary. The ACS design must still be able to cope with the resonances introduced by body flexure. In extreme cases, this can lead to a reduction in the bandwidth of the ACS or the control surface servo, with resultant loss in guidance performance.

The use of controls to provide active damping of body flexure is sometimes used in large missiles. Again, the prime object is to improve stability of the ACS rather than to give a higher system bandwidth or to reduce structural fatigue.

An allied problem to body flexure is the effect of fuel motion (fuel sloshing) encountered with liquid fuel missiles. This is the type of propulsion unit used in large, long range missiles. The main difference is that fuel sloshing frequencies are much lower than body flexure modes, and therefore much more difficult to attenuate. This problem can severely limit the ACS bandwidth and therefore considerable effort is usually invested in careful fuel tank design, i.e. addition of compartments etc. to reduce fuel sloshing effects.

6.3 Non-linearities

In order to study the effects of non-linearities, it is possible to use analytical techniques which are useful if only one non-linear element is present. If many non-linearities exist within a particular system, the most useful technique is to use simulation. Aerodynamic non-linearities do not normally pose problems except in extreme cases, e.g. controlling the turnover of a vertically launched missile where very

high incidences occur. The most common ACS non-linearities are servo rate and position limits and limits on the dynamic range of instruments.

Servo limits always exist and a cost-effective design invariably shows limits which are no greater than required. (Bang-bang servos are highly non-linear but in practice can usually be regarded as approximately equivalent to a conventional proportional servo with the respective rate and angle limits.) The rate limitation is inherent in the fact that the servo is designed to produce a certain torque which is capable of rotating the inertia of the control surface at a particular rate. Any increase in torque implies a larger servo, consuming more power which is not desirable. The effect of a rate limit is to slow the servo down when high rates of change are demanded. This in fact means that at higher rates, when the servo begins to saturate, the servo gives more phase lag than a linear version and results in a lower effective servo bandwidth. In the ACS this severely reduces the system stability unless measures are taken to ensure it cannot happen. In practice this comes back again to a reduction in the ACS bandwidth, although some compensation can be made by reducing the servo amplitude limit. This is illustrated in Fig.13 which shows how a servo with normally high bandwidth behaves as a result of rate limits and a position limit of two different values. In the first case with a high amplitude limit, the phase lag is relatively large. When the position limit is decreased, the effect of the rate limit is noticeably reduced. For this reason, servo position limits are always made as low as possible. This also serves to emphasise the need for high aerodynamic gain and hence airframe neutral stability wherever possible.

The dynamic ranges of sensors are usually selected to make sure that the maximum ACS demands or disturbances (e.g. noise) can be dealt with adequately. Sensor accuracy (scale factor, biases etc.) are generally a function of the full scale and therefore it is necessary to keep the dynamic range as low as possible. The effect of rate gyro saturation in the case of the ACS of Fig.5 (rate plus acceleration feedback) is to reduce ACS stability. This is similar in principle to the servo rate limit. The ACS must therefore be carefully designed to ensure that the rate gyro is not subject to high levels of noise or body flexure components which may cause saturation. In practice, body flexure is more difficult to cope with than noise and it can lead to gyro scale factors being about twice the value one might expect, i.e. the levels of rates due to body flexure can be double the normal maximum manoeuvres. This situation is often brought on by the use of a bang-bang servo since the resultant control surface oscillations tend to stimulate the body-bending modes. However, this situation is acceptable provided the ACS remains stable in the presence of body flexure.

Reduction of accelerometer limits tends to compensate for the loss of stability due to rate gyro saturation. Thus it is essential to fix the accelerometer full scale at the lowest possible value without impairing the missile lateral acceleration capability such that guidance accuracy will suffer.

Im summary, the effects of non-linearities are generally to degrade stability. Compensation by reduction of servo position limit or accelerometer limit can be of some value but usually non-linearities have the end result of a lower ACS bandwidth to regain stability and hence an overall reduction in guidance accuracy.

7. UNMANNED AIRCRAFT

Unmanned aircraft (UMA) can be defined as an unmanned vehicle which is basically similar to an aircraft in layout. Such vehicles are generally of monowing configuration and often of low lateral acceleration capability or low speed. Many vehicles are loosely classed as UMA, for example, model aircraft target vehicles, remotely piloted vehicles (RPVs) and cruise missiles.

Airframe control systems for UMA are often very similar to those used in missiles. One difference is in the control of horizontal motion. With a monowing configuration, horizontal manoeuvre is achieved either by use of the rudder whilst keeping the wings level or by rolling the airframe using aileron control. Use of the rudder is very sluggish but often adequate for gentle turns, e.g. for mid-course navigation. This also has advantages if it is essential to keep the wings level, which may be the case if a radar altimeter is in use to give a height keeping ability. Banked turns using ailerons are capable of giving higher horizontal accelerations but some means of controlling height is necessary in order that the elevator angles are increased to compensate for the loss in vertical lift.

The same type of sensors as already described are likely to be used in UMA. However, considerable effort is presently being used in the development of new low-cost sensors for use in small UMA and RPV applications. For example, a low-cost laminar flow jet rate sensor is in the process of being developed by British Aerospace Dynamics Group (Ref.6). Novel techniques have been tested such as electrostatic sensors for attitude stabilisation in pitch and roll. Although these devices work quite well, they are unfortunately prone to noise and electrostatic potential inversions during certain weather conditions. The main difference between UMA and missiles is that the monowing configuration typical of UMA often calls for attitude stabilisation. This requires some form of low-cost attitude reference which is more reliable than electrostatic sensors. Such a device is not available at the present time.

The various flight modes used for UMA and RPVs can be summarised as follows:

(a) open loop airframe

(b) airframe control system in circuit

(c) automatic flight control

(d) guidance

If an ACS is used, it has to perform well for all the functions required. For example, the vehicle may be required to respond to pilot commands from a ground station; this may be in mode (b) with reversion to mode (a) in case of emergency or failure. It may also have some automatic flight control (avionics) in the form of height-lock and heading hold system or a beacon navigation device. The ACS may then finally be required to operate in a homing guidance system. The airframe and ACS requirements can consequently be very

complicated and likely to end in considerable compromise. Similarly the aerodynamic requirements of the airframe can also be of a varied nature. Generally, if an open loop airframe is likely to be used, the airframe must be given a satisfactory degree of stability to avoid problems of remote pilot control, particularly at launch or during landing. If the same airframe is to be used in a guidance or avionics system, then any performance limitations must be accepted. In practice, the effect of airframe stability is not very critical with the type of applications normally considered here, since the vehicles are mostly of low speed.

Avionics sensors constitute attitude gyros and magnetometers for heading-hold systems and barometric or radar altimeters for height lock or terrain-following systems. A typical magnetometer based heading-hold system is shown in Fig.14. This uses a phase advance shaping network to stabilise the control loop. It is worth noting that the heading-hold loop controls the vehicle rudder and not the ailerons. This is because the vehicle is roll stabilised for this application and the aircraft is limited to flat turns. This is in order to ensure no loss of sensitivity from the magnetometer; since the vehicle was to be flown in areas where the magnetic vector was some 70^{o} to the horizontal, no more than 20^{o} roll angle could be tolerated.

A typical height lock loop is shown in Fig.15. The height sensor is given some datum value which, in the case of a barometric sensor is a function of the prevailing meteorological conditions. The height lock loop is also stabilised using phase advance shaping although this may not be needed in some cases. It is worth noting that the ACS design for both height lock and heading-hold systems is usually required to be well damped. This is necessary in order to ensure the eventual avionics loops also end up with sufficient stability. A different approach to height lock is to employ aircraft principles and use the throttle to control height whilst controlling speed using the elevators with air speed indicator feedback. This technique works well but requires a reasonably good engine throttling capability with ample power. Similar techniques have been applied to RPV helicopters with successful results.

8. RESUME

This review of missile airframe control systems is necessarily limited, but hopefully it gives some insight into the control techniques and concepts applied to missiles and how they may relate to similar problems with manned aircraft. One must remember that, although techniques may be similar in manned aircraft, generally missile airframe control system design problems are on a smaller scale. This is because the usual constraints on size, complexity and mass give rise to necessarily similar and cheaper solutions. The guidance and overall system design problems really constitute the major areas of difficulty which are not really covered in any detail here. However, active control technology (ACT) has been used virtually exclusively in missile systems which is regarded as a classic application of ACT.

Currently, considerable interest is being expressed in the use of modern control principles in guided weapon systems control problems, e.g. optimal control, Kalman filtering, on-line identification and adaptive control, particularly in conjunction with digital techniques and especially in the case of guidance systems. As ACT in aircraft becomes more widely applied, the modern control approach may well find more applications in missile systems as well as in manned aircraft airframe control systems.

Missile systems are characterised by the need to maintain high performance and stability over a wide range of aerodynamic conditions often in the presence of large amplitudes of electronic noise. These problems would seem parallel to the use of active control technology for stability augmentation and ride comfort. Similarly, the application of control configured vehicle design expertise to weapons such as long range cruise missiles would seem quite appropriate. Perhaps the advent of active control technology in aircraft will see missile and aircraft techniques brought closer together in the future.

REFERENCES

1. P. Garnell and D.J. East — Guided Weapon Control Systems. Pergamon Press, 1977.

2. D.V. Stallard — Classical and Modern Guidance of Homing Interceptor Missiles. MIT Seminar, April 1968.

3. D.J. Frary — The Prediction of Autopilot Behaviour in the Presence of Roll Motion. BAC Report ST.5686, May 1971.

4. D.J. Frary — A Comparative Study of Autopilot Configurations for Anti-Aircraft Guided Missiles. The Hatfield Polytechnic, M.Sc. Project Report, November 1972.

5. F.R.J. Spearman — The Derivation and Use of Aerodynamic Transfer Functions of Airframes. Journal of the Royal Aeronautical Society, November 1955.

6. J.M. Franks — Summary of Development of the Laminar Flow Jet Rate Sensor for RPVs. BAe Dynamics Group Report ST.19690, January 1978.

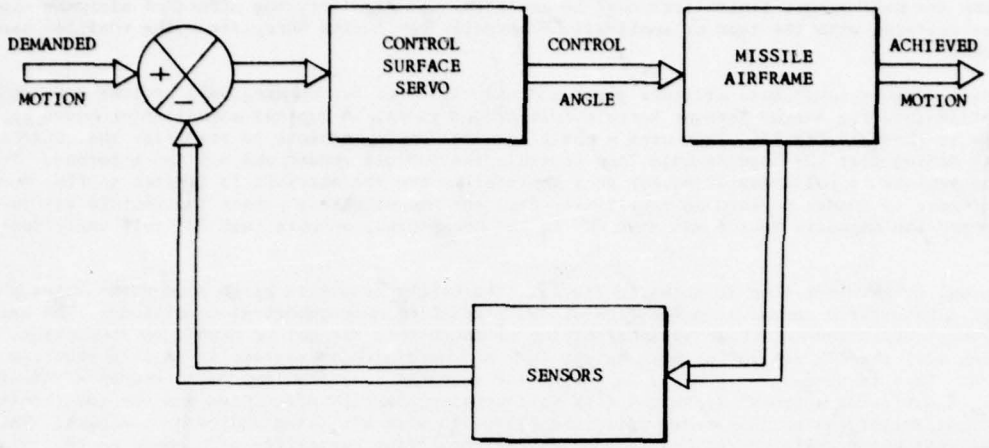

FIGURE 1. AIRFRAME CONTROL SYSTEM

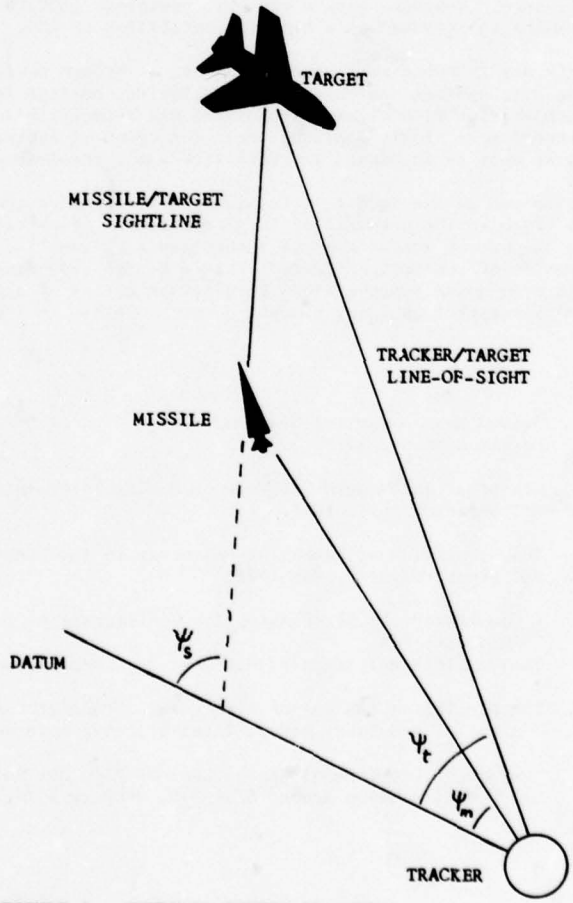

FIGURE 2. GUIDANCE SYSTEM GEOMETRY

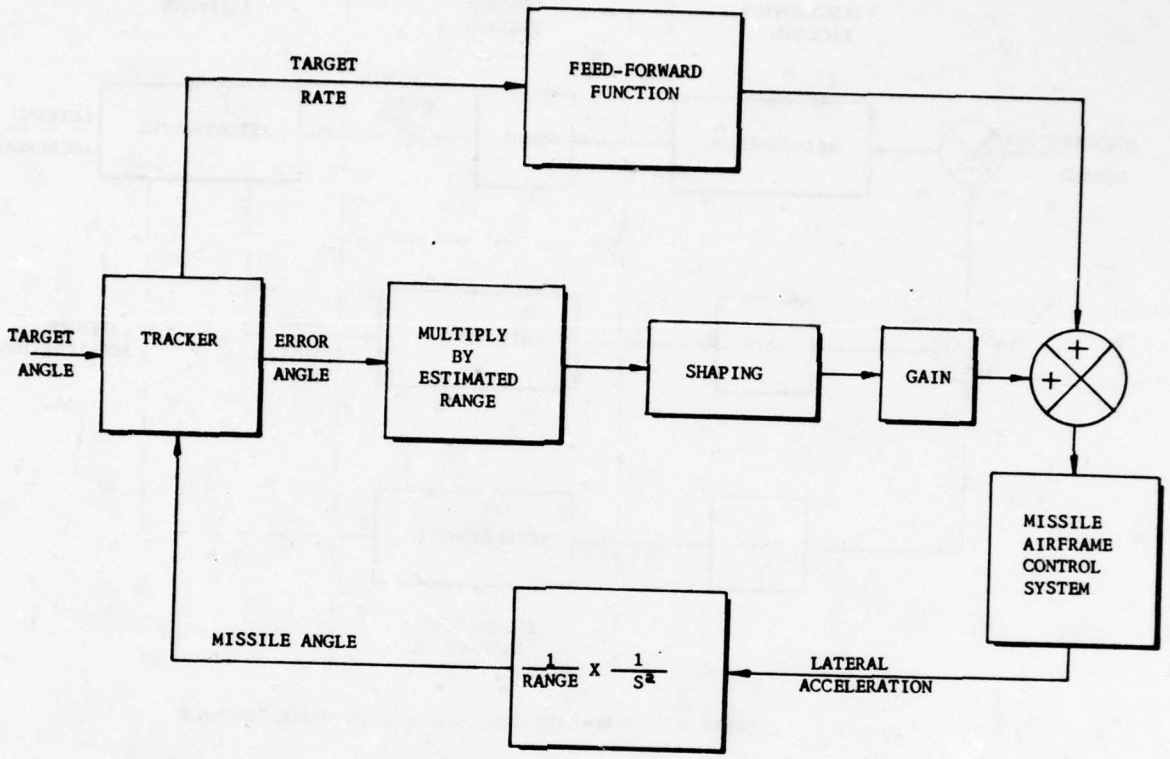

FIGURE 3. CLOS GUIDANCE LOOP

$$a_d = \lambda^* \dot{\psi}_s$$

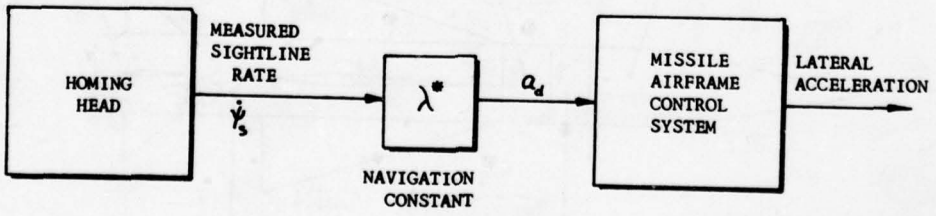

FIGURE 4. PROPORTIONAL NAVIGATION GUIDANCE SYSTEM

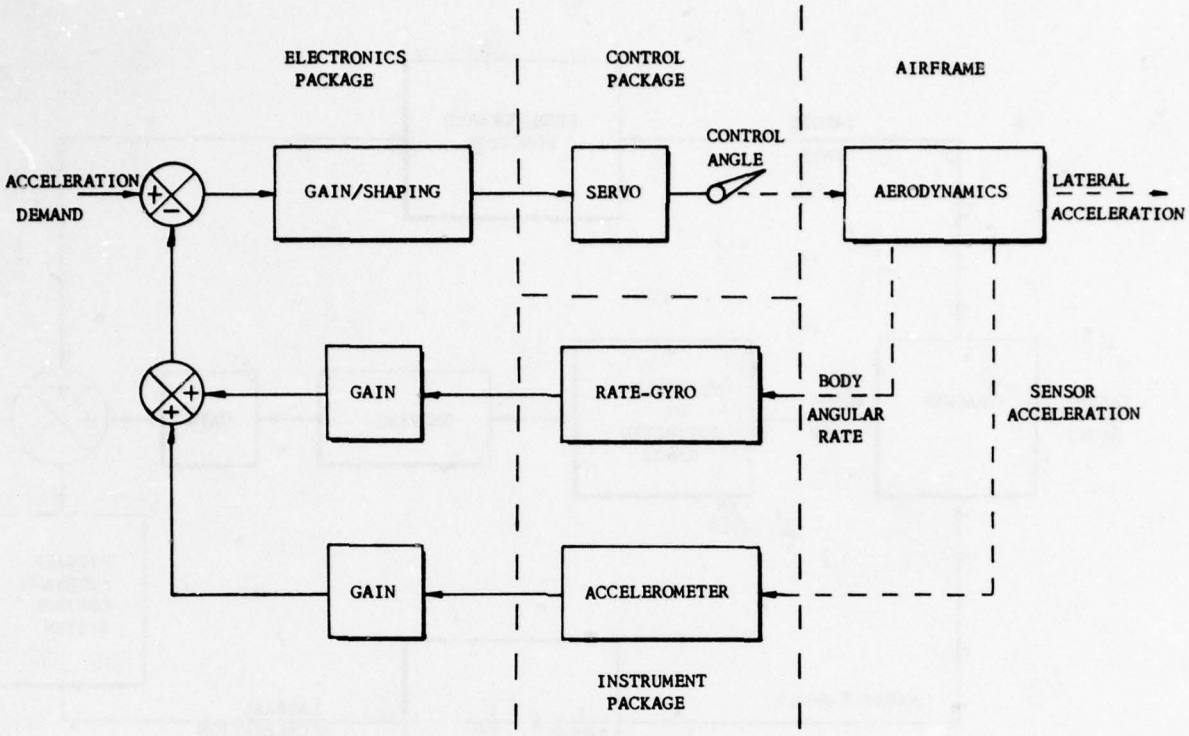

FIGURE 5. LATERAL ACS USING RATE GYRO AND ACCELEROMETER FEEDBACK

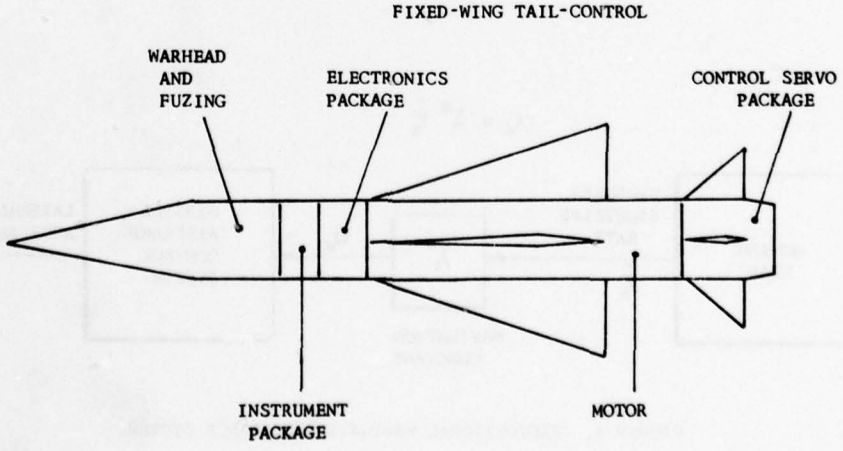

FIGURE 6. TYPICAL CLOS BODY LAYOUT

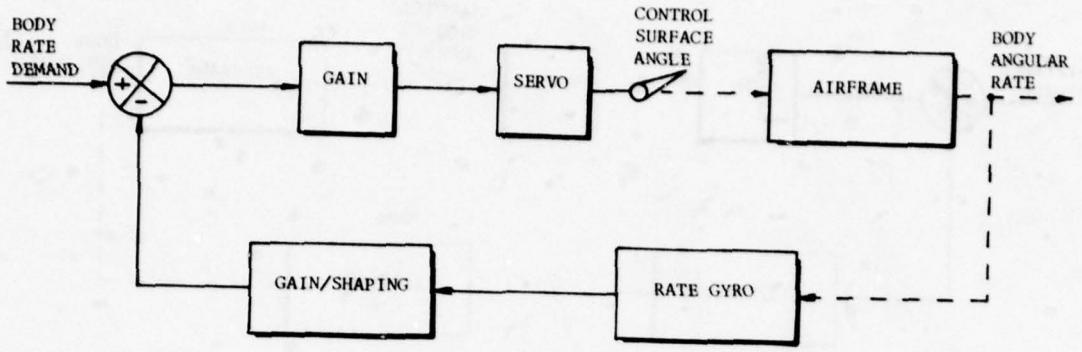

FIGURE 7. LATERAL ACS USING SINGLE RATE GYRO FEEDBACK

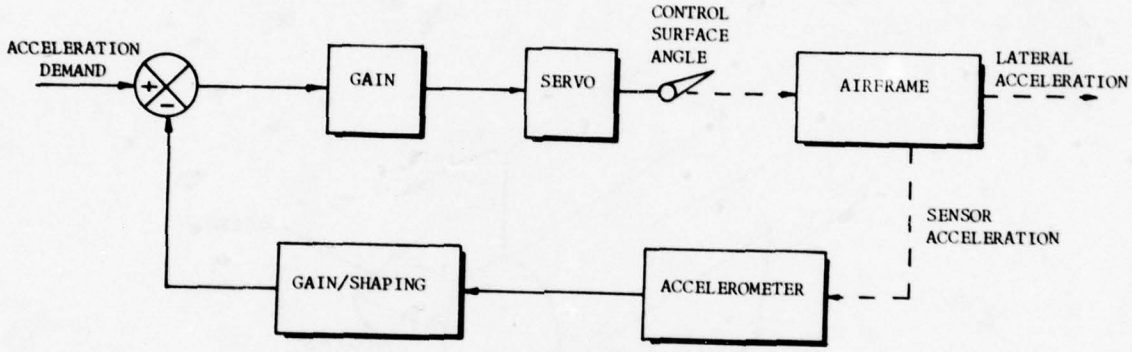

FIGURE 8. LATERAL ACS USING SINGLE ACCELEROMETER FEEDBACK

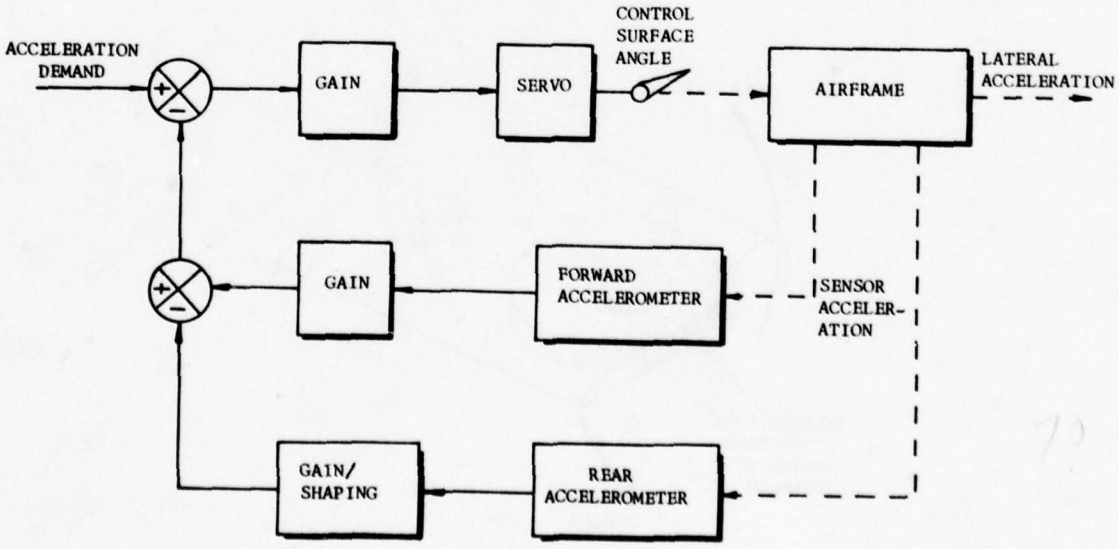

FIGURE 9. LATERAL ACS USING TWIN ACCELEROMETER FEEDBACK

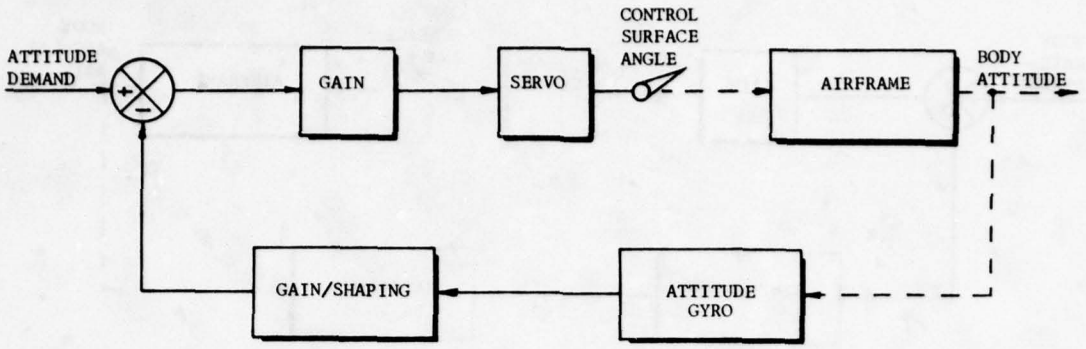

FIGURE 10. LATERAL ACS USING ATTITUDE GYRO FEEDBACK

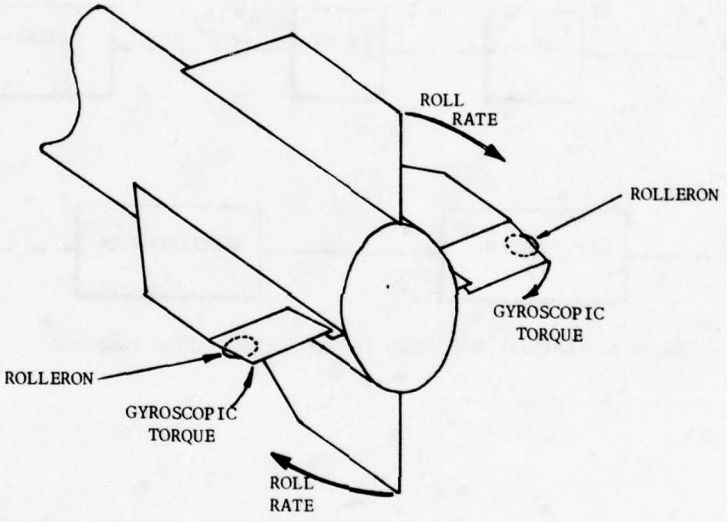

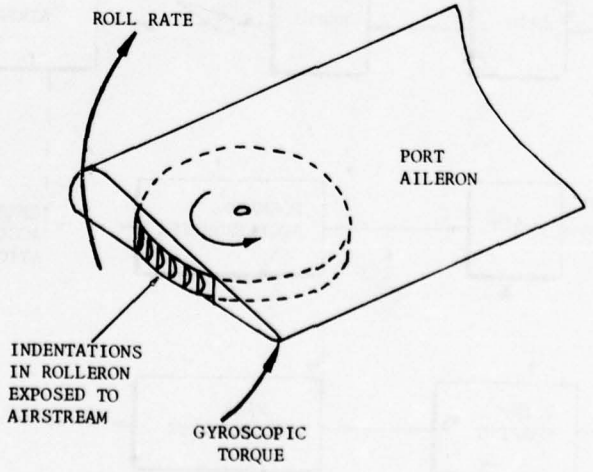

FIGURE 11. ROLLERONS USED FOR ROLL RATE CONTROL

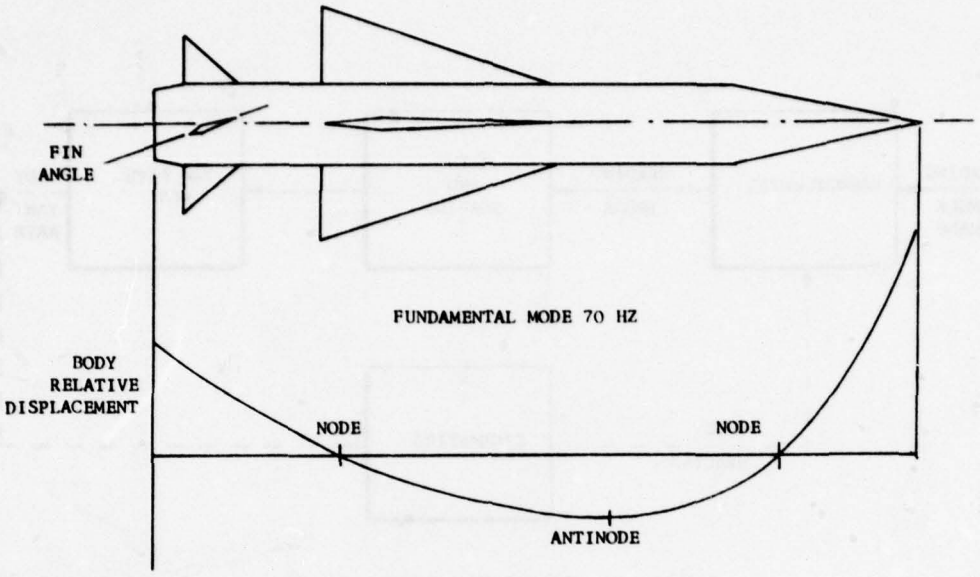

FIGURE 12. TYPICAL BODY FLEXURE MODE

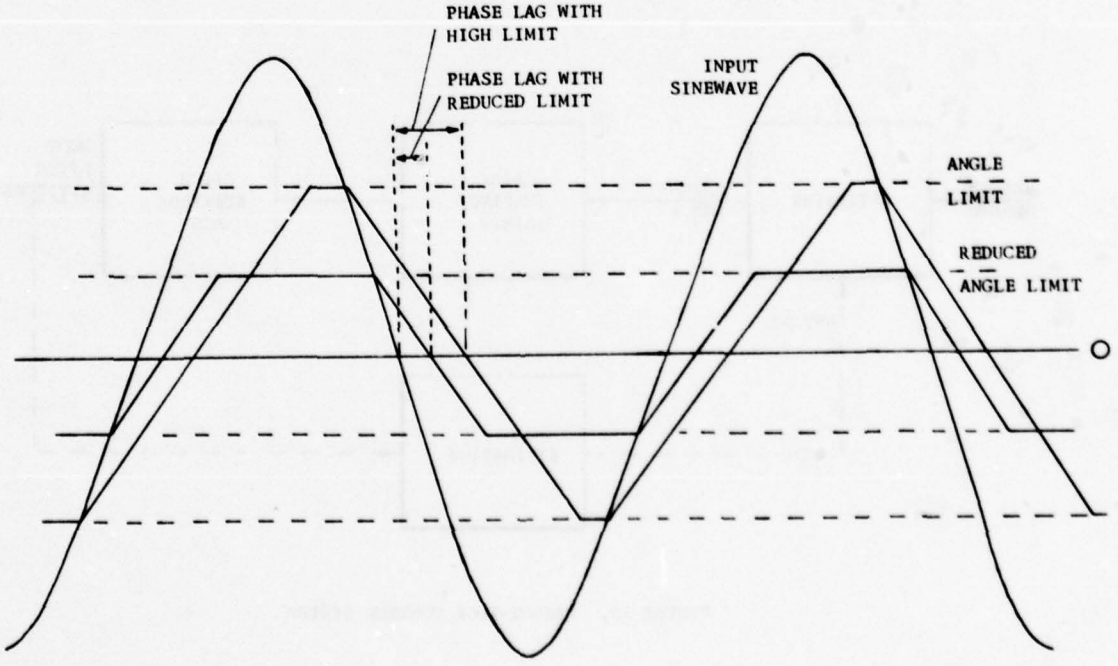

FIGURE 13. EFFECT OF SERVO RATE AND ANGLE LIMITS

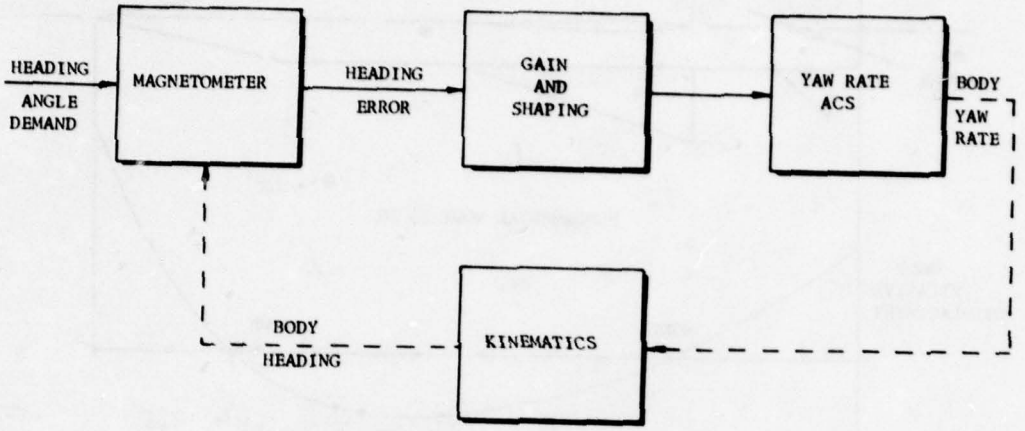

FIGURE 14. HEADING-HOLD CONTROL SYSTEM

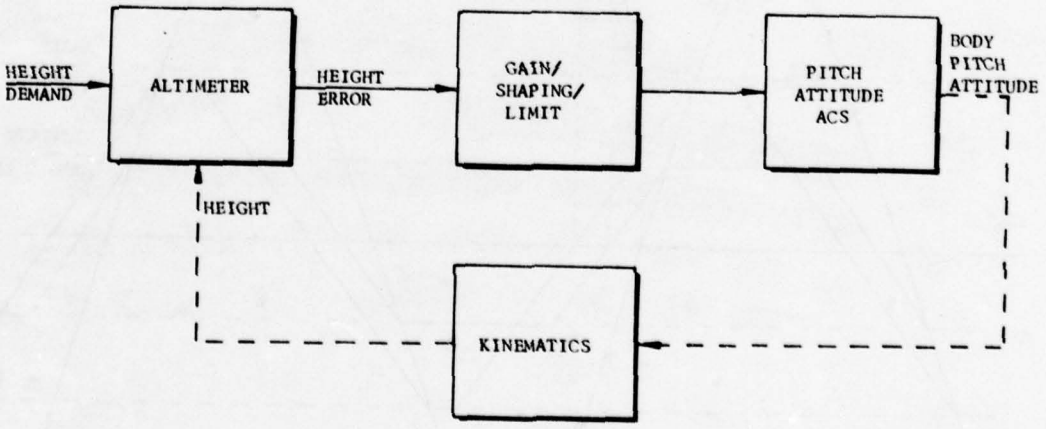

FIGURE 15. HEIGHT-LOCK CONTROL SYSTEM

ENHANCED FIGHTER MISSION EFFECTIVENESS BY USE OF INTEGRATED FLIGHT SYSTEMS

John H. Watson* and Willie S. Bennett II+
General Dynamics
Fort Worth Division
Fort Worth, Texas 76101

ABSTRACT

The performance of the modern fighter aircraft and its flight systems is truly fantastic. This performance has been increased in the last few years to the extent that it hardly seems possible to improve further. However, further improvement in effectiveness is possible through proper functional integration of the pilot, his crew station, and the flight systems. The extent of this possible improvement in effectiveness is significant. The improvement can be realized by the incorporation of advanced control modes, the integration of avionic systems and the flight control system, and the unification of all aircraft functions under the control of a flight management system. This results in a reduction in pilot workload and, at the same time, an increase in mission effectiveness. The ability of the pilot to change all pertinent system characteristics with one switch action relieves him of countless routine actions and provides him with mission-segment-tailored flight characteristics and displays. This system characteristic transforms the pilot from a system operator into a system manager and director. Optimization of the flight characteristics by mission segment eliminates the design compromises required in the past. The decoupling of a fighter aircraft attitude from its flight path vector makes it possible to maximize tracking time and reduce the control problem from a second-order to a first-order control task in both the pitch and yaw axes. A director fire control system used in conjunction with a coupler to the flight control system can greatly improve the target tracking and weapon delivery capability of the fighter aircraft with an accompanying reduction in pilot workload over that demonstrated for manual control.

1. INTRODUCTION

The judicious coupling of certain flight systems can result in significant benefit in terms of fighter mission effectiveness. As fighter aircraft performance has increased in the past three decades, the list and complexity of vital systems needed to support this increased performance has grown considerably. These systems fall naturally into two categories. The first category, support systems, will not be discussed in this paper. The second category, direct mission-related systems, will be alluded to only briefly. The main topic of this paper is the effective integration of the flight systems within the overall aircraft system design. The list of flight systems is exhaustive; however, those discussed in this paper have a direct bearing on particular disciplines, as depicted in Figure 1. Some of the mature flight systems to be discussed, along with their

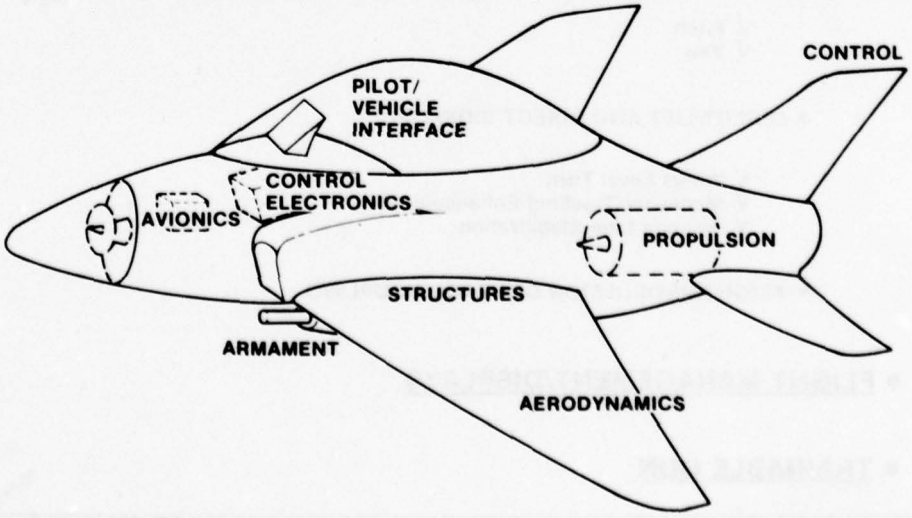

Figure 1 INTEGRATED FLIGHT SYSTEMS FOR ENHANCEMENT OF FIGHTER MISSION EFFECTIVENESS

* Digital Flight Control System Program Manager
\+ Engineering Specialist

benefits, are illustrated in Figure 2. Near-mature technologies that are candidates for incorporation in advanced aircraft design are listed in Figure 3. The complexity of each system has grown to the point where the conventional design team is extended to its limits to achieve individual system objectives. Each system requires specialists to solve the growing problems, and these specialists are organized by technology departments. Thus, a void exists between the technologies because of communication gaps and undefined areas of responsibility. The elimination of these technology gaps is the essence of effective flight systems integration, as illustrated in Figure 4. The trend in fighter aircraft size, weight, and cost was on the increase through the early 1970s. The key to reversal of this trend has been effective integration of flight systems into the overall fighter aircraft system design as illustrated in Figure 5. More can be done, however.

MATURE FLIGHT SYSTEM TECHNOLOGIES	
• STABILITY & CONTROL AUGMENTATION	• RELAXED STATIC STABILITY
• FLY-BY-WIRE FLIGHT CONTROL – SIDE STICK CONTROLLER	• GUST ALLEVIATION
BENEFITS	
• EXCELLENT WEAPON DELIVERY MISSION EFFECTIVENESS	• REDUCED DRAG DURING CRUISE AND MANEUVERING FLIGHT
• EXCELLENT HANDLING/TRACKING	• SUSTAINED G'S AND MISSION DURATION/RANGE

Figure 2 MATURE FLIGHT SYSTEMS

- **SIX DEGREES-OF-FREEDOM AIRCRAFT FLIGHT CONTROL**
  - FUSELAGE POINTING
    - √ Pitch
    - √ Yaw
  - DIRECT LIFT AND DIRECT SIDEFORCE
    - √ Wings Level Turn
    - √ Maneuver/Tracking Enhancement
    - √ Weapon Line Stabilization
  - FLIGHT/PROPULSION CONTROL COUPLING
- **FLIGHT MANAGEMENT/DISPLAYS**
- **TRAINABLE GUN**

Figure 3 NEAR-MATURE FLIGHT SYSTEMS

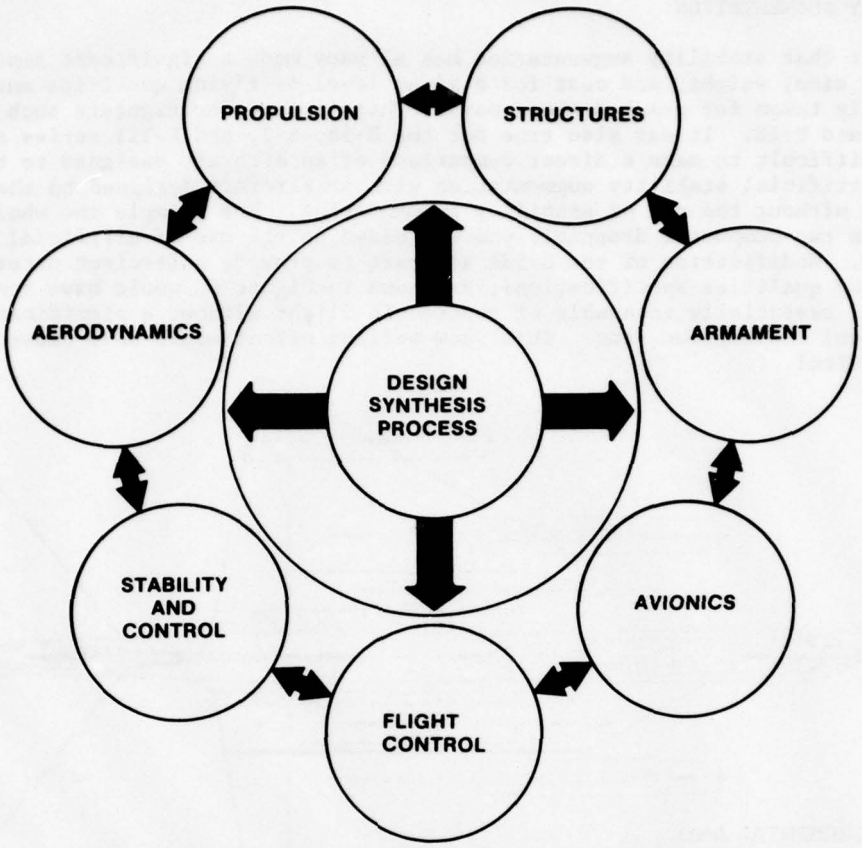

Figure 4 TECHNOLOGY DEVELOPMENT BETWEEN ENGINEERING DISCIPLINES – THE ESSENCE OF EFFECTIVE FLIGHT SYSTEMS INTEGRATION

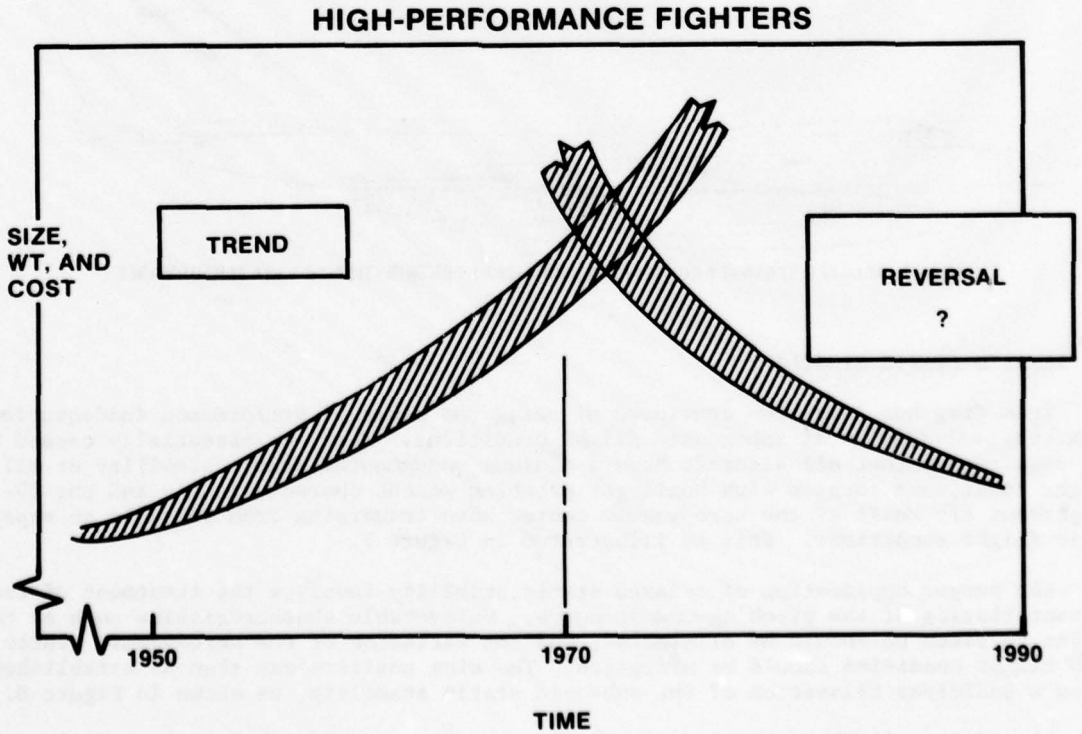

Figure 5 EFFECTIVE FLIGHT SYSTEMS INTEGRATION – THE KEY TO IMPROVED, HIGH-PERFORMANCE FIGHTER CONFIGURATION TRENDS

2. STABILITY AUGMENTATION

The fact that stability augmentation has already made a significant impact on reducing aircraft size, weight, and cost for a given level of flying qualities and performance is essentially taken for granted these days. This is true for fighters such as the F-14, F-15, F-16, and F-18. It was also true for the B-58, B-1, and F-111 series aircraft. It is very difficult to make a direct comparison of an aircraft designed to take full advantage of artificial stability augmentation with an aircraft designed to the same requirements except without the use of stability augmentation. For example the whole B-58A concept with its two-component droppable pod was based on the use of artificial stability augmentation. Modification of the B-58A aircraft to provide sufficient natural stability to meet flying qualities specifications, as shown in Figure 6, would have rendered the Mach-2 bomber essentially incapable of supersonic flight without a significant escalation of thrust, fuel consumption, etc. This snow-balling effect would have caused the design to be impractical.

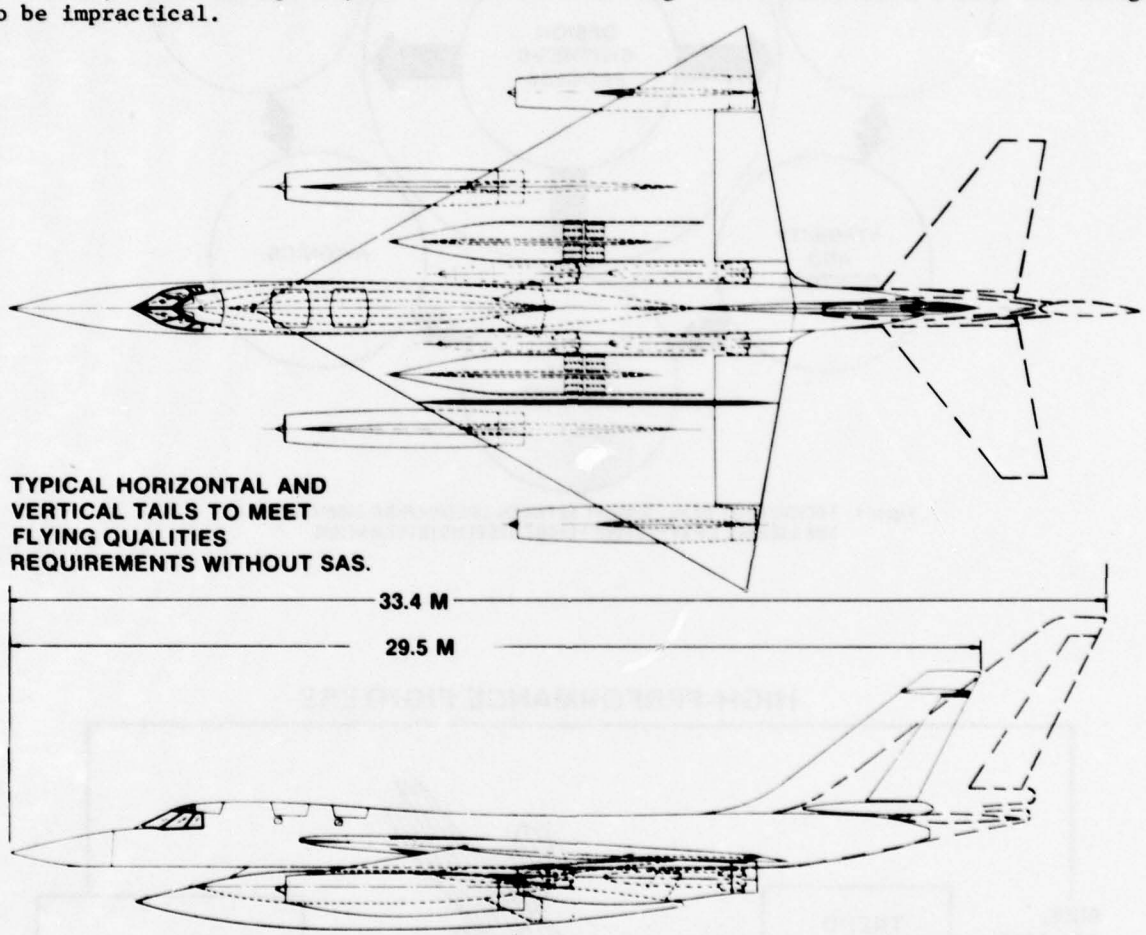

Figure 6 RELAXED STABILITY CONCEPT – A SIGNIFICANT CONTRIBUTION TO B-58A PERFORMANCE

3. RELAXED STATIC STABILITY

Trim drag has long been convicted of being the cause of performance inadequacies of fighters, especially at supersonic flight conditions. This was essentially caused by the requirement that all aircraft have a minimum unaugmented static stability at all flight conditions coupled with nonlinear pitching-moment characteristics and the 20- to 25-percent aft shift of the aerodynamic center when traversing from subsonic to supersonic flight conditions. This is illustrated in Figure 7.

The proper application of relaxed static stability involves the treatment of the characteristics of the pitching-moment curve. Unfavorable characteristics such as tendencies to pitch up should be eliminated, and the variation of the aerodynamic center with flight condition should be minimized. The wing position can then be established to allow a judicious relaxation of the subsonic static stability, as shown in Figure 8.

Closed-loop flight control system design can then provide the airplane flying qualities without paying the penalty of a statically stable design.

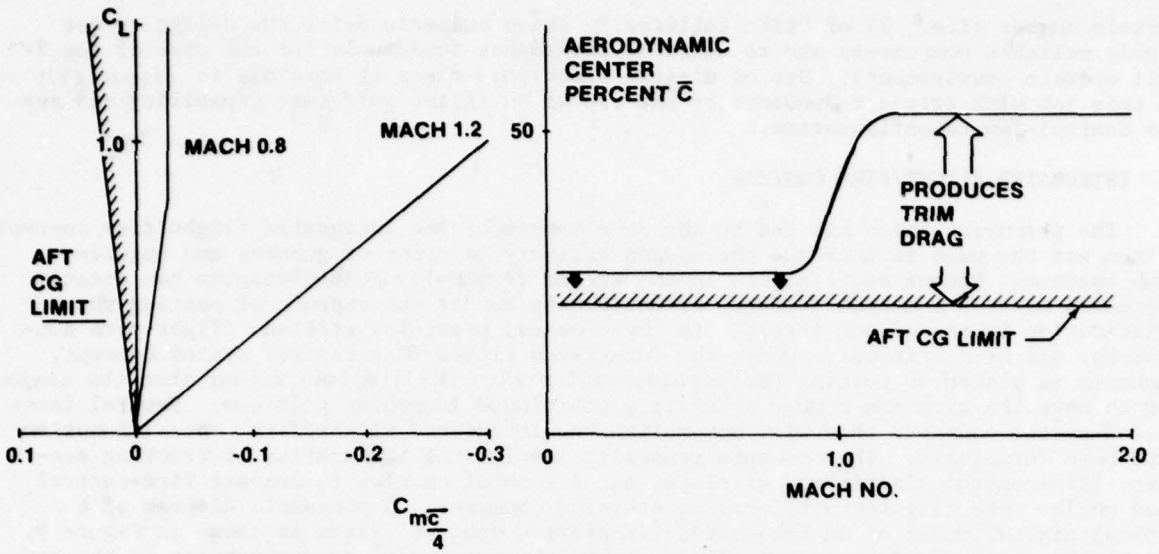

Figure 7 REPRESENTATIVE CONVENTIONAL STABILITY/TRIM DRAG RELATIONSHIP

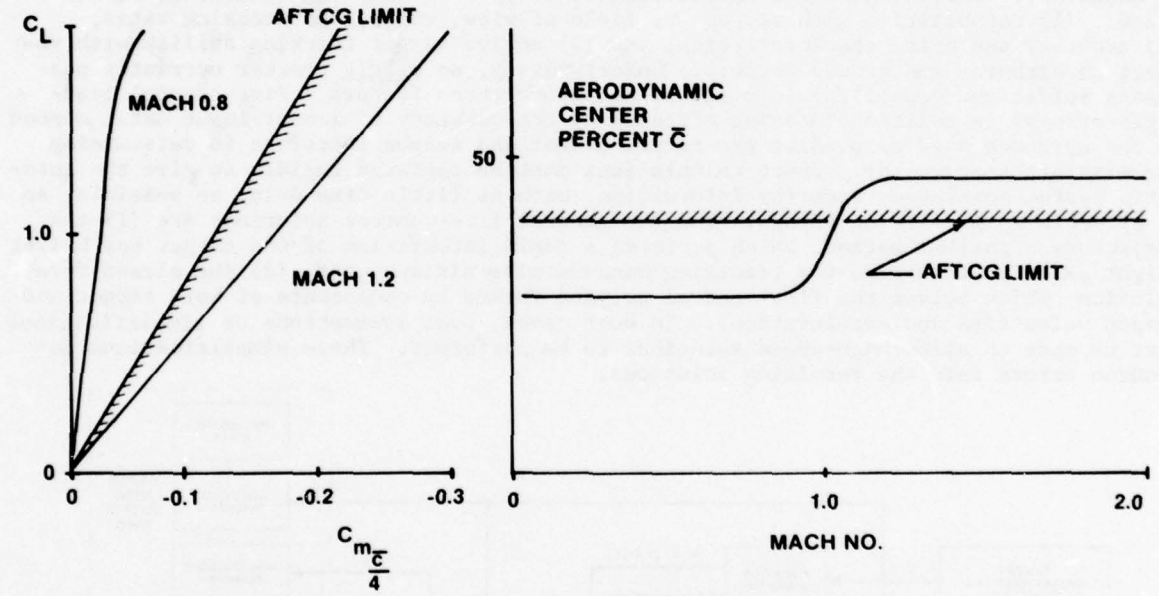

Figure 8 REPRESENTATIVE RELAXED STABILITY/TRIM DRAG RELATIONSHIP

4. FLY BY WIRE

A case for the use of fly-by-wire flight control can be made for a conventionally balanced airplane on the basis of volume, weight, and cost. A conservative designer may elect to stay with mechanical flight control, augmented to meet the more stringent flying qualities requirements. However, when the designer "bites the bullet" and incorporates relaxed static stability into his airplane configuration design, he has committed himself to providing stability augmentation at such a high reliability level that he might as well decide to go fly by wire from the beginning. Fly-by-wire flight control and relaxed static stability are natural considerations to be conducted concurrently in an integrated design effort. The level of reliability required for fly by wire and relaxed static stability drives the design to triple or quadruple redundant parallel systems with a suitable redundancy management scheme. A discussion of the various design considerations for a fly-by-wire flight control system is contained in Reference 1 (AIAA Paper No. 76-1915).

5. REDUNDANCY MANAGEMENT

Redundancy management is a logic scheme that votes, monitors, and switches electronic or mechanical signals to eliminate or minimize the effects of failures. The redundancy management scheme is established to meet certain reliability and failure criteria. The two most common criteria are (1) specification of the number of flying hours before a loss of control or mission abort and (2) specifications of operation after a

certain number (i.e., 2) of "like failures." These criteria drive the design to use highly reliable components and to multiple redundancy (quadruple for the case of the 2-fail operate requirement). Use of digital processors makes it possible to essentially do this job with triple redundancy by the use of an inline self-test capability and system control-law reconfiguration.

6. INTEGRATED FLIGHT/FIRE CONTROL

The precursor which has led to the development of the integrated flight/fire control system was the need to increase the weapon delivery accuracy of gunnery and unguided-bomb systems. Recent developments in the use of terminally guided weapons has greatly increased missile and bomb delivery effectiveness but at the expense of putting the sophistication in the weapon itself. In these cases, precision airplane flight-path control has not been critical. Under the integrated flight/fire control system concept, emphasis is placed on putting the sophistication into the airplane rather than the weapon and to make the airplane a more accurately positioned launching platform. Several integrated-system concepts that will accomplish the integrated flight/fire control function have been formulated. The concepts generally involve the integration of tracking sensors, fire-control algorithms, displays, and a form of coupler to convert fire-control lead angles into flight-control-system steering commands. A schematic diagram of a typical digital model of an integrated flight/fire control system is shown in Figure 9. The tracking sensor plays a most vital role in the successful accomplishment of the integrated flight/fire control function in that precise knowledge of the target location is mandatory. Three major factors determine the types of tracking systems to be utilized: (1) capabilities with respect to field of view, range, and tracking rates, (2) accuracy and noise characteristics, and (3) active target tracking ability with respect to airborne and ground targets. Unfortunately, no single tracker currently possesses sufficient capabilities in all of the above three factors. Fire-control lead-angle errors, in addition to being affected by the accuracy of sensor input data, depend on the approach used to predict the future target and weapon locations in determining the miss-distance vector. These calculations must be repeated rapidly to give the automatic system continuous steering information, with as little time delay as possible, so as to minimize prediction errors. The two general fire-control solutions are (1) the trajectory algorithm method, which performs a rapid integration of the target and bullet flight paths to determine the resulting minimum miss distance,and (2) the closed-form solution, which solves the fire-control polygon formed by components of both target and weapon velocities and accelerations. In both cases, some assumptions or simplifications must be made to allow high-speed solutions to be performed. These simplifications introduce errors into the resulting solutions.

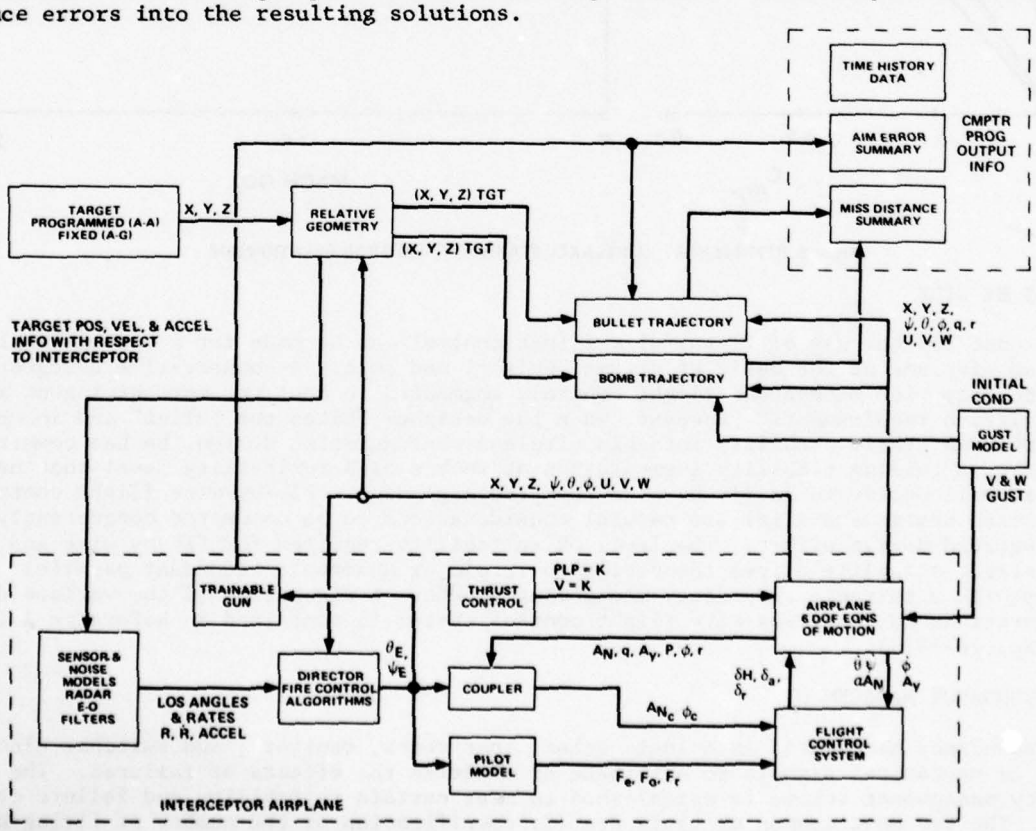

Figure 9 SCHEMATIC OF INTEGRATED FIRE/FLIGHT CONTROL DIGITAL MODEL

The fire-control-system output data is in terms of elevation and azimuth lead angles and lead-angle errors. The lead-angle data is utilized by the head-up display for pilot cueing and monitoring and by the automatic system, i.e., the flight-control coupler, to generate the airplane flight-control-system command inputs. Significant improvement in tracking-error response can be provided by automatic integrated flight/fire control (relative to manual operation), as shown in Figure 10. The dramatic improvement in tracking at small angles (where it is important) provided by automatic integrated flight/fire control is compared in Figure 11 to manual operation with a director solution and with a lead-computing optical sight. With the conventional flight control system, the basic logic of the coupler is to null the azimuth pointing error through positioning the attacker roll attitude and to null the elevation pointing error through rotation of the flight-path vector about the pitch axis. With advanced flight control configurations, additional control modes plus separate control of the airplane flight path and attitude become available to perform error removal by fuselage pointing and wings-level turns in addition to the conventional maneuvering. The use of independent gun pointing in lieu of or in addition to fuselage pointing is compatible with the integrated flight/fire control system. It should be noted that the coupler is the only new component required to implement the integrated flight/fire control concept, as illustrated in Figure 12. Additional discussion of the integrated flight/fire control concept is contained in Reference 2 (AIAA Paper No. 77-1078).

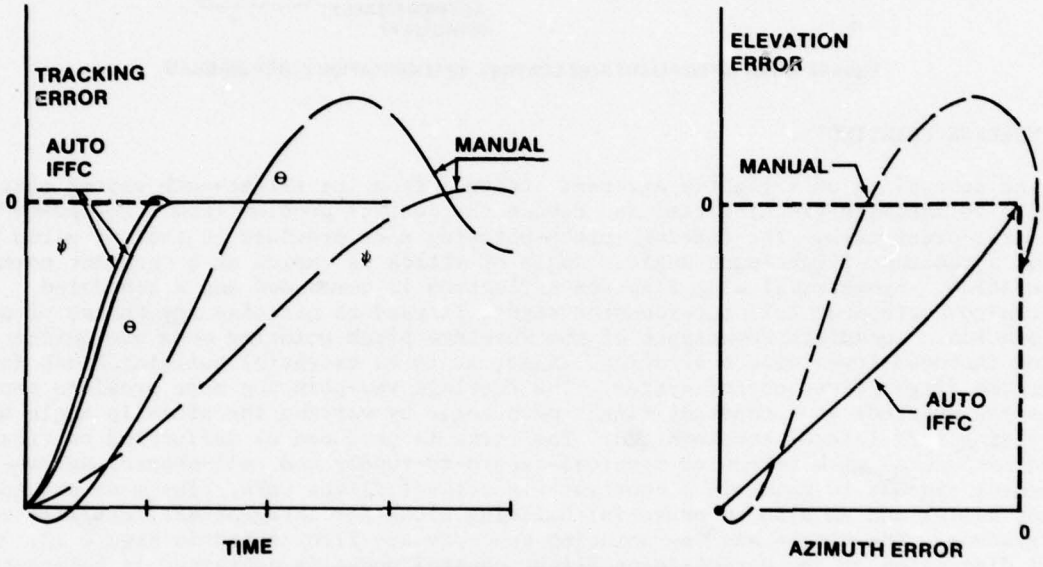

Figure 10 AUTOMATIC IFFC/MANUAL TRACKING ERROR COMPARISON

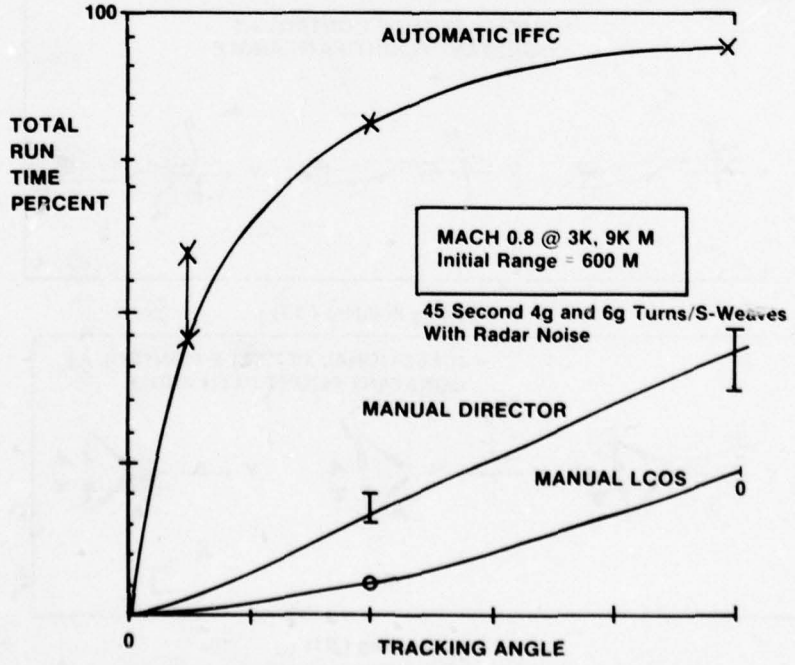

Figure 11 REPRESENTATIVE AUTOMATIC IFFC TRACKING EFFECTIVENESS

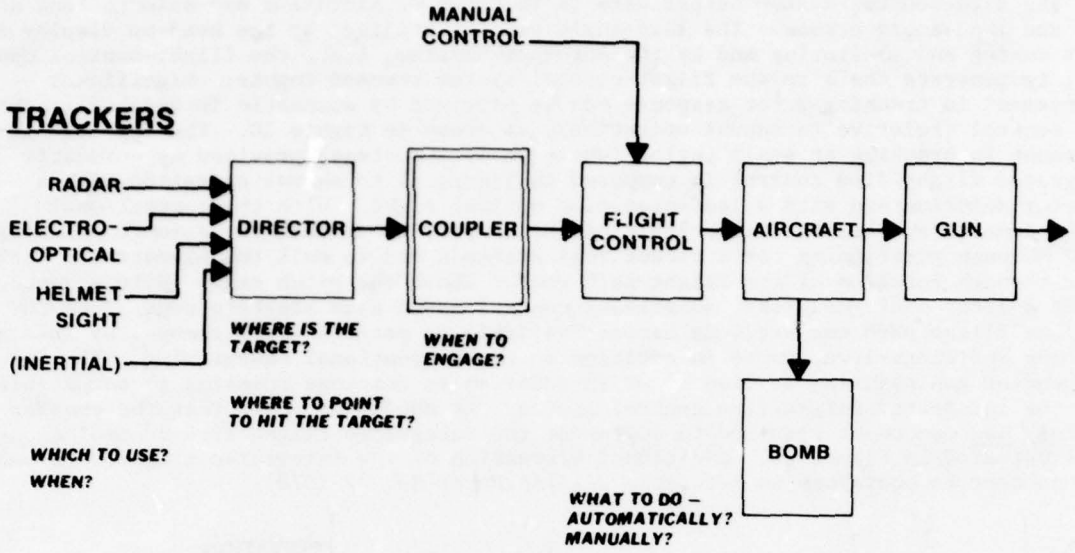

Figure 12 INTEGRATED FLIGHT/FIRE CONTROL IMPLEMENTATION BLOCK DIAGRAM

7. FUSELAGE POINTING

The decoupling of a fighter aircraft attitude from its flight-path vector makes it possible to maximize tracking time and reduce the control problem from a second-order to a first-order task. The fuselage pitch-pointing mode provides control of pitch attitude at a constant flight-path angle. Angle of attack is varied at a constant normal acceleration. Symmetrical wing-flaperon deflection is commanded and a scheduled flaperon-to-horizontal tail interconnect signal is used to minimize any change of normal acceleration. Immediate advantages of the fuselage pitch pointing mode are quicker aiming and improved low-altitude strafing. Also, it is an essential building block for the integrated flight/fire control system. The fuselage yaw-pointing mode provides control of the yaw attitude at a constant flight-path angle by varying the sideslip angle while maintaining zero lateral acceleration. The force is produced by deflecting vertical-canard surface(s) with scheduled vertical-canard-to-rudder and roll-control-surface interconnect signals to maintain a constant directional flight path. The mode provides quicker aiming and is also an essential building block for integrated flight/fire control systems. The pitch- and yaw-pointing concepts are illustrated in Figure 13. Additional discussion of the direct-force flight control modes is contained in Reference 3 (AIAA Paper No. 77-1119).

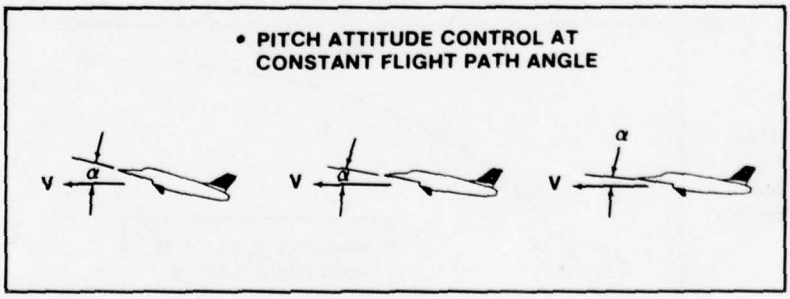

a. Pitching Pointing (α 1)

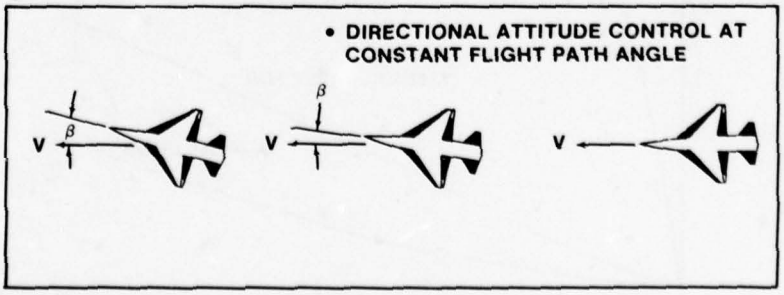

b. Yaw Pointing (β 1)

Figure 13 FUSELAGE POINTING

8. GUN POINTING

A gun that can be decoupled from the airframe and is capable of being directed by the fire control system appears intuitively to offer better accuracy and faster response. The lead-angle errors in the director fire control system are used to command the automatic gun control system to null the gun-pointing errors. The fire control outputs are also presented on the head-up display to cue the pilot for steering, or the commands can be routed through the flight control coupler, where they are converted to automatic flight control commands. Either of these two control loops serve as course steering controls while the fire control outputs are simultaneously fed to the gun control servo to minimize the residual error. The limits of gun authority in pitch and yaw need to be addressed from the standpoint of (1) airplane physical limitations and their resulting performance penalties and (2) a parametric effectiveness determination establishing the knee of the effectiveness-versus-gimbal-limits relationship. The increase in firing accuracy provided by automatic gun-pointing authority (with automatic IFFC and with manual flight path control) is illustrated in Figure 14 as a function of the gun gimbal limits. These data show that ±25- to ±50-milliradian gun gimbal limits are adequate for use with an automatic integrated flight/fire control system but that gun gimbal limits of ±100 milliradians would be warranted if this gimbal angle did not otherwise overly degrade airplane performance.

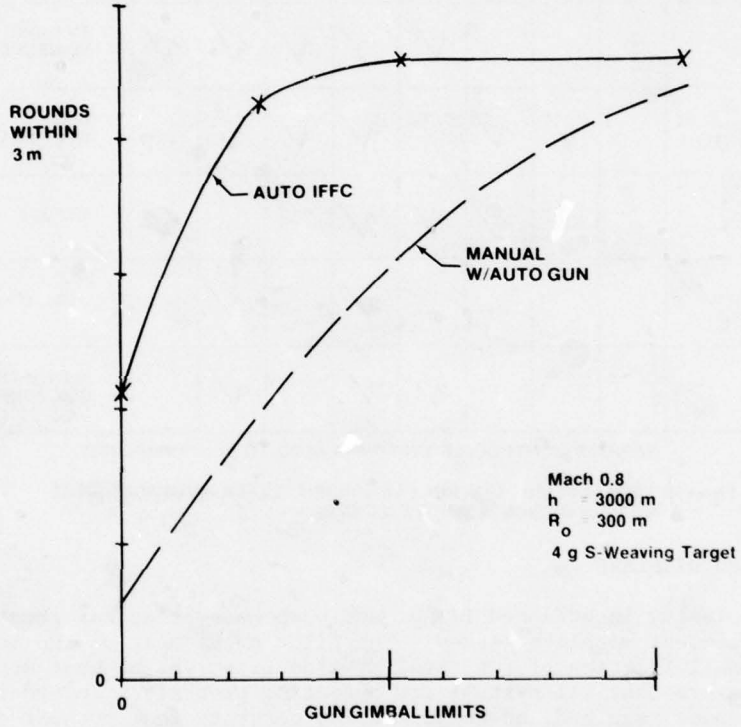

Figure 14 GUN POINTING FIRING ACCURACY COMPARISON

9. MISSION-TAILORED CONTROL

Up until now, the flight control laws and strategies for high-performance fighters have been essentially selected to provide the best overall flying qualities and tracking performance for the entire flight envelope and loading configurations of the airplane. This is usually limited to simple gain variations as a function of air data parameters such as static pressure and/or dynamic pressure. With the development of the direct-force flight-path flight control modes and the emerging availability of digital flight control computers, the effective use of mission-tailored control is imminent. In the development of this concept for particular airplane mission combinations, several operations must be conducted. First, the missions must be defined in detail. The various mission segments for which candidate control laws and/or strategies are to be considered must be identified. Typical mission-segment elements are (1) takeoff/climb, (2) cruise, (3) air-to-surface bomb, (4) air-to-surface gunnery, (5) air-to-air gunnery, (6) air-to-air missile, (7) refuel, and (8) approach/landing. Second, the candidate flight control laws must be identified and defined. Typical of these are (1) normal, (2) direct force, (3) maneuver enhancement, (4) translation, (5) fuselage pointing, and (6) gun pointing. Development of most of these control modes is further discussed in Reference 3 (AIAA Paper No. 77-1119) and Reference 4 (AGARD Paper 51, G/C 26, May 1978). The control strategies involve a determination of how the various control laws and controllers will

be implemented and integrated. This is done through analytical and pilot-in-the-loop simulations of the various combinations of control laws and strategies and mission segment elements, as shown in Figure 15. The candidate controllers must be selected, designed, and implemented in the pilot/vehicle interface cockpit simulator. An important consideration in the development of mission-tailored control is that every element must be found worthy of its cost. For example, are the increases in effectiveness of the fuselage pointing and/or gun pointing features over the basic integrated flight/fire control sufficient to warrant the cost of their incorporation? The answer to this question could well depend on the airplane's configuration/mission requirements.

MISSION SEGMENT ELEMENTS / FLIGHT CONTROL LAW	TAKE OFF/ CLIMB	CRUISE	REFUEL	AIR-TO-SURFACE BOMB	AIR-TO-SURFACE GUNNERY	AIR-TO-AIR MISSILE	AIR-TO-AIR GUNNERY	APPROACH/ LANDING	REMARKS
NORMAL	✓	✓						✓	BASELINE
DIRECT FORCE				✓	✓	✓	✓	✓	EVASIVE MANEUVERS
MANEUVER ENHANCEMENT		✓	✓		✓	✓	✓		GUST ALLEVIATION
DIRECT TRANSLATION			✓	✓	✓			✓	REFUEL
FUSELAGE POINTING					✓		✓		AUTO IFFC
GUN POINTING					✓		✓		AUTOMATIC GUN POINTING

VARIOUS CONTROLLER TYPES ARE ALSO TO BE CONSIDERED

Figure 15 TYPICAL FLIGHT CONTROL LAW CANDIDATES FOR INVESTIGATION AT VARIOUS MISSION SEGMENT ELEMENTS

10. MISSION-RELATED DISPLAYS

Increased complexity in advanced flight and weapons systems has greatly expanded the number of independent displays needed. The pilot needs most of the independent displays only for a small fraction of the total-mission time, yet he must monitor all of them in order to ensure that all systems are operating properly. In order to reduce the amount of display space required, advanced display concepts that present only the information required to perform each particular mission segment plus notification of any out-of-tolerance conditions are being developed. The pilot can then concentrate on mission-critical information. The mission-related displays provide the pilot with the vital information needed for integrated selection of the flight control mode, fire control mode, sensor mode, and weapons. Selections tailored to each mission segment are accomplished by a single switch action. Other functions are flight plan and fuel management, monitoring of sensors, check lists, and emergency procedures. The head-up display, containing all essential information needed for terminal combat encounters, is easily the most important fighter display. The fuselage pointing and/or gun pointing capability requires a large instantaneous field-of-view head-up display that is also useful in minimizing symbology clutter. The use of a high-acceleration cockpit seat further reduces the already limited available space for displays. Also, a significant requirement in the design of mission-related displays is the ability to see the displays while in a reclined position.

11. PILOT AIR-VEHICLE INTERFACE

Pilot/air-vehicle interface development is the key to successful integration and advanced flight systems. The performance of the pilot is becoming more critical as aircraft performance and system complexity continue to escalate. The pilot's work station must help him to overcome both physiological and functional limitations, as illustrated by Figure 16. Three cockpit considerations are essential to improve the pilots work

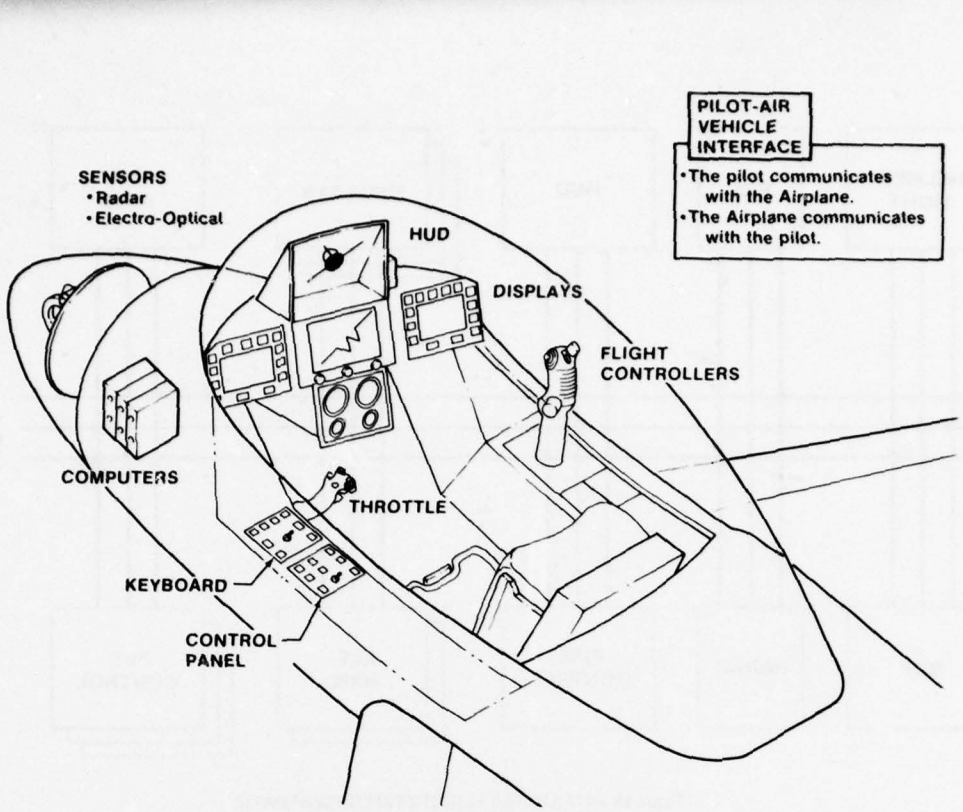

Figure 16 PILOT–CREW STATION INTERFACE

station, (1) increased g tolerance, (2) improved integrated displays, and (3) improved integrated controllers. Typical increased-g tolerance and improved integrated-display concepts are illustrated in Figure 17. To minimize pilot workload, he must interface with an integrated set of flight systems and controls. These flight systems are integrated through a redundant multiplex bus controlled by flight management computers, as illustrated in Figure 18.

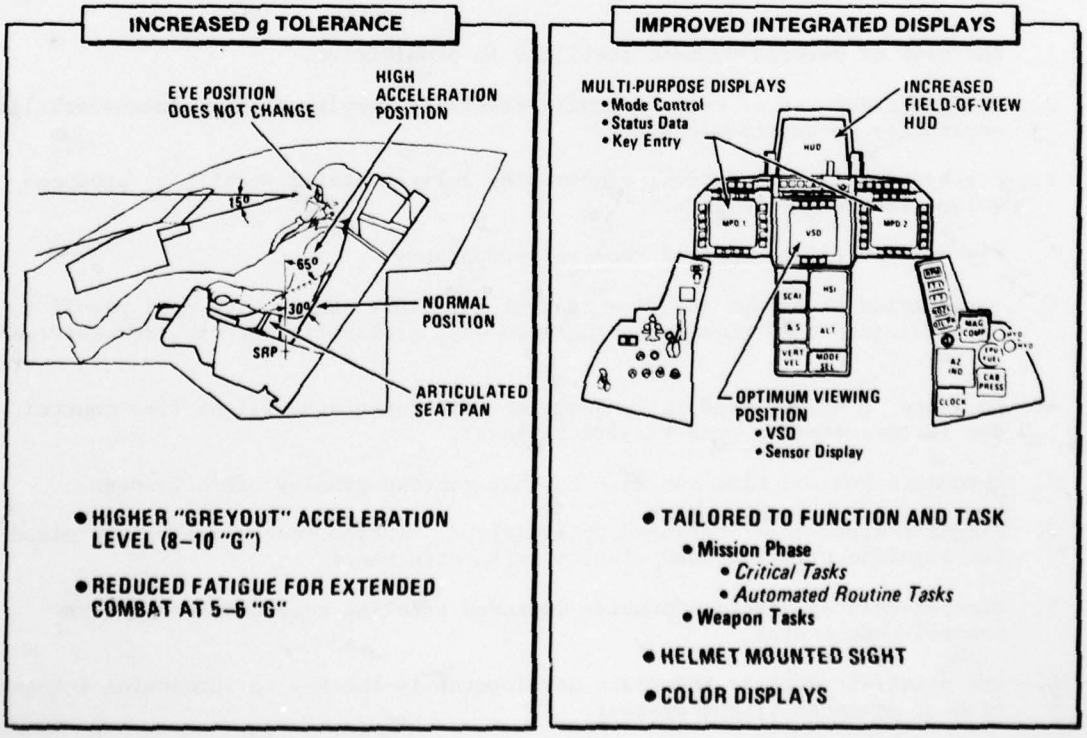

Figure 17 PILOT-AIR VEHICLE INTERFACE

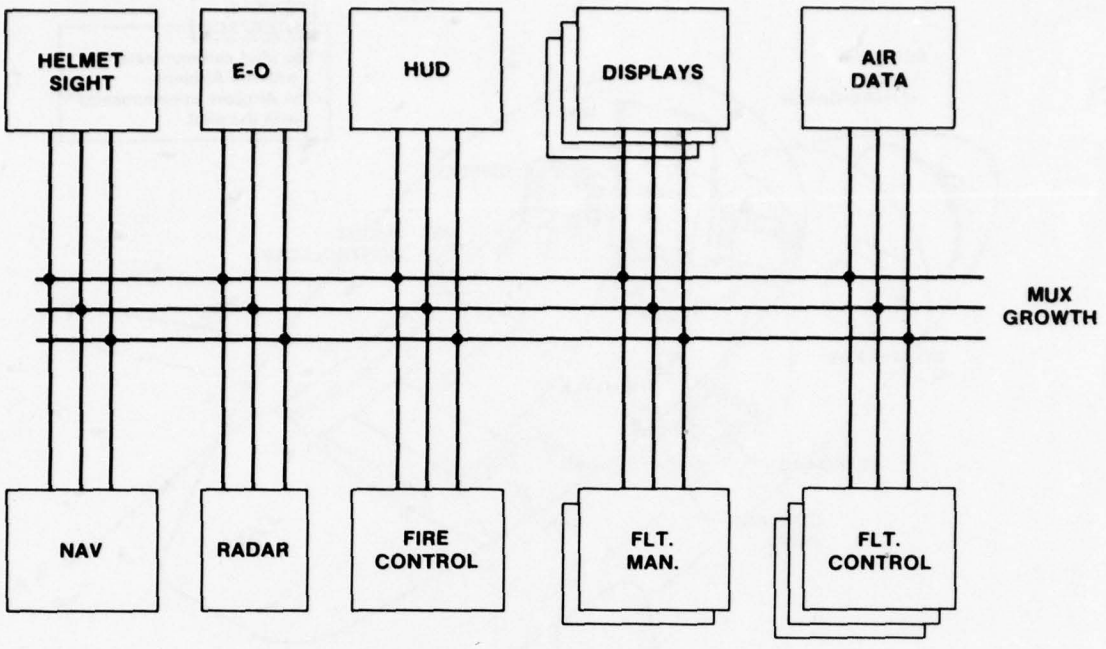

Figure 18 INTEGRATED FLIGHT SYSTEMS SCHEMATIC

12. CONCLUSIONS

Hard and fast conclusions are difficult to render on such an all-inclusive subject as "Enhanced Fighter Mission Effectiveness by Use of Integrated Flight Systems." This is because the extent of the truth of this statement depends on configuration and requirements, and the total task remains to be accomplished in its entirety. Yet, parts of the job have been done to such an extent that the judicious accomplishment of the overall design of a fighter aircraft using the concepts presented herein can lead to considerable improvement in mission effectiveness. Some of the pertinent conclusions the authors have come to believe are as follows:

1. The cost of natural dynamic stability is prohibitive.
2. The judicious use of relaxed static stability results in high maneuverability, especially at supersonic speeds.
3. Fly-by-wire flight control. required by relaxed static stability, produces volume and weight payoffs.
4. Fly-by-wire flight control requires redundancy.
5. Integration of flight and fire control functions can provide real payoff in target acquisition time, tracking accuracy, probability of hit, and survivability.
6. Fuselage pointing, used in conjunction with integrated flight/fire control, can further improve gunnery effectiveness.
7. Automatic gun pointing can also further improve gunnery effectiveness.
8. Flight control laws, tailored to individual mission tasks, can be optimized for significantly improved mission task performance.
9. Mission-related displays provide improved tracking cues and interactive control-mode status.
10. The pilot/air vehicle interface development is the key to successful integration of advanced flight systems.
11. The successful integration of multiple advanced flight systems depends on digital-computer computational power.

REFERENCES

1. Watson, John H., "Fly-by-Wire Flight Control System Design Considerations for the F-16 Fighter Aircraft," AIAA Paper 76-1915, Guidance and Control Conference, San Diego, Calif., August 1976.

2. Watson, John H., George J. Komechak, "Development of an Integrated Fire/Flight Control System for a High Performance Fighter Aircraft," AIAA Paper 77-1078, Guidance and Control Conference, Hollywood, Florida, August 1977.

3. Watson, John H., Jack D. McAllister, "Direct-Force Flight-Path Control - The New Way to Fly," AIAA Paper 77-1119, Atmospheric Flight Mechanics Conference, Hollywood, Florida, August 1977.

4. Ramage, James K., and Frank R. Swortzel, "Design Considerations for Implementing Mission-Tailored Flight Control Modes," presented at the 26th AGARD Guidance and Control Panel Symposium, Sandefjord, Norway, May 1978.

RESULTATS RELATIFS A L'EXPERIMENTATION SUR SIMULATEUR ET EN VOL D'UN SYSTEME DE COMMANDES DE VOL ELECTRIQUES GENERALISABLES

par

A. CAZENAVE et J. IRVOAS
S.N.I.Aérospatiale
316, route de Bayonne, TOULOUSE, FRANCE

RESUME

L'étude des performances d'un avion de transport à voilure élancée, dont le contrôle longitudinal est assuré par l'intermédiaire d'élevons, montre l'intérêt d'un recul du centre de gravité pour améliorer la finesse aux basses vitesses : le centrage optimal se situe au-delà de la limite arrière opérationnellement acceptable pour le pilotage avec des commandes de vol classiques.

Il a donc été développé, et expérimenté sur simulateur puis en vol sur l'avion T.S.S. CONCORDE n° 1, un système de commandes de vol électriques destinées à permettre le pilotage dans les conditions d'instabilité prononcées, au travers d'un minimanche. Nous décrirons la forme des lois de pilotage considérées, ainsi que les améliorations apportées à la suite de leur expérimentation sur simulateur. Les caractéristiques et les résultats obtenus en vol seront également présentés : ils seront comparés aux prévisions.

1 OBJECTIF

C'est en 1974 qu'à débuté sous contrat des Services Officiels français (D.G.A.C., Service Technique de l'Aéronautique et Centre d'Essais en Vol) l'étude d'un ensemble de commandes de vol électriques généralisables (C.D.V.E.), dont le but principal a été de définir un moyen permettant d'optimiser au point de vue performances et sécurité l'ensemble des systèmes de pilotage d'un avion.

Pour réaliser cet objectif, plusieurs actions ont été entreprises, avec comme aboutissement une expérimentation en vol sur un avion moderne :

-a- Concevoir des lois de pilotage permettant le vol à des centrages très arrières, inaccessibles avec des commandes classiques, et ayant des performances nettement supérieures.

-b- Miniaturiser les organes de pilotage.

-c- Etudier et réaliser un schéma général de commandes de vol à base de calculateurs numériques dont l'architecture et la technologie soient suffisamment élaborées pour être généralisables à d'autres domaines du contrôle actif généralisé.

CONCORDE a été choisi comme support de l'étude pour différentes raisons :

- pour ce type d'avion supersonique, il est très avantageux au point de vue performances, d'avoir un centrage très arrière par rapport au foyer aérodynamique, à basse vitesse. Il s'impose donc une aide au pilotage que peuvent fournir des commandes de vol électriques.

- Ce type d'avion possède un domaine de vol très étendu nécessitant une adaptation des aides au pilotage spécifique à chaque cas de vol. Cette adaptation est plus facilement réalisable avec des commandes de vol électriques.

- Enfin, le CONCORDE n° 1 était disponible pour des essais et disposait des équipements nécessaires pour une telle expérimentation (servocommandes, commandes de secours, transfert de carburant).

NOTA : On remarquera que CONCORDE possède déjà des commandes de vol électriques (voir Planche 1). La commande principale se compose de deux chaînes (bleue + verte) qui commandent électriquement les servocommandes. Une commande mécanique permet le pilotage dans le cas de panne des commandes électriques. L'autostabilisation n'est alors plus active. On voit donc que dans toutes les configurations, la gouverne reproduit la position du manche, d'où la difficulté de pilotage entraînée par le vol à des centrages très arrières.

2 HISTORIQUE

Les travaux se sont échelonnés sur un peu plus de quatre années comme l'indique le graphique ci-dessous :

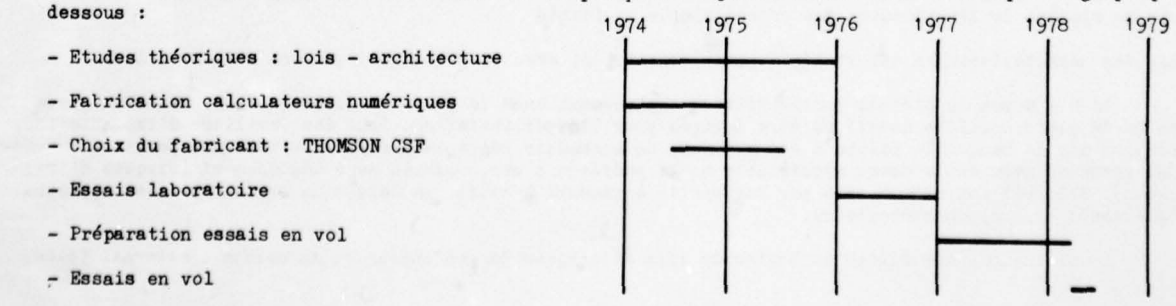

Jusqu'au choix des calculateurs numériques, les études ont été menées à la fois chez l'avionneur pour la définition des lois et chez les fabricants d'équipements pour la réalisation et la mise au point des calculateurs.

3 CONCEPTION GENERALE DE L'ENSEMBLE

L'ensemble commandes de vol tout électrique (C.D.V.E.) peut être envisagé sous deux aspects :

- aspect lois de pilotage
- aspect système.

Examinons successivement chacun d'eux.

3.1 Aspect lois de pilotage.

Axe de profondeur.

Un des buts principaux a été de faire voler l'avion aux centrages arrières. On a donc étudié essentiellement le pilotage en tangage.

La loi de pilotage adoptée est une loi à retours gyrométrique (q) et accélérométrique (Δnz) (voir planche 2). Le pilote commande un facteur de charge.

Un intégrateur dans la chaîne directe donne à cette loi un gain statique infini, ce qui permet d'obtenir par principe :

- des efforts par g constants dans tout le domaine de vol
- une insensibilité aux perturbations atmosphériques et aérodynamiques.

Des gains fonctions de la vitesse permettent d'obtenir des temps de réponse et des amortissements du mode courte période compatibles avec les objectifs fixés, en tout point du domaine de vol.

Pour satisfaire aux règlements, un retour en vitesse (V_c) fournit la stabilité statique, et masque les imperfections du système, telles que les hystérésis des détecteurs et les faux zéros.

Au "sol" l'intégrateur, le retour en Vc, et le retour en Δnz sont sans effet.

On a admis dès le début de l'étude, que le domaine des hautes incidences ne serait pas exploré. On n'a donc pas mis au point de système assurant la protection dans cette zone.

Axe de gauchissement.

On donne planche 3 les schémas de la loi adoptée en C.D.V.E. et la loi CONCORDE.

Par rapport à CONCORDE, les calculateurs et les vérins de sensation musculaire ainsi que le système de neutralisation des élevons externes, sont remplacés par des gains variables fonction de la vitesse et très facilement programmables dans les calculateurs numériques. Le minimanche est rappelé au zéro par une bielle à ressort. Ce principe de commande C.D.V.E. amène donc comme avantages :

- un gain de masse et une fiabilité plus grande,
- une possibilité d'homogénéisation des vitesses de roulis dans tout le domaine de vol, pour un même braquage du minimanche, donc pour le même effort, par ajustement des gains fonction de la vitesse.

3.2 Aspect système.

Il comprend :

- l'ensemble minimanche
- l'ensemble calculateurs numériques de C.D.V.E.

De telles commandes de vol tout électriques s'accomodent d'organes de pilotage miniaturisés. Pour cela un minimanche deux axes tangage et roulis a été développé à partir des objectifs suivants :

- permettre une accessibilité correcte aux planches de bord
- avoir un système de transmission des ordres simple et fiable
- avoir des caractéristiques effort-déplacement compatibles avec le pilotage d'un gros avion civil.

Il n'y a pas eu d'étude particulière d'emplacement dans le poste de pilotage, car, seule la place pilote ou la place copilote devait en être équipée pour l'expérimentation. Pour des facilités d'implantation, la fixation sur la banquette pilote a été retenue. Un accoudoir réglable permet au pilote une position correcte. Une commande avec déplacement appréciable a été préférée à une commande sans déplacement (risques d'imprécision). Elle est rappelée à zéro par une bielle à ressort à seuil. La détection se fait par des capteurs de déplacement type synchrodétecteurs.

Le minimanche est équipé du bouton de trim électrique de profondeur et du bouton d'alternat (planche 4).

NOTA : Une minicommande 3 axes tangage-roulis-lacet n'a pas été envisagée pour cette expérimentation. Sa mise au point fera l'objet d'une étude ultérieure.

Restait à définir la complexité du système reliant l'organe de pilotage aux gouvernes. Pour cela, un exemple de schéma complet certifiable a été étudié. On en donne planche 5 le principe :

- 3 calculateurs numériques surveillés attaquent électriquement les servocommandes,

- 1 calculateur de secours, soit numérique, soit analogique, entraîne un servomoteur relié mécaniquement à l'entrée des servocommandes

La solution expérimentale retenue pour notre étude est représentée en traits pleins.

Le minimanche fournit les ordres de profondeur et de gauchissement à deux calculateurs numériques qui élaborent les braquages des gouvernes. Un boitier de changement de gains permet de faire varier aisément les gains et constantes de temps des lois.

Une surveillance très efficace de l'ensemble a été établie de telle sorte que tout défaut détecté fait déconnecter les calculateurs. Elle s'exerce sur la validité des signaux d'entrée des calculateurs, sur les calculateurs eux-mêmes, sur la validité des signaux de sortie et sur la partie puissance de la chaîne de commande.

Une surveillance supplémentaire (boitier de protection) de la réaction de l'avion a été adoptée, par détection d'une vitesse limite de roulis ou d'une combinaison limite de vitesse de tangage et de facteur de charge.

Les calculateurs utilisés sont des THOMSON CSF "Comvol", dont les caractéristiques principales sont données planche 6. Leur choix a été déterminé principalement pour leur programmation très facile et pour leur autosurveillance très efficace.

3.3 Avantages qu'apporterait le système C.D.V.E. sur un Supersonique type-Concorde.

Outre les intérêts de pilotabilité et d'aménagement du poste que nous venons de voir, l'application du système général de C.D.V.E. à un Concorde entraînerait les avantages essentiels suivants :

- gain de performance au décollage. En effet, la possibilité de décoller à des centrages très arrières (abstraction faite de la position du train d'atterrissage) apporterait un gain de finesse appréciable par diminution de la traînée dûe aux braquages des gouvernes (voir planche 7)

- gain de masse et de complexité par suppression des commandes mécaniques, des servomoteurs de trim, des vérins de sensation musculaire

- gain de fiabilité et de maintenance par intégration de différentes fonctions avec possibilité d'extension à d'autres domaines du contrôle actif.

Pour informations, sur Concorde, le gain de masse dû aux équipements peut être évalué environ à 500 kg.

4 IMPLANTATION DE L'ENSEMBLE C.D.V.E. SUR CONCORDE

Le schéma d'implantation de l'ensemble de commandes de vol sur Concorde est donné planche 8.

La commande des élevons de Concorde se compose de deux voies parallèles et indépendantes : Une chaîne de commande bleue et une chaîne de commande verte. En cas de panne de la voie bleue, qui est la commande normale, une commutation automatique active la chaîne verte.

Pour l'expérimentation en vol on a remplacé la voie bleue par le système C.D.V.E. La commande électrique verte non modifiée constitue donc une chaîne de secours utilisable en place copilote.

Les ordres élaborés par cette chaîne sont en permanence synchronisés sur ceux de la chaîne principale. Elle doit permettre le pilotage de l'avion dans tout le domaine de vol exploré lors de l'expérimentation.

De même, la commande mécanique de secours de Concorde est utilisable en place copilote. Les ordres élaborés par cette chaîne sont en permanence synchronisés sur ceux de la chaîne principale.

Le contrôle de la gouverne de direction est assuré par les commandes de vol Concorde.

La commutation commande C.D.V.E. - commande verte se fait soit volontairement par un bouton situé sur le manche copilote, soit automatiquement à la suite d'une panne de calculateur. La planche 9 donne une vue du poste de pilotage modifié.

5 MISE AU POINT DE L'ENSEMBLE C.D.V.E. SUR SIMULATEUR

5.1 Installation d'essais disponible.

Les essais de mise au point au laboratoire des commandes de vol tout électriques ont rendu nécessaires l'étude et la réalisation de divers moyens d'essais :

- une cabine de pilotage Concorde équipée d'une instrumentation et d'organes de pilotage représentatifs de ceux de la solution expérimentale,

- une visualisation

- une simulation de l'avion sur calculateur numérique

- une simulation analogique des commandes de vol pouvant être remplacée par les éléments réels du banc général de commandes de vol

- un banc d'essais partiels des calculateurs numériques de C.D.V.E. et de leurs équipements associés

- un ensemble pour la réalisation des programmes, leur mise au point et leur contrôle, qui a été développé et amélioré dans le but essentiel d'augmenter la rapidité et la sûreté de la programmation.

Cette installation d'essais (voir planche 10) a été conçue de façon à apporter le plus de souplesse possible dans son utilisation, en particulier au niveau du banc d'essai partiel des calculateurs numériques C.D.V.E. Il a été possible en effet d'étudier le fonctionnement d'un calculateur soit seul, soit couplé à d'autres équipements (capteurs, deuxième calculateur, boîtier de changement de gain), soit intégré dans les chaînes de commandes de vol Concorde réelles ou simulées.

5.2 Mise au point sur simulateur.

Vu le peu d'heures de vol envisagées pour cette expérimentation, beaucoup d'importance a été donnée à l'étude sur simulateur.

L'expérience Concorde a permis de montrer qu'il était très bien représentatif de l'avion, ce qui nous a incités à l'utiliser au maximum pour faire une mise au point très poussée des lois de pilotage et du système complet.

Les premiers essais entrepris ont porté sur le choix d'une loi de pilotage en profondeur. Le domaine d'étude a été celui de Concorde avec une plage de centrages arrières nettement reculée, notamment à basses vitesses (de l'ordre de 2,5 % de la corde centrale de l'aile, en approche).

Plusieurs lois ont été envisagées comportant toutes un intégrateur dans la chaîne directe, mais donnant au pilote la possibilité de piloter soit une vitesse de tangage (retour purement gyrométrique), soit un facteur de charge associé à une vitesse de tangage (loi C*). La simulation dans cette première phase s'est faite analogiquement. Le choix des pilotes s'est porté sur le dernier type de loi, dont la description est donnée au § 3.1.

En effet, à basses vitesses, le temps de réponse de l'avion à une sollicitation minimanche et l'amortissement du mode courte période ont semblé plus compatibles avec les exigences d'un gros avion civil tel que Concorde.

La deuxième phase d'essais de cette loi de pilotage a été menée avec les calculateurs numériques et les équipements réels. Elle a surtout porté sur l'optimisation des gains de stabilisation dans la zone des basses vitesses, et sur l'adaptation du trim électrique et du retour de stabilité statique.

Au point de vue logique de fonctionnement ce sont surtout les phases décollage-atterrissage-remise des gaz qui ont nécessité le plus d'essais.

Une trentaine de vols avec plusieurs pilotes ont permis de figer une loi de profondeur et une loi de gauchissement associées à une logique de fonctionnement, qui ont été programmées pour les essais en vol.

Parallèlement à l'étude des lois de pilotage, les pilotes ont effectué la mise au point du minimanche. En effet, celui-ci a été disponible dès le début des essais sur simulateur et amélioré surtout pendant la phase de simulation analogique.

Les objectifs principaux ont été d'obtenir une très bonne homogénéité en effort sur les deux axes, avec un minimum de couplages, notamment pour les grands débattements. On a veillé en plus à assurer une bonne protection en effort pour éviter les facteurs de charge excessifs sans compromettre le confort de pilotage, et à avoir des efforts par g bien adaptés, et des vitesses de roulis homogènes pour un effort donné, dans tout le domaine de vol.

Le meilleur compromis a été obtenu en jouant sur les parties mécaniques (bielles à ressort - débattement) et sur la partie électronique par introduction de gains variables. La planche 2 donne la loi d'effort-déplacement obtenue sur l'axe de profondeur ainsi que la courbe d'efforts/g.

L'étude sur simulateur s'est poursuivie par la mise au point du système complet tel que monté sur avion. Elle a permis de vérifier en particulier que les calculateurs numériques couplés n'entraînaient pas de déconnexions intempestives, (pour faciliter la détection d'erreurs de logiciel, chaque calculateur est programmé par une équipé différente) et que le fonctionnement des protections était correct.

L'ensemble expérimental de C.D.V.E. a fait l'objet d'une analyse de pannes très poussée, permettant de s'assurer que les objectifs de sécurité fixés étaient bien vérifiés quelle que soit la configuration de vol. L'influence de différentes pannes (simples ou combinaisons de pannes simples) sur le pilotage de l'avion a été déterminée par essais, et les cas les plus significatifs présentés aux pilotes. Leurs conséquences ont entraîné la mise à jour des procédures d'utilisation du système de C.D.V.E. et l'adjonction d'une signalisation indiquant à tout moment le mode de pilotage actif et l'état d'engagement des calculateurs numériques de C.D.V.E.

En fin de mise au point, un vol spécial avec un équipage des Services Officiels et du C.E.V. (Centre d'Essais en Vol) a permis de présenter les lois de pilotage définies, ainsi que différents cas de pannes avec le système complet d'expérimentation en vol. L'ensemble a été entériné le 18.01.78 et autorisé à être essayé en vol sur Concorde n° 1.

6 ESSAIS EN VOL

Après l'étude très complète effectuée en simulation, on s'est proposé d'évaluer en vol le comportement global du système C.D.V.E. et de juger les améliorations apportées par le minimanche et les lois de pilotage.

Pour des raisons de sécurité, une première phase d'essais sur un T.S.S. non modifié a permis d'ouvrir avec les commandes de vol classiques, le domaine de centrage principalement pour les centrages arrières. La deuxième phase a été consacrée aux vols C.D.V.E. proprement dits.

6.1 Phase d'essais préliminaires.

La conception du système d'expérimentation en vol est tel qu'en cas de panne des commandes de vol tout électriques (chaîne bleue) on revient automatiquement en commandes classiques. Il a donc fallu s'assurer que dans le domaine de centrages retenus en C.D.V.E., le pilotage avec les commandes actuelles était acceptable.

Pour celà, un vol a eu lieu permettant de définir les limites de centrages arrières (surtout à basses vitesses) où le contrôle de l'avion pouvait s'effectuer sans dégradation notable des performances. Les essais ont eu lieu successivement :

- en commande électrique Concorde avec stabilisateurs

- en commande mécanique.

Le couloir de centrage adopté pour les essais en C.D.V.E. est donné planche 7.

6.2 Phase d'essais en vol C.D.V.E.

Le temps alloué pour les essais en vol a été d'environ 10 heures. Compte tenu du nombre limité de vols, les essais ont été conduits principalement dans la partie du domaine de vol la plus susceptible de poser des problèmes de pilotage, c'est-à-dire en subsonique et en particulier aux vitesses d'approche et d'atterrissage.

Les vols aux grandes incidences ont été exclus, ainsi que l'étude systématique de pannes. La campagne d'essais a comporté huit vols dont le programme est donné ci-après :

VOL	DATE	P R O G R A M M E
1	16.03.78	- Engagement du système C.D.V.E. en vol - Essai des protections - Essai de pilotabilité aux centrages normaux de vol - Atterrissage en C.D.V.E. (X_G = 53,5 %)
2	03.04.78	- Essai de pilotabilité aux centrages normaux de vol jusqu'à M = 2,04 - Atterrissage en C.D.V.E. (X_G = 53,5 %) - Décollage et tour de piste en C.D.V.E. (X_G = 53,5 %)
3	05.04.78	- Décollage en C.D.V.E. (X_G = 53,5 %) - Etude de la pilotabilité aux centrages arrières - Touch and go aux centrages arrières (X_G max AR = 54,5 %) - Atterrissage en C.D.V.E. (X_G = 53,5 %)
4	13.04.78	- Etude d'amélioration de l'approche et de l'arrondi - Atterrissage en C.D.V.E. (X_G = 54 %)
5	24.04.78	- Etude de l'amélioration de l'approche et de l'arrondi (présentation à un deuxième pilote) - Touch and go aux centrages arrières (X_G = 55 %)
6	27.04.78	- Etude de l'amélioration de l'approche - Touch and go aux centrages arrières (X_G = 55,5 %) - Etude influence du mode à 1 Hz aux centrages avants
7	27.04.78	- Présentation des C.D.V.E. à un troisième pilote - Tours de piste (55 %)
8	02.05.78	- Présentation des C.D.V.E. au C.E.V. et au S.T.Aé - Montée VMo - Tours de piste (X_G = 55,5 %)

7 RESULTATS

Le programme de vol établi avant les essais a été réalisé intégralement. Comme indiqué sur la planche 11, un balayage en centrage très complet de toute la zone subsonique a été réalisé et en particulier dans les plases critiques approche-atterrissage-remise des gaz. Vu le peu de problèmes rencontrés au niveau système, le domaine supersonique a été ouvert jusqu'à M = 2,04, mais il n'a pas été fait d'étude systématique de l'influence du centrage dans cette zone.

Les principaux enseignements que l'on peut tirer de cette expérimentation sont les suivants :

7.1 Comportement du système.

Le comportement du système a été jugé excellent. Il s'est caractérisé par :

- l'absence de déconnexions intempestives des calculateurs numériques. Les passages en commandes de secours ont été dûs, soit à une action intentionnelle de l'équipage (procédures de changement de gain par exemple), soit au boîtier de protection dans le cas de fortes turbulences ou de manoeuvres pilotées dépassant les seuils de surveillance.

- une très bonne disponibilité ; une seule panne d'équipement (effacement mémoire morte) est survenue pendant les essais. Elle a été détectée par la check-list d'avant vol et n'a entraîné aucun retard dans la programmation des vols.

- une très grande facilité à programmer les calculateurs numériques. La grande souplesse apportée par cette technologie a été la cause essentielle du succès de l'expérimentation. En effet, si l'on considère que la disponibilité de l'avion était limitée à un mois et demi et que le nombre d'heures de vol ne devait pas dépasser dix heures, on ne pouvait prétendre résoudre définitivement tous les problèmes rencontrés. L'idée principale a donc été d'acquérir le maximum d'informations de façon à posséder après les vols tous les éléments susceptibles de conduire à une solution définitive ; il s'en est suivi un grand nombre de modifications au niveau des lois de pilotage ou des logiques de fonctionnement, qui auraient été difficilement envisageables avec une technologie différente.

La procédure utilisée après chaque vol était la suivante :

- analyse des résultats avec les pilotes puis à partir des enregistrements

- recherche d'une solution au simulateur

- programmation de la modification dans les calculateurs (chacun d'eux est programmé par une équipe différente)

- vérification sur banc partiel et sur simulateur des logiciels modifiés

- vérification sur avion

Ces trois dernières phases n'ont jamais dépassé un cycle de 3 jours.

7.2 Comportement de la commande et des lois de pilotage.

L'impression générale des pilotes a été une amélioration importante du confort de pilotage par rapport à Concorde, dont on connait déjà les qualités de vol intrinsèques, et surtout une très grande facilité d'adaptation à ce nouveau type de commande. En effet :

- le minimanche a apporté une très bonne précision, permettant un pilotage reposant et souple. Les lois effort-déplacement sur les deux axes, qui avaient été définies sur simulateur ont donné entière satisfaction. Seuls quelques problèmes d'ergonomie ont été rencontrés avec l'emplacement des boutons de trim et d'alternat et avec le réglage de l'accoudoir.

- l'homogénéité des axes de profondeur et de roulis s'est révélée excellente. De plus, comme l'avaient laissé prévoir les essais en simulation la dispersion en maniabilité a été diminuée dans toute la gamme de vitesses étudiées. Si l'on regarde par exemple, le temps de réponse de l'avion aux 2/3 à un échelon de manche (planche 12), on voit qu'aux bornes du domaine de vol, et pour les centrages arrières C.D.V.E., T 2/3 varie dans des proportions bien moindres que sur Concorde. Cette conclusion est aussi confirmée sur l'axe de roulis comme le montre la planche 13 donnant la réponse de l'avion en vitesse de roulis (p) à un échelon de minimanche.

- la stabilité en assiette est parfaite notamment en approche. La sensibilité aux variations de centrage n'est pas perceptible par le pilote. Il en est de même des effets des irrégularités en tangage, dans la zone transsonique et à la réduction des moteurs à M = 2.

- les efforts par g sont pratiquement constants dans tout le domaine de vol. On a relevé des efforts par g de 7 daN $\pm$ 0,5 daN/g. Pour mémoire, sur Concorde certifié, ils varient de 20 à 40 daN/g.

7.3 Problèmes rencontrés.

Deux problèmes particuliers ont été rencontrés et ont fait l'objet d'améliorations pendant plusieurs vols.

Le premier concerne le pilotage en phase arrondi. La loi de tangage comportant un intégrateur à gain élevé, les pilotes ont constaté dès les premiers atterrissages que le déplacement à cabrer du minimanche dans la phase arrondi était très peu perceptible comparativement à un avion classique. Il s'en suivait une certaine difficulté à obtenir le point d'impact visé avec précision.

On a donc envisagé une nouvelle loi différente de la loi nominale par suppression de l'intégration et du retour en Δnz . Elle a été jugée parfaite en arrondi. Essayée en approche, depuis la capture glide jusqu'à l'impact, elle s'est avérée plus précise que la loi nominale, mais a entraîné des efforts par g plus importants et une utilisation trop importante du trim surtout en approche à vitesse non stabilisée.

Le deuxième problème rencontré concerne l'apparition de modes oscillatoires en vol et au sol, liés à la souplesse de l'avion.

En configuration vol, un mode de période proche d'1 seconde apparaît en subsonique. Il se caractérise par une amplitude faible, et est plus ou moins bien organisé suivant le cas de vol. Ce résultat n'est pas spécifique aux commandes de vol tout électriques car il se rencontre aussi sur Concorde un mode P.A. en haut subsonique.

Des essais ont permis de montrer que la diminution du gain de stabilisation était bénéfique, mais difficilement envisageable car on est vite limité dans ce sens par les exigences de pilotabilité.

Au sol, lors des premiers roulages, on a retrouvé comme sur Concorde, mais de manière plus marquée, des oscillations importantes de gouverne dont l'effet est peu perçu au poste de pilotage.

En effet, l'avion sur ses trains est soumis à un mouvement de translation suivant l'axe vertical, entraînant une participation de la souplesse du fuselage. La position des gyromètres est telle qu'un signal apparaît à leur niveau et par l'intermédiaire du bouclage de stabilisation à gain élevé entraîne les gouvernes qui accentuent le phénomène.

Une diminution importante de ce gain tant que les trains principaux sont écrasés a permis de retrouver un fonctionnement très acceptable.

Un deuxième problème d'oscillation de fréquence proche de 7 Hz est apparu dès les premiers essais au sol avion arrêté.

Pour un braquage important du minimanche, un couplage manche-structure se produisait à travers le bras et la main du pilote. L'élimination de cet effet a été obtenue au niveau calculateurs, par filtrage de l'entrée minimanche, et par l'utilisation de bloqueurs d'ordre zéro en sortie des calculateurs numériques.

7.4 Validité des résultats obtenus en simulation.

L'ensemble des vols C.D.V.E. a permis de confirmer de façon très précise la représentativité du simulateur de vol. En effet, les lois de pilotage, les réglages du minimanche, et le système en général, qui avaient été mis au point au laboratoire, ont subi très peu de modifications sur avion. Cependant, les problèmes rencontrés en vol permettent de conclure :

- qu'il est très difficile d'obtenir une bonne représentation de l'environnement extérieur au sol ou à proximité du sol (arrondi, abattée, roulage)

- que la non-simulation de l'avion souple ne permet pas au stade de mise au point de s'affranchir des problèmes d'oscillations aux fréquences supérieures à 1 Hz.

8 PERSPECTIVES

Le résultat très positif apporté par cette expérimentation en vol, notamment au point de vue maîtrise de la technologie numérique, permet d'envisager de nombreuses études, utilisant les commodités apportées par une telle technique.

Dans l'immédiat, un des premiers objectifs est d'approfondir et de résoudre à partir de tous les résultats d'essais, les principaux problèmes rencontrés en vol, à savoir, l'optimisation de la loi de pilotage en approche et le problème plus général de la suppression des oscillations à 1 Hz en vol et au sol.

Un deuxième objectif est de définir à partir de cette loi de base, d'autres principes de pilotage, tels que manche relaché, l'assiette et/ou la pente acquises sont maintenues automatiquement.

Il est certain que dans cette optique, le point de vue réglementaire devra être aussi abordé car les exigences actuelles de stabilité statique seraient difficilement applicables.

Toutes ces études doivent déboucher sur une deuxième campagne d'essais sur Concorde.

A plus long terme, l'exemple des C.D.V.E. pourra être étendu à d'autres concepts du contrôle automatique généralisé. On peut envisager par exemple des systèmes permettant l'augmentation des vitesses limites de flottement, ou une meilleure répartition des efforts sur la voilure.

Ces concepts peuvent également trouver un champ d'application dans les avions de transport subsonique pour lesquels le principal objectif est la réduction des efforts sur la voilure principale : soit en répartissant les charges aérodynamiques différemment sur la voilure principale, soit en transférant une partie de ces charges sur la voilure secondaire.

CONCEPTION GENERALE

PRINCIPE DES C.D.V.E. DE CONCORDE ACTUEL

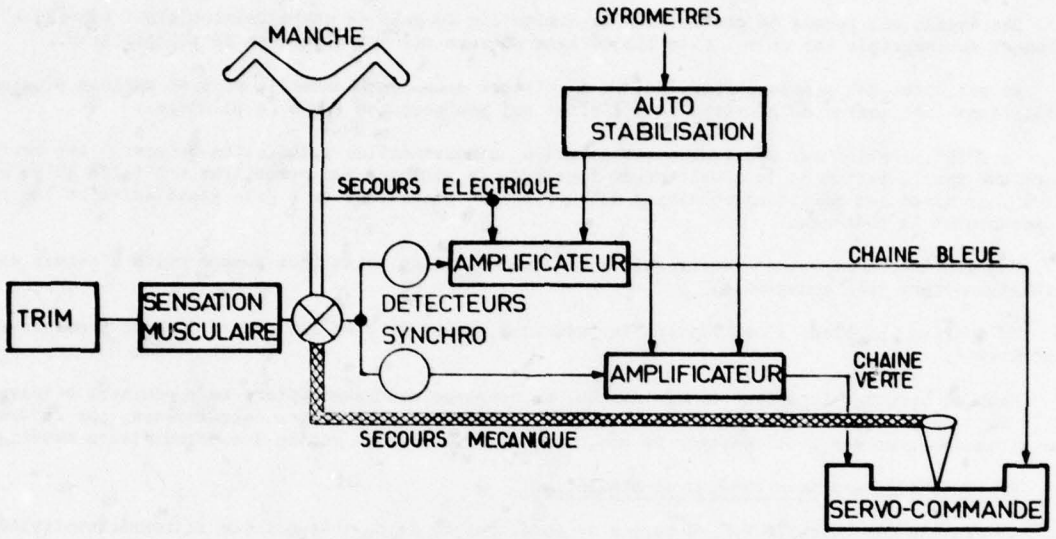

PL. 1

LOIS DE COMMANDE

AXE DE PROFONDEUR

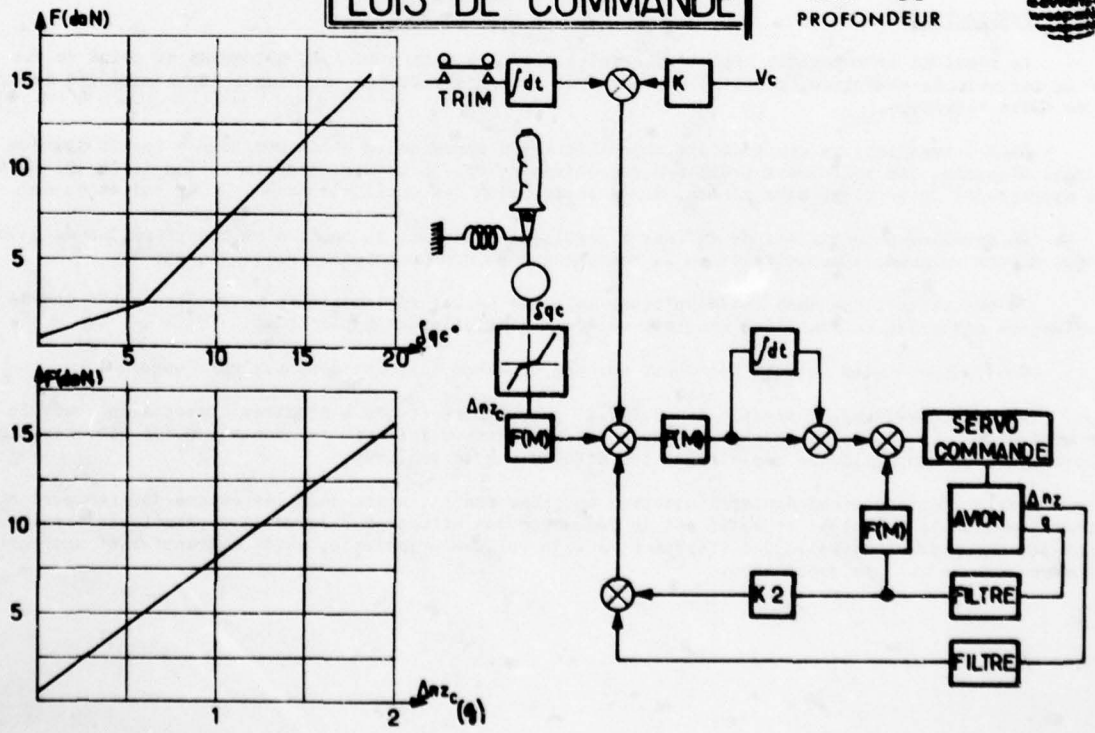

PL. 2

LOIS DE COMMANDE

Axe de Gauchissement

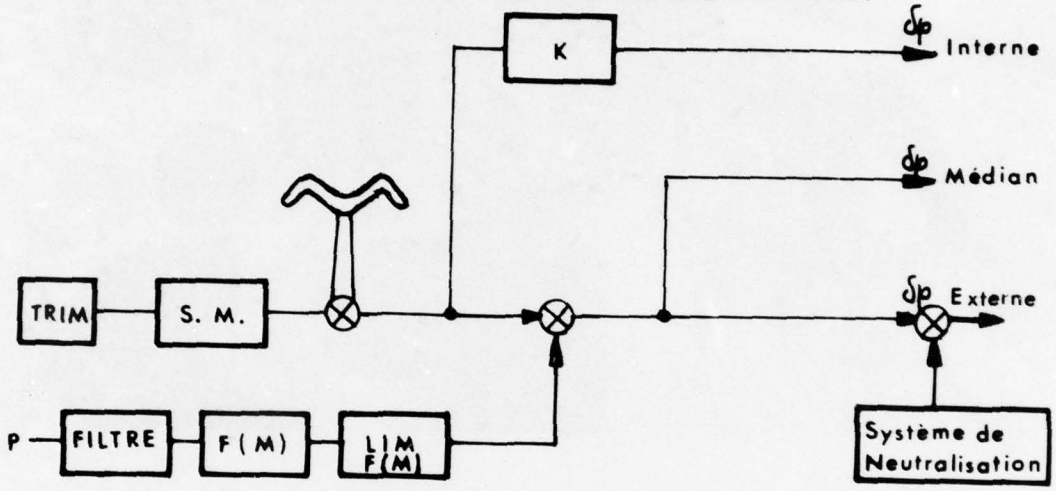

PRINCIPE CONCORDE (Commande électrique)

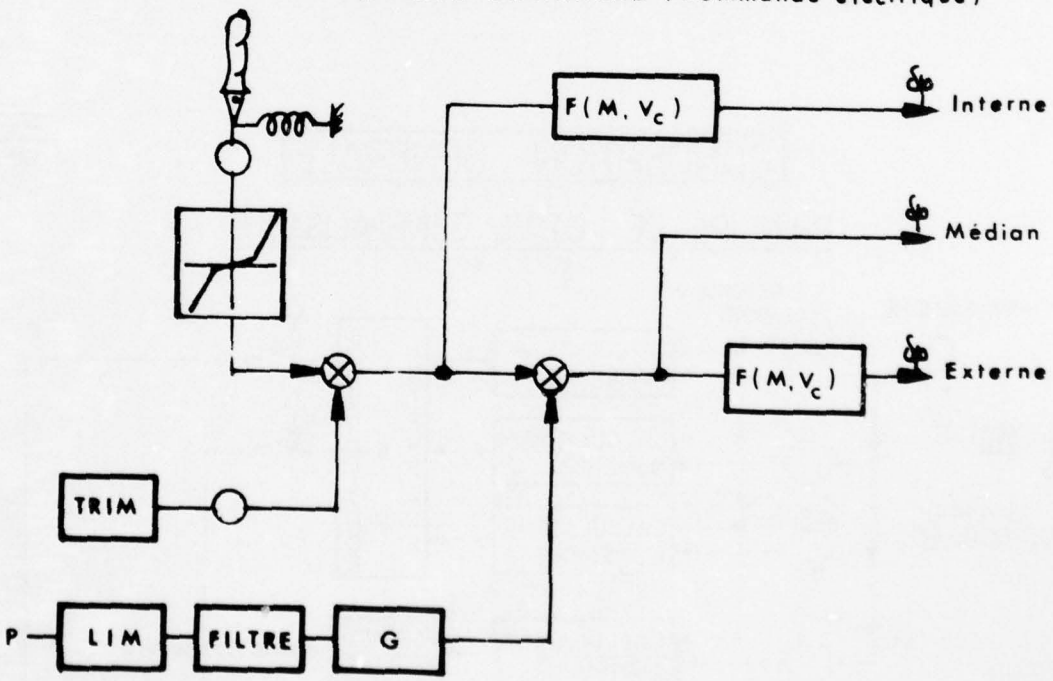

PRINCIPE CONCORDE C.D.V.E.

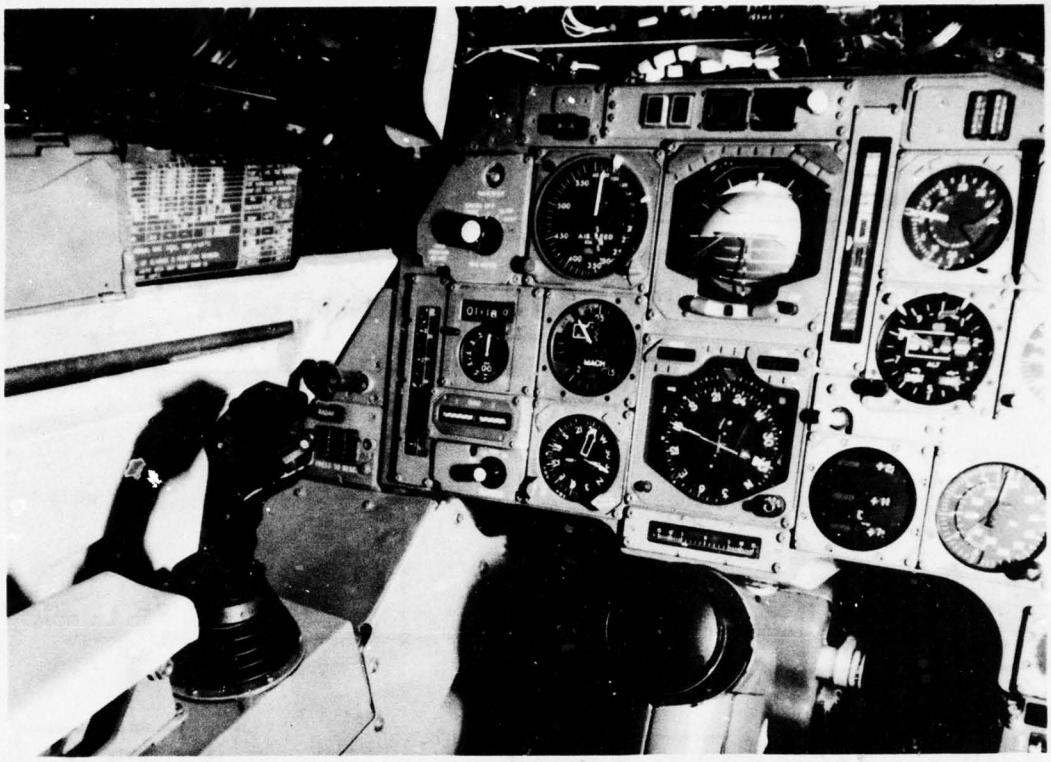

PL. 4

CONCEPTION GENERALE

PRINCIPE DE C.D.V.E GENERALISABLE

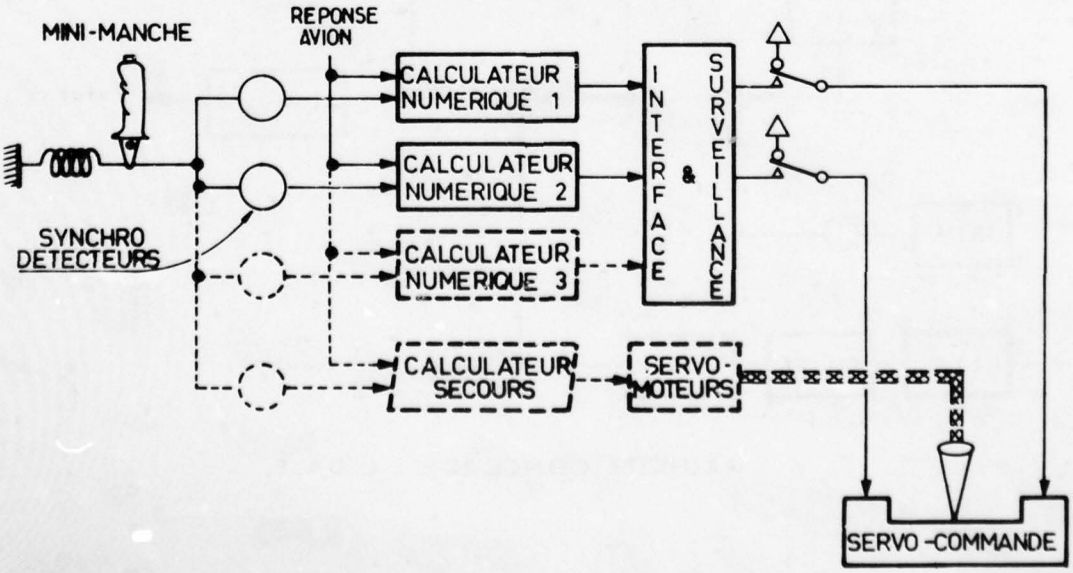

PL. 5

AD-A071 709 ADVISORY GROUP FOR AEROSPACE RESEARCH AND DEVELOPMENT--ETC F/G 1/3
STABILITY AND CONTROL.(U)
MAY 79
UNCLASSIFIED AGARD-CP-260 NL

2 OF 4
AD A071709

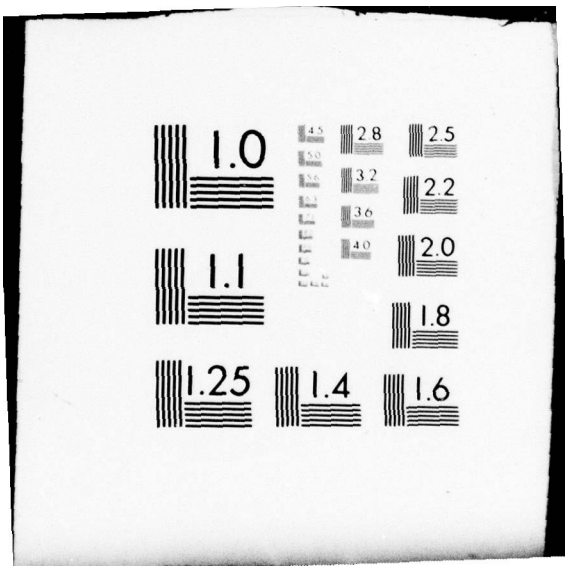
1.0
1.1
1.25
1.4
1.6
1.8
2.0
2.2
2.5
2.8
3.2
3.6
4.0
4.5
5.0
5.6

CALCULATEUR NUMERIQUE CSF COMVOL

CARACTERISTIQUES

TYPE: SPECIFIQUE

ARCHITECTURE: 2 UNITES DE CALCUL TRAVAILLANT EN PARALLELE.
- 1 UNITE DE CALCUL OPERATIONS LONGUES (Vectoring, Racine carrée)
- 1 UNITE DE CALCUL OPERATIONS COURTES (Addition, Soustraction)

* EXECUTION SIMULTANEE D'UNE OPERATION LONGUE ET DE TROIS OPERATIONS COURTES.

MODE DE CALCUL: SERIE, VIRGULE FIXE SUR MOTS DE 16 BITS, PROTECTION CONTRE DEBORDEMENTS.

NOMBRE D'INSTRUCTIONS: 26

TYPE D'INSTRUCTIONS: SPECIALISEES: VECTORING, ROTATION 53,3 µs.
DE BASE: ADDITION, SOUSTRACTION, OU, ET : 10,6 µs.

ECHANGES AVEC EXTERIEUR: ACCES DIRECT MEMOIRE

CAPACITE DE LA MEMOIRE PROGRAMME: 10K OCTETS.

NOMBRE D'ENTREES/SORTIES:

	ENTREES	SORTIES
ANALOGIQUES	72	7
DISCRETES	64	32
NUMERIQUES	8	1

AUTOSURVEILLANCE : EFFICACE

PROGRAMMATION : FACILE

PL.6

CONCEPTION GENERALE

* STABILISATION D'UN AVION INSTABLE : Exemple CONCORDE

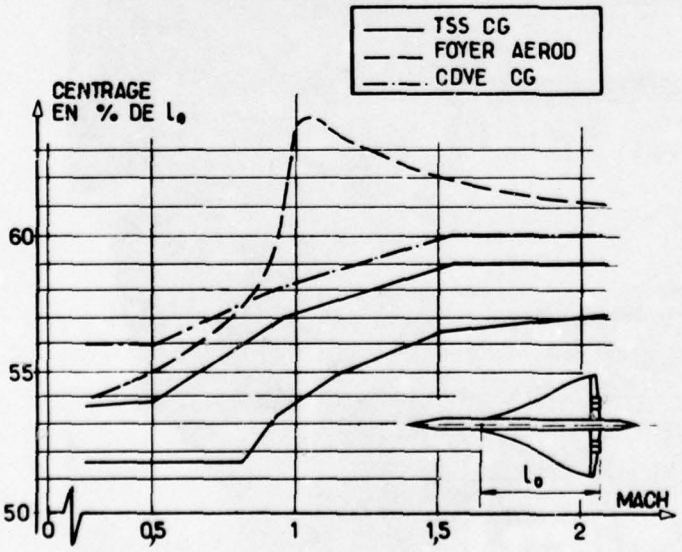

PLAGE DE CENTRAGE

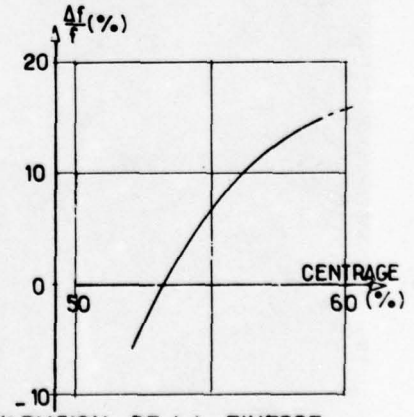

VARIATION DE LA FINESSE AERODYNAMIQUE A BASSE VITESSE EN FONCTION DU CENTRAGE

PL.7

IMPLANTATION SUR CONCORDE

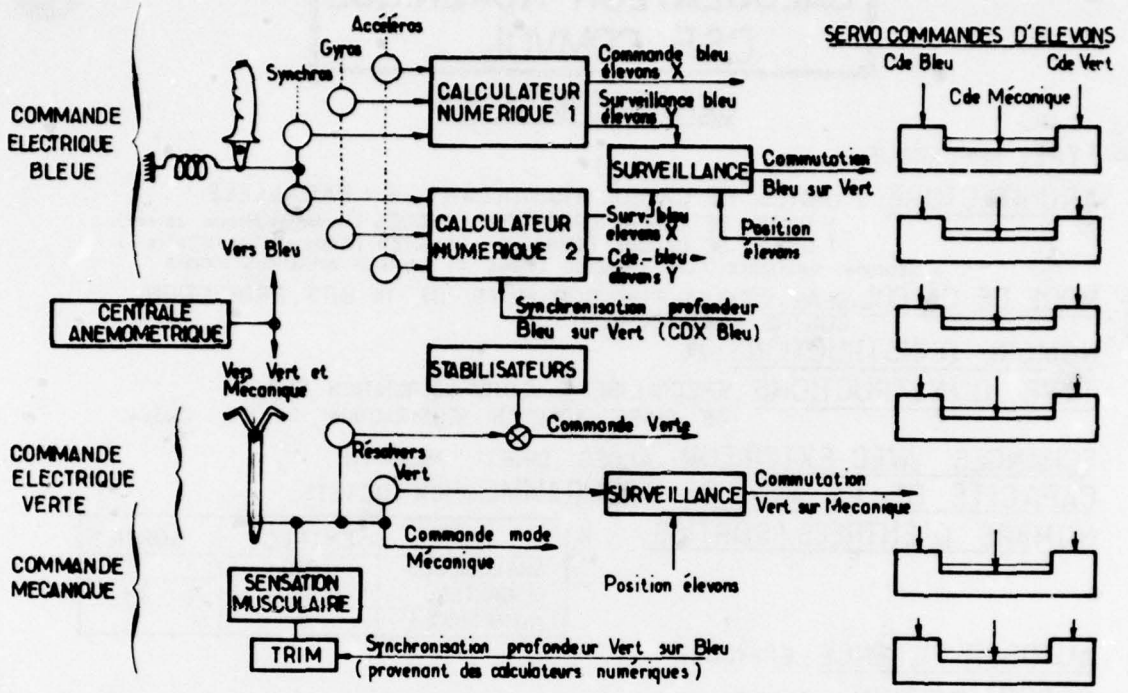

PL. 8

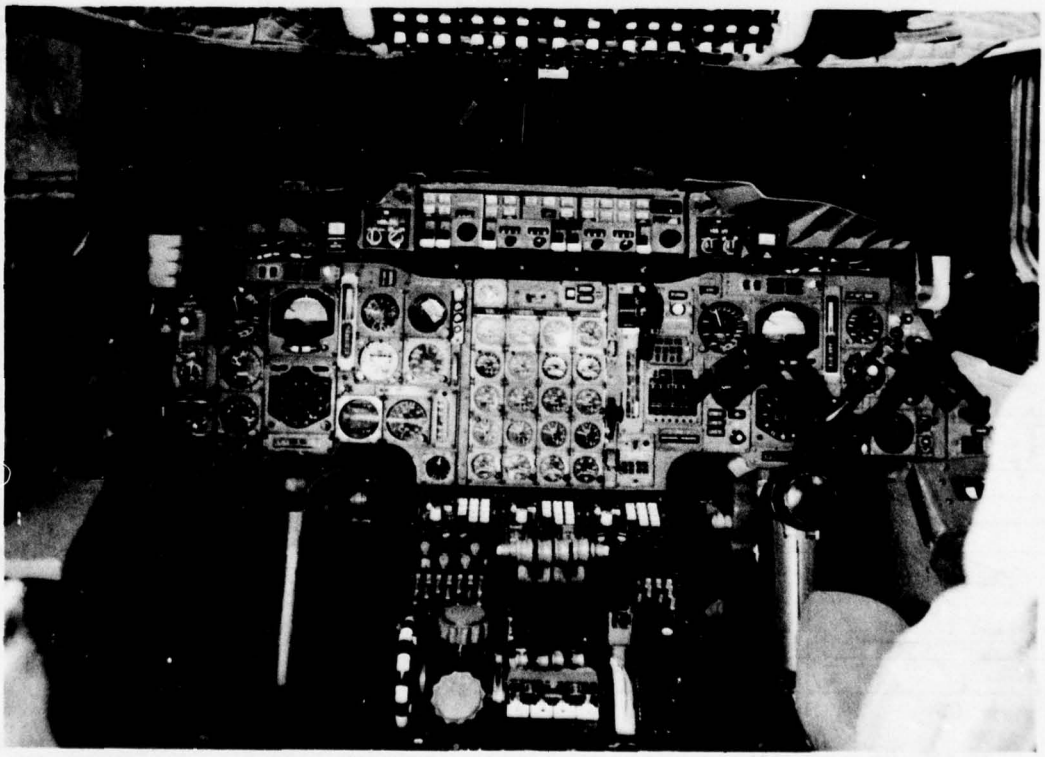

PL.9

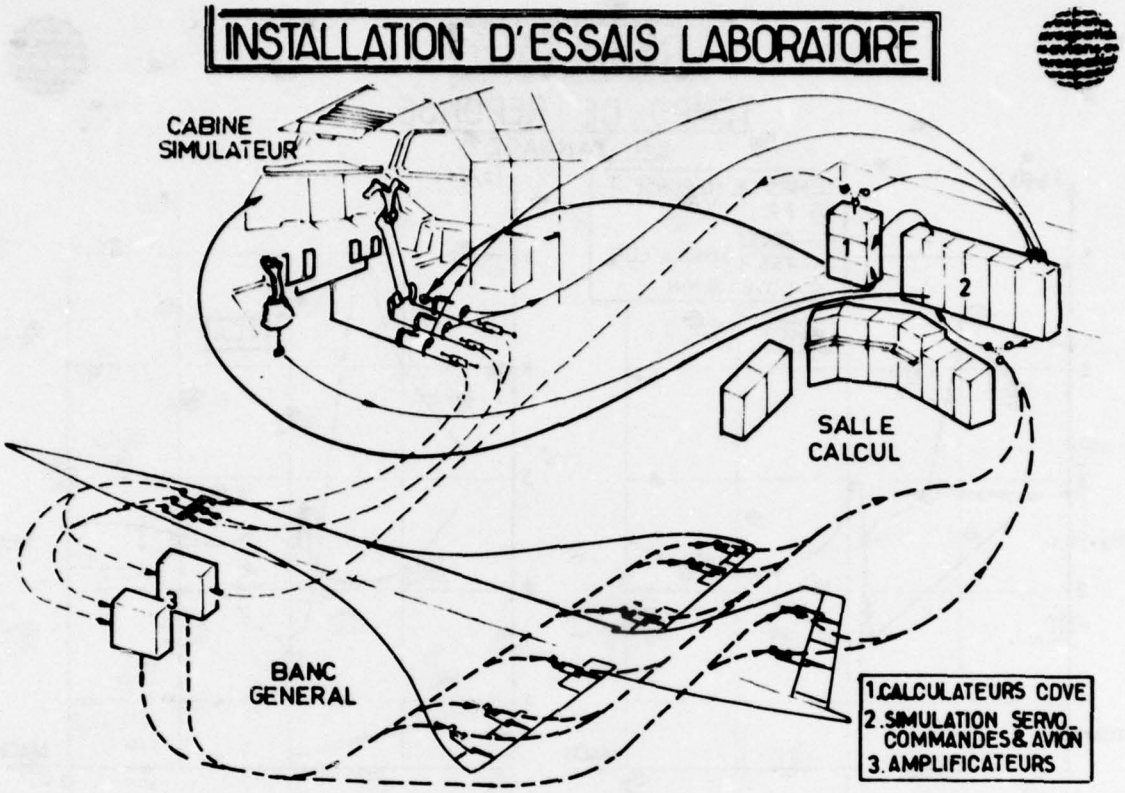
INSTALLATION D'ESSAIS LABORATOIRE
CABINE SIMULATEUR
SALLE CALCUL
BANC GENERAL
1
2
3
1.CALCULATEURS CDVE
2.SIMULATION SERVO-COMMANDES & AVION
3.AMPLIFICATEURS

PL.10

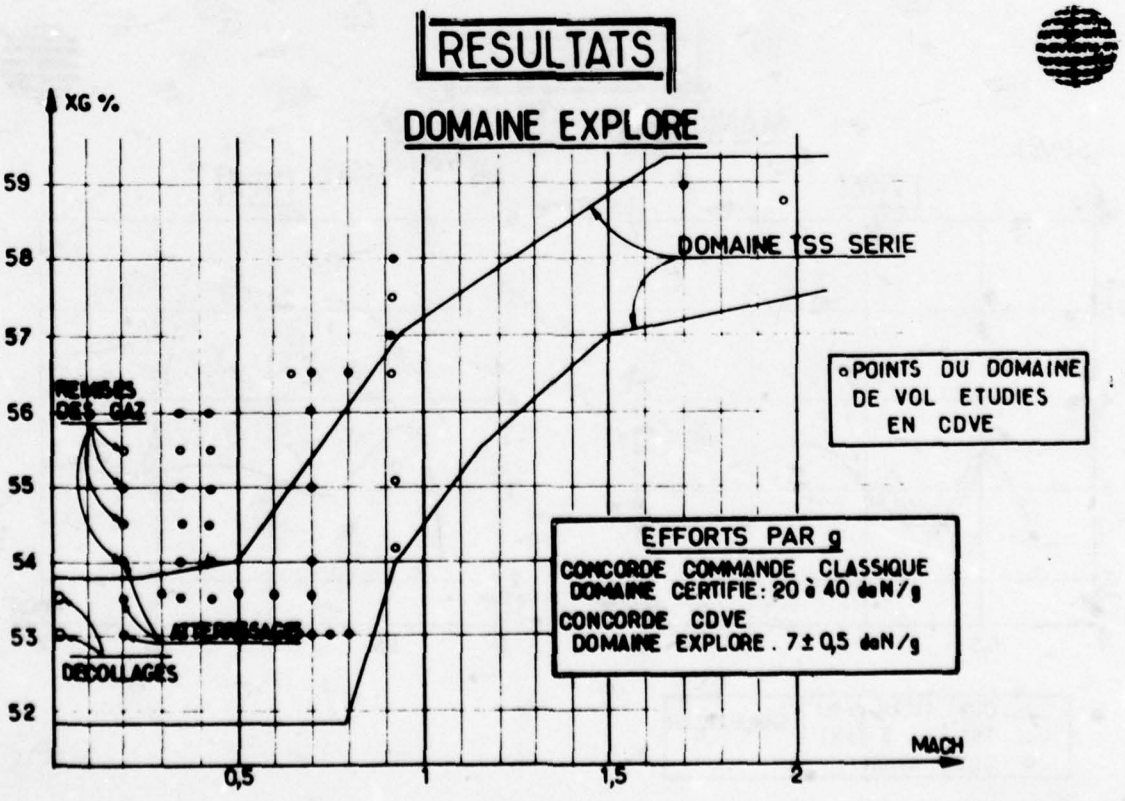
RESULTATS
DOMAINE EXPLORE
XG %
59
58
57
56
55
54
53
52
0,5
1
1,5
2
MACH
DOMAINE TSS SERIE
REMISES DES GAZ
ATTERRISSAGES
DECOLLAGES
o POINTS DU DOMAINE DE VOL ETUDIES EN CDVE
EFFORTS PAR g
CONCORDE COMMANDE CLASSIQUE
DOMAINE CERTIFIE: 20 à 40 daN/g
CONCORDE CDVE
DOMAINE EXPLORE. 7 ± 0,5 daN/g

PL.11

RESULTATS

TEMPS DE REPONSE EN TANGAGE

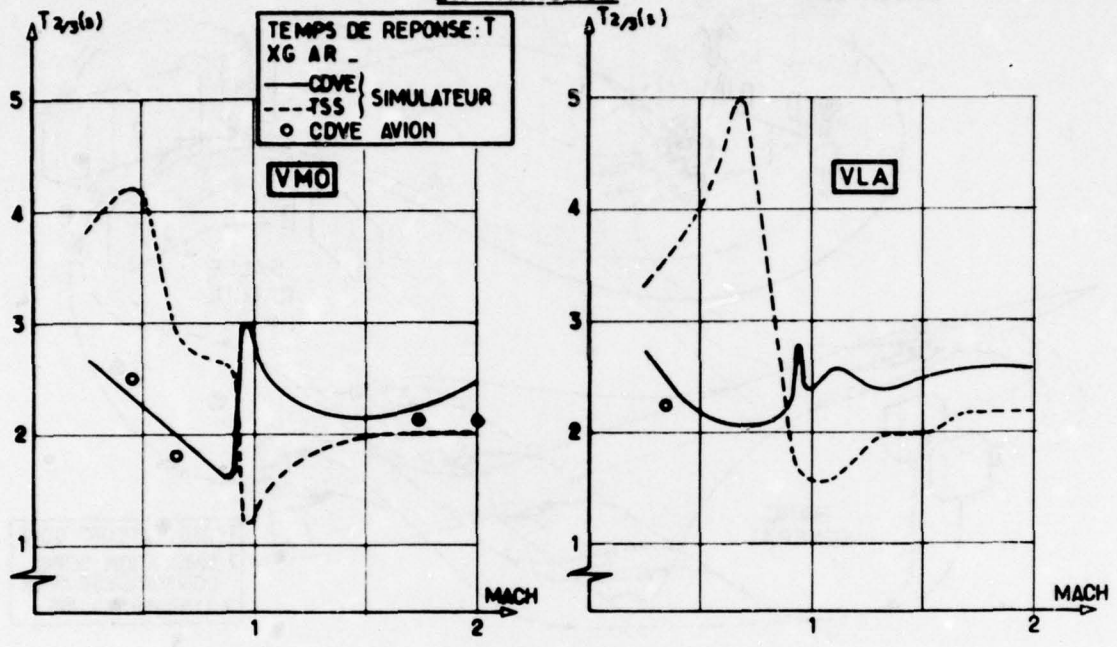

PL. 12

RESULTATS

MANIABILITE EN ROULIS

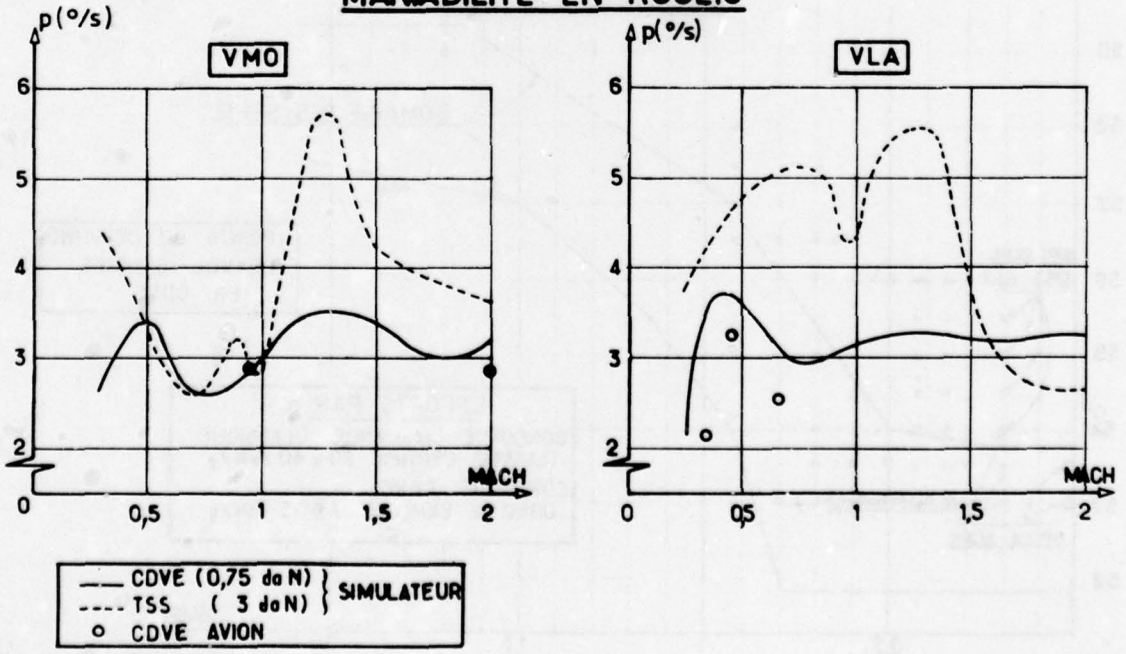

PL. 13

GENERAL CONCEPT

PRINCIPLE OF CONCORDE FLY BY WIRE SYSTEM IN DAY TO DAY OPERATIONS

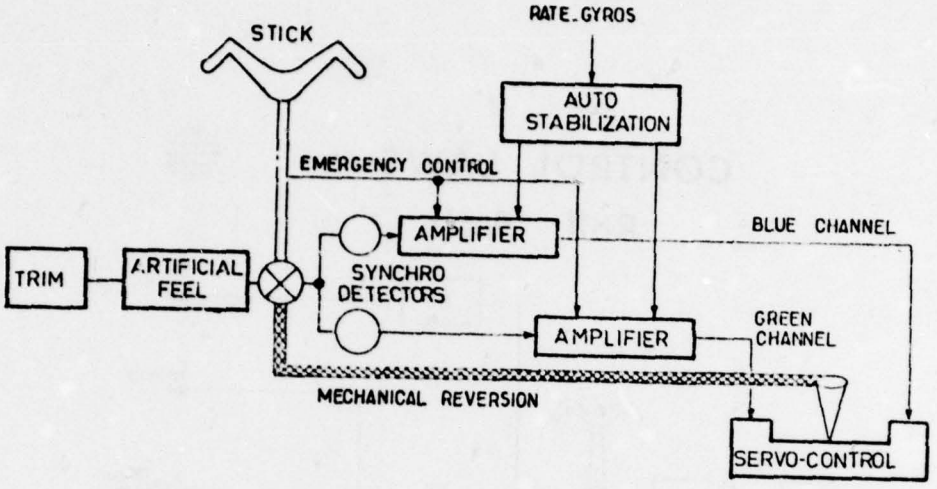

PL. 1

CONTROL LAWS

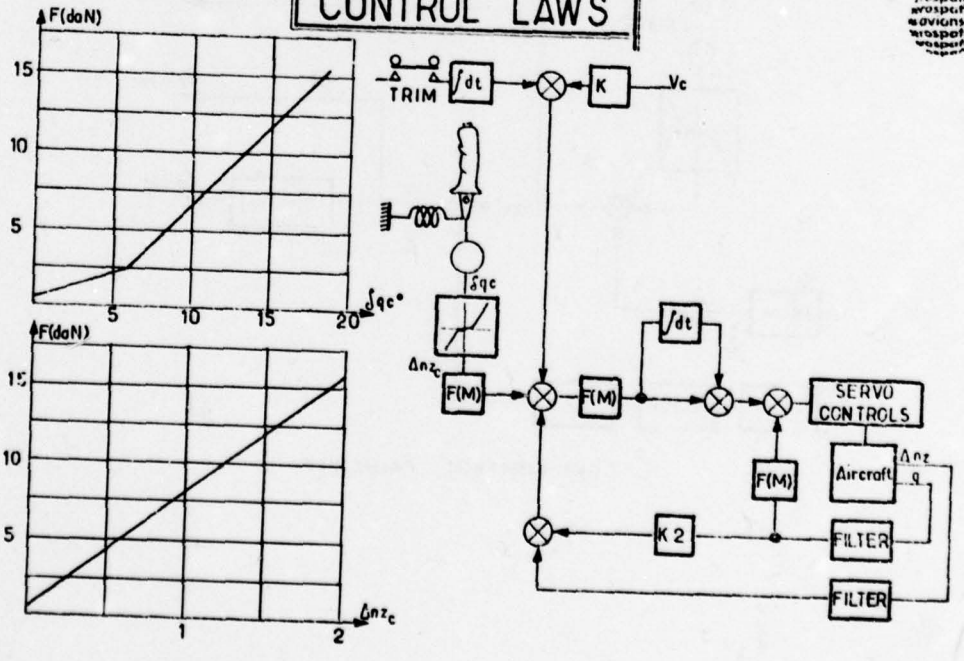

PL.2

CONTROL LAWS
Roll Axis

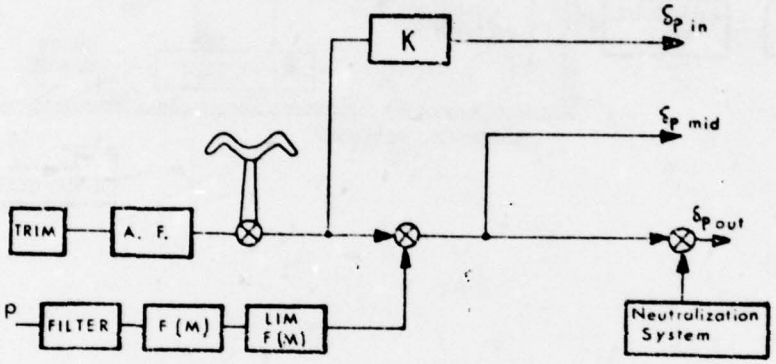

CONCORDE ELECTRIC CONTROL PRINCIPLE

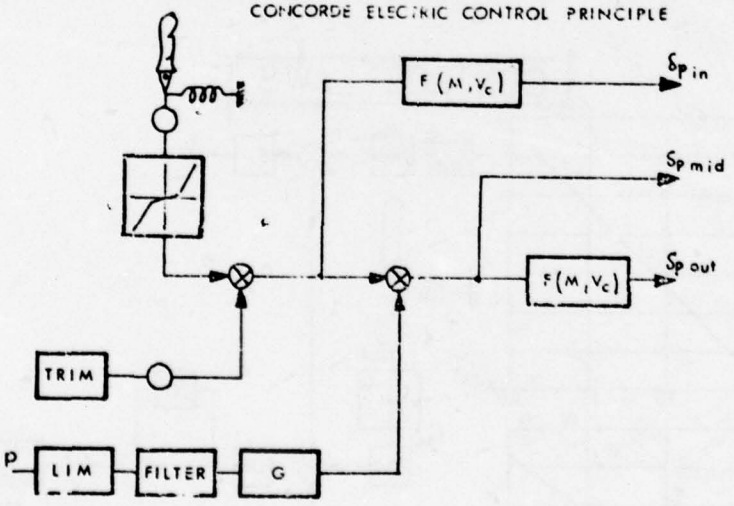

CDVE CONTROL PRINCIPLE

PL.3

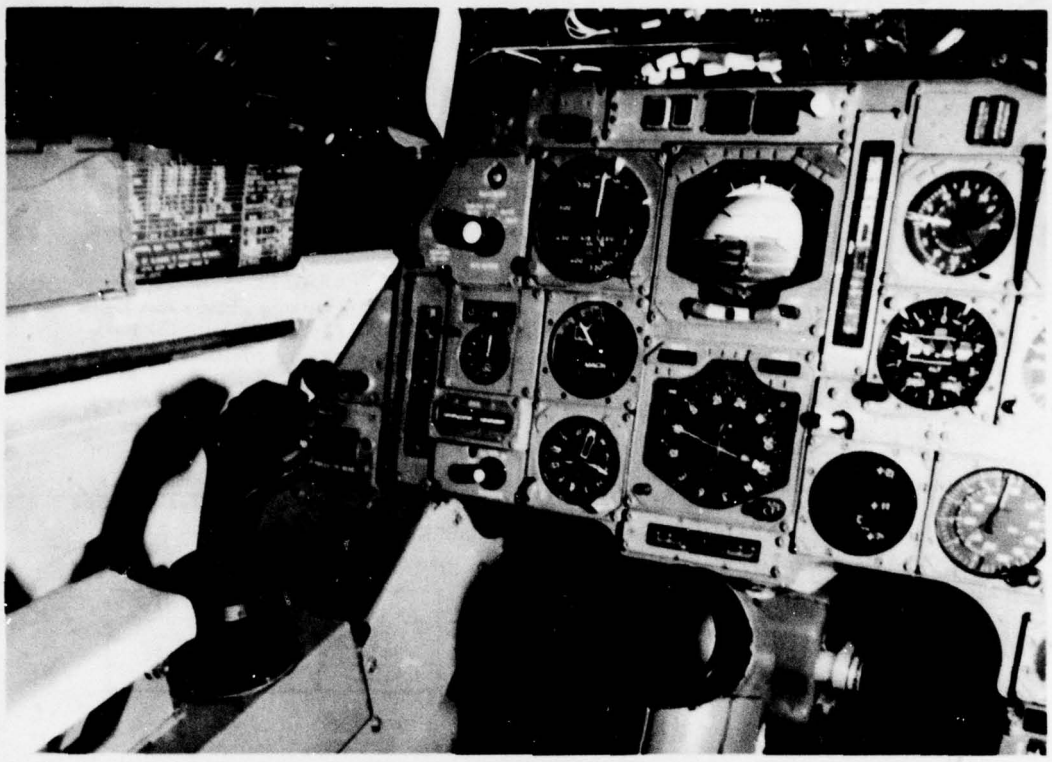

PL.4

GENERAL CONCEPT

PRINCIPLE OF GENERALIZABLE FLY BY WIRE SYSTEM

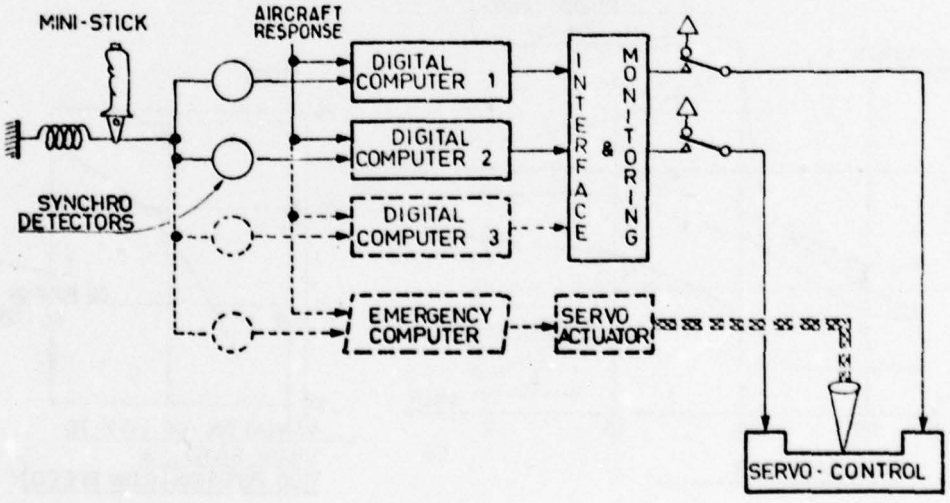

PL.5

DIGITAL COMPUTER CSF COMVOL

CHARACTERISTICS

TYPE : SPECIFIC

ARCHITECTURE : 2 COMPUTER UNITS OPERATING IN PARALLEL.
- 1 COMPUTER UNIT FOR LONG OPERATIONS (Vectoring, Square root)
- 1 COMPUTER UNIT FOR SHORT OPERATIONS (Addition, Subtraction)

* ONE LONG OPERATION AND 3 SHORT OPERATIONS CARRIED OUT SIMULTANEOUSLY.

COMPUTATION MODE
SERIES, FIXED POINT ON 16 BIT WORDS, OVERFLOW PROTECTION.

NUMBER OF INSTRUCTIONS : 26

TYPE OF INSTRUCTIONS : SPECIALIZED INSTRUCTIONS : VECTORING, ROTATION 53,3 µs
BASIC INSTRUCTIONS : ADDITION, SUBTRACTION, OR, AND : 10,6 µs

EXCHANGES WITH OUTSIDE : DIRECT MEMORY ACCESS.

PROGRAMME MEMORY CAPACITY : 10 K 8 BIT BYTES

NUMBER OF INPUTS / OUTPUTS

	INPUTS	OUTPUTS
ANALOG	72	7
DISCRETE	64	32
DIGITAL	8	1

MONITORING

PROGRAMMING : EASY

PL.6

GENERAL CONCEPT

STABILIZATION

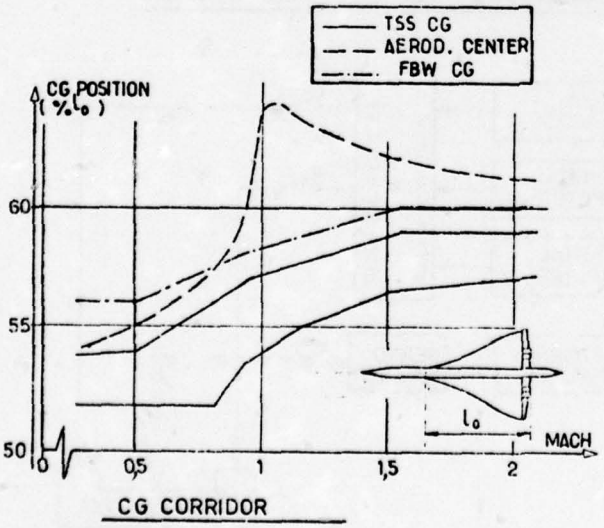

CG CORRIDOR

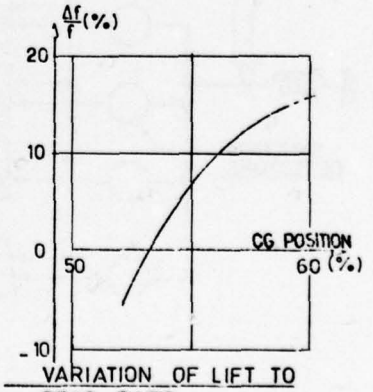

VARIATION OF LIFT TO DRAG RATIO = f(CG POSITION) (LOW SPEED)

PL.7

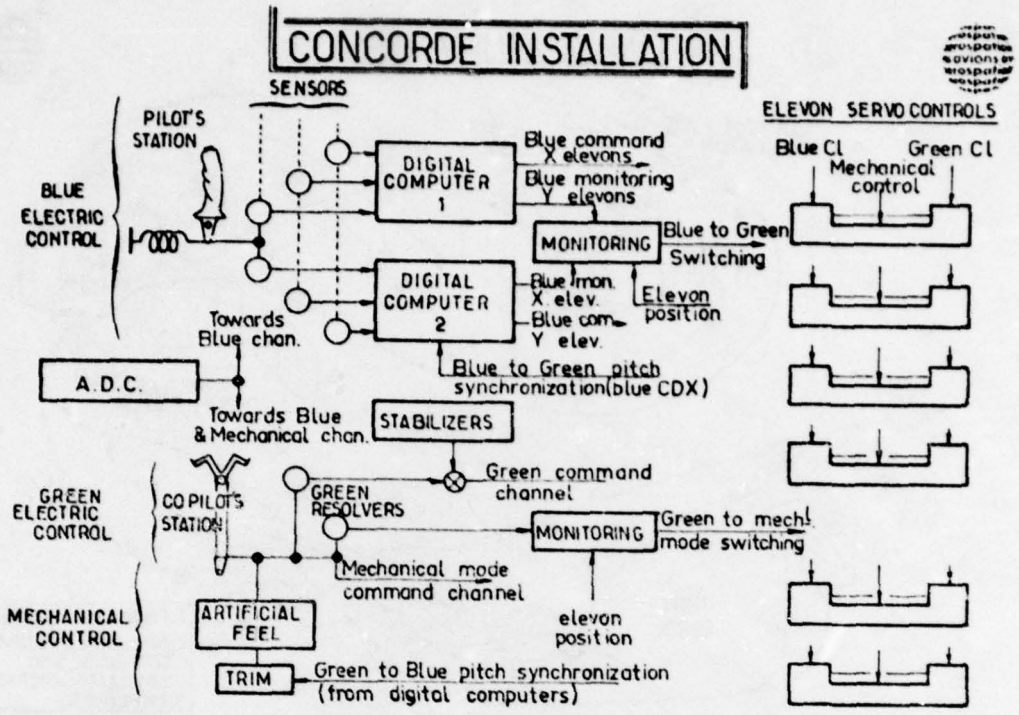
CONCORDE INSTALLATION
SENSORS
ELEVON SERVO CONTROLS
PILOT'S STATION
BLUE ELECTRIC CONTROL
DIGITAL COMPUTER 1
DIGITAL COMPUTER 2
Blue command X elevons
Blue monitoring Y elevons
MONITORING
Blue to Green Switching
Blue mon. X elev.
Blue com. Y elev.
Elevon position
Towards Blue chan.
A.D.C.
Blue to Green pitch synchronization(blue CDX)
Towards Blue & Mechanical chan.
STABILIZERS
Blue Cl
Green Cl
Mechanical control
GREEN ELECTRIC CONTROL
CO PILOT'S STATION
GREEN RESOLVERS
Green command channel
MONITORING
Green to mech! mode switching
Mechanical mode command channel
elevon position
MECHANICAL CONTROL
ARTIFICIAL FEEL
TRIM
Green to Blue pitch synchronization (from digital computers)

PL.8

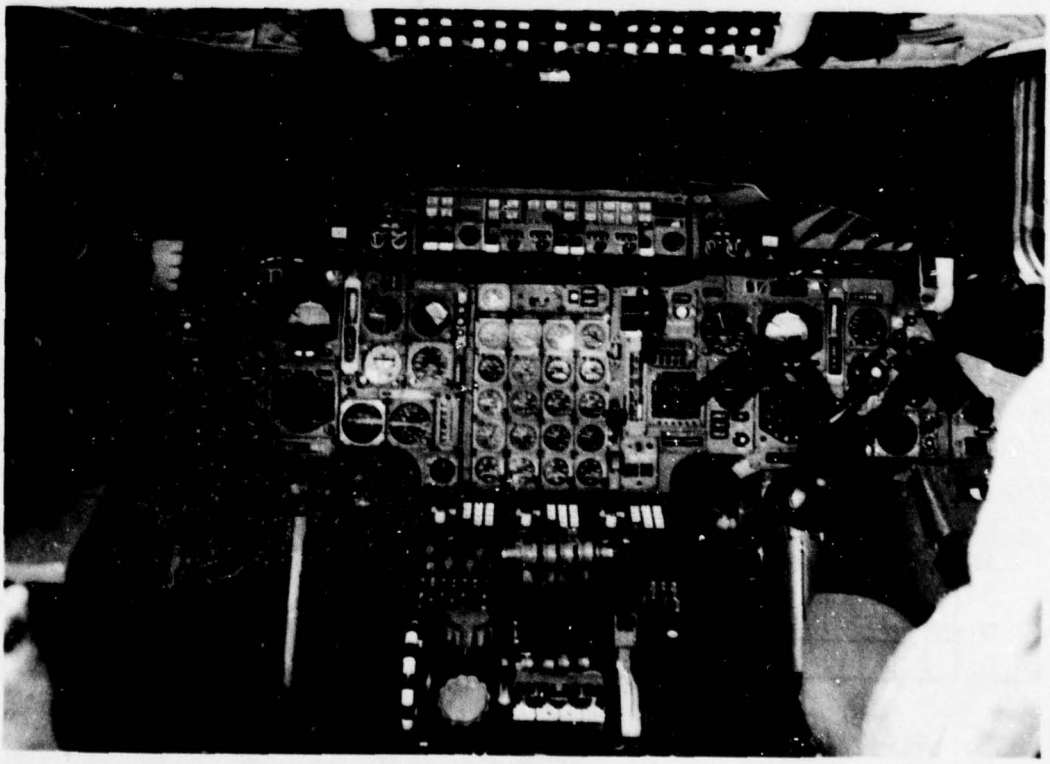

PL.9

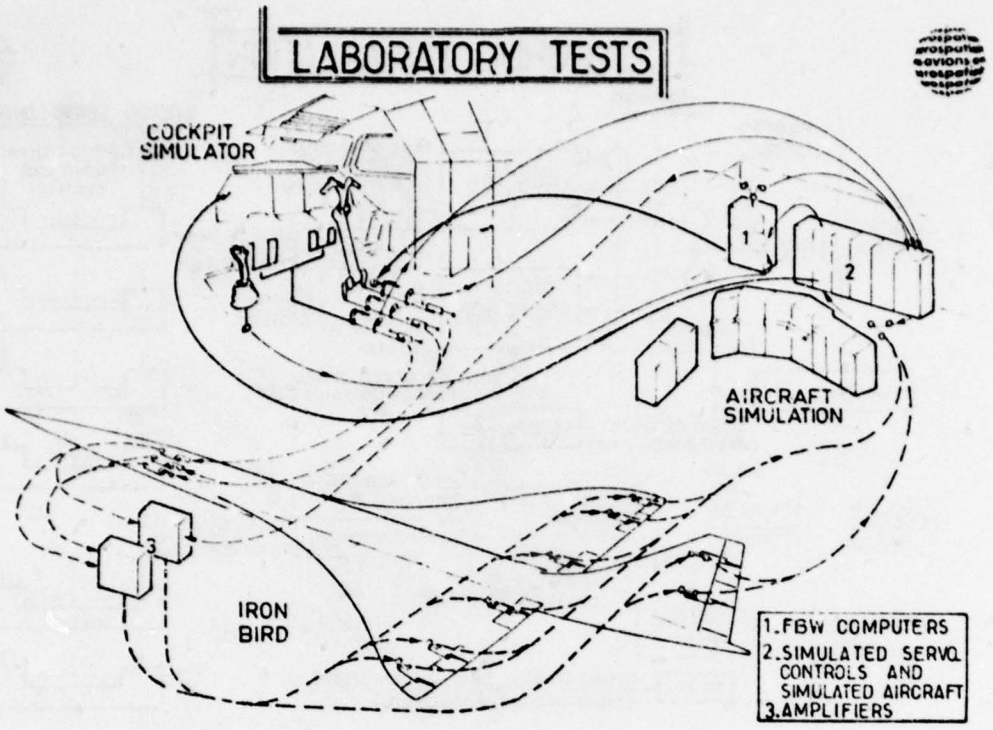
LABORATORY TESTS
COCKPIT SIMULATOR
AIRCRAFT SIMULATION
IRON BIRD
1
2
3
1.FBW COMPUTERS
2.SIMULATED SERVO CONTROLS AND SIMULATED AIRCRAFT
3.AMPLIFIERS

PL.10

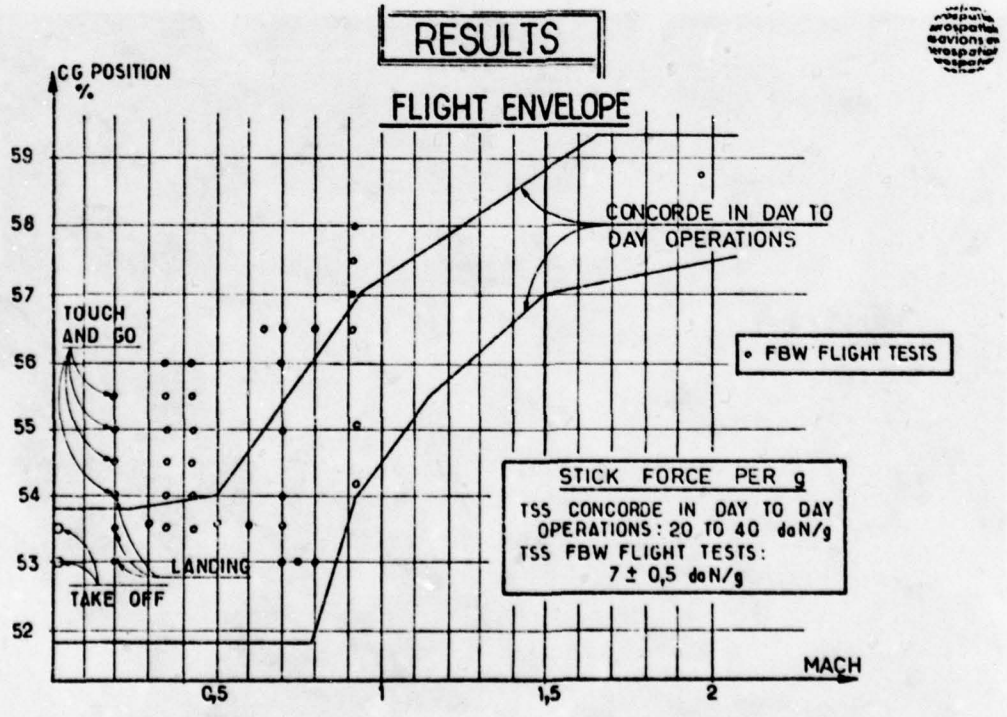
RESULTS
FLIGHT ENVELOPE
CG POSITION %
59
58
57
56
55
54
53
52
TOUCH AND GO
LANDING
TAKE OFF
CONCORDE IN DAY TO DAY OPERATIONS
• FBW FLIGHT TESTS
STICK FORCE PER g
TSS CONCORDE IN DAY TO DAY OPERATIONS: 20 TO 40 daN/g
TSS FBW FLIGHT TESTS: 7 ± 0,5 daN/g
0,5
1
1,5
2
MACH

PL.11

RESULTS

RESPONSE TIME

PITCH AXIS

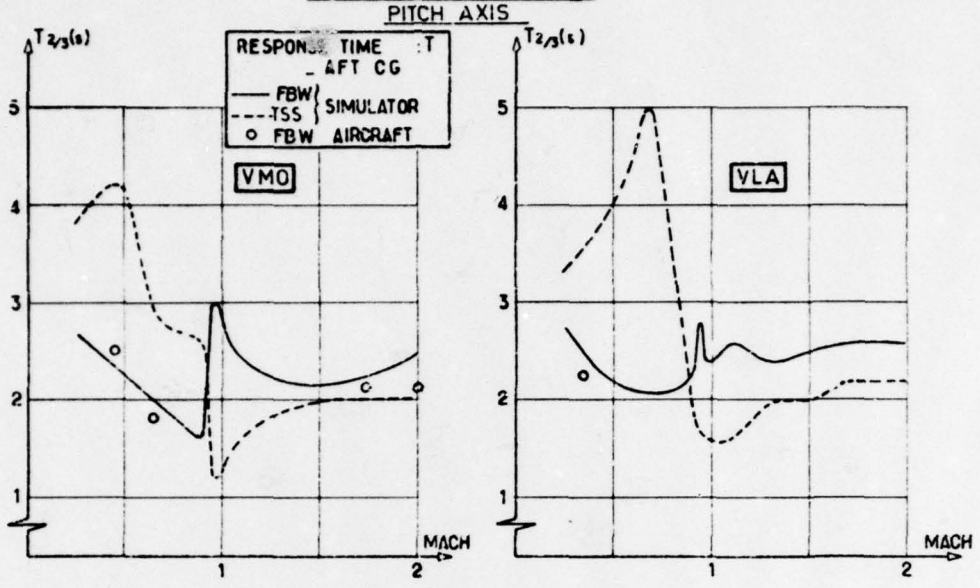

PL.12

RESULTS

ROLL MANŒUVRABILITY

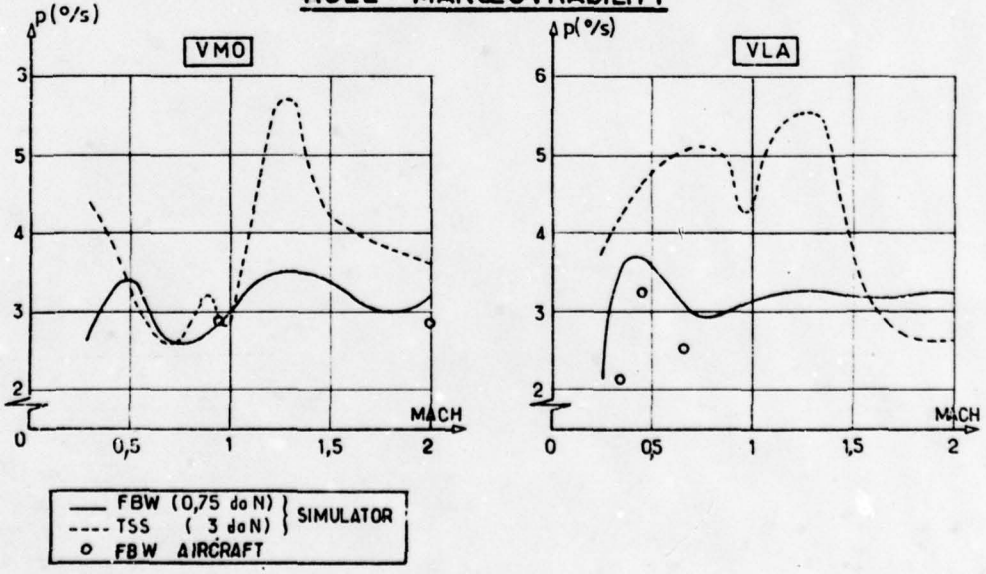

PL.13

IMPROVEMENT OF FIGHTER AIRCRAFT MANEUVERABILITY THROUGH EMPLOYMENT OF CONTROL CONFIGURED VEHICLE TECHNOLOGY

Janusz Stalony-Dobrzanski*
and
Naren Shah**

Northrop Corporation
Aircraft Group
Hawthorne, California, USA

September 1978

SUMMARY

The Control Configured Vehicle (CCV) design concept employing concurrently the traditional disciplines as well as full authority automatic control system design, is shown to offer a very large combat performance improvement over conventional design approach. This improvement is due primarily to the freedom, under CCV concept, of designing statically longitudinally unstable configurations. The configuration selected for the evaluation is a tailless clipped delta employing advanced structure and engine technologies. The performance gains are achieved simultaneously with decreased aircraft and fuel weight for the same mission.

The feasibility of designing a Stability and Command Augmentation System (SCAS) for the statically unstable configurations is demonstrated. The full authority SCAS provides excellent flying qualities in general flying and target tracking modes. The departure prevention feature permits true "head-out-of-cockpit" flying without the pilot having ever to consult flight instruments for safety. The system was evaluated extensively on a moving base simulator. The practical limitations to the degree of static instability are discussed.

1. INTRODUCTION

The basic idea in the Control Configured Vehicle (CCV) design concept is to use automatic control devices as design elements right from the beginning of a new aircraft design in the conceptual and preliminary design phases. The automatic control and stability aspects are then considered in parallel with the aerodynamic and structural design. The objective of the early incorporation of automatic control devices into a new design is the optimization of the overall system in the sense of either increased maneuverability or reduced aircraft weight and cost for a given level of flight performance.

The following CCV concepts are main contributors to the improved maneuverability of a highly maneuverable combat aircraft design:

a. Negative Static Longitudinal Aerodynamic Stability
b. Reduced Directional Aerodynamic Stability
c. Automatic Camber Control (automatic leading- and trailing-edge flap control as a function of Mach number and angle of attack)

The performance advantages of camber control, whether by pilot selection or more recently by automatic operation, have been well established for quite some time and will not be discussed in this paper. Furthermore, it is an open loop type of control without much interaction with the Stability and Command Augmentation System (SCAS).

This paper is concerned with the gains in maneuverability and/or reduction in weight due to reduced or negative static stability. A statically unstable configuration involves, of course, in a most profound fashion the design of the automatic stabilization system. Thus, the main purpose of this paper is to show that the very substantial performance improvement achievable with unstable configurations is a practical proposition with properly designed SCAS.

2. NEGATIVE STATIC LONGITUDINAL STABILITY

In the past conventional design procedure, it has been necessary to satisfy the requirement for static longitudinal stability margin. Complying with this requirement at subsonic speeds results in trim drag penalty which becomes even more severe at supersonic speeds due to the aft movement of the aerodynamic center.

---

*Director, Advanced Technology Integration
**Engineering Specialist

The major change under the CCV design concept is the removal of the requirement for static longitudinal stability. This became possible with the much improved reliability of the electronic hardware providing automatic stability. With the ground rules thus changed, it is feasible to design aircraft which are subsonically statically unstable and have reduced static margin at supersonic speeds.

All aircraft configurations gain in combat performance by designing for negative static stability, but a tailless delta is a particularly interesting configuration because of the conjunction of aerodynamic characteristics and the practical possibilities of automatic stabilization systems. The shift of the aerodynamic center with Mach number on a tailless clipped delta configuration is much less than for a conventional air superiority fighter as illustrated in Figure 1. Locating the CG at the supersonic aerodynamic center minimizes the supersonic trim drag of the tailless configuration and in subsonic regime the static margin is about -15% which can be automatically stabilized with a realistic SCAS design providing good handling qualities*. Employing static margin (SM) more negative than -15% is likely to lead to design and hardware problems discussed in the latter part of this paper.

The unstable delta in subsonic flight trims with down elevon with much improved aerodynamic efficiency compared to stable delta trimming with up elevon. This concept, in which subsonic elevon down trim is reminiscent of conventional configuration maneuvering trailing-edge flap, is illustrated in Figure 2. Additional advantages of design simplicity and consequent reduction in weight make the tailless design even more attractive. The CCV 15% unstable advanced clipped delta design, selected for performance evaluation and for the design of SCAS, is shown in Figure 3. Advanced technologies of composite structures, advanced engines with 2-dimensional nozzles, avionics and armament have been integrated in this design with negative static stability. The thrust-to-weight ratio selected is 1.4. The design mission provides for approximately 30% increase in combat persistence and military payload compared to current air superiority fighters.

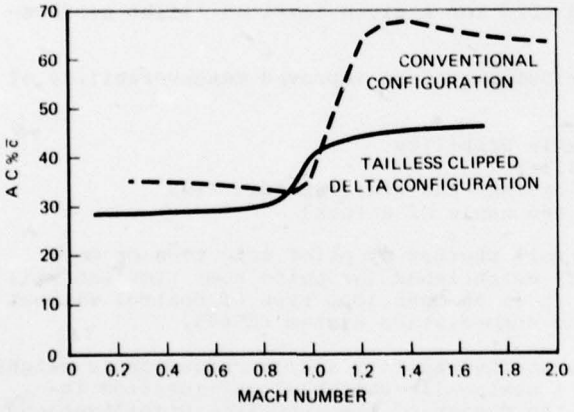

FIGURE 1. AERODYNAMIC CENTER MOVEMENT WITH MACH NO.

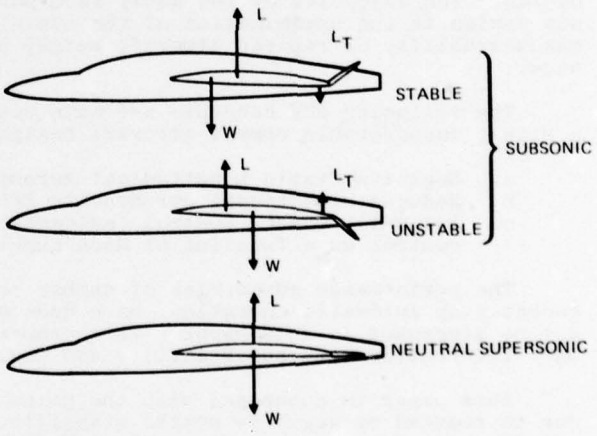

FIGURE 2 . NEGATIVE STABILITY WITH TAILLESS DESIGN

*The static margin for the purposes of this investigation refers to static margin at low speed and low angle of attack.

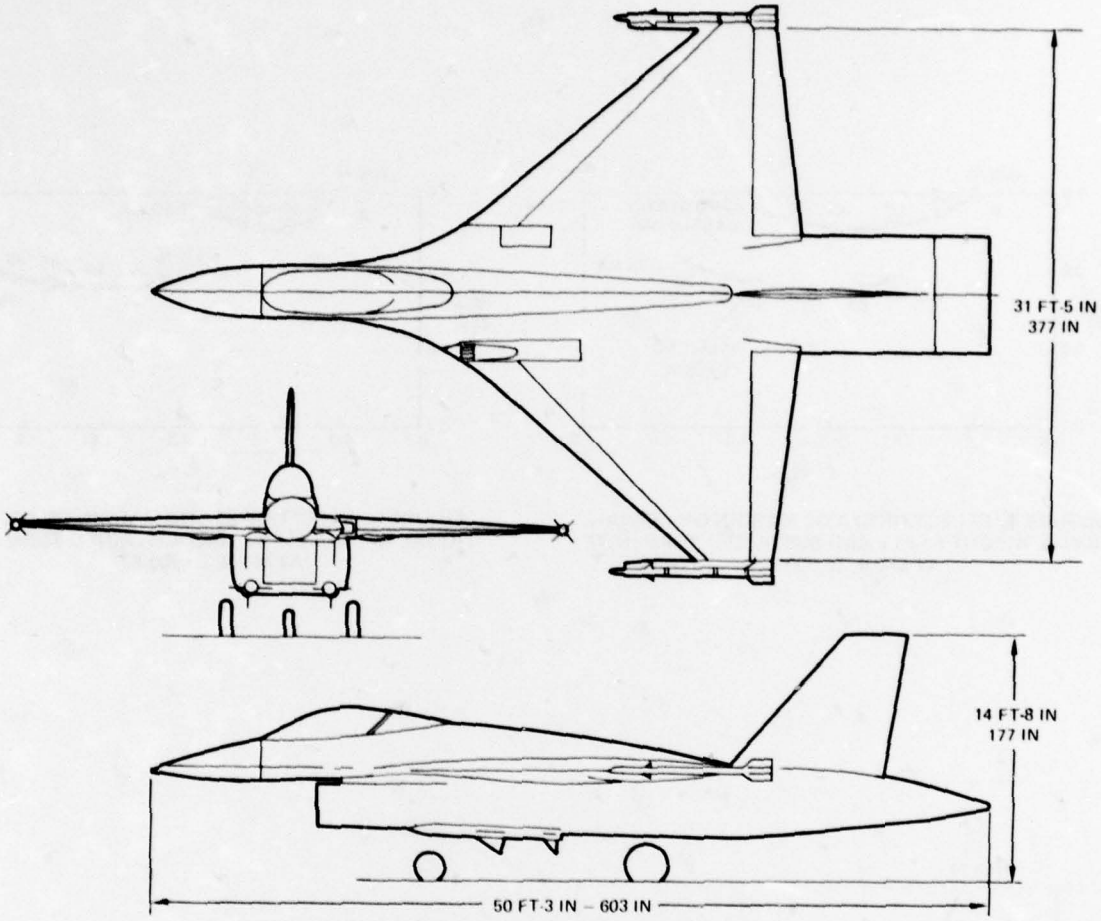

FIGURE 3 . ADVANCED TAILLESS CLIPPED DELTA CONFIGURATION

The sustained turning performance and operational weight empty (OWE) of the neutrally stable (zero static margin) configuration are compared to those of the configuration with -15% SM in Figure 4 at M 0.9, 30,000 ft. All designs on this and subsequent figures satisfy the same mission requirements and their performance is shown relative to the neutrally stable design A with wing loading of 70 psf. The supersonic sustained turn performance at M 1.2, 30,000 ft., is shown in Figure 5. A large improvement in turning performance, particularly at supersonic speed, with negative stability is evident. For the selected design, with wing loading of 40 psf, the increase in sustained turn rate at M 0.9 is about 20% and it is 54% at M 1.2 entirely due to change from zero to -15% SM. At the same time, the OWE is reduced by 7.5% and the fuel weight is reduced by 17%, Figure 6, most noteworthy in view of the life cycle cost. The acceleration time from M 0.9 to M 1.6 at 30,000 ft., for the selected design, increased by 8% due to the negative SM as shown in Figure 7 which is acceptable.

Further increases in turning performance, relative to the selected design, are possible by employing even lower wing loading with very little increase in OWE and actually a decrease in fuel weight. However, design at a wing loading of 40 psf is a good compromise of the various considerations involved in the selection process. One of the more important of these considerations is flight in turbulence. The ride discomfort index was evaluated at M 1.1 and 500 ft. and was found satisfying the requirements of MIL Spec F-9490D.

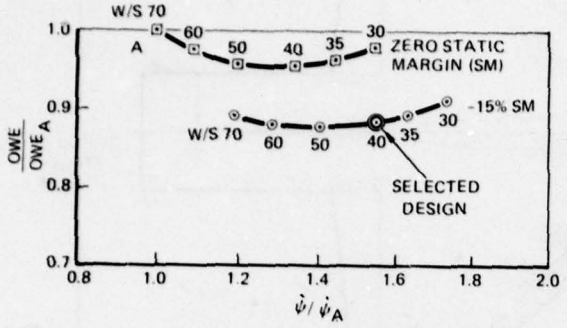

FIGURE 4. EFFECT OF STATIC MARGIN ON OPERATIONAL WEIGHT EMPTY AND SUSTAINED TURN RATE AT M 0.9, 30,000 FT

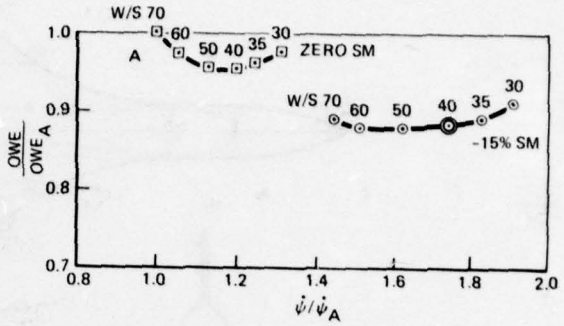

FIGURE 5. EFFECT OF STATIC MARGIN ON OPERATIONAL WEIGHT EMPTY AND SUSTAINED TURN RATE AT M 1.2, 30,000 FT

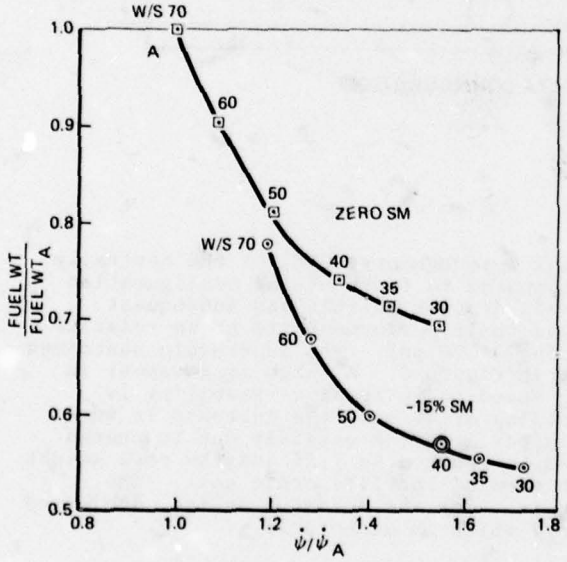

FIGURE 6. EFFECT OF STATIC MARGIN ON FUEL WEIGHT AND SUSTAINED TURN RATE AT M 0.9, 30,000 FT

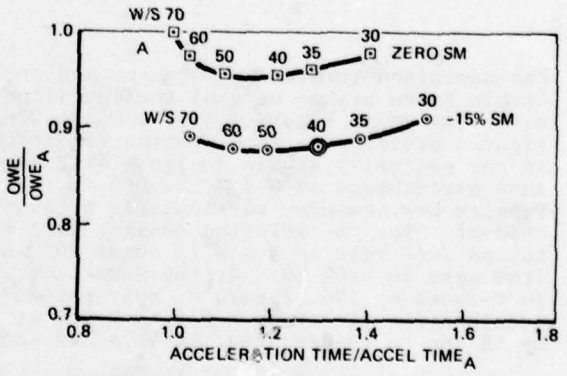

FIGURE 7. EFFECT OF STATIC MARGIN ON OPERATIONAL WEIGHT EMPTY AND ACCELERATION TIME FROM M 0.9 TO M 1.6 AT 30,000 FT

3. REDUCED DIRECTIONAL STABILITY

The current air superiority fighters are utilizing vortex flow to improve lift performance. At high angle of attack, the vortices produce strong cross-flow at aft fuselage which makes it difficult to provide adequate static directional stability. A frequent present solution is to provide large fixed twin verticals with rudders. With the acceptance of static instability in the CCV design approach, automatic stability can be provided by a single all-movable vertical which usually can be smaller in size than one of the fixed twin verticals. The feasibility of this solution depends on adequate control effectiveness of the single movable vertical which wind-tunnel tests have shown to be available up to angles of attack higher than the angle-of-attack limit imposed by the departure prevention considerations. Furthermore, the effectiveness is little affected by the angle-of-attack. This makes the design of this feature of the automatic stabilization fairly simple.

The use of an all-movable vertical reduces slightly drag and weight compared to twin verticals. However, the improvement in performance due to reduced directional stability is much smaller than that due to negative longitudinal stability. The reason for this is that for a practical design, considering such requirements as one engine out or cross-wind landing, the directional stability usually ends up being slightly positive or neutral due to required directional control.

The main advantages of relaxing the static directional stability requirement and of using a single all-movable vertical are the reduced development problems since it is difficult to find a location for the twin verticals with rudders providing adequate static stability and control effectiveness at high angles of attack.

4. STABILITY AND COMMAND AUGMENTATION SYSTEM DESIGN FOR CCV AIRCRAFT

Requirements and Design Techniques

As discussed in preceding sections, significant performance advantages have forced advanced fighter aircraft design towards aerodynamically statically unstable configurations. The feasibility of such designs, however, depends completely on the ability to design, and eventually to demonstrate in flight, automatic Stability and Command Augmentation Systems (SCAS) which would assure good handling qualities for these aircraft. The SCAS becomes as essential an element of the overall aircraft system as the structure.

In design of the SCAS for CCV aircraft, the traditional relationship between the pilot's and SCAS' authority is reversed: For stable aircraft, the SCAS authority was limited and means were provided for pilot's override of malfunctioning SCAS; for unstable aircraft, pilot authority is limited by the SCAS. Pilot commands must be monitored and limited to prevent departure which, depending on the particular aircraft configuration, can be a fatal unrecoverable departure. Also, in the combat engagement of one-on-many, even a recoverable departure may be tactically fatal. The additional requirement for high reliability through redundancy, monitoring and fault-tolerant computer operation stems from the total dependence on a properly functioning SCAS, not only for good flying qualities but also for the basic safety of flight, since these statically highly unstable configurations cannot be flown at all by the pilot without adequate augmentation.

The unstable aircraft-SCAS system is a high order nonlinear dynamic system and does not lend itself easily to traditional linear stability analysis. The objective is to design a departure safe aircraft for arbitrary control inputs so that the pilot can concentrate on combat without monitoring flight instruments. This results in a highly nonlinear control system in addition to nonlinear aerodynamic characteristics and inertial and engine gyroscopic coupling. Experience at Northrop has been in the course of SCAS designs over the last five years, for unstable configurations of conventional and advanced tailless aircraft, to employ to a large extent time domain analysis. A C* criterion (Ref. 1) was found very useful for large maneuvers in general flying. The MIL-F-8785B (Ref. 2) and Neal and Smith frequency domain criteria (Ref. 3) for pilot closed-loop precision tracking task were used to supplement the time domain analysis. The unstable aircraft with SCAS systems designed by this approach were evaluated extensively on the Northrop moving base simulator.

The full authority Fly-by-Wire SCAS design was influenced by several ground rules. Design simplicity was stressed for improved reliability. All the gain scheduling, with one exception, was done with compressible dynamic pressure only. Another design goal was to make closed-loop performance relatively insensitive to changes in CG location, air speed and altitude. For combat maneuvering, excellent high-angle-of-attack performance was provided by using roll-yaw cross-feed. Roll reversal tendency, which results due to high adverse yaw at high angles of attack, was eliminated. The control system parameters were optimized for both general flying and precision tracking with multimode capability to enhance mission performance.

The two most important control design parameters for safe operation of highly augmented unstable aircraft are control surface rate and authority. Both are affected by the following factors:

a. Static Margin
b. Turbulence and Gusts
c. Recovery Moment at α Limit
d. Aerodynamic and Inertia Coupling in Large Combat Maneuvers

Trade studies were conducted to minimize the required control rates and authority resulting from an envelope over the demands created by these factors individually and in combination. Higher rates and deflections increase weight and power demands of primary control system, and thus performance is adversely affected by higher aircraft weight and decrease in engine power available for maneuver.

A departure prevention system is required for safe operation of statically unstable aircraft. The departure may result due to lack of control power available to counteract moments due to inertial and aerodynamic cross-coupling, engine gyroscopic effects and thrust offset. The protection is provided by limiting angle of attack (alpha). The lift and turn rate capability is maximized by using a nonlinear control system to push the alpha limit as high as possible. The system is designed truly for "head-out-of-cockpit" flying so that the pilot can use any combination of control inputs without the danger of ever departing the aircraft. Thus, the pilot can concentrate on air combat rather than having to monitor the instruments. For structural protection, the SCAS limits the maximum load factor that the pilot can command.

A six-degree of-freedom nonlinear large amplitude digital simulation was used to develop and test the control laws. The aero data, modified by static elastic effects, was mechanized without any linearization. For example, lift, drag and moment coefficients were mechanized as three-dimensional functions of angle of attack, elevon position and Mach number. The control system was mechanized with all important nonlinearities such as control surface rate, deflection and hinge moment limits. Engine dynamics and thrust characteristics were mechanized. The pilot and turbulence were also simulated. The selected SCAS configuration was mechanized on Northrop's moving base simulator for pilot-in-the-loop evaluation. The feel system and tracking mode parameters were optimized on the simulator. Excellent Cooper-Harper ratings of 1 and 2 were obtained from test pilots, some of whom have flown the stable YF-17. An interesting conclusion of these investigations of highly augmented systems was that with properly designed SCAS, it is possible to obtain response and good flying qualities which are independent of the aircraft configuration; for example, in Figure 8, the load factor response of the conventional aircraft at the pilot station is compared to that of an advanced tailless aircraft at two different flight conditions. The response is practically identical, and depends only on the degree of static instability, which in this case was -15%. These responses were obtained with pilot-in-the-loop. The effect of negative static margin on improving the load factor response is shown in Figure 9.

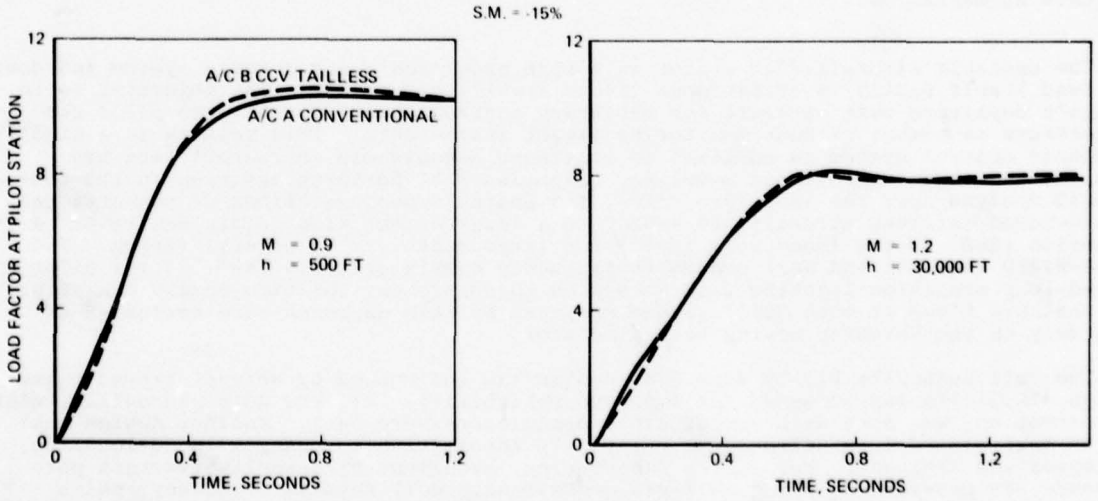

FIGURE 8. COMPARISON OF DYNAMIC RESPONSE WITH PILOT-IN-THE LOOP

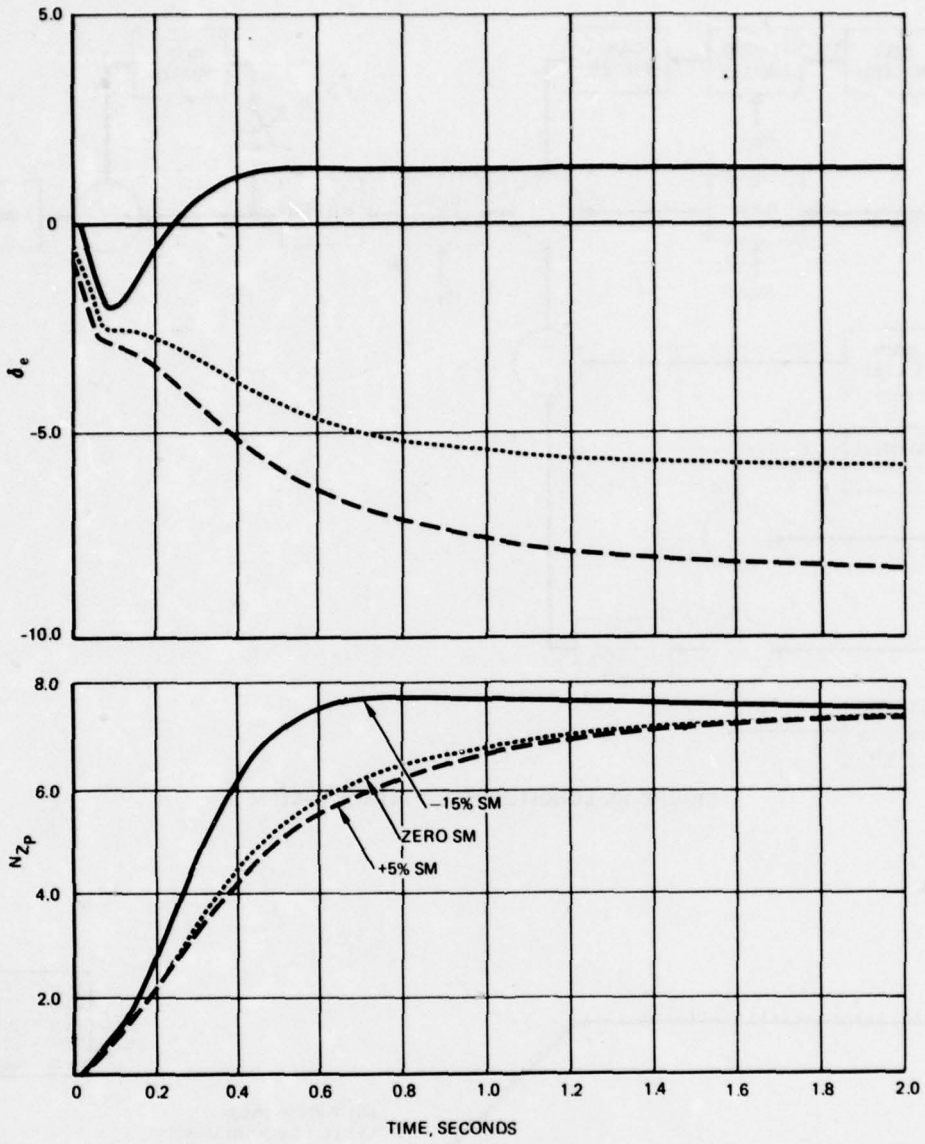

FIGURE 9. EFFECT OF STATIC MARGIN ON RESPONSE AT M 0.9, 500 FT

Longitudinal Control System

The block diagram for the longitudinal control system with departure prevention feature is shown in Figure 10. The pitch rate and normal acceleration feedback are normally used. When the angle of attack exceeds the specified bias, the difference between the two is also used as feedback to provide angle of attack limiting. The bias value is modified as a function of body rates to compensate for inertial cross-coupling. The filtered pitch control surface position is added to the angle of attack feedback to provide a lead effect. Nonlinear gains used in the departure prevention system maximize performance. A fast forward loop integrator provides neutral speed stability. It automatically compensates for elevon trim changes due to changes in airspeed or altitude. Also, with a forward loop integrator and with the proper blend between pitch rate and normal acceleration feedbacks, relatively constant stick force per G is obtained for the entire flight envelope as shown in Figure 11. The control system provides fast and well-damped responses, as illustrated in Figure 9.

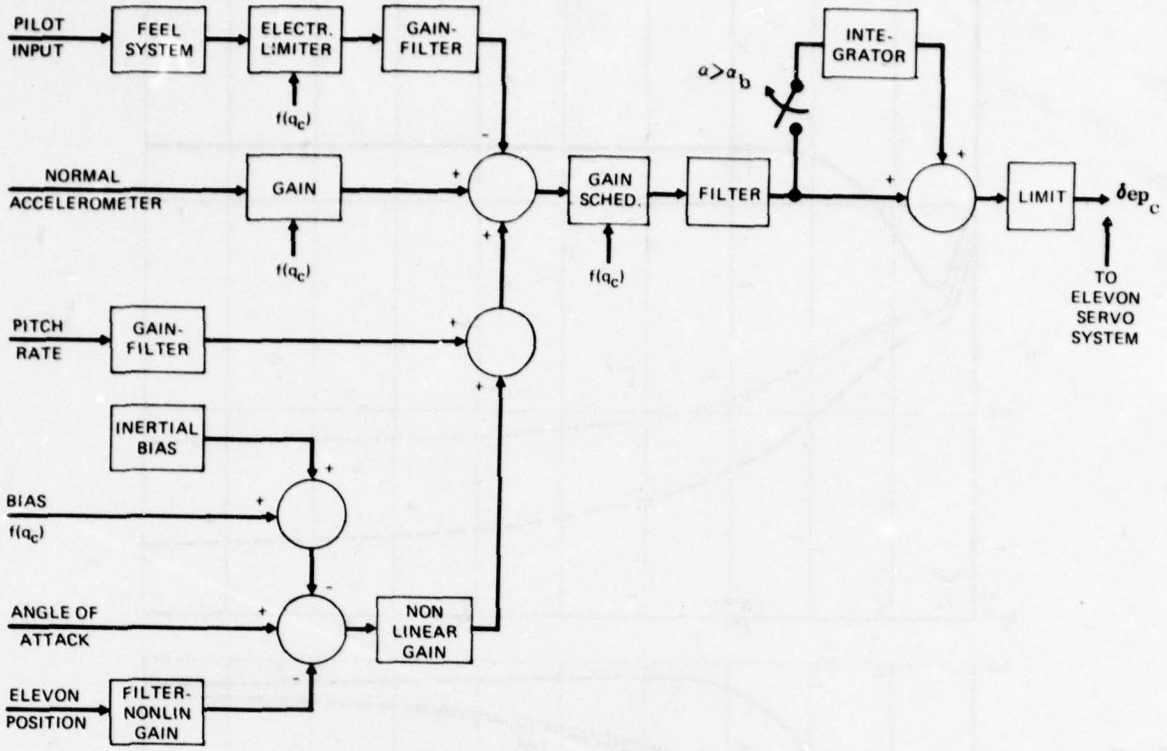

FIGURE 10. LONGITUDINAL CONTROL SYSTEM

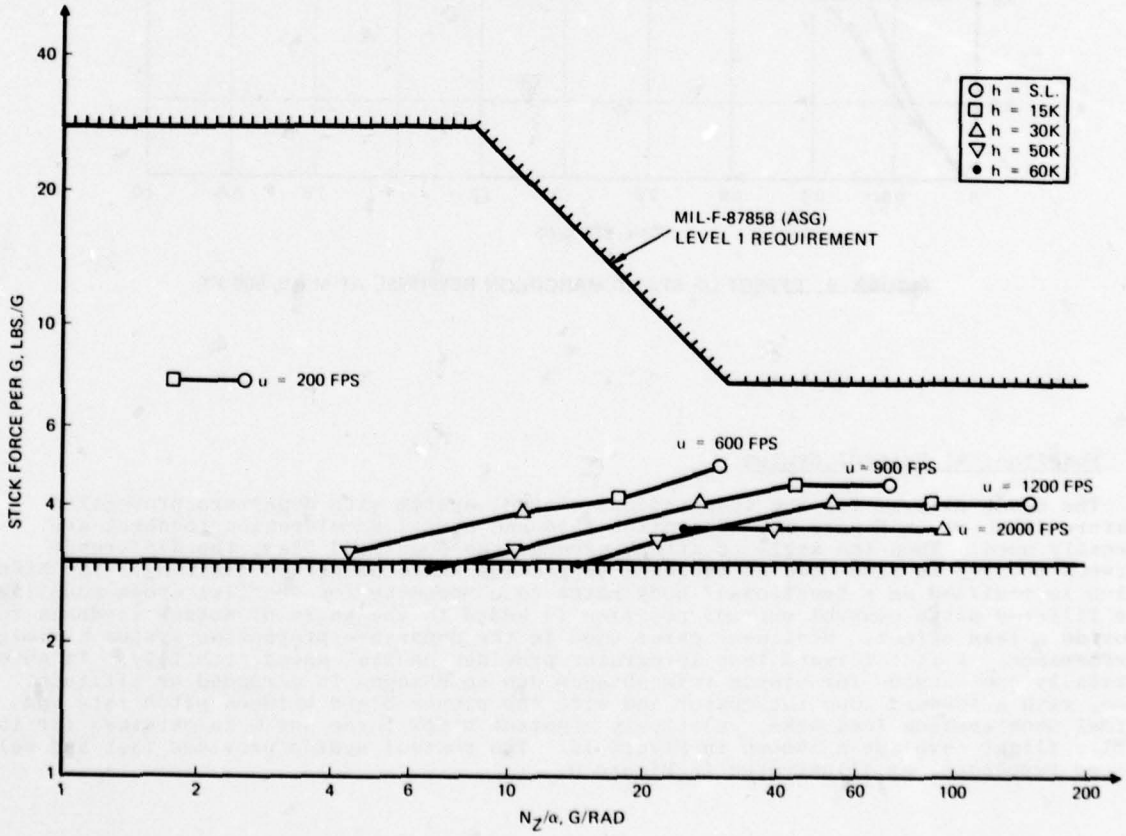

FIGURE 11. STICK FORCE PER G WITH NOMINAL GAINS

Figure 12 shows the short-period frequency, as a function of N_z/α , for representative flight conditions. Again, the specification requirements are easily satisfied. The short-period damping at all flight conditions was greater than 0.5. The requirement is for minimum damping of 0.35. The control system parameters are scaled such that the maximum load factor that a pilot can command is limited to 11 G.

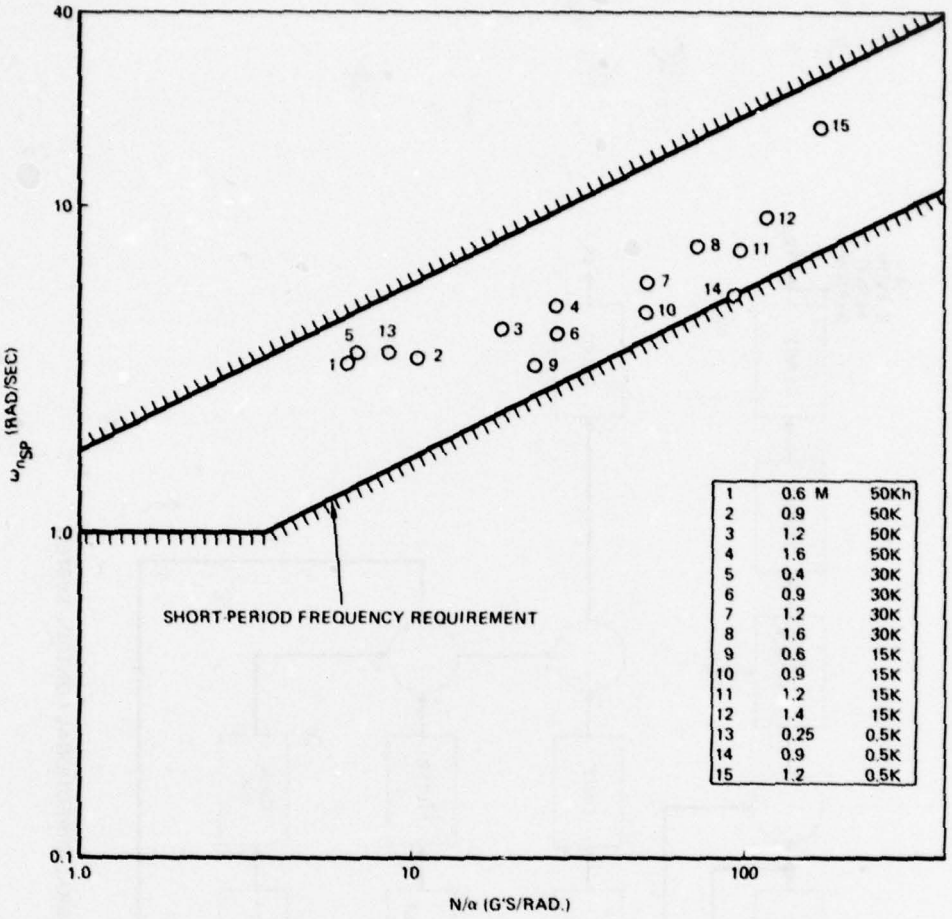

FIGURE 12. SHORT PERIOD FREQUENCY

Lateral Directional Control

The lateral-directional control system block diagram is shown in Figure 13. The roll system uses roll rate gyro feedback and forward loop scheduling with q_c. The yaw damping is provided by using yaw rate feedback. Lateral acceleration modified with a gravity term feedback is used to limit sideslip and side force excursions. The roll-to-yaw crossfeed is provided by using roll stick position and angle of attack. The gains are scheduled with compressible dynamic pressure, q_c. This control system provides excellent lateral-directional performance even at the high roll rates which are typical of this aircraft configuration. Figure 14 shows the time required to roll through 90 degrees and the peak sideslip excursions with maximum roll stick input. The results are shown as a function of Mach number for altitudes ranging from 500 feet to 50,000 feet. The performance exceeds specification requirements at all flight conditions. In the air combat regime, roll rates up to 380 degrees per second are achieved but the sideslip excursions are still less than 2 degrees. The dutch-roll damping and frequency are shown in Figure 15 for representative flight conditions. Again, the specification requirements are exceeded.

The elevon servo system and pitch-roll mixing are shown in Figure 16. Note that at high angles of attack more authority is provided for pitch control. This is to ensure that sufficient control power is available for recovery from stall.

Control System Evaluation

The control system parameters were adjusted to minimize roll to pitch coupling at high angles of attack. Maximum roll rate maneuvers were examined at high G trim conditions to ensure that the resulting load factor structural limits were not exceeded, as shown in Figure 17.

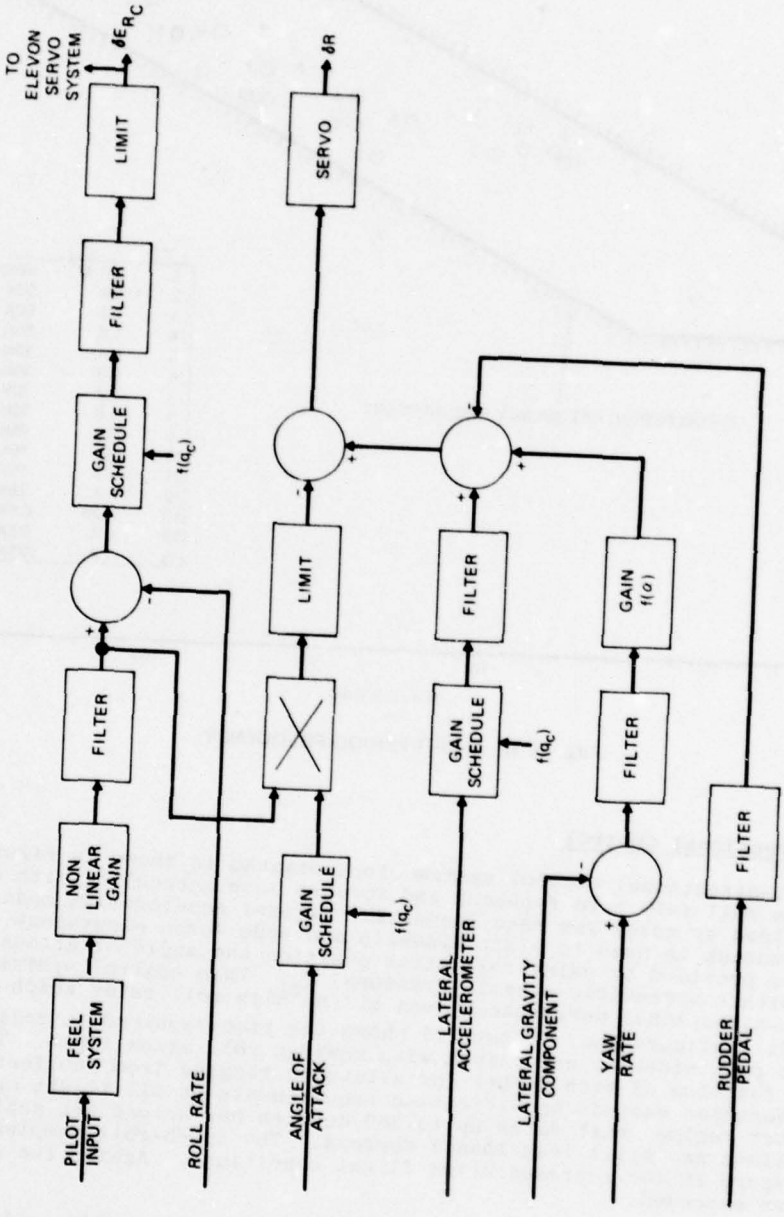

FIGURE 13. LATERAL-DIRECTIONAL CONTROL SYSTEM

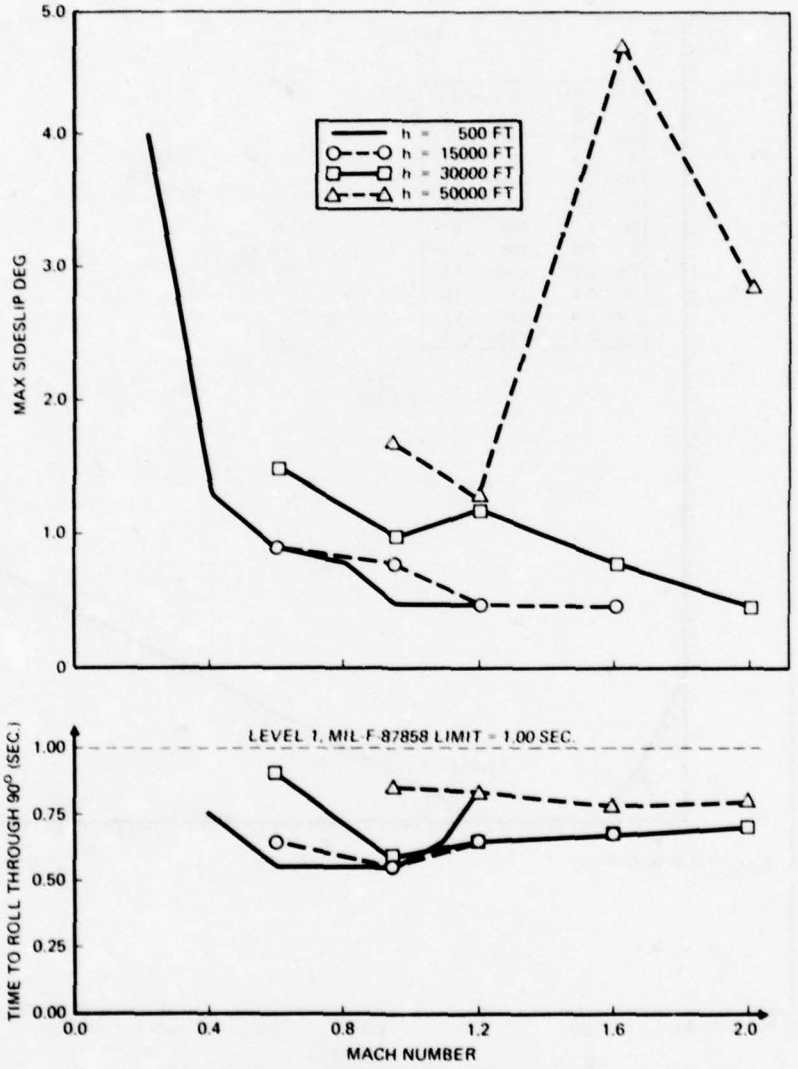

FIGURE 14. PEAK SIDESLIP EXCURSION AND TIME TO ROLL THROUGH 90 DEGREES MAXIMUM ROLL STICK INPUT AT 1 G

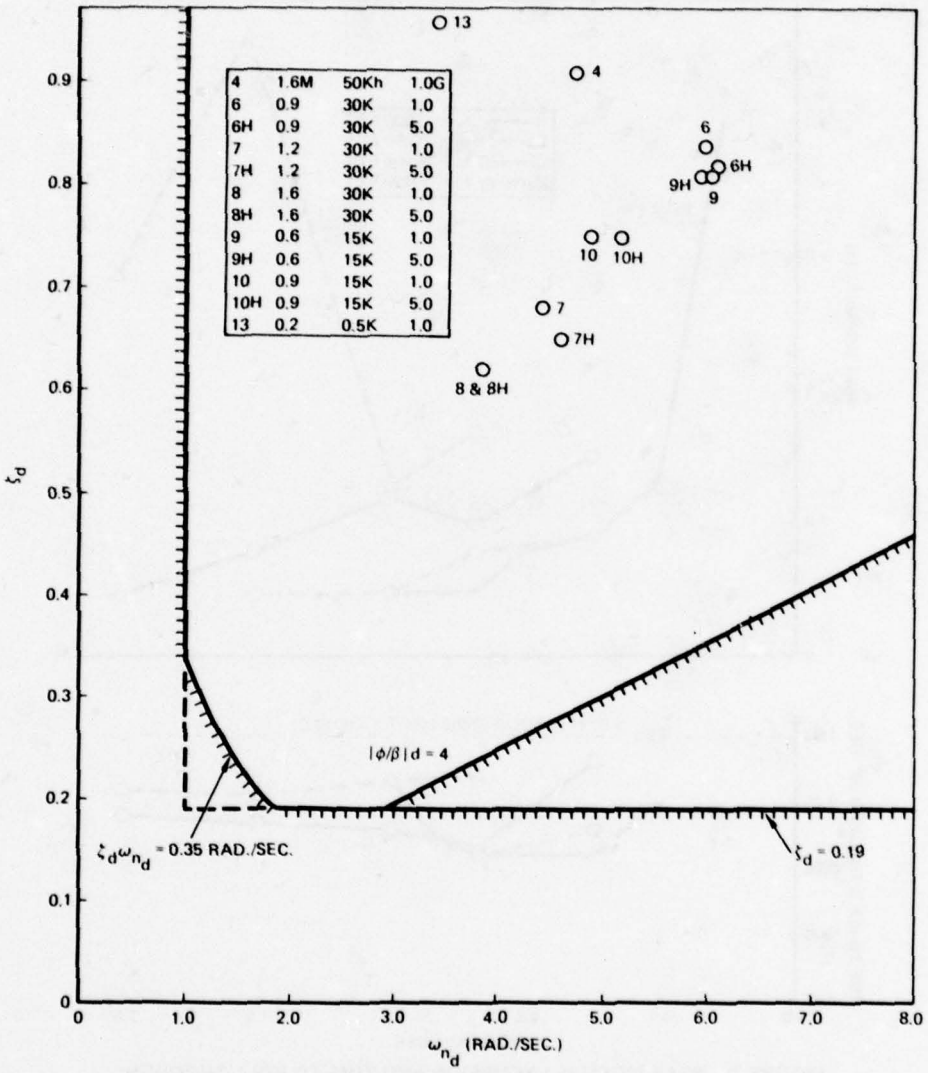

FIGURE 15. DUTCH ROLL DAMPING AND FREQUENCY

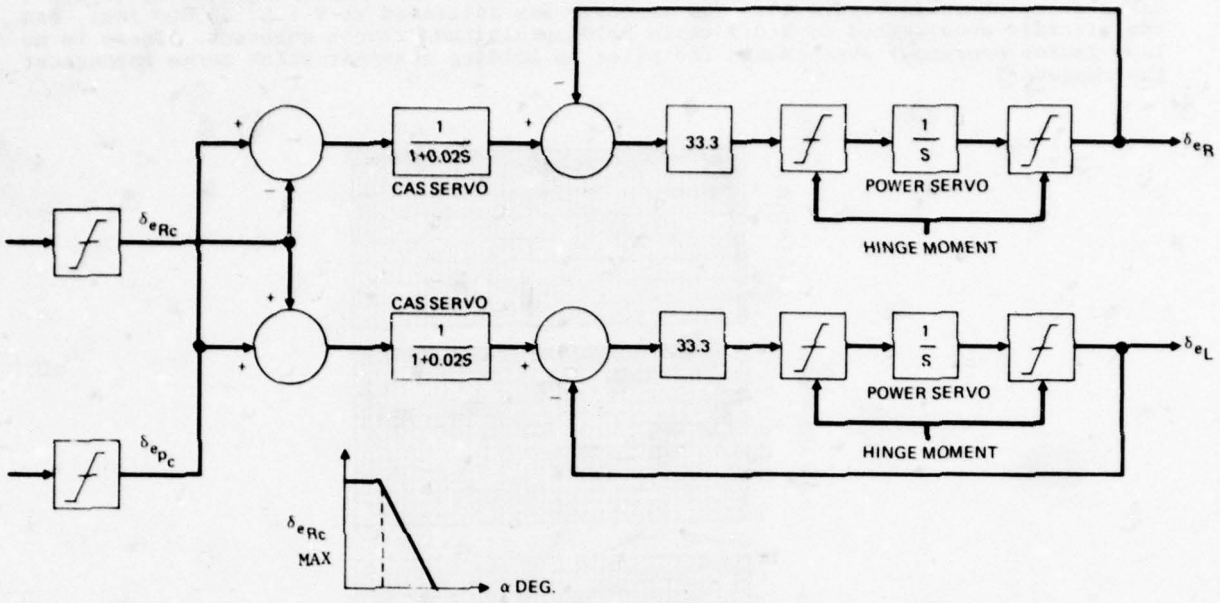

FIGURE 16. ELEVON SERVO SYSTEM AND PITCH-ROLL CONTROL MIXING

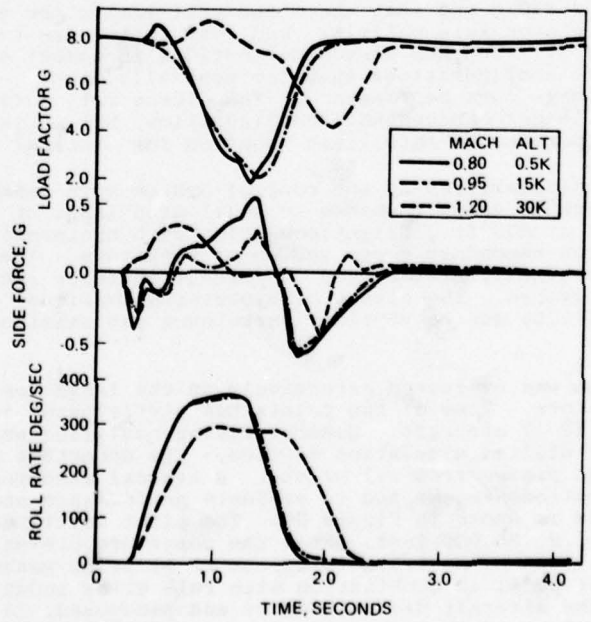

FIGURE 17. MAXIMUM ROLL RATE MANEUVER AT 8G TRIM

The system provides excellent protection against the load factor overshoots which generally occur when decelerating from the supersonic to subsonic region due to the large change in elevon trim condition. A typical five G decelerating wind-up turn maneuver is shown in Figure 18. The maneuver was initiated at M 1.2, 30,000 feet, and the aircraft decelerated to M 0.7 while holding altitude almost constant. There is no load factor overshoot even though the pilot is holding constant stick force throughout the maneuver.

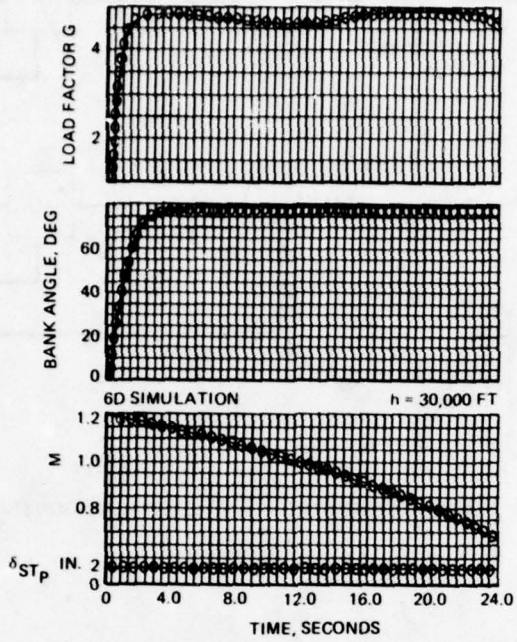

FIGURE 18. 5G DECELERATING WIND-UP TURN

The evaluation studies were conducted in the presence of turbulence and discrete gusts to ensure that the load factor activity at the pilot station is acceptable and that sufficient control power is available for safe operation. The load factor excursions due to 80-foot-per-second discrete gusts are listed in Table I for neutrally stable and 15 percent unstable configurations. Note that there is not much difference between the two configurations and that the structural limits are not exceeded. The RMS elevon deflection, elevon rate activity, and load factor due to vertical turbulence are summarized in Table II. The RMS elevon deflections in combat conditions, although higher for -15% unstable configurations than for neutrally stable, are small and would not affect adversely combat turn performance. The elevon rate activity is about two to three times higher for 15 percent unstable configuration, but it is not significant compared to the 90-degree-per-second rate limit required for critical stability conditions.

The effects of nonlinearities in the control system were examined and were found to be negligible. Figure 19 shows response to small step input at worst case (high dynamic pressure, M 1.1 at 500 ft.) flight condition with hysteresis, 0.05 degree to peak, between each elevon secondary servo and power actuators. The results are given for 5 percent stable, neutrally stable, and 15 percent unstable configurations. There are no sustained limit cycles. The effect of hysteresis amplitude on RMS load factor and control surface activity due to vertical turbulence was examined and found insignificant.

The control system was evaluated extensively on the large amplitude moving base simulator by current pilots. Some of the pilots had participated in simulator and flight test evaluation of the YF-17 aircraft. General flying qualities were found to be excellent as predicted by digital simulation studies. The departure prevention feature, in particular, drew high praise from all pilots. A typical maneuver which pilots used to test departure prevention systems and to evaluate performance and handling qualities at high angles of attack is shown in Figure 20. The pilot initiated vertical climb maneuver starting at M 1.2, 35,000 feet. When the departure prevention system took over at low dynamic pressure, the pilot tried to oppose it by using maximum pitch stick. He also applied full rudder pedal in combination with roll stick input which he cycled from one stop to another. The aircraft did not depart and recovered. A maximum pull-up maneuver followed by maximum roll stick input is shown in Figure 21. The maneuver was initiated at M 1.2, 30,000 feet, with full-aft stick input which resulted in about 11 G load factor. The maximum roll-stick input was applied when dynamic pressure dropped to 140 psf and was left in. The aircraft performed 4.5 successive 360-degree rolls without

TABLE I. RESPONSE TO 80 FPS DISCRETE GUST
(PER MIL-F-8785B)

FLIGHT CONDITION			S.M. 0	-15%
MACH NO.	ALTITUDE 1000 FT	N_z TRIM G	MAX G MIN G	MAX G MIN G
.2	.5	1	1.6 0.4	1.9 0.1
.9	.5	1	2.7 -0.7	3.4 -1.5
1.1	.5	8	10.2 5.7	10.9 4.8
.9	30	1	1.5 0.6	2.7 0.3
.9	30	5	5.4 4.3	5.6 4.2
1.2	30	5	5.3 4.6	5.6 4.3

TABLE II. RMS ACTIVITY DUE TO VERTICAL TURBULENCE WITH PROBABILITY OF EXCEEDANCE = 0.01

MACH NO.	ALTITUDE x 10^{-3} FT	RMS ACTIVITY, CG = 28.5 %			RMS ACTIVITY, CG = 43.5 %		
		$\Delta\delta_h$ DEG	$\dot{\delta}_h$ DEG/SEC	N_{ZP} G	$\Delta\delta_h$ DEG	$\dot{\delta}_h$ DEG/SEC	N_{ZP} G
0.2	0.5	0.44	2.2	0.07	1.3	6.8	0.12
0.6	0.5	0.20	4.5	0.18	0.45	11.1	0.25
0.9	0.5	0.12	3.1	0.24	0.28	9.1	0.38
0.6	15.	0.13	1.9	0.07	0.23	4.7	0.09
0.9	15.	0.07	1.4	0.08	0.13	4.1	0.13
0.6	30.	0.17	1.7	0.04	0.25	4.3	0.06
0.9	30.	0.08	1.0	0.05	0.11	2.5	0.09
1.2	30.	0.12	1.4	0.07	0.11	2.6	0.11

NOTE : $\Delta\delta_h$ = STABILIZER DISPLACEMENT ABOUT TRIM CONDITION

$\dot{\delta}_h$ = STABILIZER RATE ACTIVITY

N_{ZP} = INCREMENTAL NORMAL ACCELERATION AT PILOT STATION

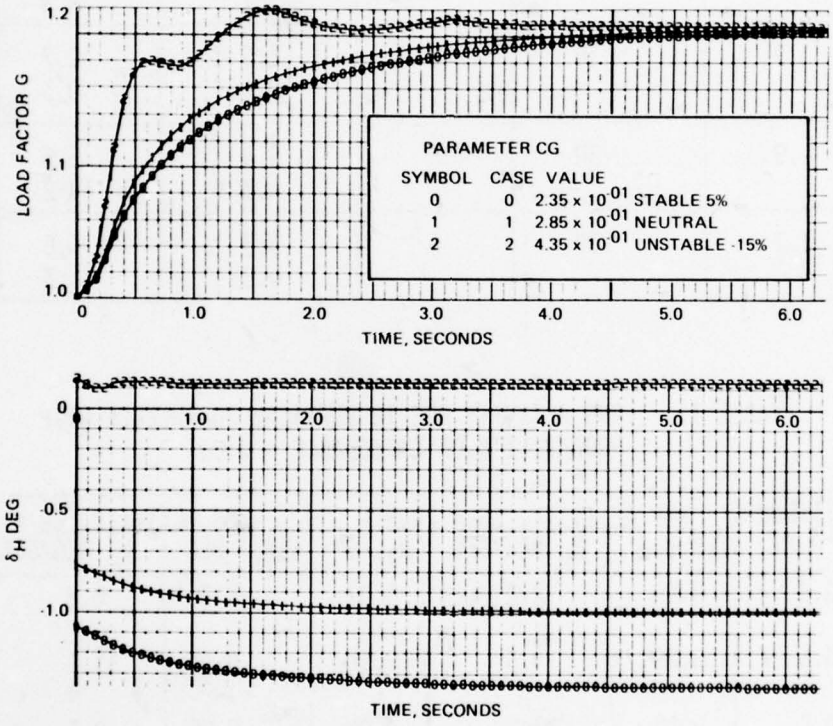

FIGURE 19. EFFECT OF 0.05 DEGREE PEAK-TO-PEAK HYSTERESIS BETWEEN SECONDARY AND POWER SERVOS ON STEP RESPONSE AT M1.1, 500 FT

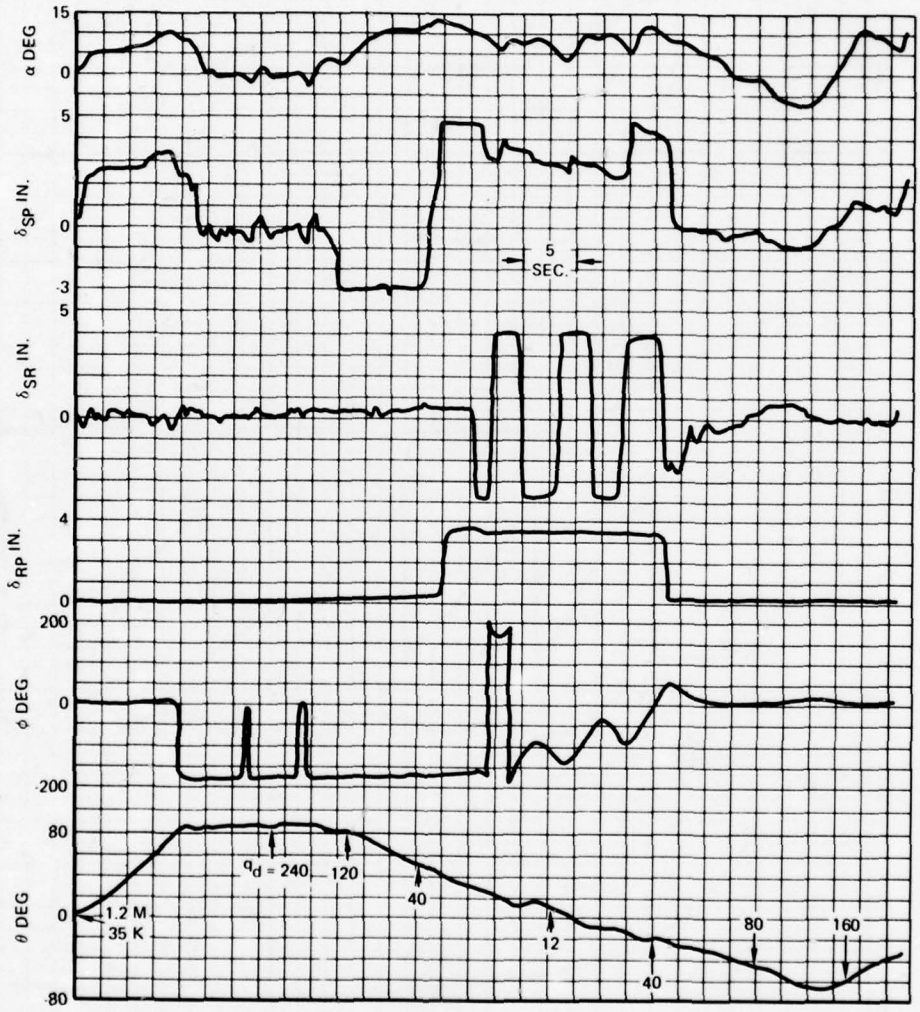

FIGURE 20. VERTICAL CLIMB MANEUVER FOLLOWED BY PITCH STICK, ROLL STICK, AND RUDDER PEDAL INPUTS

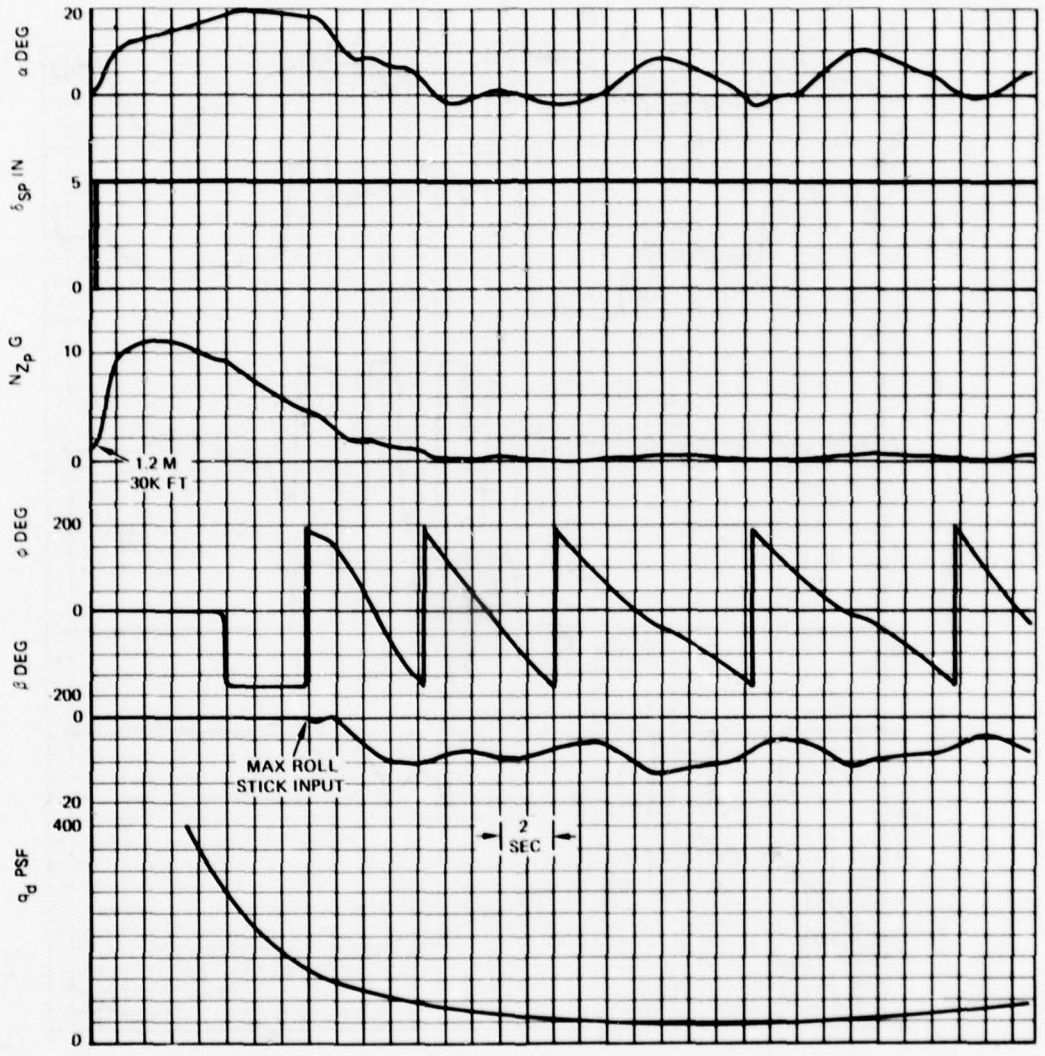

FIGURE 21. MAXIMUM PULL-UP MANEUVER, INITIATED AT M1.2, 30,000 FT FOLLOWED BY MAXIMUM ROLL STICK INPUT

any tendency to depart. During the maneuver, the dynamic pressure dropped down to 30 psf but the sideslip excursion did not exceed 13 degrees. The Figure 22 shows a typical low speed stall maneuver. The pilot used pitch and roll stick inputs and commanded about ±50 degrees bank angle changes. The angle of attack was limited to about 15 degrees and the aircraft recovered when the pilot removed the control inputs.

The precision-tracking-mode parameters were optimized on the simulator. Generally, 25 to 50 percent higher pitch rate and roll rate gains, compared to those used for general flying, were found to be more optimum. No other control system changes were necessary. The pilots reported excellent tracking performance. Even at close range, both pitch and roll damping were adequate with no PIO tendency. An on-line computer program was used to calculate average and RMS tracking errors and average range to target for each 10-second interval. These statistical measurements were used for optimizing tracking mode parameters. Typical statistical performance results are shown in Figure 23. The tracking errors are small, usually less than 4 mil RMS, except when target is executing a roll-reversal maneuver from 5 G left to 5 G right. An extensive air combat simulation has been recently conducted on the Northrop moving base simulator in which the pilot was engaged in a gun fight with an interactive target. This target, computer controlled, takes defensive as well as offensive action. The resulting maneuvering was very realistic with the aircraft driven to its performance limits. In a total of more than 500 combat engagements, flying the 15-percent unstable tailless delta aircraft, not a single departure has occurred.

Control Power Requirements

The control power requirements were investigated by subjecting the aircraft to the following:

1. Limiting level-probability of exceedance 10^{-5} of turbulence and discrete gusts as specified by MIL-F-9490D. (Ref. 4)

2. Large-amplitude maneuvers, resulting in stall and recovery from stall, by using a combination of pitch stick, roll stick and rudder pedal inputs.

3. Large check-pitch maneuvers used for testing structural integrity of the airplane.

The maneuvering in turbulence and large stall recovery maneuvers were investigated on the simulator with pilot-in-the-loop. The control surface rate and travel authority requirements for flight in turbulence were highest during simulated landing (approach and flare), and they were very sensitive to approach and landing airspeed. With a design touchdown speed of 110 knots, the elevon rate authority of ±90 degrees per second and travel authority of ±30 degrees were required to prevent any uncontrolled departures and oscillations. With a stable airplane, ±30 degrees per second rate authority should be sufficient. These authority limits were found to be just adequate for large maneuvers which resulted in stall and subsequent automatic recovery by the control system with pilot purposely trying to oppose it. Generally, the control power requirements were highest for maneuvers resulting in low dynamic pressure and employing idle power with speed brake (or maximum power with thrust reverser) and maximum control inputs (pitch stick, roll stick, and rudder pedal). A typical maneuver, as illustrated in Figure 20, consisted of vertical climb maneuver starting with supersonic airspeed and low angle of attack with maximum use of all three control inputs at very low dynamic pressure.

The discrete gust and check-pitch structural test maneuvers were evaluated by using a digital simulation. The rate requirements to counteract a discrete gust were found to be low, less than 30 degrees per second. The authority requirements for check-pitch maneuvers were found to be comparable to those demanded by large stall recovery maneuvers.

Limitations to Negative Longitudinal Stability

For the tailless delta configuration, discussed in this paper, 15% negative static margin realizes maximum possible combat performance. However, for some conventional configurations, performance improvement continues well beyond -15% SM, particularly at supersonic speed. Therefore, from purely performance point of view, even further aft CG locations may be desirable. There are, however, the following practical design aspects to be considered:

a) Response limitations of electro-hydraulic actuators. High gain associated with high negative static margin will eventually lead to hardware instability.

b) Excessive rate demand on control surfaces results in higher hydraulic system weight and drain on engine power.

c) Coupling with structural modes may occur.

d) Maximum automatic angle of attack limit, to prevent departure, will be lower with increasing negative static margin.

The trade-off studies of these considerations resulted in selecting -15% SM as a reasonable practical limit.

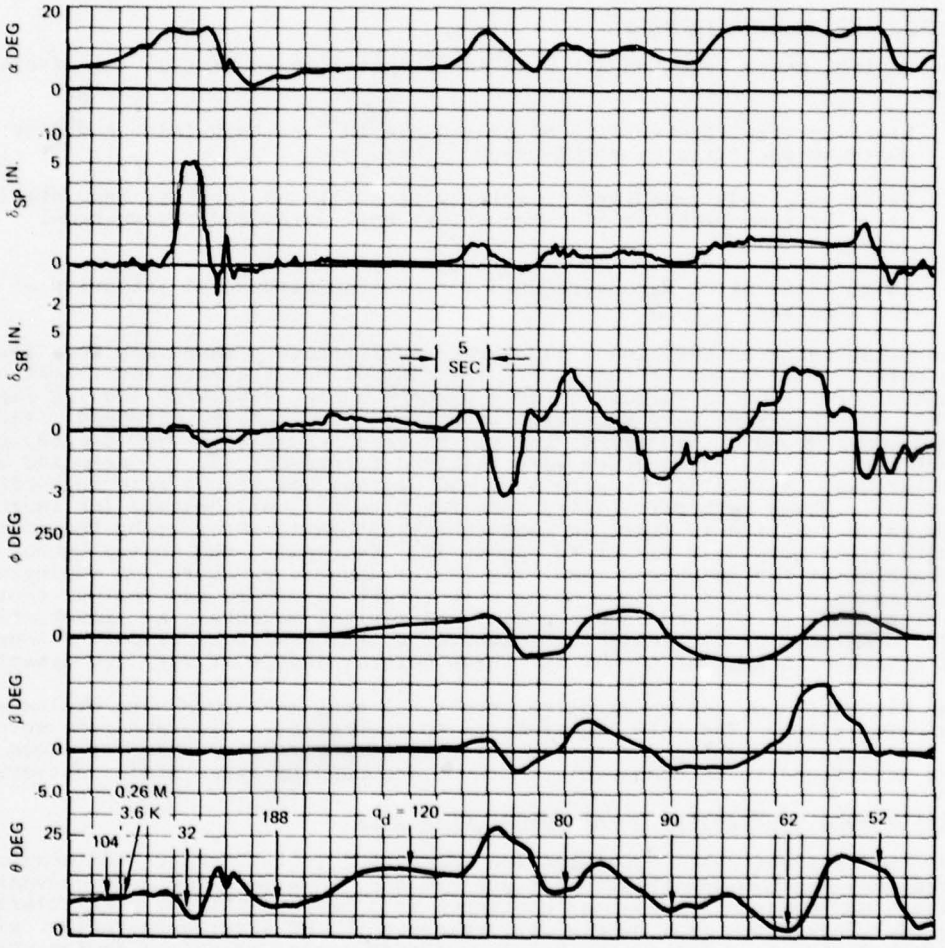

FIGURE 22. LOW SPEED STALL MANEUVER

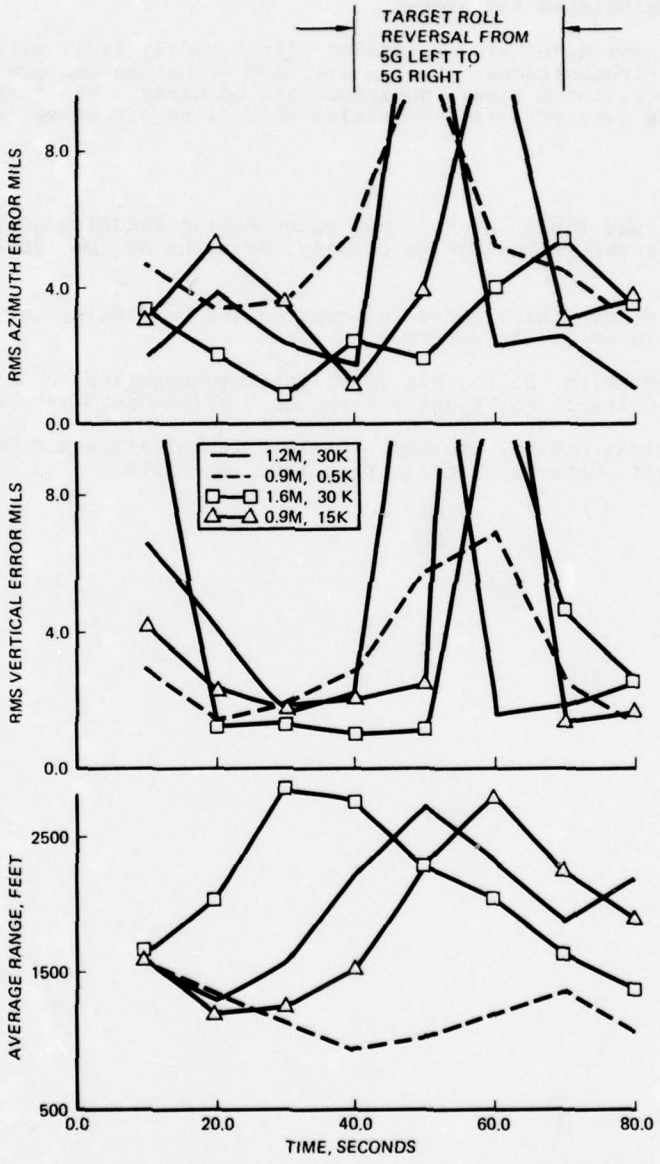

FIGURE 23, TRACKING MODE STATISTICAL PERFORMANCE SUMMARY

5. CONCLUSIONS

The CCV concept of negative longitudinal static stability provides very large improvements in combat performance in terms of sustained turn rates in the combat arena. At the same time, these performance gains are obtained with aircraft and fuel weights much lower than for the statically stable aircraft designed for the same mission.

The realistic design limit for negative static stability level has been established as -15%. At this limit, the tailless configuration realizes its full potential performance.

The feasibility of designing practical full-authority FBW SCAS providing excellent handling qualities in general flying and tracking, for 15 percent statically unstable advanced technology tailless aircraft, has been demonstrated by using digital simulation techniques and pilot-in-the-loop simulator evaluation. The design and evaluation techniques have been established and proven.

The departure-prevention system enabled pilots to fly truly with "head-out-of-cockpit" under all circumstances. During over 500 combat encounters on the Northrop moving base simulator, not a single departure has occurred. The target was computer-controlled employing very effective defensive as well as offensive tactics.

REFERENCES

1. Malcolm, L. G. and Tobie, N. N., "New Short Period Handling Quality Criteria for Fighter Aircraft," The Boeing Company, Document No. D6-17841 T/N, October 1965.

2. Chalk, C. R., et al, "Background Information and User Guide for MIL-F-8785B (ASG)," AFFDL-TR-69-72, August 1969.

3. Neal, T. P. and Smith, R. E., "An In-Flight Investigation to Develop Control System Design Criteria for Fighter Airplane," AFFDL-TR-70-74, June 1970.

4. MIL-F-9490D Flight Control Systems - Design, Installation and Test of Piloted Aircraft, General Specification for, June 1975.

LATERAL STABILITY AT HIGH ANGLES OF ATTACK, PARTICULARLY WING ROCK

by

A. Jean Ross

Flight Systems Department
Royal Aircraft Establishment,
Farnborough, Hampshire, England

SUMMARY

The Gnat aircraft exhibits wing rock at high subsonic Mach numbers, but the onset of wing rock is delayed to higher angles of attack if fuel tanks are carried on the wings. Flight responses of Dutch roll and wing rock oscillations in steady turns have been analysed to give the variation of the stability derivatives with angle of attack at various Mach numbers for both aircraft configurations, and the results show that the onset of wing rock occurs when the damping of the Dutch roll mode is zero, due mainly to loss in damping-in-roll derivative at high angle of attack. The stability derivatives from flight tests are compared with wind tunnel results, and show the same trends with angle of attack. The values of the linear derivatives have been used as a basis for evaluating the effects of various added aerodynamic nonlinearities, both to explore the possible mechanisms for the limit cycle type of wing rock responses, and to calculate the changes in response due to an idealised stability augmentation system.

LIST OF SYMBOLS

AXES	A geometric-body system of axes is used, with x-axis forward along the fuselage datum, and z-axis down. Origin is at the mean CG position
a_1, b_1, c_1, d_1	coefficients of lateral stability quartic
a_3, b_3, c_3, d_3	coefficients of cubic terms
a_y, a_z	lateral and normal accelerations
b_x, b_z	$(I_y - I_z)/I_x$, $(I_x - I_y)/I_z$
C_N	coefficient of normal force
C_ℓ, C_n	rolling and yawing moment coefficients
e_x, e_z	I_{xz}/I_x, I_{xz}/I_z
$Ep, Er, E\beta, Ea_y$	off-set errors in instruments recording p, r, β, a_y
g	acceleration due to gravity
g_2, g_3	$g \sin \Theta_e$, $g \cos \Theta_e \cos \Phi_e$
h	height
i_x, i_z, i_{xz}	non-dimensional inertia coefficient, I_x/ms^2 , etc
I_x, I_y, I_z	moments of inertia in roll, pitch and yaw
I_{xz}	product of inertia
k_D, k_R	damping index of Dutch roll and roll subsidence
$K_{p\xi}, K_{r\zeta}$	roll/aileron and yaw/rudder gearings
ℓ_v, ℓ_p etc	rolling moment derivative due to sideslip, roll rate etc
ℓ_{v1}, ℓ_{v3} etc	nonlinear rolling moment coefficients due to sideslip etc
m	aircraft mass
M	Mach number
n_v, n_p etc	yawing moment derivative due to sideslip, roll rate etc
$n_{v_{dynamic}}$	$n_v - (i_z/i_x)\ell_v \sin \alpha$
p,q,r	rate of roll, pitch, yaw
S	reference wing area
s	semi-span of wing
$\hat{t}$	aerodynamic unit of time, $m/\rho SV$
v	sideslip velocity
V	aircraft velocity
x_1, y_1, z_1	position of lateral accelerometer
x_3, y_3, z_3	position of sideslip vane
y_v, y_p etc	sideforce derivative due to sideslip, roll rate etc
α	angle of attack
β	angle of sideslip
ζ	rudder angle

ζ_D	damping ratio of Dutch roll mode
λ	local damping factor
Θ	pitch attitude angle
ρ	relative density, $m/\rho Ss$
ξ	aileron angle
μ_2	air density
τ_R	time constant of roll subsidence mode
Φ	bank angle
Ψ	heading angle
ω	local frequency
ω_D	frequency of Dutch roll mode
Suffices, etc	(applied to arbitrary letter X)
X_e	steady state value in turn
X_{eff}	effective value of derivative
$\overset{\circ}{X}$	derivative in dimensional form, divided by appropriate mass or inertia
X_s	steady value in limit cycle
X^*	nonlinear equivalent of linear quantity

1 INTRODUCTION

It is now well-known[1,2] that many combat aircraft do not have satisfactory handling qualities at the flight conditions needed for superiority in combat, at high angle of attack/high subsonic Mach numbers, and that adverse lateral behaviour, such as nose slice, roll off, or wing rock often limit the potential manoeuvre performance. In order to alleviate these handling problems, the aircraft designer needs to know which parameters are significant, and then to find means of keeping these parameters within design limits, either by aerodynamic or control system features. Two such criteria are extensively used[3], $C_n(\beta)_{dynamic}$, and LCDP, and zero values of these are usually associated with departure conditions. The significant parameters for the occurrence of wing rock are not so well defined, and it seems that the phenomenon may be due to any of several different mechanisms, depending on the particular aircraft. For the Phantom, $C_n(\beta)_{dynamic}$ is zero near the onset of wing rock and the pitching moment due to sideslip also seems significant[4], while oscillatory rolling moments have been measured on wind tunnel models of Harrier[5] at angles of attack and Mach numbers corresponding to the occurrence of wing rock in flight. From the work to be described in this Paper, the wing rock of the Gnat aircraft is shown to be the dynamically unstable Dutch roll mode, the loss of damping being caused by the large changes in damping-in-roll derivative with angle of attack.

The Gnat has been particularly useful as a test aircraft, in that the flight behaviour depends on the configuration, the onset of wing rock being delayed to higher angles of attack at given Mach number if the slipper fuel tanks are carried on the wing. The aircraft was flown in the two configurations, clean and tanks on, to obtain Dutch roll and wing rock responses in steady turns throughout the angle of attack and Mach number ranges, and these responses have been analysed to give the variation of derivatives with angle of attack. The test programme and results are described and discussed in section 2, where the analysis is confined to lateral responses which can be represented by linear aerodynamic derivatives. This analysis covers only the Dutch roll responses, and the onset and the initial growth of wing rock. The values of the derivatives identified from the flight records are compared with wind tunnel results, and used to study theoretically the effects of a roll damper on the responses.

In common with other combat aircraft, the wing rock of the Gnat is limited at finite amplitude, rather than diverging continuously, particularly at the lower Mach numbers, indicating that nonlinear forces and/or moments become significant. Some possible forms of nonlinearities are considered in section 3, the aims being to reproduce theoretically the wing rock type of response, and to see if such nonlinearities affect the efficiency of stability augmentation systems. Responses have been computed, and an approximate analysis method applied to highlight the important parameters.

2 WING ROCK OF GNAT AIRCRAFT

2.1 Flight tests and analysis techniques

A Gnat aircraft was used for the flight tests, the GA being shown in Fig 1, with tanks on. The leading geometric data are given in Table 1, and the CG is taken to be at a mean position of $0.23\bar{c}$, the change during flight being only $\pm 0.008\bar{c}$.

The flight variables recorded were h, V, α, β, a_y, a_z, p, r and ξ, with q and ζ also in the later flights. (The space available in the rear cockpit for experimental instrumentation is very limited, so some compromises had to be made, to allow for a parallel research programme on the aircraft.) The pilot's instrumentation was standard, with the addition of α and β presentation from independent vanes, as sideslip had to be monitored, and lateral responses with angle of attack held constant were required. These lateral responses were either induced by a rudder pulse (followed by aileron doublet in the later flights) applied during steady turns at various g-levels and various constant Mach numbers for the Dutch rolls, or obtained without deliberate lateral inputs for the wing rocks, at the higher angles of attack. The steady

turns (which had to be diving to maintain the higher Mach numbers), were executed at mean heights of 24K, 30K and 36K ft for the clean aircraft, and 30K ft for the aircraft with tanks on.

Typical flights records of a Dutch roll oscillation in buffet, and wing rock onset are shown in Fig 2a&b, for the clean aircraft. The example of Dutch roll is taken from the last series of flight tests, when the pilot was asked to apply an aileron doublet after the rudder pulse, so the roll subsidence mode is apparent in the roll rate response. The yaw rate and roll rate are plotted to the same scale, to show more clearly the predominance of roll. The wing rock at this Mach number was preceded by a definite wing drop (Fig 2b), and the resulting divergent oscillation led to large roll rates after 3 or 4 cycles, so that the pilot reduced angle of attack to regain control. The developed wing rock, where the initially divergent oscillation becomes one of near-constant amplitude, is discussed later in section 3.

For the aircraft with tanks on, the achievable angle of attack is limited by a longitudinal motion described as porpoising by the pilots, with 'untidy' wing rock superimposed at the higher incidences, shown in Fig 3. The roll rate record does not show a regular oscillation, and is of relatively small amplitude, whereas the pitch rate record shows a periodic response. As the angle of attack is increased further, the lateral oscillation is more apparent (but not periodic), and the longitudinal oscillations have large amplitudes. Unfortunately, the traces for pitch rate and angle of attack reached their limits, so normal acceleration is also shown in Fig 3, to indicate the changes from the nominally steady flight condition.

Examination of the flight records showed that the angle of attack at which wing rock occurs on the clean aircraft is a function of Mach number (Fig 4), but with no measurable dependence on altitude. The characteristics of the oscillatory responses were also derived from the portions of record with no control inputs, to give period, damping, amplitude ratios, and phase angles of Dutch rolls and wing rocks. The results are discussed in the next section, and indicate that the wing rock motion is closely related to the Dutch roll oscillation, and so the mathematical model chosen to represent the response was based on small perturbation lateral motion about the steady turning flight path, with linear aerodynamic derivatives. The values of these derivatives were identified using the simplest Output Error Method of Weighted Least Squares[6]. (Some responses were also used with a computer program based on Maximum Likelihood, giving similar results.) The equations of motion are given in Appendix A1, together with the mathematical model of the instrument readings, and some discussion on applying the programs.

2.2 Results and discussion

The results from the analysis of the flight records are described fully in Ref 7*, and only those derivatives of prime importance to the lateral stability are discussed here, *ie* moment derivatives due to sideslip and rate of roll. The sideforce derivatives are either well-behaved or negligible, and the moments due to yaw rate do not have large effects at high angles of attack. The flight values of the derivatives are first compared with wind-tunnel results obtained from 1/6-scale models of the Gnat aircraft[8,9], and then the results are used to evaluate the lateral stability characteristics.

2.2.1 Moments due to sideslip

The results for ℓ_v and n_v from flight, static tunnel tests and oscillatory rig tests are shown in Fig 5a-d. The mean Mach numbers chosen for the flight values, 0.7 and 0.8, are the same for the clean aircraft and with tanks on, but the ranges of Mach number about the mean are slightly different. A mean line has been drawn through each set of flight results, using twice the standard deviation for guidance, the magnitude of the latter being indicated by the length of the vertical bar.

The values of ℓ_v from flight are, in most cases, close to the results obtained from the oscillatory rig model, but the static model results are smaller in magnitude. Although the levels of ℓ_v are different, all the results show the same increase then decrease in magnitude with increasing angle of attack, departing from the linear variation with angle of attack near buffet onset, to give losses in magnitude of ℓ_v.

For $M \approx 0.7$, clean aircraft, the flight values of n_v are fairly evenly scattered about the tunnel values (Fig 5a), although a group of results between $\alpha = 2^o$ and 3^o seem to show consistently lower values than the tunnel results, as do the results at $M \approx 0.8$, (Fig 5b) and for tanks on. All results show that the mean level of n_v is reasonably independent of angle of attack, although the flight values at $M = 0.7$ begin to show losses in the wing rock region.

2.2.2 Moments due to roll rate

At present, the tunnel experiments** have had to be restricted to those angles of attack where the aerodynamic damping is sufficient to control the motion of the model. The available tunnel results do show a small loss in damping-in-roll at high angles of attack, and at higher angles the model oscillates too violently for accurate readings to be taken, indicating near-zero values of damping. The rig is being modified to extend the range by introducing additional known damping.

Although the flight values of ℓ_p are generally larger in magnitude (Fig 6), they give stronger evidence for this loss on the clean aircraft, which begins to occur at similar angles of attack in flight and in the tunnel. With tanks on, flight and tunnel results for ℓ_p both show (Fig 6c&d) an initial small increase in magnitude as angle of attack increases, but the loss in damping is delayed and is less abrupt than for the clean aircraft.

---

* The moments of inertia in roll and pitch have recently been measured on a ground rig, and preliminary results indicate that the estimated inertia in roll used in Ref 7 was too small. The rolling moment derivatives have been corrected, so the results in Figs 5 and 6 differ from those of Ref 7.

** Two sets of results from the oscillatory rig are shown for $M = 0.7$, clean aircraft obtained in two series of tests. These are discussed in Ref 8. For clarity, the derivatives are referred to as ℓ_p and n_p, but see Appendix A1 for discussion on the combined derivatives $\ell_p + \ell_{\dot{v}} \sin\alpha$ and $n_v - n_{\dot{v}} \cos\alpha$.

The results for n_p agree very well in the mid-angle of attack range, Fig 6a-d, both for the clean aircraft and with tanks on. At low angles of attack, less than about 4^o, the tunnel results are more positive, but at high angles of attack they are more negative than the flight values. However, the two changes of slope in the variation of n_p with angle of attack, from negative to positive to negative, are apparent in all the sets of results.

It is demonstrated in Ref 7 that estimates of the derivatives based on the simple empirical methods, using measured lift and drag forces to modify the linear theoretical values of rolling and yawing moments respectively, do show the same trends with angle of attack as the experimental results. Thus the variation at high angles of attack can be associated with flow separation effects.

2.2.3 Dynamic n_v

The occurrence of wing rock on some American aircraft has been attributed to the fact that the parameter $C_{n_\beta}{}_{dynamic} \equiv$ 'dynamic n_v' $= n_v - (i_z/i_x)\ell_v \sin\alpha$ tends to zero[3] near the angles of attack for the onset of wing rock. Dynamic n_v has been calculated for the Gnat on the basis of the mean values of ℓ_v and n_v from the flight results (Fig 5), and the results are shown plotted as functions of angle of attack, for mean Mach numbers of 0.7 and 0.8, in Fig 7. It is evident that the onset of wing rock does not correlate with dynamic n_v tending to zero. The 'onset region' is taken from Fig 4 for the appropriate range of Mach number, *eg* values for the clean aircraft at $M \approx 0.7$ are based on results with $0.65 < M < 0.74$, giving the angle of attack range 11^o to 8.5^o for the onset of wing rock. With tanks on, 'dynamic n_v' shows similar increase with increasing angle of attack, followed by slight decrease for $M \approx 0.7$.

2.2.4 Dutch roll characteristics

The mean values of the derivatives obtained from the flight responses of both Dutch roll and wing rock oscillations have been used to calculate the frequency, damping, Dutch roll ratio and p-r phase angle, for flight at 30K ft, with mean weight appropriate to clean aircraft or with tanks on. The effect of the steady pitch rate in the turn was obtained from C_N, and has been included by using effective derivatives, as given in Appendix A2. The calculated characteristics of the oscillations have been compared with those obtained by graphical analysis of the flight records actually used to obtain the derivatives, and the parameters used most commonly in handling criteria are presented.

The frequency, ω_D, increases initially as angle of attack increases, Fig 8, and then decreases slightly, the calculated values for the Dutch roll oscillation giving a satisfactory mean to those obtained directly from the measured Dutch roll and wing rock responses. Also shown, for the clean aircraft at $M \approx 0.7$, is the approximate value of frequency, *ie*

$$\omega_D \approx \frac{1}{\hat{\tau}}\left\{\frac{\mu_2}{i_z} n_{v_{dynamic}}\right\}^{\frac{1}{2}} . \qquad (1)$$

This approximation (see Appendix A2, equations (A2-13) and (A2-15)) agrees well with the actual frequency, and shows the same trends with angle of attack; the similarity in trends is also present for the other sets of results, for $M \approx 0.8$, both for clean aircraft and with tanks on.

The damping of the Dutch roll, expressed as damping ratio ζ_D, is shown in Fig 9, and negative values of ζ_D (divergent oscillation) occur in the wing rock regions for the clean aircraft. The damping is zero in or very close to the onset region for wing rock, also shown in Fig 9, so that the identification of the onset of the wing rock oscillation as a divergent Dutch roll is substantiated. No attempt has been made to calculate the damping for $\alpha > 12^o$, as the derivatives seem to be more dependent on Mach number at the highest angles of attack, and it is not possible to specify mean flight values for ℓ_v and ℓ_p. The increase of Dutch roll damping at the moderate angles of attack is very marked, but the increase is smaller for the aircraft with tanks on, and the tendency to zero damping is delayed. It is interesting to note that the wing rock did in fact occur in flight (with tanks on) at $\alpha = 10^o$, $M = 0.82$ and $\alpha = 14^o$, $M = 0.78$, so that the calculated damping at $M = 0.8$ shows appropriate tendency to zero. The flight records of these wing rocks have not been used with the derivative extraction computer program, as the longitudinal porpoising motion is of large amplitude, causing significant changes in angle of attack.

The Dutch roll ratio and p-r phase angle show similar agreement, and do not vary significantly between Dutch roll and wing rock. This further confirms that the wing rock can be identified as an undamped Dutch roll for the Gnat aircraft.

2.2.5 Roll subsidence mode

Although there is some evidence in the later flight records of the roll subsidence mode being excited by aileron input, it has not been possible to determine its damping k_R directly from the responses. The calculated values, based on the derivatives identified from the Dutch roll responses, are shown in Fig 10. The roll 'subsidence' mode is calculated to be divergent at the highest angles of attack for the clean aircraft, the angle of attack at which this occurs being slightly greater than that for zero Dutch roll damping (marked on Fig 10a). This divergence is possibly supported by flight evidence, in that continuous rolls did occur at higher angles of attack than wing rock onset. The flight conditions for 'roll off' given by the pilot are $\alpha = 10^o$ at $M = 0.72$ and $\alpha = 9^o$ at $M = 0.82$ for the clean aircraft, which are certainly in the range where $k_R = 0$. The steady rolling of the aircraft with tanks on occurred at higher Mach numbers, *eg* $\alpha = 8.5^o$ at $M = 0.84$, a value not inconsistent with the trends shown in Fig 10b. The large values of k_R (*ie* short time constant) at the lower angles of attack probably indicate the reason for lack of success in obtaining significant contribution of the roll subsidence mode to the flight responses using an aileron doublet.

2.2.6 Effects of stability augmentation systems

In the past, the damping of the Dutch roll mode has been augmented by a yaw damper, but this is not very effective when the response is mainly in roll, as at high angles of attack. A roll damper is now often used as an alternative, provided that roll control power is reasonably effective. The aerodynamic data for two of the wing rocks analysed have been used to demonstrate theoretically the effect of an idealised roll damper with no lags, $\xi = K_{p\xi}p$, for various levels of gearing $K_{p\xi}$. The results are shown in Fig 11, as variation of Dutch roll damping with $K_{p\xi}$. The Dutch-roll damping varies almost linearly with $K_{p\xi}$ (Fig 11), and becomes positive (stable) within acceptable levels of gearing ratio for both cases, but the higher gearing needed for stability at the higher angle of attack causes the roll subsidence and spiral modes to combine and give a stable lateral phugoid oscillation (Fig 11).

The approximation for the damping of the Dutch roll mode given in Appendix A2, equation (A2-17), may be extended to include the effects of the roll damper by adding increments of $K_{p\xi}(V/s)\ell_\xi$ and $K_{p\xi}(V/s)n_\xi$ to $\ell_{p_{eff}}$ and $n_{p_{eff}}$ respectively. Then it is easily seen that

$$\frac{dk_D}{dK_{p\xi}} \approx -\frac{1}{2\hat{t}}\frac{V}{s}\frac{\ell_v}{i_x}\left[\frac{\ell_\xi}{i_x}\sin\alpha - \frac{n_\xi}{i_z}\cos\alpha\right]\Bigg/\left(\frac{n_v}{i_z}\cos\alpha - \frac{\ell_v}{i_x}\sin\alpha\right) \quad . \tag{2}$$

Although the approximation does not give the level of damping very accurately it does lead to remarkably good agreement with the variation of damping with gearing ratio, as shown in Fig 11. At the high angles of attack where $n_\xi > 0$, this expression shows that the aileron yaw enhances the effect of rolling moment ($\ell_\xi < 0$) on the Dutch roll damping. However, at lower angles of attack, where ℓ_ξ remains negative but n_ξ is also negative, it would be necessary to schedule $K_{p\xi}$ to zero, or introduce an aileron-rudder interconnect, since the applied yawing moment could overcome the stabilising rolling moment contribution. It is also apparent that a roll damper would not be beneficial at angles of attack where ℓ_v tends to zero. (Note that the approximation derived in Appendix A2 is only valid if either ℓ_v or n_v remains non-zero.)

A corresponding expression may be obtained to show the variation of Dutch-roll damping with gearing ratio $K_{p\zeta}$ for a yaw damper,

$$\frac{dk_D}{dK_{r\zeta}} \approx -\frac{1}{2\hat{t}}\frac{V}{s}\frac{n_v}{i_z}\left[\frac{n_\zeta}{i_z}\cos\alpha - \frac{\ell_\zeta}{i_x}\sin\alpha\right]\Bigg/\left[\frac{n_v}{i_z}\cos\alpha - \frac{\ell_v}{i_x}\sin\alpha\right] \quad . \tag{3}$$

For the two wing rocks considered, with rudder moments extrapolated from tunnel results, $K_{r\zeta}$ would have to be about six to eight times larger than $K_{p\xi}$ to achieve the same level of damping. However, since the Dutch roll ratio $|p/r|$ lies in the range 5 to 9, the aileron or rudder deflections needed for roll or yaw damper respectively would be approximately the same.

Since the roll subsidence mode can be expected to be modified by a roll damper, the approximation method of Appendix A2 was used to give (in the notation of Appendix A2), the damping index $k_R \approx c/b$, so that

$$\frac{dk_R}{dK_{p\xi}} \approx \frac{V}{s\hat{t}}\cos\alpha\left[\frac{n_v}{i_z}\frac{\ell_\xi}{i_x} - \frac{\ell_v}{i_x}\frac{n_\xi}{i_z}\right]\Bigg/\left[\frac{n_v}{i_z}\cos\alpha - \frac{\ell_v}{i_x}\sin\alpha\right] \quad . \tag{4}$$

Both numerical cases considered exhibit adverse aileron yaw characteristics, $n_v - \ell_v(n_\xi/\ell_\xi) < 0$, so that the roll damper actually reduces the level of damping of the roll subsidence mode, as shown in Fig 11. Thus it is evident that the efficient design of a stability augmentation system for high angle of attack depends highly on the particular values of the aerodynamic derivatives, for the best compromises to be made.

3 MODELLING WING ROCK AS A LIMIT CYCLE OSCILLATION

3.1 Background

The Gnat shows the same behaviour as some other combat aircraft, in that the wing rock can become a sustained oscillation of near-constant amplitude, which can be held for several cycles. This behaviour cannot, of course, be explained by the linear analysis given in the previous section, and it is necessary to postulate some nonlinearity to explain this feature of the wing rock phenomenon. The severity of the wing rock as a handling problem is clearly related to the magnitude of the limit cycle and not just to the fact that it occurs, so it is important to be able to predict the steady state amplitude for a realistic assessment of the problem, and also to specify realistic requirements for stability augmentation. In particular, the type of nonlinearity causing the limit cycle could have repercussions on the methods used to alleviate the wing rock. Wind tunnel tests show that rolling and yawing moments due to sideslip tend to become highly nonlinear at large angles of attack, and the same can be expected for moments due roll rate (and perhaps yaw rate). It is possible to simulate limit cycles with any such nonlinearities, and those due to sideslip and roll rate have been investigated separately.

The possibility of coupling between the longitudinal and lateral response being a contributory factor in the limit cycle behaviour is currently being investigated, but preliminary results show expected trends, and are not described here.

The nonlinear phenomena outlined above have been modelled to obtain responses on an analogue computer, and approximate analytic solutions have also been obtained, using the method suggested by Beecham[11,12]. For this, it is assumed that a mode of the form $a\cos\theta$ exists, where the local 'damping' is defined as $\lambda = \dot{a}/a$ and local 'frequency' is $\omega = \dot{\theta}$, both being functions of the local amplitude a. If the variation in damping and frequency over one cycle is small, then averaging techniques may be applied, to give relationships between λ, ω and a. The process is described in Appendix A3. Another promising approximation method, based on using two time scales, used by Padfield[13] for the analysis of similar lateral motions

on a slender-wing aircraft, could also be applied to the present mathematical models, but there has not been opportunity as yet to complete this analysis.

3.2 Effects of nonlinear rolling moments due to roll rate

The rolling moment due to roll rate may be expected to be nonlinear with roll rate at high angles of attack due to flow separation effects, and a possible representation is by an additional cubic term,

$$C_\ell \left(\frac{pb}{2V}\right) = \ell_{p1} \left(\frac{pb}{2V}\right) + \ell_{p3} \left(\frac{pb}{2V}\right)^3 \qquad (5)$$

for moderate values of roll rate.

The characteristics of the responses due to such a nonlinearity have been investigated, for cases where ℓ_{p1} gives dynamically unstable Dutch roll at very small amplitudes, using both the approximation theory outlined in Appendix A3, and parametric studies on an analogue computer. The approximate theory gives two interesting results for the frequency and amplitude of the limit cycle, namely that the frequency is independent of ℓ_{p1} and ℓ_{p3}, and that the amplitude is given by

$$\ell_{p1} + \tfrac{3}{4}\ell_{p3} \left(\frac{pb}{2V}\right)^2 = \text{const} \quad . \qquad (6)$$

The latter relation is obtained from the condition that Routh's discriminant be zero, but with ℓ_p replaced by $\ell_{p1} + \frac{3}{4}\ell_{p3}(pb/2V)^2$.

The parametric studies confirmed these results, as shown in Fig 12. A range of values of $\ell_{p1} > -0.095$ was used in the analogue computations, where the linear derivatives give zero Dutch roll damping with $\ell_p = -0.095$, and ℓ_{p3} was adjusted to give a final steady amplitude of 0.68 rad/s in roll rate. (Sideslip and yaw rate then have corresponding steady amplitudes, with $\beta_s = 0.023$ rad, $r_s = 0.026$ rad/s.) The responses shown in Fig 12 were all obtained using an initial condition of $\beta = 0.002$, $p = r = 0$. The initial rate of growth to the limit cycle changes with ℓ_{p1} (Fig 12a), but the frequency remains unchanged. The values of ℓ_{p3} obtained from the analogue computations are compared with the approximate theoretical relationship in Fig 12b, and are seen to give good agreement. The value of ℓ_{p1} for zero ℓ_{p3} is given by the condition for zero Dutch roll damping, and equation (6) gives the theoretical line of slope $\frac{3}{4}(pb/2V)^2$. It is interesting to note that the constant of equation (6) is the value of $\partial C\ell/\partial(pb/2V)$ at $p = p_s/2$, *ie* the local damping-in-roll derivative at half the steady state amplitude, for which Routh's discriminant is zero.

Also of interest is the variation in local growth rate of the envelope of the oscillatory mode. The nonlinear representation of damping is given by $\lambda = |\dot{p}|/|p|$, where $||$ denotes amplitude, and λ is a function of p. Two results from analysing the analogue records are shown in Fig 13, the envelopes from which the slopes have been obtained being plotted in Fig 13a. The nonlinear damping factor has been divided by the Dutch roll damping λ_0, ($\ell_{p3} = 0$) at small amplitudes, and it may be seen that $|\dot{p}|/|p|$ remains fairly close to λ_0 for amplitudes up to half the steady state amplitudes. This fact can be used in the extraction of nonlinear derivatives from flight responses; analysis of the initial growth of the wing rock response gives a linear value for ℓ_p, which can then justifiably be used for the initial guess of ℓ_{p1} in the identification of a complete wing rock record (*ie* initial growth and limit cycle motion). The steady amplitude and the rate of growth then give sufficient information in the response to identify ℓ_{p1} and ℓ_{p3} separately. An example of the fit obtained between flight and computed responses for one wing rock of Gnat, using such a nonlinear model in an extension of the computer programs described in Ref 6 is shown in Fig 14, for rate of roll and sideslip vane records. The derivatives ℓ_v, ℓ_ξ, n_v, n_p, y_v, were also identified, and remained almost the same as the values obtained from the first 3.6 seconds of record, using the linear model for damping-in-roll. The results are encouraging, although it should be noted that angle of attack is still increasing during the initial growth, so that a good match cannot be expected there. More analysis needs to be done to attempt to identify responses which include significant variation of angle of attack, but the general success of this match suggests that the assumed type of nonlinearity in damping in roll appears a plausible explanation for the limit cycle behaviour of the wing rock motion of the Gnat.

It is also probable that yawing moment due to roll rate has a significant effect on the damping of the Dutch roll mode at high angle of attack, and can be expected to be nonlinear. There has not been opportunity to investigate the effects of n_{p1} and n_{p3} on the responses, but they should be similar in character to those of ℓ_{p1} and ℓ_{p3}.

If this assumed model of the aerodynamics is correct, it is evident that using a roll damper to augment ℓ_p by a linear increment (ℓ_{p1} more negative) would reduce the amplitude and growth rate of the limit cycle and, if sufficiently powerful, prevent wing rock altogether.

3.3 Effects of nonlinearities in sideslip

Although the assumption of a nonlinearity in the rolling moment due to roll rate considered above has led to a plausible explanation of the limit cycle nature of the wing rock of the Gnat aircraft, this does not exclude other aerodynamic nonlinearities as possible causes. Also there is the possibility that other aircraft may exhibit limit cycle behaviour in a lateral oscillation which cannot be related to $C_\ell(p)$. For instance, strong nonlinearities have been observed in $C_\ell(\beta)$ and $C_n(\beta)$ measured in wind tunnels and aircraft with such characteristics do experience wing rock. So it was considered worthwhile to examine this class of nonlinearity, although the static tunnel results[9] for Gnat remain reasonably linear in the wing rock region.

It does not seem possible to obtain limit cycles through nonlinearities of a single-valued stiffness term in a second order differential equation, but it is possible to obtain them in a multimode system

(higher order equations), where the stiffness-type terms, such as n_v and ℓ_v, affect both the frequency and distribution of damping between the modes in the linear motion. In passing, it is worth remarking that hysteresis in stiffness can cause limit cycles in a single oscillatory mode, and there are indications from wind-tunnel results[14] that $C_n(\beta)$ and $C_\ell(\beta)$ can exhibit hysteresis in some separated flow conditions. As such behaviour implies sudden large changes in flow separation-reattachment conditions, it is probably better to seek an aerodynamic solution to this problem, to reduce the hysteresis, rather to develop a sophisticated control system to correct the resulting response. The work in the Control Division at RAE has been concentrated mainly on sideslip characteristics which can be represented by polynominal expressions, again using an analogue computer for parametric studies and approximate theory to interpret the results.

The examples discussed here are confined to cubic representations of rolling and yawing moments due to sideslip, with sideslip expressed as β(rad) = sideslip velocity/V ,

$$C_\ell(\beta) = \ell_{v1}\beta + \ell_{v3}\beta^3 \tag{7}$$

$$C_n(\beta) = n_{v1}\beta + n_{v3}\beta^3 \quad . \tag{8}$$

The solution for the amplitude of the limit cycle is given by

$$R^* = a^*b^*c^* - a^{*2}d^* - c^{*2} = 0 \quad , \tag{9}$$

and a^*, b^*, c^*, d^* are obtained by replacing the derivatives ℓ_v and n_v by the expressions $(\ell_{v1} + \frac{3}{4}\ell_{v3}\beta_s^2)$, $(n_{v1} + \frac{3}{4}n_{v3}\beta_s^2)$ respectively in the coefficients of the linear lateral stability quartic, *ie* R^* is quadratic in β_s^2 . The corresponding frequency of the limit cycle is then given by

$$\omega_s^2 = \frac{c^*}{a^*} \quad . \tag{10}$$

In the first example, ℓ_{v1} and n_{v1} were chosen to retain their usual signs ($\ell_v < 0$, $n_v > 0$) and the other derivatives such that the linear Dutch roll oscillation is undamped. With n_{v3} positive, the effective stiffness increases with increasing sideslip amplitude, and a limit cycle results for a large range of values of ℓ_{v3} , the approximate theoretical results being in remarkably close agreement with those obtained from the analogue computations (Fig 15). However, for $\ell_{v3} < 117$, the approximation for β_s^2 is negative, *ie* the limit cycle does not exist, and this is substantiated by the analogue solutions, which continued to grow in amplitude or diverged. When a softening spring characteristic was used for $C_n(\beta)$, *ie* $n_{v3} < 0$ (value of -70), the range for which limit cycles exist is reduced to $\ell_{v3} > 191$, and a non-oscillatory divergence occurred in the analogue computations, as shown in Fig 15c. This divergence corresponded to solutions of equations (9) and (10) giving $\beta_s^2 > 0$, $\omega_s^2 < 0$, the latter condition being interpreted as an exponential mode (see Appendix A3). The solution of the approximate equations has various branches, but the agreement with the analogue results is very good, if the critical amplitude in sideslip is assumed to occur when the roll rate response shows sudden change, as indicated in Fig 15c. Thus it seems that the approximate theory will reveal the presence of divergences as well as limit cycles, and this has application in the design of augmentation systems.

The characteristics of the motion are mainly determined by the values of the local sideslip derivatives, $dC_\ell/d\beta$, $dC_n/d\beta$, evaluated at $\beta = \beta_s/2$, as for the nonlinear rolling moment due to roll rate. (NB. Nonlinearities with respect to two or more response variables cannot be treated by the approximate method in its present stage of development, and it is not possible to derive an equivalent R^* for such equations of motion.) As wind tunnel results indicate that there are possibilities of any combinations of signs for n_{v1}, n_{v3}, ℓ_{v1}, ℓ_{v3} , it can be useful to consider some families based on these local derivatives. The linear lateral stability diagram, where the boundary is given by R = 0, then corresponds to conditions $R^* = 0$ for limit cycles of amplitude β_s or divergence at β_s , where $\ell_v = \ell_{v1} + \frac{3}{4}\ell_{v3}\beta_s^2$, and $n_v = n_{v1} + \frac{3}{4}n_{v3}\beta_s^2$. The boundary between limit cycles and divergence is given by $\omega_s^2 = 0$, *ie* $c^* = 0$, since a is independent of ℓ_v and n_v , and is positive for conservative systems.

Since this type of nonlinearity in $C_\ell(\beta)$ and $C_n(\beta)$ can lead to divergences as well as limit cycles, both phenomena must be considered in the design of augmentation systems. In particular, it is evident that a roll damper will be able to control the oscillatory instability, as with the nonlinear $C_\ell(p)$, but it may not materially affect the divergence. For the second example, with roll damper, values of ℓ_{v1}, ℓ_{v3}, n_{v1}, n_{v3} were chosen to give a softening spring for rolling moment and stiffening spring for yawing moment, with $\ell_{v1} = -0.15$, $\ell_{v3} = 137$, $n_{v1} = 0.05$, $n_{v3} = 44$. The responses with various levels of p/ξ gearing ratio, $K_{p\xi}$, were simulated, and the effects of several initial conditions were investigated. Plausible values of $\ell_\xi < 0$ and $n_\xi > 0$ were assumed, typical of high angle of attack values, and some results were obtained assuming $n_\xi = 0$. For $K_{p\xi} < 0.008$, the linear small amplitude motion is dynamically unstable, and small initial conditions on β lead to limit cycles, while larger initial conditions lead to divergences similar to that of Fig 15c. For $K_{p\xi} > 0.008$, the small amplitude motion is a damped oscillation, but the response to large initial conditions diverges. For $K_{p\xi} > 0.05$, this divergence is oscillatory, (Fig 16b) but at intermediate values of $K_{p\xi}$ it is difficult to discern the type of divergence from the analogue computations. The approximate theory, using effective derivatives of the form $\ell_p + K_{p\xi}\ell_\xi$ and $n_p + K_{p\xi}\ell_\xi$, indicates that an exponential divergence is possible at $K_{p\xi} = 0.02$, but that no real solution for β_s exists at $K_{p\xi} = 0.03$, and an undamped oscillation can occur at large amplitudes for $K_{p\xi} > 0.04$. There is remarkably close agreement (Fig 16a), between the critical sideslip amplitude given by the approximate theory, and the least initial condition on sideslip which causes the oscillation to be divergent, although the roll damper does damp out the responses from smaller initial conditions. Thus nonlinearities in sideslip derivatives can have significant effects on moderate amplitude motions, and so need to be considered at the design stage of augmentation systems.

4 CONCLUSIONS

Flight records of Dutch roll and wing rock oscillations of the Gnat aircraft in steady turns have been obtained, both for clean aircraft and with external fuel tanks, over a range of Mach numbers and

heights. Analysis of the characteristics of the oscillations indicates that the wing rock encountered on this aircraft is a Dutch roll type motion, and the usual mathematical model for this mode, with linear aerodynamic derivatives, has been used to obtain values of the derivatives through the angle of attack range, up to and well into the wing rock region. Although the magnitudes of the derivatives are somewhat different to the tunnel results, the trends with angle of attack are in broad agreement, including the effects due to flow separation at high angles of attack.

It has been shown that such trends in derivatives cause the damping of the Dutch roll mode to become zero near angle of attack and Mach number conditions for which wing rock onset occurs in flight on the clean aircraft, so that the wing rock is an undamped Dutch roll for the Gnat.

The parameter 'dynamic n_v' (zero values of which have been associated with the onset of wing rock on other aircraft) remains well positive, and it is the moment derivatives due to roll rate which are more significant in this case. In particular, the damping in roll derivative becomes first zero and then positive as angle of attack increases into the wing rock region. The influence of the external fuel tanks on these derivatives and on Dutch roll characteristics has been demonstrated to be consistent with the fact that the flow separation effects are delayed to higher angles of attack. It has also been found that the calculated damping of the roll subsidence mode can become near-zero at the highest angles of attack, which may account for the rolling divergences sometimes encountered in flight, both for clean aircraft and with tanks on.

A simple theoretical assessment has been made of the effects of a roll damper, showing that acceptable levels of roll rate/aileron gearing would achieve damped Dutch roll oscillations, and so eliminate wing rock where at present this phenomenon is a limiting factor. However, the roll subsidence mode can be driven unstable for large gains, and in addition the effects of the roll damper at low angle of attack would need to be considered, including possibly aileron/rudder interconnect and scheduling with angle of attack.

Extending the mathematical models to include possible nonlinear effects has yielded some interesting results, from analogue computations and approximate theory. Nonlinear rolling moment due to roll rate can obviously cause limit cycle type responses, and a few of the Gnat wing rock records have been analysed, showing that such a nonlinearity is a plausible explanation of the behaviour, with reasonable matching between computed and flight responses. Nonlinearities in moments due to sideslip can also cause limit cycles, but it is possible to find divergence conditions, of either exponential or oscillatory type, which cannot be contained by roll damper alone. The approximate theory gives the solutions for the amplitudes of limit cycles and the critical amplitudes for divergence, which agree well with the analogue computations.

Table 1

GEOMETRIC DATA

Wing				
Area (gross)		16.26 m^2		175 ft^2
Span	b	7.315 m		24 ft
Geometric mean chord,	$\bar{c}$	2.22 m		7.29 ft
Aerodynamic mean chord,	$\bar{\bar{c}}$	2.31 m		7.57 ft
Taper ratio,	λ		0.5	
Sweepback of ¼-chord,	$\Lambda_{\frac{1}{4}}$		40°	
Tail				
Area (gross)		3.45 m^2		37.1 ft^2
Span		3.30 m		10.83 ft
λ			0.4	
$\Lambda_{\frac{1}{4}}$			46°	
Fin				
Area (gross)		2.73 m^2		29.4 ft^2
Height (exposed)		1.46 m		4.8 ft
λ			0.4	
$\Lambda_{\frac{1}{4}}$			45°	

CG — Mean CG position for flight tests is 1.47 m (4.83 ft) behind the reference position marked on Fig 1, which is situated at 25% root chord. With the leading edge of the aerodynamic mean chord at a distance 0.73 $\bar{\bar{c}}$ behind leading edge of root chord, then the CG is at 0.23 $\bar{\bar{c}}$.

Positions of transducers, relative to mean CG

	x(positive, forwards)	y(positive, starboard)	z(positive, down)
Angle of attack vane	6.25 m (20.5 ft)	-0.10 m (-0.33 ft)	0.36 m (1.17 ft)
Angle of sideslip vane	6.25 m (20.5 ft)	0 (0)	0.25 m (0.83 ft)
Normal accelerometer	0.90 m (2.96 ft)	-0.165 m (-0.54 ft)	-0.61 m (-2.0 ft)
Lateral accelerometer	0.88 m (2.88 ft)	-0.05 m (-0.17 ft)	-0.55 m (-1.79 ft)

REFERENCES

1. The effects of buffeting and other transonic phenomena on manoeuvring combat aircraft. AGARD Advisory Report 82 (1975

2. Fluid dynamics of aircraft stalling. AGARD CP 102 (1972)

3. Stall/spin problems of military aircraft. AGARD CP 199 (1976)

4. D.E. Johnston, I.L. Ashkenas and J.R. Hogge. Investigation of flying qualities of military aircraft at high angle of attack. AFFDL-TR-74-61 (1974)

5. C.L. Bore. Post-stall aerodynamics of the Harrier Gr 1. Paper 18 of AGARD CP 102 (1972)

6. A. Jean Ross and G.W. Foster. Fortran programs for the determination of aerodynamic derivatives from transient longitudinal or lateral responses of aircraft. RAE Technical Report 75090 (1975)

7. A. Jean Ross, G.W. Foster and T. Turvey. An investigation of Dutch roll and wing rock oscillations of a Gnat Trainer aircraft: flight results and linear analysis. RAE Technical Report 78032 (1978)

8. C. O'Leary. Wind-tunnel measurements of lateral aerodynamic derivatives using a new oscillatory rig and comparisons for a Gnat aircraft. RAE Technical Report 77159 (1977)

9. P.J. Haynes and S. Lineham. RAE Technical Report (to be published)

10. G.W. Foster and A. Jean Ross. An investigation of lateral oscillation of a Gnat aircraft at high angles of attack: nonlinear analysis. RAE Technical Report (to be published)

11. L.J. Beecham and I.M. Titchener. Some notes on an approximate solution for the free oscillation characteristics of nonlinear systems typified by $\ddot{x} + F(\dot{x},x) = 0$. ARC R&M 3651 (1969)

12. A. Jean Ross and L.J. Beecham. An approximate analysis of the nonlinear lateral motion of a slender aircraft (HP 115) at low speeds. ARC R&M 3674 (1971)

13. G.D. Padfield. The application of perturbation methods to nonlinear problems in Flight Mechanics. Cranfield Institute of Technology, PhD Thesis (September 1976). See also Paper 31 of AGARD CP 235 (1978)

14. T. Cord. Hysteresis-induced wing rock. AFFDL-TM-75-76-FGC (1975)

15. L.T. Nguyen. Evaluation of the importance of lateral acceleration derivatives in the extraction of lateral-directional derivatives at high angles of attack. NASA TN D-7739 (1974)

References quoted are not necessarily available.

Copyright ©, Controller HMSO, London 1978

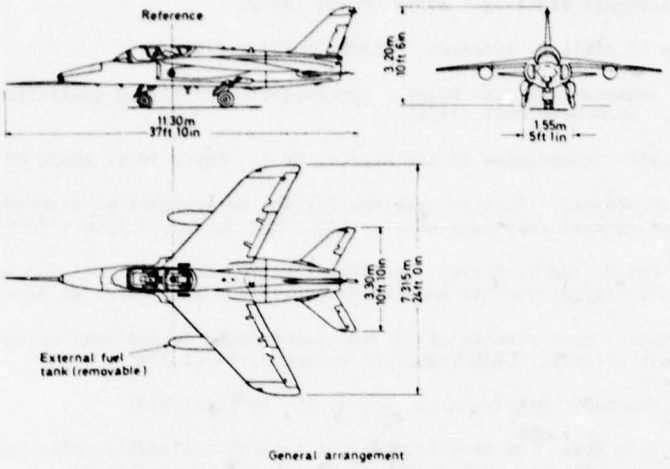

Fig 1 Gnat aircraft

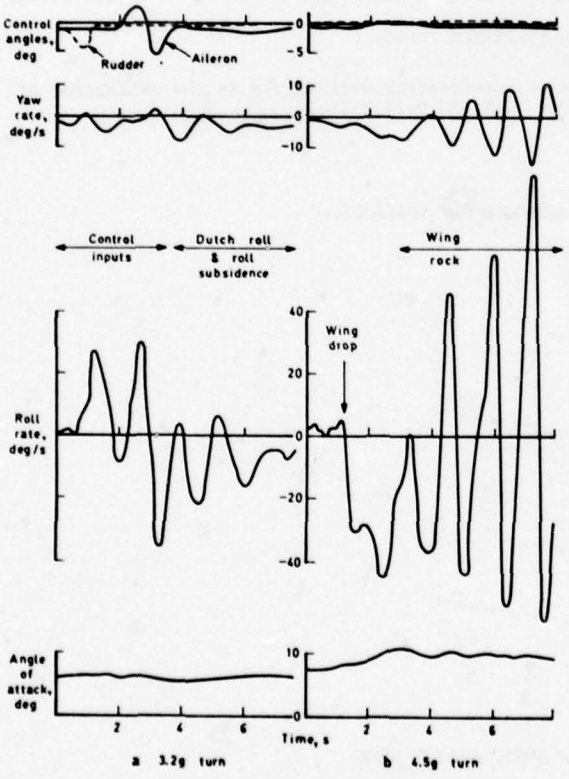

Fig 2 Responses in turns. Clean aircraft, M = 0.78

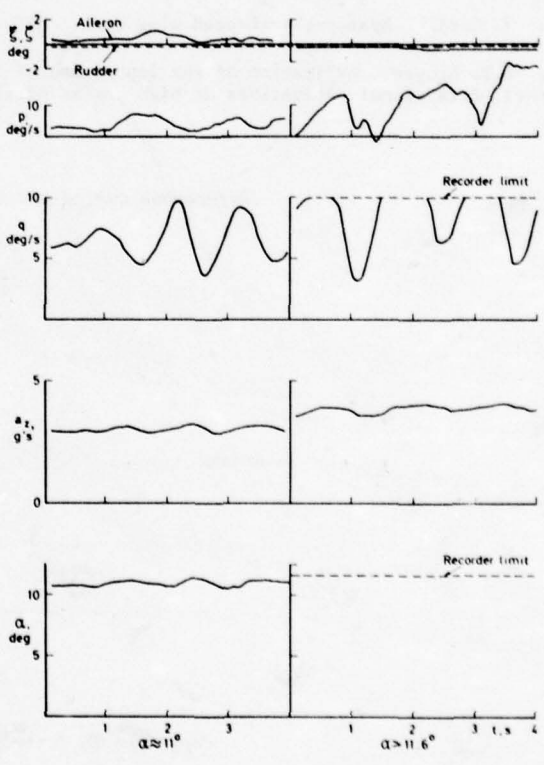

Fig 3 Porpoising motion, beginning and end of test run. Tanks on, M ≈ 0.7

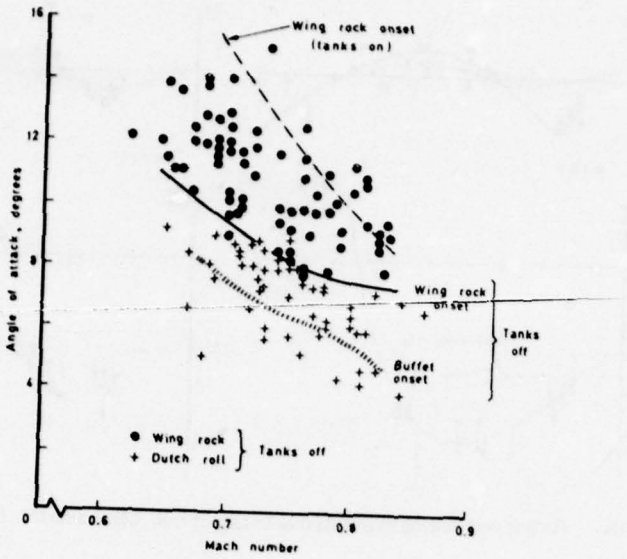

Fig 4 Boundaries, onset of wing rock

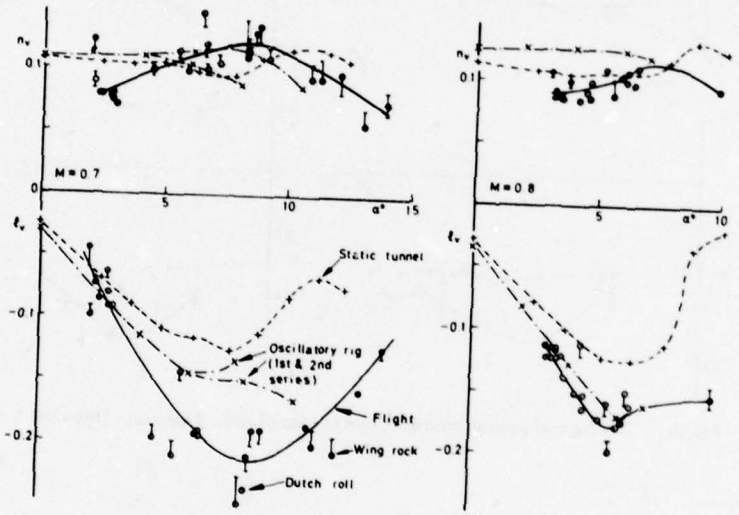

Fig 5a Rolling and yawing moments due to sideslip. Clean aircraft. (Interim)

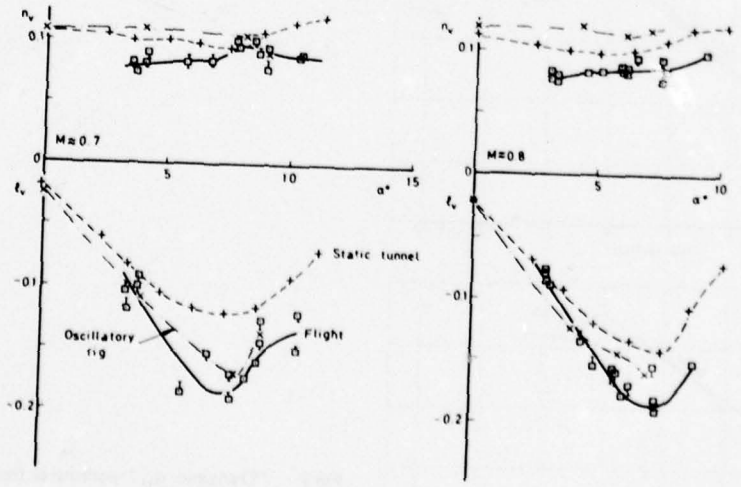

Fig 5b Rolling and yawing moments due to sideslip. Tanks on. (Interim)

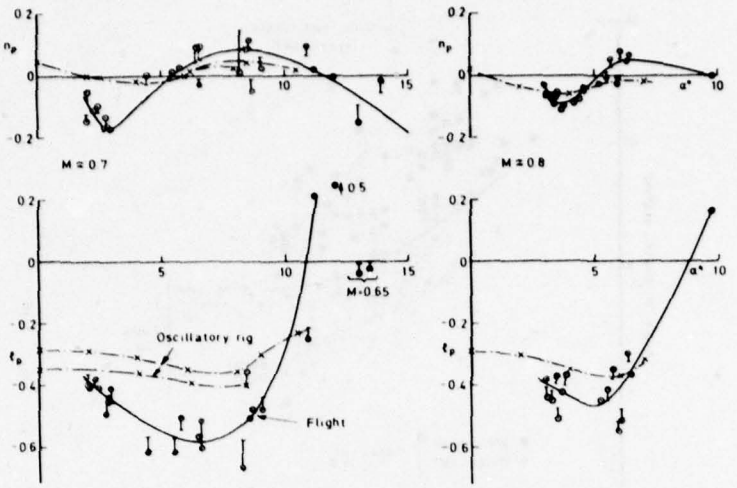

Fig 6a Rolling and yawing moments due to rate of roll. Clean aircraft. (Interim)

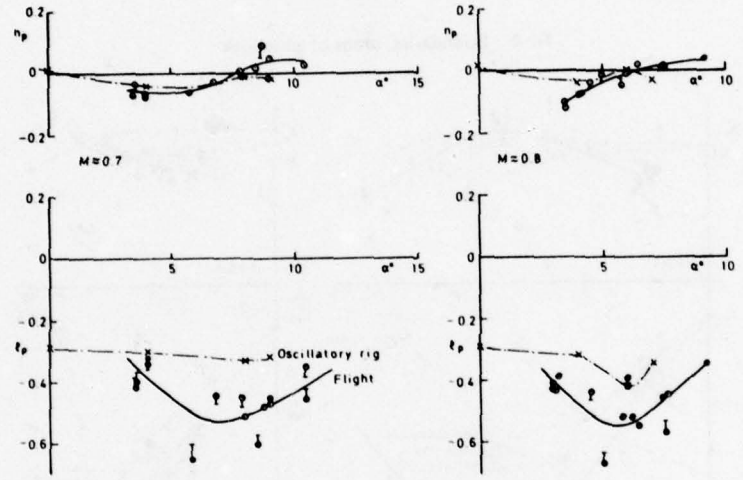

Fig 6b Rolling and yawing moments due to rate of roll. Tanks on. (Interim)

$$n_{v_{dynamic}} = n_v - \frac{I_z}{I_x} \ell_v \sin\alpha$$

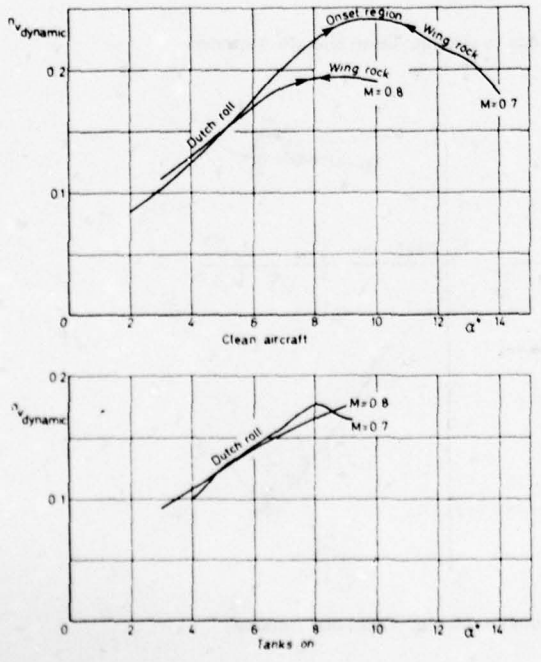

Fig 7 "Dynamic n_v" parameter from flight derivatives

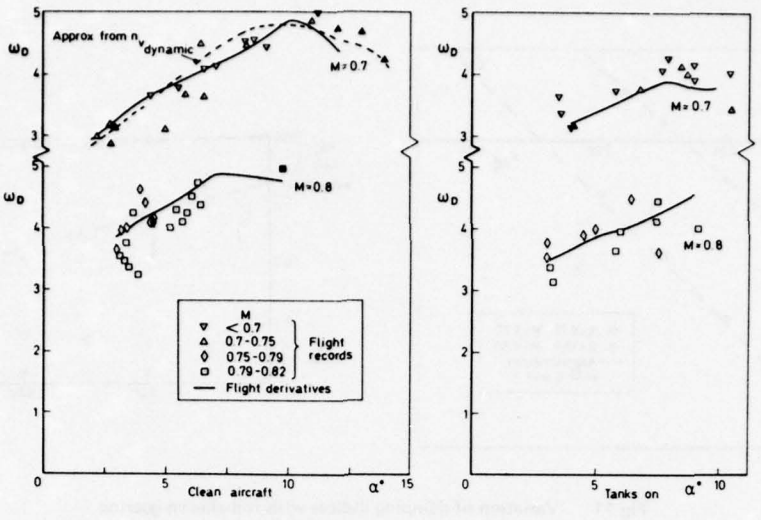

Fig 8 Frequency of Dutch roll oscillation from flight records and derivatives

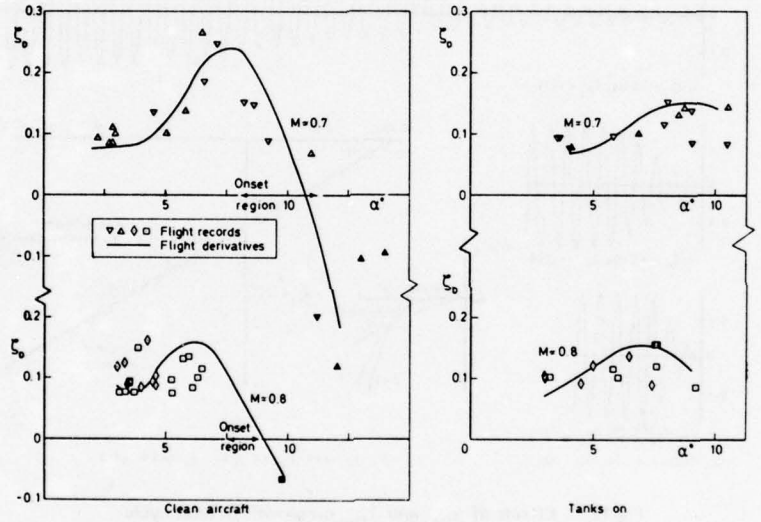

Fig 9 Damping of Dutch roll oscillation from flight records and derivatives

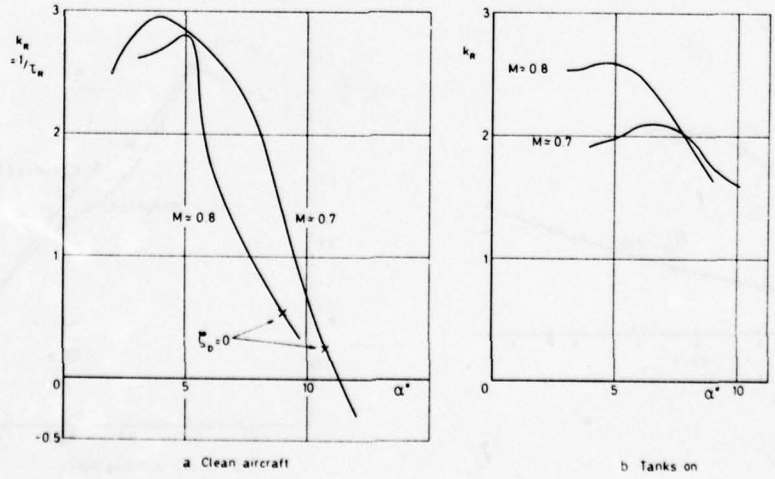

Fig 10 Damping index of roll subsidence mode

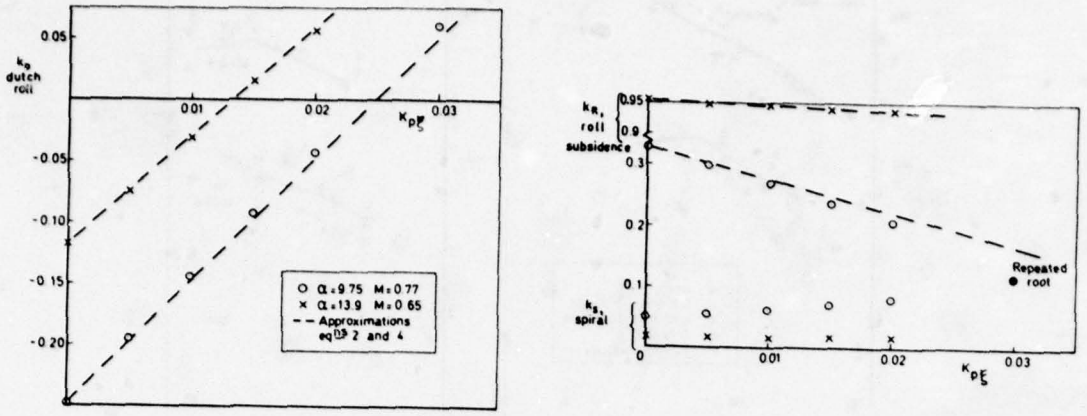

Fig 11 Variation of damping indices with roll-aileron gearing

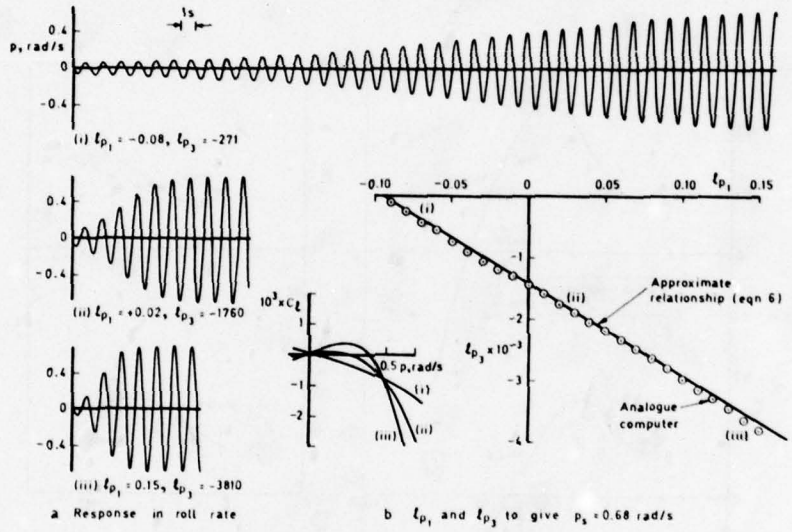

Fig 12 Effects of ℓ_{p_1} and ℓ_{p_3} on growth to limit cycle

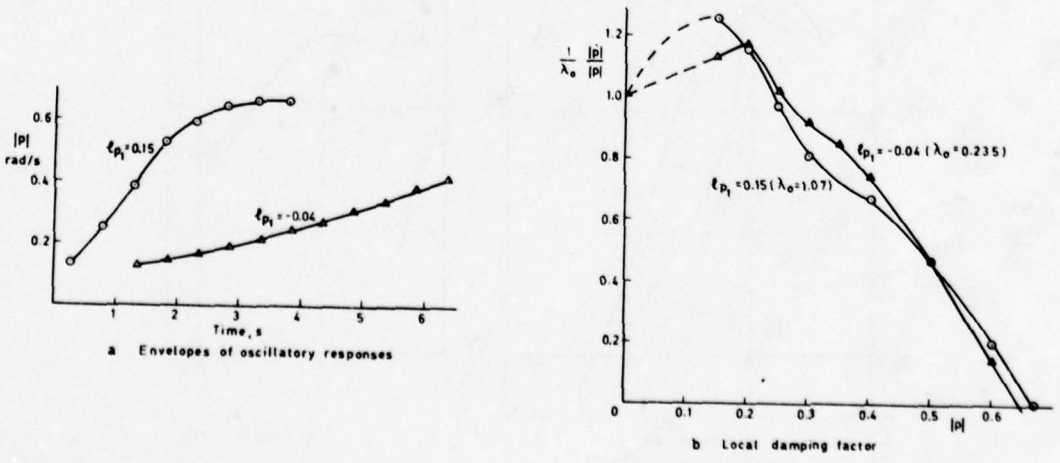

Fig 13 Change in damping during growth to limit cycle

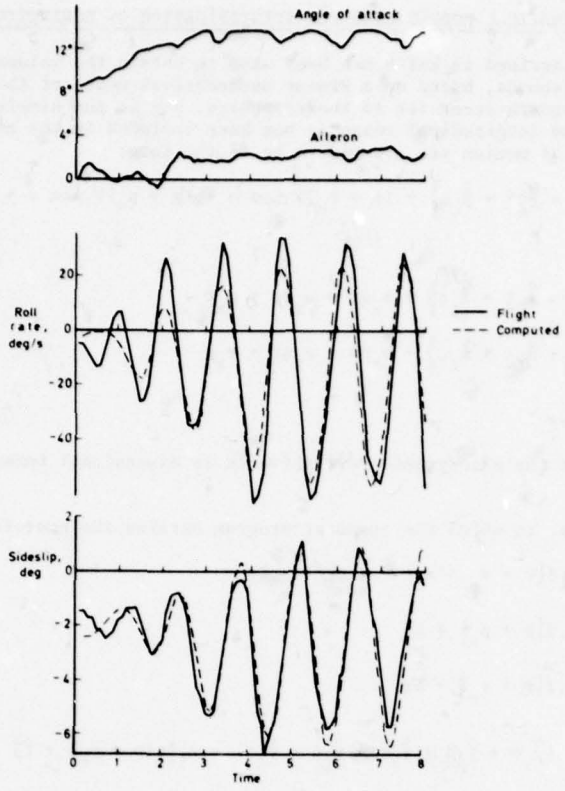

Fig 14 Flight and computed response for wing rock of Gnat

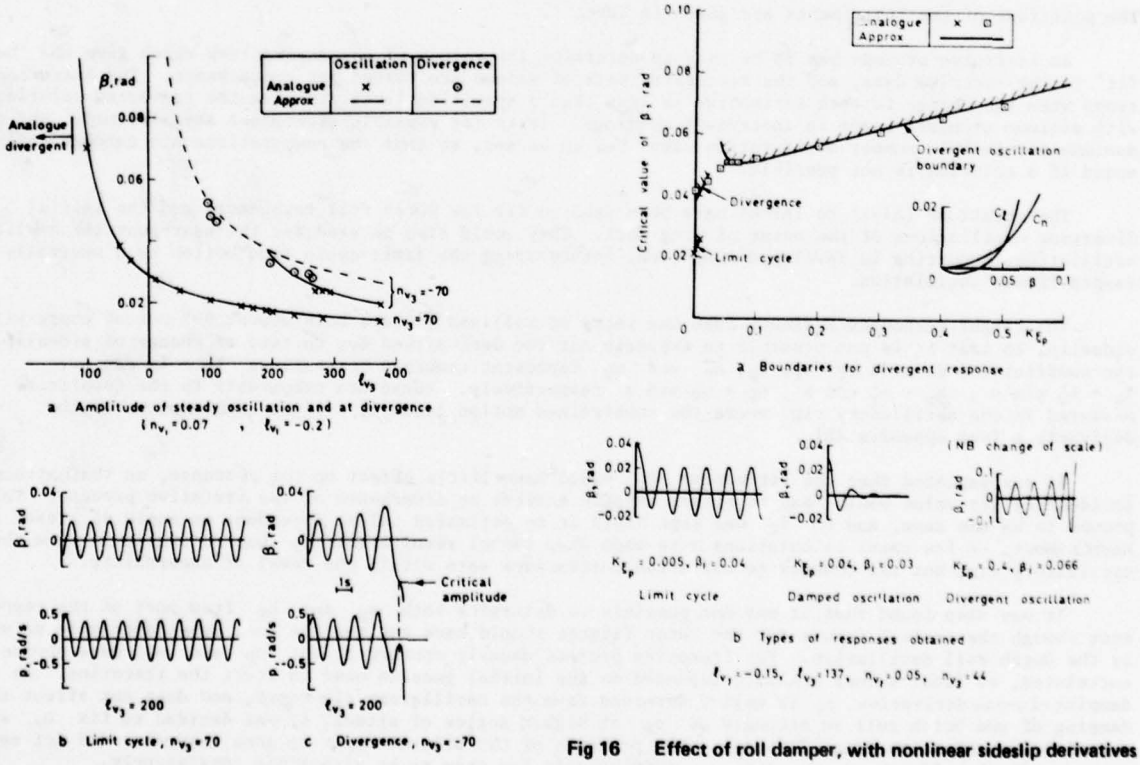

Fig 16 Effect of roll damper, with nonlinear sideslip derivatives

Fig 15 Characteristics of responses with cubic nonlinearities in sideslip

Appendix A1

MATHEMATICAL MODELS USED FOR IDENTIFICATION OF DERIVATIVES

The computer program described in Ref 6 has been used to obtain the values of the aerodynamic derivatives from the flight records, based on a linear mathematical model of the aerodynamics. The method gives the generalised least-square error fit to the responses, and is the simplest of the Output Error Methods. The influence of the longitudinal response has been included in the kinematic 'second-order' terms, so that the equations of motion are assumed to be of the form:

$$\dot{v} = -\left\{\overset{\circ}{y}_v v + \overset{\circ}{y}_p p + \overset{\circ}{y}_r r + \overset{\circ}{y}_\xi \xi + \overset{\circ}{y}_\zeta \zeta\right\} - (r + r_e)V \cos\alpha + (p + p_e)V \sin\alpha + a_{y_e} g + g \cos\theta_e \sin\Phi \; . \qquad \text{.....(A1-1)}$$

$$\dot{p} = -\left\{\overset{\circ}{\ell}_v v + \overset{\circ}{\ell}_p p + \overset{\circ}{\ell}_r r + \overset{\circ}{\ell}_\xi \xi + \overset{\circ}{\ell}_\zeta \zeta\right\} + b_x qr + e_x qp + e_x \dot{r} \qquad \text{(A1-2)}$$

$$\dot{r} = -\left\{\overset{\circ}{n}_v v + \overset{\circ}{n}_p p + \overset{\circ}{n}_r r + \overset{\circ}{n}_\xi \xi + \overset{\circ}{n}_\zeta \zeta\right\} + b_z qp - e_z qr + e_z \dot{p} \qquad \text{(A1-3)}$$

$$\dot{\Phi} = p + r \cos\Phi_e \tan\Theta_e \; . \qquad \text{(A1-4)}$$

The superfix $^\circ$ denotes that the aerodynamic derivative is in dimensional form, and is divided by appropriate mass or inertia.

The instrument readings, to which the computer program obtains the best fit, are expressed as

$$\beta^\circ_{\text{vane}} = 57.3\{v + v_e + x_3 r - z_3 p\}/V + E\beta \qquad \text{(A1-5)}$$

$$p^\circ/s = 57.3\{p + p_e\} + Ep \qquad \text{(A1-6)}$$

$$r^\circ/s = 57.3\{r + r_e\} + Er \qquad \text{(A1-7)}$$

$$a_y = \Big\{-(\overset{\circ}{y}_v v + \overset{\circ}{y}_p p + \overset{\circ}{y}_r r + \overset{\circ}{y}_\xi \xi + \overset{\circ}{y}_\zeta \zeta) + x_1[q(p + p_e) + \dot{r}] - y_1\left[(p + p_e)^2 + (r + r_e)^2\right] + z_1[q(r + r_e) - \dot{p}]\Big\}/g + Ea_y + a_{y_e} \qquad \text{(A1-8)}$$

where (x_1, y_1, z_1) and (x_3, y_3, z_3) denote the positions of the lateral accelerometer and the sideslip vane relative to the CG and $E\beta$, Ep, Er and Ea_{y_e} are the zero-offset errors of the respective instruments. The positions of the instruments are given in Table 1.

An iterative process has to be used to determine the values of the derivatives which give the 'best fit' to the recorded data, and the successive sets of values are tested for convergence. The iteration stops when the change in each derivative is less than a specified level, to give the converged solution with minimum standard error in instrument readings. Tests for possible divergence are also made, and the maximum permissible number of iteration steps has to be set, so that the computations are automatically ended if a solution is not possible.

The equations (A1-1) to (A1-8) have been used to fit the Dutch roll responses, and the initial divergent oscillations of the onset of wing rock. They could also be used for the near-constant amplitude oscillations occurring in developed wing rock, interpreting the limit-cycle type motion as a neutrally damped linear oscillation.

The flight responses indicate that the rates of roll and yaw are both almost 90° out of phase with sideslip, so that it is not possible to separate out the derivatives due to rate of change of sideslip, and the coefficients denoted by ℓ_r, ℓ_p, n_r and n_p represent combined derivatives $\ell_r - \ell_{\dot{v}} \cos\alpha$, $\ell_p + \ell_{\dot{v}} \sin\alpha$, $n_r - n_{\dot{v}} \cos\alpha$, $n_p + n_{\dot{v}} \sin\alpha$ respectively. These are comparable to the quantities measured in the oscillatory rig, where the constrained motion leads to similar combinations of the derivatives (see Appendix A2).

It was expected that the derivative ℓ_r would have little effect on the response, so that attempts to identify its value would lead to either erratic answers or divergence of the iterative process. This proved to be the case, and so ℓ_r was kept fixed at an estimated value, dependent on angle of attack and Mach number. A few check calculations were made when tunnel results for ℓ_r become available from the oscillatory rig, but the changes to extracted derivatives were within the level of uncertainty.

It was also found that it was not possible to determine both n_p and n_r from most of the responses even though the control inputs for the later flights should have excited the roll subsidence mode as well as the Dutch roll oscillation. The iterative process usually converged, but n_p and n_r were obviously correlated, so final values probably depended on the initial guesses used to start the iteration. As the damping-in-yaw derivative, n_r is well-determined from the oscillatory rig tests, and does not affect the damping of the Dutch roll so strongly as n_p at higher angles of attack, it was decided to fix n_r at the tunnel value and so to determine n_p. The presence of the aileron input in some responses did not appear to uncouple the effects of n_p and n_r sufficiently for them to be determined consistently.

Appendix A2

VARIOUS APPROXIMATIONS USED IN LATERAL STABILITY ANALYSIS

A2.1 Effect of derivatives due to rate of sideslip

The equations of motion for small perturbations about the steady turning motion may be written in a form corresponding to the equations in Appendix A1.

$$\dot{v} = -\left\{\overset{\circ}{y}_v v + \overset{\circ}{y}_p p + \overset{\circ}{y}_r r + \overset{\circ}{y}_{\dot{v}} \dot{v} + \overset{\circ}{y}_\xi \xi + \overset{\circ}{y}_\zeta \zeta\right\} - Vr \cos\alpha + Vp \sin\alpha + g_2\phi + g_2\psi \qquad (A2\text{-}1)$$

$$\dot{p} = -\left\{\overset{\circ}{\ell}_v v + \overset{\circ}{\ell}_p p + \overset{\circ}{\ell}_r r + \overset{\circ}{\ell}_{\dot{v}} \dot{v} + \overset{\circ}{\ell}_\xi \xi + \overset{\circ}{\ell}_\zeta \zeta\right\} + b_x q_e r + e_x q_e p + e_x \dot{r} \qquad (A2\text{-}2)$$

$$\dot{r} = -\left\{\overset{\circ}{n}_v v + \overset{\circ}{n}_p p + \overset{\circ}{n}_r r + \overset{\circ}{n}_{\dot{v}} \dot{v} + \overset{\circ}{n}_\xi \xi + \overset{\circ}{n}_\zeta \zeta\right\} + b_z q_e p - e_z q_e r + e_z \dot{p} \qquad (A2\text{-}3)$$

$$\dot{\phi} = p \quad \text{and} \quad \dot{\psi} = r .$$

The terms in the sideforce equation due to the steady turn have been balanced by the gravity term, which is replaced by the perturbations in gravity components, expressed* in terms of the deviation angles ϕ and ψ, with $g_2 = g \sin\Theta_e$, $g_3 = g \cos\Theta_e \cos\Phi_e$. The derivatives due to rate of change of sideslip have also been included.

It is easier to see the relative magnitudes of the contributions if the sideslip velocity, v, is replaced by sideslip angle, $\beta = v/V$ (in radians), and if the concise derivatives are expanded in their aerodynamic form, to give

$$\dot{\beta} = \frac{\rho VS}{m}\left\{y_v\beta + y_p\frac{ps}{V} + y_r\frac{rs}{V} + y_{\dot{v}}\frac{\dot{\beta}s}{V} + y_\xi\xi + y_\zeta\zeta\right\} - r\cos\alpha + p\sin\alpha + \frac{g_3}{V}\phi + \frac{g_2}{V}\psi \qquad (A2\text{-}4)$$

$$\dot{p} = \frac{\rho V^2 Ss}{I_x}\left\{\ell_v\beta + \ell_p\frac{ps}{V} + \ell_r\frac{rs}{V} + \ell_{\dot{v}}\frac{\dot{\beta}s}{V} + \ell_\xi\xi + \ell_\zeta\zeta\right\} + b_x q_e r + e_x q_e p + e_x\dot{r} \qquad (A2\text{-}5)$$

$$\dot{r} = \frac{\rho V^2 Ss}{I_z}\left\{n_v\beta + n_p\frac{ps}{V} + n_r\frac{rs}{V} + n_{\dot{v}}\frac{\dot{\beta}s}{V} + n_\xi\xi + n_\zeta\zeta\right\} + b_z q_e p - e_z q_e r + e_z\dot{p} \qquad (A2\text{-}6)$$

It is usual to assume that y_p and y_r have a negligible effect on the response, and if $y_{\dot{v}}$ is also neglected, it is possible to eliminate $\dot{\beta}$ from equations (A2-4) to (A2-6) to give

$$\dot{p} = \frac{\rho V^2 Ss}{I_x}\left\{\left[\ell_v + \frac{y_v\ell_{\dot{v}}}{\mu_2}\right]\beta + \left[\ell_p + \ell_{\dot{v}}\sin\alpha\right]\frac{ps}{V} + \left[\ell_r - \ell_{\dot{v}}\cos\alpha\right]\frac{rs}{V} + \left[\ell_\xi + \frac{y_\xi\ell_{\dot{v}}}{\mu_2}\right]\xi \right.$$
$$\left. + \left[\ell_\zeta + \frac{y_\zeta\ell_{\dot{v}}}{\mu_2}\right]\zeta + \ell_{\dot{v}}\frac{s}{V}\left[\frac{g_3}{V}\phi + \frac{g_2}{V}\psi\right]\right\} + b_x q_e r + e_x q_e p + e_x\dot{r} , \qquad (A2\text{-}7)$$

where $\mu_2 = m/\rho Ss$, with an analogous equation for $\dot{r}$. The relative density, μ_2, is usually large, so that the derivatives due to sideslip and control deflections may be considered unchanged, and the combined derivatives, $\ell_p + \ell_{\dot{v}}\sin\alpha$, $\ell_r - \ell_{\dot{v}}\cos\alpha$ replace the derivatives ℓ_p and ℓ_r respectively. Thus for large μ_2, the perturbation equations of motion may be written

$$\dot{\beta} = \frac{\rho VS}{m}\left\{y_v\beta + y_\xi\xi + y_\zeta\zeta\right\} - r\cos\alpha + p\sin\alpha + \frac{g_3}{V}\phi + \frac{g_2}{V}\psi \qquad (A2\text{-}8)$$

$$\dot{p} = \frac{\rho V^2 Ss}{I_x}\left\{\ell_v\beta + (\ell_p + \ell_{\dot{v}}\sin\alpha)\frac{ps}{V} + (\ell_r - \ell_{\dot{v}}\cos\alpha)\frac{rs}{V} + \ell_\xi\xi + \ell_\zeta\zeta \right.$$
$$\left. + \ell_{\dot{v}}\frac{s}{V}\left[\frac{g_3}{V}\phi + \frac{g_2}{V}\psi\right]\right\} + b_x q_e r + e_x q_e p + e_x\dot{r} \qquad (A2\text{-}9)$$

$$\dot{r} = \frac{\rho V^2 Ss}{I_z}\left\{n_v\beta + (n_p + n_{\dot{v}}\sin\alpha)\frac{ps}{V} + (n_r - n_{\dot{v}}\cos\alpha)\frac{rs}{V} + n_\xi\xi + n_\zeta\zeta \right.$$
$$\left. + n_{\dot{v}}\frac{s}{V}\left[\frac{g_3}{V}\phi + \frac{g_2}{V}\psi\right]\right\} + b_z q_e p - e_z q_e r + e_z\dot{p} . \qquad (A2\text{-}10)$$

The gravity terms are usually small and do not have significant effects on the Dutch roll or roll subsidence modes so that the additional gravity contributions to the moment equations may be neglected. Thus a valid approximation to the effect of the derivatives due to acceleration in sideslip is to use the combined derivatives, as measured by an oscillatory rig, in place of those due to rates of roll and yaw**. By the same argument, the derivatives obtained from matching the flight records may be interpreted as being the combined derivatives, for direct comparison with the tunnel results. These remarks have to be modified for lateral responses which include a large contribution from the spiral mode[15].

---

* The alternative expressions in terms of the increments in bank angle, etc are not so convenient for non-zero steady bank angles.

** The physical explanation for this approximation is that the lateral displacement is constrained to be small for a model on an oscillatory rig, and is also usually small in the Dutch roll and roll subsidence modes.

A2.2 Effect of steady turn

If the small perturbation equations are used to obtain the lateral stability roots, then the effect of the steady turn may be incorporated by using effective derivatives in the moment equations,

where

$$\left.\begin{aligned} \ell_{p_{eff}} &= \ell_p + \ell_{\dot{v}} \sin\alpha + \frac{I_{xz}}{\rho V s^2} q_e \\ n_{p_{eff}} &= n_p + n_{\dot{v}} \sin\alpha + \frac{(I_x - I_y)}{\rho V s^2} q_e \end{aligned}\right\} \qquad (A2\text{-}11)$$

$$\left.\begin{aligned} \ell_{r_{eff}} &= \ell_r - \ell_{\dot{v}} \cos\alpha + \frac{(I_y - I_z)}{\rho V s^2} q_e \\ n_{r_{eff}} &= n_r - n_{\dot{v}} \cos\alpha - \frac{I_{xz}}{\rho V s^2} q_e \quad . \end{aligned}\right\} \qquad (A2\text{-}12)$$

The most important change is in the effective value of n_p, where the negative increment due to $q_e(I_y > I_x)$ is usually destabilising in the Dutch roll mode. This may be demonstrated by considering a first approximation to the Dutch roll damping, valid if ℓ_v and n_v do not tend to zero together. The lateral stability quartic, $\lambda^4 + a\lambda^3 + b\lambda^2 + c\lambda + d$, is assumed to be factorised as two quadratics $(\lambda^2 + 2k_D\lambda + \omega_D^2)(\lambda^2 + G\lambda + H)$, with H small. Then

$$\omega_D^2 \approx b, \quad G \approx \frac{c}{b} \text{ and } 2k_D \approx a - \frac{c}{b} \qquad (A2\text{-}13)$$

are the first approximations, which have then to be further simplified by including only major terms of a, b, c in terms of the derivatives. It is usually sufficient (for μ_2 large and i_{xz} small) to assume that

$$a \approx \frac{-1}{\hat{t}}\left\{y_v + \frac{\ell_{p_{eff}}}{i_x} + \frac{n_{r_{eff}}}{i_z}\right\} \qquad (A2\text{-}14)$$

$$b \approx \frac{1}{\hat{t}^2}\left\{\frac{\mu_2 n_v}{i_z}\cos\alpha - \frac{\mu_2 \ell_v}{i_x}\sin\alpha\right\} \qquad (A2\text{-}15)$$

$$c \approx \frac{1}{\hat{t}^3}\left\{\frac{\mu_2 n_v}{i_z}\left(-\frac{\ell_{p_{eff}}}{i_x}\cos\alpha - \frac{\ell_{r_{eff}}}{i_x}\sin\alpha - \frac{g_2\hat{t}}{V}\right) + \frac{\mu_2 \ell_v}{i_x}\left(\frac{n_{p_{eff}}}{i_z}\cos\alpha + \frac{n_{r_{eff}}}{i_z}\sin\alpha - \frac{g_3\hat{t}}{V}\right)\right\} \qquad (A2\text{-}16)$$

where $\mu_2 = \frac{m}{\rho S s}$

and $\hat{t} = \frac{m}{\rho S V}$.

The approximation for the damping index of the Dutch roll is then given by

$$k_D \approx -\frac{1}{2\hat{t}}\left\{y_v + \left[\frac{n_v}{i_z}\left(\frac{n_{r_{eff}}}{i_z}\cos\alpha - \frac{\ell_{r_{eff}}}{i_x}\sin\alpha - \frac{g_2\hat{t}}{V}\right) + \frac{\ell_v}{i_x}\left(\frac{n_{p_{eff}}}{i_z}\cos\alpha - \frac{\ell_{p_{eff}}}{i_x}\sin\alpha - \frac{g_3\hat{t}}{V}\right)\right] \Big/ \left[\frac{n_v}{i_z}\cos\alpha - \frac{\ell_v}{i_x}\sin\alpha\right]\right\} . \qquad (A2\text{-}17)$$

Although this approximation does not always give values of damping index very close to the actual level of damping, it does seem to give reasonable indication of the variation of damping with the derivatives. In particular,

$$\frac{\partial k_D}{\partial n_{p_{eff}}} \approx -\frac{1}{2\hat{t}}\frac{\ell_v}{i_x}\frac{\cos\alpha}{i_z}\frac{1}{\left[\frac{n_v}{i_z}\cos\alpha - \frac{\ell_v}{i_x}\sin\alpha\right]} , \qquad (A2\text{-}18)$$

which is positive for usual values of the sideslip derivatives, so that the effect of the steady pitch rate in the turn is to reduce the damping index of the Dutch roll mode.

The corresponding approximation for the damping of the roll subsidence mode is given by

$$k_R \approx G \approx -\frac{1}{\hat{t}}\left\{\frac{n_v}{i_z}\left(\frac{\ell_{p_{eff}}}{i_x}\cos\alpha + \frac{\ell_{r_{eff}}}{i_x}\sin\alpha + g_2\frac{\hat{t}}{V}\right) - \frac{\ell_v}{i_x}\left(\frac{n_{p_{eff}}}{i_z}\cos\alpha + \frac{n_{r_{eff}}}{i_z}\sin\alpha - g_3\frac{\hat{t}}{V}\right)\right\} \Big/ \left(\frac{n_v}{i_z}\cos\alpha - \frac{\ell_v}{i_x}\sin\alpha\right) . \qquad (A2\text{-}19)$$

Appendix A3

MATHEMATICAL MODELS USED IN SECTION 3

A3.1 Linear model

The basic linear model for the equations of motion are derived from those given in Appendix A1, with zero perturbation in control angles. The steady terms in the sideforce equation are balanced by the gravity component in a coordinated turn, so that p_e and r_e do not have to appear explicitly. In the moment equations, the terms containing q_e may be combined with the aerodynamic derivatives, to give effective values, *eg* $\overset{\circ}{\ell}_{p_{eff}} = (\overset{\circ}{\ell}_p - e_x q_e)$. With the assumption that y_p and y_r are small, the equations may be arranged to give

$$\dot{v} = \overset{\circ}{y}_v v + V \sin\alpha\, p - V \cos\alpha\, r + g_1\phi + g_2\psi \qquad \text{(A3-1)}$$

$$\dot{p} = \overset{\circ}{\ell}_v v + \overset{\circ}{\ell}_{p_{eff}} p + \overset{\circ}{\ell}_{r_{eff}} r - e_x \dot{r} \qquad \text{(A3-2)}$$

$$\dot{r} = \overset{\circ}{n}_v v + \overset{\circ}{n}_{p_{eff}} p + \overset{\circ}{n}_{r_{eff}} r - e_z \dot{p} \ . \qquad \text{(A3-3)}$$

The lateral stability quartic obtained from equations is of the form

$$D^4 + a_1 D^3 + b_1 D^2 + c_1 D + d_1 = 0 \ , \qquad \text{(A3-4)}$$

where a_1, b_1, c_1, d_1 are the usual combinations of derivatives.

A3.2 Nonlinear models

The nonlinear equations of motion considered have either the sideslip contributions, $\overset{\circ}{\ell}_v\dot{v}$ and $\overset{\circ}{n}_v v$, replaced by $\overset{\circ}{\ell}_{v1}v + \overset{\circ}{\ell}_{v3}v^3$ and $\overset{\circ}{n}_{v1}v + \overset{\circ}{n}_{v3}v^3$ respectively in equations (A3-2&3), or the rolling moment due to roll rate, $\overset{\circ}{\ell}_p p$, replaced by $\overset{\circ}{\ell}_{p1}p + \overset{\circ}{\ell}_{p3}p^3$ in equation (A3-2). Both resulting sets of equations may be reduced to the form

$$\frac{d^4x}{dt^4} + \frac{d^3}{dt^3}(a_1x + a_3x^3) + \frac{d^2}{dt^2}(b_1x + b_3x^3) + \frac{d}{dt}(c_1x + c_3x^3) + d_1x + d_3x^3 = 0 \ , \qquad \text{(A3-5)}$$

where a_1, b_1, c_1, d_1 have $\overset{\circ}{\ell}_v$ and $\overset{\circ}{n}_v$ replaced by $\overset{\circ}{\ell}_{v1}$ and $\overset{\circ}{n}_{v1}$ respectively, or $\overset{\circ}{\ell}_p$ replaced by $\overset{\circ}{\ell}_{p1}$. The coefficients a_3, b_3, c_3, d_3 may be derived by inspection, taking the factors of $\overset{\circ}{\ell}_v$, etc in a_1, b_1, c_1, d_1 , and multiplying them by $\overset{\circ}{\ell}_{v3}v^2$ etc.

An approximate analytic solution for the oscillatory mode is obtained by representing x by $X\cos\Psi$, where $d\Psi/dt = \omega(X)$ and $dX/dt = X\lambda(X)$. The average value of equation (A3-5) over one cycle ($\Psi = 0$ to 2π) is taken to be zero, with the assumption that ω and λ do not vary significantly during one cycle, and may be replaced by their value at mid-amplitude. It is shown in Ref 12 that the amplitude of a limit cycle X_s , (*ie* when $\lambda(X_s) = 0$) is given by an equivalent Routh's discriminant being zero,

$$R_1^* = a_1^* b_1^* c_1^* - a_1^{*2} d_1 - c_1^{*2} = 0 \ , \qquad \text{(A3-6)}$$

where

$$a_1^* = a_1 + \tfrac{3}{4}a_3X^2 \ldots, \ . \ d_1^* = d_1 + \tfrac{3}{4}d_3X^2 \ . \qquad \text{(A3-7)}$$

The frequency of the limit cycle is given by

$$\omega_s^2 = c_1^*/a_1^* = (c_1 + \tfrac{3}{4}c_3X_s^2)/(a_1 + \tfrac{3}{4}a_3X_s^2) \qquad \text{(A3-8)}$$

The solution of equation (A3-6) gives values of X_s^2 , either positive, or negative, or complex, of which the first possibility is the only one of interest. However, with positive X_s^2 , it is still possible to have positive or negative values of ω_s^2 , depending on the signs of c_3 and a_3 . If $X_s^2 > 0$ and $\omega_s^2 > 0$, then a limit cycle can occur, the type of solution originally being considered to represent wing rock. The combination $X_s^2 > 0$ and $\omega_s^2 < 0$ has also been obtained, and correlates with the existence of a divergence, X_s now being the critical amplitude above which divergence occurs. This is physically and mathematically acceptable, as the cos term, in $x = X\cos\Psi$, becomes a pair of exponential modes, $e^{\pm\omega_s t}$, one of which is necessarily divergent.

It is also possible to obtain equations relating local 'damping' and local 'frequency' with local amplitude X , assuming that $d\lambda/dX$ and $d\omega/dX$ are negligible. The equations are of the form

$$\omega^3(a_1 + \tfrac{3}{4}a_3X^2 + 4\lambda) = \omega\left[c_1 + \tfrac{3}{4}c_3X^2 + 2\lambda(b_1 + \tfrac{9}{4}b_3X^2) + 3\lambda^2(c_1 + \tfrac{27}{4}c_3X^2) + 4\lambda^3\right] \qquad \text{(A3-9)}$$

$$\omega^4 - \omega^2\left[b_1 + \tfrac{3}{4}b_3X^2 + 3\lambda(a_1 + \tfrac{9}{4}a_3X^2) + 6\lambda^2\right] + d_1 + \tfrac{3}{4}d_3X^2$$
$$+ \lambda(c_1 + \tfrac{9}{4}c_3X^2) + \lambda^2(b_1 + \tfrac{27}{4}b_3X^2) + \lambda^3(a_1 + \tfrac{81}{4}a_3X^2) + \lambda^4 = 0 \ . \qquad \text{(A3-10)}$$

If $\omega \neq 0$, then ω^2 may be eliminated, to give an equation relating λ and X , which is sextic in λ , and bicubic in X , so cannot be solved analytically.

STALL BEHAVIOUR EVALUATION FROM FLIGHT TEST RESULTS

by

Prof. Dr.-Ing. G. Sachs
Hochschule der Bundeswehr
München
D-8014 Neubiberg

Dipl.-Ing. H. Wünnenberg
Dornier GmbH
Postfach 1420
D-7990 Friedrichshafen

SUMMARY

By comparing the dynamic stall behaviour of a combat aircraft with a simulation a special type of discrepancy in roll was found. The simulation was based on the best wind tunnel data available. The examination leads to the conclusion, that the aircraft is disturbed by random-type "fluctuation"-forces and moments. The order of magnitude was estimated from the scattering region of the wind tunnel data beyond C_{Lmax}. Introducing these effects into the mathematical model it is possible to simulate the pilot in the loop dynamic stall behaviour with the aid of a simple mathematical pilot model. For a general application in the design stage of a new project, new wind tunnel test techniques including the measurement of the time-dependent parameters will be necessary.

1. INTRODUCTION

The stall and departure behaviour of an aircraft is one of the most important aspects of stability and control especially for fighter aircraft. This flight regime, which is normally outside the operational envelope of transport aircraft, has to be used by the fighter pilot for tactical maneuvers. Therefore a good behaviour within this regime, especially in the high speed case, will lead to extended maneuver boundaries, which is an important performance aspect, too.

Due to these facts a lot of efforts have been directed towards the physical understanding of the different phenomena and towards their prediction from wind tunnel test results to aid the design engineer in a proper configuration optimisation. Nevertheless, up till now there were merely "static" design criteria available, which lead to a certain probability of achieving good stall characteristics. These criteria are:

- no unstable pitching moments in the stall region
- no flow separation starting at the outer wing
- $C_{N_{\beta dyn}}$-criteria and LCDP to avoid uncontrollable motions and spin-sensitivity.

The physical background of the different phenomena like wing drop, wing rock and nose slice, which are caused by dynamic effects, is only partly known. There remains a large field for research including the need of expanding and improving the wind tunnel test techniques, which are necessary for the prediction of the phenomena and improving their characteristics prior to the first flight.

The objectives of a study, sponsored by the German Ministry of Defense, were to obtain an understanding of the physics of the dynamic low speed stall behaviour of a fighter aircraft and to assess their predictability from wind tunnel data. The results of this study are summarized in this paper.

2. DESCRIPTION OF THE ANALYSED PHENOMEN

The analysed phenomena were low speed 1g-stalls, typical parameters of which are given in Fig. 1:

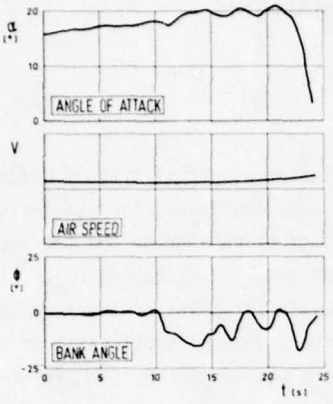

Fig. 1 TYPICAL STALL BEHAVIOUR

The pilot slowly increased the angle of attack. At a certain value of α the airplane suddenly develops a bank angle of medium magnitude. A further increase in angle of attack leads to a roll oscillation with small amplitudes (wing rock). To study this behaviour, a 6 DOF-digital simulation was used.

The mathematical model of the aircraft was improved by taking into account all the available wind tunnel results, especially at the higher angles of attack beyond C_{Lmax}. The flight test data were available on magnetic tape. The activity of the pilot in form of the deflections of the different control surfaces was taken as an input for the simulation directly from the flight test tape. The task was accomplished by matching the time histories of flight test and simulation through the following three step procedure:

- modification of the static derivatives
- modification of dynamic derivatives
- estimation of random-type influences.

For the evaluation several flights in cruise and landing configuration have been examined.

3. COMPARISON BETWEEN FLIGHT TEST AND SIMULATION

The Fig. 2a and b show the results of the comparison.

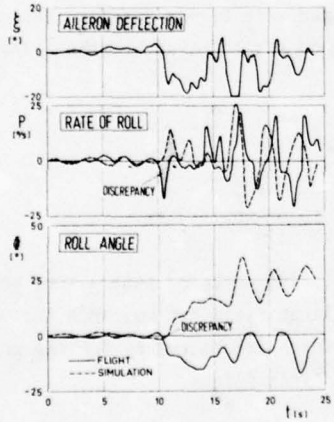

Fig. 2a DISCREPANCY BETWEEN FLIGHT TEST AND SIMULATION AT STALL

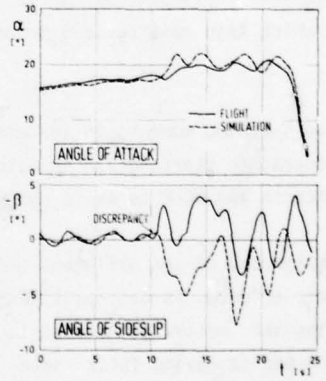

Fig. 2b DISCREPANCY BETWEEN FLIGHT TEST AND SIMULATION AT STALL (continued)

The upper trace on the Fig. 2a shows the aileron input for both the flight test and the simulation. At a time shortly after the 10 sec-mark the pilot made a large, nearly abrupt negative aileron input. This negative aileron input should result in a positive roll rate. This is true for the simulation trace, whereas the flight test trace shows the opposite. The discrepancy can be seen even more clearly in the time histories of the bank angle. In the flight test a roll to the left occurs, but the simulation produces a roll to the right. If this situation is examined in more detail, it can be seen, that shortly before the aileron is activated, an abrupt negative roll rate occurs. The pilot reacts with his aileron in-

put only to a sudden roll disturbance. The cause of this disturbance is not clear, as the excursions of the side slip angle can be correlated with the aileron deflections.

This situation leads to the conclusion that there are aerodynamic moments in the stall regime which appear suddenly with alternating sign and will therefore be called "fluctuation" moments.

4. ORDER OF MAGNITUDE OF THE "FLUCTUATION" MOMENTS

For the estimation of these disturbing moments the wing stall characteristics from the wind tunnel results were examined. Fig. 3 shows the flow separation area on the wing with increasing angle of attack. The figure shows two important features:

- Due to a sawtooth the separation area remains nearly at the same spanwise station with increasing angle of attack.
- The ailerons remain effective during the stall.

Fig. 4 shows some typical examples of the lift curve slope, and from tests with a half model the corres-

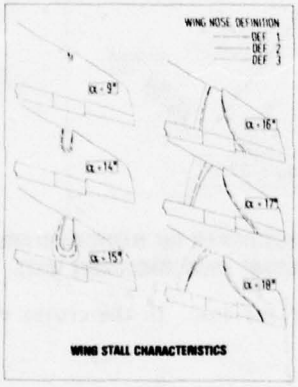

Fig. 3

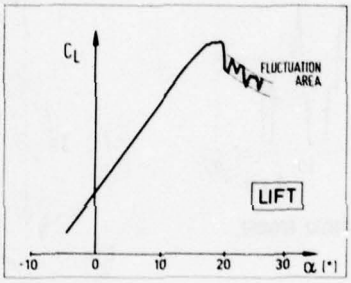

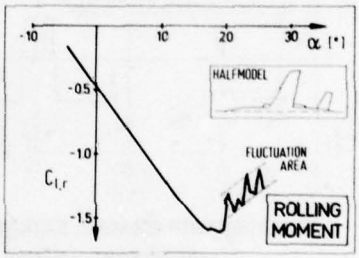

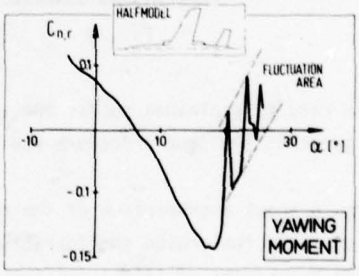

Fig. 4

FLUCTUATION AREAS OF LIFT, ROLLING AND YAWING MOMENT COEFFICIENTS FROM WINDTUNNEL TESTS

ponding rolling and yawing moment coefficients. It can be seen that there are certain areas beyond the C_{Lmax} for all three parameters, where the values are no longer steady but change within certain limits. It means, that within the stall regime changes in lift and drag up to certain maximum values are possible. These "fluctuation"-regions correspond to each other and also to the lift losses which can be derived from the flow separation areas of Fig. 3.

This examination allows an assessment of the order of magnitude of the fluctuation lift-, rolling- and yawing moment coefficients disturbing the aircraft. They will be taken into account in the subsequent analysis.

5. SIMULATION WITH AN EXPANDED MATHEMATICAL MODEL

By introducing these fluctuation lift and moment coefficients in a proper manner, Fig. 5 , it is possible to get a good agreement between simulation and flight test results. The ratios between the three coefficients remain constant, which corresponds to the wind tunnel results shown in Fig. 4.

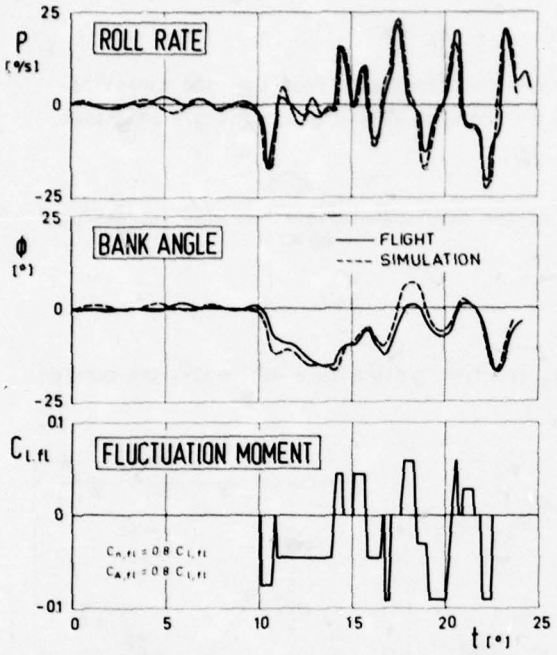

SIMULATION WITH ENLARGED MATHEMATICAL MODEL. LANDING CONFIGURATION

Fig. 5

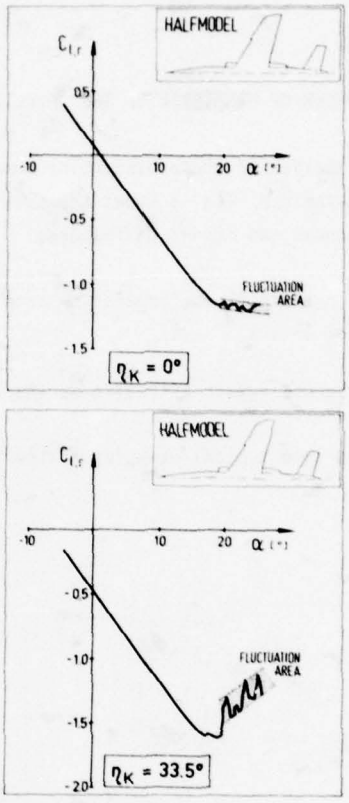

Fig. 6

INFLUENCE OF FLAP DEFLECTION ON THE FLUCTUATION AREA OF THE ROLLING MOMENT FROM WINDTUNNEL TESTS

The results explained so far are valid for the landing configuration with flaps down. In the cruise configuration the same procedure was used with similar results.

Fig. 6 shows a comparison of the rolling moment fluctuation regions for cruise and landing configurations. For the cruise configuration the fluctuation amplitudes are smaller. It is evident that the amplitude bandwidths of lift-, rolling- and yawing moment coefficients are different for the two flap deflections, but also that the bandwidths are constant with angle of attack.

Fig. 7 shows the corresponding comparisons of the flight test data and the simulation results obtained with the classical mathematical model and the expanded model which takes into account lift and moment fluctuations. It can be seen that the stall is controlled only by elevator and aileron with nearly no use of the rudder. The introduction of fluctuation effects leads to a good agreement not only for the roll parameters, but also for side slip and yaw rate.

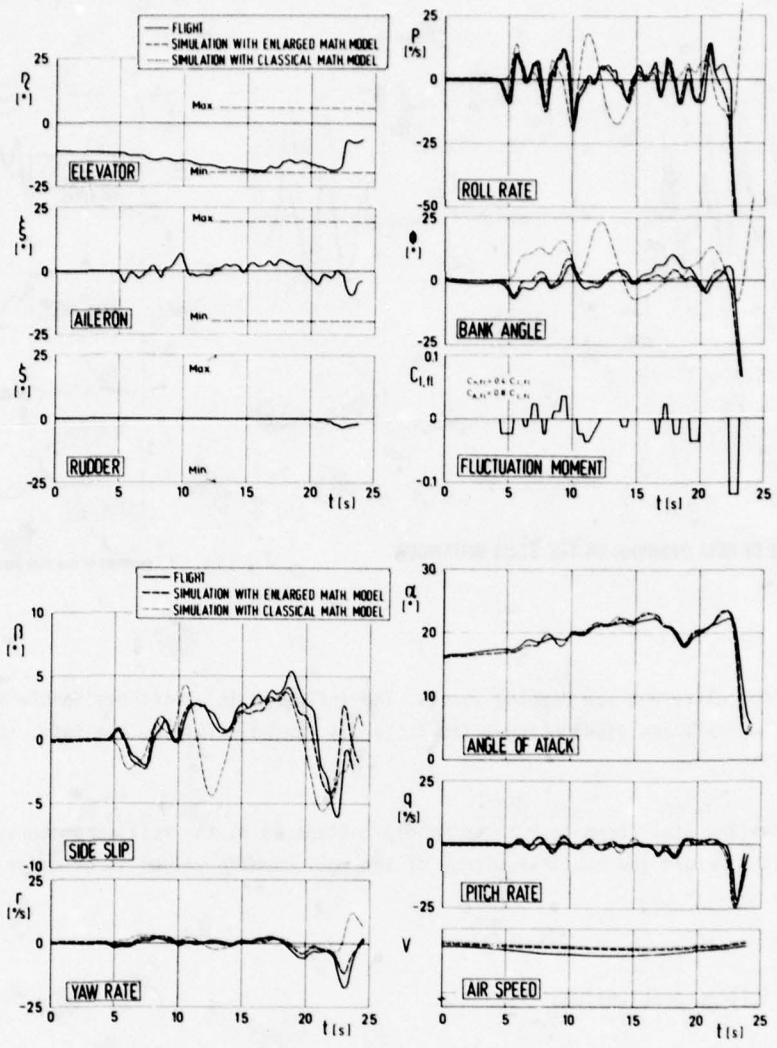

Fig. 7 **STALL BEHAVIOUR IN CRUISE CONFIGURATION**

From the Fig. 7 it can also be seen, that the stall behaviour for this aircraft is mainly influenced by the lateral motion degrees of freedom as the longitudinal motion is not effected by these additional inputs. The longitudinal motion is of minor importance. In the flight mechanical sense this means a separation of the longitudinal and lateral motions in the case where the stall behaviour is mainly characterised by the wing rock phenomena.

6. INFLUENCE OF THE DYNAMIC DERIVATIVES ON THE STALL BEHAVIOUR

Fig. 8 shows the influence of roll damping on the simulated stall behaviour with fluctuation moments. There is a strong effect of roll damping on the amplitudes of the rolling parameters and on the side slip angle. But there is no phase shift or deviation in the traces comparable to the effects of the fluctuation moments.

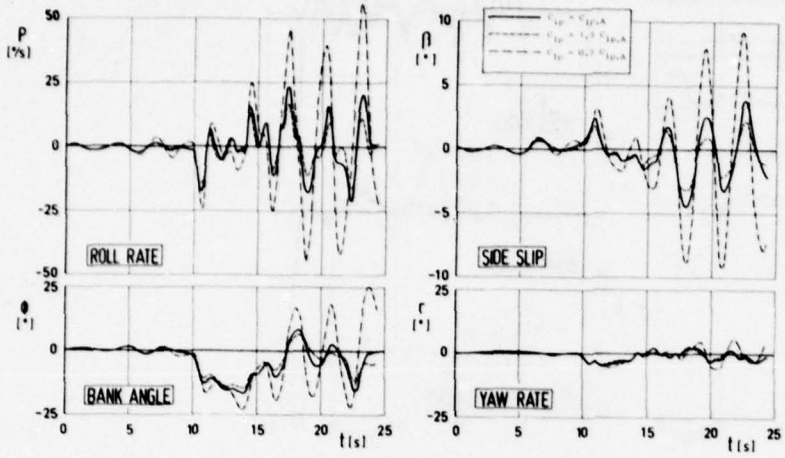

Fig. 8 **INFLUENCE OF ROLL DAMPING ON THE STALL BEHAVIOUR**

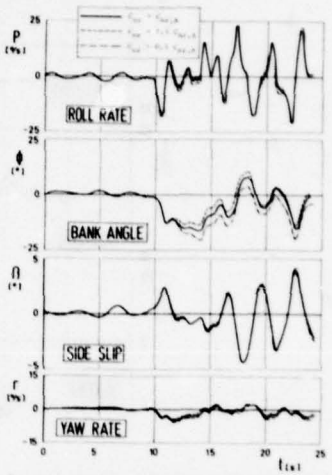

Fig. 9 **INFLUENCE OF YAW DAMPING ON THE STALL BEHAVIOUR**

Fig. 9 shows the same for different yaw damping values. The influence is almost negligible excepting the bank angle which shows a small amplitude change. The latter is caused mainly by the fact, that the yaw rates at stall are small.

Since these results show the stall behaviour to be mainly influenced by the roll parameters, it must be concluded that for this aircraft the exact knowledge of the roll damping values is of major importance.

7. POTENTIAL PRACTICAL APPLICATIONS

Although the introduction of the fluctuation moments has served to illustrate the wing rock-type stall behaviour of this aircraft, the question remains how this can be used in practice. As the main interest is directed towards the prediction of the stall behaviour, an attempt was made to use a mathematical pilot model. The question was: Will it be possible, provided the fluctuation forces and moments can be measured in the wind tunnel, to simulate the stall behaviour with the pilot in the loop?

The task of introducing a mathem. pilot model controlling the stall was relatively simple. As already pointed out, there is almost no coupling between the longitudinal and lateral motions. The fluctuation lift changes are small in comparison to the available lift at stall. The pitching moments are negligible due to the fact that the flow separation occurs at a wing station which is located near the center of gravity and outboard of the tail. Therefore the control of the longitudinal motion by the pilot can be regarded as a control task without feedback. For this reason the elevator or the angle of attack time history need not be controlled by the pilot model but can be used as given.

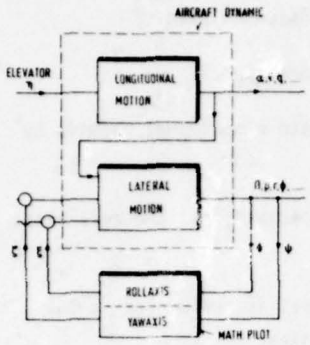

BLOCKDIAGRAM OF THE OPERATION OF THE MATHEMATICAL PILOT

Fig. 10

Those considerations result in a simple pilot model, which operates as described in Fig. 10. The mathematical pilot is working only in roll and yaw, controlling the bank angle in roll and the azimuth angle in yaw. The elevator input is taken from the original flight test tape to have a reference in angle of attack which influences the lateral derivatives.

The pilot model itself is the wellknown transfer function from Ref. [12].

$$Y_p(s) = K_p \frac{1 + T_L s}{1 + T_I s} \cdot \frac{e^{-\tau s}}{1 + T_N s}$$

As the roll axis is dominant, the comparison was done with and without the yaw pilot. The results are shown on the Fig. 11 for the pilot's acitivity and on Fig. 12 for the motion parameters. The figures show that even with the roll pilot alone the agreement with the flight test results is excellent.

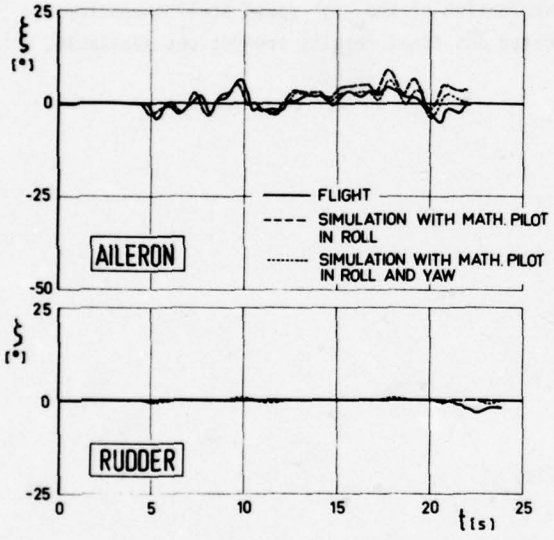

Fig. 11 **STALL CONTROLING BY A MATHEMATICAL PILOT**

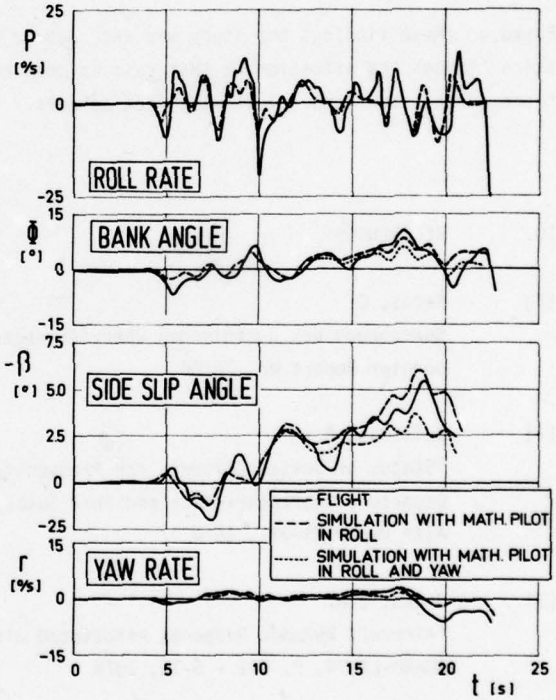

Fig. 12 **STALL CONTROLING BY A MATHEMATICAL PILOT**

This result leads to the conclusion that it will be possible to calculate the probable stall characteristics with the pilot in the loop, if the disturbing forces and moments are known. This information can only be obtained through improved wind tunnel measuring techniques, where the time dependent forces and moments rather than averaged values can be measured.

8. SUMMARY AND CONCLUSTIONS

- The dynamic stall behaviour of an aircraft cannot be completely characterized by steady-state aerodynamic forces and moments, time-dependent contributions, have to be considered also.
- These time dependent excursions, called fluctuation moments, are of random type.
- The maximum values of the fluctuation can be derived from the steady-state wind tunnel results by the scatter width of the values beyond the C_{Lmax}.
- The fluctuation effects are important mainly for the lateral motion, especially for the roll axis; the influence on the longitudinal motion is nearly negligible.
- The longitudinal motion is independent of the lateral, whereas the lateral is influenced by the longitudinal motion through the angle-of-attack-dependent lateral derivates.
- For the prediction of the dynamic stall behaviour from wind tunnel tests it is necessary to extend the measuring techniques to resolve time-dependent effects.
- With these effects it is possible to simulate the probable stall behaviour by simple mathematical pilot models where the control of the roll axis is important.

Based on these findings the study was extended to the examination of the high speed stall characteristics. Though the situation in that case is more complicated and final results are not yet available, there is the same tendency if wing rock appears.

10. REFERENCES

[1] Sachs. G.
Berechnung des dynamischen Oberziehvorgangs
Dornier Report Nr. 76/88

[2] Weissman, R.
"Status of Design Criteria for Predicting
Departure Characteristics and Spin Susceptibility",
AIAA Paper 74-791, 1974

[3] Jones, J.G.
"Aircraft Dynamic Response Associated with Fluctuating Flow Fields",
AGARD-LS-74, P. 5-1 - 5-15, 1975

[4] Johnston, D.E., Hogge, J.R.,
The Effect of Non-Symmetric Flight on Aircraft High Angle of Attack
Handling Qualities and Departure Characteristics",
AIAA Paper 74-792, 1974

[5] Pelikan, R.J.
"Evaluation of Aircraft Departure Divergence Criteria with a Six-
Degree-of-Freedom Digital Simulation Program",
AIAA Paper 74-68, 1974

[6] Lamers, J.P.
"Design for Departure Prevention in the YF-16",
AIAA Paper 74-794, 1974

[7] Bihrle, W. jr., Meyer, R.
"F-14A Flight Characteristics at High Angles of Attack",
AIAA Paper 75-170, 1975

[8] Weissman, R.
"Preliminary Criteria for Predicting Departure Characteristics/
Spin Susceptibility of Fighter-Type Aircraft",
Journal of Aircraft, Volume 10, Nr. 4,
P. 214-219, 1973

[9] Schoenstadt, A.L.
"Nonlinear Relay Model for Post-Stall Oscillations",
Journal of Aircraft, Volume 12, Nr. 7, P. 572-577, 1975

[10] Thomas, H.H.B.M.
"On Problems of Flight over an Extended Angle-of-Attack Range",
Aeronautical Journal, S. 412-423, 1973

[11] AGARD-LS-74, Aircraft Stalling and Buffeting,
März 1975

[12] Etkin, B.
"Dynamics of Atmospheric Flight",
John Wiley, New York, 1972

[13] Kalriste, Juri
"Aircraft Stability at High Angles of Attack
AGARD-FDP Symposium, Athens, Greece, 1978

[14] Skow A.M., Titiriga A.
"A Survey of analytical and experimental Techniques to predict
Aircraft dynamic Characteristics at high Angles of Attack
AGARD-FDP Symposium, Athens, Greece, 1978

HYBRID COMPUTER INVESTIGATION OF DISCRETE GUST AND WINDSHEAR EFFECTS ON AUTOMATIC LANDING SYSTEM PERFORMANCE

by

K.W. Rosenberg

Flight Controls Division

Marconi Avionics

Airport Works, Rochester, Kent, England.

SUMMARY

Operational experience has shown that during the landing approach particular patterns of gusts or windshear can result in unexpected system behaviour with increased probability of poor landing performance or hazard to the aircraft.

Consideration has been given to the certification of Automatic Landing Systems by assessing the response to single and pairs of discrete gusts of various shapes and timings in addition to the current practice of using random turbulence, described by power spectral density considerations, with fixed pattern windshear.

An Automatic Landing System has many non-linearities arising from the Aerodynamic Model and the Autopilot control laws, also the gust scale length varies with altitude making the determination of critical gust patterns a complex problem. Hence an automatic search employing a hybrid computer provides a means of identifying critical cases when there are many variables for the designer to consider.

A hybrid computer investigation is described which includes a search routine which allows the gust parameters and point of application of the gust to be varied so that the limiting touchdown range and vertical velocity for a given gust intensity can be determined.

The results are discussed and compared with the performance assessment using conventional certification criteria. The feasibility of this method as a general design tool for flight control systems is also discussed.

1. INTRODUCTION

Over recent years some doubts have been expressed as to the completeness with which aircraft Automatic Landing Systems can be assessed using turbulence models defined by Power Spectral Density methods. Once the primary decision has been taken as to which of the many turbulence models should be adopted there must always be doubts regarding the accuracy of the chosen model. Clearly since no single turbulence model covers all aspects of atmospheric disturbances the turbulence model chosen must be that which is best suited to the application under consideration.

Continuing analysis of measured atmospheric disturbances, especially in the earth's boundary layer, suggests that the Power Spectral Density models may be pessimistic in the average situation but have no adequate representation of the squall condition where large atmospheric disturbances can occur completely unrelated to the average situation. Further, analysis of simulation results obtained using Power Spectral Density turbulence models indicate a strong correlation between the occurrence of extreme flight parameters following the random occurrence of an extreme gust pattern.

In the aircraft Automatic Landing analysis it is the extreme occurrences, which can lead to an aircraft incident, that are of particular interest. This leads to two observations regarding analysis by Power Spectral Density methods. Firstly, since it is the unusual events which are of interest, the majority of work will only contribute to the information background. Secondly, in atmospheric turbulence, the extreme events are those which are least well represented by the Power Spectral Density models.

One approach to these problems has been the development of a statistical discrete gust model which takes a discrete ramp gust as the basic element, Ref (1). From these elements realistic gust patterns can be built and related to a probability of occurrence.

This approach is particularly relevant to situations where the system is highly non-linear such as the landing approach of an aircraft. The aerodynamic coefficients are not only non-linear in themselves but ground effects cause additional changes in the later stages of the approach. The autopilot and autothrottle control will contribute to

the non-linearity of the problem as the modes progress through capture to track and finally automatic flare out with possibly an associated programme throttle closure phase. Coupled with these effects are the non-linearities of the ground based ILS equipment leading to an overall system of such complexity that not only is the gust shape important but the point of application is highly critical.

The simulation of these effects on the automatic landing performance of a modern transport aircraft has been studied on a hybrid computer. The aim of the MOD funded study was to evaluate the discrete gust, or pattern of gusts, together with the gust intensity corresponding to critical values of touchdown parameters. Figure 1 shows a block diagram of the major functional components of the simulation. The optimisation routine was developed by MOD, and was used to optimise the discrete gust parameters to maximise the aircraft touchdown parameter deviations. The advantage of a hybrid simulation is that the problem may be readily timescaled to run very much faster than real time for the search routine, or at real time to produce time histories of particular gust patterns.

2. TURBULENCE INTENSITY

As an overall measure of atmospheric disturbances, a scalar reference intensity $\bar{\sigma}$ is defined, Ref (2) and Ref (3). Although having the dimension of an rms turbulence velocity, and in some cases being identical with the rms values of actual turbulence velocity components, $\bar{\sigma}$ is strictly only a general scaling factor relating to either a power spectral or a discrete gust model.

Figure 2 gives guidance on the probability of turbulence equalling, or exceeding, a given reference intensity $\bar{\sigma}$ for specific altitudes, Ref (3). The probabilities presented are based on global statistics and contain contributions from all types of turbulence (clear air, storm, boundary layer, etc).

It is assumed that there is a finite probability of conditions existing with zero turbulence reference intensity $\bar{\sigma} = 0$. This produces a step in the distribution function at $\bar{\sigma} = 0$ and explains why the curves in figure 2 do not tend to the value 1.0 as $\bar{\sigma}$ tends to zero.

Above 75m $\bar{\sigma}$ varies smoothly with altitude and values for altitudes between those shown in figure 2 may be found by interpolation. Below 75m $\bar{\sigma}$ remains constant.

3. DISCRETE GUST MODEL

The discrete gust model is intended to cover two contingencies, Ref (3). Firstly the case of the large gust embedded in continuous turbulence, where the reference intensity of the turbulence and that of the discrete gust are related, and secondly, the isolated event such as a squall where the intensity acts merely as a parameter relating the discrete gust amplitude to its probability of occurrence.

The discrete gust models are compatible with the energy distribution of the von Karman form of the power spectrum and define families of gusts of equal probability. Two distinct gust patterns are considered: a single ramp gust as the fundamental model and a sequence of two such ramps, of opposite sign, for cases where a resonant build-up of response is possible.

The general form of the single ramp gust is shown in figure 3(a). This form is applicable to all three components of turbulence, forward, cross and vertical with Vg_m then taking the corresponding particular values of ug_m, vg_m or wg_m.

For conditions defined by given values of the reference intensity $\bar{\sigma}$ and scale lengths Lu, Lv and Lw, a family of equiprobable gusts if formed by varying the gradient distance H, and hence gust amplitude ug_m, vg_m, and wg_m such that the following relationships are satisfied:

$$ug_m = 1.25\, J \left(\frac{H}{750}\right)^{1/3} \bar{\sigma} \qquad H \leq Lu$$

$$ug_m = 1.25\, J \left(\frac{Lu}{750}\right)^{1/3} \bar{\sigma} \qquad H > Lu$$

$$vg_m = 1.45\, J \left(\frac{H}{750}\right)^{1/3} \bar{\sigma} \qquad H \leq Lv$$

$$vg_m = 1.45\, J \left(\frac{Lv}{750}\right)^{1/3} \bar{\sigma} \qquad H > Lv$$

$$wg_m = 1.45\, J \left(\frac{H}{750}\right)^{1/3} \bar{\sigma} \qquad H \leq Lw$$

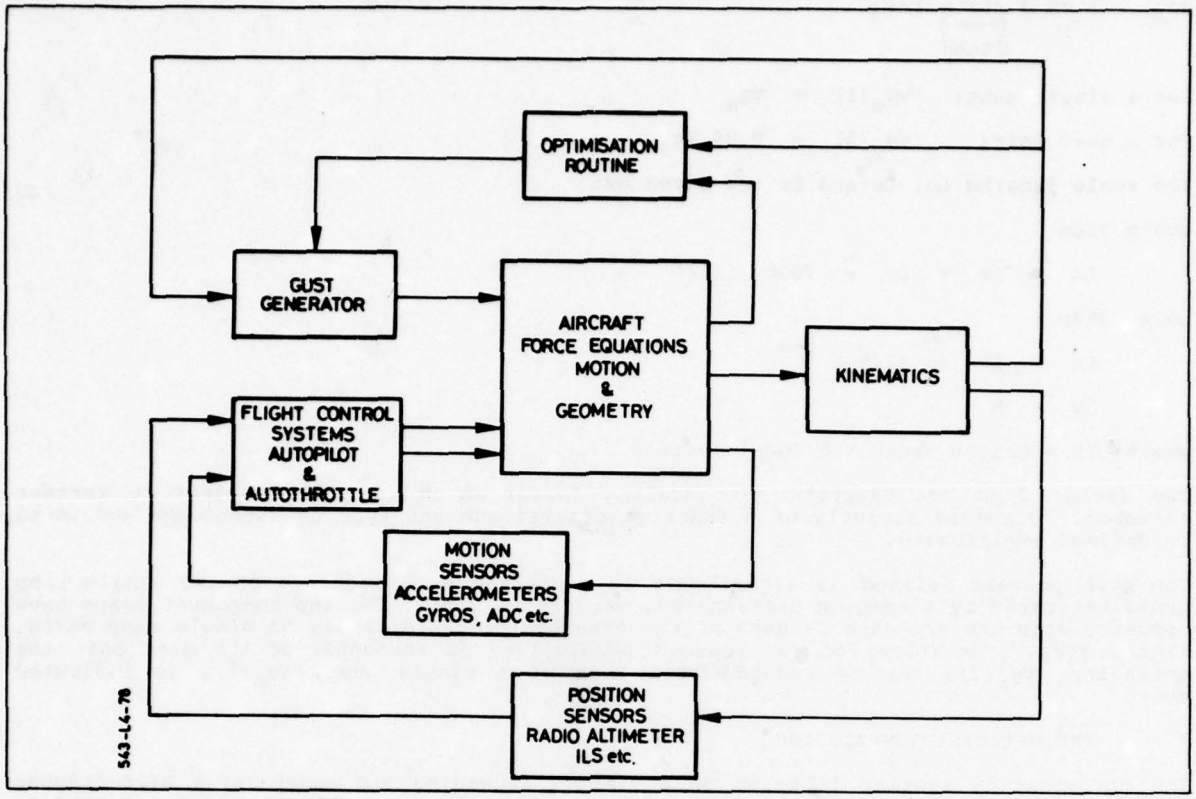

Figure 1 System Schematic

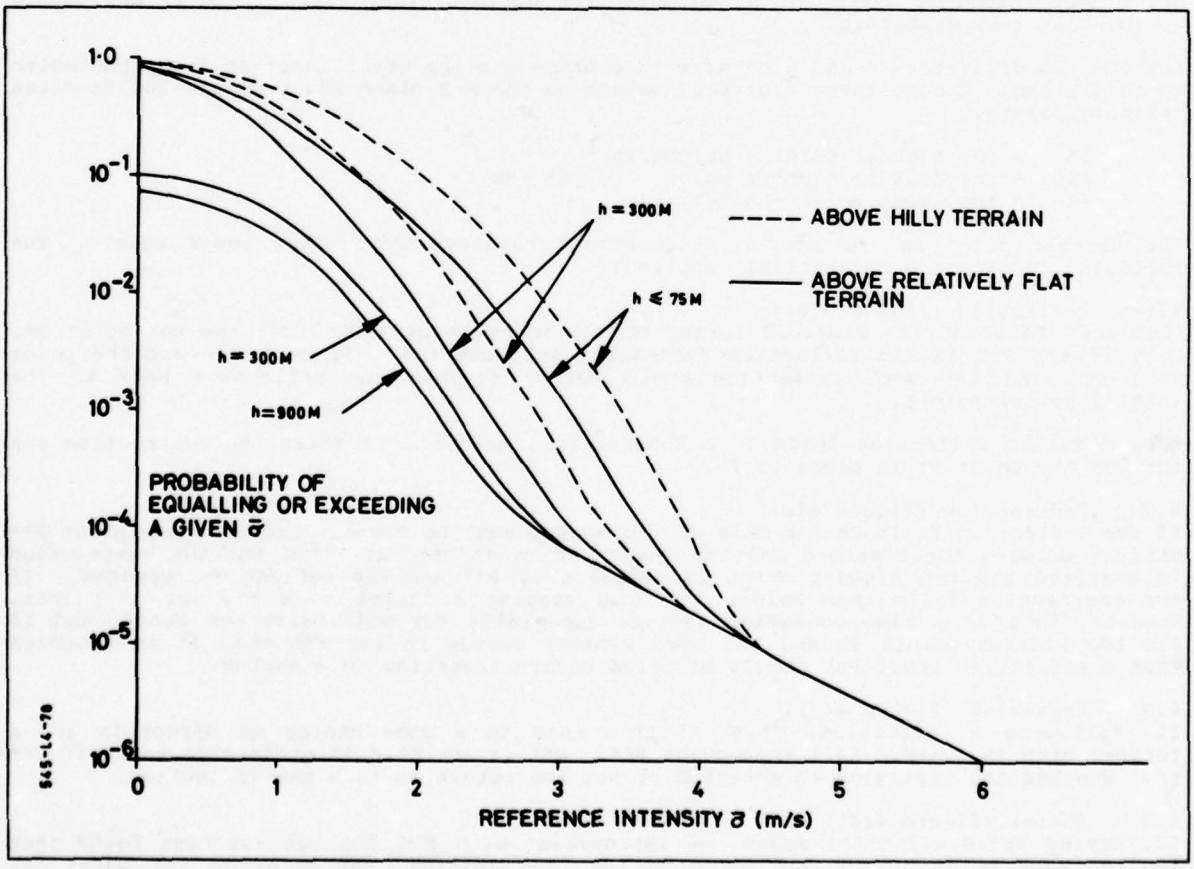

Figure 2 Probability of Turbulence Equalling or Exceeding a Given Reference Intensity at Specific Altitudes

$$wg_m = 1.45\ J \left(\frac{Lw}{750}\right)^{1/3} \bar{\sigma} \qquad H > Lw$$

For a single gust: $Vg_m(1) = Vg_m$

For a gust pair: $Vg_m(2) = 0.85\ Vg_m$

The scale lengths Lu, Lv and Lw are given by:

above 750m

$$Lu = Lv = Lw = 750m$$

below 750m

$$Lu = Lv = 82.5\ h^{1/3}$$

$$Lw = h$$

where: h = height above the local terrain

The factor J is the discrete gust scaling factor which is still subject to further research. J should strictly be a function of altitude and type of turbulence and is to be defined empirically.

The gust pattern defined as a gust pair is conceived as a sequence of two single ramp gusts separated by a spacing distance Hs, see figure 3(b). The two component ramps have opposite sign and are each members of the same equiprobable family of single ramp gusts, figure 3(c). To allow for the reduced probability of encountering the gust pair the intensity, $Vg_m(2)$, may be reduced from that of a single gust, $Vg_m(1)$, as indicated above.

4. THE OPTIMISATION ROUTINE

The optimisation routine is based on a simplex expanding and contracting hill-climber algorithm developed by Nelder and Mead. Although called a hill-climber the method is used in reverse to descend to a minimum and is basically a means of locating the minimum of a multi parameter function by means of an ordered series of function evaluations. A brief description is given for a two parameter optimisation. The method is applicable up to about ten parameters.

Let the two parameters A and B be axes in a plane and the error function F perpendicular to this plane. Choose three arbitrary points on the A-B plane and evaluate the function at these points:

Ph - the highest point - height Fh
Pnh - the next to highest point - height Fnh
Pl - the least point - height Fl

The highest point in the set is successively replaced by another lower point. The following tactics are repetitively applied:

4.1 Reflection (figure 4(a))

'Reflect' Ph about the centroid formed by all points except Ph. Call the new point P*. Only if F* < Fnh is the reflection successful and accepted. If F* > Fnh and the point were accepted the next reflection would merely reverse the reflection back to the initial set of points.

Thus a failed reflection leads to a contraction, however, if F*<Fh the contraction can include the point P* in place of Ph.

4.2 Contraction (figure 4(b))

If the reflection fails then a more cautious step must be taken. Choose a new point P** halfway between the centroid and the lesser of Ph or P*. If F** < Fnh the contraction is accepted and the highest point is replaced by P** and the reflection repeated. If the contraction fails then Nelder and Mead suggest a shrink to a new set of points. However, this is a time consuming tactic, especially for multiparameter cases, and if the two highest points Ph and Pnh have similar values Fh and Fnh then it is proposed that a reflection about Pnh should be tried before resorting to a shrink.

4.3 Expansion (figure 4(c))

If, following a reflection, F* < Fl then this is a good choice of direction and a further step is tried. Call this point P**. P** is accepted in preference to P* if F**< F*. Whether the expansion is accepted or not the return is to a new reflection.

4.4 Shrink (figure 4(d))

If, having tried all other means, an improvement with F < Fnh has not been found then replace each point by the mid-point of the line joining that point to the point Pl. Evaluate new function values and sort into order before proceeding with a new reflection.

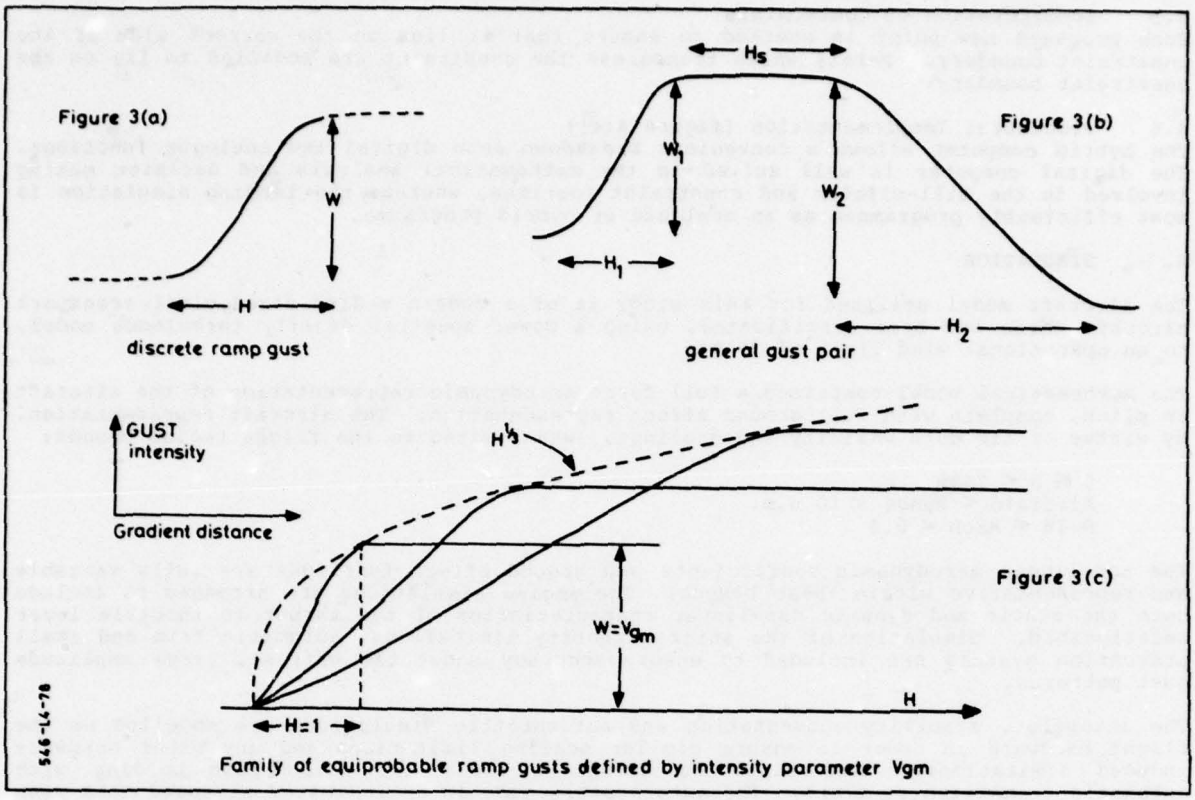

Figure 3 Discrete Gust Models

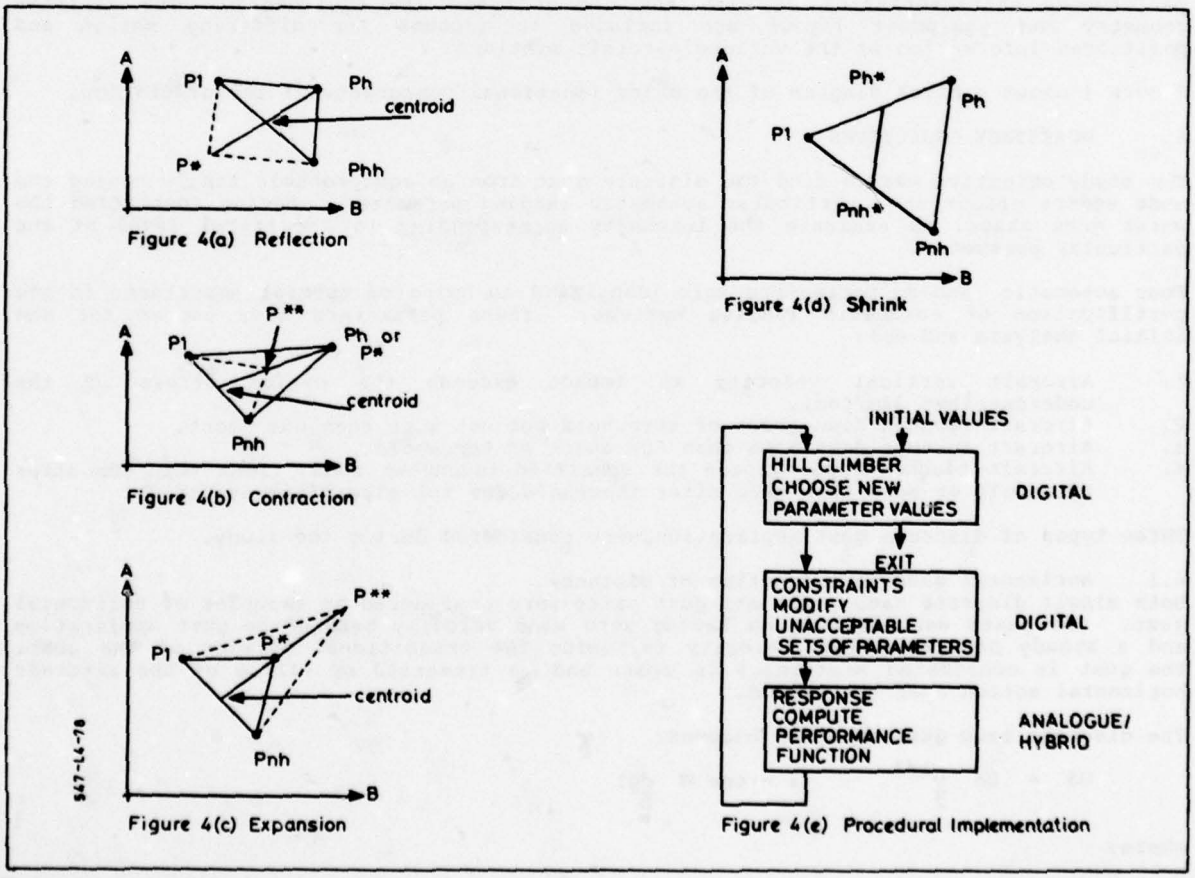

Figure 4 Optimisation Routines

4.5 Incorporation of Constraints
Each proposed new point is checked to ensure that it lies on the correct side of the constraint boundary. Points which transgress the constraint are modified to lie on the constraint boundary.

4.6 Procedural Immplementation (figure 4(e))
The hybrid computer allows a convenient breakdown into digital and analogue functions. The digital computer is well suited to the mathematical analysis and decision making involved in the hill-climber and constraint routines, whereas the landing simulation is most efficiently programmed as an analogue or hybrid programme.

5. SIMULATION

The aircraft model utilised for this study is of a modern medium-sized civil transport aircraft which has been certificated, using a power spectral density turbulence model, to an operational wind limit of 25 kts.

The mathematical model comprised a full force aerodynamic representation of the aircraft in pitch, complete with full ground effect representation. The aircraft representation, by virtue of its data validity and scalings, was limited to the flight regime bounds:

$0 \leq h < 750m$
Airfield $<$ Range $<$ 10 n.m.
$0.18 <$ Mach < 0.4

The non-linear aerodynamic coefficients and ground effect functions are fully variable and representative within these bounds. The engine simulations are arranged to include both the static and dynamic non-linear characteristics of the thrust to throttle lever relationship. Simulation of the stick authority limitations, automatic trim and stall prevention systems are included to ensure accuracy under the extreme, large amplitude gust patterns.

The autopilot, stability augmentation and autothrottle simulations are modelled on the flight hardware in order to ensure similar scaling limitations and any other hardware induced limitations. The simulated autopilot modes are glide path holding with automatic transition to flare. The autothrottle mode is an indicated airspeed hold with programmed throttle closure during the flare phase.

The equipment sensors are simulated to include any non-linearities, limits and dynamic performance characteristics as with the ground based ILS equipments. The airframe geometry and equipment layout are included to account for differing motion and positioned information at the various aircraft stations.

Figure 1 shows a block diagram of the major functional components of the simulation.

6. WORKSTUDY OBJECTIVES

The study objective was to find the discrete gust from an equiprobable family having the most severe effect on a particular automatic landing parameter. Having identified the worst gust shape, to evaluate the intensity corresponding to a critical level of the particular parameter.

Four automatic landing parameters were identified as being of special importance in the certification of automatic landing systems. These parameters were chosen for the initial analysis and are:

1. Aircraft vertical velocity at impact exceeds the design stress of the undercarriage (4m/sec).
2. Aircraft touches down short of threshold but not more than 60m short.
3. Aircraft touches down more than 60m short of threshold.
4. Aircraft touches down outside the specified touchdown zone. (less than 60m after threshold or more than 805m after threshold for the aircraft considered).

Three types of discrete gust application were considered during the study.

6.1 Horizontal gust as a function of distance.
Both single discrete ramp gusts and gust pairs were considered as examples of horizontal gust. The gusts were defined as having zero wind velocity before the gust application and a steady head/tail wind velocity following the transitional portion of the gust. The gust is considered stationary in space and is traversed by virtue of the aircraft horizontal motion over the ground.

The discrete ramp gust equation becomes:

$$Ud = Un \left(\frac{D}{2}\right)^{1/3} \left(1 - \cos \pi \frac{dg}{D}\right)$$

where:

Un = Gust intensity
D = gradient distance $0 < D < 184h^{1/3}$
dg = ground distance into gust $0 < dg < D$

h = local aircraft height.

6.2 Horizontal gust as a function of height
Again both single gusts and gust pairs are to be considered. The gusts have zero wind velocity before application and a steady head/tail wind velocity following the transitional part of the gust. The gust is considered to be stationary in space and is traversed by virtue of the aircraft vertical motion through the atmosphere.

The discrete ramp gust equation becomes:

$$Uh = Un \left(\frac{H}{2}\right)^{1/3} (1 - \cos \pi \frac{hg}{H})$$

where:

H = gradient height
hg = height distance into gust $0 < hg < H$

6.3 Vertical gust as a function of distance
Vertical gusts are only considered as gust pairs since a steady vertical draught will not occur over infinite distance. However, there is no restriction that the aircraft cannot land during the gust pair. The gust pair was defined as having zero vertical draught before and after the entire gust pair. The vertical draught may be in an upward or downward direction. The gust pair is considered stationary in space and is traversed by virtue of the aircraft horizontal motion over the ground.

The discrete gust pair is made up of two ramp gusts separated by a distance ds. The two ramp gusts are of opposite sign and each has the form:

$$Wd = U2 \left(\frac{D}{2}\right)^{1/3} (1 - \cos \pi \frac{dg}{D})$$

ds = separation $0 \leq ds < 5 \times (SL)$

where:

D = gradient distance $0 < D < SL$
SL = scale length = h at 2nd ramp gust start

7. RESULTS

Initially it was considered possible that the error functions would exhibit a single minimum and that by initialising the optimisation routine at two or three extremes, a positive identification of the most critical gust would be achieved. The results, however, soon showed this to be untrue. Random starting points led to convergence on differing local minima and a more systematic selection of starting points had to be adopted.

For the case of the single discrete gust, a raster scan of the two parameters, gust initiation point and gust gradient distance, enabled contour plots of the touchdown parameters to be constructed. Using these contour plots for guidance, it becomes a relatively simple matter to initialise the optimisation routine in the vicinity of the critical gust pattern.

For the discrete gust pair, however, this approach is not feasible. With two gusts the number of independent variables increases to four and the number of runs required to cover a full raster scan of all parameters becomes prohibitive. Also a five dimensional summary of the results is impracticable. The preliminary investigations showed that the optimisation routine was most critical to the initial gust application point and that the initial gust gradient lengths were of minor importance. This is because the local minima in the error functions tend to occur as functions of the gust application point and the optimisation routine will converge to the nearest local minimum. The approach adopted for gust pairs was to consider permutations of three first gust application points coupled with three second gust application points with a nominal value for the gust gradient lengths. This gives a selection of nine predefined starting points for the optimisation routine.

7.1 Horizontal Gust as a Function of Distance
The three criteria of hard touchdown, short touchdown and long touchdown ranges were investigated. Table 1 summarises the results and includes the approximate peaks indicated by the single gust parameter scan and the true peaks found by the optimisation routine. Figures 5 and 6 show examples of typical results obtained from the raster scans. Shaded regions are included to indicate the area of gust parameter combinations which result in a discrete gust sufficient to cause an exceedance of the glide beam monitor. For the discrete gust pairs the optimisation routine was initiated at each of the predefined starting points and allowed to coverge to a minimum. This resulted in several equally severe gust shapes being found which at first sight seemed unrelated. However, further analysis showed that one of the elements of the discrete gust pairs was almost identical in each instance and correlated with the most critical single discrete gust. Figure 7(a) shows a selection of these critical single gust and gust pair shapes which result in a hard touchdown. Figure 7(b) and 7(c) show the equivalent information for short touchdown range and long touchdown range. The gust shapes have been

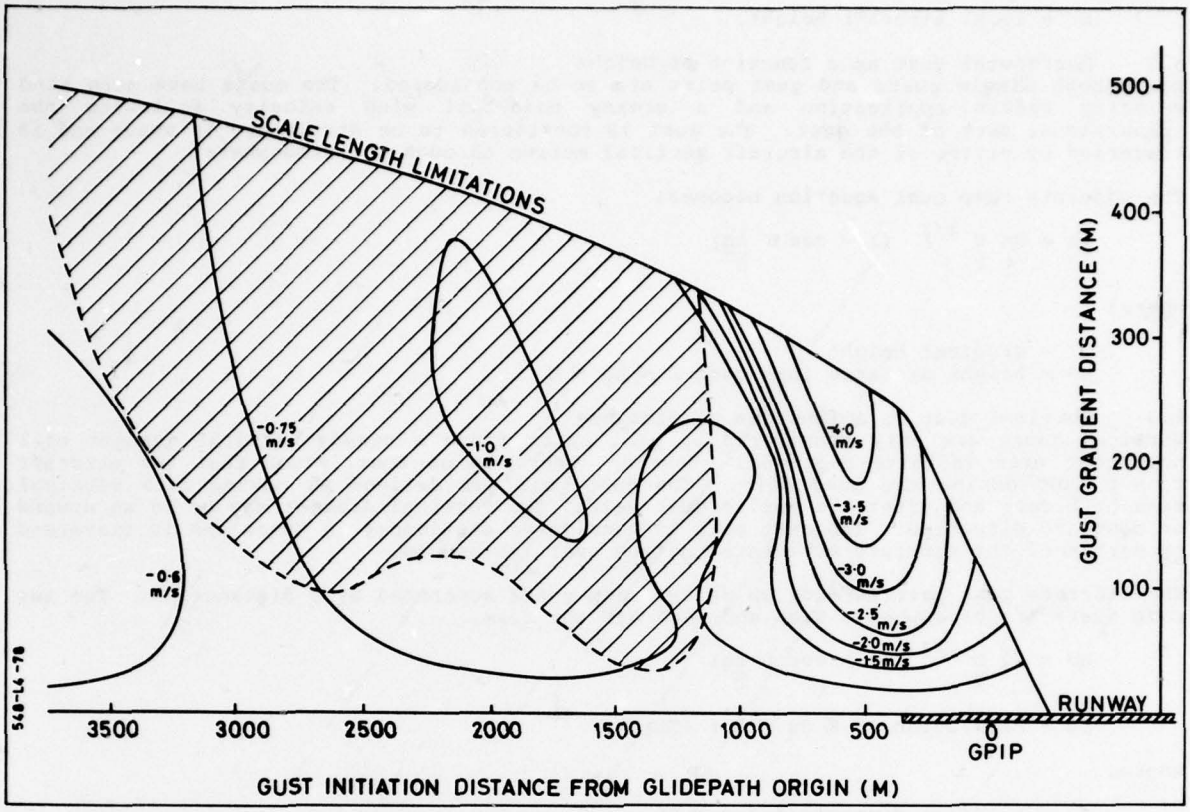

Figure 5 Height Rate at Touchdown(m/s) for Single Horizontal Gust U_o = 4 Tailwind

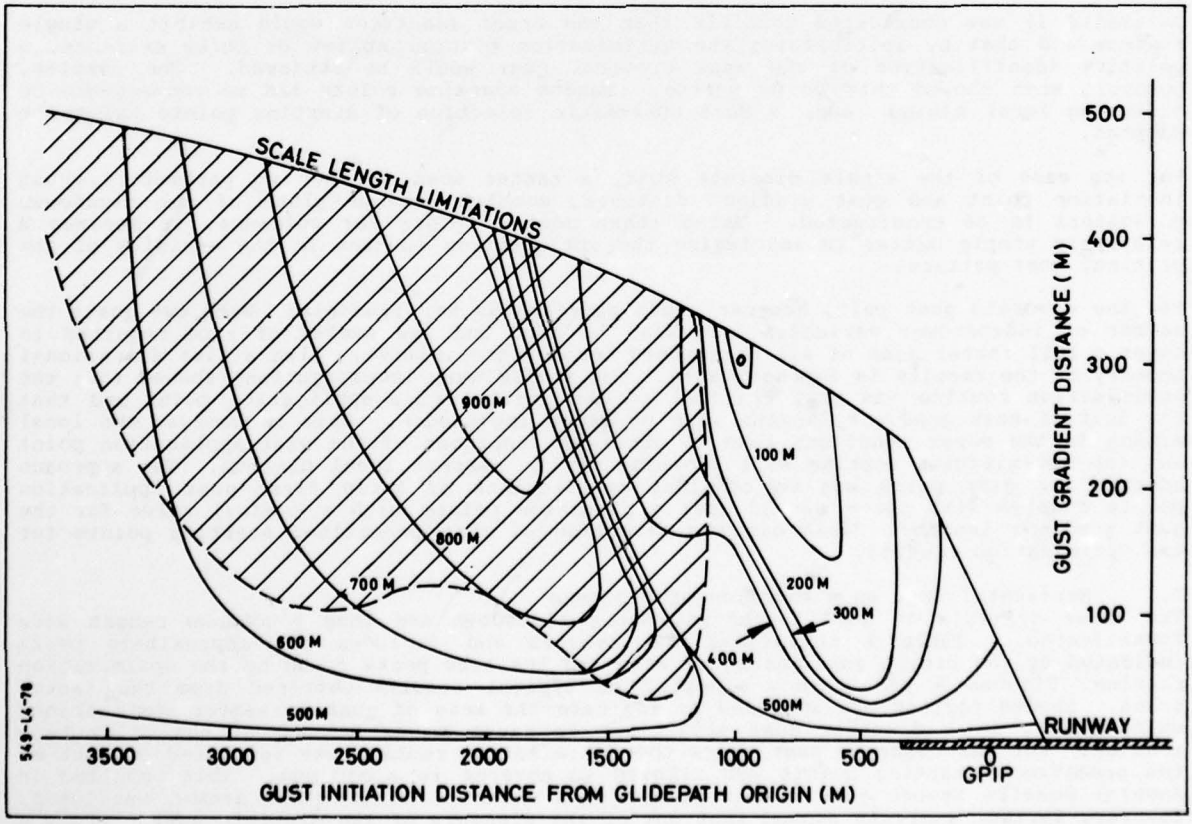

Figure 6 Touchdown Range Past Threshold(m) for Single Horizontal Gust U_o = 4 Tailwind

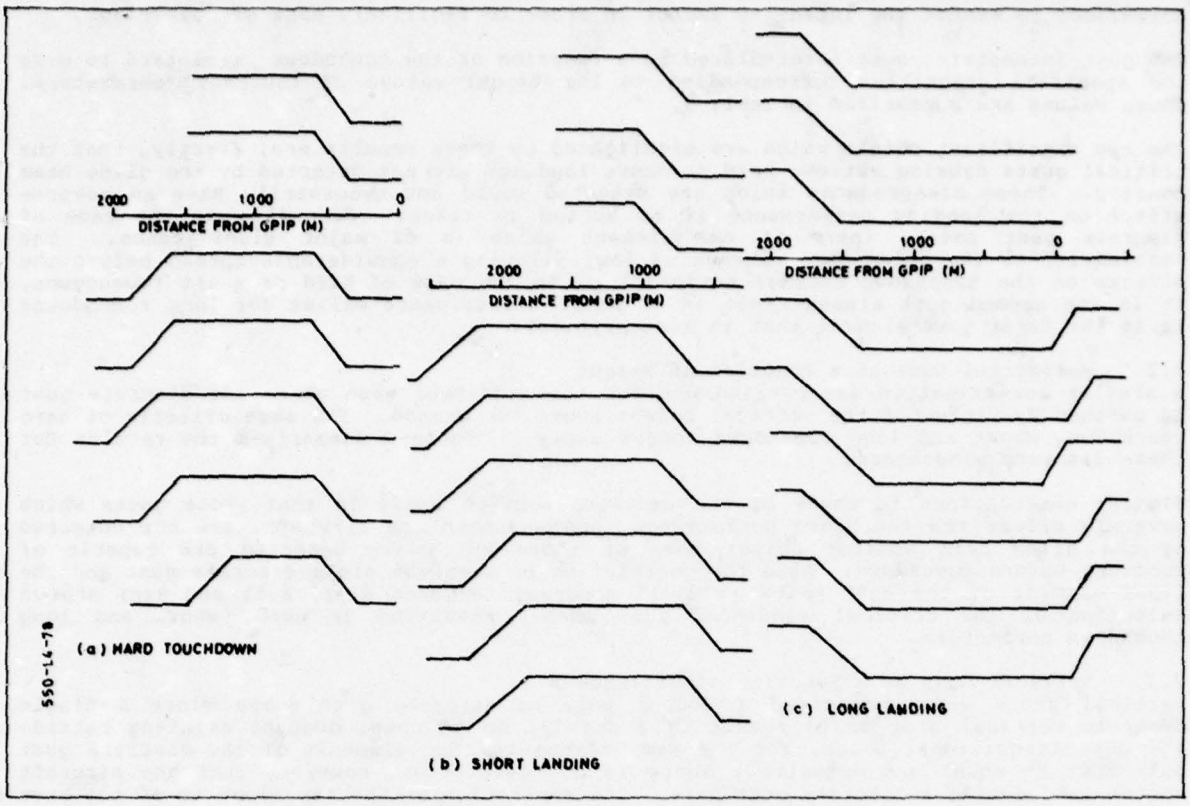

Figure 7 Critical Horizontal Gusts as a Function of Distance

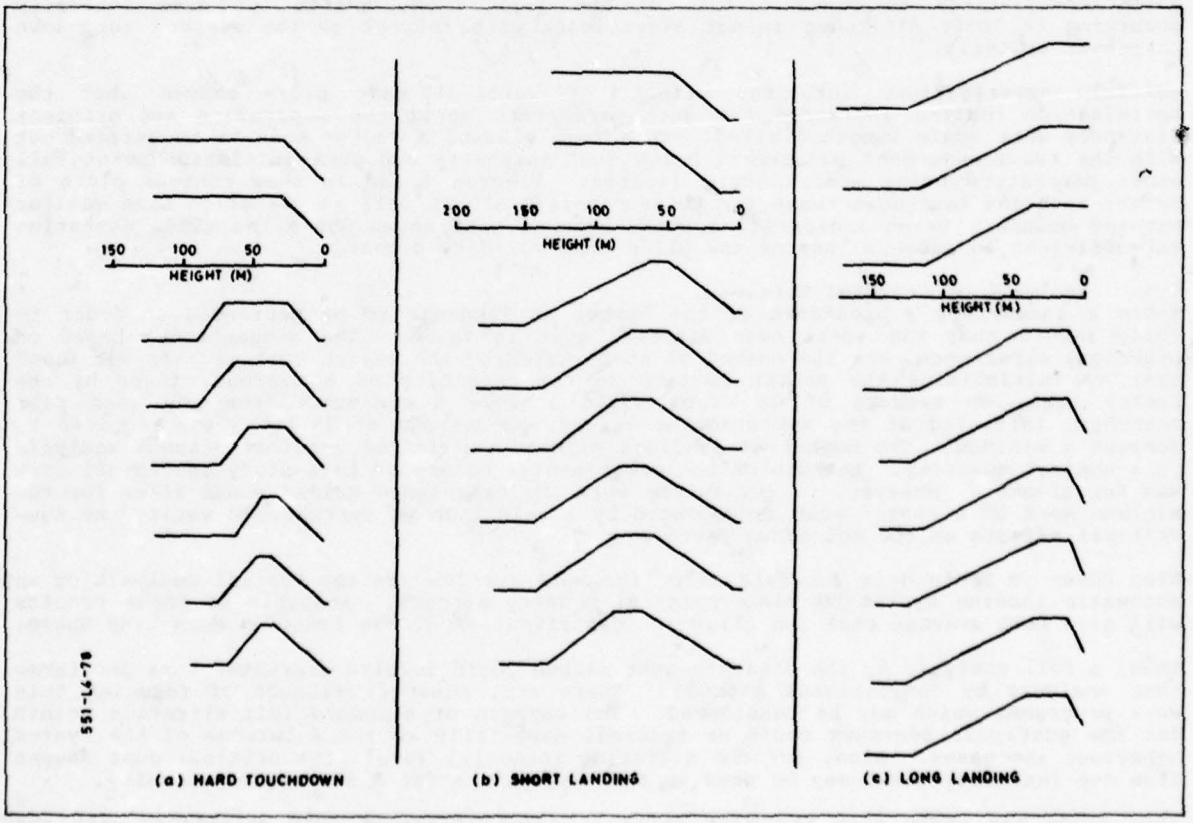

Figure 8 Critical Horizontal Gusts as a Function of Height

normalised to remove the intensity factor in order to facilitate ease of comparison.

The gust intensities were interpolated as a function of the touchdown parameters to give the specific intensities corresponding to the target values of touchdown parameters. These values are summarised in Table 3.

The two significant points which are highlighted by these results are, firstly, that the critical gusts causing extreme hard or short landings are not detected by the glide beam monitor. Those disturbances which are detected would not necessarily have an adverse effect on the landing performance if no action is taken. Secondly, in the case of discrete gust pairs, there is one element which is of major significance. The sensitivity to the other gust element is low, allowing a considerable spread before the effects on the touchdown becomes noticeable. In the case of hard or short touchdowns, it is the second gust element that is of major significance whilst for long touchdowns it is the first gust element that is most critical.

7.2 Horizontal Gust as a Function of Height

A similar investigation was carried out for the windshear case where the discrete gust is defined by virtue of the vertical height above the ground. The same criteria of hard touchdown, short and long touchdown ranges apply. Table 2 summarises the results for these discrete windshears.

Similar observations to those of the previous section apply in that those gusts which severely affect the touchdown performance, and endanger the aircraft, are not detected by the glide beam monitor whilst some of those which are detected are capable of recovery before touchdown. Also the correlation between the singe discrete gust and the final element of the gust pairs is still apparent. Figures 8(a), 8(b) and 8(c) show a selection of the critical windshear gust shapes resulting in hard, short and long touchdown parameters.

7.3 Vertical Gust as a Function of Distance

Vertical gusts were considered to occur only as discrete gust pairs since a single discrete vertical gust would result in a steady, up or down, draught exisitng outside the gust transitional phase. For the same reason the two elements of the discrete gust pair must be equal and opposite. There is no restriction, however, that the aircraft cannot land during a discrete gust pair. The separation of the two elements of the gust pair was limited to five scale lengths where the scale length was computed from the aircraft position at the start of the second gust element. This results in the gust duration, together with the gust amplitude, being progressively reduced by the scale length limitation as the gust initiation height reduces. Thus for a fixed intensity, a discrete gust pair occurring early in the glide phase can produce an aircraft deviation sufficiently large to cause a loss of the glide beam, whilst the same intensity occurring at lower altitudes is not significant with respect to the various touchdown parameter criteria.

Initial investigations into the effects of vertical gust pairs showed that the optimisation routine increased the gust parameters until the separation and gradient distances were scale length limited. This fact allowed a raster scan to be carried out with the two independent parameters being gust intensity and gust initiation point, all other parameters being scale length limited. Figures 9 and 10 show contour plots of height rate and touchdown range for these conditions. As well as the glide beam monitor warning boundary being indicated, a cross-hatched area shows where the glide deviation is sufficient to cause a loss of the glide beam validity signal.

7.4 Analysis of Computer Workload

Table 4 summarises a breakdown of the number of landings to be performed in order to fully ensure that the worst case discrete gust is found. The assumptions, based on practical experience, are the number of steps taken by the search routine. It was found that by initialising the search routine in the proximity of a minimum, found by the raster scan, an average of 25 steps would achieve a minimum. For the gust pair searches, initiated at the set starting values, an average of 75 steps was required to achieve a minimum. The number of landings allowed for in the vertical draught analysis is a nominal quantity. Because of the experimental nature of this study the actual work was far greater. However, in any future work the experience gained would allow for the minimum work of a raster scan accompanied by a selection of searches to verify the non-critical effects on the touchdown performance.

Also shown in Table 4 is a breakdown of the work involved in the typical analysis of an automatic landing system by Power Spectral Density methods. Analysis of these results will give both average risk and allow an identification of the limiting Mean Wind Speed.

Thus, a full analysis by the discrete gust method could involve a greater work programme than analysis by conventional methods. There are, however, methods of reducing this work programme which may be considered. The numbers of standard initialisation points for the gust pair searches could be reduced, especially as the knowledge of the system behaviour increases. Also, for the differing intensity levels the critical gust shapes from one intensity level may be used as starting points for a different intensity.

This study has shown that the most critical single discrete gust correlates with the dominant element of the critical discrete gust pairs. Also the single discrete gust analysis accounts for only about one tenth of the total workload. Thus the technique proposed would be to analyse the single gust case with a raster scan followed by

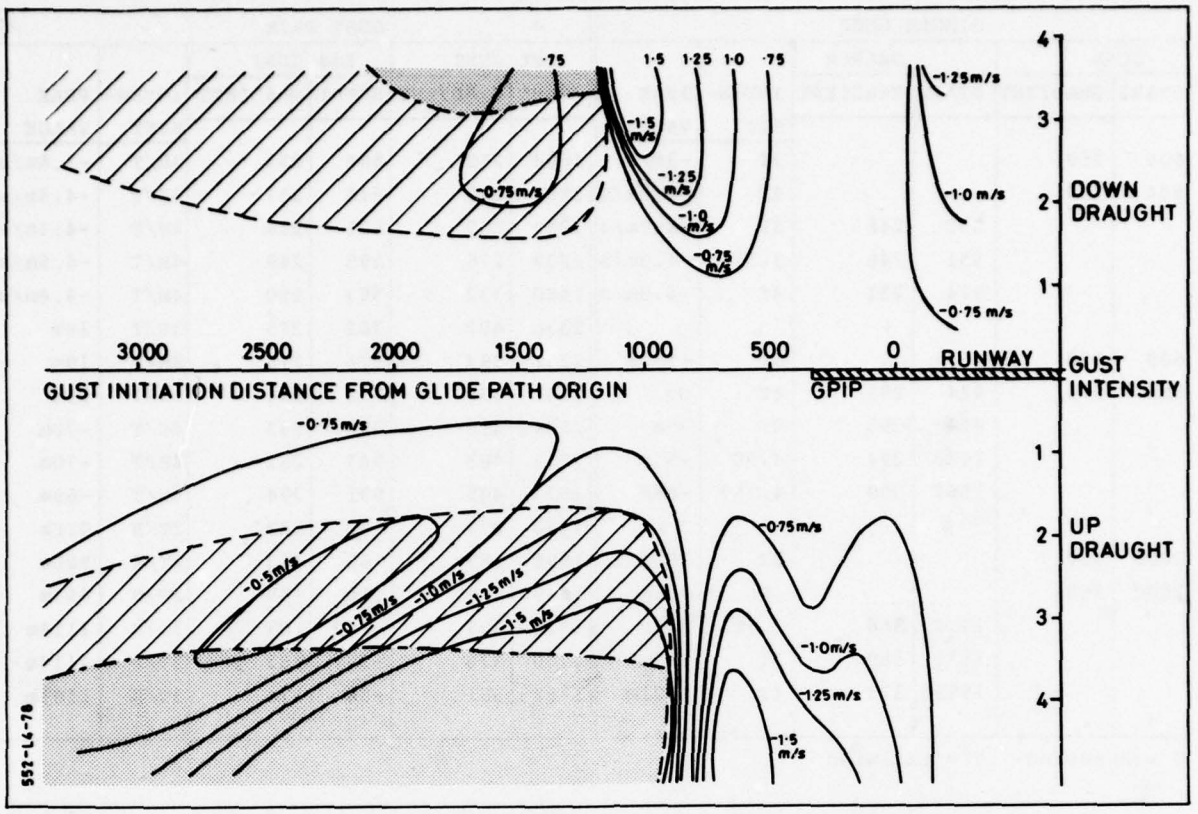

Figure 9 Height Rate at Touchdown(m/s) for Scalelength Limited Vertical Draughts

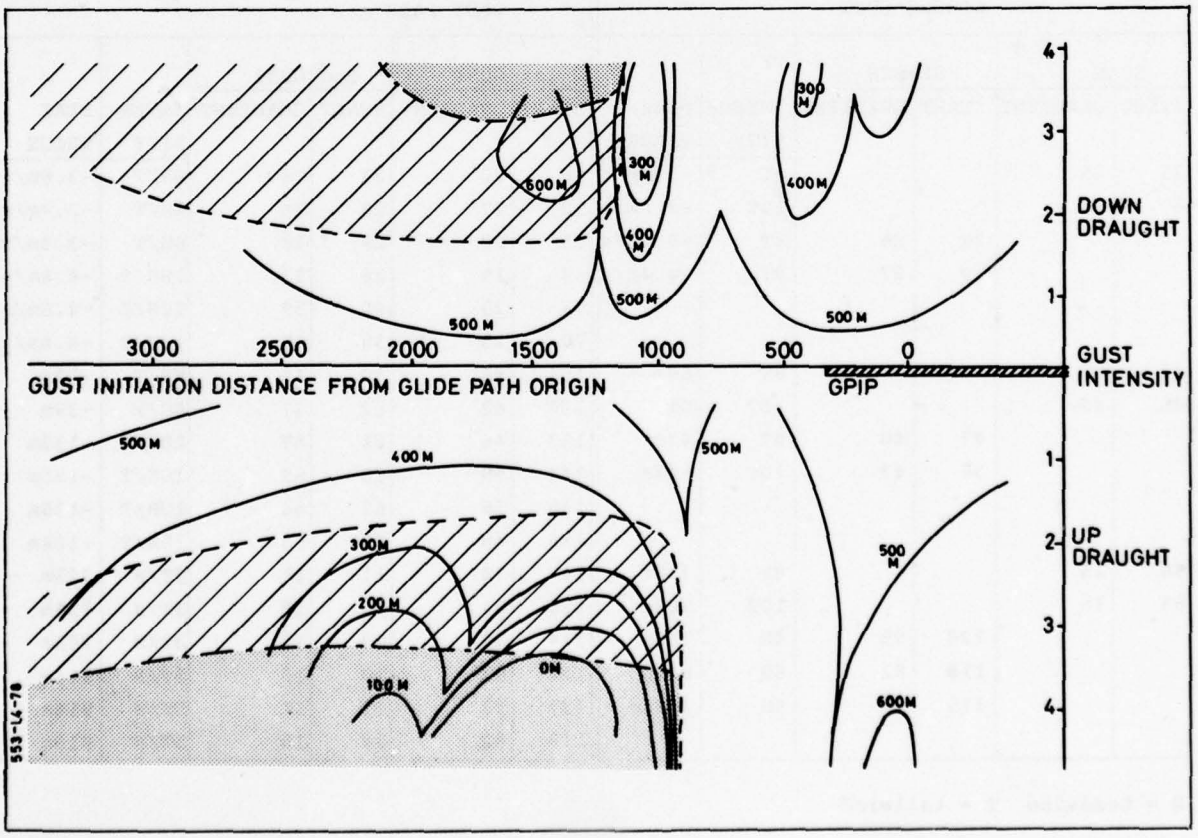

Figure 10 Touchdown Range Past Threshold(m) for Scalelength Limited Vertical Draughts

SINGLE GUST						GUST PAIR					
SCAN		SEARCH				1st GUST		2nd GUST			
START	GRADIENT	START	GRADIENT	INTEN-SITY	PEAK VALUE	START	GRADIENT	START	GRADIENT	INTEN-SITY	PEAK VALUE
600	250			3T	-3m/s	1868	262	594	253	3H/T	-3.6m/s
600	250			4T	-4.5m/s	1888	285	616	257	4H/T	-4.5m/s
		550	248	3T	-3.7m/s	2059	355	621	258	4H/T	-4.5m/s
		551	248	3.5T	-4.3m/s	1827	276	595	249	4H/T	-4.5m/s
		574	251	4T	-4.8m/s	1480	332	563	250	4H/T	-4.4m/s
						2336	402	762	275	3H/T	19m
600	250			3T	+150m	2251	393	771	275	3H/T	19m
900	275	944	295	4T	0m	2251	395	753	264	3H/T	23m
		944	295	4T	-5m	2604	416	929	293	4H/T	-70m
		1033	294	4.5T	-55m	2533	403	937	292	4H/T	-70m
		1067	309	4.75T	-86m	2523	405	931	294	4H/T	-69m
						1756	374	42	183	2T/H	910m
2000	350			3T	750m	1906	389	-66	183	2T/H	900m
2000	350			4T	900m	1649	359	110	155	2T/H	893m
		1770	366	2.5T	823m	1814	388	-142	183	3T/H	1114m
		1811	369	3T	897m	1750	378	-39	183	3T/H	1114m
		1889	373	4T	1071m	1768	381	-56	174	3T/H	1109m

H = headwind T = tailwind

TABLE 1 - HORIZONTAL GUST AS A FUNCTION OF DISTANCE

SINGLE GUST						GUST PAIR					
SCAN		SEARCH				1st GUST		2nd GUST			
START	GRADIENT	START	GRADIENT	INTEN-SITY	PEAK VALUE	START	GRADIENT	START	GRADIENT	INTEN-SITY	PEAK VALUE
25	25			8T	-3.5m/s	90	20	27	24	8H/T	-3.8m/s
30	30			10T	-4.5m/s	90	27	28	25	8H/T	-3.9m/s
		28	26	8T	-3.9m/s	75	20	29	28	8H/T	-3.9m/s
		29	27	9T	-4.4m/s	64	19	36	33	10H/T	-4.8m/s
						77	29	40	39	10H/T	-4.8m/s
						70	23	38	37	10H/T	-4.8m/s
40	30			8T	60m	151	88	50	45	8H/T	-37m
45	45			10T	0m	137	62	52	47	8H/T	-39m
		47	40	8T	43m	133	46	64	57	10H/T	-132m
		56	43	10T	-47m	144	59	66	65	10H/T	-136m
						145	58	62	56	10H/T	-138m
						136	48	69	65	10H/T	-104m
90	15			8T	750m	117	74	11	11	3T/H	753m
85	15			10T	900m	120	84	10	10	3T/H	756m
		128	98	4H	763m	114	78	12	12	3T/H	753m
		116	82	6H	889m	124	92	10	10	5T/H	914m
		115	77	8H	1036m	127	93	11	11	5T/H	914m
						119	82	10	10	5T/H	916m

H = headwind T = tailwind

Table 2 - HORIZONTAL GUST AS FUNCTION OF HEIGHT

Touchdown parameter	INTENSITY U(Distance)		INTENSITY U(height)	
	Single gust	Gust pair	Single gust	Gust pair
Descent rate = 4m/s	3.25 T	3.45 H/T	8.10 T	8.20 H/T
Range past threshold = 60m	3.40 T	2.60 H/T	7.40 T	6.00 H/T
Range at threshold	4.00 T	3.20 H/T	8.90 T	7.20 H/T
Range before threshold = 60m	4.50 T	3.90 H/T	10.30 T	8.40 H/T
Range past threshold = 800m	2.40 T	1.50 T/H	4.70 H	3.65 T/H

H = headwind T = tailwind

Table 3 - CRITICAL GUST INTENSITIES

DISCRETE GUST ANALYSIS		POWER SPECTRAL DENSITY ANALYSIS	
Raster Scan U1(d)	100		
Search U1(d) h max (25 x 2)	50	6 samples (1000 landings)	
Search U1(d) short (25 x 2)	50	for mean wind speeds	
Search U1(d) long (25 x 2)	50	10 kts tailwind to 15kts headwind	
Search U2(d) h max (75 x 9)	675	at 5 kt intervals	6,000
Search U2(d) short (75 x 9)	675		
Search U2(d) long (75 x 9)	675	3 samples (1000 landings)	
		for 15kts to 25 kts headwind	
Total/Intensity level	2,275	at increased V Ref.	3,000
Similar exercise U(h)		TOTAL LANDINGS	9,000
Total/Intensity level	2,275		
Total U(d) and U(h)	4,550		
2 Intensity levels	9,100		
+ W2(d) analysis	900		
TOTAL LANDINGS	10,000		

Table 4 - COMPUTER WORKLOAD COMPARISON

searches initiated in the proximity of the minima. Using these critical single discrete gusts as starting points the discrete gust pairs analysis should be greatly reduced.

8. CONCLUSIONS

This study, which was initiated following a series of incidents attributed to the occurrence of large windshears during the approach and landing phase, raises some interesting observations. The most critical horizontal discrete gusts and wind shears are those occurring during the final stages of the approach and occur too late to be detected by the glide beam monitor. Some of those gusts which are detected by the glide beam monitor may safely be allowed to continue to an acceptable landing. Some other form of system performance monitor would be required to provide a warning of those critical gusts.

For vertical draughts, the nature of the discrete gust model dictates that the maximum permissible gust reduces with altitude. Thus a scale length limited gust occurring at altitude can disturb the aircraft sufficient to cause a loss of the glide beam whilst the same intensity gust occurring during the later stages of the approach would be scale length limited to a value having an insignificant effect on the aircraft performance. These large vertical draughts occurring at high altitudes were outside the scope of this study since they caused an automatic disconnection through the glide beam validity signal. The recovery from these situations would be dependent on pilot intervention and would require a pilot in the loop simulation.

As a means of attaining certification this study has suggested that the workload, in ascertaining the most critical gust pattern, can be at least as great as that required to determine the limiting Mean Wind Speed by conventional means unless a logical approach is adopted. The procedure that is recommended, based on the experience gained during this study, is to perform a raster scan followed by an optimisation to evaluate the most critical discrete single gust. Using this critical single gust as the initial value of the relevant element of a discrete gust pair, optimise to find the most critical discrete gust pair.

The problems associated with this method are, firstly, of defining the relationships between the most critical gust intensity and the Mean Wind Speed Limit, and secondly, building up a background of experience within the industry and the certification authorities to accept this novel technique as a means to provide for the certification of an aircraft.

As a design tool to aid in the development of the automatic landing control laws of an aircraft the discrete gust pattern response could be used to identify over sensitive areas which may require modification. For this purpose the single discrete gust, using the raster scan and search technique, should be sufficient since an absolute value of limiting gust intensity is not required.

References

1. J. G. Jones: Notes on the application of the statistical discrete gust method to autoland assessment.
RAE FS 129 (1977)

2. J.G. Jones: Influence of atmospheric gusts and turbulence on aircraft flying qualities at low altitude.
RAE Technical Memos FS 64, 85 (1976)

3. Joint Airworthiness Committee: Flying qualities requirements.
JAC 925 (1975)

AIRCRAFT RESPONSE TO WINDSHEARS AND DOWNDRAUGHTS

by
J.C. van der Vaart

Delft University of Technology
Department of Aerospace Engineering
Kluyverweg 1
2629 HS Delft - The Netherlands

SUMMARY

After a short review of current methods of modelling low altitude random atmospheric turbulence and variations of mean wind with altitude (windshears), a decription is given of an analytical method to find deterministic wind or turbulence time-histories that cause largest deviations of aircraft motion variables. Some numerical examples illustrate that small variations of wind, in particular of horizontal wind, may cause relatively large deviations relative to a desired aircraft trajectory.
Finally it is shown that the problem of finding "worst case" response to deterministic changes in wind can be reduced to that of the statistics of a random white noise driven linear system.

1. INTRODUCTION

Although low altitude atmospheric turbulence has been of some concern from the early days of aviation, the atmospheric phenomena usually denoted by windshears and downdraughts have increasingly gained attention in recent years. Specifically on final approach, windshears have been a factor in more than one accident per year since 1972 (Ref. 1).

The calculation of aircraft response to given (deterministic) wind time-histories as well as the evaluation of aircraft r.m.s. response to random atmospheric turbulence with known spectral properties have both become a matter of routine.
Theoretical investigations into the response to low altitude, low frequency turbulence, i.e. to windshears and downdraughts are, however, seriously handicapped by lack of appropriate mathematical models.

A different way to study windshear and downdraught response is trying to find horizontal or vertical wind time-histories that, under certain restrictions, cause maximum deviations of particular aircraft variables from a required flight path.

After a short review of methods commonly used to model aircraft response to changes in winds, the present paper describes a simple method to find worst case wind time-histories and to calculate the resulting deviations.

2. CURRENT METHODS OF MODELLING LOW ALTITUDE ATMOSPHERIC TURBULENCE AND WINDSHEARS

Current low altitude turbulence models present the atmospheric disturbance components as a superposition of a variation of the mean wind with altitude and a fluctuating part which is the result of the prevailing atmospheric turbulence, see Fig. 1.
The fluctuating part is usually considered as a random process, the properties of which can be modelled by the Von Karman, Dryden or other mathematical descriptions of power spectral densities (Ref. 2). As the governing parameters in these models (turbulence r.m.s. level and integral scale length) are functions of altitude, a climbing or descending aeroplane experiences turbulence with altitude-dependent and hence, time-dependent statistical and spectral properties.

If it is assumed that the random turbulence is a gaussian or normal process and that the aircraft can be considered as a linear system, then the calculation of aircraft r.m.s. response due to the fluctuating part, also in the case of time-dependent turbulence properties, is a relatively simple matter using todays computing techniques. Refs. 3 and 4.
The variation of mean wind with altitude can mathematically be modelled as a function of the prevailing meteorological conditions (neutral, stable or unstable atmosphere).
The responses of aircraft due to changes in mean wind experienced when climbing or descending is what is generally called windshear response. Two distinct factors appear to hamper a proper mathematical modelling of the mean wind.

The first is related to the fact that theoretically derived wind profiles as the one shown in Fig. 1, are by no means proper representations of actual mean wind variations.
In practice local terrain features, large buildings around airports or the presence of an inversion may cause mean winds to deviate markedly from the theoretical profiles, see Fig. 2.

Moreover, it is obvious that local weather phenomena such as the occurence of thermals, the passage of squall lines and thunderstorms will influence mean wind. Here a second uncertainty in mean wind modelling presents itself, as it is difficult to make a clear distinction between "stationary mean wind" and the low frequency part of "random turbulence". Perhaps changes in wind due to local weather phenomena should be considered as low frequency random turbulence.

Still, it will be evident that what matters to the aeroplane during approach or take-off is the time-history of the wind as experienced, independent of the fact whether it is caused by random turbulence, changing mean wind, or a combination of these, see Fig. 3.

One way of generating realistic time-histories is of course using measured and recorded (or reconstructed) wind time-histories of a typical approach trajectory.
More ideally still, one would like to have a reliable model of the ensemble characteristics of random turbulence, covering the entire frequency range of interest for aircraft motions and representative of all changes in relative wind, including those due to changes in mean wind, as experienced by a climbing of descending aircraft at low altitudes. Some efforts in this direction are being undertaken elsewhere (Ref. 5).

Unfortenately, however, even the theoretical power spectra presently available for turbulence at a given altitude, are unreliable in the low frequency range particularly of interest for windshear response (Refs. 6 and 7). Consistent experimental data are lacking and will probably remain scarce due to the long registration times involved.

Until more reliable models are available, deterministic methods of studying aircraft response to given time-histories of low frequency turbulence are still worthwhile.
The next Chapter gives a short recapitulation of the different methods presently used.

3. AIRCRAFT RESPONSE TO DETERMINISTIC CHANGES IN WIND

Many efforts have been undertaken to evaluate aircraft response to deterministic changes in wind, all involving some degree of simplification of the actual mean wind profiles or the low frequency turbulence.

Theoretically derived profiles, also combined with stepwise changes in horizontal wind as occuring in strong inversions were used in a study by Luers and Reeves, Ref. 8.
Mean wind is also very often modelled as a shear layer of given thickness characterized by a constant, linear wind gradient. Responses to the gradients, combined with stepwise increases in horizontal wind and a sustained downdraught are given in Ref. 9.
Interesting theoretical analyses, also assuming constant linear wind profiles were given by Gera (Ref.10) and Sherman (Ref. 11).
These studies have definitely been a great asset in understanding the peculiarities of general behaviour of aircraft in windshears and downdraughts. Bearing in mind the many possible shapes of mean wind profiles, or better still the many different time-histories (realisations) of actual low altitude winds, the modelling by constant linear wind profiles or stepwise changes should be considered as rather gross approximations.
Stepwise changes or linear wind profiles will probably never be encountered in practice. Moreover, it appears that not only the magnitude, the duration or the rate of change in wind is important but that the succession of changes, or more exactly, the time-history of the wind plays an important part.
This is illustrated by a simple example in Fig. 4 where the response of indicated airspeed, vertical speed and altitude is shown as a result of a single step and two opposed, successive steps in horizontal wind speed. Although the integal of the changes in wind experienced becomes zero after 40 secs in the case of the double step unput, excursions of indicated airspeed, vertical speed and altitude are remarkably larger than in the single step case.

A similar difference can be found in the time-history of the vertical speed in the case of a single linear shear and two opposed, successive shears, see Fig. 5.

The importance of the shape of the wind time-history was also stressed in a recent publication by McCarthy et al, Ref. 12.

The foregoing chapters can be summarized as follows. Neither the deterministic models of mean wind, nor the stochastic description of random turbulence give a fair representation of low altitude, low frequency changes in actual wind along an approach path or take-off trajectory. The deterministic models mentioned above (stepwise changes in wind, linear wind profiles) are too gross approximations while moreover the shape of the wind time-histories appears to be important.

As some wind time-histories are known to be worse than others,the question arises whether it would be possible to find worst case wind time-histories that, under certain restrictions, cause maximum deviations of for instance flight speed, altitude or sink rate.
Efforts along these lines have been undertaken by Corbin, Ref. 13, who derived worst case wind time-histories by a search procedure to find combinations of sines and cosines that caused maximum deviations of touch-down variables for an automatic landing.
The present paper deals with worst case time-histories derived analytically, using basic principes of modern system theory.

4. WORST CASE WIND TIME-HISTORIES

From theoretical work on aircraft response to deterministic changes in wind it is well known that, for touch-down errors for instance, the instant at which changes in wind occur prior to touch-down, is an important parameter. The question can of course then be raised wether there would be anything like a critical instant or altitude for such a change in wind to occur in order to be most effective in causing touch-down errors and, further, whether a particular continuous series of wind changes - a wind profile or wind time-history - could be found that is most critical for a given aeroplane.

This problem appeared to be very straightforwardly formulated and solved by using basic concepts of linear system theory. For the sake of completeness the necessary system theory formulation of aircraft dynamics is summarized in Appendix 1 together with a brief derivation of worst-case wind time-histories. In the following, the matter is dealt with in a more descriptive way. For further details the reader is referred to Ref. 14.

If it is assumed that the aircraft is a constant linear system, is initially in stationary equilibrium but being perturbed by a single input signal $v(t)$, for instance a change in wind speed, then the value of a deviation at instant t, of a particular aircraft motion variable x_i relative to a stationary flight condition, is given by the following expression:

$$x_i(t) = \int_0^t h_i(t - \tau)v(\tau).d\tau \qquad (1)$$

Here $h_i(\tau)$ is the response of x_i to a unit impulse input signal at $\tau=0$:

$$v(\tau) = \delta(0)$$

Therefore $h_i(t-\tau)$ in eq.(1) is in fact the time-reversed impulse response. The integrand of eq. (1) has been visualized in Fig. 6. The function $h_i(t-\tau)$ can be considered as a measure of the contribution of v at instant τ to the value of x_i at instant t.
The instants at which single changes in wind speed are most critical clearly stand out as the peaks in the time-reversed impulse response of this example.
Without a formal derivation it is also easily seen form eq. (1) and Fig. 6 that for a fixed value of t_1 of t and for instance a given maximum amplitude of the wind excursions, the absolute value of $x_i(t_1)$ will be maximal if $v(\tau)$ is exactly matched to the function $h_i(t_1-\tau)$. Thus the worst case wind time-history is given by

$$v(\tau) = k.h_i(t_1-\tau) \qquad (2)$$

where k is a positive or negative constant. In Appendix 1 it is shown that this result can formally be derived as the solution of a variational problem with a single constraint on the time-history $v(\tau)$.
As all state variables, or motion variables, of a system have differing impulse responses, separate and differing worst case wind time-histories, causing greatest deviations of each particular variable, at a given t_1, will be found. It will be evident that horizontal, vertical as well as lateral worst case wind time-histories can be found by using the appropriate impulse responses in eqs. (1) and (2).

5. AIRCRAFT RESPONSE TO WORST CASE TIME-HISTORIES. SOME NUMERICAL EXAMPLES

The wind time-histories according to eq. (2) can indeed be shown to be very effective in causing deviations of aircraft motion variables. Fig. 7 shows worst case horizontal wind controls-fixed responses of an example aircraft, particulars of which are summarized in Table 1.
Although the maximum wind excursions are at or below 1 m/sec (approx. 2 knots), the wind time-histories are seen to induce an air speed loss of 3 m/sec (6 knots) an altitude loss of 25 m (80 ft) and to cause an excess sink rate of 2.3 m/sec (450 ft/min).
The wind signals very efficiently excite the aircraft's natural modes, in particular the phugoid mode. The example aircraft, a typical present-day jet transport, was not artificially stabilized and no pilot action was supposed to be involved. Of course a vigilant pilot would, in some stage of the perturbed flights illustrated in Fig. 7, have taken corrective action and these examples of responses of fairly long duration represent worst cases in more than one sense. Worst case signals of shorter duration, however, are equally effective in causing large perturbations, see Fig. 8.

It will be apparent form the foregoing that the worst case concept is also readily applicable to downdraughts. Responses to vertical wind, however, differ somewhat from those to changes in horizontal wind. To illustrate this, flight speed and altitude responses to equal stepwise changes of horizontal and vertical wind have been compared in Fig. 9.
In the case of a stepwise change in horizontal wind both flight speed and altitude time-histories are dominated by the phugoid mode. A stepwise downdraught of equal magnitude causes much smaller flight speed excursions but induces a remarkably larger altitude loss. The time-history of altitude is, moreover, much less influenced by the phugoid mode and it can be seen form Fig. 9 that the aircraft, as far as altitude is concerned, may well be considered as an almost pure integrator of vertical wind speed.
Also shown in Fig. 9 is the change in total energy as expressed by energy height h_E.
Changes in total energy will be dealt with in some more detail in the next Chapter but is may already be concluded here that changes in total energy due a change in horizontal wind are negligable if compared to those caused by a change in vertical wind of equal magnitude.
Bearing in mind these characteristic differences of horizontal and vertical wind response, it will not be amazing that a worst case downdraught, see Fig. 10, will not be quite so effective in inducing large filght speed excursions as a worst case horizontal wind time-history, see Fig. 7.
As the aeroplane can roughly be considered as a pure integrator of vertical wind speed as far as altitude response is concerned, the worst case vertical wind time-history causing the maximum altitude loss, see Fig. 10, tends to a continuous downdraught in which periodic features are less dominating, see also Fig. 7.

6. WORST CASE RESPONSE, TOTAL ENERGY AND ON-BOARD WINDSHEAR MONITORS

In Chapter 2 it was stated that neither the current theoretical models of low frequency turbulence as encountered during an approach or take-off, nor the available models of mean wind are proper mathematical descriptions of actual changes of low altitude winds. Of course the same goes for the worst case time-histories presented in this paper.
Nonetheless the wind signals and their effects shown in the preceding Chapter well stress the fact that the severity of the response is not necessarily exclusively determined by the maximum wind excursion alone. For example, in one well known case resulting in an accident (Boston, 1973), at no time was the performance capability of the aeroplane challenged (Ref. 15).
It will be readily admitted that some problems caused by severe shears and downdraughts should be formulated in terms of performance rather than of stability and control. In another well known case, occuring six minutes before the J.F.K. Airport accident (1975), an L-1011 aircraft needed full climbing performance to counteract the combined effect of shears and downdrauhgts (Refs. 15 and 16).

The fact that the aircraft's performance has, in a number of cases, been the decisive factor in windshear and downdraught encounters, has inspired the development, elsewhere, of on-board instruments called "windshear monitors" of "windshear detectors".
In one type of windshear monitor (Refs.17 en 18), the wind speed at the aircraft's altitude, computed from air speed and inertial speed, is compared with reported wind speed at runway level. This gives an estimate of the total change in mean wind to be met with somewhere along the approach path. As to the exact shape of the wind profile, or the wind time-history to be encountered, no information is available.
Another proposed on-board windshear detector uses the instantaneous excess rate of change of the aircraft's total energy to alert pilots of possible windshear or downdraught hazards (Ref. 19). It is therefore worthwhile to consider changes of total energy in some more detail.

It became already apparent from Fig. 9 that, in general, changes in total energy due to horizontal winds were far less important than those caused by vertical winds. As for the worst cases of this paper, they were derived by setting a constraint on the wind excursions and hence on the energy content of the wind signals, see Appendix 1 .
It may therefore be expected that the level of changes of the total energy brought about by worst case horizontal wind time-histories is also low. This can indeed be seen in Fig. 11 where the change in total energy is given together with the contributions caused by changes in inertial speed and altitude. Total energy is expressed here as energy height h_E, a definition of which can be found in Appendix 2.
Energy in this case (worst case for flight speed) is almost being continuously exchanged between the speed and altitude perturbations of the phugoid mode.

The change of total energy as a result of a worst case downdraught, see Fig. 12, is much larger and is mainly caused by the loss of altitude alone.
Total energy, or its rate of change appears indeed an appropriate parameter to use in a "windshear monitor" as far as vertical winds are concerned. In some special cases of horizontal wind response, where the transient behaviour is dominating, see Fig. 11, the way in which total energy is, at a given instant, distributed among motion variables (mainly speed and altitude) appears far more important than change, or rate of change, of total energy.
A still different on-board system, called a "windshear detection system" Ref. 20, is reported to use indicated airspeed and inertial data to compute the wind downdraught angle and the rate of change of horizontal wind. A go around alarm is automatically given if the aircraft has experienced a sustained rate of horizontal wind change, a sustained downdraught angle (or a combination of the two) exceeding a certain preset value. A typical (sustained) rate of change of horizontal wind to trigger the alarm is reported to be 1,5 m/sec^2. No doubt such a system is very useful in warning a pilot in a sufficiently early stage if large shears and especially downdraughts are encountered. However, in those cases where the aircraft's transient behaviour rather than its performance is decisive, large deviations may occur without the alarm being triggered. This is illustrated by two worst case examples in Fig. 13 where an indicated airspeed loss of 10 m/secs (20 knots) and an altitude loss of 40 m (130 ft) is seen to occur within 20 secs while for no lenght of time the rate of change of horizontal wind exceeded $\pm$ 1 m/sec^2, which is two thirds of the reported typical preset value.
In some publications, Refs. 18 en 26 for instance, the possible future use of ground based wind monitoring systems has been mentioned. Ideally these would measure, by remote sensing techniques, wind velocities along the glide path so that warnings could be broadcast in the case of large shears. If such systems become operational in the future, it may be useful to scan the measured profiles not merely for large shears, but also for less extreme profiles with features that would appear "worst cases" for the class of incoming aircraft.

7. COMPUTING AND MINIMIZING WORST CASE RESPONSE

If one wishes to know all maximum deviations caused by the related worst case input time-histories, a possible solution would of course be to determine the responses by analogue or digital techniques.
There is, however, a different and more direct method for obtaining all maximum deviations at once and for a large range of durations (t_1) of the worst case signals.
This method relates the deterministic worst case responses to statistical properties of responses to certain stochastic inputs, as will become apparent in the following.
The response of the variable x_i to its particular worst case wind time-history is according to equations (1) and (2):

$$x_i(t_1)_{max} = k \int_0^{t_1} h_i^2(t_1-\tau)d\tau$$

By considering Fig. 6 it is easily seen that this is equal to

$$x_i(t_1)_{max} = k \int_0^{t_1} h^2(\tau)d\tau \qquad (3)$$

It has been shown elsewhere, see Refs. 21 en 22, that the integral in eq. (3) is equal to the variance $\sigma^2_{x_i}$ of the variable $x_i(\tau)$ of a linear time-invariant system on which a white noise input-signal of unit intensity has been acting from $\tau = 0$ up to $\tau = t_1$:

$$\int_0^{t_1} h_i^2(\tau)d\tau = \sigma^2_{x_i}(t_1) \qquad (4)$$

The calculation of the variance as a function of time, of an output signal of a white noise driven system can be performed by a number of routines. The impulse response method described in Ref. 22, sometimes also referred to as the equivalent deterministic input technique (Ref. 23), actually uses eq. (4) to compute variances of variables.

A still more effective way is to use a routine in which the complete covariance matrix as a function of time is calculated, see Refs. 3 en 4. In this way all maximum deviations caused by their respective worst case input signals are then obtained as variances of output signals.

The covariances, the off-diagonal elements in the covariance matrix are then obtained simultaneously, which is another advantage.
It is easily shown, see Ref. 14 en Appendix 1 of this paper that the value of a non-maximally deviating variable x_j caused by the worst case input that causes the greatest deviation of another variable x_i, is proportional to the covariance $\sigma_{x_j x_i}(t_1)$ in the stochastic, white noise driven case.

The relation between deterministic worst case response and mean square response in the random white noise driven case has been schematically visualized in the diagram of Fig. 14. The upper part of the Figure represents the worst case input time-history $u_g(\tau)$ which is the input to the linear system characterized by the impulse response $h(t)$, yielding a maximum deviation of the variable x at t_1.
The lower part of the Figure depicts the growth in time of the variance σ_x^2 of the same variable of the same system in the white noise driven case.
It should be emphasized that the formulation of the aircraft as a system driven by random white noise turbulence has no immediate relation with physical reality, but is only to be considered as a computational tool.

Some examples of results obtained by such a calculation have been given in Fig. 15.
Maximum deviations of flight speed, vertical speed and altitude are given as a function of t_1, the duration of the worst case horizontal wind time-histories causing these deviations. The constant k in eqs. (2) and (3) was kept constant for all t_1 and was given a value such that the maximum wind excursions were 1 m/sec in each case.

The examples given in this paper, apart from being only concerned with symmetric aircraft motions, were restricted to the unstabilized (controls-fixed) case. The formulation and the computational method just described open the possibility to use modern control theory to design glide slope couplers, autothrottles etc. especially for the purpose of minimizing or allevating the response to worst case windshears and downdraughts. Some work along these lines is presently in progress.

8. CONCLUSIONS

Difficulties related to the theoretical modelling of the low frequency atmospheric phenomena denoted by windshears and downdraughts can be circumvented by considering worst case, amplitude constrained turbulence time-histories causing maximum deviations of particular aircraft motion variables.
By using worst case turbulence (or wind) time-histories derived straightforwardly form basic concepts of linear system theory, it was shown by some examples of a controls fixed aeroplane, that in particular small changes of horizontal wind (windshears) may cause large deviations of flight variables. The resulting changes of the aircraft's total energy were shown to be negligable in the horizontal wind cases.
Downdraught response was shown to be characterized by losses of total energy and is therefore likely to pose performance problems.
Finally the maximum deterministic deviations due to the worst case wind time-histories of this paper were shown to be proportional to the variances of these deviations in the stochastic case if the aircraft is considered to be perturbed by random white noise. This similarity means an important simplification of worst case response calculation, especially for the purpose of minimizing windshear and downdraught response of automatically controlled aeroplanes.

9. REFERENCES

1. C.A. Whitmore, R.C. Stokely, Windshears on final approach. Proceedings of the 29th International Air Safety Seminar on Take off, Approach and Landing-Accident Prevention.October 1976, Anaheim, California.

2. AGARD Report No. 632 on Approach and Landing Simulation, 1975.

3. J.C. van der Vaart, H.L. Jonkers, F.K. Kappetijn, The calculation of RMS values of deviations of aircraft controlled to fly along a desired flight path. AGARD CP No. 220 on Application of Advances in Navigation to Guidance and Control, 1977.

4. J.L. Jonkers, F.K. Kappetijn, J.C. van der Vaart, Digital calculation of the propagation in time of the aircraft gust covariance matrix. Report LR 266, Delft University of Technology. Department of Aerospace Engineering, 1978.

5. L.D. Reid, A.B. Markov, W.O. Graf, The application of techniques for predicting STOL aircraft response to windshear and turbulence during the landing approach. UTIAS Report No. 215, Institute for Aerospace Studies, University of Toronto, 1977.

6. J.A. Dutton, Effects of turbulence on aeronautical systems. In: D. Küchemann (ed.) Progress in Aerospace Sciences, Vol. 11 Pergamon Press, Oxford - New York - Toronto - Sydney - Braunschweig, 1970.

7. R.H. Rhyne, Flight assessment of an atmospheric turbulence measurement system with emphasis on long wavelenghts. NASA TN D-8315 (1976).

8. J.K. Luers, J.B. Reeves, Effect of shear on aircraft landing. NASA CR-2287 (1973).

9. C.T. Snyder, Analog study of the longitudinal response of a swept-wing transport airplane to wind shear and substained gusts during landing approach.

10. J. Gera, The influence of vertical wind gradients on the longitudinal motion of airplanes. NASA TN D-6430 (1971).

11. W.L. Sherman, A. theoretical analysis of airplane longitudinal stability and control as affected by windshear. NASA TN D-8496 (1977).

12. J. McCarthy, E. Blick, R.R. Bensch, Effect of wind turbulence and shear on landing performance of jet transports. AIAA Paper 78-249.

13. M.J. Corbin, Turbulence time-histories causing greatest touch down errors following an automatic flare. RAE Techn. Memo Avionics 152 (1973).

14. J.C. van der Vaart, Worst case wind time-histories causing largest deviations from a desired flight path. An analytical approach. Report LR 267, Delft University of Technology, Department of Aerospace Engineering, 1978.

15. R.S. Bray, Factors influencing tolerance to wind shears in landing approach. In: Aircraft safety and operating problems. NASA SP-416 (1976).

16. T.Th. Fujita, Spearhead echo and downburst near the approach end of a John F. Kennedy airport runway, New York City. S.M.R.P. Research Paper 137 (1976).

17. W.C. Wetmore, Onboard windshear monitor developed. Aviation Week & Space Technology, August 22, 1977.

18. K.J. Stein, FAA Intensifies windshear R&D effort. Aviation Week & Space Technology, September 12, 1977.

19. R.G. Joppa, Windshear detection using measurement of aircraft total energy change. NASA CR-137839 (1976).

20. R.A. Greene, A wind shear detection system for airline aircraft. Shell Aviation News 445, 1978.

21. B. Etkin, A simple method for the analogue computation of the mean square response of airplanes to atmospheric turbulence. UTIA Technical Note no. 32, 1960.

22. J.C. van der Vaart, The impulse response method for the calculation of statistical properties of aircraft in random atmospheric turbulence. Report VTH-197, Delft University of Technology, Department of Aerospace Engineering, 1975.

23. L.D. Reid, A.B. Markov, W.O. Graf, A comparison of techniques for estimating aircraft response to low altitude turbulence. Aeronautical Quarterly, November 1977.

24. H. Kwakernaak, R. Sivan, Linear optimal control systems. Wiley-Interscience Inc., New York-London-Sidney-Toronto, 1972.

25. B.S. Gottfried, J. Weisman, Introduction to optimization theory. Prentice-Hall Inc., Englewood Cliffs, New Yersey, 1973.

26. G. Beaulieu, The effects of wind shear on aircraft flight path and methods for remote sensing and reporting of wind shears at airports. UTIAS Technical Note No. 216, 1978.

Table I. Aircraft data used in the numerical example

$W = 96160$ kg		$V = 71.24$ m/sec	
$S = 260.68$ m^2		$\mu_c = 49.315$	
$\bar{c} = 6,10$ m		$K_y^2 = 2.354$	
$b = 42.67$ m		$\rho = 0.125$ kg sec^2/m^4	
$x_{c.g} = 0.36\ \bar{c}$			
$C_{X_o} = -0.0507$	$C_{Z_o} = -1.163$		
$C_{X_u} = -0.370$	$C_{Z_u} = -2.326$	$C_{m_u} = 0$	
$C_{X_\alpha} = 0.655$	$C_{Z_\alpha} = -5.04$	$C_{m_\alpha} = -0.72$	
	$C_{Z_{\dot\alpha}} = -0.395$	$C_{m_{\dot\alpha}} = -1.218$	
	$C_{Z_q} = -4.65$	$C_{m_q} = -8.622$	
	$C_{Z_\delta} = -0.342$	$C_{m_\delta} = -1.055$	

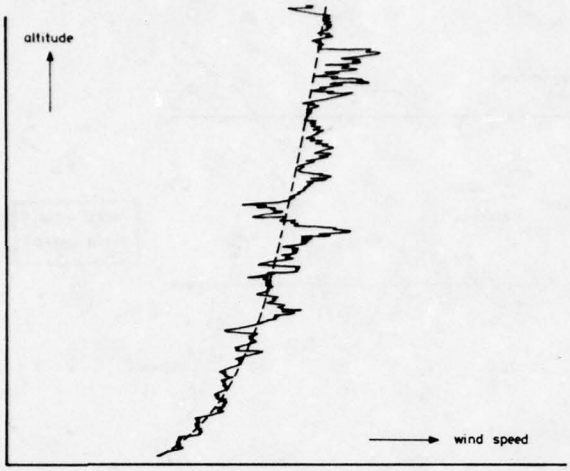

Fig.1 Mean wind profiles superimposed by altitude dependent random turbulence.

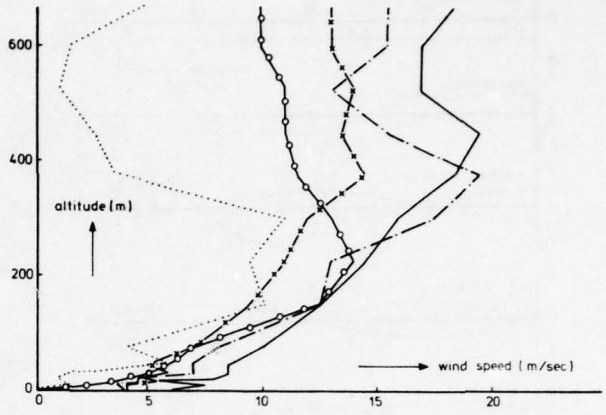

Fig.2 Examples of measured mean wind profiles, taken from Reference 2.

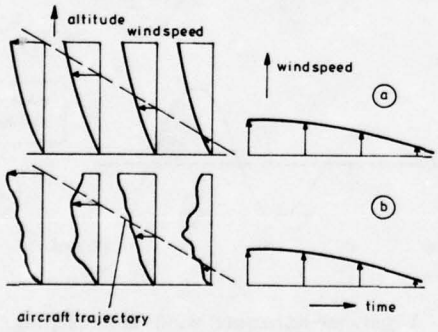

Fig.3 Relative wind as experienced by a descending aeroplane.
(a) Constant wind profiles
(b) Changing wind profiles (random turbulence).

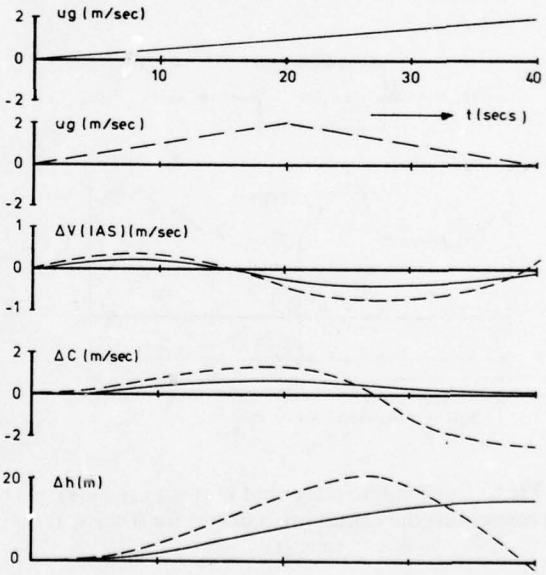

Fig.4 Response of indicated airspeed, vertical speed and altitude to single and double stepwise changes of horizontal wind.

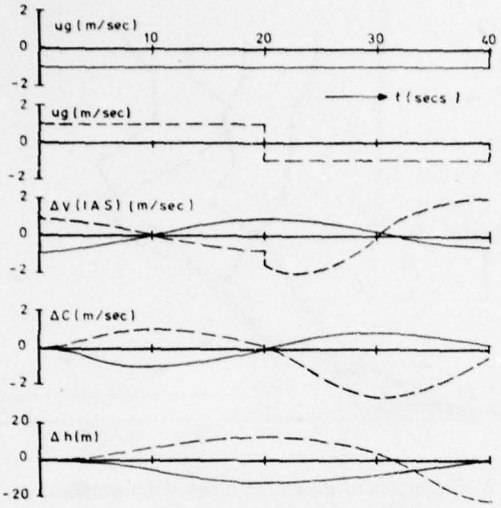

Fig.5 Response of indicated airspeed, vertical speed and altitude to single and double linear shears.

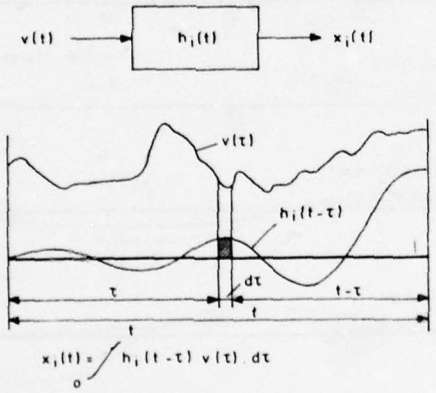

Fig.6 Convolution integral of $h_i(t-\tau)$ and $v(\tau)$ representing the contribution of $v(\tau)$ for $0 \leqslant \tau \leqslant t$ to $x_i(t)$.

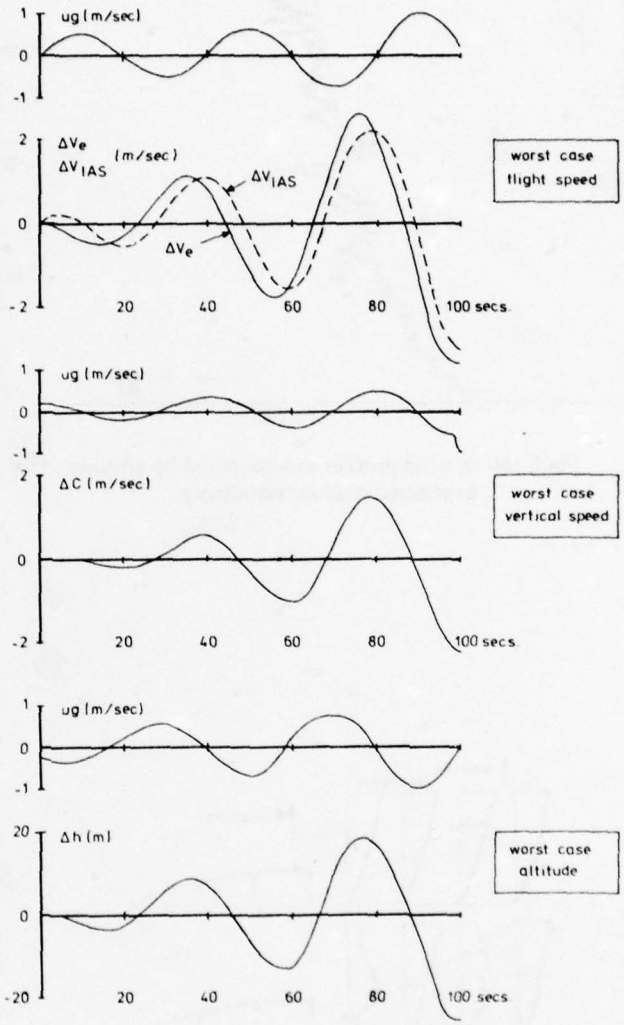

Fig.7 Worst case horizontal winds and resulting deviations of flight speed, vertical speed and altitude. Duration of wind signals 100 secs.

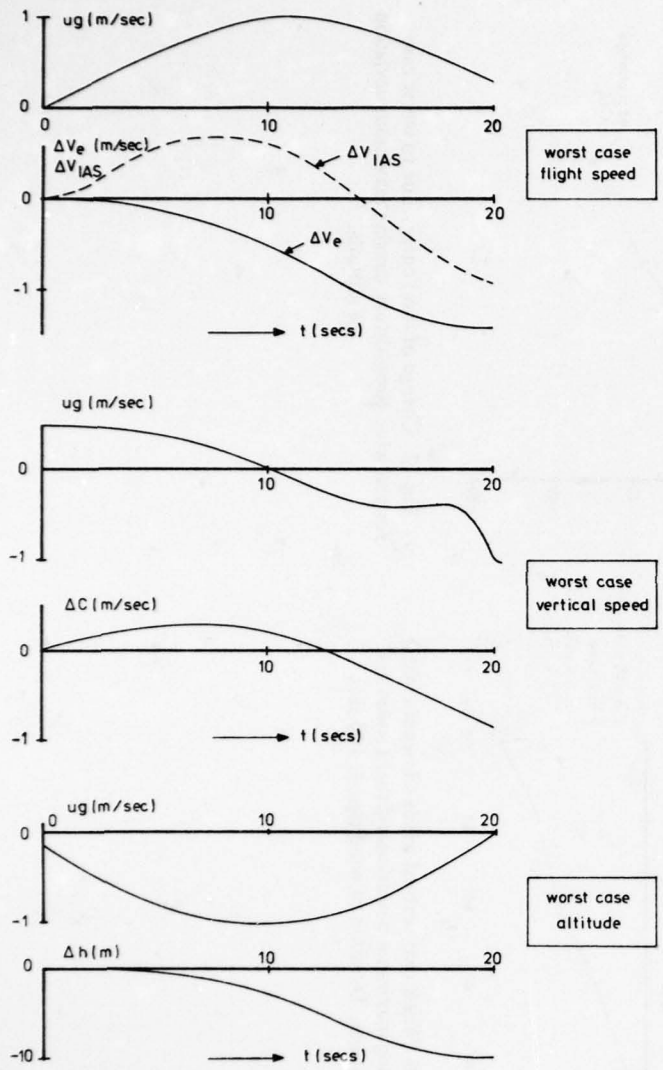

Fig.8 Worst case horizontal winds and resulting deviations of flight speed, vertical speed and altitude. Duration of wind signals 20 secs.

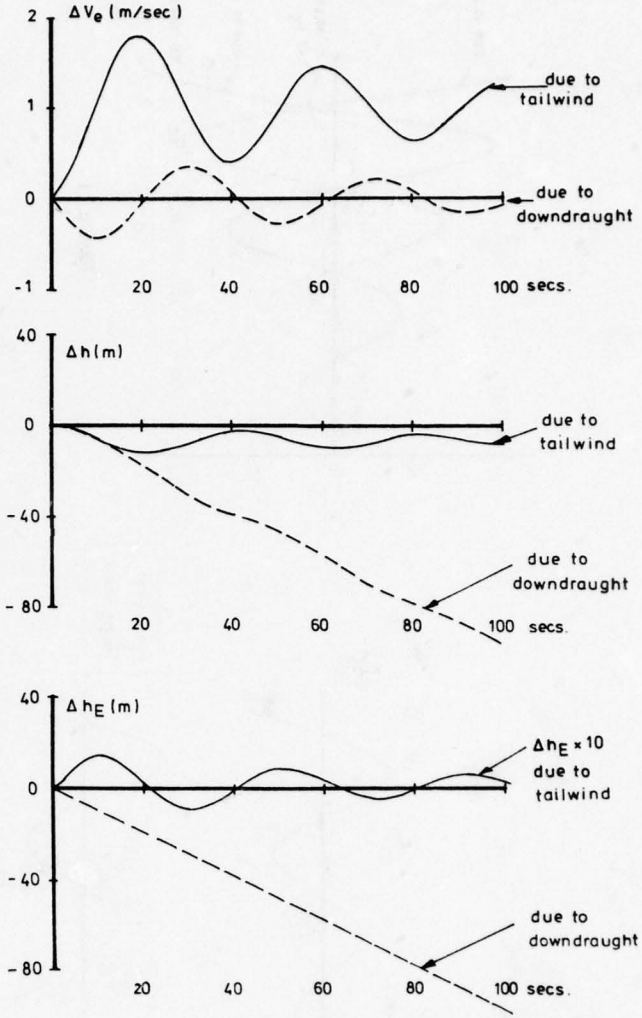

Fig.9 Comparison of speed, altitude and energy height responses to stepwise changes of horizontal and vertical winds. Magnitude of step 1 m/sec in both cases.

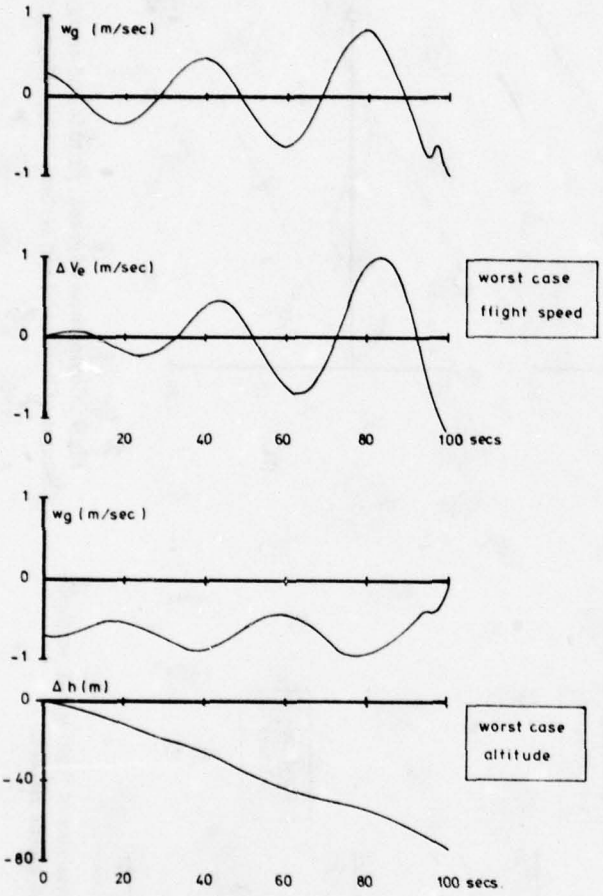

Fig.10 Worst case vertical winds (downdraughts) causing maximum deviations of flight speed and altitude. Duration of wind signals 100 secs.

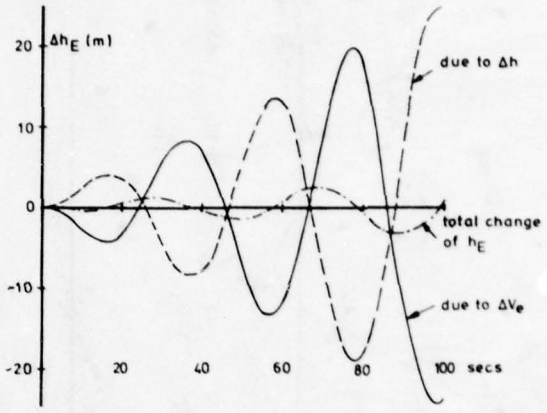

Figure 11

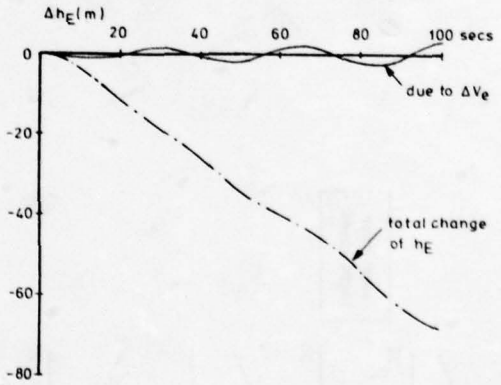

Fig.12 Change of total energy due to worst case vertical wind time-history causing maximum deviation of altitude.

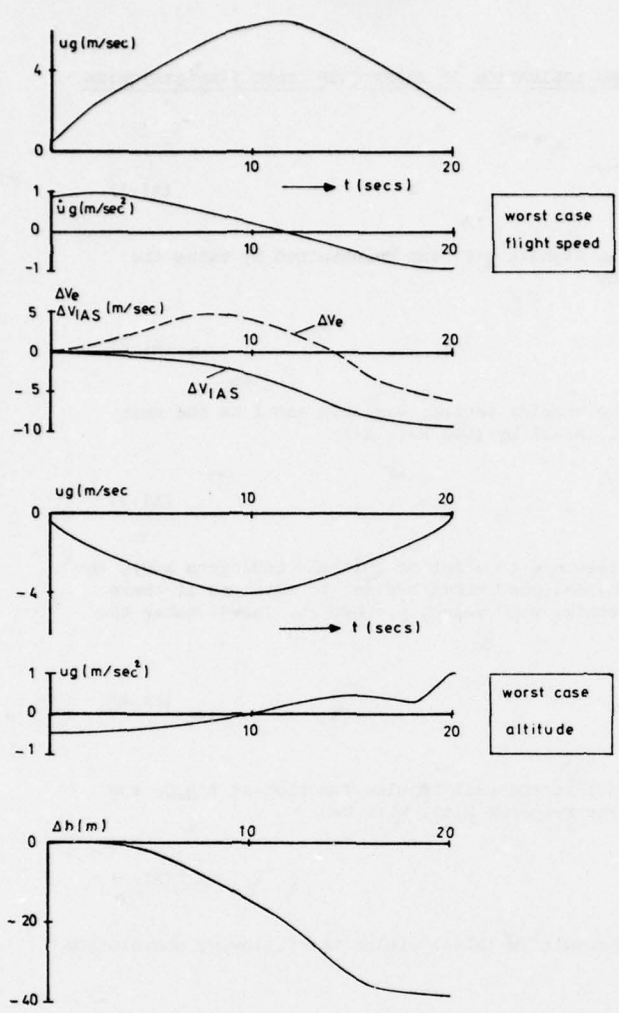

Fig.13 Examples of worst case response to wind time-histories, rate of change not exceeding 1 m/sec².

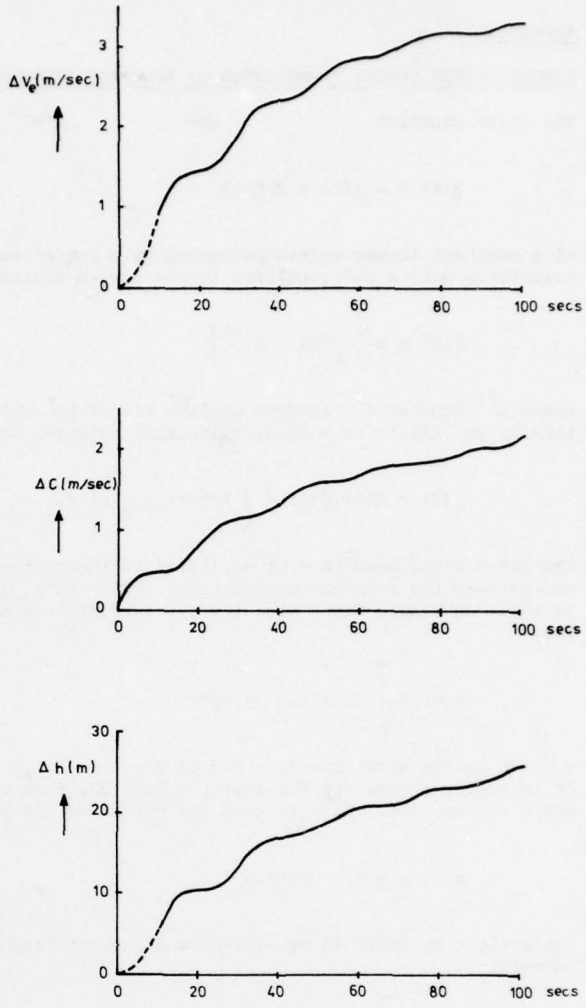

Fig.14 Relation between maximum deviation x at t_1 (worst case, deterministic) and the variance $\sigma_x^2(t_1)$ of x(t) in the white noise driven stochastic case.

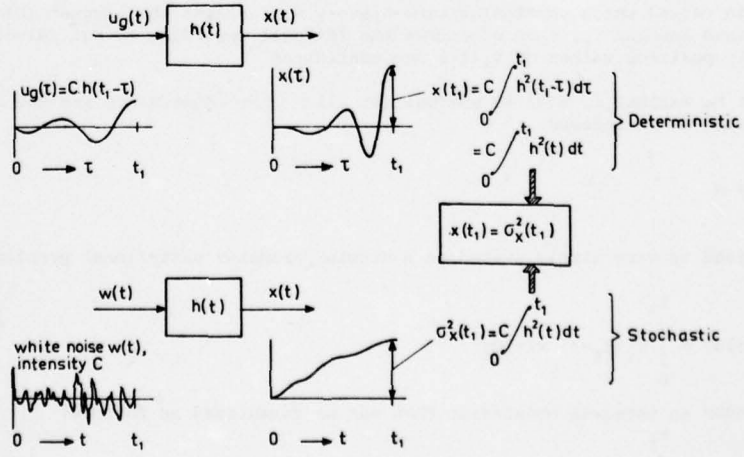

Fig.15 Maximum deviations of flight speed, vertical speed and altitude as a function of the duration t_1 of the worst case wind signals.
Maximum amplitude of wind signal 1 m/sec for all t_1.

APPENDIX 1

LINEAR SYSTEM THEORY FORMULATION OF AIRCRAFT DYNAMICS AND DERIVATION OF WORST CASE INPUT TIME-HISTORIES

The state equation

$$\dot{\underline{x}}(t) = A.\underline{x}(t) + B\,\underline{v}(t) \tag{A1-1}$$

of a constant linear system perturbed by a set of driving signals $\underline{v}(t)$ can be obtained by using the transition matrix F(t), related to the system matrix A by

$$F(t) = L^{-1}\left[\{PI - A\}^{-1}\right] \tag{A1-2}$$

where L^{-1} denotes the inverse Laplace transform, P is the complex Laplace variable and I is the unit matrix. Eq. (A1-1) is solved, using F(t) as given by eq. (A1-2) by (see Ref. 24):

$$\underline{x}(t) = F(t).\underline{x}(0) + \int_0^t F(t-\tau).B.\underline{v}(\tau).d\tau \tag{A1-3}$$

The first right hand term of eq.(A1-3) is the system's response to a set of initial conditions $\underline{x}(0)$, the second term the response to the input vector $\underline{v}(\tau)$. If initial conditions are set to zero and if there is only one single input signal $v(\tau)$, for instance horizontal wind velocity, then eq. (A1-3) takes the form

$$\underline{x}(t) = \int_0^t F(t-\tau).\underline{b}\; v(\tau).d\tau \tag{A1-4}$$

where $\underline{b}$ is the appropriate vector of B.
It is easily shown, see for instance Ref. 22, that if $v(\tau)$ is the unit impulse function at $\tau = 0$, the state vector $\underline{x}(t)$, which is then the vector of the impulse response $\underline{h}(t)$, will be

$$\underline{x}(t) = \underline{h}(t) = F(t).\underline{b} \tag{A1-5}$$

Replacing t by $(t-\tau)$ in eq. (A1-5) and substituting the result in (A1-4) yields the following convolution integral

$$\underline{x}(t) = \int_0^t \underline{h}(t-\tau).v(\tau).d\tau$$

In particular one element $x_i(t)$ of x(t) will then be given by

$$x_i(t) = \int_0^t h_i(t-\tau).v(\tau).d\tau \tag{A1-6}$$

The variable $x_i(t)$, may be for instance the deviation of flight speed, at instant t, caused by a horizontal wind time-history $v(\tau)$.
If now the question is raised which particular time-history $v(\tau)$ causes the largest absolute deviation of x_i at a certain fixed instant t_1, then of course the integral according to eq. (A1-6) should be maximal if for the moment only positive values of $x_i(t_1)$ are considered.

Of course $x_i(t_1)$ will be maximal if $v(\tau)$ is maximal for all τ if no constraints are set for $v(\tau)$. Therefore the following constraint is introduced

$$\int_0^{t_1} v^2(\tau)d\tau = C \tag{A1-7}$$

The question just raised is very simply stated as a single parameter variational problem where the objective function

$$I = \int_0^{t_1} \Phi(v,\tau)d\tau = \int_0^{t_1} h_i(t_1-\tau)\; v(\tau)d\tau \tag{A1-8}$$

is to be maximized under an integral constraint that can be formulated as follows:

$$G = \int_0^{t_1} \psi(v,\tau)d\tau = \int_0^{t_1} v^2(\tau)d\tau - C =$$

$$= \int_0^{t_1} (v^2(\tau) - D)d\tau = 0 \qquad \text{(A1-9)}$$

The solution of the variational problem is given by the Euler - Lagrange equation, see Ref. 25,

$$\frac{\partial \Phi}{\partial v} + \lambda \frac{\partial \psi}{\partial v} = 0 \qquad \text{(A1-10)}$$

From eqs: (A1-8) and (A1-9) it follows that

$$\Phi(v,\tau) = h_i(t_1-\tau).v(\tau) \qquad \text{(A1-11)}$$

and

$$\psi(v,\tau) = v^2(\tau) - D \qquad \text{(A1-12)}$$

From eq. (A1-9) it follows that D is a constant as t_1 is fixed.
Applying (A1-10) to (A1-11) and (A1-12) yields

$$h_i(t-\tau) + 2\lambda.v(\tau) = 0$$

Hence

$$v(\tau) = \frac{1}{2\lambda} h_i(t-\tau) \qquad \text{(A1-13)}$$

Althought till now only positive values of $x_i(t_1)$ were considered, the foregoing more generally holds for maximum absolute values of $x_i(t_1)$. The result of eq. (A1-13) can therefore be formulated as

$$v(\tau) = k\, h_i(t_1-\tau) \qquad \text{(A1-14)}$$

where k is either a positive or negative constant.
No restrictions have been formulated on the stability of the system so that eq. (A1-14) also holds for neutrally stable or unstable impulse response if, in these cases, t_1 is kept finite.
Substituting eq. (A1-14) into eq. (A1-6) yields the maximum value of $x_i(t_1)$:

$$x_i(t_1)_{max} = k \int_0^{t_1} h_i^2(t_1-\tau)d\tau$$

which can be shown to be equal to

$$x_i(t_1)_{max} = k \int_0^{t_1} h_i^2(\tau)d\tau \qquad \text{(A1-15)}$$

As mentioned in Chapter 7 of this paper, (see also Refs. 21, 22 and 23) the integral in eq. (A1-15) is equal to the variance $\sigma^2_{x_i}(t_1)$ of x_i at t_1 in the (imaginary) white noise signal from $\tau = 0$ onwards:

$$\int_0^{t_1} h_i^2(\tau)d\tau = \sigma^2_{x_i}(t_1) \qquad \text{(A1-16)}$$

The constant C in eqs. (A1-7) and (A1-9) now becomes

$$C = k^2 \int_0^{t_1} h_i^2(t_1-\tau)d\tau = k^2 \int_0^{t_1} h_i^2(\tau)d\tau = k^2\sigma^2_{x_i}(t_1)$$

Then, if k is assumed positive

$$k = \frac{\sqrt{C}}{\sigma_{x_i}(t_1)} \qquad \text{(A1-17)}$$

From eqs. (A1-15), (A1-16) and (A1-17) it follows that

$$x_i(t_1)_{max} = \sqrt{C}.\sigma_{x_i}(t_1) \qquad \text{(A1-18)}$$

It is concluded from eq. (A1-18) that if the integral of the worst case input signal squared is kept constant, the deviation caused by a worst case wind time-history is proportional to the standard deviation in the white noise driven, stochastic case.
Now consider a different, non-maximally deviating variable x_j.
At t_1 its value, due to the worst case time-history for x_i, will be

$$x_j(t_1)_{x_i max} = k \int_0^{t_1} h_j(t_1-\tau)v(\tau)d\tau = k \int_0^{t_1} h_j(t_1-\tau)h_i(t_1-\tau)d\tau$$

Again this may be written as

$$x_j(t_1)_{x_i max} = k \int_0^{t_1} h_j(\tau)\ h_i(\tau)d\tau \qquad \text{(A1-19)}$$

Quite similar to the significance of the integral in (A1-15) the integral in (A1-19) is equal to the covariance $\sigma_{x_i x_j}(t_1)$ in the white noise driven case, see Ref. 21.

$$\int_0^{t_1} h_j(\tau)\ h_i(\tau)d\tau = \sigma_{x_i x_j}(t_1)$$

A non-maximum deviation $x_j(t_1)$ is then, using eq. (A1-17):

$$x_j(t_1)_{x_i max} = \sqrt{C}.\ \frac{\sigma_{x_j x_i}(t_1)}{\sigma_{x_i}(t_1)} \qquad \text{(A1-20)}$$

This result can now be compared with the maximum deviation of x_j caused by its own particular worst case $v(\tau)$:

$$x_j(t_1)_{max} = \sqrt{C}.\sigma_{x_j}(t_1) \qquad \text{(A1-21)}$$

The constant C is taken to be equal in eqs. (A1-20) and (A1-21).
Introducing the correlation coefficient $\rho_{ji}(t)$:

$$\rho_{ji}(t) = \frac{\sigma_{x_j x_i}(t_1)}{\sigma_{x_j}(t_1).\sigma_{x_i}(t_1)} \qquad \text{(A1-22)}$$

and bearing in mind that

$$|\rho_{ji}(t_1)| \leq 1$$

it follows that

$$\left|\frac{x_j(t_1)_{max}}{x_j(t_1)_{x_i max}}\right| = \left|\frac{1}{\rho_{ji}(t_1)}\right| \geq 1$$

Unless two stochastic variables are fully correlated ($|\rho| = 1$) the absolute value of ρ is always less than unity. This confirms that the maximum deviation of a variable caused by its own particular worst case input signal is always greater than, or equal to, the deviation caused by any other worst case input history under the constraint assumed.

For practical applications some choice has to be made as to the value of the constant C. Up till now the upper boundary of integration t_1 was kept fixed so C was constant and hence the factor k could be considered constant.

If all variances and covariances, as a function of time of the motion variables in the white noise driven case are given and one wants to evaluate the influence of the duration t_1 of the worst case wind signals, then either of two approaches may be taken.

A first one is to keep C constant for all variables and all t_1. This implies that the integral of the wind signal squared according to eq. (A1-7) is kept constant for all t_1 and all variables. The deviations are then given by eqs. (A1-18) and (A1-20). The constant value of C is then a basis of comparison but the factor k has become a function of t_1, see eq. (A1-7).

Provided that all impulse responses are known, another possibility would be to give k, for each particular variable, a different value, constant for all t_1 considered.
The values of k could then be chosen such that for example, the maximum amplitudes for all worst case input signals were equal.

APPENDIX 2

TOTAL ENERGY AND ENERGY HEIGHT

When neglecting the contribution of the aircraft's rotations, then its total energy E, i.e. the sum of kinetic and potential energy relative to an earth-fixed frame of reference can be written as:

$$E = \frac{1}{2}m(V^2 + C^2) + mgh \qquad \text{(A2-1)}$$

where m is the aircraft's mass
g is the acceleration due to gravity
V is the horizontal speed
C is the vertical speed
h is the height above a reference plane.

The specific energy, the energy per unit of weight or the energy height h_E may be written as:

$$h_E = \frac{E}{mg} = \frac{1}{2g}(V^2 + C^2) + h \qquad \text{(A2-2)}$$

If small perturbations ΔV, ΔC and Δh relative to unperturbed straight flight at a speed V_o, a vertical speed C_o and at an altitude h_o are considered, then eq. (A2-2) becomes

$$h_E = \frac{1}{2g}\{(V_o + \Delta V)^2 + (C_o + \Delta C)^2\} + h_o + \Delta h$$

which, after linearisation, may be written as

$$h_E = \frac{1}{2g}(V_o^2 + C_o^2) + h_o + \frac{1}{g}(V_o.\Delta V + C_o.\Delta C) + \Delta h$$

The change in energy height h_E relative to unperturbed flight is then

$$\Delta h_E = \frac{V_o}{g}.\Delta V + \frac{C_o}{g}.\Delta C + \Delta h \qquad \text{(A2-3)}$$

In a typical approach the flight path angle is -3^o and as a consequence the unperturbed sink rate C_o is roughly 5% of the flight speed. Therefore the second term in eq. (A2-3) may well be omitted for a first approximation:

$$\Delta h_E = \frac{V_o}{g}\Delta V + \Delta h$$

GUST ALLEVIATOR FEASIBILITY STUDY FOR G91Y

by R. CARABELLI
AERITALIA - COMBAT AIRCRAFT GROUP
TORINO, Italy

1. SUMMARY

A feasibility study has been carried out of an active system to alleviate the turbulence effects on a light attack aircraft during the penetration phase of a ground attack mission.
The study was tailored to the G91Y and the conclusions were that proceeding through an experimental research by developing a flying prototype would be preferable, the risks implicit in the achievement of the required accuracy in measuring the gust velocity being very high.
The proposed system is working on two axes. An open loop sub-system driven by the normal component of the gust velocity on the pitch axis and a roll damper on the lateral is indicated as an adequate solution to meet profitable cockpit 'g' reductions and weapon delivery accuracy improvement as well.

2. INTRODUCTION

Some basic concepts were postulated at the beginning of the study to define the guidelines along which to proceed.

- The high manoeuvrability is a characteristic which cannot be given up. Therefore, any solution even potentially impairing like increased wing load by reduction of wing area or gust alleviating system limitations implying reduced maximum attainable 'g's had to be rejected.
- The time spent by a G91Y class aircraft at low altitude and high speed is fairly short and the g's felt by the pilot are more an annoying factor during tracking than a fatiguing one as resulting in prolonged missions. Therefore, the maximum alleviation effort had to be performed in the low frequency band of the gust spectrum where the energy contents is higher.
- Enhancement in weapon delivery accuracy had to be gained.
- Active systems had to be considered as the most promising one.
- The minimum impact on other systems had to be pursued.

3. SYSTEM DESIGN PHILOSOPHY

According to the last concept of point 2, a promising design philosophy to get a minimum impact on the remnant of the control system of the aircraft is an open loop control process based upon a measured value of the gust velocity feeding the controls actuation system.
On the G91Y the application of such philosophy to both pitch and lateral axis was rejected for two reasons.

- A roll damper is the most cost-effective in damping out lateral low frequency gust disturbances. A minimum of yaw damper control law reoptimization will be required to provide Dutch Roll lev.1 MIL-F-8785 B (ASG) requirements compliance.
- Cancelling of the aircraft side and yaw motions from the sideslip sensor output to generate a lateral gust velocity signal poses more problems than in pitch. This because Cy_β is smaller than $C_{L\alpha}$, thus the lateral acceleration intensity will be smaller and more difficult to measure with accuracy. Otherwise, the lateral acceleration is necessary to cancel the side motion contribution.

The conclusion was to adopt a roll damper on the lateral and an open loop normal gust velocity driven system on the pitch axis.

4. ROLL DAMPER

The roll damper layout was defined on the basis of the lateral gust response and dynamic stability of the linearized model of the lateral-directional motion of the aircraft. Simulation of the yaw damper was provided in this model.
The root loci analysis showed an additional oscillatory mode at frequencies lower than the Dutch Roll one. This mode is due to the yaw damper and its natural frequency reduces as well as the Mach number increases. Furthermore, the φ/β amplitude is pretty higher than for the Dutch Roll, specially at high speed and the resulting sensitivity to low frequency gusts greater than for the basic aircraft.
The roll damper layout of FIG.2 provides lower lateral gust sensitivity at low frequency than with yaw damper only. Further benefits result in the Dutch Roll frequency range so that enhancements in tracking precision can be reasonably expected.

5. PITCH AXIS GUST ALLEVIATOR

The functional diagrammes of the two basic configurations investigated are shown in FIG.3.
The solution EL (Elevator only is used) assumes the normal gust velocity signal is filtered and then fed into the elevator actuation system. The filter shape is a function of the task assigned to the system i.e. normal 'g' attenuation at a given fuselage station or increased platform stability, and therefore both problems cannot find a definite solution at the same time with a single functional mode system. This is the first drawback of such configuration.
The method used for calculating the filter is that indicated by Mr.Coupry in his work already presented to AGARD. By the way, its full application was not necessary for the G91Y. A stable filter was provided by the trivial solution consisting of

$$1)\quad K(S) = k\,\frac{\text{zeroes of } Hw_g\,(S)}{\text{zeroes of } H\delta_e\,(S)} \qquad \text{where}$$

k is a suitable gain and Hw_g, δ_e the transfer function of the aircraft response to vertical gust velocity/elevator input.
The aircraft response, which can be either the normal 'g' or the longitudinal tracking error, assumes the form

$$2)\quad Hw_g\,(S) = \left[Hw_g\,(S)\right]_{\substack{\text{basic}\\ A/C}} + K(S)\,.\,H\delta_e\,(S)$$

The longitudinal tracking error transfer function is taken from Ref.1 which defines it as

$$3)\ Her_{wg}(S) = K_{\alpha} \cdot W_{wg}(S) + K_{\vartheta} \cdot \vartheta_{wg}(S)$$

where K_{ϑ} and K_{α} are weight coefficients depending on the weapon used , aircraft dive angle and speed. ϑ_{wg} and W_{wg} are the aircraft responses in attitude and normal velocity to the normal gust.
The second solution FLEV provides command inputs to the flaps and the elevator.
These inputs are simply proportional to the normal gust velocity and the gains were derived by assuming that the gust induced lift and pitching moment are set to zero by appropriate elevator and flaps displacements. The mechanization of this solution is more complicate two control surfaces being used instead of one but it has the great advantage of providing simultaneous normal 'g' alleviation at all fuselage stations and improved platform stability.
Both solution EL and FLEV do not affect the handling qualities of the aircraft if a perfect cancelling of the aircraft motion contribution to the measured gust velocity is achieved. This is a great advantage because the stability augmentation system will not suffer of the drawbacks resulting from compromise solutions trying to achieve both goals i.e. simultaneous gust alleviation and good handling.

6. NORMAL GUST VELOCITY CALCULATION

The normal gust velocity is calculated on the basis of the output of an incidence sensor to be installed slightly ahead of the root wing section leading edge on the fuselage sidewall.
This position is the result of wind tunnel data analysis and minimised sideslip induced errors and provides linear characteristics versus incidence. A fuselage location was chosen to get more practicality of the system than with nose probe installation. The front fuselage is generally housing visual aids (radar, cameras, infra-red devices) which might be disturbed by the probe.
The aircraft motion contribution to the incidence signal is cancelled according to the relationship shown in FIG.4 between gust induced incidence and sensor output.
- w is the C.G. normal velocity
- q is the pitch rate
- l is the distance between C.G. and incidence sensor.

It is obviously not essential to deal with incidence or velocity their relationship being a proportionality one.
In the FIG.4 relationship the normal load factor is the foundamental signal to be washed-out and then integrated to get the required velocity. The lateral contributions have been neglected being assumed that any lateral motion perturbation is sufficiently damped by the roll damper.
The plant view of the aircraft shows where the additional instrumentation has to be installed.

7. BASE OF COMPARISON FOR CONFIGURATION EL AND FLEV

Several characteristics concurred in defining the base of comparison for configuration EL and FLEV.
FIG.5 summarizes these characteristics and their use can be briefly justified as follows.
The pitch attitude and the normal C.G. velocity both contribute to define the longitudinal tracking error during ground attack.
The normal accelerations are necessary to monitor stress changes on parts of the airframe or on the pilot.
The maximum actuation rates and the controls position errors required were used for the system mechanization design.
All the preliminary calculations were carried out by using linearized aircraft and flight control system dynamics. The control laws were derived accordingly and their validity in presence of non-linearities checked later on. The Dryden's model of the gust was used.

8. CONFIGURATION EL

The EL System performance was checked with optimum control law and elevator actuation system dynamics as presently available on G91Y. In order to simplify the calculations the pitch damper was assumed off. This allowed an easier determination of the command filter K (S) of equation (1) the Hwg and $H\delta_e$ transfer functions to be used being of lower order. No oversimplifications were introduced in this way provided of course that the FLEV system performance with pitch damper off will be used for comparison.
Figure 6 is of interest because it shows the inadequacy of the present actuation system. When the basic aircraft normal-acceleration at the cockpit power-spectral-density are compared, the improvement looks not attractive indeed. Even though the R.M.S. 'g' is halved, the approximation of the mathematical model and the sensitivity to changes in flight conditions might reduce to zero this gain. The second step was then to study a modification to the actuation system which gave curve 2 results and a suitable phase lag compensation filter to further improve the performance. The result of this effort is the curve 3 and the definite enhancement that it represents.
The filter characteristics were defined by comparing system performances and requirements in terms of maximum actuation rate and system authority to meet these performances.
FIG.7 shows the performance reductions resulting when constraints are put on both maximum rate and authority as necessarily occur in actual systems. To get 50% R.M.S. 'g' reduction, 135°/sec of maximum actuation rate and 6° of system authority need to be provided.Such authority is roughly twice the pitch damper one and will require protection against hardover consequences.
The resulting increase in complexity is high whichever is the solution adopted to improve the system reliability.

9. CONFIGURATION FLEV

The major assumption made in carrying out calculations for configuration FLEV was to postulate improved elevator actuation system dynamics as in the last assessments of configuration EL. A preliminary mechanization study was necessary to give a realistic estimate of the flap actuation system dynamics. A bandwidth of 16 Hz was assigned as target, the resulting loss of performance of the gust alleviator being fairly small in this case.
On the basis of the R.M.S. 'g' alleviation achievable at the cockpit for each combination of the gust alleviator authorities (FIG.8) it is evident that 7-8 deg. of flaps and 1-1.5 deg of elevator authority provide quite satisfactory performances.

The authorities chosen to define further requirements were 7.5 deg for the flaps and 1.5 deg for the elevator. In this way protection against hardovers is given either in pitch or in roll, because according to the calculations the pilot can easily reduce the resulting transients.
The maximum actuation rates acceptable with the above authority limits were defined on the base of FIG.9 data.
75°/sec can be accepted for the flaps and 15°/sec for the elevator, still having a good performance of the system and a fairly flat trend of it versus the actuation rates. This is essential to minimize the system sensitivity to actuation loads.

10. COMPARISON OF CONFIGURATION EL & FLEV

Both configuration EL and FLEV use the normal C.G. velocity thus requiring integration function provision for the calculation.
An integrator implementation is not physically necessary in the EL system thanks to its control law requiring a zero in the origin. The control filter can then be split and the integration avoided by cancelling the derivative operator in that part of the filter which operates on the output of the normal C.G. velocity computing circuit. FIG.10 better illustrates this fact.
Configuration FLEV has not such a facility and an approximation is therefore necessary to avoid the integration in analogues.
The filter used in the approximation is shown in FIG.10 and an acceptable time constant was found to be 10 sec.
Next figure (11) gives evidence of the main advantage of the configuration FLEV.
The normal 'g' alleviation can be met together with improved platform stability because either the attitude response and the incidence response to gust are considerably lower than for configuration EL optimized to improve the R.M.S. 'g'.
Further points of advantage of configuration FLEV are the reduced authorities and this has been sufficiently pointed out in paragraph 9, and the reduced maximum actuation rates demanded which allow to achieve good system performances with less extensive elevator actuation system modifications.
Where the FLEV system shows significant drawbacks is the increased power consumption to feed the flaps actuators and the wing structure modifications to fit the new hinged flaps and the relevant actuation system.
The solution given to these problems were acceptable for a demonstrator aircraft but not for production.
A deeper insight of them was left to a later phase of the development programme.

11. SENSITIVITY STUDIES ON CONFIGURATION FLEV

Sensitivity analyses were carried out on configuration FLEV to evaluate the development risk.

11.1 The position control accuracy of both elevator and flaps was the first area subject to investigation. Calculations were carried out by simulating a hysteresis on the actuators output and the R.M.S. 'g' at the cockpit was used as basis for comparison (FIG.12).
If as design target accuracies .1 degree for the elevator and .05 degree for the flaps are assumed, reasonable tolerances will be available without significantly degrading the gust alleviator performance.

11.2 The sensitivity to system gains variations was assessed in the design flight condition by calculating the R.M.S. 'g' at the cockpit and by representing it as gains function (FIG.13). The gain variations can be attributed to either imperfect knowledge of the aerodynamic derivatives or to imperfect measure of the air data or both.
Loocking at FIG.13 if a 20% error is made on both gains, a large loss of performance will occur. The reduction in performance is a function of the direction of the gain changes and therefore a step by step approach to optimum gains will be necessary during flight testing for safety reasons.
A suitable path to the optimum couple of gains was defined by taking margins which guarantee that the worst performance will be better or at least equal to that of the basic aircraft.

11.3 System stability analyses were necessary because calculations showed that aperiodic instability is likely to occur due to imperfect cancelling of the aircraft motion contribution from the measured gust velocity. The resulting error makes no longer the gust alleviator an open loop system, the control inputs being now a function of the aircraft response to gust.
The rate of instability is a function of the system gains, specially the flaps one, and a suitable cure to make the system definitly stable is to introduce a wash-out first order filter on the measured gust velocity. The shape of the filter is that of a highpass one with time constant in between 7 and 10 seconds. FIG.14 shows the enhancement given by the wash-out which keeps clear of the instability due to the pseudo-integrator and gives large stability margin.
The system could be made stable with enough margin even by a time constant quite lower than 7 sec.
Loss of performance damming dictated its setting in between 7 and 10 sec.

11.4 The system layout of FIG.15 was used to define the minimum sensor characteristics to be used in the design phase and to further simplify the system.
The airstream direction detector (ADD) sensing the total incidence was found to be very critically affecting the system performance (FIG.16). The R.M.S. 'g' at the cockpit looks shallowly affected by the damping while the choice of the frequency needs to be accurately done.
The acceptable minimum accuracy, which was simulated by a hysteresis, resulted of the order of .1 deg because no more than 10% of R.M.S. 'g' at cockpit increase is produced in this case.
The pitch rate gyro (PRG) output feeds the gust velocity computer to calculate the ADD position error correction and the normal C.G. velocity. The former gives a small contributions, the distance from the C.G. being very short.
The latter has almost no effect on the gust alleviator performance but it is necessary to avoid undue system activity in manoeuvring flight. The dynamic characteristics of the series aircraft pitch damper PRG look adequate ones an enlarged range of measure is provided to prevent gust alleviator interferences during high 'g' manoeuvring.
The normal accelerometer (NA) dynamics currently provided by flight test instrumentation sets was found to be adequate. A suitable sensor location was identified as shown in FIG.4 to reduce the structural noise. This point corresponds to a node of the fuselage first bending mode.

The attitude signals (pitch and roll) contribution to the normal C.G. velocity calculation accuracy was found negligible. Therefore, although always available being an output of the air data computer (ADC), their use is not foreseen unless different indications will come out from flight tests.

11.5 Finally, performances assessments were carried out using tridimensional gust and six-degrees of freedom aircraft motion mathematical model.
The lateral gust worsens the vertical alleviation through the roll rate times lateral velocity product if no account of this term is taken when computing the normal C.G. velocity. To do that a sideslip sensor and further hardware should be added to the system whilst significant benefits result by the use of the roll damper already introduced to alleviate the lateral gust sensitivity.
In this way the roll rate response to gust is reduced and the above term contribution to the normal response considerably made weak.

12. CONCLUSIONS

- The whole system (FLEV + roll damper) is designed to provide the maximum alleviation in the low frequency band of the gust spectrum in order to enhance the tracking performance.
  The configuration FLEV can provide a high degree of gust alleviation to G91Y along the normal axis while a roll damper needs to be used to reduce the lateral gust sensitivity. As fallout lower FLEV system complexity can be retained the cancelling of the lateral motion contribution to the measured normal C.G. velocity being no longer necessary.
- The sensors accuracy required is high but acceptable for a development programme. More practicality would be achieved later on by relaxing the requirements on the basis of flight test results.
- The controls actuation characteristics required are acceptable. Higher actuation rate is necessary for the flaps but it can be met without big changes to the hydraulic power supply circuit.
- The system performance sensitivity to gains variation is fairly high thus the design gains shall be achieved step by step as flight experience advances. It is expected that an operational system will have either limited speed range in which it can be profitably used or scheduled gains if an enlarged range of operation will be requested.
- The efforts to make the system more practical by allowing certain computing errors are not impairing the manoeuvrability.
  Only a slight reduction of the initial normal 'g' response seems to be induced by the adverse flaps angle demanded.

REFERENCES

1. AD746002 June 1972 issued by NTIS
   Analysis of Piloted Weapon Delivery
   A7D Strafing Thesis.

SIMBOLS

α	:	incidence (angle of attack)
β	:	sideslip angle
φ	:	lateral attitude (bank angle)
ϑ	:	pitch attitude
g	:	gravity acceleration often used to indicate the load factor ('g')
R.M.S.	:	Root Mean Square
S	:	Laplace operator

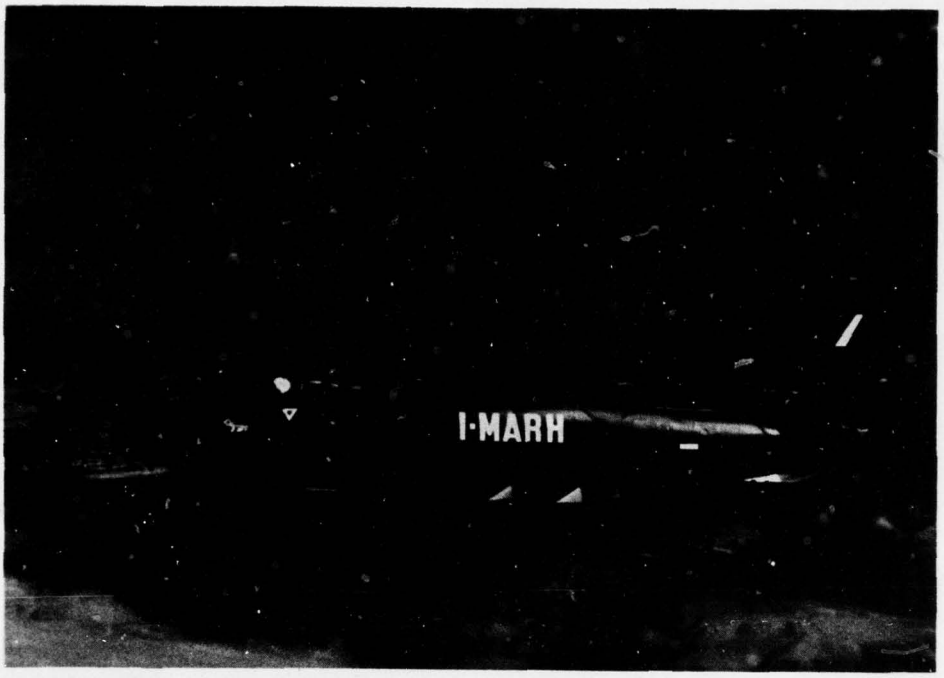

FIG. 1 - THE G91Y

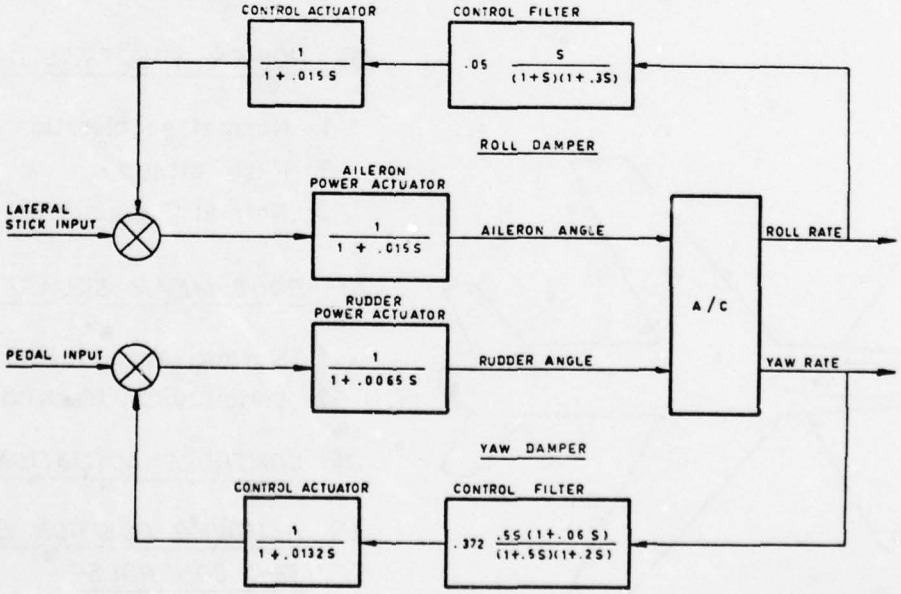

FIG. 2 - ROLL/YAW DAMPERS LAYOUT

AD-A071 709 ADVISORY GROUP FOR AEROSPACE RESEARCH AND DEVELOPMENT--ETC F/G 1/3
STABILITY AND CONTROL.(U)
MAY 79

UNCLASSIFIED AGARD-CP-260 NL

3 OF 4
AD A071709

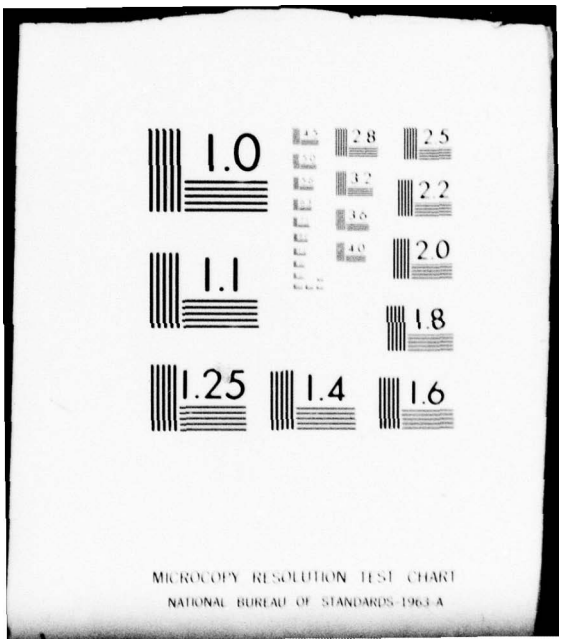
1.0
1.1
1.25
1.4
1.6
1.8
2.0
2.2
2.5
2.8
3.2
3.6
4.0
MICROCOPY RESOLUTION TEST CHART
NATIONAL BUREAU OF STANDARDS-1963-A

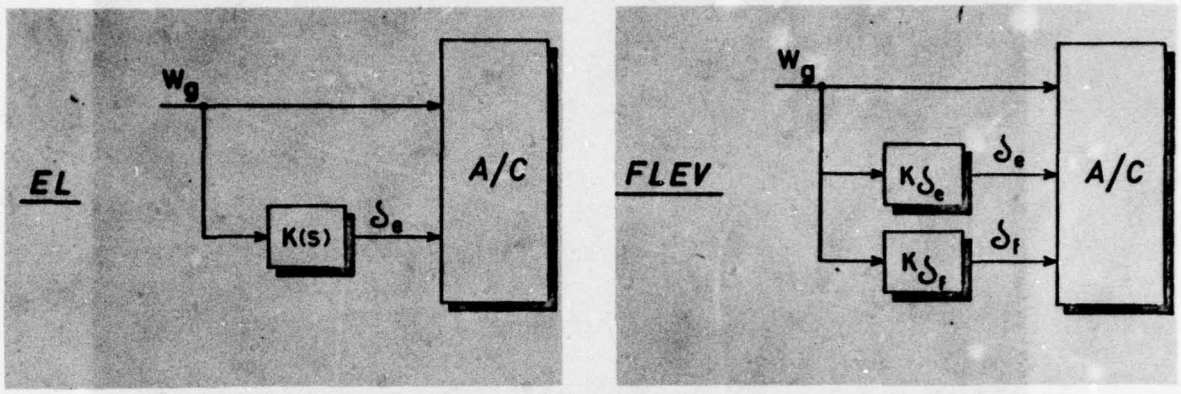

FIG. 3 - GUST ALLEVIATION CONCEPTS INVESTIGATED

1. $\alpha_g = \alpha_v - (w - q\ell) \cdot \frac{1}{U_o}$

2. $w = \int (qU_o + gn_z + g\cos\theta)\,dt$

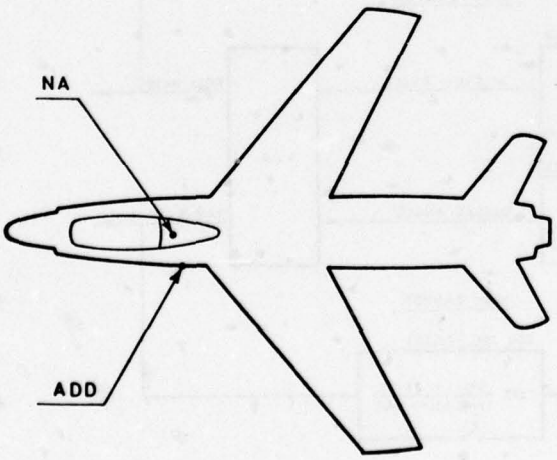

FIG. 4 - GUST INDUCED INCIDENCE CALCULATION

A) *FREQUENCY RESPONSE OF*

- .1 Normal acceleration at tailplane C.G. and cockpit
- .2 Pitch attitude
- .3 Normal C.G. velocity component

B) *POWER SPECTRAL DENSITY OF*

- .1 Normal acceleration at cockpit
- .2 Pitch attitude
- .3 Normal C.G. velocity component

C) *ROOT MEAN SQUARE OF*

- .1 Normal acceleration at cockpit
- .2 Longitudinal tracking error

D) *CONTROLS ACTUATION RATE*

E) *ALLOWED POSITION ERROR OF THE CONTROLS*

FIG. 5 - BASE FOR COMPARING EL AND FLEV SYSTEM

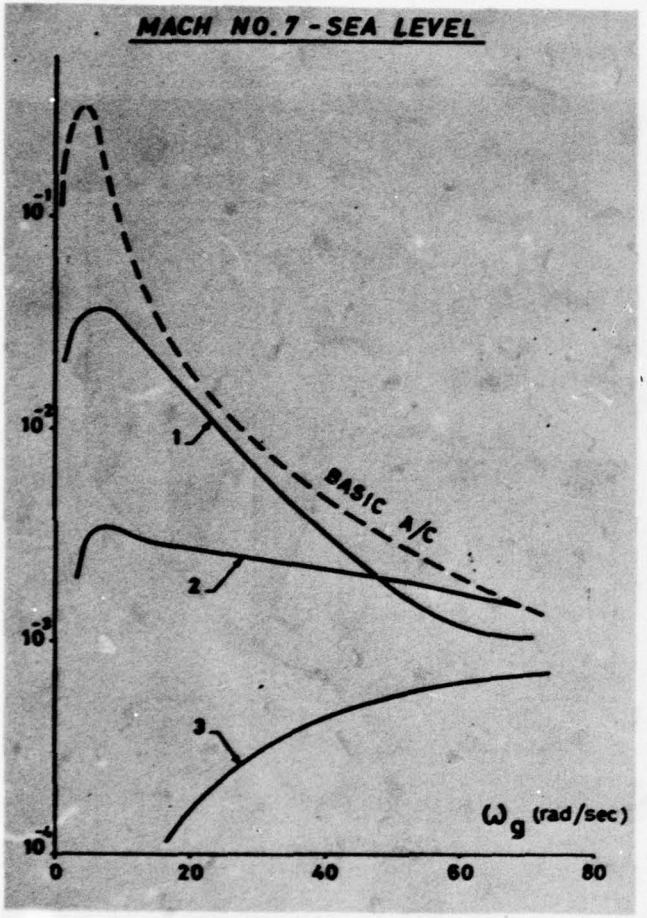

FIG. 6 - POWER SPECTRAL DENSITY OF THE NORMAL 'G' AT THE COCKPIT

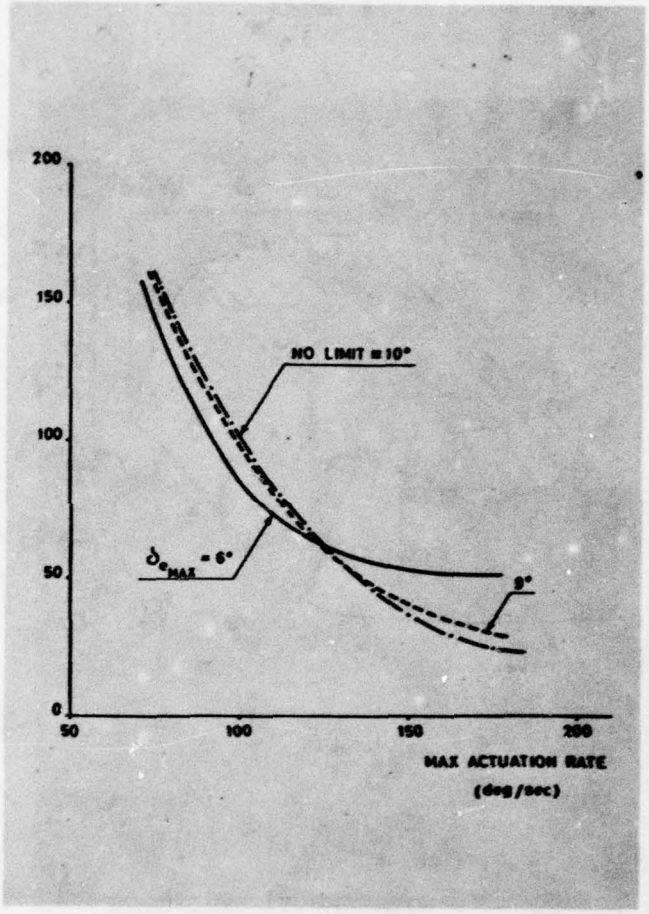

FIG. 7 - PERCENTAGE OF R.M.S. 'G' AT THE COCKPIT REFERRED TO THE BASIC AIRCRAFT

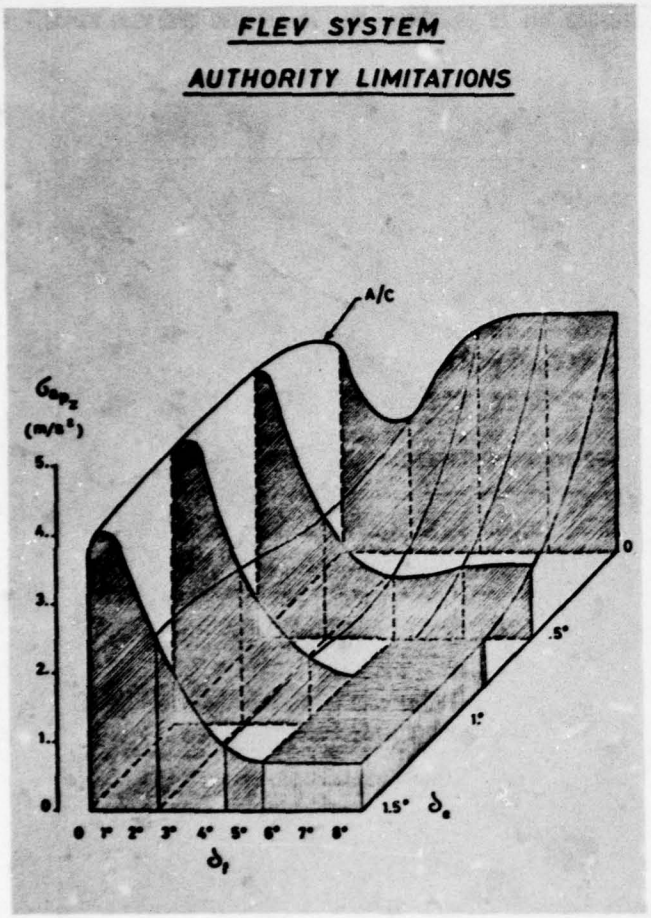

FIGURE 8

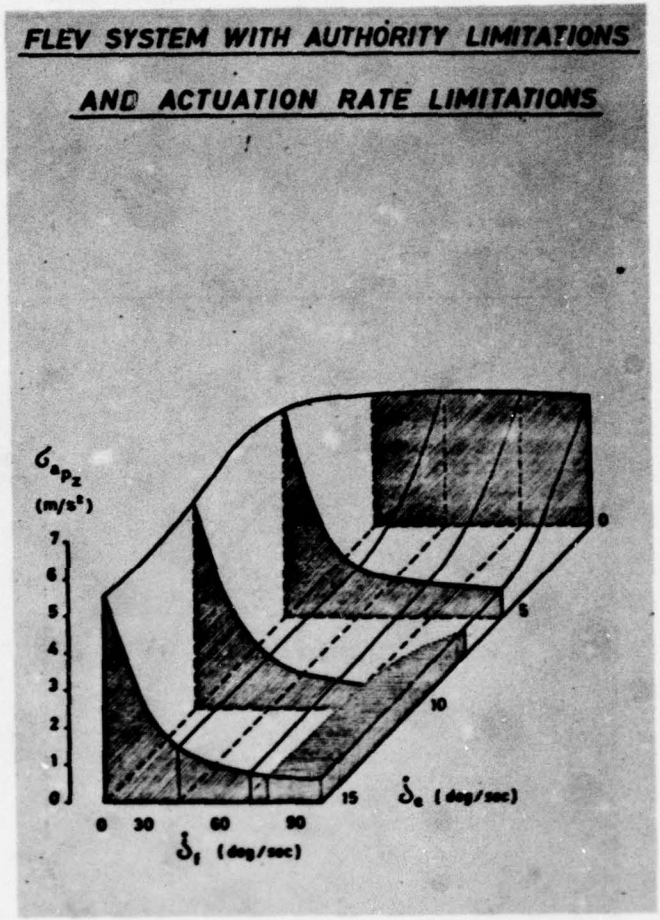

FIGURE 9

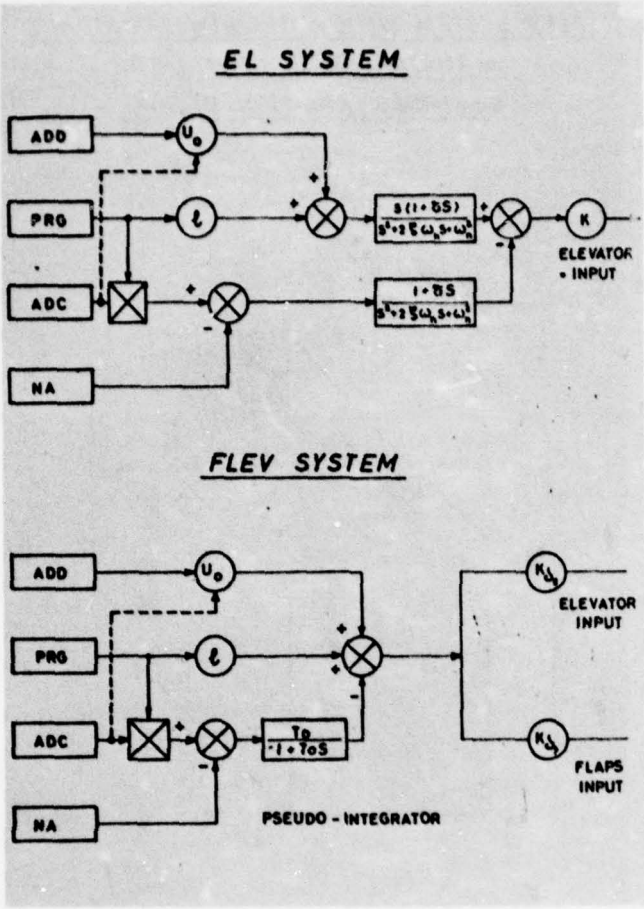

FIGURE 10

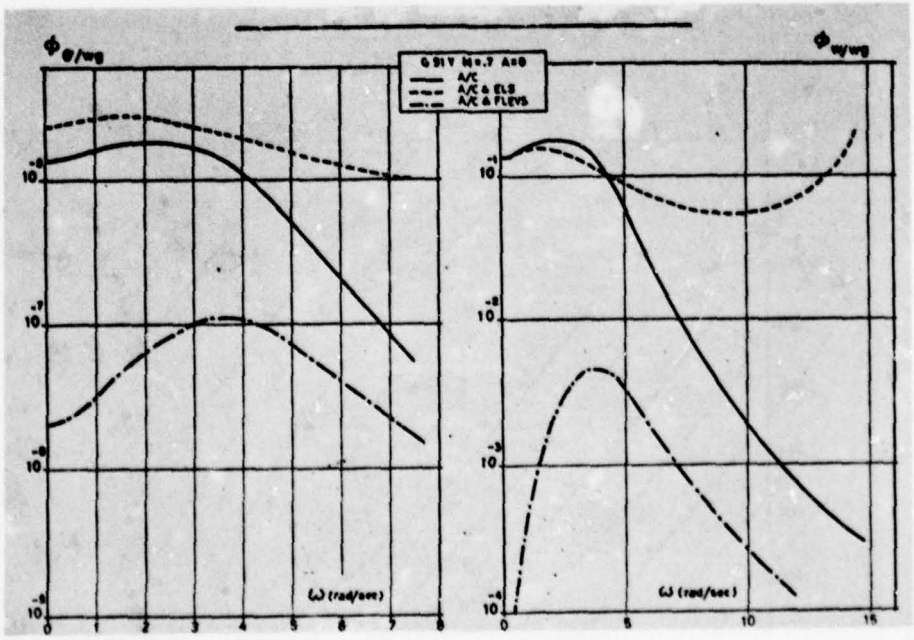

FIG. 11 - EL - FLEV SYSTEMS COMPARISON
P.S.D. OF PITCH ATTITUDE AND C.G. NORMAL VELOCITY RESPONSE TO VERTICAL GUST

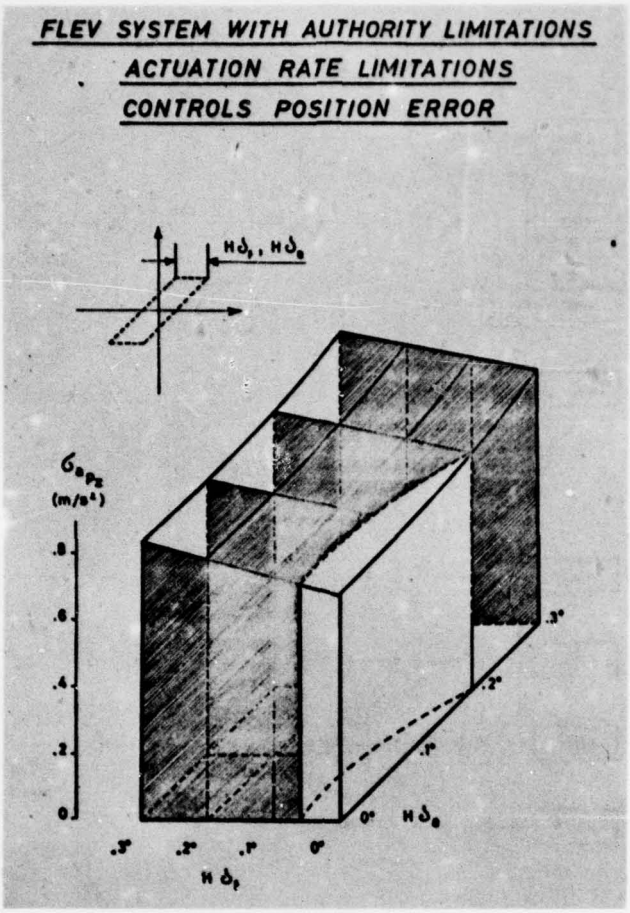

FIGURE 12

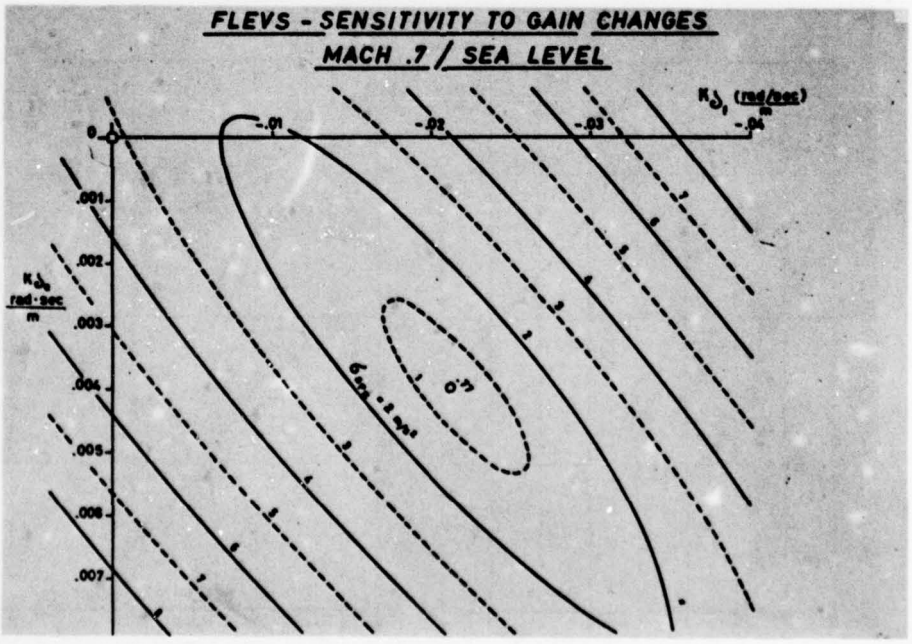

FIGURE 13

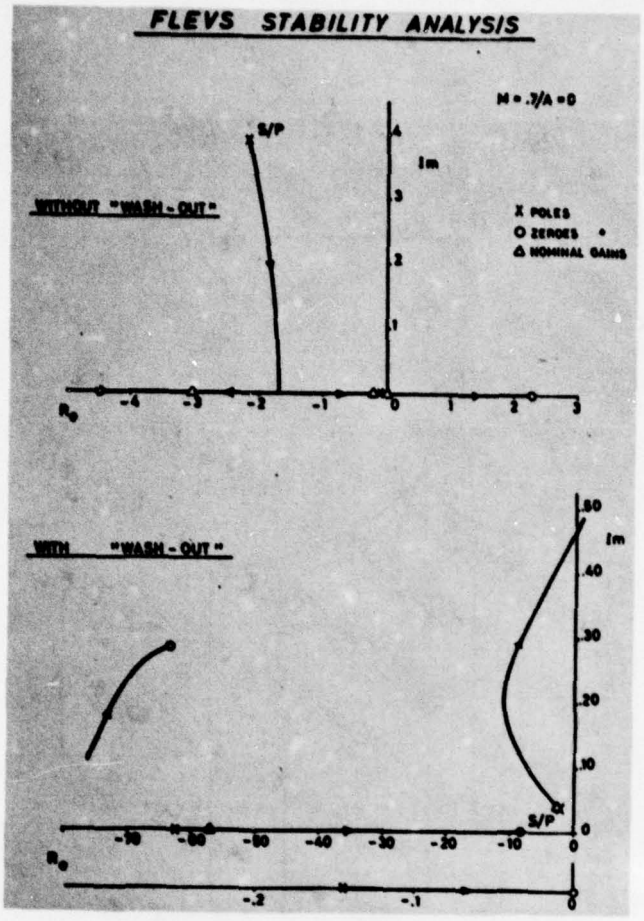

FIGURE 14

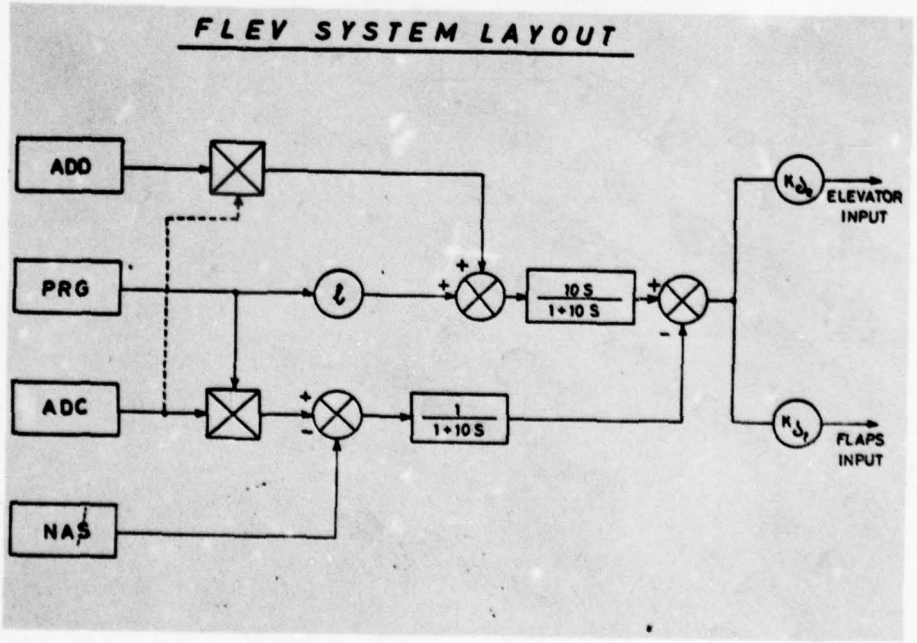

FIGURE 15

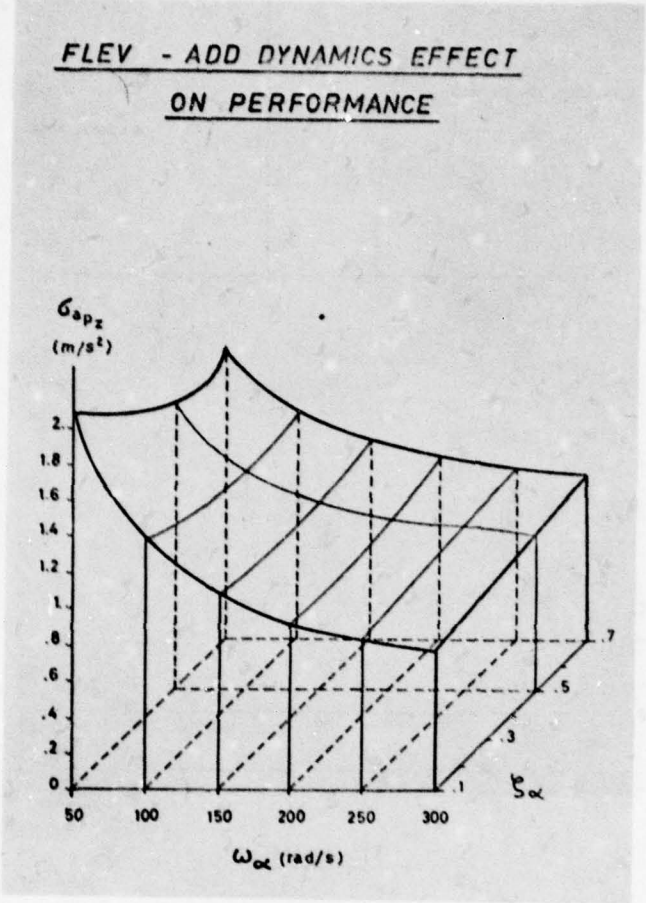
FLEV - ADD DYNAMICS EFFECT
ON PERFORMANCE
$\sigma_{a_{pz}}$
(m/s²)
2
1.8
1.6
1.4
1.2
1
.8
.6
.4
.2
0
50
100
150
200
250
300
ω_α (rad/s)
.7
.5
.3
.1
ζ_α

FIGURE 16

DESIGN CONSIDERATIONS FOR RELIABLE FBW FLIGHT CONTROL

James K. Ramage* and James W. Morris**
Air Force Flight Dynamics Laboratory
Wright-Patterson AFB, Ohio 45433

ABSTRACT

The advent of fly-by-wire (FBW) flight control systems, as validated by developments over the past several years, has established a viable technology base from which the designer can confidently explore and apply innovative flight control concepts to achieve improved overall performance capabilities and reduced cost of ownership. Adequate consideration of the critical design factors summarized in this paper can contribute to the overall success in design and implementation of a reliable FBW flight control system. Specific attention is given to experience with the FBW system developed under the USAF Survivable Flight Control System Program which represented the successful culmination of a number of developments into a major concentrated program aimed at establishing the practicality of FBW primary flight control.

LIST OF SYMBOLS AND ACRONYMS

A/D	Analog to Digital
BIT	Built-In-Test
CCV	Control Configured Vehicles
D/A	Digital to Analog
DOF	Degrees of Freedom
FBW	Fly-By-Wire
EMC	Electromagnetic Compatibility
GPC	General Purpose Computer
IFM	In-Flight Monitoring
I/O	Input/Output
LRU	Line Replaceable Unit
LVDT	Linear Variable Differential Transformer
MBU	Mechanical Back-Up
PACT	Precision Aircraft Control Technology
SFCS	Survivable Flight Control System
X_a	Actuator Coverage
X_c	Computer and I/O Coverage
X_s	Composite Sensor Coverage
X_2	Total Second Fault Coverage
λ	Channel Failure Rate
λ_a	Actuator Failure Rate
λ_c	Computer and I/O Failure Rate
λ_s	Composite Sensor Failure Rate

1. INTRODUCTION

The purpose of this paper is to highlight some of the more critical design considerations which both aircraft designers and flight control systems engineers must bear in mind in the design and implementation of fly-by-wire (FBW) flight control systems. The advent of FBW flight control systems, as validated by developments over the past years, has established a viable technology base from which the designer can confidently explore and apply innovative flight control concepts. Fly-By-Wire has paved the way for increased application of active control technology which will result in airplanes having improvements in range and maneuver performance along with smooth ride and precision tracking. Evolution of FBW flight control technology is represented in Figure 1. Additionally, FBW will permit a better integration of structural, mechanical, electrical, electronic, and aerodynamic technologies in such a way as to result in the best overall airplane from the combined standpoints of safety, reliability, maintainability, and cost of ownership.

Over a period of more than fifteen years the USAF has been involved actively in the research and development of FBW and related technologies. The Air Force Flight Dynamics Laboratory's overall flight control program has been geared toward establishing new flight control technology and demonstrating its realistic impact on aircraft design, mission effectiveness, and cost. Along these lines, the AFFDL's role in the technology development and transition process is to (a) demonstrate the practicality of promising

* Program Manager, Digital Flight Control System Advanced Development Program
** Principal Engineer, Control Systems Development Branch

technologies, (b) identify critical design considerations, (c) formulate application criteria, and (d) establish confidence based on design, fabrication, ground qualification/compatibility, and flight test experience. These efforts, along with both domestic and foreign government and industry programs, contribute to the overall broad FBW technology base from which important design considerations continue to evolve. These experiences and resulting design considerations have also contributed to the application of FBW in major systems and are currently paving the way for further exploitation in the areas of control configured vehicles, active controls, multi-mode control, and integrated fire/flight control.

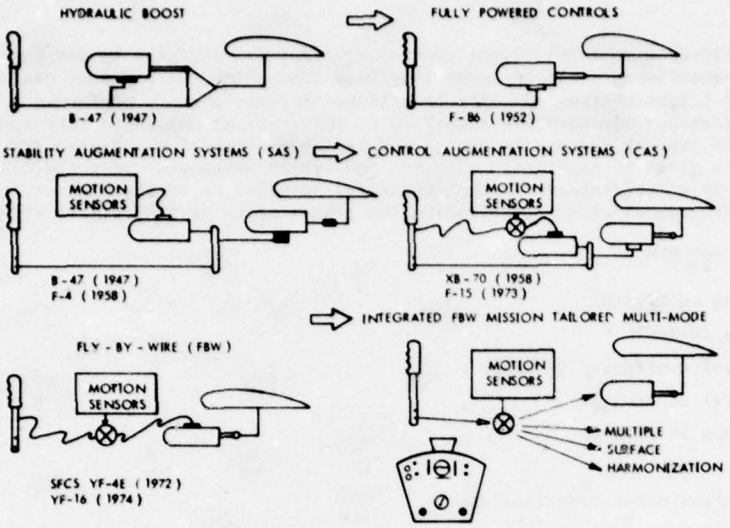

Figure 1 Evolution of FBW Flight Controls

The purpose of this technology validation is to increase the designer's options available when performing new aircraft design and trade-off studies. Design freedom has been stressed to make practical use of technologies in whatever combinations best satisfy the specific requirements, provided that sufficient confidence has been established in the technology to warrant its use. The point at which new technology has been sufficiently demonstrated for reasonably acceptable technical and cost risk is very often difficult to define.

This has indeed been the case for FBW, with the USAF's program geared at reaching that acceptable level of risk through progressively escalated developments to a point of technology acceptance and application to systems. This paper reviews briefly some of those activities leading to a full-scale USAF fly-by-wire development and flight test evaluation program with emphasis on some of the resulting design considerations. Specific attention is given to experience with the FBW system developed under the USAF Survivable Flight Control System Program, since this program represented the successful culmination of a number of developments into a major concentrated program to unquestionably establish FBW as a viable technology for aircraft primary flight control.

2. BACKGROUND

In the early 1960's, USAF development efforts were aimed at developing a reliable electric primary flight control system which used no electronics (vacuum tubes) or electro-mechanical switching. The primary goal was a simple and reliable direct electrical replacement of its mechanical flight control system counterpart. Concurrent with this development work, considerable effort was placed on developing a reliable and accurate digital capability to provide for necessary control augmentation and automatic flight control functions. Conclusions evolving from these efforts in 1962 were: (a) simple electric counterparts to mechanical flight control systems are easily achievable; (b) some form of redundancy and channel voting or signal selection can be applied to computation and signal transmission to realize safe system operation in face of individual component failures; (c) an electric/electronic flight control system would eliminate friction, stiction, backlash, and the complexities commonly associated with traditional mechanical controls; and (d) the limiting factor in developing a viable electric/electronic flight control system was primarily in the state-of-the-art of electronics (size, power, stability, weight).

During the mid 1960's we saw a dramatic revolution in electronics that has established a sound electronic technology baseline from which we could build reliable, low weight, small size, and realistically costed computers, one of the inevitable needs for realizing fly-by-wire. A continuing activity in development and trade-off studies, taking advantage of electronic and control system integration advances, was showing increasing benefits of FBW for such conceptual systems as advanced fighters, bombers and transports. One of the studies conducted in 1967 using the AMSA (Advanced Manned Strategic Aircraft) as a baseline vehicle verified some very important conclusions about FBW as a primary means for control of that vehicle. Some of the benefits indicated at that time were:

Gross weight reduction of 300 to 700 pounds

Reduction of maintenance manhours per flight hour

Reduction in design and installation time and in problems caused by vehicle geometry and compliance. Total cost savings of $80,000 per aircraft in production.

Improved mission success reliability and flight safety

Weight reductions through new configurations eliminating structural weight penalties for stability.

Some of the advertised benefits of FBW, such as design and installation savings, were being realized from the all-electric (FBW) spoiler control system on the F-111. Confidence in reliability and safety was becoming established by continued excellent operation of that system. Further confidence and acceptance of FBW was demonstrated on the AF Flight Dynamics Laboratory's B-47 FBW development and flight test program. Technical emphasis was in redundant FBW servo-actuators, direct electrical and closed loop control, and sidestick controller implementation. Flight test indicated significant reductions in pilot workload and less pilot fatigue. Instead of high pilot control forces during maneuvering conditions, simple wrist action with very small stick forces provided precise control of such a large aircraft with minimum effort. Vehicle disturbances were automatically compensated for by effective feedback closed loop control. Confidence in reliability and safety of electric/electronic control was further enhanced through a limited number of flights. In late 1969 and early 1970 applicable fighter control laws for analog FBW were aptly demonstrated under realistic mission scenarios in the F-4C Tactical Weapon Delivery (TWeaD) Program. Control augmentation comprised of high gain control with both pitch rate and normal acceleration feedback was proven through flight test evaluation to be very effective in significantly improving unguided weapon delivery performance. Control laws developed for TWeaD formed a basis for subsequent FBW control law implementation and development programs.

Experience, knowledge, and confidence gained from the aforementioned programs culminated in initiating the USAF's Survivable Flight Control System (SFCS) Program in 1969. One of the major objectives was to establish practicality of the Fly-by-Wire concept for use in military fighter aircraft to achieve improved combat survivability through dispersed redundancy and minimizing single failure points. The program included design, fabrication, qualification, and flight test evaluation of an analog quad-redundant FBW primary flight control system in a YF-4E test aircraft. Initial portion of the SFCS program was completed in mid-1973 following a successful 84 flight test program flown by McDonnell Aircraft, USAF, USMC, and NASA test pilots to evaluate the improved system and aircraft performance.

Major equipment elements of this full authority (motion command) FBW system included:

Quadruplex analog computer and voter units

Adaptive gain and stall warning computer

Master control and display panel

Built-in-test computer (self test)

Centerstick and sidestick controllers

Quadruplex secondary servo actuators

Results from this intensive FBW advanced development effort indicated actual and projected improvements in overall flight control system performance, reliability, aircraft design freedom, safety, survivability, maintainability, and cost of ownership. Additionally, the strong and credible FBW technology base developed paved the way for further aircraft design improvements through exploitation and application of advanced concepts such as Control Configured Vehicles and Multi-Mode Controls with potential system implementation advantages using digital design techniques. One of the follow-on development efforts using the F-4 SFCS test aircraft was the McDonnell Aircraft/USAF Precision Aircraft Control Technology (PACT) Program. The purpose of this effort was to flight test demonstrate the impact of relaxed static stability in conjunction with horizontal close-coupled canards on aircraft maneuvering performance. In March 1974, the Air Force Flight Dynamics Laboratory (AFFDL) contracted with McDonnell Aircraft Company to conduct an advanced digital flight control system definition study. This program included both analytical studies and manned simulations to explore potential payoffs and to establish technical feasibility of a digital Fly-by-Wire (FBW) flight control system, incorporating mission-tailored control modes, advanced multi-purpose displays and decoupled flight path control features. The baseline aircraft configuration used in these studies was the former FBW test aircraft YF-4E SN-12200, modified with differentially controlled horizontal canards. In a related effort under the Fighter Control Configured Vehicles (CCV) Advanced Development Program, AFFDL contracted with General Dynamics in December 1973 to develop and evaluate independent six degree-of-freedom decoupled flight path control techniques for improving fighter aircraft mission effectiveness. Results from these efforts have contributed significantly to the technology base required in the pursuit of advanced flight control concepts, such as decoupled flight path control, mission-tailored control modes and fault tolerant mechanizations.

3. DESIGN CONSIDERATIONS

The design considerations discussed below primarily are based upon Air Force Flight Dynamics Laboratory (AFFDL) experience from numerous FBW and related development activities. Obviously, there are many more detailed design considerations, requirements, and tradeoffs which must be made to satisfactorily implement a FBW system; however, the considerations identified below are those which are most likely to impact the ultimate success of a FBW flight control system design.

Reliability

To a large extent, the level of redundancy required to satisfy a specified mission reliability

requirement (typically on the order of 10^{-7} catastrophic failures per flight hour) is dependent on the type of failure monitoring scheme (in-line and/or cross-channel comparison), component failure probabilities, desired fail-operational capability and overall confidence in achieving the desired reliability. Existing full-authority three-axis analog FBW mechanizations typically employ quadruplex redundancy to achieve the desired mission reliability; however, with digital implementation schemes it is feasible to consider triply redundant systems which can be mechanized to confidently satisfy mission reliability requirements. Reduction in the level of redundancy not only reduces overall system complexity, but also has an appreciable impact on weight and volume savings, along with reduced acquisition and life cycle costs. From a design standpoint and based on state-of-the-art in electronics, redundancy management and implementation schemes can have the largest single impact on overall integrity, reliability and cost of ownership of a FBW system. For this reason great care must be taken during preliminary design and system specification phases to adequately include appropriate tradeoffs required to achieve a truly optimal system. The reliability requirement per channel may not have to be excessively high to meet the overall system failure probability target for a redundant system. However, if the equipment does not have a high level of intrinsic reliability, it will be unacceptable from the maintenance and long term cost of ownership viewpoints. Additionally, it is unlikely to maintain acceptability by the user since it will not engender a high confidence level. Any significant nuisance failures will aggravate the situation. Redundancy should not be allowed to detract from integrity and reliability of the subelements of a system.

In a triplex digital mechanization adequate second fault coverage is the primary concern. Probability of first fault coverage is essentially 1.0 using cross channel comparison monitoring. Coverage in this case is defined as the probability of detecting, isolating and recovering from an internal system failure. Typical second fault coverage and failure rates for critical system elements are shown in Figure 2.

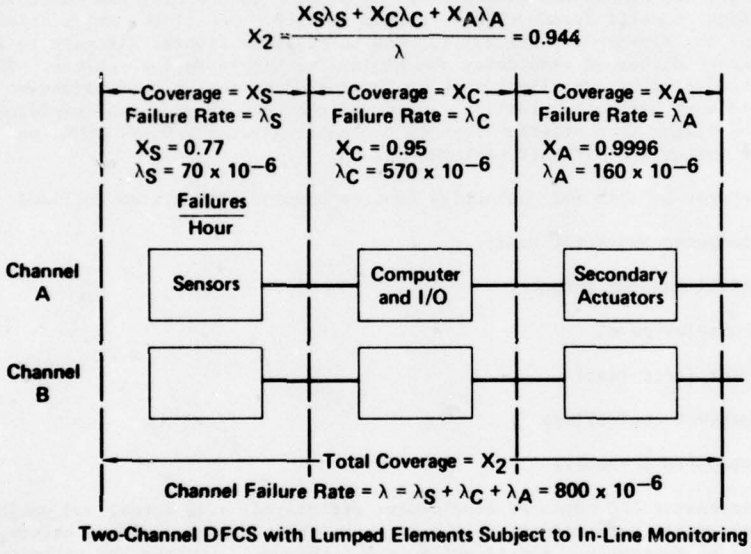

Figure 2 Second Fault Coverage (X_2) in a Triplex System

Figure 3 illustrates the relationship between second fault coverage, single channel failure rate and mission reliability, i.e., probability of loss of control. From these figures it is evident that one can achieve an overall mission reliability of 10^{-7} failures per operating hour for a triplex digital system, which has a second fault coverage of at least .944 and single channel failure rate not exceeding 800 X 10^{-6} failures per hour.

A group of generic quadruplex and triplex systems are compared in Figure 4. Quadruplex system Q-1 has a third fault coverage of 0.95. Achieving this level of coverage requires the same in-line monitoring techniques used in the triplex system. System Q-2, on the other hand, requires only a simple "heads-or-tails" test for third fault coverage. Triplex system T-1 has a second fault coverage of 0.95 which is conservative and readily achievable with known in-line monitoring techniques. It is theoretically possible to achieve a second fault coverage of 0.99 and the probability of loss of control shown by T-2. For any triplex system to have as low a probability of loss of control as quadruplex system Q-2 requires a second fault coverage of 0.9996 (system T-3) which is extremely unlikely. Based on studies and analyses conducted to date, it is considered feasible to achieve satisfactory mission reliability (10^{-7}) with a triplex digital configuration employing a combination of cross channel comparison and in-line monitoring schemes.

Quality Assurance

Quality assurance requirements for the SFCS FBW system were necessarily severe and, in retrospect, appear to have been justified. Use of high-reliability parts, burn-in and system as well as line replaceable unit (LRU) acceptance testing were employed. System testing, in particular the automatic built-in-test, proved invaluable in troubleshooting and weeding out marginal equipment.

The traditional requirements for performance testing under laboratory conditions and design approval testing are still valid, but should be more stringent for FBW systems. For example, burn-in of each deliverable item, including temperature cycling and vibration for 100 hours, was required on the SFCS equipment.

Sufficient failures associated with uninspectable workmanship and detail part infant mortality were uncovered prior to LRU and system acceptance testing to more than justify the costs of this procedure. In the area of aircraft compatibility testing, additional tests to determine susceptibility to induced electromagnetic effects due to lightning threats should be added.

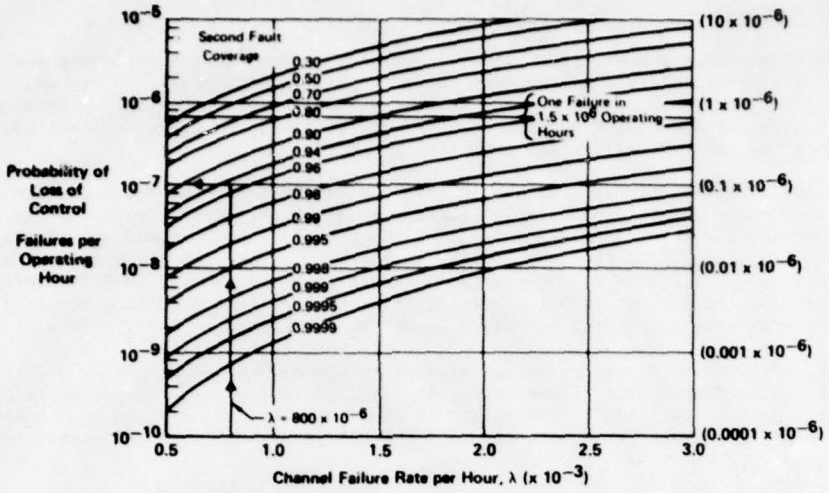

Note: First Fault Coverage = 1.0
Coverage = the Probability of Detecting, Isolating and Recovering from Failures

Figure 3 Triplex System Failure Probabilities

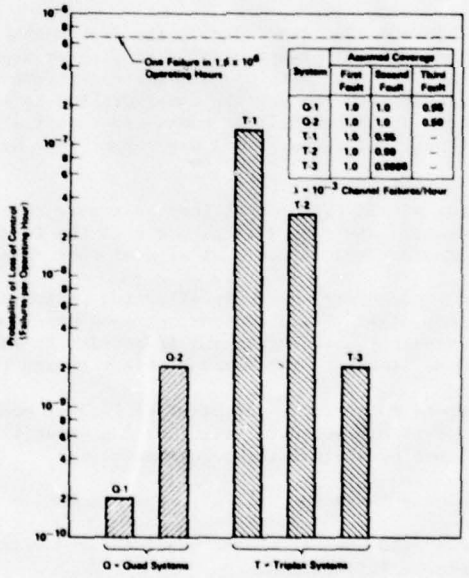

Figure 4 Comparison of Quadruplex and Triplex System Reliabilities

In addition, it is recommended that system testing as well as LRU acceptance testing be required on each set of deliverable hardware. This type of testing, which may require an individual LRU supplier to have a system bench setup simulating all other interfacing hardware, is particularly important in the case of redundant electronic units. It is nearly impossible to design and refine an LRU test specification which assures that the unit will work in the system. This situation exists today in many LRUs that are in production. In order to have tight LRU test tolerances sufficient for redundant operation, one must first produce enough units to establish the statistical nominal values. Yet the specification is frozen far in advance of this information. Consequently, the tolerances are initially left large in order to accept units that will satisfy system requirements. These tolerances are then approved, and after customer acceptance or during field operation it is found that nominal values are in error, changes at that time would most likely result in increased effort and cost. Since some level of system testing is required to validate BIT circuits and component functional operation, it is recommended that this particular phase of testing be used to evaluate actual system tolerance build ups and overall system compatibility of redundant elements.

Other aspects of quality assurance for FBW/flight safety essential systems relate not to specific requirements imposed by the specification, but result from the potential legal responsibility or liability of suppliers of such equipment. It is estimated that the inspection, test and documentation associated with production of flight safety essential equipments is three-to-one more costly than these same activities for non-essential flight controls. These costs should be recognized by the specification originator who should exercise due judgment and avoid the imposition of unnecessary special quality assurance requirements.

Single Point Failures

A single point failure analysis should be conducted during the initial conceptual design phase to identify those single points where a malfunction could cause loss of control. A second, more detailed single point failure analysis should be performed when the actual mechanization has been determined. The second analysis should consist of a detailed end-to-end study of the total FBW flight control installation including the aircraft electrical and hydraulic power supplies.

In general, single point failures should be minimized through redesign or, where this approach is impractical, back-up modes may be considered to provide an alternate control path. It is not always possible or desirable to provide for reversion to a parallel path or back-up mode to circumvent single point mechanical failures. In the case of the SFCS FBW as installed in the F-4, production hardware failures were considered highly improbable since reliability had been established through use in over 4000 aircraft and many flight hours. Where multiple single point failures are possible, such as in a secondary actuator, the probability of failure must be minimized by careful attention to design detail and to the proofing of the design.

One means of avoiding single point failures is to use channel separation. Electronic suppliers have always grouped like functions together, e.g., the amplifiers together, demodulators together, etc. In redundant flight control electronic systems the electronics should be grouped by channel. If it is necessary to incorporate components of more than one channel in one LRU, channel separation should be maintained within the LRU.

It is not always advantageous or possible to design all single point failures out of redundant FBW flight control system elements. For example it would be very difficult to disperse the elements of such items as the stick force transducer, rudder pedal transducer, and the stabilator position transducer. On the other hand, the probability of mechanical failure of these units can be low enough to accept the single point failure possibilities. Single point failure criteria should be based on good engineering judgment and supported by hard data.

System Safety

A system safety program should be initiated during the embryo phase of concept formulation for a FBW system to develop a system with minimum inherent risk. The program should initially be directed at identifying general design criteria consistent with operational requirements and then at establishing specific design requirements compatible with the vehicle configuration to limit the effects of failures, adverse environmental conditions, and the potential for human error during production, test, packaging, transportation, installation, checkout, maintenance, and operation. The design criteria should include provisions to:

Isolate the effects of failures within the control loop to assure channel survival by axis in the event of a failure. An example would be a failure within the lateral axis of a channel which will not fail the longitudinal and directional axis of that channel.

Minimize the possibilities of human error adversely affecting system operation by color coding channels and using either dissimilar connectors or connectors with dissimilar key arrangements, locating high frequency maintenance and inspection items in accessible areas, and protecting all actuators and linkages from Foreign Object Damage (FOD).

Assure positive switching command to activate any required back-up mode by deliberate pilot action and assure that the back-up has adequate trim, damping, stability augmentation, and feel to be acceptable in the most sensitive flight regimes.

Assure that transition between any two modes will not cause excessive transients.

Assure that failure of any mode such that it cannot be disengaged will not limit trim authority to a degree unacceptable for landing.

Provide electrical and hydraulic power that is truly redundant.

Provide adequate safeguards against damage due to improper charging or discharging of batteries and locate the batteries in areas isolated from hydraulic lines, electrical wiring, and other mission essential equipment.

Isolate the distribution of power to components outside of the computers so that a fault in a non-critical component will not adversely affect power supplied to critical components.

Disperse and isolate by channel where practical the rate sensors, accelerometers, and other sensors which are critical to safe flight.

Incorporate Built-In-Test (BIT) to completely check out the system for on-line maintenance trouble-shooting and ground crew preparation of aircraft. Additionally a separate, abbreviated, pilot initiated and completely automatic BIT function should be implemented for pre-flight checkout prior to takeoff. Provisions assuring BIT cannot be engaged during flight should be included.

Consider the impact of environmental factors such as lightning strike, static electricity, and EMI on the final design configuration and the selection of system components.

Back-Up Systems

The general conclusion regarding mechanical backup systems to the FBW primary flight control system is that they generally create more problems and degrade performance beyond their worth. Back-up systems should be avoided if they cannot be implemented essentially independent of the primary system. It would be more cost effective to concentrate on increasing mission reliability by emphasizing the basic integrity of the primary system and its equipment.

For the SFCS FBW system a mechanical backup (MBU) was provided for longitudinal and directional control. The MBU impacted the normal FBW mode by causing some degradation of the pitch (FBW mode) stability properties at low amplitudes. This was attributed to deadband and friction in the mechanical isolation mechanism which was used to shift between FBW mode and MBU mode. Shortly after flight test was initiated, the MBU was removed with a corresponding noticeable improvement in small amplitude stability and reduced limit cycle tendencies. Equally significant was the reduction of safety hazards with the MBU removed. Class III hazards were reduced from 12 to 1; Class IV from 2 to 1. Additional factors against mechanical back-ups is the increase in design and development costs and the added maintenance, all of which detract from the realizable benefits of FBW.

Electrical backups (open loop direct electrical signal transmission link) when considered should not be allowed to degrade the normal mode of operation. For some applications, a mechanical or electrical back-up mode would be useless, as the case where the unstable nature of an aircraft may preclude control with a simple, open loop control system. In such cases a reduced gain option in the normal FBW mode may be desirable, during early flight testing, to provide a means of avoiding structural feedback if it should occur. Unless a clear need for an open loop back-up mode can be established, none should be provided in production systems. As previously stated and emphasized again, a better approach would be to strengthen the integrity of the primary FBW mode at those points where weaknesses tend to justify a back-up.

If a back-up mode is included, a degree of complexity sufficient to allow a reasonable degree of performance should be provided. Regardless of the intent when originally conceived, if a mode of control exists it must be flyable and safe even if its use is planned only in the event of total failure of the primary mode. Although some degradation in flying qualities can be allowed, a Cooper-Harper rating no greater than 7 should be maintained at all flight conditions, and controllability should not be in question. To provide any less means the pilot could inadvertently revert to the back-up mode and suddenly find that he has an aircraft control mode which cannot be used to provide adequate vehicle control.

Primary Controllers

Pilot input to the SFCS FBW flight control system is accomplished by use of a centerstick or sidestick controller for pitch and roll commands and by rudder pedals for yaw commands. The SFCS experience produced no significant changes to yaw command input control; however, the controllers for pitch and roll command had undergone considerable development and evaluation.

The centerstick as mechanized for the SFCS used quad-redundant strain gages (force sensors) to generate the electric command signals, and was found to be acceptable for an R&D aircraft. However, the strain gages presented problems during humidity tests by failing due to separation from the support. A polysulfide coating allowed the strain gages to pass the humidity tests, but their characteristics were still adversely affected. Similarly, characteristic changes occurred during the flight test program which required recalibrations.

Another characteristic about the centerstick was that wrist articulation or "torquing" of the stick in pitch and roll results in a measure of abrupt lateral overcontrol and potentially dangerous pitch commands in the negative "g" direction. Center stick mechanization is shown in Figure 5. The pitch axis characteristic is divergent as the pilot body motion couples to the negative "g". This phenomenon was experienced during the SFCS FBW flight test while performing an abrupt 1/2 aileron, 1g entry rolling maneuver. An unintentional torquing centerstick input generated a nose down pitch command resulting in a negative 4g load factor shown in Figure 6. Subsequent ground and flight evaluations verified the susceptibility of the centerstick grip transducer design to potentially dangerous inputs (bending the grip opposite to the direction of intended stick displacement, as shown in Figure 7). Such designs leading to these conditions should be avoided for future systems. From the standpoint of poor performance, coupled with development problems of adequately matching gages in redundant systems and of achieving satisfactory compliance with other interrelated mechanical elements, strain gages are not generally recommended for future FBW applications as control stick sensors in lieu of a better alternative.

Quad-redundant position transducers (LVDT's) used in the SFCS FBW sidestick controllers were found to be entirely adequate for the R&D system and are recommended for consideration for future production applications. Position transducers are readily available in varying types and with such characteristics as to allow meeting wide range of specification requirements. Whether consideration is for a displacement stick or a fixed stick (essentially no apparent displacement from the pilot's viewpoint), LVDT's are available with high enough resolution to facilitate the design.

Simulation and Compatibility Testing

A series of simulations was used during the development and test of the SFCS FBW to assist in the design, verify equipment performance, train pilots, and correlate flight test data.

When hardware was available, it was integrated into an Iron Bird so that only the airframe equations of motion were modeled on the computer. Static gains, frequency responses, thresholds, and mode switching and failure transients were measured. Pilots then "flew" various missions to verify system performance. During this time, the project test pilots had the opportunity to study system operation with various simulated

failures. Such "survivability missions" helped the pilots to thoroughly understand the fault detection and isolation techniques and to understand system operation during such occurrences. This simulation was used to train pilots for flight, and was rated as a very high fidelity simulation by the pilots. Some system anomalies were detected during this effort and were corrected before flight testing was initiated. Pre-flight checkout procedures and flight test techniques were worked out in advance using the simulator. As a result of this extensive simulation and ground test program, a high level of pilot confidence was established prior to the initiation of the flight test program.

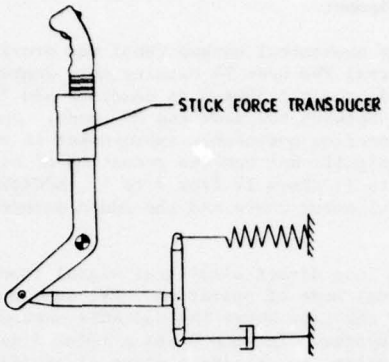

Figure 5 Center Stick Mechanization

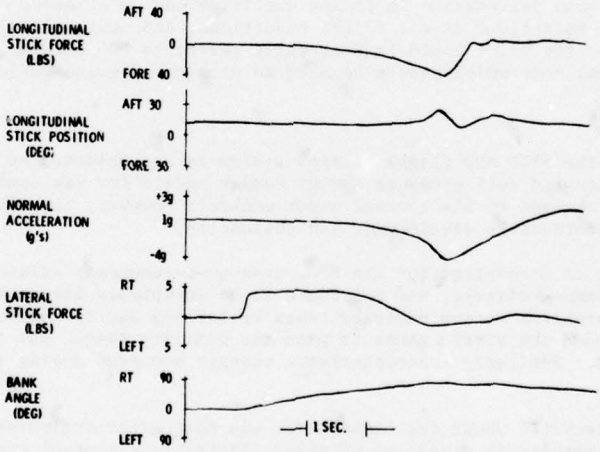

Figure 6 Inadvertent Transient Response

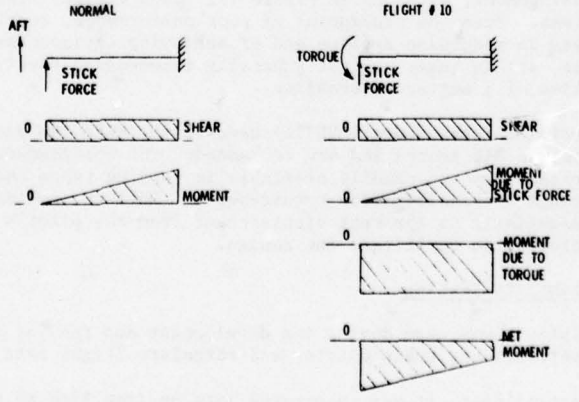

Figure 7 Center Stick Loading

For future FBW system development programs, consideration should be given to a simulation and compatibility test program as extensive as possible but commensurate with the type of system being implemented, test facilities, resources, system sophistication, pilot training need, degree of supplier testing already performed, etc. The objective of component compatibility testing is to establish compatibility between all components of the complete system including: major procured items, associated aircraft equipment, aircraft wiring, aircraft electrical system, and aircraft hydraulic system.

The SFCS component compatibility testing was accomplished on the SFCS Flight Simulator as illustrated in the functional block diagram of Figure 8; however, in the event no such control system mock-up is available, equivalent tests can be conducted on the aircraft. If the system incorporates a minimum of mechanical flight control system components, equivalent iron bird tests can also be conducted using a less sophisticated ground based test fixture. During component compatibility testing, open loop tests, closed loop tests, and verification of all modes and functions should be accomplished.

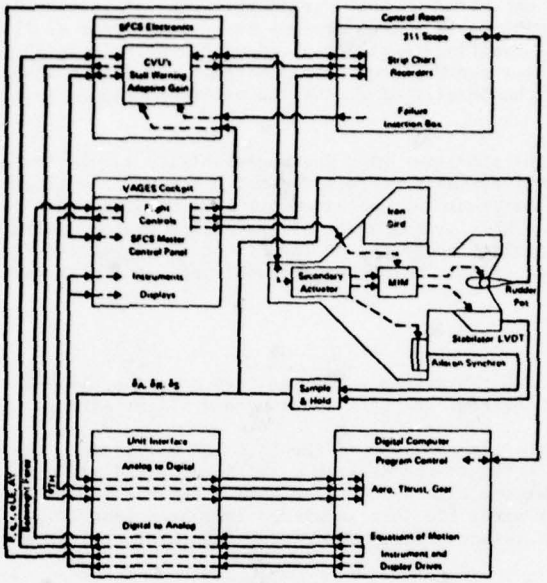

Figure 8 Iron Bird Functional Block Diagram

The objective of the open loop tests is to evaluate overall flight control system open loop performance and compatibility of flight control hardware with associated aircraft systems. The principal characteristics which should be evaluated are:

Open loop response, threshold, phase and gain margin of all actuators while being powered by aircraft systems with actual aircraft electrical and hydraulic line losses and mechanical hysteresis and deadband duplicated.

Proper functioning of all fail safe and fail operational features including measurement of the associated disengage transients.

All mode switching sequences.

Built-In-Test.

In-flight monitor.

The objective of the closed loop tests is to obtain closed loop performance data of the complete flight control system and associated aircraft systems. Tests should be performed in all operating modes and at representative flight conditions. Data obtained should be compared with earlier analytical data and all discrepancies carefully dispositioned by system changes and simulation changes. The closed loop performance data should be retained for later comparison with flight test data.

A test should be conducted to verify that all modes, functions, and switching sequences can be properly accomplished using the actual aircraft controls and to verify that all modes and functions are properly indicated on appropriate aircraft displays.

After completion of a well planned series of Supplier tests and component compatibility tests, the system as installed on the Flight Simulator or aircraft is ready for system performance verification and development using simulator techniques.

Several types of simulations used for development and evaluation of the SFCS FBW included simulations to: augment the analytical studies and design, test new hardware components, provide for closed loop testing of the aircraft installed hardware, and provide for flight test data correlation and discrepancy evaluation. Each of these types of simulations contributed to the overall development effort and is recommended for development of future FBW control systems.

Much of the initial system study and design effort can best be accomplished with small specialized simulations. However, for the total system design evaluation prior to finalized hardware mechanization, a large scale simulation of the complete system, including a man-in-the-loop, is recommended.

Various hardware components which are critical to the overall system performance require special testing that includes applying the proper simulated loads and command signals. This is especially true of actuators where compensation loops may be required to establish the desired bandwidth.

Compatibility simulation is singled out for special recommendation for future systems. The concept of assembling the control equipment as a complete system used to control the simulated aircraft offers many advantages above an all-software simulation. Of particular importance is the capability to assess actual hardware system level performance including failure detection logic, switching transients, etc., to assure proper integration of critical elements.

Pilot familiarization can be accomplished prior to flight testing during the compatibility simulation. Deficiencies which are uncovered through use of this type of testing do not endanger life or testbed and at the same time allow for suitable system changes to be made prior to flight testing. Such testing is cost effective when compared to waiting to find discrepancies during a flight test program. In addition, effects such as multiple failures can be investigated without the danger involved in simulating such multiple failures in flight. This has the benefit of giving the pilot confidence in continued system operation in this environment.

Operation of the flight simulator used for compatibility simulation should continue during the flight test program to serve as a basis for data correlation and discrepancy evaluation. Any differences between the flight test data results and the previously obtained simulation data should be examined using this simulation. The simulation can serve as a highly useful means of evaluating system faults and unexpected phenomena detected during flight test. The parallel operation of the flight simulator and flight test program will lead to a level of system evaluation capability not otherwise achievable and will enable expedient improvements in system design.

Built-In-Test (BIT)

The BIT used in the SFCS FBW system was a positive asset to the program from a number of standpoints including maintenance, system checkout and verification, and flight safety.

a. BIT Implementation - In the case of the SFCS FBW BIT design, the BIT computer was programmed with a single 4 minute program which functioned as both a maintenance aid and a pilot preflight confidence check. Subsequently, it was found that the pilots felt that this check was too long for their use, while Supplier testing, system use, and other after the fact knowledge indicated that it was not long enough to do all that was desired to satisfy its maintenance role. Therefore, the future BIT should be implemented along the following lines.

The use of lengthy test routines is best left to maintenance and preflight operations prior to arrival of the flight crew at the aircraft. Any testing done with the flight crew present should be as short as possible and make maximum use of routine operations normally accomplished by them. The multi-channel mechanization of FBW with IFM lends itself to such implementation since normal manipulation of the controls as accomplished during preflight by the flight crew to check control surface response would identify most of the active and passive type failures of immediate concern. The remaining failures, such as dead gyros, could be detected by a short, i.e., less than 10 seconds, end-to-end BIT test activated by the pilot which torques the gyros and otherwise activates the various system sensors.

For maintenance purposes two BIT programs, one with a selectable sub-routine, would be applicable. The first of these would be a maintenance pre-flight BIT directed to maximum detection of faults without regard to LRU fault isolation, preferably being run on internal APU or battery provided power to avoid engine operation. The second BIT program would be directed to LRU fault isolation. A sub-routine of this program would be activated whenever BIT indications suggest a fault exists in the hydro-mechanical portions of the flight control system. Operation of this sub-routine would require the application of either internal or external hydraulic power and, as required, full electrical power.

b. BIT Capability - Historically, the capability of BIT has been specified as a 0.95 probability of fault detection and fault isolation. To satisfy the flight safety and maintenance requirements of an electronic flight control system, the capability of the equipment to detect and isolate faults in the FBW system must be more adequately defined. It has been found that the specification of BIT capabilities involves more than simply stating quantitative probability of fault detection and isolation numbers. Ideally, these numbers should be adequately modified by suitably defining statements regarding types of faults to be detected and isolated, and by appropriate design approval and acceptance test provisions calling out specific confidence levels to be verified. Although analytically the SFCS system met the specification, it in fact fell short in fault detection and fault isolation when tested by insertion of actual faults using a cumulative binomial test plan. It is interesting to note that experience with this system's BIT capability has shown it to be more than satisfactory in operational use. In fact, such confidence is placed in this system's BIT capability that it is used as the final test of proper system and LRU performance, even after extensive and detailed manual acceptance testing is completed with satisfactory results.

While specification of high, i.e., greater than 95%, probabilities and testing confidence levels for failure detection and isolation is obviously desirable, the specification of such probabilities and confidence levels must be carefully weighed against their impact on the other areas of design. Since such probabilities and confidence levels are an exponential function, a change by even a percentage point in these areas will result in substantial changes in the amount of BIT circuitry and/or programming required. Some improvement in the fault detection and isolation capabilities of the SFCS FBW system referred to above could have been accomplished through optimizing the BIT program. This, at most, would have resulted in improvements in fault detection and isolation probabilities to perhaps 95% and 93% respectively. Attainment of 95% BIT capability for LRU fault isolation, as originally specified for the R&D SFCS, may be difficult to

achieve in light of the amount of circuitry, number of monitors and break-in points, and computer memory capacity required. Furthermore, even with adequate modifying ground rules, a 98% BIT fault detection may become an extremely difficult requirement to meet in light of recent SFCS experience.

c. Plug-In Maintenance Computer - It has been suggested that a BIT computer such as that found in the SFCS could be packaged as ground test equipment and used in a plug-in fashion to service several aircraft rather than being dedicated to a single aircraft. Although this appears to be an attractive approach, there are some offsetting factors that need to be considered. For example, enhanced maintenance flexibility during aircraft dispersal to remote bare bases for tactical deployments would emphasize the need for self-contained BIT capability. Additionally, since the BIT computer piece part count is relatively small, the value of a separate plug-in test computer may be questionable. It might be pointed out that the SFCS BIT system dedicated circuitry comprises only 15.5% of the SFCS electronics total piece part count and 11.4% of its failure rate. In addition, only 41% of the piece parts and 39% of the failure rate attributable to BIT are in the BIT computer, which is the only part of the SFCS BIT system that might be considered removable and suitable for use as a piece of ground test equipment.

d. Verification Testing - Due to the criticality of the BIT system to flight safety, it is recommended that the BIT system capabilities of future FBW systems be verified by formal design approval testing. Although such testing has not been common in the past, it appears that it will be essential in future systems having the flight safety impact of a FBW flight control system. Experience gained during the SFCS program indicates that the benefits to be gained in system confidence and maintainability are more than adequate to offset the costs of such testing.

In-Flight Monitor (IFM)

IFM provides the necessary fault detection, isolation and recovery logic to satisfy overall system reliability and fail-operational requirements. Signal selection algorithms and fault recovery strategies are key elements in the design of a fault tolerant flight control system. Achieving .95 second fault coverage with a triplex configuration requires application of both cross-channel monitoring and in-line monitoring techniques. Other more advanced concepts which could be considered are analytical redundancy and reconfiguration.

Functional implementation must address the following fundamental considerations:

Cross Channel Monitoring

- Number of Voting Planes
  - Sensor and Controller Inputs to Computer
  - Intermediate Computed Parameter
  - Computer Outputs to Actuators
- Computer Monitoring of Actuators
  - ΔP Comparison
- Redundant Data Comparison and Voting
  - Signal Selection
  - Averaging
- Computer Synchronization
  - Bit by Bit
  - Frame
  - Comparison of Intermediate Computational Results
  - Asynchronous
- Computer Interchange of Redundant Data

In-Line Monitoring

- Computer Self-Test
- Computer Test of Sensors and Controllers
  - Data Reasonableness
  - Torquers
  - Dither
- Computer Test of Actuators
  - Actuator Models
- Computer Test of I/O and Multiplex
  - Parity
  - Wraparound
  - Rebound
- Computer and Hardware Test of Power Supplies
- Data Reasonableness

Software design, programming standards, verification and control procedures must be sufficient to assure that no catastrophic single failure points exist. A case in point is the addition of multiple voting planes. Inclusion of voting planes is one of the ways by which a redundant flight control system is made fault tolerant. Theoretically, the more voting planes, the more fault tolerant the system. When the system is analog, the addition of voting planes, over and above what are needed to achieve the required system reliability, are costly due to the signal buffering required to prevent fault propagation between channels and the additional dedicated analog voters. With a digital computer, the buffering and cross channel date transfer are readily facilitated, and the same software voting algorithm can be used to vote on many different signals. Consequently, there is a temptation to consider using many voting planes to increase fault tolerance and improve system reliability. On the other hand, interconnections between redundant channels required to implement a large number of voting planes tends to increase the potential for common mode failures. For this reason, it is desirable that voting planes be limited to planes B, C, and E as shown in Figure 9. In this manner data cross-strapping is confined to a single digital data exchange bus, which can be properly buffered and monitored. In general, interconnections between redundant channels should be minimized to limit the potential for propagating system failures. Monitor thresholds at these voting planes must be sufficiently tight to limit excessive switching transients but yet loose enough to avoid frequent nuisance disconnects.

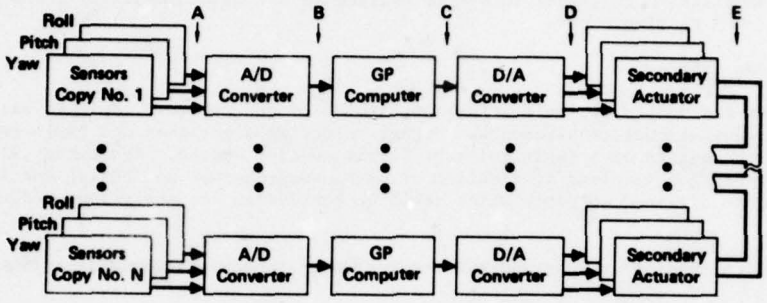

Figure 9 Potential Voting Plane Locations

One of the major advantages of a digital architecture is the ability to accommodate extensive self-test features required for implementing reliable in-line monitoring schemes. After one failure in a triplex system and two failures in a quadruplex system, in-line monitoring must be used to resolve any channel differences, if the flight control system is to continue to operate. When in-line monitoring is used, the computer must first test itself; then it is in a condition to check other system elements. Self-testing of digital computers involves a mix of hardware and software. Certain basic portions of the computer must be operable before any self-testing can be conducted, e.g., power supplies and clocks. Failure of these basic portions must be detected by hardware. With these basic portions of the computer operating, self-testing of the computer can begin. The design of the self-test program is based on the inverted pyramid test philosophy. That is, the program first tests the instructions that require a minimum of logic for their execution, and the memory locations that contain the self-test program. These verified instructions and memory locations are then used to test instructions and memory on the next higher level. This process is continued until all of the instructions, memory and I/O have been verified.

Aeroservoelastic Interaction Analyses and Tests

Experience with high gain closed-loop electronic flight control systems over the past several years has emphasized the need to define and understand the behavior and influence of the primary flight control system as it relates to dynamic interactions associated with aeroelastic phenomena. To accurately and confidently predict these interactions, overall system stability analyses must include adequate consideration of flight control system characteristics (particularly filter dynamics), structural modes and aerodynamic loads including non-linearities, unsteady flow effects, vehicle configurations (gross weight, gain level, store loadings, etc.) and flight conditions.

Historically there has been only a minimal interface between the flight control designer and the structural dynamist. As the trend continues towards closed-loop active controls, there is a very definite need for these disciplines to jointly iterate through the design analysis and testing phases to assure an efficient and successful approach for identifying and eliminating aeroelastic dynamic instabilities.

With proper consideration of all pertinent factors, modern structural dynamics and stability analysis methods are more capable of predicting the existence and nature of these highly complex interactions including both rigid body and aeroelastic coupling. However, ground testing including ground vibration (preferably with the flight control system operative), limit cycle, structural resonance and frequency response tests are necessary to provide sufficient correlation data for verifying and establishing confidence in the analytical model. It should be pointed out that demonstration of substantial gain margins (6 db or more) during ground tests does not necessarily ensure that the system is free from in-flight instabilities involving elastic mode coupling at operational gain levels. For this reason comprehensive system stability analyses complemented by appropriate ground testing offers a more complete pre-flight assessment of aeroservoelastic stability, as opposed to total reliance on ground based test results.

Actuator Dynamic Analysis

Four basic analyses are considered particularly essential to any criteria for redundant actuators. These include stability, frequency response, tolerance, and failure transient analyses. In addition, it is also considered essential that an adequate mathematical model of the actuators be formulated to evaluate the effect of actuator characteristics on the flight control system stability and dynamic performance.

a. Stability - Stability analyses of the SFCS FBW System indicated a more than adequate stability margin for the electrohydraulic secondary actuator, and this conclusion was supported by test results. This confirms past experience which has shown that small electrohydraulic servos with light inertia loads are usually very stable. An electromechanical secondary actuator, by contrast, did require stability compensation when the gains were increased sufficiently to meet frequency response requirements. The results obtained from both analysis and tests indicate that a stability analysis of redundant electromechanical actuators is essential in FBW control system design.

b. Frequency Response - Frequency response analysis, confirmed by tests, showed that frequency response characteristics generally met requirements. It was also evident that freeplay had a very detrimental effect on frequency response characteristics and considerable effort was expended in an effort to minimize the presence of freeplay. The freeplay which was most detrimental was that in the mechanical control linkage between the secondary actuator and the power control cylinder. It is therefore recommended that actuator frequency response criteria include provisions for both small amplitude and large amplitude frequency response requirements. The small amplitude frequency response will show the effects of deadband, freeplay, and friction. The large amplitude frequency response will show the effects of velocity and acceleration saturation (limiting).

c. Tolerance Analysis - A statistical tolerance analysis was performed for the redundant electrohydraulic secondary actuator in order to assess the probability of nuisance disconnect. The results indicated that the anticipated equipment tolerances were adequate and that nuisance disconnects would be infrequent. Laboratory and flight test experience has demonstrated that very few disconnects have occurred which were not traceable to either actual failures or to equipment which was significantly out of tolerance.

It is therefore recommended that a statistical tolerance analysis, assuming normal distribution, be performed for similar applications. This statistical analysis would provide significant insight relative to the probability of nuisance disconnects and would provide a more realistic estimate of tolerance effects. Such statistical analysis would help avoid stringent and unwarranted restrictions on equipment tolerances which other analytical estimates would tend to support.

d. Failure Transients - Both analyses and tests demonstrated the capability of the electrohydraulic secondary actuators to meet failure transient requirements. Since the magnitude of the transients was determined by the force fight characteristics of the secondary actuator, it was not necessary to employ rapid cutoff of failed channels to control the transients. By delaying failed channel cutoff for approximately 0.5 seconds after failure detection, the influence of actuator dynamics on failure transients is minimized. Analysis and preliminary tests of a redundant electromechanical secondary actuator employing the velocity sum concept indicated failure transient capabilities comparable to the force fight concept.

Should future applications require more stringent failure transient capabilities greater than those required for SFCS actuators, two considerations are recommended. These are an increase in gain and the use of equalization. An increase in gain generally reduces the magnitude of the transients and would be of particular consequence on third failure since aircraft sensor feedback tends to minimize the effect of first and second failures. In considering a gain increase, the effect on nuisance disconnect must be evaluated since this places one of the limitations on gain. The use of equalization on the signal selection device of the SFCS minimized the electrical transients resulting from electronic failures and tolerances. Some benefit may accrue from the use of equalization on redundant actuators.

Control Laws

The impact of FBW on overall mission performance and flying qualities is largely dependent on the control laws implemented in the basic design. The aircraft designer must translate specific mission requirements into meaningful control system and flying qualities requirements in order to establish appropriate control laws/modes. One of the primary advantages of a FBW mechanization is the ability to more easily tailor aircraft response to meet a wide range of flying qualities/mission requirements. During the past several years, numerous programs based on paper analysis, simulation and flight test assessments have addressed the development of control laws applicable to specific classes of vehicle mission requirements. Control law synthesis is an iterative process with considerable reliance on past experience, trial and error analysis and piloted simulations. Major emphasis is typically centered around the definition and assessment of feedback parameters/blending, gain scheduling, air data computations, command signal shaping, compensation filter dynamics and modes of operation. Final control law mechanization is eventually determined by overall control system performance in terms of stability, frequency response, etc., and ultimately by the impact on mission and flying qualities requirements, i.e., frequency, damping, pilot opinion, tracking, and numerous other quantitative and subjective closed loop system performance metrics. It should be pointed out that many of the classical flying qualities parameters are not completely applicable to FBW systems, since the forced response nature of closed loop systems tends to mask free airframe dynamics. Incorporation of CCV features in the context of a task-tailored multimode flight control system, adds a new dimension in the control law development process by emphasizing the need for more extensive consideration of the pilot/vehicle interface, in terms of controller harmonization, display formats, vehicle response dynamics, and overall system logic functions. For this reason great care must be exercised when establishing performance criteria, in order to assure proper evaluation of closed loop flying qualities. Pilot involvement and adequate engineering consideration of the control laws during the early phases of a major development program can alleviate many of the task/flying qualities oriented problems typically encountered during flight test. This is particularly important in light of the present trend towards more sophisticated control laws brought about by increasing demands on the flight control system to expand overall mission capabilities.

Electromagnetic Compatibility (EMC) and Lightning Protection

The integration of a fly-by-wire flight control system into an advanced aircraft is influenced by several EMC considerations such as: (a) degrading effects in the flight control system from interference created by other electronic systems onboard the aircraft, (b) degrading effects in the flight control system from interference created by an external environment, and (c) degrading effects in other onboard electronic systems from interference created by the flight control system.

EMC is generally achieved by: (a) minimizing extraneous noise generation and susceptibility to unwanted signals, (b) electrically bonding the fly-by-wire equipments, (c) properly grounding circuits, (d) using electrical shielding and wire twisting techniques, and (e) separately routing incompatible signals.

Statistics on lightning strikes on various aircraft types indicate substantial differences between the number of lightning strikes reported per flight hour for various types of aircraft. These statistics indicate that some aircraft configurations are inherently less vulnerable to lightning strikes and that some aircraft configurations are less prone to initiate the strike.

During the period 1965-1974, more than 700 lightning-related incidents to USAF aircraft were documented. USAF experience indicates 5 lightning strikes for 100,000 flight hours whereas U.S. commerical airline experience shows approximately 33 strikes per 100,000 flight hours. Although there is an appreciable difference between military and commercial experience, even the lowest incident rate warrants attention to the effects of lightning on continued and safe operation of an aircraft with a FBW system (a flight-essential function). Earlier vacuum tube electronics were relatively immune to lightning induced transients or surges in aircraft electrical circuits. However, during the past several years the trend has been toward discrete solid-state and then to integrated circuit electronics. As this trend continues, application of microcircuitry including large scale integrated circuits, microprocessors, etc., appears to be the next step.

The newer generations of modern, solid-state microcircuitry are more susceptible to upset or damage from induced current effects and may require additional protective measures. These effects are of particular importance where performance, safety, and reliable operation are driving considerations. An additional contributing factor is the projected increased use of composite materials in aircraft structures. These materials provide considerably less electromagnetic shielding as compared to conventional materials (all metal airplanes) and hence sensitive electronic flight controls may be exposed to higher levels of induced electromagnetic energy.

Limited experience to date suggests that electric/electronic flight control systems for all metal aircraft can be designed, installed, and adequately protected against electrical hazards. There is little evidence indicating difficulty with lightning effects on control systems of operational aircraft, such as F-111, having high authority control augmentation and partial FBW. In a continuing effort to assess the effects of lightning on FBW systems, low level lightning tests using the transient analyzer technique were conducted on the SFCS FBW F-4. Test set-up is shown in Figure 10. The results indicate that the FBW system, as designed and installed in that aircraft, does not exhibit a level of vulnerability to lightning that would result in catastrophic loss of control. AFFDL sponsored programs are continuing to assess the potential adverse electromagnetic effects and development of appropriate protective methods for aircraft employing both advanced composite structural materials and electronic flight controls.

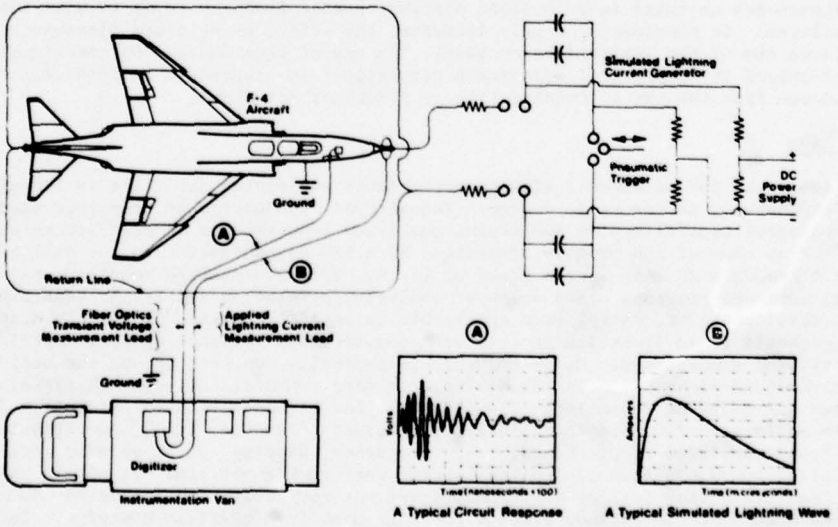

Figure 10 Simulated Lightning Induced Voltage Test

4. SUMMARY

The advent of FBW flight control systems, as validated by developments over the past several years, has established a viable technology base from which the designer can confidently explore and apply innovative flight control concepts to achieve improved overall performance capabilities and reduced cost of ownership.

Continued development and application of advanced concepts, such as CCV, Integrated Fire/Flight Control and task-tailored control modes further emphasizes the need for highly reliable/fault-tolerant FBW flight control system mechanizations. Adequate consideration of the critical design factors summarized in this paper can contribute to the overall success in the design and implementation of a reliable FBW flight control system.

REFERENCES

1. V.C. Sethre, R.E. Schenbeck, R.L. Kerber, Design Techniques and Laboratory Development of an Electrical Primary Flight Control System, ASD/TDR-62-46, Flight Control Laboratory, Aeronautical Systems Division, Wright-Patterson AFB, Ohio, April 1962.

2. J.J. Fleck, D. Hogan, and E.A. Shemeta, Demonstration of the Application of Majority Logic for Increased Reliability of Automatic Flight Control Systems, ASD-TDR-63-275, Air Force Flight Dynamics Laboratory, Wright-Patterson AFB, Ohio, July 1963.

3. F.L. Miller and J.E. Emfinger, Fly-by-Wire Techniques, AFFDL-TR-67-53, Air Force Flight Dynamics Laboratory, Wright-Patterson AFB, Ohio, July 1967.

4. L.V. Nardi, G.R. Toomey, and D. Koziol, Phase I, AMSA System Task S-14C, Fly-by-Wire Study, Final Report to USAF under Contract No. AF33(613)-15343, 1968.

5. D.S. Hooker, R.L. Kisslinger, G.R. Smith, and M.S. Smyth, Survivable Flight Control System Final Report, AFFDL-TR-73-105, Air Force Flight Dynamics Laboratory, Wright-Patterson AFB, Ohio, December 1973.

6. F.M. Krachmalnick, et al, Survivable Flight Control System; Active Control Development, Flight Test, and Application, AGARD Conference Proceedings No. 157 on Impact of Active Control Technology on Airplane Design, October 1974.

7. J. Flannigan and J. Emfinger, Production Design Requirements for Fly-by-Wire Systems, AGARD Conference Proceedings No. 157 on Impact of Active Control Technology on Airplane Design, October 1974.

8. R.C. Ettinger, R.L. Majoros and C.W. Powell, Air Force Evaluation of the Fly-by-Wire Portion of the Survivable Flight Control System ADP, Final Report FTC-TR-73-32, Air Force Flight Test Center, Edwards AFB, California, August 1973.

9. D.S. Hooker, et al, Definition Study for an Advanced Fighter Digital Flight Control System, AFFDL TE-75-59, Air Force Flight Dynamics Laboratory, Wright-Patterson AFB, Ohio, June 1975.

10. J.K. Ramage and F.R. Swortzel, Design Considerations for Implementing Integrated Mission-Tailored Flight Control Modes, AGARD Conference on Impact of Integrated Guidance and Control Technology on Weapon Systems Design, May 1978.

OPEN/CLOSED LOOP IDENTIFICATION OF STABILITY AND CONTROL CHARACTERISTICS OF COMBAT AIRCRAFT

by

R. Koehler
M. Marchand

Institut für Flugmechanik

Deutsche Forschungs- und Versuchsanstalt
für Luft- und Raumfahrt e.V. (DFVLR)
3300 Braunschweig Flughafen, West Germany

SUMMARY

In this paper some general aspects of assessing flying qualities of augmented aircraft using system identification methods are discussed. The aircraft under test is equipped with a stability augmentation system which has a complex dynamic behavior. The dynamics influenced the flying qualities as well as the applicability of investigation methods. Therefore, the influence and recognizability of the stability augmentation system dynamics on handling quality evaluations and system identifications were inquired and pilot-in-the-loop investigations were made using the system identification results.

INTRODUCTION

To asses flying qualities of a modern combat aircraft flight test data were evaluated applying two different techniques (figure 1):

- The characteristic motions were evaluated to determine the dynamic characteristics - eigenvalues and eigenvectors - of the system. The results were compared with flying qualities requirements of MIL-F-8785.

- A system identification was done based on the flight test data. From the resulting mathematical model, the dynamic response including eigenvalues and eigenvectors was computed and then compared with the MIL-requirements.
  In addition an assessment concerning aspects of system theory was done.

The dynamic behavior of an aircraft can be assessed using MIL-F-8785 requirements when the aircraft is unaugmented or when the dynamic behavior is similar to an unaugmented aircraft. This condition is not met, when the augmentation system dynamics influence the dynamic response of the aircraft. Quantitative assessment based on the MIL specification may give conflicting results when compared to pilot rating evaluations. Therefore, the question, whether it is possible to recognize the dynamics of the control system during evaluation is of general interest. First, some experiences from evaluation of characteristic motions shall be discussed.

EVALUATION OF CHARACTERISTIC MOTION

For the determination of eigenvalues and eigenvectors from characteristic motions a computer program was developed. Using an iterative process, this program computes eigenvalues using a gradient method and eigenvectors using regression analysis.

In the following some examples of evaluation results will be given. Figure 2 shows time histories of the lateral directional characteristic motion. Flight test data are plotted using solid lines. The crosses represent the best fit possible using a second respectively fourth order model. For this dutch roll example, yaw rate and sideslip angle are matched fairly well, whereas the fit for roll rate is unsatisfactory using a second order model. A satisfactory fit was obtained using a fourth order model consisting of two conjugate complex pole pairs. One of these pole pairs represents the dutch roll motion the other pair represents the control system dynamics. Another data run is shown in figure 3. As can be seen, the unsatisfactory roll rate fit using a second order model is again improved when a fourth order model is used. In this case also better fits for yaw rate and angle of sideslips are obtained with the fourth order model.

In the two examples shown in figure 2 and 3, the SAS dynamics could be detected during the evaluation of characteristic motions. The flight test engineer is warned: The stability augmentation system has significant dynamic behavior. The response of the augmented aircraft does not conform to the basic assumptions of the MIL Spec 8785 and these criteria cannot be readily applied.

Similarly the SAS for the longitudinal axis also had a dynamic behavior which significantly influenced handling qualities. However, in all cases, the longitudinal characteristic motions evaluated could be satisfactorily modeled using a second order short period model (Examples are shown in figure 4). Thus, the augmentation system dynamics could not be detected during characteristic motion evaluations, and the flight test engineer may apply the handling criteria without being warned. But, the quantitative assessment based on the MIL-Specification would give conflicting results when compared to pilot rating evaluations.

CLOSED LOOP SYSTEM IDENTIFICATION

To overcome the deficiencies of handling qualities investigations based on characteristic motion evaluations, system identification methods were applied. A modified maximum likelihood identification method which can be started without knowledge of a priori values for the unknown parameters was used. The flight test data was obtained using various pilot applied control inputs (mainly steps and doublets). However, special input signals designed for system identification were not employed. During these manoeuvers the SAS was engaged. Signals were measured at points A, B and C shown in the sketch of figure 5.

The flight test data measured at the points A and B were used to identify the SAS. The outputs from the identification were the SAS parameters. Elevator surface deflection and aircraft response, points B and C, were used to determine the aerodynamic derivatives of the basic aircraft. The results of the two identifications can be used to calculate the behavior of the closed loop model. In addition, a system identification of the augmented aircraft from point A to C was done using an unaugmented aircraft model structure. This identification yields so called equivalent derivatives.

The results of some representative flight test data time histories and corresponding system identification curve fittings are shown on figure 6. The curve fittings based on the identification of the aerodynamic derivatives on the left of figure 6 are satisfactory. On the right hand side, equivalent derivative curve fittings are shown. The pitch rate fit is unsatisfactory, while the vertical acceleration fit is acceptable but not good. The deficiencies are caused by the inadequate model structure which did not include the augmentation system dynamics.

As a check, two models were used for identification of the control system. On the left of figure 7 results using the complete dynamic model are shown. On the right are results using a simplified model which neglected augmentation system dynamics. The poorer fit on the right again shows the influence of the augmentation system dynamics.

Another time sequence is shown in figure 8. Again as shown on the left, identification of aerodynamic derivatives yielded satisfactory fits. The model structure is equal to the system structure. As shown on the right, identification of equivalent derivatives also yielded satisfactory fits. Although the model structure is not equal to the system structure, the fits are still good. The flight test engineer may assume that the influence of the stability augmentation system dynamics is small and can be neglected for handling qualities assessment.

In figure 9 the corresponding identification results for the stability augmentation system are shown. On the left, the identified model included the SAS dynamics. On the right, the identified model did not include SAS dynamics. It is clear that the SAS dynamics should not be neglected.

For the cases where a good fit of aircraft response was possible using equivalent derivatives, the augmentation system dynamics were approximated by modifying the derivatives. It turned out the modification of the derivatives was dependent on the particular input signal used. Therefore, the identified equivalent derivatives could not be used to predict aircraft responses for other arbitrary input signals.

In figure 10 poles of the short-period motion for both the open and closed loop cases are shown. Three different regions can be distinguished. The poles of the basic aircraft are at relatively low frequencies. The poles of the augmented aircraft which were calculated from both the identified SAS and basic aircraft models, are at relatively high frequencies. In between are the poles of the aircraft modeled with equivalent derivatives. These poles should be in the same region as the poles for the augmented aircraft. Thus, aircraft models using equivalent derivatives can lead to erroneous conclusions during handling qualities investigations. All aircraft configurations investigated showed similar results.

PILOT-IN-THE-LOOP INVESTIGATION

In the last part of the presentation, pilot-in-the-loop investigations using identification results will be discussed (figure 11). The complete model of the dynamic stability augmentation system and the basic aircraft is used to describe the dynamic behavior of the augmented aircraft. This control loop is supplemented by a pilot model. The pilot's activities during a specific task are assumed to be similar to the output of a constant feedback system which uses normal acceleration as input and longitudinal stick deflection as output. In combat aircraft with tandem seat arrangements normal acceleration is different for the two pilot locations (figure 12). As frequency is increased more and more above the short period frequency, the motions can be approximated more and more by a rotation around a fixed axis. The rotation is a function of both the normal acceleration and the pitch acceleration, both caused by elevator deflection.

Root locus curves of the pilot/augmented aircraft loop are shown on figure 13. With increasing pilot gain the damping decreases. Compared to the front seat pilot loop, the back seat pilot loop has less damping and is even unstable for high gains. As shown in figure 14, these curves depend on the augmentation system model used in the identification. Different augmentation system models result in different root locus curves. As example, curves for the two pilot positions are shown with and without time lag in the control system model.

- With time lag in the control system the pilot-in-the-loop system is poorly damped, and the handling qualities will be noted as bad.

- Without time lag in the control system model, the pilot-in-the-loop system is well damped and the handling qualities will be noted as good.

Therefore, the exact modelling of augmentation system dynamics and the identification of control system time lag is necessary for the evaluation of pilot-in-the-loop-handling qualities. In doing so, a good correlation of evaluated handling qualities characteristics and pilot ratings was achieved.

CONCLUDING REMARKS

Five subjects of handling qualities investigation methods were discussed.

- Characteristic motion evaluations:
  The influence of pole pairs produced by the augmentation system dynamics could be detected in some instances. But, in investigations using another augmentation system, these influences could not be detected.

- Estimation of equivalent derivatives:
  To evaluate flight test data for an augmented aircraft, an unaugmented aircraft model structure was used. Time history matching ranged from good to unsatisfactory. In all cases the augmentation system dynamics significantly influenced the time histories.

- System identification:
  Augmented aircraft flight test was used to identify both the basic aircraft and the dynamic stability augmentation system. Time history matching was satisfactory in all cases.

- Open/closed loop eigenvalues:
  There were significant differences between the eigenvalues computed using the equivalent derivatives and the eigenvalues calculated using the augmented aircraft model.

- Pilot-in-the-loop investigations based on identification results for basic aircraft and augmentation system dynamics were done.

To conclude, when identifying an aircraft with a dynamic stability augmentation system, the following points are important (figure 15):

- Evaluation of flight test data may yield satisfactory curve fits but give unsatisfactory results for closed loop handling qualities investigations. In particular the flight test engineer must be aware of the shortcomings of characteristic motion evaluations, equivalent derivative estimations, and investigations based on equivalent derivatives. Using these methods, augmentation system dynamics and its influence cannot be detected in all cases.

- Satisfactory fits and also satisfactory results can be obtained using expanded models and methods. System identification of the basic aircraft and the dynamic stability augmentation system yields a correct mathematical model. Pilot-in-the-loop investigations based on the identification results gave a good insight into the relationship of handling qualities and dynamic characteristics of the aircraft. Separate identification of basic aircraft and SAS instead of using equivalent derivatives showed to be absolutely necessary and lead to good correlation of flight test data evaluations and pilot ratings.

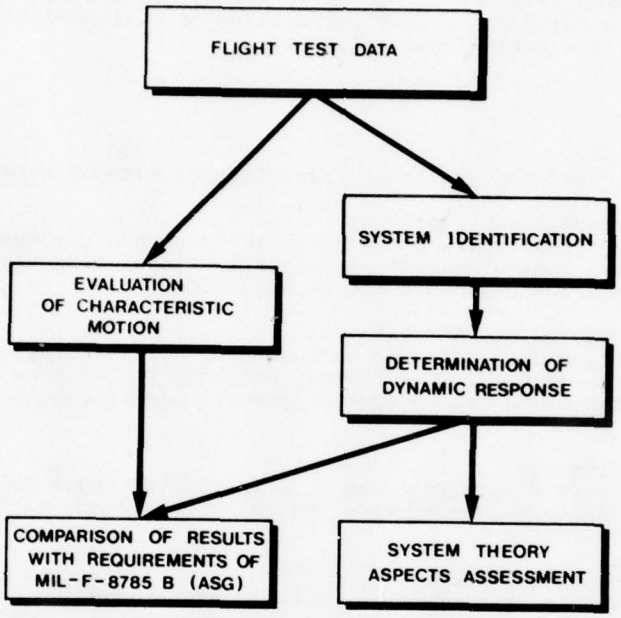

Fig. 1 Evaluation Methods

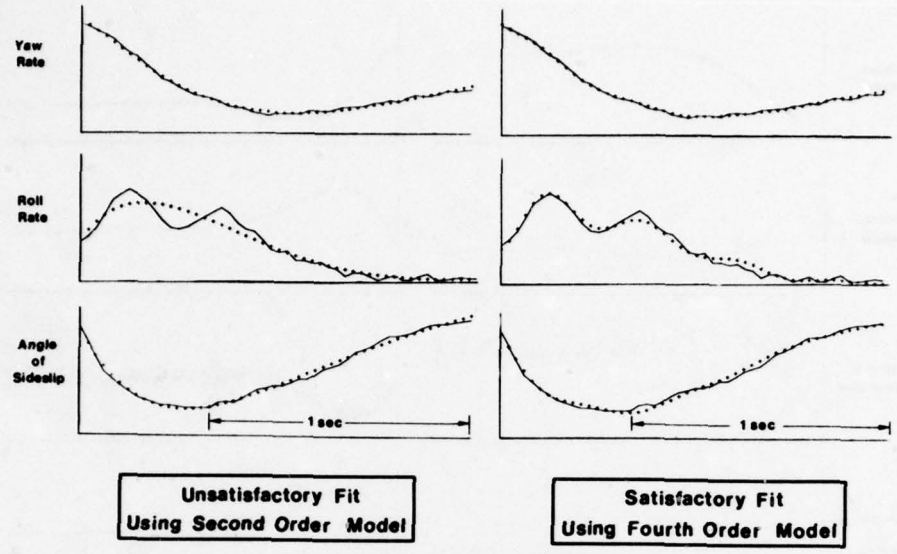

Fig. 2 Comparison of Fits Using Second and Fourth Order Models
——— flight test data
+ + + model output

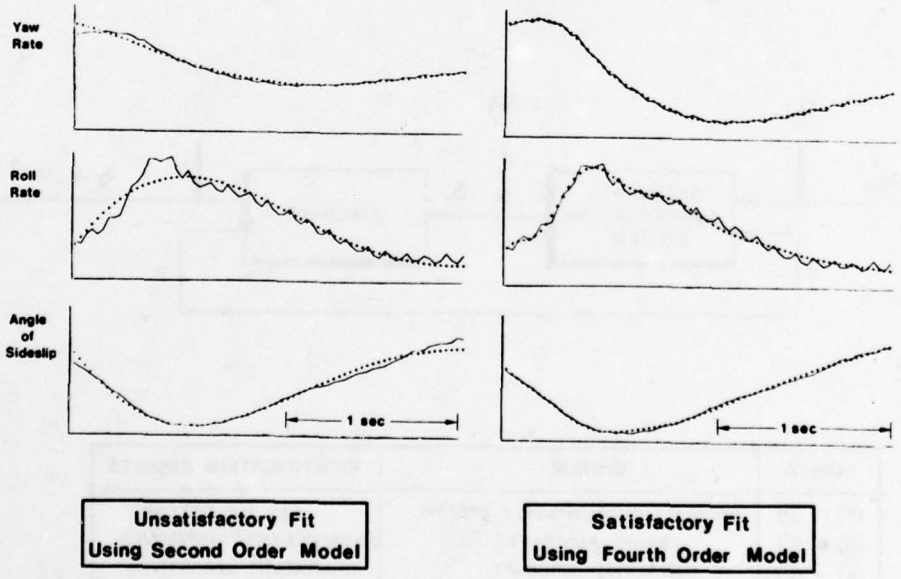

Fig. 3 Improvement of Fits in Three Output Signals Using a Fourth Order Model
——— flight test data
+ + + model output

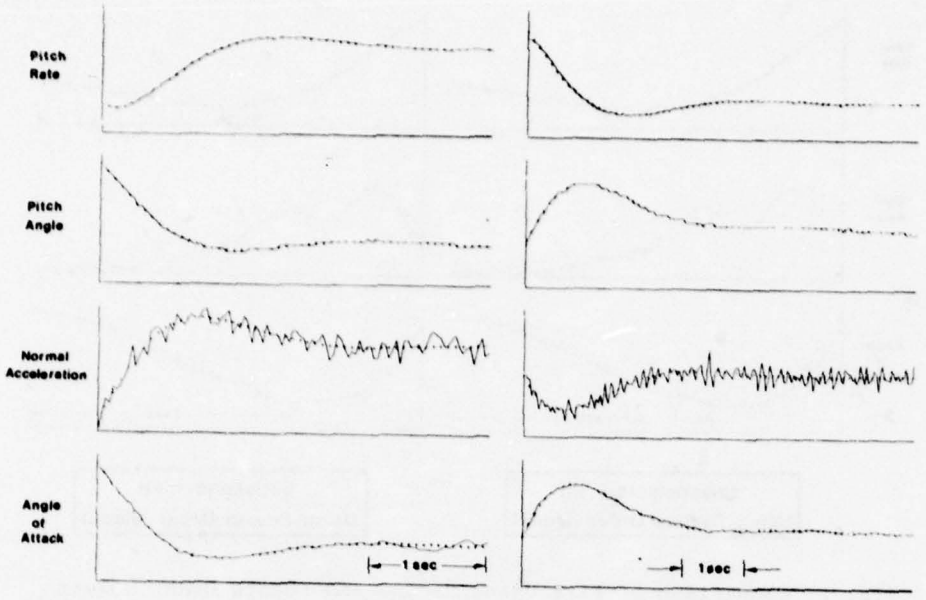

Fig. 4 Examples of Satisfactory Fit Using Second Order Model
——— flight test data
+ + + model output

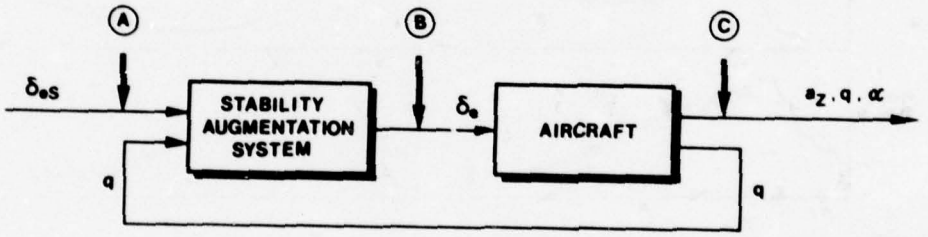

POINTS	SYSTEM	IDENTIFICATION RESULTS
(A) – (B)	STABILITY AUGMENTATION SYSTEM	SAS PARAMETERS
(B) – (C)	BASIC AIRCRAFT	AERODYNAMIC DERIVATIVES
(A) – (C)	AUGMENTED AIRCRAFT	EQUIVALENT DERIVATIVES

Fig. 5 Closed Loop System Identification

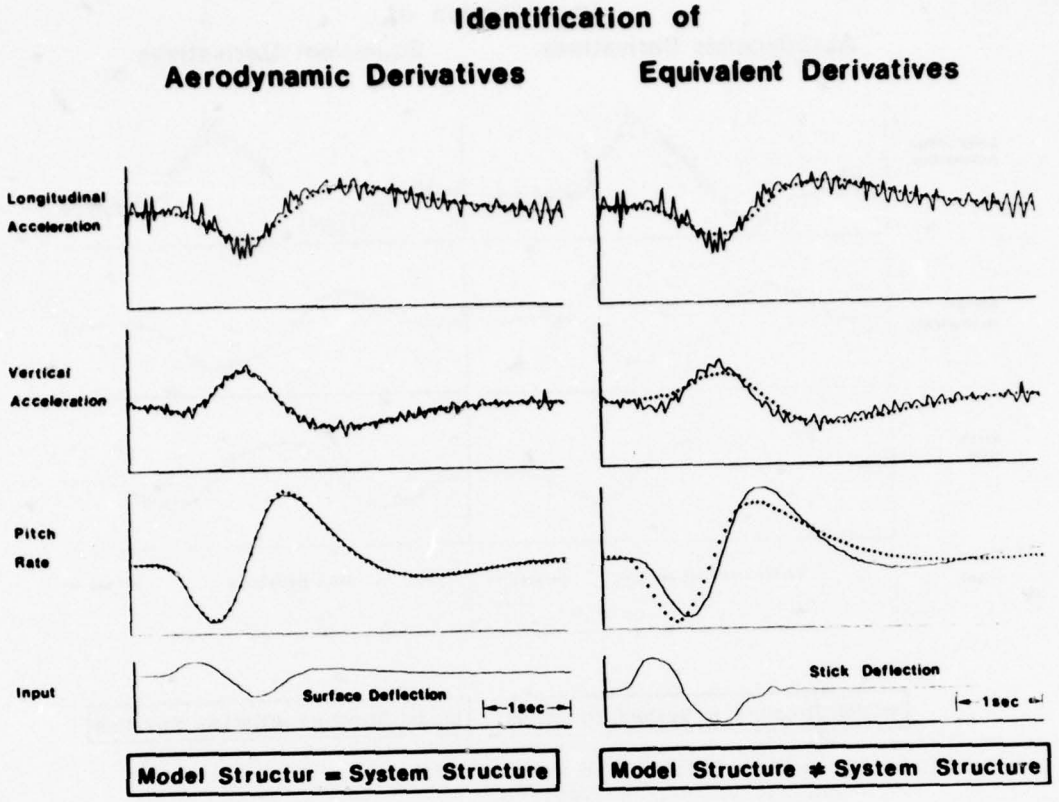

Fig. 6 Example of Degraded Fits in Identification of Equivalent Derivatives

——— flight test data
+ + + model output

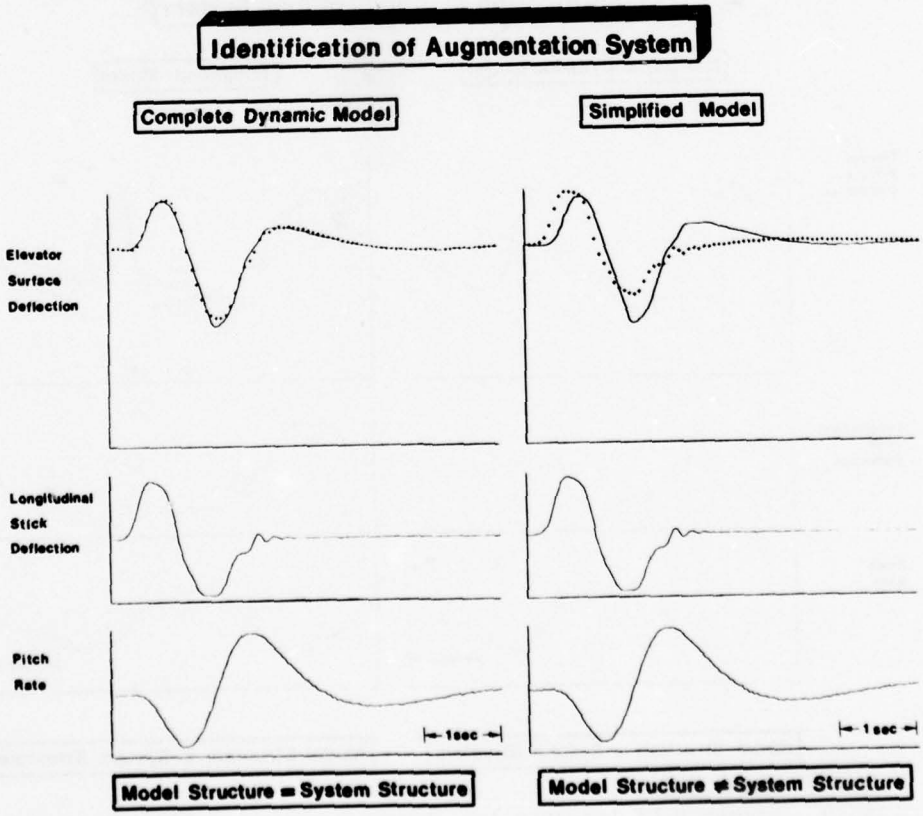

Fig. 7 Comparison of Fits in Identification of the Augmentation System

——— flight test data
+ + + model output

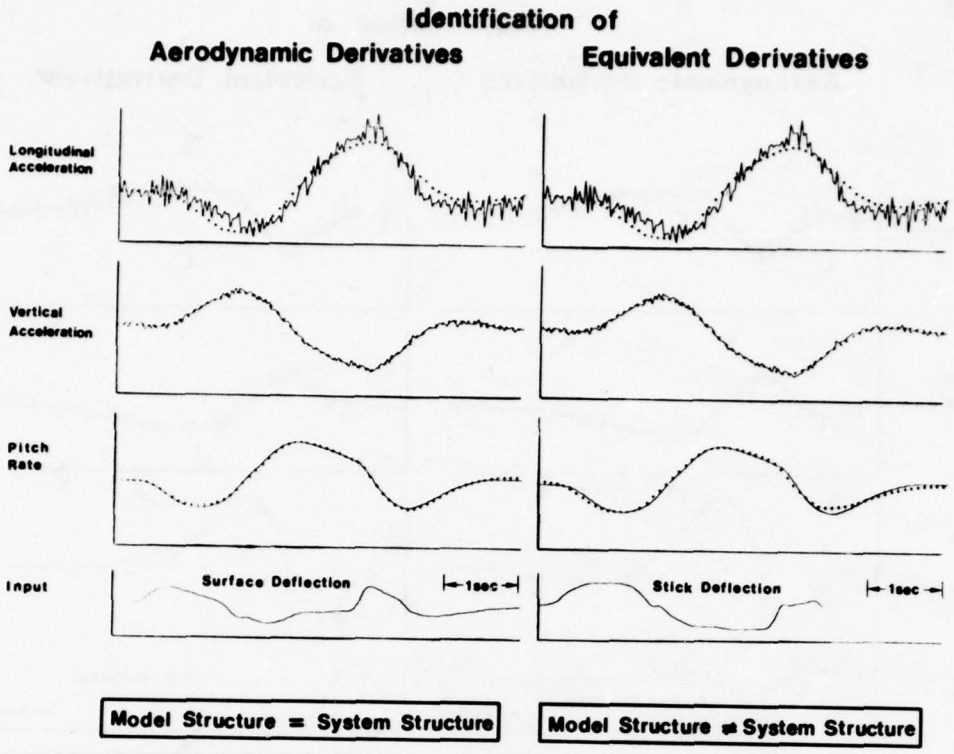

Fig. 8 Example of Good Fits in Identification of Aerodynamic and Equivalent Derivatives

——— flight test data
+ + + model output

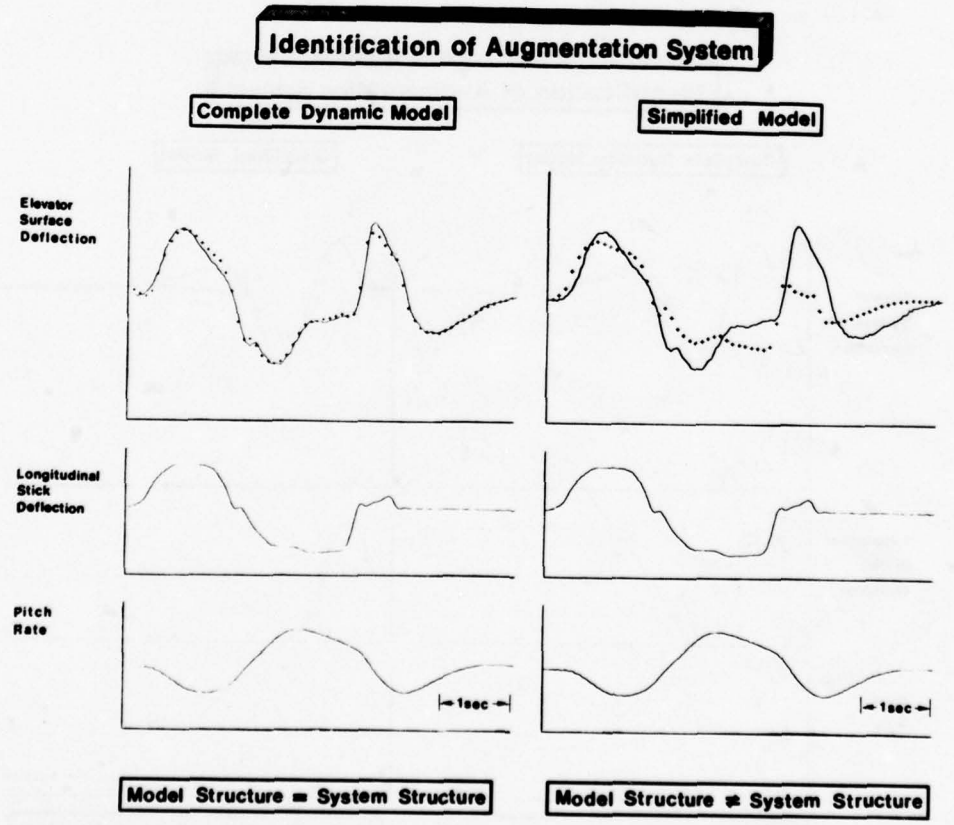

Fig. 9 Influence of Augmentation System Dynamics on Time Histories

——— flight test data
+ + + model output

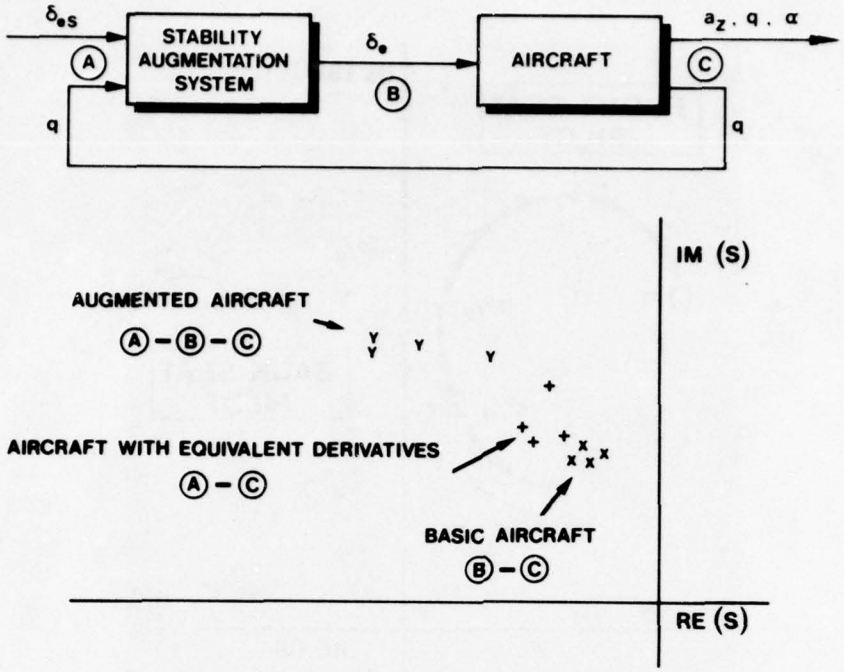

Fig. 10 Poles of Short Period Motion in Open and Closed Loop System

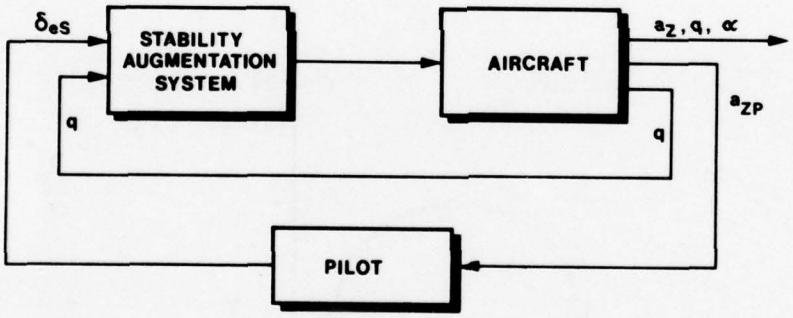

Fig. 11 Pilot-in-the-Loop System

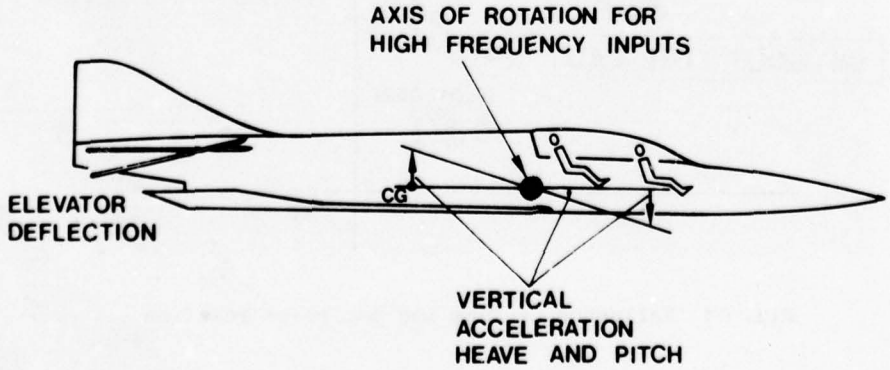

Fig. 12 Vertical Acceleration Due to High Frequency Inputs

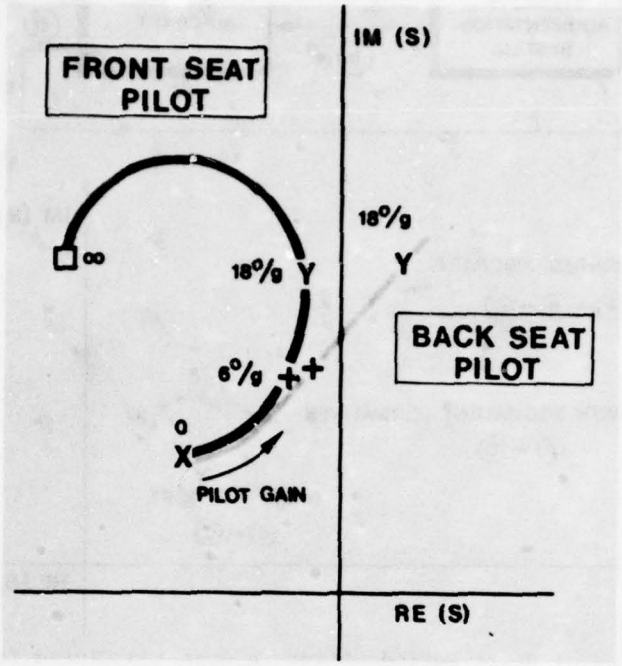

Fig. 13 Influence of Pilot Position on Stability of Pilot-in-the-Loop System

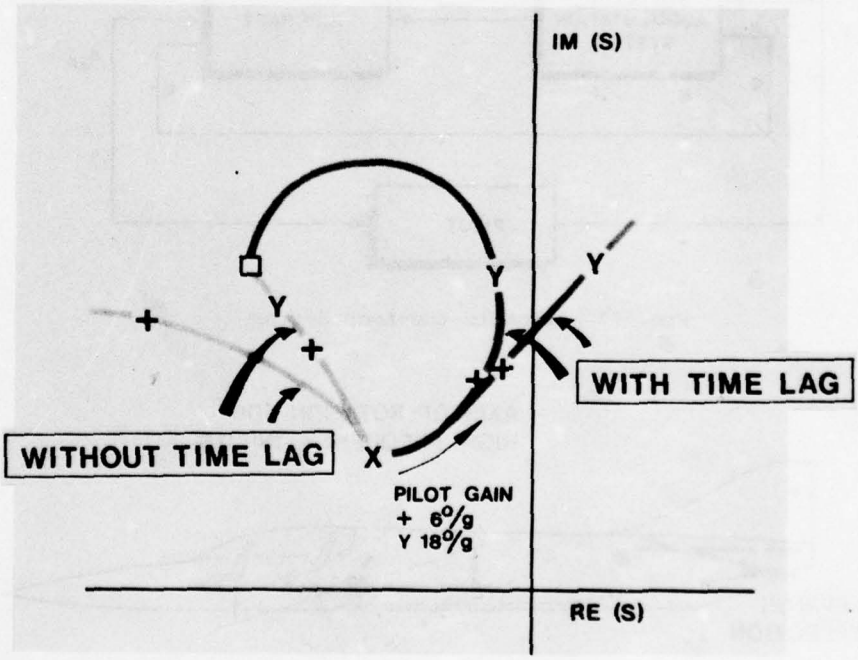

Fig. 14 Influence of Time Lag and Pilot Position

Satisfactory Fit but Unsatisfactory Results

- Characteristic Motion Evaluation
- Estimation of Equivalent Derivatives
- Investigations Based on Equivalent Derivatives

Satisfactory Fit and Satisfactory Results

- System Identification of
  - Basic Aircraft and
  - Dynamic Augmentation System under Flight Conditions
- Pilot–in–the–Loop Investigations

Fig. 15 Conclusions

DYNAMIC WINDTUNNEL SIMULATION OF ACTIVE CONTROL SYSTEMS

P.G. Hamel
B. Krag

Institut für Flugmechanik

Deutsche Forschungs- und Versuchsanstalt
für Luft- und Raumfahrt e.V. (DFVLR)
3300 Braunschweig Flughafen, West Germany

Summary

Research studies were conducted by the DFVLR to demonstrate the application potential of the Dynamic Simulation in Windtunnels test facility. Elastic mode control and ride smoothing systems were scaled to model frequency and tested in the DFVLR 3 m subsonic gust windtunnel. An open loop active control ride smoothing system was optimized for the Dornier-TNT light transport aircraft experimental program. Dynamic windtunnel flight tests of this program have been successfully completed.

1. Introduction

Stability and Controllability as Handling and Ride Qualities have, for many years, constituted a major area of interest of the Flight Mechanics Specialists and consequently of the AGARD Flight Mechanics Panel. Increased attention has been focused on this area of flight dynamics because of the latest progress in the field of active control technology [Ref. 1].

The application of active control systems is not only advantageous in the area of vehicle flight dynamics but seen from an energy efficiency standpoint it also offers a means for improving vehicle flight performance and operational flexibility. In order to obtain real benefits from advanced or active control technology it must be considered as an integral element in the whole flight vehicle design procedure. This design philisophy has become known as the control configured vehicle concept [Ref. 2].

The technical panels of AGARD have put a good deal of effort in to continuously stimulating advances in the field of active control technology and exchanging relevant scientific and technical information within the NATO community [Ref. 3 and 4].

The development and flight testing of flight vehicles with integrated active control ("ACT") systems have to consider not only combined aerodynamics, flight dynamics and control system dynamics but also structural and aeroelastic influences. In addition, there is a need for sophisticated measurement and data-processing techniques to extract a maximum of precise flight test data from the overall flight vehicle system. The extent, the complexity and the cost of flight testing have substantially increased and, consequently, analytical, simulation and windtunnel model testing methods have to be improved to offer alternative opportunities for more cost-effective preliminary designing and testing of advanced flight vehicles with integrated active control systems.

Running dynamic windtunnel programs with free flying and controllable models at NASA Langley RC [Ref. 5], IMFL and ONERA [Ref. 6], MBB München [Ref. 7] and DFVLR Braunschweig Ref.[8, 9] demonstrate the efforts undertaken to fill the needs for more cost-effective experimental results. The experiments also show the effectiveness of active systems for improving the flight mechanic and aeroelastic behaviour.

This paper describes some recent results of active control system testing using the DFVLR Dynamic Simulation Windtunnel Test facility in Braunschweig. The results have demonstrated the feasibility of conducting safe, realistic and reproducable flight testing of dynamically scaled aircraft configurations with integrated active control systems.

2. Test Facility Description

In recent years the DFVLR-Institut für Flugmechanik has performed special windtunnel flight testing of dynamically scaled aircraft models with integrated active control systems. The method of Dynamic Simulation in Windtunnels is especially well suited for investigating interdisciplinary problem areas of CCV-concepts. This technique synthezises the methods of computer simulation, windtunnel and flight testing including realistic hardware components. The disadvantages of inadequate mathematical models for computer simulation as well as expensive and complex full scale flight tests are excluded.

The model flies in a special suspension frame which allows freedom of motion in pitch, yaw, roll and heave. This is sufficient for simulating the short period longitudinal motion of conventional aircraft. The models may have inertial and elastic scaled properties which give them a dynamic response behaviour similar to the original aircraft. The experimental installation includes a gust generator and a measurement container which houses the model control devices, the measurement data processor, and various monitoring devices. The advantage of this type of simulation is the good observability of all state and disturbance variables which act on the model. The test time can be as long as necessary to perform a detailed measurement of all important parameters. All standard test routires for dynamic response evaluation, such as harmonic, impulsive and stochastic excitations, can be performed. Either the gust generator and/or the control surfaces can be used to excite the model. The response can be evaluated using time history, frequency response or power spectrum analysis.

One of the main features of this installation is the gust generator. The two gust generator flaps are driven by an electro-hydraulic actuator. This device allows a deflection of the airstream within the test-section of up to 10 degrees. The gust generator can generate gusts in the frequency range from zero to fifteen Hertz. It is possible to generate various types of gust profiles, such as impulsive or stochastic gusts.

The properties of the gust generator allow the simulation of a scaled stochastic gust field with Dryden - or v. Kármán characteristics. The output signal of a noise generator is passed through a shaping filter to obtain the desired turbulence characteristics. The parameters of the shaping filter depend on the altitude and speed of the aircraft and can be found, for example, from the relevant MIL-F-8785 specifications. The filtered signal drives the gust generator and produces an artificially stochastic gust-field. There is a strong correlation between the measured power spectrum of the gust angle of attack and the shaping filter output. This correlation can be maintained up to frequencies of about 8 Hertz [Ref. 10 and 11].

Another important feature is the aircraft model suspension system. A servo-controlled vertical force generator can produce constant vertical forces intependent of the model motion in order to simulate a different reference model flight condition by varying the effective model weight. For example, a constant increase of vertical force allows for model flight testing at reduced reference angles of attack and unchanged windtunnel speeds. Again, the model flight dynamics is unaffected by this simulated change of model gravity [Ref. 12].

3. Test Programs

Recently conducted active control system testing included an experimentel program for evaluating Ride Smoothing Systems (RSS) and Elastic Mode Suppression System (EMS) for wing and fuselage bending modes of a flexible combat-type multipurpose aircraft model. This program was sponsored by the Federal Ministry of Defense BMVg (ZTL-program BASE).

In the field of light transport aircraft a common Dornier/DFVLR windtunnel test program was accomplished using a rigid experimental light transport aircraft model to investigate a low cost Ride Smoothing System (RSS). This program was sponsored by the Federal Ministry of Research and Technology BMFT (ZKP-program OLGA).

Some of the test results obtained from these two programs will be presented in the following.

4. SAS, RSS and EMS testing of a combat-type multipurpose aircraft model

Structural vibrations can contribute to the degradation of ride qualities of combat aircraft during flights near ground in the same order as the rigid body mode excitation. In this case, ride quality control leading to improved crew comfort has to be mechanized by a combination of a rigid body ride smoothing system (RSS) and a fuselage elastic mode suppresion system (body-EMS).

Fig. 2 shows the dynamically scaled aircraft model equipped with active lift (A), symmetric aileron (B), elevator (C) and canard (D) control surfaces. From fig. 3 the selected combinations of active control surfaces for evaluating stability augmentation systems (SAS), ride smoothing systems (RSS) and wing-and body-elastic mode suppression systems (EMS) can be identified. The optimum gust response alleviation achieved in different frequency regimes is evident.

5. SAS and RSS testing of a light transport aircraft model

In a joint effort the Dornier Aircraft Company and DFVLR are developing a low cost ride smoothing system (RSS) for future application in a small twin-engined light transport aircraft. The preliminary flight testing was performed in the DFVLR Dynamic Simulation test facility using a dynamically scaled replica of the Dornier-TNT light transport experimental aircraft. This model is built completely from carbon fiber reinforced material, which results in a low-weight and highly rigid structure (fig. 4).

The active control surfaces (inner flaps (A), symmetric ailerons (B) and horizontal tail (C)), are driven by electro-mechanical torque motors. The model is well equipped with rate gyros, accelerometers, pressure transducers, potentiometers for control surface and rigid body deflections and various angle of attack probes at different locations. Built-in test equipment is applied for computer controlled dynamic component diagnosis. Power supply, control signals and measured data are transferred to and from the model via an umbilical cable (fig. 5).

From fig. 6 the selected combinations of active control surfaces applicated for evaluating stability augmentation (SAS) and variable stability systems, and especially for rigid body ride smoothing systems (RSS) are apparent. The influence of maximum control surface rates (0,30 and 60 deg/sec) and gust probe locations (I and II) on the RSS effectiveness within the motion-sickness frequency band (full-scale frequency band: 0.3 to 0.8 Hz) is shown schematically.

The dynamic response behaviour of the Dornier/DFVLR-TNT model, when flying through a dynamically scaled stochastic windtunnel gust field is shown in fig. 7. The time histories obtained from windtunnel tests of the optimized ride smoothing system show efficient reductions of both vertical and pitching accelerations when the RSS is engaged.

Fig. 8 shows the measured vertical acceleration frequency response of the model flying in a harmonic windtunnel gust field. Again, the strong gust response alleviation effect of the active control ride smoothing system (RSS) is apparent. This is especially true in the region of motion sickness (model-scale frequency band: 0.8 to 2.0 Hz).

Finally, from fig. 9 the measured power spectra of the vertical acceleration indicate nearly equal performance in gust response attenuation of two ride smoothing systems having digital and analog filters. These filters simulate the residual dynamics or residual time delay resulting from the difference of the combined equivalent time delay effects due to gust penetration phenomena, sensor and control surface actuator dynamics and the flight mechanics time delay. This time delay is defined by the dimensions of individual aircraft and reference flight speed. A more detailed description and discussion of dynamic residual filter design for ride smoothing system optimization is contained in References 11 and 13.

(In the oral version of this paper a movie clip was used to show some of the effects of active controls on the dynamic response of the dynamically scaled Dornier/DFVLR-TNT light transport aircraft model here discussed).

6. Concluding Remarks and Future Outlook

Research studies were conducted by the DFVLR to demonstrate the application potential of the Dynamic Simulation in Windtunnels technique. The following general conclusions can be drawn:

Successful basic research has been accomplished in the field of

(1) Generation of various types of gust profiles, such as impulsive, harmonic and stochastic gusts.

(2) Adjustment of various steady flight conditions without changing aircraft geometric or inertial characteristics.

(3) Identification of rigid and elastic body dynamic response characteristics due to control and disturbance inputs.

(4) Reproducable dynamic response testing under fully defined environmental conditions.

(5) Improvement of rigid and elastic body dynamic response by application of active control techniques.

(6) Development and testing of a low-cost ride smoothing system for a Dornier light transport aircraft project.

For the future the following research objectives can be projected:

(1) Active control system testing for guaranteeing handling and ride quality harmony of future CCV aircraft.

(2) Application of system identification techniques for active control surface optimization.

(3) Improvement of control input design for system identification applications.

(4) Identification of unsteady aerodynamic effects of lifting and control surfaces (cooperation with IMFL, France).

(5) Prediction of mission load spectra of future active control aircraft.

(6) Industry aircraft project support.

7. References

1. Statler, I.C. Flight Mechanics - A Review of the Activities of the AGARD Flight Mechanics Panel. AGARD Highlights 78/1 (1978).

2. Wanner, J.C. The CCV Concept AGARD Highlights 72/2 (1976).

3. ANON. Impact of Active Control Technology Airplane Design. AGARD-CP-157 (1975).

4. ANON. Structural Aspects of Active Control. AGARD-CP-228 (1977).

5. Reed, W.H. Comparisons of Flight Measurements with Predictions from Aeroelastic Models in the NASA Langley Transonic Dynamic Tunnel. AGARD-CP-187 (1976), Paper No. 6.

6. Gobeltz, J. Simulation de Vol par Maquettes de Vol libre en Laboratories. AGARD-CP-187 (1976), Paper No. 14.

7. Hönlinger, H., Sensburg, O. Dynamic Simulation in Windtunnels. Part I: Active Flutter Suppression. AGARD-CP-187 (1976), Paper No. 5-1.

8. Subke, H., Krag, B. Dynamic Simulation in Windtunnels Part II: Gust Alleviation and elastic Mode Control. AGARD-CP-187 (1976), Paper No. 5-17.

9. Hoffmann, G. Stabilisierung, Böenkompensation und Schwingungsdämpfung am elastischen, beweglichen Flugzeugmodell im Windkanal. Deutsche Luft- und Raumfahrt, Forschungsbericht DLR-FB 76-44 (1976).

10. Krag, B. Gust-Vehicle Parameter Identification by Dynamic Simulation in Windtunnels. AGARD-Workshop: Dynamic Stability Parameter, Athen, 22-24 May 1978.

11. Krag, B. The Windtunnel Behaviour of a Scaled Model with a Gust Alleviation System in a Deterministic Gust Field. Symposium: Dynamic Analysis of Vehicle Ride and Maneuvering Characteristics. The Institute of Measurement and Control, London, 28-30 November 1978.

12. Subke, H. Test Installations to Investigate the Dynamic Behaviour of Aircraft with Scaled Models in Wind Tunnels.
Symposium: Dynamic Analysis of Vehicle Ride and Maneuvering Characteristics.
The Institute of Measurement and Control, London, 28-30 November 1978.

13. Krag, B. Active Control Technology for Gust Alleviation.
VKI-Lecture Series: Active Control Technology, Brussels, 4-8 December 1978.

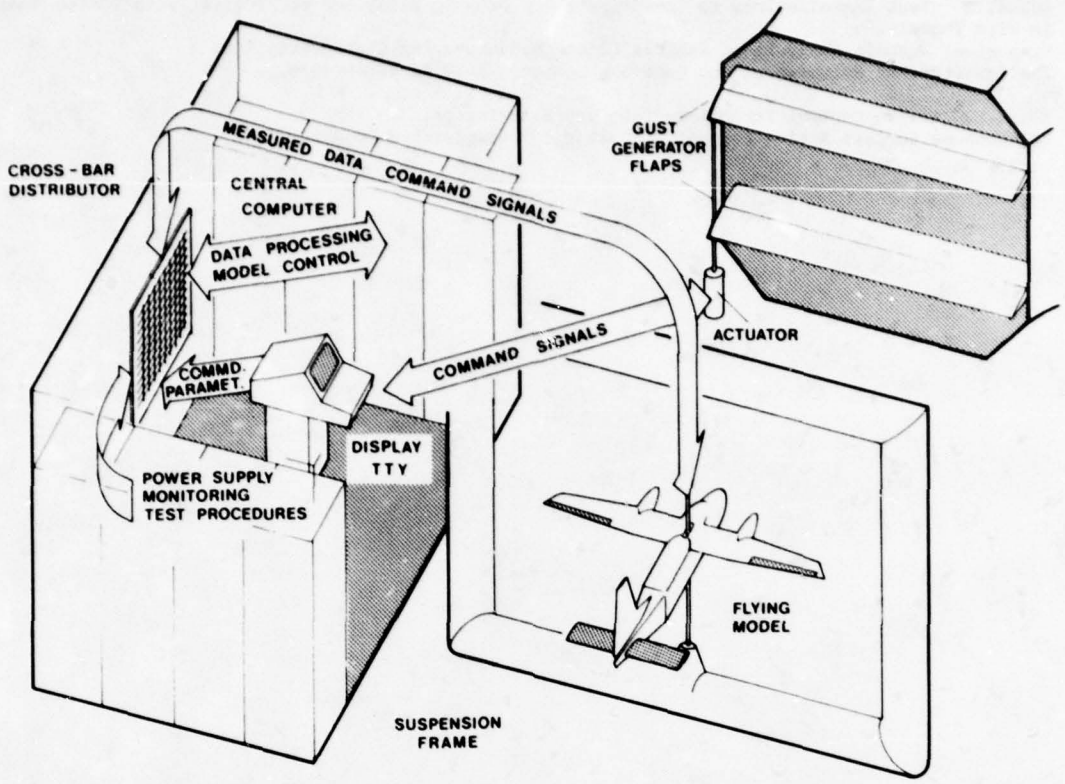

Fig. 1 DFVLR test facility for dynamic simulation in windtunnel of flight vehicles with integrated active control systems

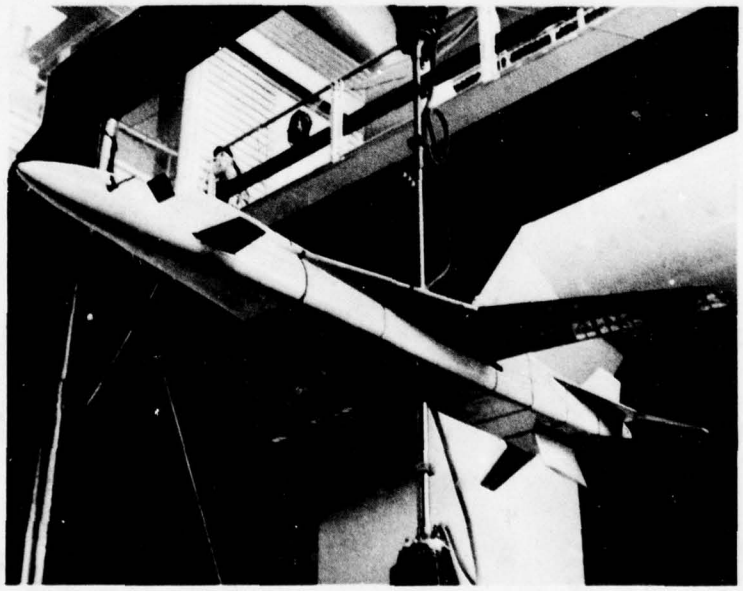

Fig. 2 DFVLR-ZTL dynamically scaled and controllable multipurpose aircraft model

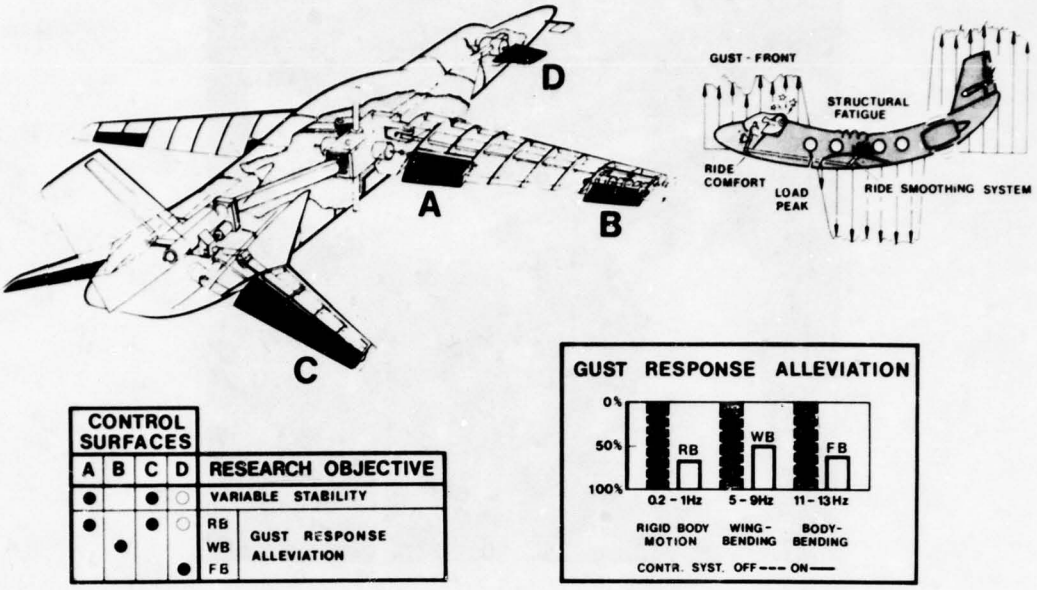

CONTROL SURFACES				RESEARCH OBJECTIVE
A	B	C	D	
●		●	○	VARIABLE STABILITY
●		●	○	RB
	●			WB — GUST RESPONSE ALLEVIATION
			●	FB

Fig 3 Active control surfaces for testing stability augmentation (SAS) ride smoothing (RSS) and elastic mode suppression systems (EMS)

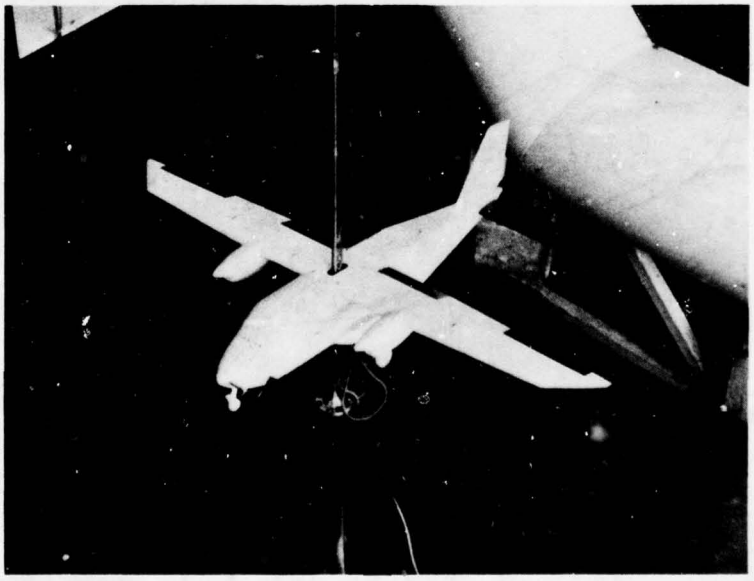

Fig. 4 Dornier/DFVLR-TNT light transport aircraft experimental model

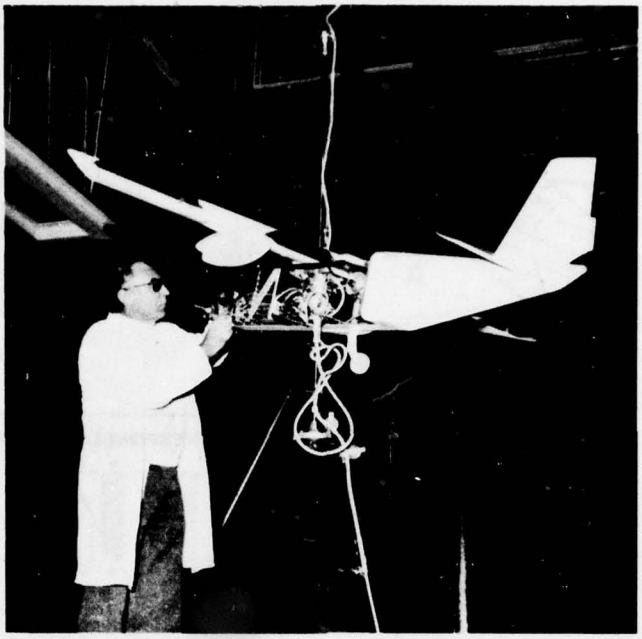

Fig. 5 Dornier/DFVLR-TNT model: active control system integration

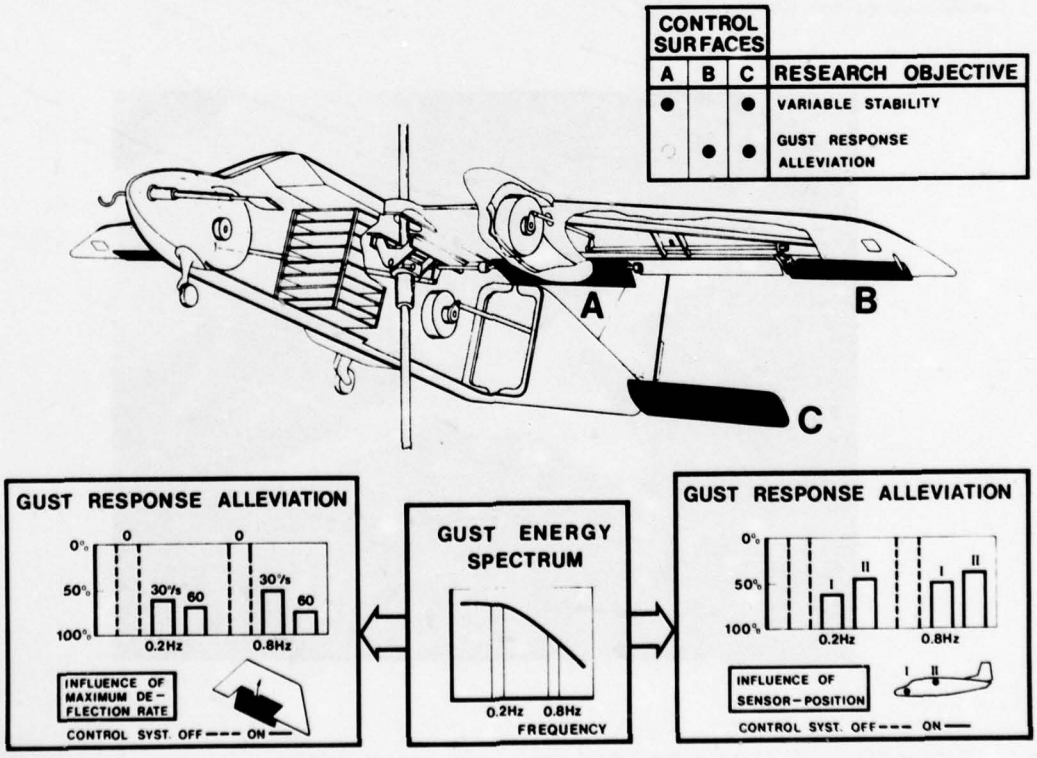

Fig. 6 Active control surfaces for testing stability augmentation (SAS) and ride smoothing systems (RSS). Influence of control surface rates and sensor locations.

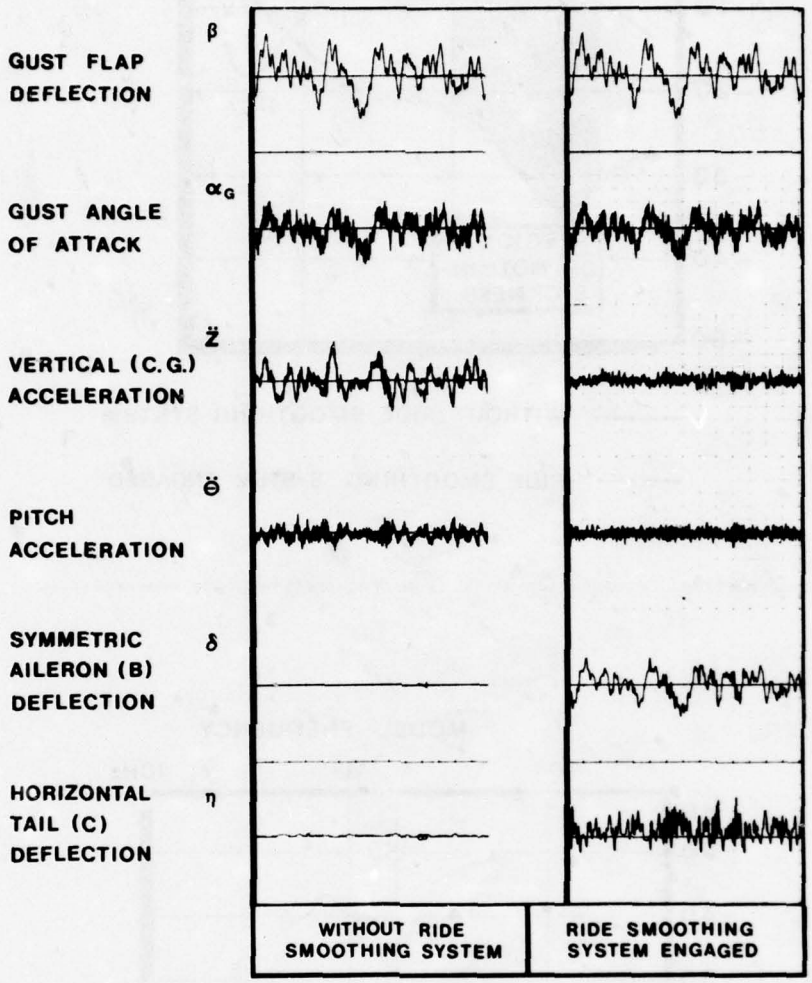

Fig. 7 Dynamic response of Dornier/DFVLR-TNT model in simulated windtunnel turbulence environment.

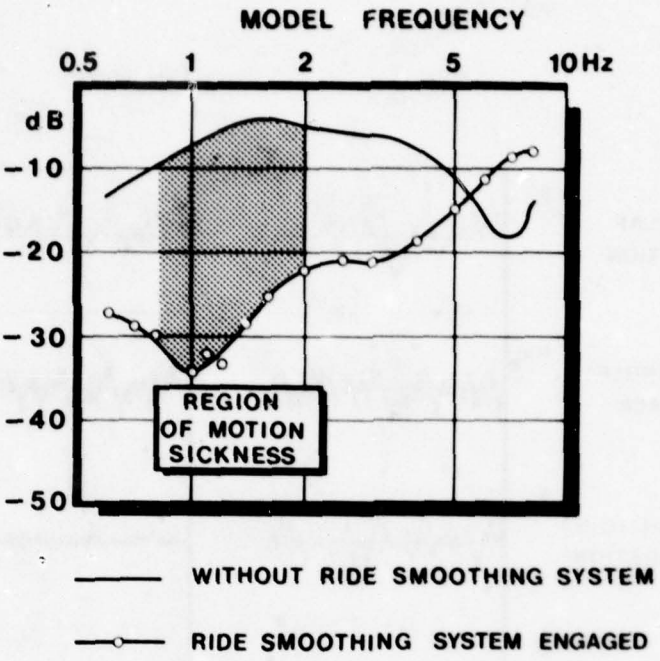

Fig. 8 Modulus of vertical acceleration at CG from frequency response measurements.

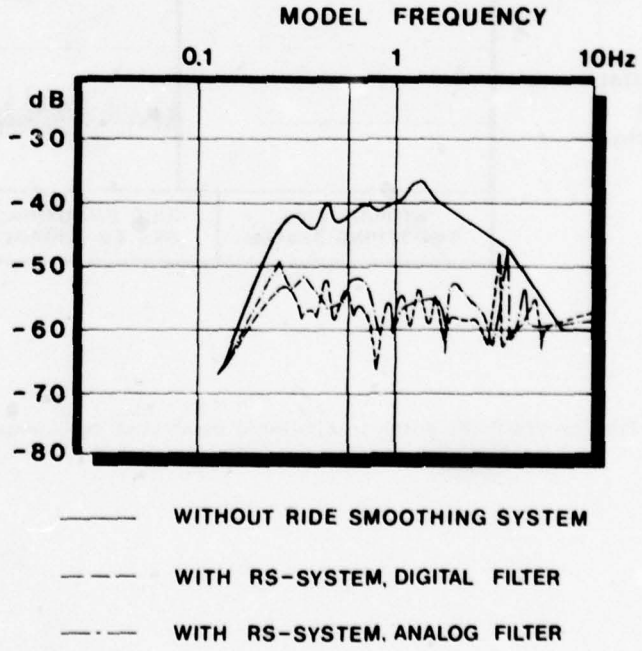

Fig. 9 Power spectrum of vertical acceleration at CG from stochastic analysis of windtunnel test data

STABILITY AND CONTROL ASPECTS OF THE CCV-F104G

by

H. Beh*, U. Korte** and G. Löbert***

Messerschmitt-Bölkow-Blohm GmbH
Military Aircraft Division
8012 Ottobrunn, Germany

SUMMARY

In Dec. 1974 a German CCV-Demonstrator Program based on the F104G supersonic combat aircraft was launched. The objectives of this program are

- development of an advanced CCV-flight control system
- investigation of FCS-performance and demonstrator handling qualities in the complete flight envelope up to 20 % negative static margin.

The desired degree of instability is obtained by mounting a canard surface above the forward fuselage and adding 600 kg aft ballast. In an emergency situation the demonstrator aircraft can be restabilised by dropping the aft ballast and transferring fuel from the tip tanks to the main fuel tank.

The CCV-FCS is characterised by

- four-channel redundancy
- digital signal processing and system monitoring
- implementation of multi-variable control theory
- integration of ADC, CSAS, Autopilot, Navigation and BITE functions in each computer
- central inertial sensors with strap-down capability
- skewed flow-direction sensors
- modular, selfmonitoring secondary actuators

The CCV command system and its implementation, and the design of the control laws are described. The superior flight-mechanical performance of the CCV-FCS is compared with that of the basic F 104G on the basis of simulator results. Finally, the validity of these results is demonstrated by comparing the principal characteristics of longitudinal and lateral motion measured in flight with the corresponding predicted values.

1. INTRODUCTION

In December 1974 a German CCV-Demonstrator Program, based on the F104G supersonic combat aircraft was launched. The objectives of this program are to develop and flight test a quadruredundant digital fly-by-wire flight control system and to investigate the stability and control characteristics of a supersonic combat aircraft throughout the complete flight envelope with up to 20 % negative static margin. Demonstration of the performance improvement resulting from relaxed static stability was not considered an objective since the effectiveness of this CCV-concept can be predicted on the basis of windtunnel testing with sufficient confidence.

A brief outline of the F104G-CCV Program will be given in Section 2. Thereafter the design of the newly developed CCV-FCS will be described in detail. In Section 4 some results of the current flight test program and comparisons with predictions will be presented.

---

* Specialist, Guidance and Control
** Deputy Chief, Guidance and Control
*** CCV Program Manager

2. PROGRAM DESCRIPTION

2.1 Demonstrator Aircraft, Destabilisation Concept

Availability considerations dictated the use of a single-seater F104G as the CCV-demonstrator aircraft. Due to the high positive static margin of the F104G in the clean configuration (approx. 20 % MAC), the negative margin aimed for can only be obtained by the combination of the following two measures:

- 600 kg aft ballast to move the centre of gravity (c.g.) to the tip-up aft limit
- An F104G horizontal tailplane mounted as a canard surface above the fuselage immediately behind the ammunition compartment (see Fig. 1). This moves the aerodynamic centre (a.c.) forward by approximately 35 % MAC.

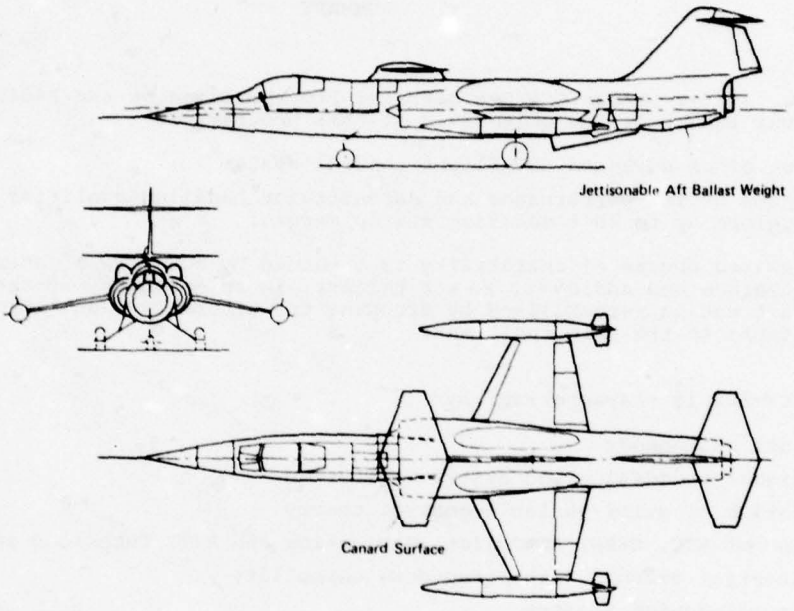

Fig. 1 DESTABILISATION CONCEPT

2.2 Aerodynamic Characteristics of the Modified Aircraft

The incidence angle of the canard surface is fixed at - 4°. At this setting wing and canard are lift-free at the same angle of attack.

Although the canard carries some 20 % of the airplane weight, the addition of this surface has little effect on the total untrimmed lift coefficient at a constant angle of attack (see Fig. 2). This is of course due to the fact that the downwash flow produced by the lifting canard is nearly completely cancelled by the wing. Canard lift is thus practically nullified by a corresponding down-load on the wing.

Fig. 3 shows the effect of the canard on the pitching-moment characteristics of the F104G clean configuration. In the lower angle of attack range the force couple acting on the canard and the wing destabilises the airplane to the desired degree. At α = 11°, the canard configuration reassumes positive stability due to the onset of flow separation on the canard upper surface. When the wing stalls at 16° angle of attack, both configurations exhibit the well-known pitch-up instability.

On the basic F104G, penetration of the pitch-up boundary is prevented by a stick-kicker which moves the control stick forward when the angle of attack - increased by a suitable fraction of the unsteady component of the pitching velocity - reaches 14°. Artificial stall warning is provided by a stick-shaker system, which under steady conditions is triggered at α = 12°.

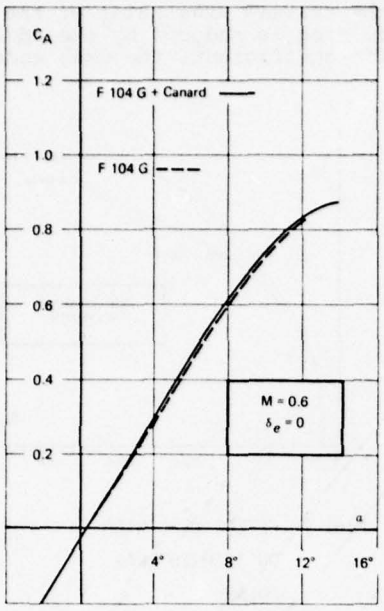

Fig. 2 EFFECT OF CANARD SURFACE ON UNTRIMMED LIFT

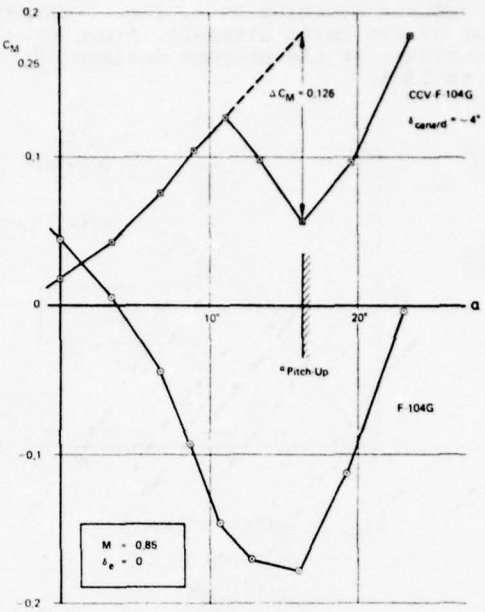

Fig. 3 EFFECT OF CANARD SURFACE ON PITCHING-MOMENT

The horizontal canard surface not only destabilises the longitudinal motion but also reduces the directional stability of the airplane considerably, as can be seen in Fig. 4. This is due to

a) the side forces induced on to the fuselage in the vicinity of the canard and

b) an increased sidewash at the vertical tail as is evidenced by the reduced dihedral effect (see Fig. 5).

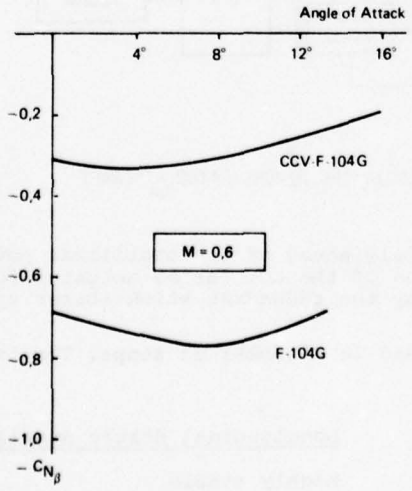

Fig. 4 EFFECT OF CANARD SURFACE ON DIRECTIONAL STABILITY

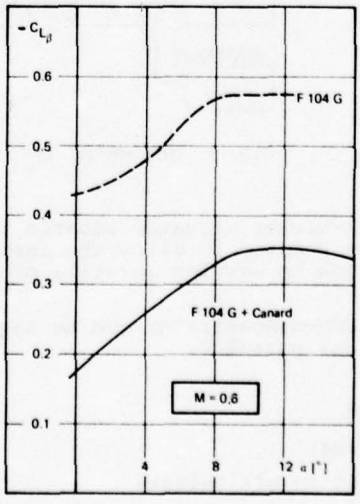

Fig. 5 EFFECT OF CANARD SURFACE ON DIHEDRAL EFFECT

Trimmed lift coefficient is of course increased considerably by the reversal of the loading of the horizontal tail, as can be seen in Fig. 6. As a result, shaker speed will be reduced by about 10 %. Fig. 7 compares the trimmed drag polar of the CCV-F104G with that of the basic aircraft. Above C_L = 0.34, drag is reduced by the addition of the canard surface. At the present maximum usable lift coefficient, the drag reduction amounts to 23 %.

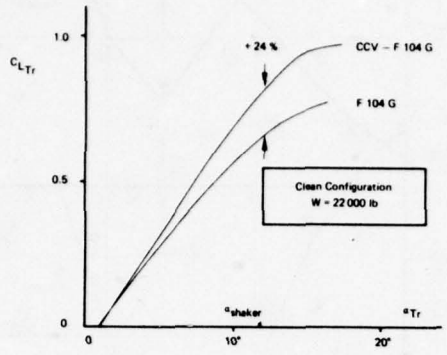

Fig. 6 EFFECT OF CANARD ON TRIMMED LIFT COEFFICIENT

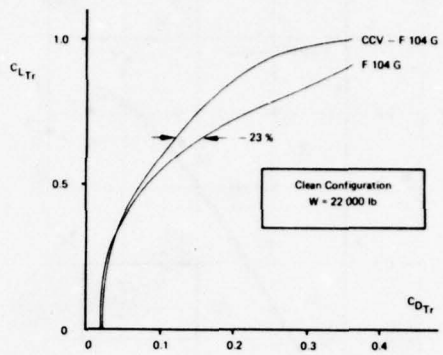

Fig. 7 EFFECT OF CANARD ON TRIMMED DRAG POLAR

2.3 Safety Measures

While a mechanical back-up FCS is considered undesirable in an operational aircraft, the lack of an iron-bird ground test rig dictated the incorporation of such a system in the F104G experimental program. This mechanical back-up is provided by the original F104G FCS. Slight modifications of this system were of course unavoidable:

- In the mechanical linkage between the artificial feel spring and the power actuator input lever of each control surface a switch-over unit was installed by means of which the power actuators can be connected to either the mechanical or the CCV-FCS (see Fig. 8).

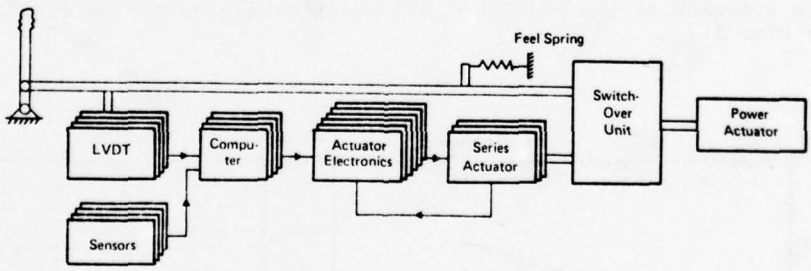

Fig. 8 INTEGRATION OF THE CCV-FCS IN THE DEMONSTRATOR AIRCRAFT

- The stick-kicker actuator located immediately ahead of the stabilizer power actuator had to be removed to allow the installation of the CCV series actuator for pitch control. Pitch-up warning is still provided by the redundant stick-shaker system.

The CCV-demonstrator can be destabilised in a number of steps. The following configurations are possible:

Configuration	Longitudinal Static Stability
B 1: Basic F104G	highly stable
B 2: B 1 + 600 kg aft ballast	moderately stable
E 1: B 1 + canard + forward ballast	marginally stable
E 2: E 1 + 400 kg aft ballast	moderately unstable
E 3: E 1 + 600 kg aft ballast + fuel transfer	highly unstable

Fig. 9 shows the c.g.-movement as a function of fuel usage for these five configurations. The most forward subsonic a.c. of the basic airplane and that of the canard configuration are also shown. Configuration E1 is ballasted such that the airplane is marginally stable under zero-fuel conditions. For configurations B2 and E3 the normal sequence of fuel usage (tip tank fuel before internal fuel) is reversed in order to obtain a more rearward c.g.-location in flight. Before landing, the tip tank fuel is transferred to the internal fuel tanks, thus moving the c.g. forward to the aft limit of 22 % MAC.

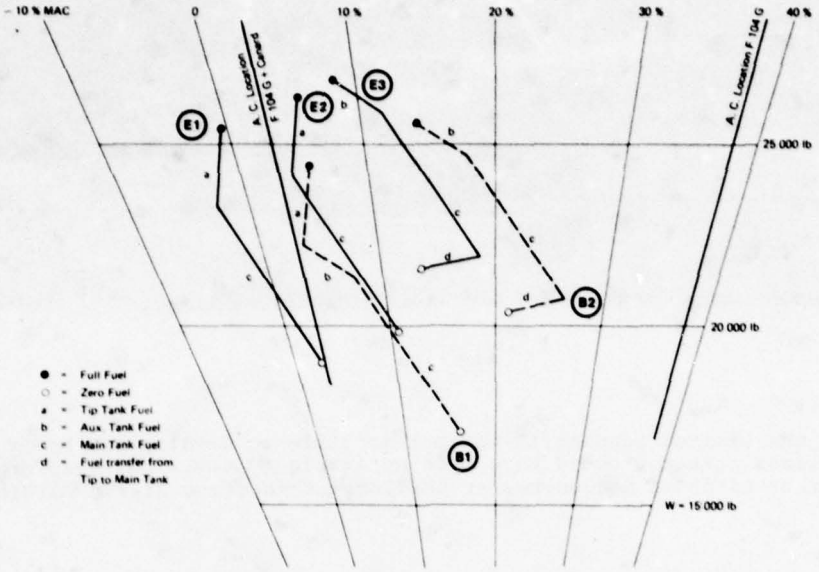

Fig. 9 CENTRE OF GRAVITY LOCATION AS A FUNCTION OF FUEL USAGE FOR THE FIVE CONFIGURATIONS OF THE CCV- F 104 G

The unstable configuration E 2 can be restabilised in an emergency situation by jettisoning the aft ballast (lead shot).

E 3 additionally requires the transfer of fuel, which takes about two minutes. Recovery from a hard-over system-failure is not possible in this configuration and in all other configurations at a high dynamic pressure flight condition. A partial system failure of course poses no problem in any of the five configurations.

Further details of the switch-over process (synchronisation, transients etc.) are given in section 4.

2.4 CCV Flight Control System

The newly-developed CCV-FCS is described in detail in Ref. 1. For completeness, the highlights of this system are repeated here.

- Double fail-operational redundancy (Quadruplex System)
- Digital data processing and system monitoring
- Application of multivariable, optimal control principles
- Skewed flow-direction sensor
- Centralisation of all inertial sensors (one set of sensors for all inertial quantities)
- Strap-down navigation
- Newly developed electro-hydraulic series actuators composed of three identical modules (each with its own failure detection capability) and a hydraulically operated redundant switch-over unit.

The series actuators for the elevator and rudder were installed on one side of the fin. The protruding parts were covered by a fairing which extends over the lower 50 % of one side of the fin (see Fig. 10). The thickness of the fin is nearly doubled by this measure.

The aileron series actuators are mounted at each side at the fuselage and are housed in two sizeable fairings (see Fig. 10).

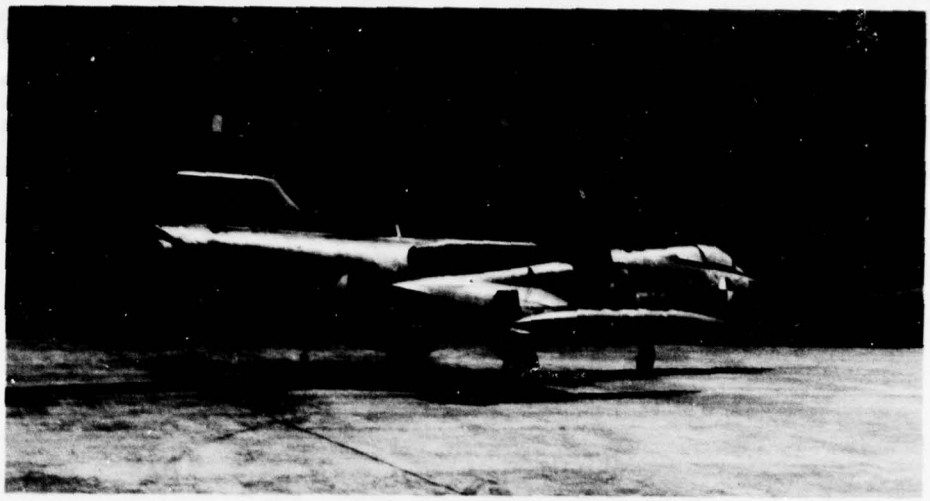

Fig. 10

Due to the limited funding it was not possible to develop new power actuators. A faster stabilizer actuator would have been desirable to cover high-performance take-offs and high-rate pitching manoeuvres at the largest negative static margin.

2.5 Flight Envelope, Flight Test Sequence

As can be seen in Fig. 11 the flight envelope of the CCV-demonstrator has been reduced from that of the basic F104G. This is mainly due to cost considerations. The maximum Mach number was set at 1.3 since most of the transonic change in longitudinal stability occurs below this Mach number. The indicated air speed was limited to 650 knots because from the Manching test facility in Germany supersonic flight testing is not possible below 36 000 ft altitude.

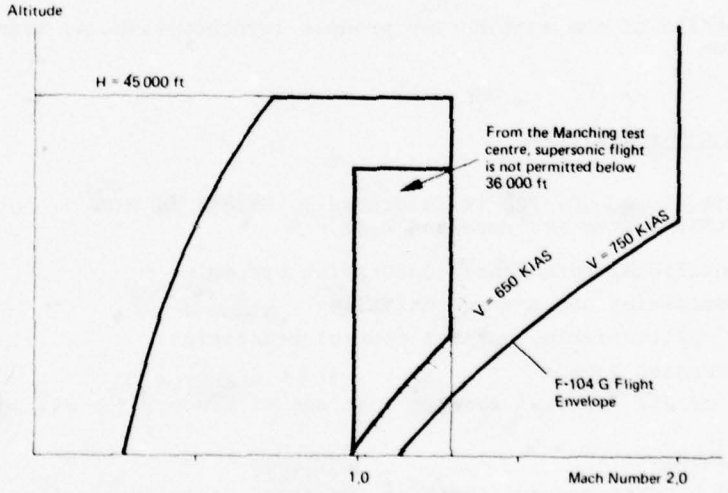

Fig. 11 FLIGHT ENVELOPE OF THE CCV-F 104 G

Fig. 12 shows the sequence in which the various demonstrator configurations will be flight-tested. The right half of the diagram depicts the relationship between the c.g.-range and a.c.-location for the five configurations.

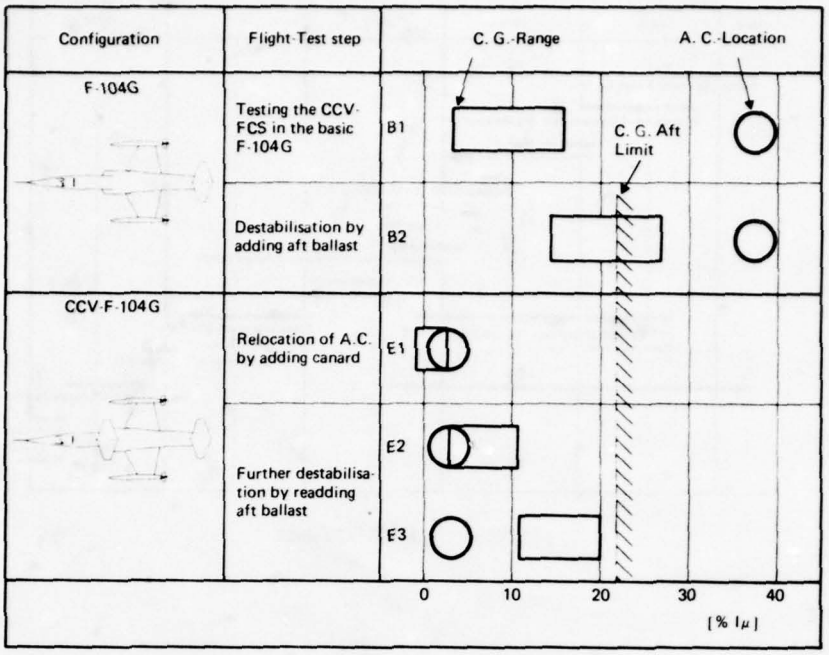

Fig. 12 FLIGHT TEST SEQUENCE

The B 1 test phase is subdivided into open-loop testing to establish confidence in the newly developed system, direct link test flights and closed loop-flight testing of the CCV-FCS.

Destabilisation of the CCV-demonstrator will begin after sufficient system confidence has been gained. In configuration B 2 aeroelastic and ballast jettison test will be conducted in addition to the standard handling qualities flight test program.

The aerodynamic and stability and control characteristics of the canard configuration will be flight-tested in the stable canard configuration E 1 both in the mechanical and in the fly-by-wire control mode. Additionally the aeroelastic stability of the canard surface will be demonstrated. In this and all subsequent canard configurations the principal structural loads will be monitored by means of strain gauges.
The demonstrator aircraft will then be destabilised further until the program objective of 20 % negative static margin is reached. In total, 135 flights are planned for the complete program.

In general, pitching rate and tailplane angle of attack will have to be closely monitored at high angles of attack and high roll rates to ensure that the maximum stabilizer deflection rate (20 deg/sec) is not reached and a safe margin to the stabilizer stall angle is maintained. As is well known, tail plane stall is catastrophic regardless of the sign and degree of stability.

2.6 Time Schedule, Program Status

Fig. 13 shows the time schedule for the program. Between 1974 and May 1977 the CCV-FCS and the associated safety system were developed and installed in the flight test vehicle. In October 1976 the aerodynamic and inertial sensors of the newly developed FCS were flight tested. Ground check-out of the installed system began in June 1977 and continued till November 1977. First flight of the CCV-F104G with the complete CCV-FCS was in Dec. 1977.

After four shake-down flights, in which the influence of the actuator and ballast fairings on the stability and control characteristics of the basic F104G was investigated, 15 further open-loop test flights were conducted to establish confidence in the CCV-FCS. Due to an unusually high failure rate in two components of this system, the program slipped by four months in this phase of flight-testing. In August and September 1978 seven flights in the direct link mode of the CCV-FCS followed.

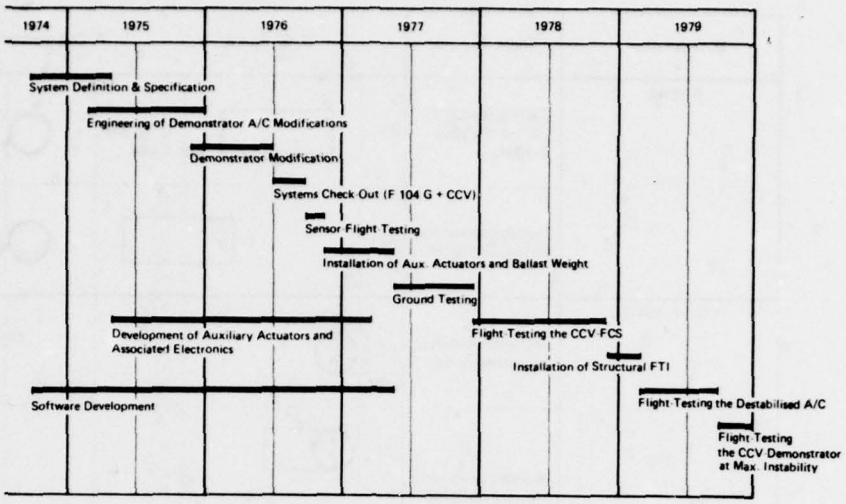

Fig. 13 TIME SCHEDULE

The first closed-loop flight will be conducted in the coming week after structural coupling ground test have shown adequate stability of the complete system.

Flight testing in the basic configuration B 1 will be completed in November 1978. After that the demonstrator aircraft will be destabilised successively.

From December 1978 until February 1979, the airplane will be layed up for the installation of further FTI-equipment which is needed for aeroelastic flight testing and the monitoring of structural loads. Flight testing in the most unstable configuration E 3 is scheduled for the fourth quarter of 1979.

3. DESCRIPTION OF THE CCV-FLIGHT CONTROL SYSTEM

The concept and the design of the CCV guidance and control system were determined by the following objectives:

- o Stabilization of the naturally unstable aircraft in order to obtain the benefits of improved aircraft performance
- o Solution of the safety problems existing with unstable aircraft
- o Development of an advanced, integrated guidance and control system with growth potential

To fulfill these tasks it was decided to choose a digital fly-by-wire system with 100 % authority. The following operational requirement was stipulated:

- o Continuation of mission without loss of performance after any first failure
- o Safe return to base after any further critical failure

This $(\text{fail-op})^2$-requirement led to a quadruplex system with parallel redundancy in which failures are detected, localised and isolated by majority vote.

3.1 The Quadruplex System

The redundancy concept and the hardware of the system have already been described elsewhere (1). Therefore only a short overview is shown in Fig. 14.

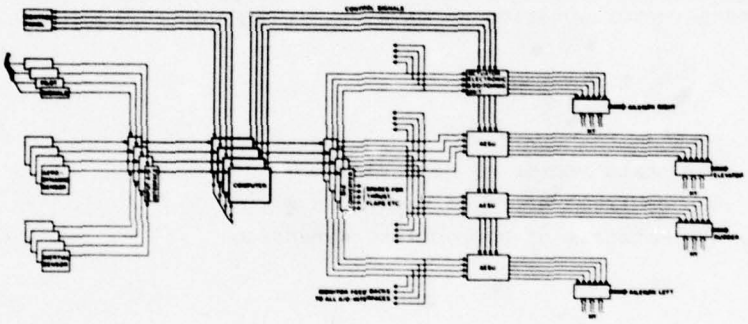

Fig. 14 SYSTEM OVERVIEW

All units (sensors, computer, interfaces etc.) have been quadruplexed with the exception of the series actuators.

For the series actuators-they are used in conjunction with the existing power actuators and had to be developed new because the series actuators of the basic F-104 damper system have only limited authority - the operational requirement is observed by using self monitoring triplex actuators.

The four identical computers are 16 bit computers with 16 K memory. They communicate with each other via fast data lines (DMA - direct memory access). Each computer performs the following functions

- o Stabilization and Control
- o Autopilot
- o Air Data Computation
- o Inertial Navigation (Strap Down)
- o Preflight Checkout
- o Redundancy Management

The necessary signals for the guidance and control system are supplied by inertial strap down sensors, airflow direction sensors (only 4 vanes for α and β are necessary instead of 8 because of a skewed arrangement), pitot static tubes and position pick-offs for pilot inputs. A list of the measured variables is given below:

α – angle of attack		$\dot{h}$ – vertical velocity	
β – angle of sideslip		V_{GSP} – ground speed	
p – roll rate	body fixed	χ – ground track angle	
q – pitch rate	body fixed	γ – flight path angle	
r – yaw rate	body fixed	Δy – cross track error	
Φ – roll angle		Φ^* – geographic latitude	
Θ – pitch angle		λ – geographic longitude	
Ψ – heading		P_s – static pressure	
V – total velocity		q_c – dynamic pressure	
h – altitude		T_t – total temperature	

It contains not only the information needed for stabilisation but for autopilot modes, navigation, air data computation as well.

3.2 Control system design

The design of the control system is based on linear control theory for multivariable systems. It was done in the discrete time domain using state vector methods.

To get the state vector description, the equations of motion have been linearised in the usual way for a reference condition of steady rectilinear flight. This leads to two sets of linear differential equations-one for the longitudinal and one for the lateral motion. In state vector notation we have

$$\dot{x} = F x + G u$$

where

x - state vector of dimension n

u - control vector of dimension m

F, G - matrices of appropriate dimension

by discretisation we get

$$x (kT+T) = A x (kT) + B u (kT) \qquad K = 0,1 , \ldots , n$$

or in short hand notation

$$x_{k+1} = A x_k + Bu_k \qquad A = e^{FT} , \; B = \int_0^T e^{Fv} G dv$$

The sampling period T for the CCV is 60 ms. This is rather large, but faster sampling was not possible because of system constraints out of the scope of the design engineer.

3.3 Control laws

For the control law design a computer aided design system has been used that has been developed by MBB (2) over a period of serveral years. It contains a variety of different design procedures. The methods chosen here were pole assignment for the longitudinal motion and linear optimal control (with quadratic performance index) for the lateral motion.

Optimal control theory leads to the linear discrete control law

$$u_k = K (x_k - x_d) + u_d \qquad K = \text{control matrix}, \; d = \text{desired}$$

where the complete state vector x is used for feedback.
For the longitudinal motion we have

$$x^T = (V, \alpha, q, \vartheta)$$

$$u = \eta \text{ elevator angle}$$

and for the lateral motion

$$x^T = (\beta, p, r, \phi)$$

$$u^T = (\zeta, \xi) \qquad \zeta = \text{rudder angle}, \quad \xi = \text{aileron angle}$$

3.4 The command system

It has already been mentioned that the CCV guidance and control system is a fly-by-wire system with full authority. In this system there is no longer a direct relationship between the position of the stick/pedals and the control surface deflections. The pilot now commands desired values of the aircraft's state variables:

Stick position is proportional to the commanded values of normal acceleration n_{z_d} and roll rate p_d respectively, pedal position is proportional to sideslip angle β_d.

From the commanded values the computer generates the control inputs u_k for the actuators that are necessary to reach the desired state.

For small deviations from the steady reference flight condition, the desired values x_d, u_d can be computed from the equation

$$\dot{x} = 0 = Fx_d + Gu_d$$

For large attitudes as they are encountered in real flight, this linear equation is not valid anymore and cannot be used. This difficulty can be overcome with a newly developed concept for the command system which functions as follows:

A reference frame-called the command system - is defined, which is rotating with the angular rates p_d, q_d, r_d. The aircraft's motion is now described with respect to the rotated reference system, which at the moment is thought fixed. If small deviations are assumed linearisation is possible. The linear equations obtained in this way are the same for all attitudes.

The attitude of the rotating system relative to the earth-fixed coordinate system is given by the Euler angles ϕ_d, θ_d, ψ_d. The aircraft itself rotates with p, q, r. Its attitude relative to the earth is described by ϕ, θ, ψ.

Ideally, the two coordinate systems should be in coincidence, that is the differences $\Delta\phi = \phi - \phi_d$, $\Delta\theta = \theta - \theta_d$, $\Delta\psi = \psi - \psi_d$ should be zero. To fulfill this task the linear controller

$$u_k = K (x_k - x_d) + u_d$$

is used.

It is well known that with the use of Euler angles there exists and ambiguity problem in some special flight manoeuvres i.e. loopings and rolls.

To avoid this difficulty, in the CCV control system quaternions are used instead of Euler angles and the feedback variables are expressed in the quaternion notation. Thus full aerobatics are possible with the fly-by-wire control system although attitudes are used for feedback.

Fig. 15 shows the CCV guidance and control system in principle.

The command values are given in a coordinate system fixed to the flight path. Via α_d, β_d these values are transformed into a body-fixed system. From them the command quaternions are computed and compared with the actual quaternions delivered by the inertial measurement units.

The feedback coefficients k_{ij} have been evaluated for different Mach numbers and altitudes:

for the take-off and landing configuration

at Ma = 0.3, Sea level

for the clean configuration

at Ma = 0.6 0.9 0.98 1.05 1.2
Alt = 5000 ft 20 000 ft 40 000 ft

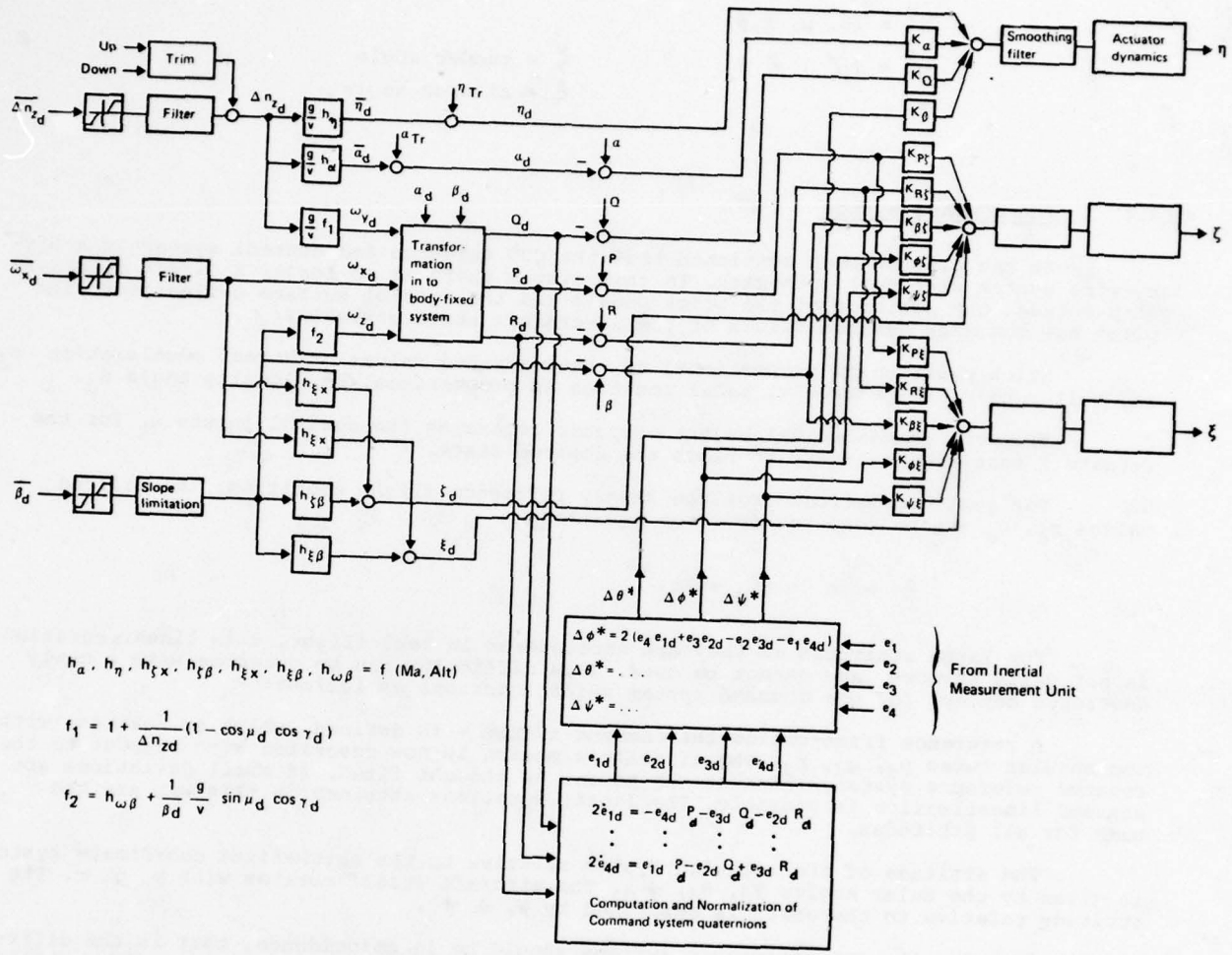

Fig. 15 CCV-Guidance and Control System (Schematic)

They are stored in the computer memory and used according to the actual Mach number and altitude. Between the reference points the coefficients are linearly interpolated.

The initially computed feed back coefficients had to be corrected for the effects of filters and actuator dynamics in order to fulfill the requirements of the MIL Spec F 8785 B. Below, some examples for damping ratio and natural frequency w_n of the short period oscillation and the dutch roll mode that finally resulted are given.

		Short period	Dutch roll
M = 0.3 Alt = sea level	unaugmented	$\zeta = 0.29$ $\omega_n = 1.7$	$\zeta = 0.02$ $\omega_n = 2.0$
	augmented	$\zeta = 0.64$ $\omega_n = 2.0$	$\zeta = 0.63$ $\omega_n = 2.3$
M = 0.6 Alt = 5000 ft	unaugmented	$\zeta = 0.23$ $\omega_n = 3.9$	$\zeta = 0.06$ $\omega_n = 3.2$
	augmented	$\zeta = 0.61$ $\omega_n = 5.5$	$\zeta = 0.62$ $\omega_n = 4.3$
M = 0.9 Alt = 5000 ft	unaugmented	$\zeta = 0.27$ $\omega_n = 5.9$	$\zeta = 0.06$ $\omega_n = 4.8$
	augmented	$\zeta = 0.54$ $\omega_n = 7.6$	$\zeta = 0.60$ $\omega_n = 7.0$

The results obtained for the other reference points were similar. Here one remark is necessary: To take the MIL F 8785 B as a guideline for the design is not very satisfactory because this specification was not written for aircraft with complex fly-by-wire control systems. It will be the task of future research work to find more suitable requirements.

3.5 Results from computation and simulation

Due to an unforeseen slippage in the time schedule of our flight test program most of the result we can present here are from computation and simulation.

In a linear analysis (eigenvalue computation) it was checked for the whole flight envelope that with the CCV-system for all c.g.-positions (most forward and most aft) the requirements of the MIL Spec regarding damping ratio and natural frequency are fulfilled. A comparison with the basic damper system showed equal or better results for the short period mode and a significant improvement for the dutch roll mode with CCV.

A parameter sensitivity study showed that no problems are to be expected in this respect.

The new command system was tested in a nonlinear simulation with fast ramp inputs in Δn_{z_d}, ω_{x_d} and β_d. When these tests proved to be satisfactory the whole system was "flown" by test pilots on a fixed-base simulator in order to get their opinions on the unfamiliar new control system.

The simulator "flights" led to some modifications but the basic structure of the control system was not changed. For example the pilots asked for a trimming device (trim button) in pitch-expecially for the approach phase. This had been thought unnecessary in an acceleration (rate) command system.

Generally, pilot comments were that the new system could be flown without difficulty. Comments were very favourable with regard to the good turn coordination (small sideslip) that is reached with the new control system.

A handling qualities analysis (defined input signals in pitch and roll) confirmed pilot comments. Behaviour in pitch was similar to the aircraft with damper whereas improvements were reached in the lateral motion. In Fig. 16, 17, 18 some roll manoeuvres for different Mach number and load factor are shown.

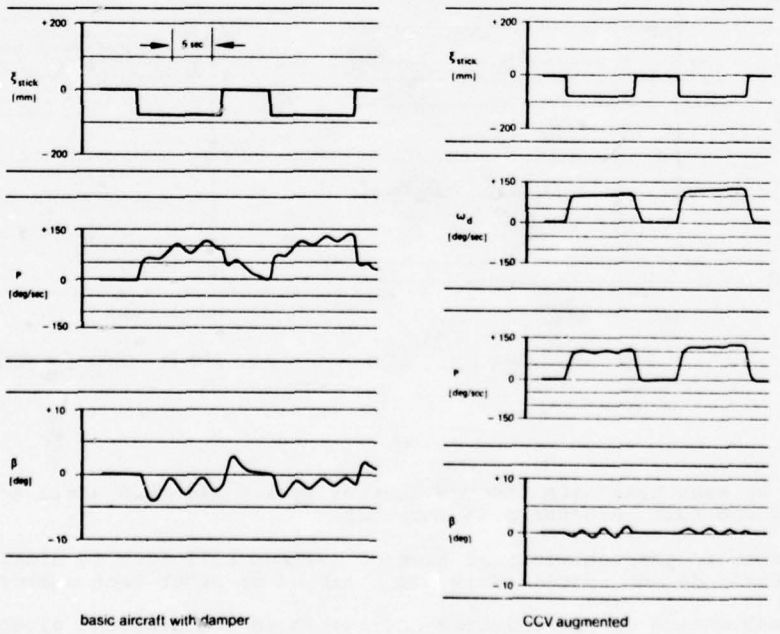

Fig. 16 FULL ROLLS AT M = 0.6 / 20 000 ft 1g

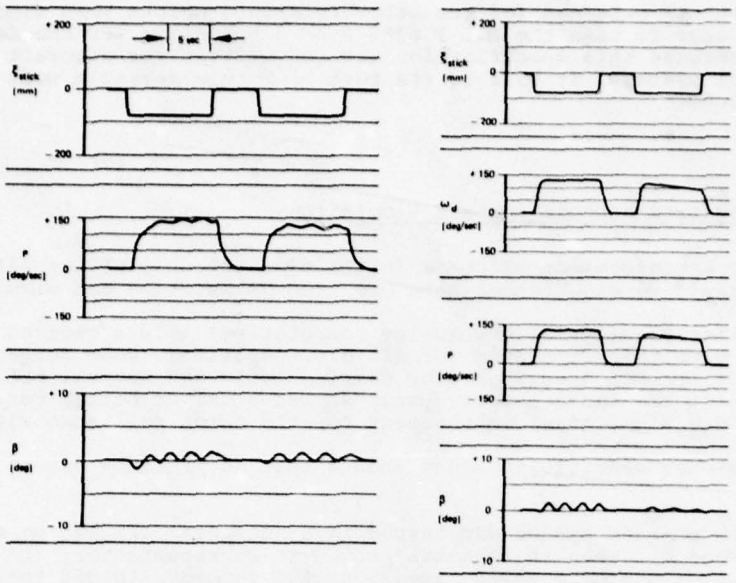

Fig. 17 FULL ROLLS AT M = 0.9 / 20 000 ft 1g

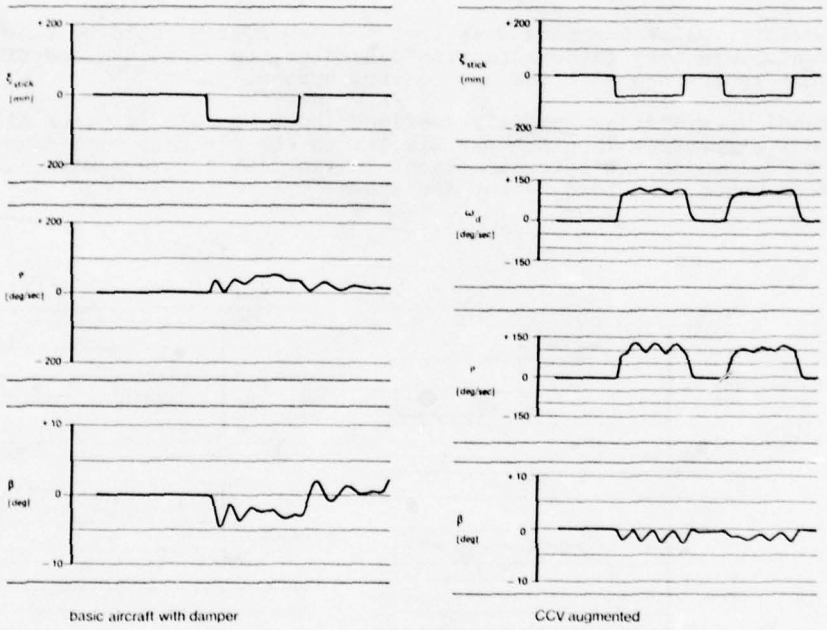

Fig. 18 FULL ROLLS AT M = 0.9 / 20 000 ft FROM 3 g PULL-UP

It can be seen that with the CCV control system sideslip angle ß is partly considerably smaller and roll response p is smoother.

Remarkable is the behaviour at high g: maximum roll rate is significantly higher than with the basic damper system. This was observed at other Mach numbers as well.

One disadvantage of the existing CCV-system is the somewhat slower initial response which became evident when T_{90} (time to reach 90° bank) was computed. This slower initial reaction is due to the phase lag introduced by the slow sampling computer and the smoothing filter in front of the series actuator.

A PIO-analysis indicates that because of this additional phase lag there might be a problem in the roll axis during landing approach. This has to be checked by flight test. In pitch no PIO-problem is expected.

4. FLIGHT TEST RESULTS

Up to now 25 flights have been conducted with the complete CCV-FCS installed and operating. These flights were devoted to shake-down flight testing of the modified aircraft, recalibration of the aerodynamic sensors, open-loop flight testing of the CCV-FCS, and flight testing in the direct link control mode. Fig. 19 shows the CCV-F104 during one of these flights.

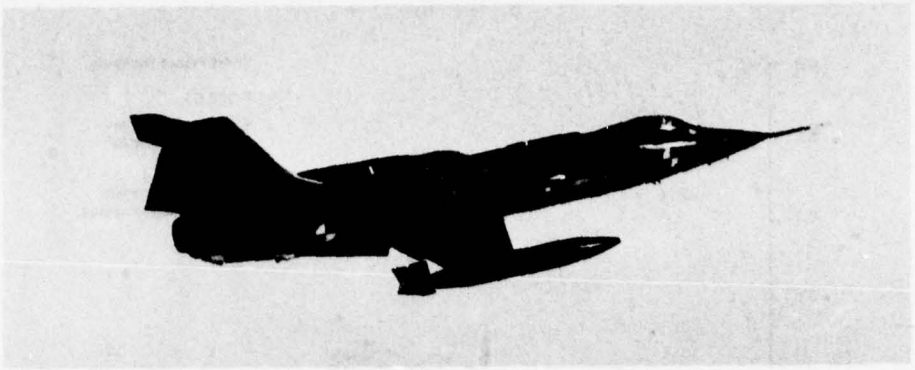

Fig. 19 . The CCV-F 104G in Flight in the Configuration B1

Due to the slippage in the program, the final step of the B1 test phase, namely closed-loop flight testing of the CCV-FCS, has not been achieved as yet. As a consequence the original intention of presenting a comparison between the predicted stability and control characteristics of the F104G augmented by the CCV-FCS and the actual aircraft behaviour has to be modified somewhat. The comparison between the flight test results and predicted aircraft behaviour will be made on the basis of the clean F104G with and without artificial damping. This gives an indication of the validity of the simulator results described in the previous section.

4.1 Longitudinal Motion

Fig. 20 shows the short period frequency of the clean airplane in configuration B1 at 15 000 and 36 000 ft altitude in comparison to the predicted values. The agreement is quite good at all Mach numbers.

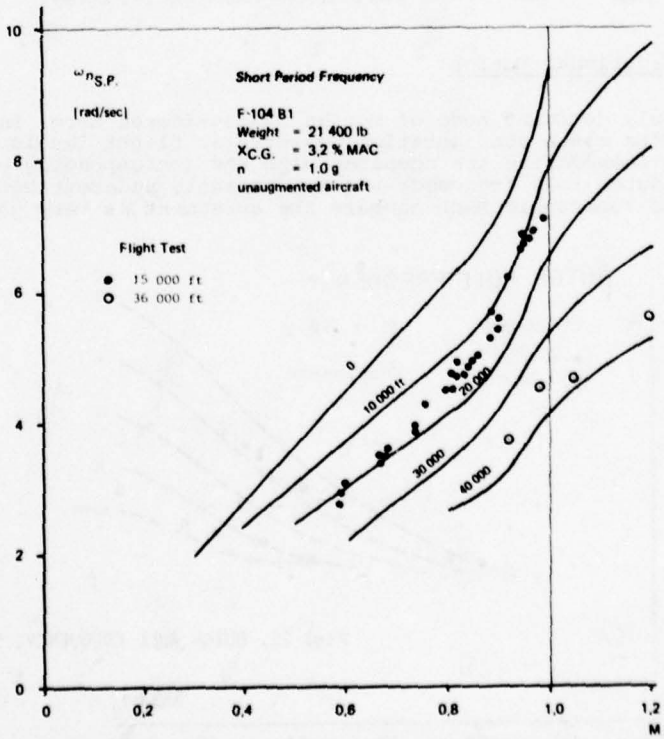

Fig. 20 SHORT PERIOD FREQUENCY,CONFIGURATION B1, CLEAN

The corresponding comparison of the short period damping with and without pitch damper is shown in Fig. 21. As is to be expected, the results for damping scatter more than those for frequency. Within the accuracy of the test results the agreement is again quite good with the exception of the high subsonic speed range ($0.92 < M < 1,0$) where the measured damping is less than predicted and the testpoints for $M = 1,05$ where the opposite is true. This is most likely caused by the addition of the large fairings above the wing roots. Lift loss in this region and the associated reduced downwash at the tail are qualitatively in accordance with the increased frequency and reduced damping at high subsonic speeds.

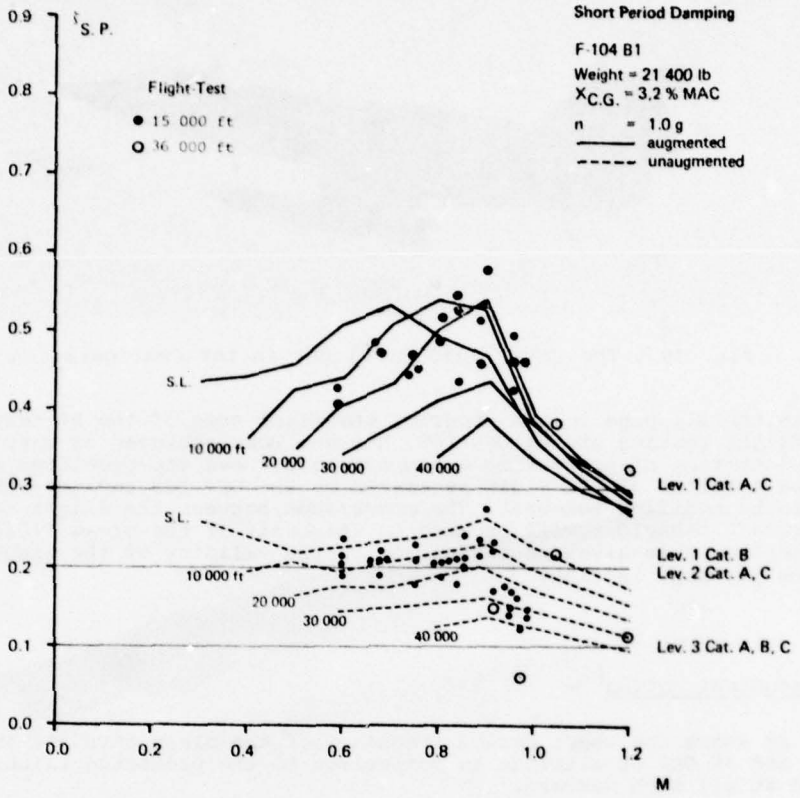

Fig. 21 SHORT PERIOD DAMPING, CONFIGURATION B1, CLEAN

4.2 Lateral / Directional Motion

As before, only dominant mode of motion is considered here. In Fig. 22 the dutch-roll frequencies of the clean configuration measured at flight levels 100 and 360 with the roll/yaw dampers inoperative are compared with the corresponding predicted values. At subsonic speeds the dutch roll frequency was consistently underestimated by approximately 6 %. At transonic and supersonic Mach numbers the agreement is very good.

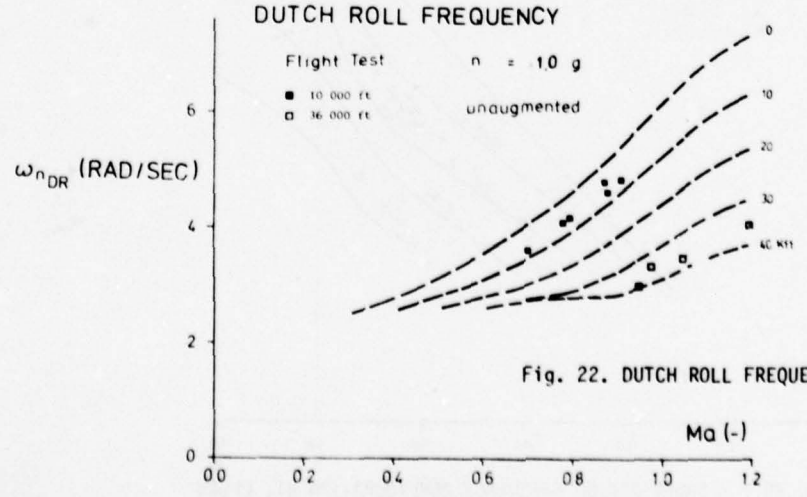

Fig. 22. DUTCH ROLL FREQUENCY, CONFIGURATION B1, CLEAN

Fig. 23 compares the measured dutch roll damping ratios for the clean configuration with dampers on and off at 10 000 and 36 000 ft altitude with the analytical predictions. For the unaugmented aircraft the damping ratio was generally underestimated by approximately 0,03 at subsonic speeds. At supersonic Mach number a better agreement was obtained.

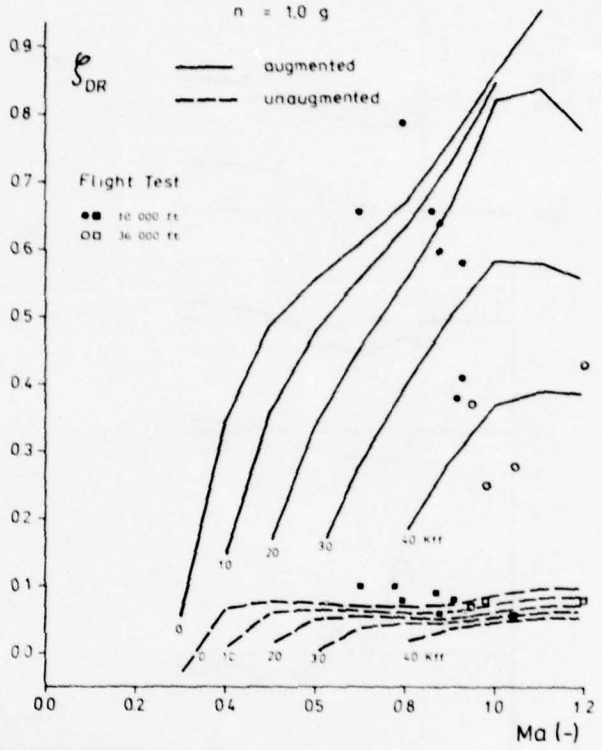

Fig. 23 DUTCH ROLL DAMPING, CONFIGURATION B1, CLEAN

The rapid reduction in damping of the augmented aircraft above M = 0.9 is indicative of a significant reduction in rudder effectiveness caused by shock-induced flow separation in the region of the actuator fairing that covers the lower half of one side of the fin. It is interesting to note, that this transonic phenomenon is considerably less pronounced at high altitude i.e. at large values of the parameter (boundary layer thickness)·(streamwise curvature). This is in accordance with the results of Pearcey and Osborne.

4.3 Switch-Over from the Electrical to the Mechanical Control Mode and vice versa

For a fly-by-wire FCS with mechanical back-up the reliability and flight mechanical safety of the switch-over-process from one system to the other is of utmost importance.

It is important that no large step inputs to the control surfaces are introduced especially at high dynamic pressure and low altitude. In order to avoid such steps switch-over is not instantaneous. During a preselectable time period the computer synchronises the CCV-actuator with the mechanical linkage. After a preselectable time delay which is presently set at 1 second the systems are switched over. Switch-over is completely independant of the computers.

The functioning of the switch-over unit was tested during the first fly-by-wire flights in the direct link mode. The results were very satisfactory. Even after deliberate mistrims only moderate transients occurred. Fig. 24 shows the transient for a minstrim of 1.2° stabilizer angle and a synchronisation time of 0.1 sec. at an equivalent airspeed of 400 knots. During switch-over no corrective action was taken by the pilot. Under these conditions the maximum transient was $\Delta n = 0{,}65$ g.

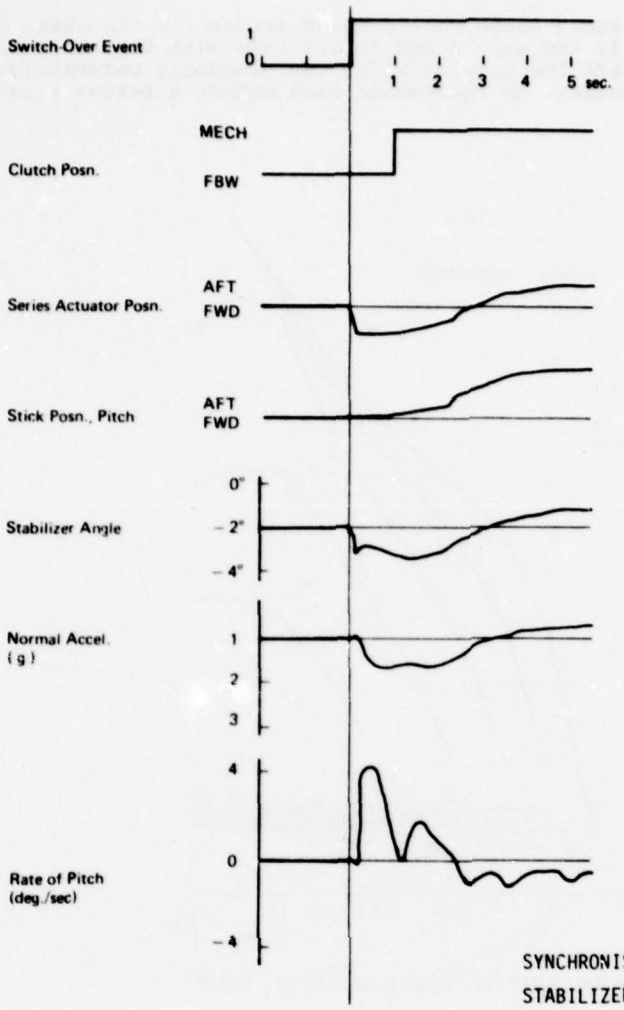

Fig. 24

SYNCHRONISATION TRANSIENT FOR A MISTRIM OF 1.2°
STABILIZER ANGLE AT 400 KEAS

5. CONCLUSION

For a F-104G CCV test aircraft an advanced, integrated, full authority fly-by-wire control system has been developed. It has been decided for several reasons to choose a digital system. Therefore the realization of a new unfamiliar complex command system was possible.

The system was "flown" by test pilots on a fixed-base simulator. The results were promising.

Data received from shake-down flights and fly-by-wire direct link flights confirm the validity of the theoretical description underlying the control law design. Therefore similar results as those obtained from simulation are expected from the flight tests which will begin within the next weeks.

6. REFERENCES

1 Kubbat, W.: A Quadruredundant Digital Flight Control System for CCV Application
AGARD-Symposium Flight Mechanics Panel and Guidance and Control Panel,
16.10.1974 Paris
MBB-UFE report 1116 (Ö)

2 Kubbat, W. and Oesterhelt, G.: Entwurf von Regelungssystemen mit Hilfe von Computer Aided Design und ihre Anwendung
DGLR-Jahrestagung, Kiel, 17.-19.09.1974
MBB report GD-8-74 (Ö)

DESIGN GUIDANCE FROM FIGHTER CCV FLIGHT EVALUATIONS

By

Frank R. Swortzel
Air Force Flight Dynamics Laboratory (FGX)
Wright-Patterson AFB, Ohio 45433 (USA)

and

Dr. Jack D. McAllister
General Dynamics Corporation - Fort Worth Division
Fort Worth, Texas 76101 (USA)

SUMMARY

Flight testing of the Fighter Control Configured Vehicle (CCV) marked the first exploitation of six degree-of-freedom flight control concepts for "a new way to fly". General Dynamics under contract to the Air Force Flight Dynamics Laboratory conducted an 87 flight, 125 flight hour test program on a modified YF-16. Validation of the new control concepts was accomplished and significant capabilities to improve overall mission effectiveness of fighter aircraft were demonstrated. This program included pilot evaluation of the CCV control modes applied to air-to-air and air-to-ground mission oriented tasks.

The primary thrust of the Fighter CCV Program was to generate uncoupled six degree-of-freedom aircraft motion. Resulting control features included direct force control, independent fuselage aiming and translation, maneuver enhancement and gust alleviation. Performance benefits of relaxed static stability were also evaluated.

Early flight testing demonstrated that the modes function in flight, produce the desired responses and have good handling qualities. Subsequent flight testing identified specific benefits provided by the unique control modes in air-to-air and air-to-ground pilot tasks. These operational evaluations identified the desirability for automated operation of the control features, simplified pilot controllers, and tailoring the mode implementations to the specific combinations of pilot task and flight regime of interest.

1. INTRODUCTION

The continuing development of active control technology has paved the way for expanding traditional aircraft design boundaries and exploiting the performance and mission effectiveness capabilities of Control Configured Vehicles. The Air Force Flight Dynamics Laboratory (AFFDL) has conducted a continuing active control technology development thrust that has produced a number of flight test validation programs. The recent Fighter Control Configured Vehicles (CCV) Program was one which focused on development and validation of advanced flight control technology that could significantly contribute to improved maneuverability and overall mission effectiveness of fighter aircraft. The Fighter CCV Program was conducted by General Dynamics, Fort Worth Division, under contract to the AFFDL. Mr. F.R. Swortzel, AFFDL CCV Program Manager, and Dr. J.D. McAllister, General Dynamics CCV Program Manager, have collaborated to produce this summary of the Fighter CCV development and flight test, and to provide a discussion of some significant design guidelines developed from the fighter CCV program.

2. FIGHTER CCV PROGRAM DESCRIPTION

In December 1973, the AFFDL contracted to General Dynamics to develop a demonstrator CCV (Figure 1) with features that focused on specific new control degrees of freedom and relaxed static stability (RSS). This program offered the first true test of decoupled, six degree-of-freedom (6DOF), flight path control. The ability to independently control vehicle translational and rotational degrees of freedom by employing independent control surfaces for each response axis, can create unique maneuvering capabilities: direct lift and sideforce, fuselage elevation and azimuth pointing independent of flight path, vertical and lateral translation, and more precise maneuvering control. These capabilities, when applied to the fighter air-to-air and air-to-ground attack tasks, have potential for significant improvements in maneuverability, weapon delivery and survivability. The Fighter CCV Program objectives were to implement decoupled 6DOF control concepts and quantify the benefits of relaxed static stability on a YF-16 aircraft, and to then validate the resultant performance advantages of these control technology features through flight testing. The broader objective of the program was to provide user/builder acceptance of CCV control technology, design criteria, and a better defined technical base for applications and additional experiments.

3. CONFIGURATION DEVELOPMENT

An extensive configuration selection process, airframe and flight control system design and modification, and ground testing were performed by General Dynamics leading to the flight test program (Figure 2). Results of the total program are documented by References 1, 2 and 3. Configuration selection centered on choosing an approach using either horizontal or vertical canard surfaces to provide the aerodynamic force generators to decouple aircraft motions. Table 1 presents a comparison of the two configuration approaches which formed the basis of selection of the vertical canard configuration for development. General arrangement of the Fighter CCV is shown in Figure 3.

The CCV YF-16 configuration changes are illustrated in Figure 4. The only external change to the aircraft is the addition of the inlet mounted canards. The capability to symmetrically deflect (± 15 degrees) the wing trailing-edge flaperons was provided without the need for mechanical modification. Fuel system changes were made to accomplish the desired, precise inflight center-of-gravity (c.g.) control to investigate RSS in terms of both handling qualities and performance variations with c.g.

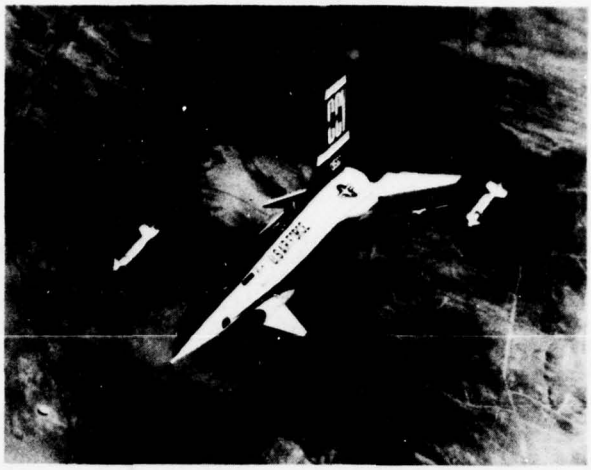

Figure 1 CCV YF-16

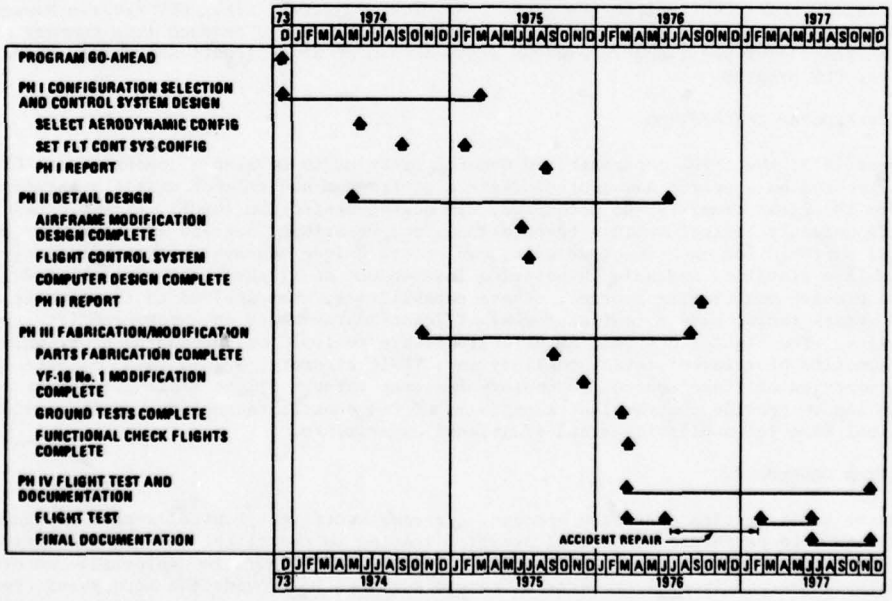

Figure 2 Program Schedule

ITEM	VERTICAL CANARDS	HORIZONTAL CANARDS
• Direct Lift	No Adverse Effects	Double Trimmed ΔC_L Available from the Trailing Edge Flaps
• Direct Side Force	Superior at High Speeds and Low α's at Low Speed	Differential Deflection Provides Usable Control to High α
• Relaxed Longitudinal Stability	Small Fwd Aerodynamic Center Shift	Fwd ac Shift Plus Increased Control Power Yield ~ 18% MAC Additional RSS Capability
• Directional Stability	Generally Better at Critical High α's	Strong Variation in Stability with Canard Deflection
• Airframe & Systems Changes	Easily Accomplished within the Capabilities of the Basic Fuselage	Requires Major Equipment Relocation and Structural Changes
• Wind Tunnel Testing	Within Scope of the Basic Program	Significant Additional Testing Required to Develop Configuration

Table 1 Comparison of Configuration Approaches

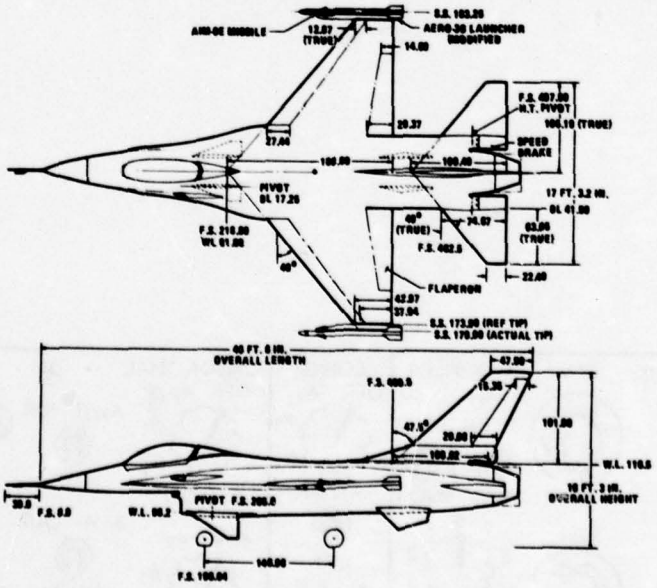

Figure 3 Fighter CCV General Arrangement

The CCV control laws were generated in an auxiliary flight control computer. The basic YF-16 flight control system was retained as a baseline to assure high operational reliability and provide suitable closed loop compensation for the statically unstable aerodynamic characteristics. A design requirement was to always be able to disconnect the CCV auxiliary computer signals and revert to the basic airplane control system. Control system modifications allowed the pilot to select the CCV modes of his choice through a control panel (Figure 5). A description of the CCV YF-16 features follows.

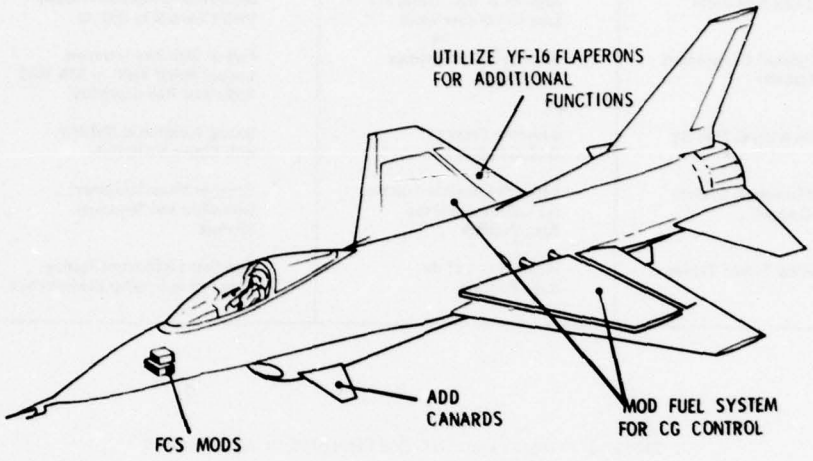

Figure 4 Fighter CCV Configuration Approach

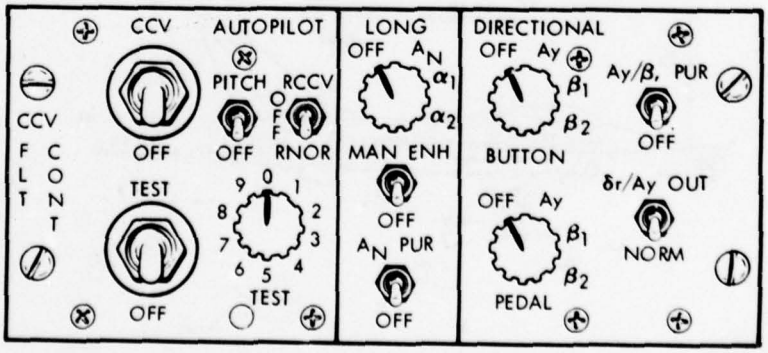

Figure 5 CCV Mode Control Panel

4. DIRECT FORCE CONTROLS

Direct force control is provided through multiple control surface inputs about a single axis so that trimmed aerodynamic force levels can be varied independent of angle of attack or sideslip. Command of flap deflection with coordinated horizontal tail deflection produces Direct Lift that controls vertical flight path at constant angle of attack (Figures 6 and 7). Similarly, command of vertical canard deflection with coordinated rudder inputs produces Direct Sideforce that controls directional flight path at zero sideslip angle.

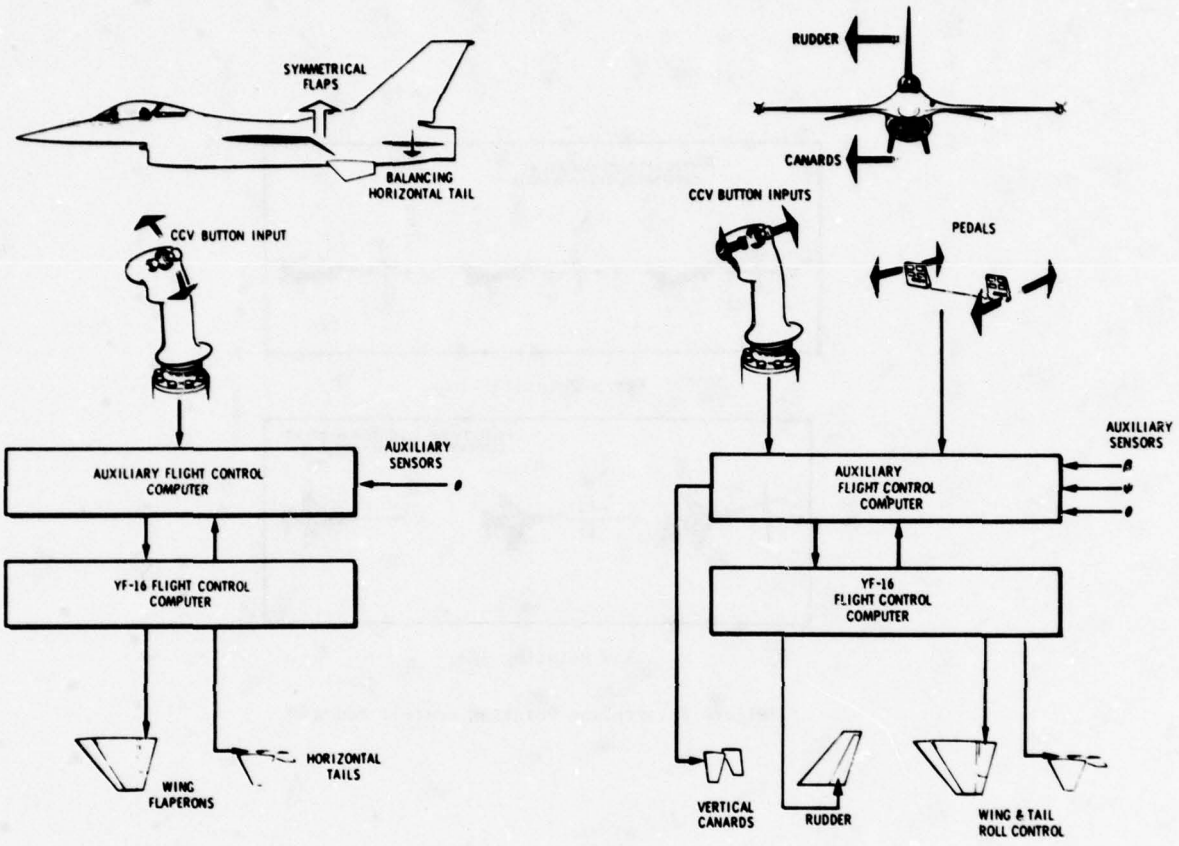

Direct Lift Implementation

Direct Sideforce Implementation

Figure 6 Direct Force Control

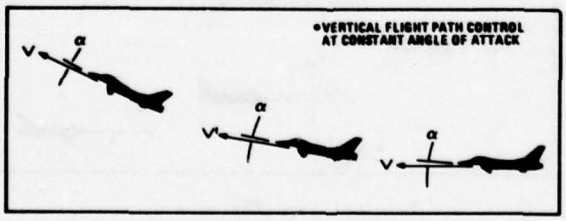

Direct Lift - A_N

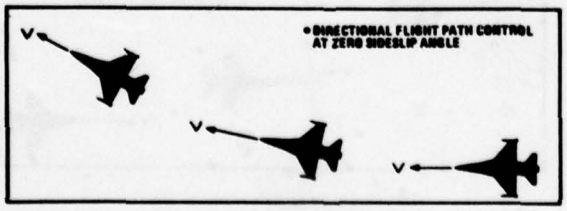

Direct Sideforce - A_Y

Figure 7 Direct Force Control Modes

Alternate use of these paired control surfaces can be made to vary angle of attack or sideslip independent of trimmed aerodynamic force levels. Maintaining constant flight path, pitch and yaw attitude can be varied to provide fuselage pointing (Figure 8). Vertical and lateral translation modes can be mechanized by altering the corresponding direct force mode such that body axis angular position is essentially invariant (Figure 9).

On the CCV YF-16, each of these modes was implemented through open loop command by a two-axis, proportional force controller that replaced the trim switch on the sidestick controller. Input commands were proportional over a ±3 pound force range. Lateral mode inputs could also be input through the rudder pedals.

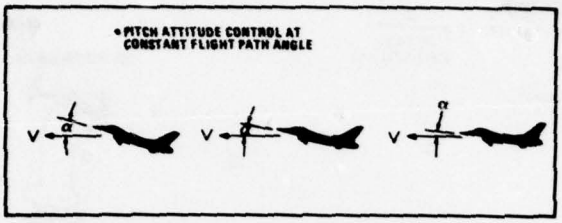

Pitch Pointing - α_1

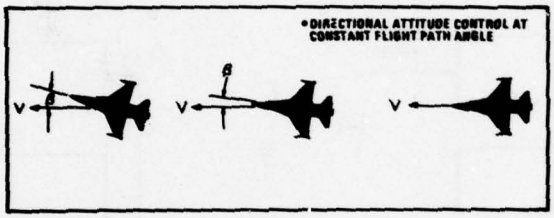

Yaw Pointing - β_1

Figure 8 Airplane Pointing Control Modes

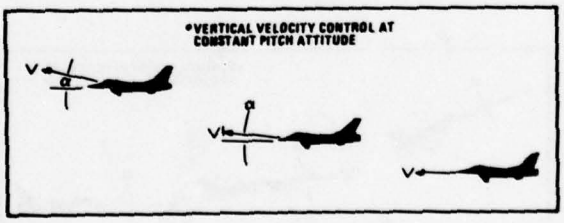

Vertical Translation - α_2

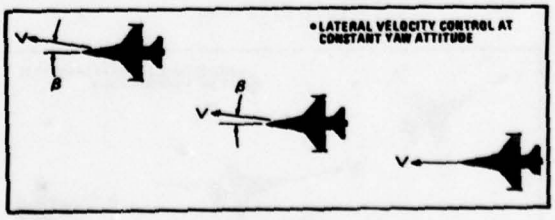

Lateral Translation - β_2

Figure 9 Airplane Translation Control Modes

5. BLENDED FORCE CONTROLS

The one closed-loop control mode implemented on the CCV YF-16 was called Maneuver Enhancement (M.E.). Direct Lift was blended into the basic longitudinal control loop to improve transient response characteristics. Flap deflection was commanded by the error between pilot commanded normal acceleration and sensed aircraft acceleration(s). The result was quickened g response, a better balance between g and pitch rate response, and a measure of gust alleviation. The aircraft's response to turbulence appears as uncommanded g and Maneuver Enhancement opposes the gust response. Figure 10 illustrates the blended control modes, and Figure 11 shows its mechanization. The manual direct force modes were usable, individually or in combination, with Maneuver Enhancement engaged.

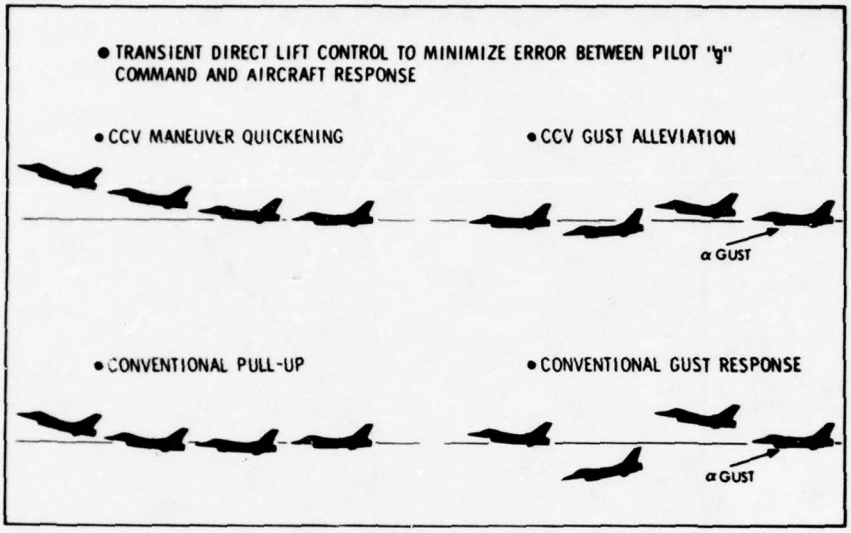

Figure 10 Blended CCV Control Mode

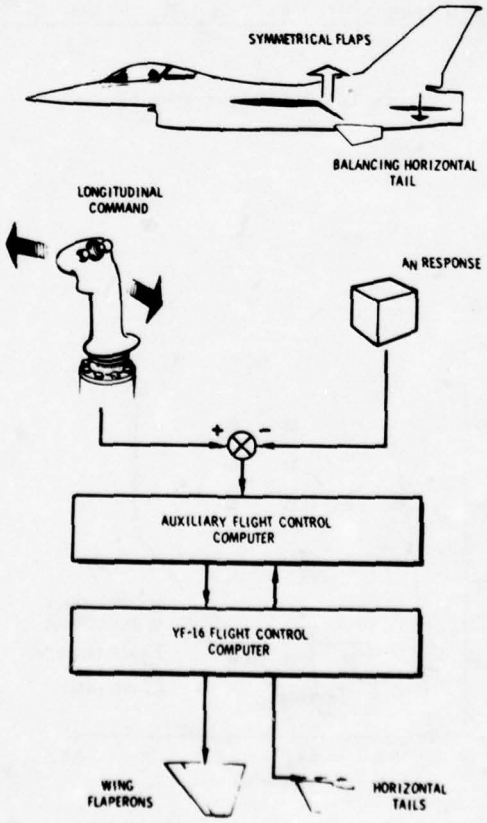

Figure 11 Maneuver Enhancement Implementation

6. CCV FLIGHT TESTING

A comprehensive flight test program consisting of 87 test flights (125 flight hours) was conducted during the periods of March-June 1976 and February-June 1977 (Figure 12). The break in testing resulted from a landing accident that required extensive repair of the airplane. This accident and other flight aborts were caused by various malfunctions not associated with the CCV modifications or features.

A phased flight test program was conducted; the first phase, system checkout, verified CCV hardware operation and cleared the flight envelope (Figure 13). Engineering evaluations established CCV mode gain characteristics and maneuver capabilities. In conjunction with the gathering of engineering data, Air Force and Contractor Project Pilots explored use of the unique decoupled control modes to accomplish basic piloting tasks, generally initiated from lg trimmed flight. These maneuver evaluations were the first step in assessing how well the pilot could actually utilize the new control modes.

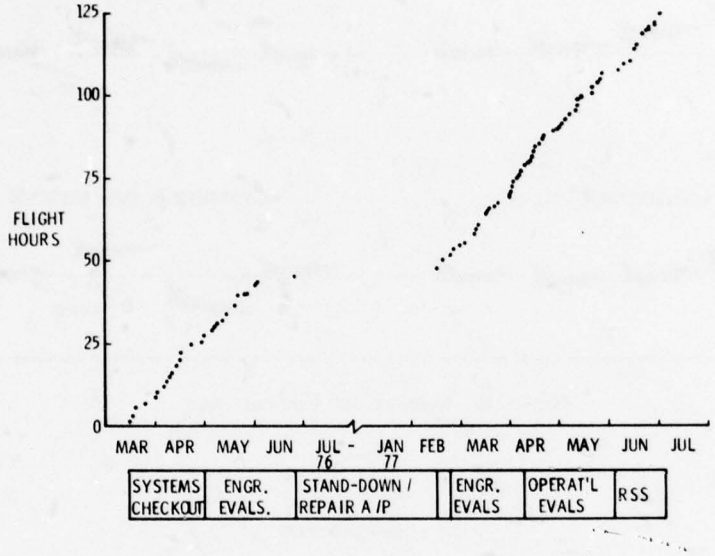

Figure 12 CCV Flight Testing

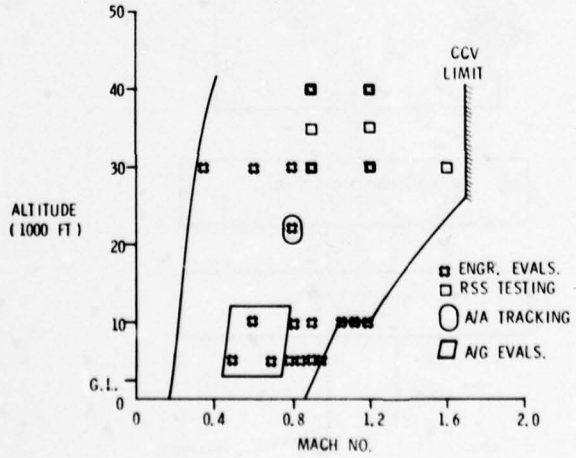

Figure 13 Primary CCV Test Points

All of the CCV control modes were 100 percent functional; no in-flight failures were experienced during the test program. Good response characteristics were obtained for each mode. Flight derived optimization of surface interconnect gains and bias signals to the basic flight control computer was effective in eliminating minor mode impurities. A lag was added to the maneuver enhancement command path to slightly slow the normal acceleration buildup for rapid pilot inputs.

Evaluations of basic flight maneuvers using the new modes revealed that the direct lift and sideforce modes are the most powerful and easiest for pilot control. Simple pointing tasks were quickly and accurately accomplished with the pitch and yaw pointing modes. Small position corrections were readily adapted to formation flight using either the vertical translation or the direct lift mode. For large position changes (greater than about 500 feet) the direct lift and sideforce modes were preferred due to quicker responses than those of the translation modes. The benefits of automatic maneuver enhancement for precision pilot control are illustrated in the tracking comparison of Figure 14. These data, from back-to-back handling qualities runs during tracking on the same flight, exhibited several key effects. Stick force inputs are reduced in magnitude with maneuver enhancement active - an indication of reduced pilot workload. The normal acceleration response with maneuver enhancement active more directly follows stickforce variations - this corresponds to pilot comments that maneuver enhancement provides a very precise and highly predictable longitudinal control mode. The improvements in tracking performance are evident in the smoother angle of attack responses and 25 percent reduction in rms pitch rate response. The small additional control surface activity automatically provided by the CCV commands to the horizontal stabilizer and flaperons result in these significant improvements.

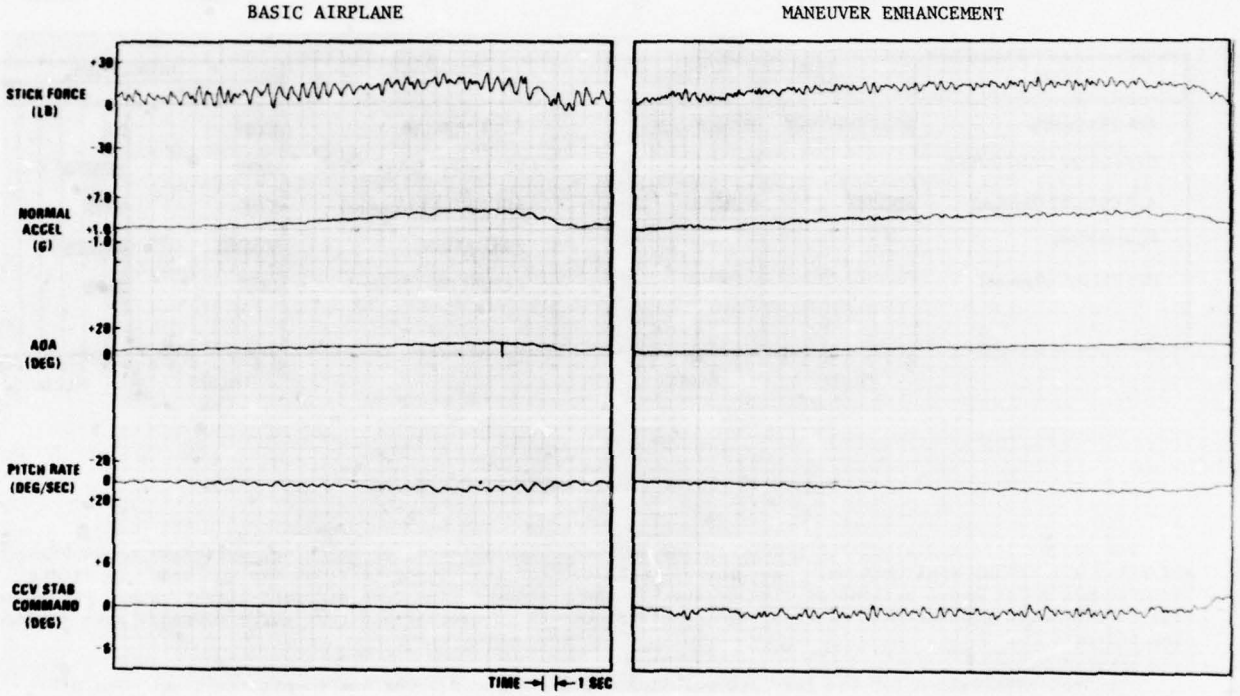

Figure 14 Wind-Up Turn Tracking Comparison - 0.8M 22,000 Ft (6700 M)

7. OPERATIONAL APPLICATIONS

The demonstrated capability to decouple the aircraft degrees of freedom with a mechanization readily controllable by the pilot enabled considerable emphasis to be placed on "operational" type evaluations. This was accomplished in two subphases: first air-to-air tasks and then air-to-surface tasks. Nine flights were used to explore and validate specific air-to-air tracking tasks with emphasis upon the Handling Qualities During Tracking (HQDT) technique (Reference 4). The formal air-to-air evaluation consisted of two flights by each of three Air Force test pilots in the F-16 Joint Test Force. Information gained by the project pilots during air-to-air development/validation was also included in the resulting data base. Significant information was obtained in three general categories: HQDT statistical data, pilot subjective evaluations of the military potential for the various mode-task combinations, and recommendations for improvements to enable better utilization of the new control modes in operational type tasks for fighter aircraft.

Figure 15 is a summary of the air-to-air endorsements for the various mode-task combinations explored by the six pilots accomplishing two or more air-to-air flights. Because of the short pilot exposure to these "new ways to fly" and the learning curve effects evident from the results of all evaluation flights, potential improvement (rather than demonstrated numerical differences) was the metric used to assess mode-to-mode differences. Each test sequence included runs using the basic YF-16 flight control system mode to establish a firm baseline for qualitative and quantitative comparisons. The pilot-qualitative potential benefits and key measured numerical differences are presented below in this section. Recommended alternate mechanizations are covered under the subsequent Design Criteria and Guidelines section.

Maneuver enhancement was rated as the most beneficial mode for air-to-air operations. Note that the quickened response and improved control precision were found useful for most of the tasks evaluated. The ride quality effects (automatic gust alleviation) of this mode were also considered to be desirable.

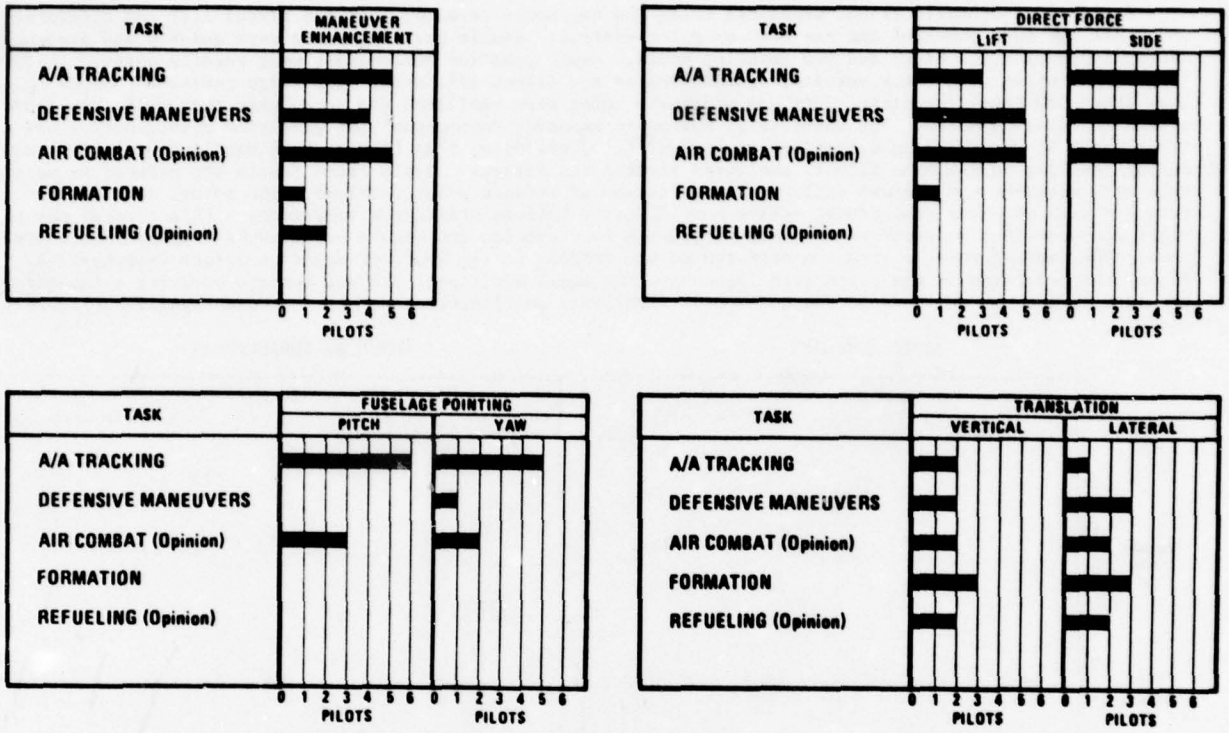

Figure 15 Pilot Endorsements of CCV Modes

The direct lift and sideforce modes (A_N and A_Y) were highly rated for tracking, defensive maneuvering, and gross air combat applications. The general technique for tracking situations was to "beep" in direct force commands for short periods of time to quickly and precisely fine tune aircraft flight path. For offensive or defensive gross combat maneuvering the technique was to use large direct force commands over extended time periods.

The best application for the fuselage pointing modes (α_1 and β_1) was air-to-air tracking. The pilot consensus was that an automatic implementation (such as an integrated fire control/flight control mechanization) is the preferred method of achieving the full potential of these modes.

The preferred air-to-air application for the vertical and lateral translation modes was formation flight. The potential for other applications shown in Figure 15 was contingent upon providing major increases in steady-state translation velocities and quicker initial responses.

The Air Force project pilot found the direct force modes to significantly improve tracking precision while following the target aircraft through a windup turn, Figure 16. A "beeping" technique of quick, short time, direct force commands was used to quickly and precisely eliminate small flight path errors as they developed during the tracking runs. Note also that use of the automatic maneuver enhancement mode resulted in a very significant improvement in tracking precision over that obtained using the basic flight control system. This improved precision with maneuver enhancement was also generally evident in the scored HQDT runs of the other pilots. Figure 17 summarizes statistically the tracking error data obtained from all pilots for each of the pertinent flight control modes. These data substantiate the pilots opinion that two HQDT flights per pilot were not sufficient to span the training/learning curve phase of tracking with the advanced control modes. However, as discussed in the following section, this brief exposure was sufficient to obtain major insights into the types of task-oriented mechanizations desired for CCV air-to-air military usages.

The air-to-ground operational evaluation concentrated upon the tasks indicated in Figure 18. Some evaluation pilots elected to include other maneuvers such as pop-up and pitch-back deliveries and simulated cross wind landings. The rating scheme employed and pilot sample was the same as discussed previously for the air-to-air evaluation.

The rating summary (Figure 18) graphically demonstrates the dominant usefulness of the direct sideforce (A_Y) mode. Consensus improvement ratings for the A_Y mode were given for eight of the eleven tasks, a remarkable preference since the mode has not, as yet, been optimized for specific air-to-ground tasks or air-to-ground operations in general. It is interesting to note that usefulness of the direct lift (A_N) mode was

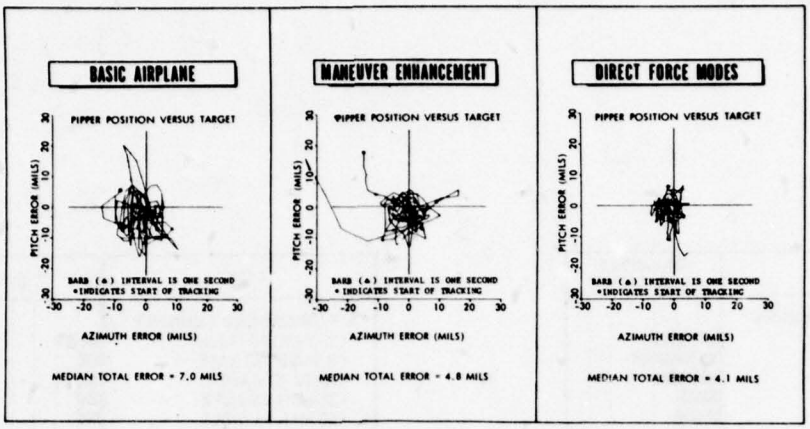

Figure 16 Wind-Up Turn Tracking Comparison - 0.8M 22,000 Ft (6700 M)

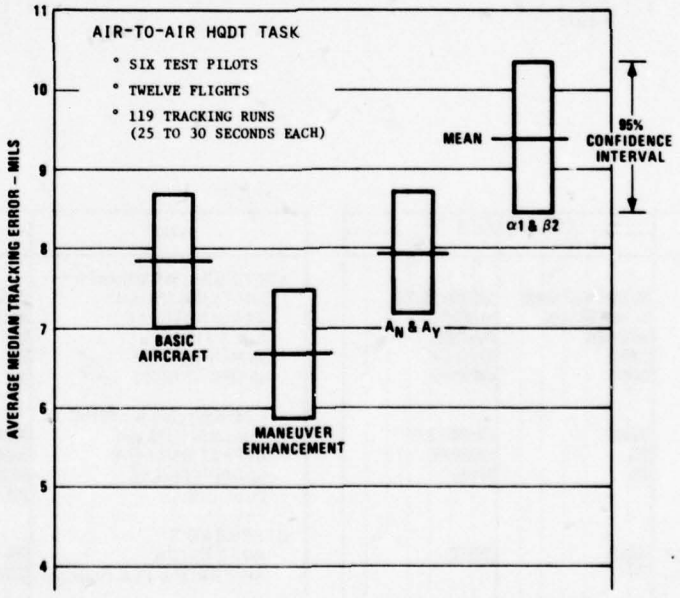

Figure 17 Tracking Error Comparison of CCV Modes

rated much lower. Subjective pilot comments were that the basic longitudinal control system was quite satisfactory for the tasks flown. The notable benefit for the direct lift mode was the quickening of pull-up maneuvers.

Ratings for the lateral and vertical translation (β_2 and α_2) modes exhibit similarities to those for A_Y and A_N. Translation laterally has greater potential for air-to-ground than translation vertically. This again attests to the relative ease of accomplishing the tasks with the basic longitudinal control system. Comparison of the ratings for the β_2 and A_Y modes suggest a modes preference for the A_Y mode. However, it must be remembered that the modes are yet to be optimized for specific tasks. Until this is done, both modes should be considered logical for air-to-ground tasks.

Potential use of the fuselage pointing (α_1 and β_1) modes in air-to-ground operations centers around low angle strafing applications. A major side benefit was observed for the α_1 mode. By using nose-down pointing during low angle passes, the minimum altitude while tracking was increased from a nominal 200 feet to about 400 feet. Pilots reported this additional minimum altitude made the runs more comfortable and easier to accomplish. In general, pilots who emphasized the operational technique of gradually working the pipper toward the target to obtain an aiming solution at the simulated firing range rated the pointing modes higher than pilots who continuously aimed at the target throughout the runs. This suggests that the relative ratings between modes for a given task can be strongly dependent upon the details of the operational pilot technique employed.

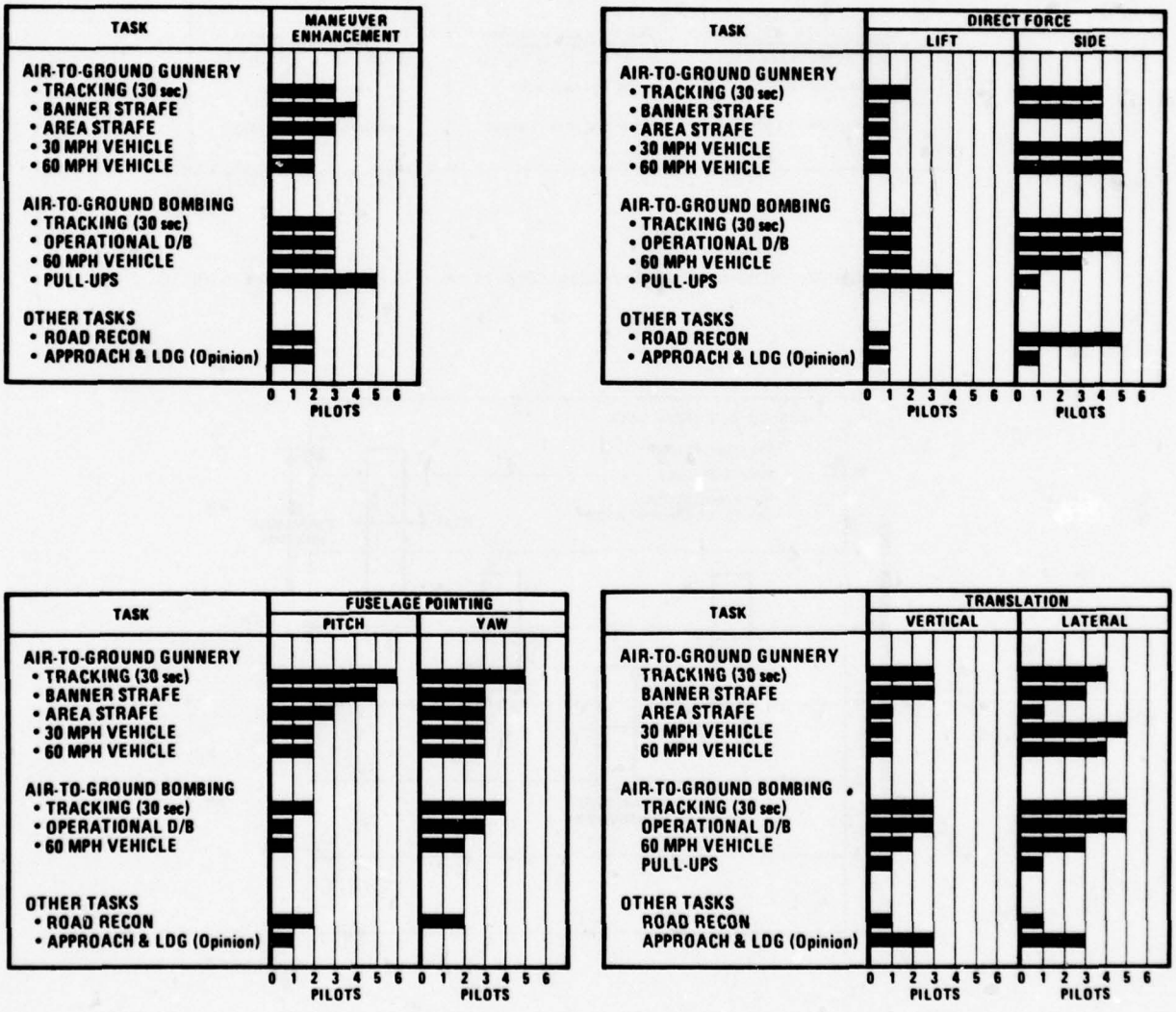

Figure 18 Pilot Endorsement of CCV Modes - Air-to-Ground

In general, the air-to-ground tasks selected for evaluation had only minimal requirements for longitudinal control changes during a run. Hence, the quickening of airplane response to pilot stick commands via automatic maneuver enhancement was generally not required during an air-to-ground run. Five of the six evaluating pilots did affirm the benefits of maneuver enhancement in quickening aircraft response in the pull-ups associated with dive recovery at the end of bombing runs. Several pilots also commented on the gust response attentuation effect of maneuver enhancement. This effect is illustrated by the response data obtained from back-to-back 1g penetrations of low altitude atmospheric turbulence (Figure 19). Note that maneuver enhancement reduces the major normal acceleration transients and increases the primary frequency of the response to atmospheric turbulence. All pilots felt that maneuver enhancement has potential as a gust alleviation feature; however, the majority would desire an improved version over that actually mechanized on the aircraft.

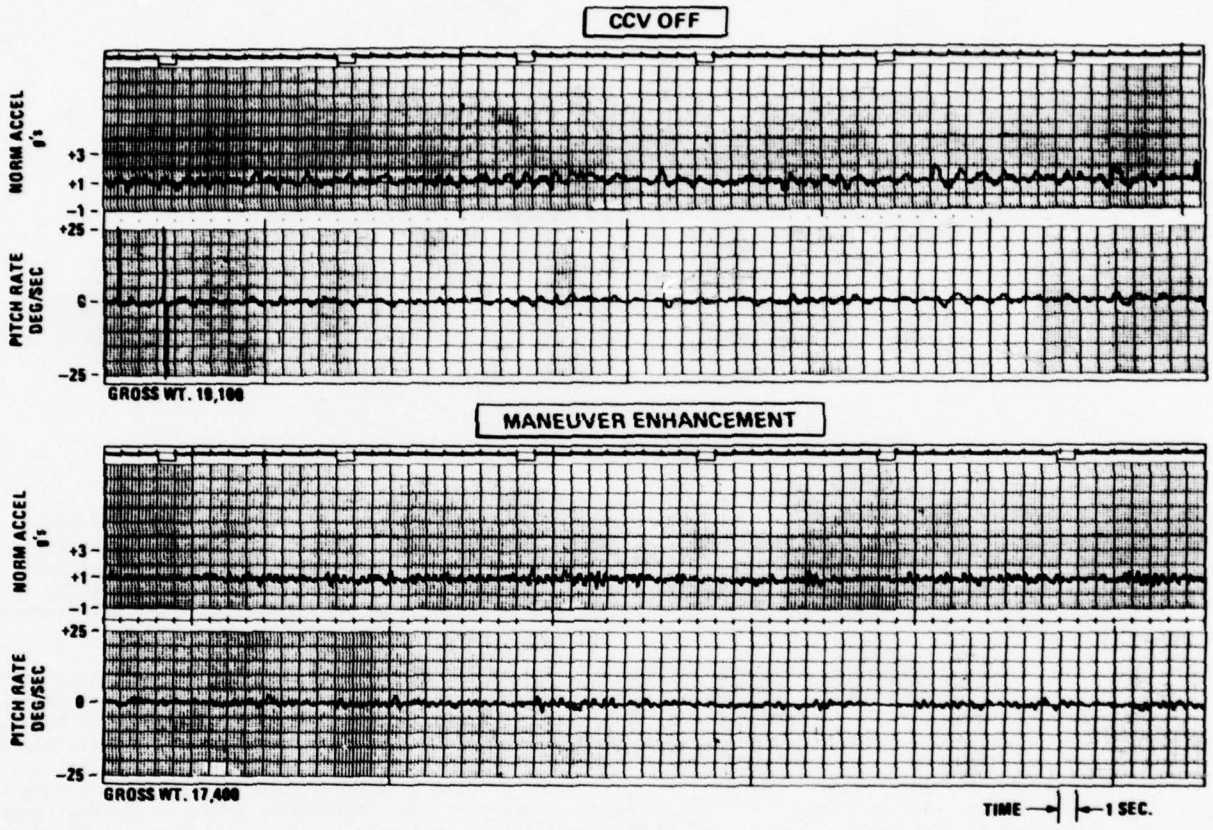

Figure 19 1g Gust Run - 0.85 Mach at 2,000 (610 M) Feet Above Ground Level

8. RELAXED STATIC STABILITY EVALUATIONS

Evaluations of relaxed aerodynamic static longitudinal stability (RSS) was accomplished in two parts. First, with a spin recovery parachute installed, progressively more aft c.g. loadings were checked for handling qualities to establish allowable operating conditions for the subsequent standard performance testing with the spin parachute removed. In both instances, the vertical canards were removed and CCV auxiliary computer deactivated to obtain the basic YF-16 configuration with respect to both aerodynamics and flight control system characteristics.

The YF-16 flight control system provides full fighter aircraft maneuver capability with center of gravity locations as far aft as 35 percent MAC. The approach employed for RSS flight testing was to restrict the test maneuvers (principally to half lateral stick roll rate commands and 18 degrees maximum angle of attack) in order to accomplish the desired RSS test maneuvers at more aft center of gravity loadings. The relationships between the aerodynamic neutral point, RSS test conditions and the pertinent center of gravity limits are depicted in Figure 20. The findings of the RSS handling qualities checks are particularly infor-

mative in terms of the nature and rapidity with which key characteristics can deteriorate as the center-of-gravity is progressively moved further and further aft. These results (obtained from standard stability and control maneuvers, modified split-S performance tests and simulated landing approaches) are best summarized by the pilot qualitative evaluations presented below. Additional technical information is contained in Reference 3, Volume II.

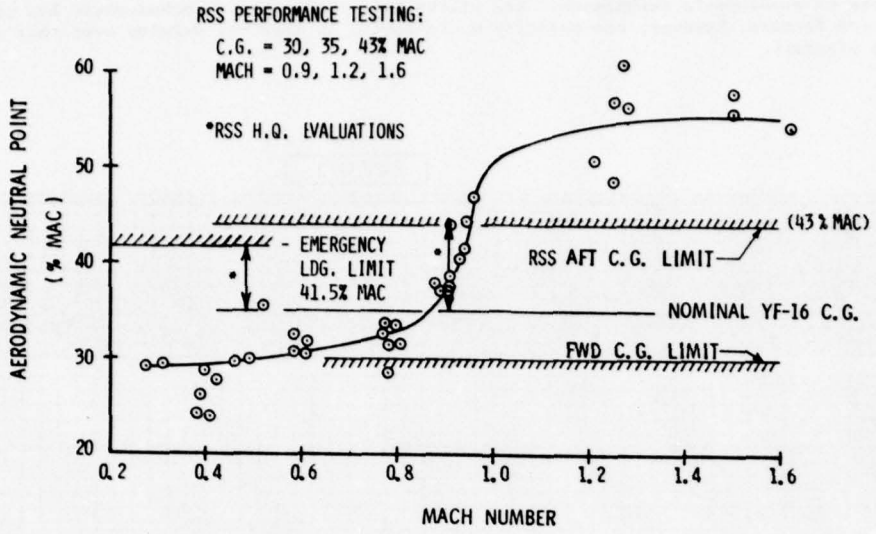

Figure 20 Aerodynamic Neutral Point/C.G. Relationship

In the clean airplane configuration (landing gear retracted), the pilot reported: "A considerable loss of precision in pitch control was evident while operating with the center-of-gravity at 44 percent MAC. Based on the specific changes seen in rolling behavior and the loss of precision in pitch control, the writer believes that the "end point" has been reached as regards aft center-of-gravity testing for this program. The airplane should not be used for subsequent performance testing with the center-of-gravity aft of 43.0 percent MAC."

In the landing configuration, the pilot reported: "The airplane exhibited some rather unpleasant flying qualities in 1g, 9 degrees, and 13 degrees angle-of-attack landing configuration flight with the center-of-gravity at 41.5 percent MAC. A horizontal tail deflection of approximately 8 degrees trailing edge down was required for trim at 1g. Very mild pitch disturbances produced large positive horizontal tail deflections during damping. In this flight condition, the airplane appears to respond very unfavorably to turbulence. Pitch control is very imprecise and the lateral-directional damping is somewhat weak. The piloting task is such that almost constant reference must be made to the angle-of-attack indicator. Based on the test runs flown (pitch-yaw-roll pulses and a simulated landing approach), performing an actual landing with the center-of-gravity at 41.5 percent MAC would be challenging in calm air and quite hazardous in turbulence. Landing configuration flight with the center-of-gravity of 41.5 percent MAC is to be avoided if at all possible and, if no alternative is available, should be approached with caution, especially in turbulence." Previous YF-16 landing experience had shown that approaches with a c.g. of 38 percent MAC were no different than landings at 35 percent MAC, the nominal prototype center-of-gravity. Initial RSS testing at 39 percent MAC confirmed these findings. Thus, a rather abrupt deterioration in handling qualities during landing approach occurred between 39 and 41.5 percent MAC.

Analysis of the in-flight measured RSS performance data trends with c.g. variation confirmed very precisely the predicted data. Here again considerable additional technical data and detailed discussion is provided in Volumes II and III of Reference 3. Taken as a whole in terms of mission performance, the data of Figure 21 graphically illustrate that RSS makes a significant positive contribution to energy efficient maneuvering of modern fighter aircraft.

9. DESIGN CRITERIA AND GUIDELINES

The flight experience gained by experienced test pilots, all with relevant operational military fighter aircraft backgrounds, has provided a technical beachhead for the establishment of design criteria and general guidelines relevant to future applications of active control technology to Fighter Aircraft. The more salient points of the data base documented in Reference 3 are reviewed below.

Mode Authorities - Table II is a consensus summary of the mode authorities desired by the pilots who evaluated in-flight the Fighter CCV Vehicle. The Fighter CCV levels used as a baseline are documented in Reference 3 and typical levels are shown in the subsequent discussion of aerodynamic characteristics and interactions.

Any evaluation of these pilot desires must take due consideration of the fact that in several instances the pilots noted that lesser mode authorities would be quite adequate for specific tasks such as precision tracking and vernier correction of normal aircraft motions. Several trade-off assessments will be necessary

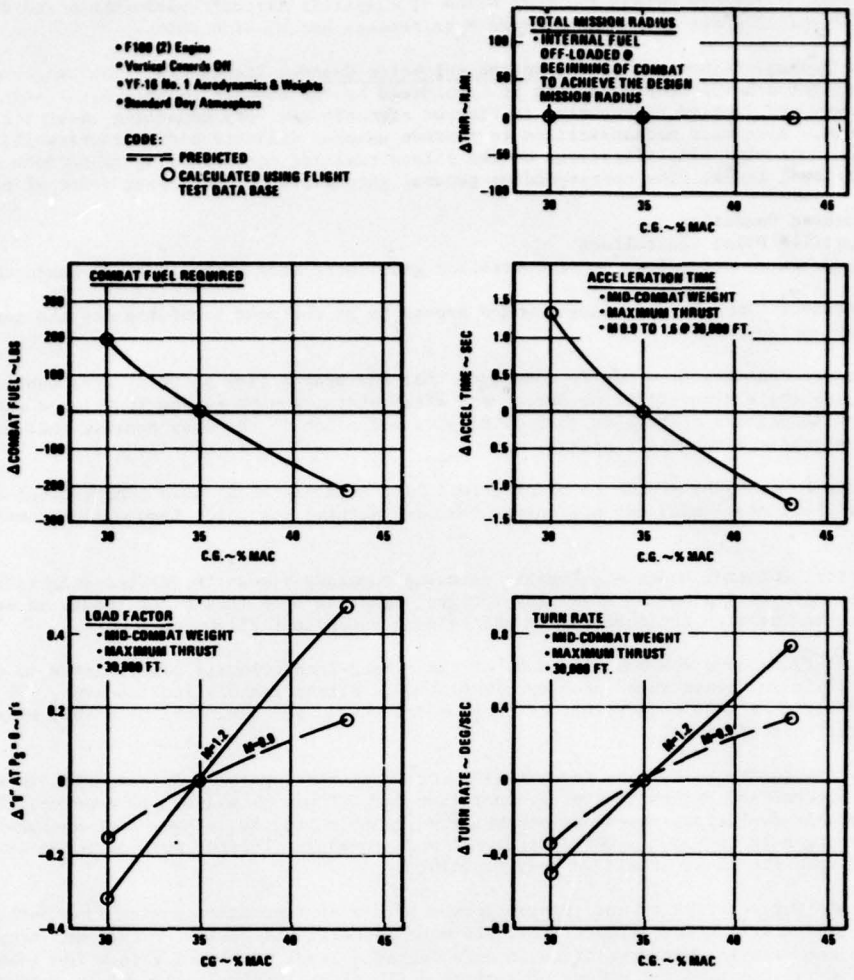

Figure 21 CCV YF-16 RSS Benefits

CCV Flight Control Mode	Recommended Authority	
Maneuver Enhancement	Fighter CCV	
Direct Lift	1.0 to 2.0 X Fighter CCV	
Direct Sideforce		
Air Combat	Greater than Fighter CCV; 2g offensively and 3g defensively	
Air-to-Ground	Same as Fighter CCV (Approximately 1g)	
Pitch Pointing	2 X Fighter CCV (±5 degrees)	
Yaw Pointing	Fighter CCV (±5 degrees)	
Vertical Translation	Equal to or Greater than Fighter CCV (1500 fpm)	
Lateral Translation		
Formation, Aerial Refuel	10 Knots	Typical Fighter CCV Capability: 30 Knots
Landing in Crosswind	30 Knots	
Air-to-Ground Weapon Delivery in Crosswind or Against Moving Target	50 to 80 Knots	

Table II Control Mode Authorities

in specific applications to obtain the best blend of classical aircraft performance and decoupled mode capabilities for a specific set of fighter design requirements and mission rules.

Improved Mechanizations and Manual versus Automatic Control Trade-Offs - The proper perspective for viewing fighter flight control mechanizations is considered by the authors to be: Air-to-Air and Air-to-Surface weapons delivery and evasive maneuvering in fighter aircraft are very demanding tasks for highly skilled military pilots. Alternate mechanizations to improve weapons delivery and/or survivability must be implemented with accompanying simplifications of the pilots task and corresponding reductions in his workload for the key operational tasks. The corresponding general guidelines in decreasing order of priority is thus:

1. Automated Operation
2. Simplified Pilot Controllers
3. Task-Oriented determination of controller gradients, mode authorities, dynamic characteristics, etc.

At the present time the following changes appear to be the most promising for the current fighter CCV control mechanization:

1. Maneuver Enhancement - Modify mode such that the weapon line pointing axis exhibits minimum disturbance and steady state standoff error during and after excitation by random turbulence and nominal wind shears. Work to harmonize primary controller characteristics and pilot in the loop dynamic characteristics in the presence of automatic direct lift operation.

2. Direct Force Modes - Seek to blend direct lift commands with basic longitudinal stick commands. Provide controllers or blended mechanizations that are natural for pilot inputs to accomplish vernier flight path changes.

3. Aircraft Pointing Modes - Automatic pointing commands via an Integrated Flight/Fire Control Mode. A less complex alternative may be to employ integral commands such that pilot inputs in essence retrim the aircraft pitch and heading attitudes while maintaining a constant flight path.

4. Translation Modes - Modes should be of the closed-loop velocity command type to quicken initial response and minimize "coast down" upon termination of a direct translation maneuver. If at all possible, the automatic attitude hold constraints of these modes should be eliminated to enable usage over a wider range of operating conditions.

An exception to the guidelines for striving for automatic control mode operation is that the rudder pedals are a natural and extremely useful controller for CCV manual modes. In essence, throughout all the Air-to-Air and Air-to-Surface maneuvers accomplished in this program, it was feet-on-the-floor unless the pedals were being used to input a CCV directional mode command. Further work on force levels and gradient tailoring for specific tasks should be very fruitfull.

Aerodynamic Characteristics and Interactions - With a configuration having five movable control surfaces (wing leading and trailing edge flaps (TEF), all movable horizontal tails, rudder and canards), the efficient definition of aerodynamic characteristics to an acceptable level of accuracy is a formidable challenge. The task of considering the expected ranges of surface deflections, individually and in increasingly complex combinations, is realistically constrained by the wind tunnel test time available to a program. The following few examples are presented to offer initial guidance for such a task.

Predicted and flight measured steady state mode characteristics at 0.8 Mach number are presented in Figures 22 through 25. Both the Direct Lift and Pitch Pointing data (Figures 22 and 23) suggest that the wind tunnel derived prediction of decreased flaperon effectiveness, beyond 6 degrees trailing edge down deflection, is less severe and in some instances non-existent (Reference 3 - Volume II). It is suspected that the difference resulted from flow separation at the upper surface wing-flaperon juncture present at the moderate Reynolds number conditions of the AEDC and NASA LRC wind tunnel tests. The directional mode capabilities as illustrated in Figures 24 and 25 were in reasonable to good agreement with predictions.

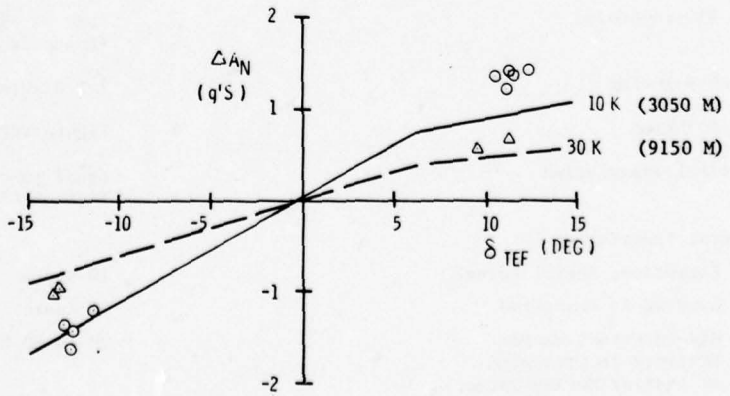

Figure 22 CCV YF-16 Flight Test Data vs. Predictions - Direct Lift Mode - M=0.8

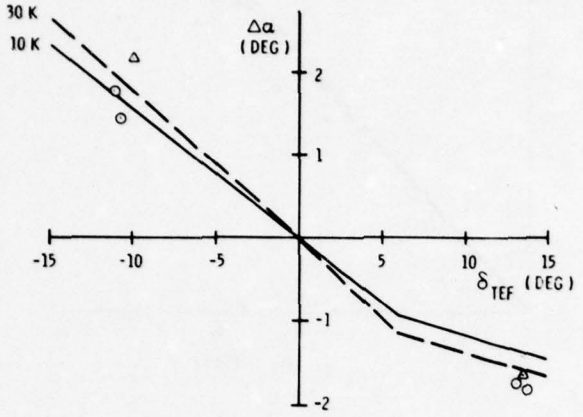

Figure 23 CCV YF-16 Flight Test Data vs. Predictions
Pitch Pointing Mode - M=0.8

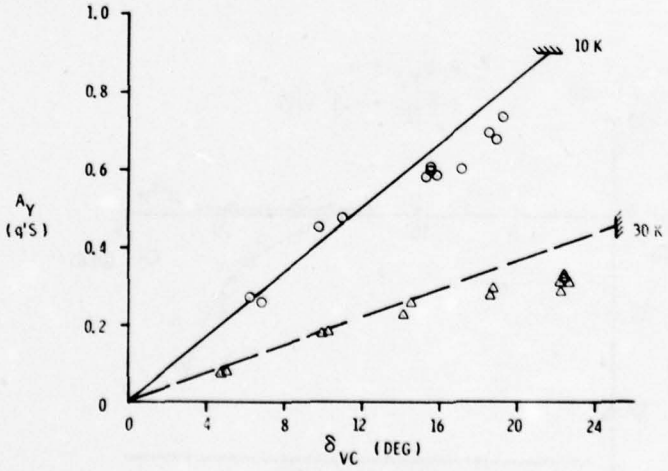

Figure 24 CCV YF-16 Flight Test Data vs. Predictions
Direct Sideforce Mode - M=0.8

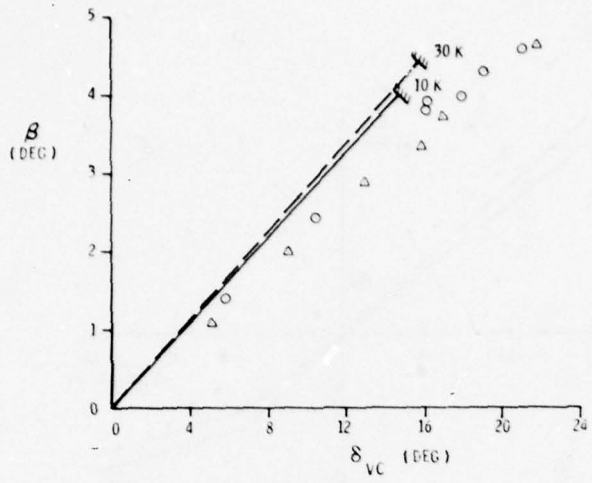

Figure 25 CCV YF-16 Flight Test Data vs. Predictions
Yaw Pointing Mode - M=0.8

The subject of aerodynamic interactions for the Fighter CCV vehicle was covered in considerable detail by R.A. Whitmoyer, Reference 5. Only the most significant interactions will be reviewed here to emphasize that such effects can become more than a minor annoyance or small reduction in anticipated capability. During accomplishment of wind-up turns with up-deflected trailing edge flaperons, it was noted that the horizontal tail deflection (δ_H) necessary to trim increased rapidly as angle of attack increased above 18 degrees, where as only very small trim changes occurred in similar maneuvers with the flaperons undeflected (Figure 26). Such large positive horizontal tail deflection increases are indicative of diminishing aircraft nose-down pitch recovery power. This is due to both decreased horizontal tail effectiveness and decreases in incremental surface deflections to reach the maximum surface deflection. The general guideline during the Fighter CCV program was to terminate the specific test maneuver if the steady state horizontal tail deflection exceeded +10 degrees (trailing edge down). The characteristics shown in Figure 26 prompted a temporary 15 degree angle of attack limit for longitudinal CCV modes, until an automatic longitudinal CCV fader was added to reduce to zero the flaperon symmetrical commands in the 15 to 18 degree angle of attack range. Subsequent reanalysis of the available wind tunnel data revealed that similar effects were to be found in the limited number of deflection combinations for horizontal tail, trailing edge flaps and leading edge flaps (Figure 27). However, sufficient wind tunnel data was not available for either a direct comparison with flight characteristics or detailed predictions of the entire scope of the interactions.

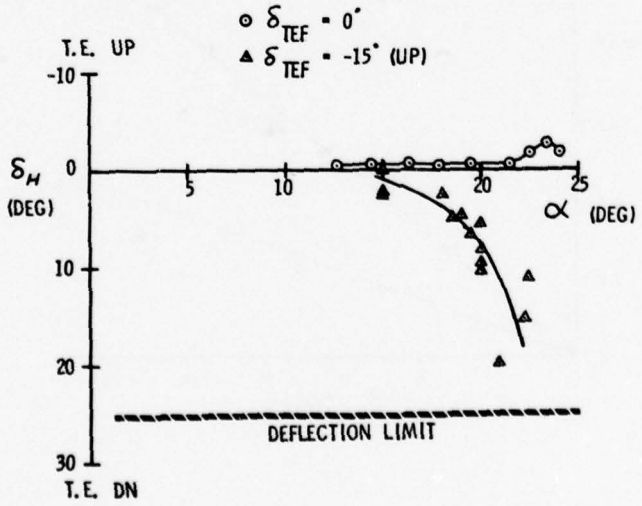

Figure 26 CCV YF-16 Flight Test Data - Trim Tail
Deflection vs Angle-of-Attack - M = 0.7

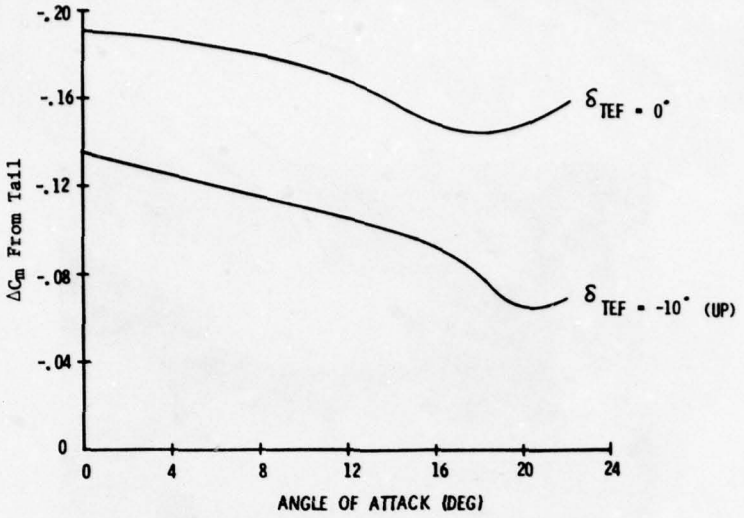

Figure 27 CCV YF-16 Wind Tunnel Data - Tail Pitching Moment Coefficient (ΔC_m) vs Angle-Of-Attack - M ≈ 0.6

10. FUTURE DEVELOPMENT ACTIVITIES

The Fighter CCV program demonstrated that decoupled 6DOF control can be effectively used to provide innovative capabilities and improved mission effectiveness for fighter aircraft. Significant applications and design guidance were established from the development and flight testing. However, this program was certainly just the initial step in full validation of the CCV potential. The testbed vehicle provided a unique demonstration capability; however, specific operational task-oriented mechanizations were outside the scope of the program. The use of different modes, controller preference, control gradients, mode authorities, and dynamic characteristics were found to be highly dependent upon the specific task. Task-tailored multimode control law implementation and selection capability is clearly required in future applications. Close attention must be given to the entire pilot/vehicle interface problem, especially in the context of specific operational tasks and tactics. An urgent need exists for development of appropriate flying qualities criteria.

The AFFDL has initiated a program to develop flying qualities criteria reflecting closed-loop requirements for decoupled 6DOF airplane motion. Correlation of existing data, analyses and substantiating piloted simulation experiments are being applied to this effort that will proceed through 1979 and 1980.

The AFFDL is also continuing to expand the CCV technology development based on the lessons learned from CCV YF-16 flight testing. A simulation effort is underway to evaluate new and modified CCV YF-16 control laws, controller characteristics, and display interactions. General Dynamics is providing analysis and design support for the control law development task. The Laboratory's Large Amplitude Multimode Aerospace Research Simulator (LAMARS) is being used (Figure 28).

The effects of a moving base versus the previous fixed based simulators for decoupled 6DOF control development will be an important experimental finding of this effort. Another important thrust of the simulation is the establishment of flying qualities criteria. Operational simplicity is a requisite to useful task application and this requires careful consideration of vehicle dynamics, logic functions, control law blending, gain schedules, feedback parameters, display formats, and controller harmonization.

Digital technology is particularly suited for implementing the sophisticated control loop functions, logic schemes, and complex interfaces with controls, displays and other subsystems (Reference 6). Digital technology can offer flexibility and growth potential for system changes through software rather than hardware modifications and offers the opportunity to reduce system redundancy from quadruplex to triplex while retaining acceptable mission reliability and fault coverage. Development of a multimode digital flight control system is being conducted by the AFFDL as a major portion of the Advanced Fighter Technology Development and Integration Program (AFTI Tech Set I).

AFTI Advanced Development Program - The purpose of the AFTI program is to provide a demonstrator aircraft for flight demonstration and validation of integrated technologies in a system configuration that permits functional assessment of the technologies in a tactical environment. The program will permit individual development of selected technologies, criteria development, and then their functional integration and validation in a manner that minimizes the number of testbeds and accelerates technology convergence at reduced cost. Selection will be made from either an F-15 or an F-16 aircraft for the starting point to obtain the demonstrator vehicle.

A major thrust of the AFTI program is the development and integration of Digital Flight Control System (DFCS) and Integrated Flight/Fire Control System (IFFC) technologies. DFCS will feature task-tailored multimodes including direct force control and weapon line pointing. IFFC will integrate the DFCS with an advanced fire control system, controls and displays, and weapons. The IFFC ties attack sensors/trackers,

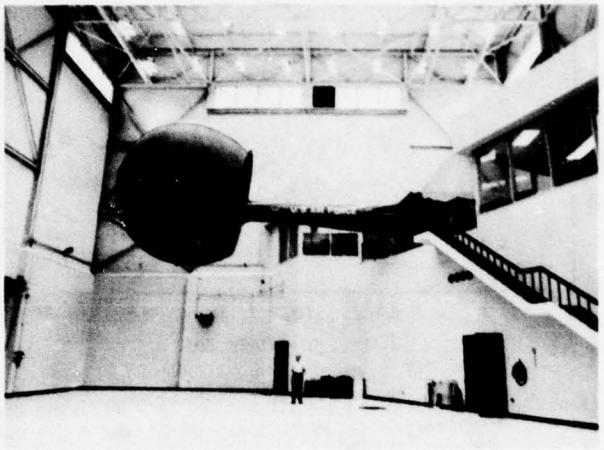

	DISPLACEMENT	NO-LOAD VELOCITY	STALL ACCELERATION
BEAM-VERTICAL	± 10 FT	13 FT/SEC	± 3 G
BEAM-LATERAL	± 10 FT	10 FT/SEC	± 1.65 G
SPHERE-PITCH	± 25 DEG	60 DEG/SEC	± 400 DEG/SEC^2
SPHERE-YAW	± 25 DEG	50 DEG/SEC	± 200 DEG/SEC^2
SPHERE-ROLL	± 25 DEG	60 DEG/SEC	± 460 DEG/SEC^2

Figure 28 LAMARS Motion Capability

a director fire control system, the DFCS, pilot and weapons into an integrated system. Dramatic improvements in air-to-air and air-to-surface weapon delivery effectiveness and survivability are anticipated. Results of this integration for design guidance to future fighters will become available in tne 1983 time period.

11. CONCLUSIONS

The Fighter CCV program was accomplished to develop design guidance and user/builder acceptance of active control concepts by demonstrating functional flight control hardware and by validating the resultant performance advantages provided by this hardware. Specific tests were conducted to evaluate the CCV implementations in numerous operational tasks. Results of this flight test program suggest the following conclusions.

1. Direct force flight-path control concepts have proven to be useful in flight. Specific modes have been validated for decoupled control of:

   a. Flight Path
   b. Fuselage Pointing
   c. Translation

2. Automated implementation of direct lift is simultaneously beneficial for enhancement of longitudinal maneuvering response and gust alleviation.

3. Direct force flight-path control concepts have significant applications for essential operational tasks of advanced fighter aircraft.

4. Further development of control modes is warranted to maximize their uses for operational weapon delivery tasks on fighter aircraft. Primary emphasis should be placed upon optimization and refined implementation to fully exploit:

a. Automated operation
b. Simplified pilot controllers
c. Task-oriented controller gradients, mode authorities, and dynamic characteristics.

REFERENCES

1. McAllister, J.D., et al, (General Dynamics Corp.), Fighter CCV Phase I Report, AFFDL-TR-75-106, Air Force Flight Dynamics Laboratory, Wright-Patterson AFB, Ohio, September 1975.

2. McAllister, J.D., et al, (General Dynamics Corp.), Fighter CCV Phase II Report, AFFDL-TR-76-119, Air Force Flight Dynamics Laboratory, Wright-Patterson AFB, Ohio, October 1976.

3. McAllister, J.D., et al, (General Dynamics Corp.), Fighter CCV Phase IV Report, AFFDL-TR-78-9, Air Force Flight Dynamics Laboratory, Wright-Patterson AFB, Ohio, February 1978.

4. Twisdale, T.R., and Franklin, D.L., Captain, USAF, Tracking Test Techniques for Handling Qualities Evaluation, AFFTC-TD-75-1, Air Force Flight Test Center, Edwards AFB, California, May 1975.

5. Whitmoyer, R.A., Aerodynamic Interactions On The Fighter CCV Test Aircraft, AGARD CP-235, Conference on Dynamic Stability Parameters, Athens, Greece, May 1978.

6. Ramage, J.K., and Swortzel, F.R., Design Considerations for Implementing Integrated Mission-Tailored Flight Control Modes, AGARD Paper No. 51, 26th AGARD Guidance and Control Panel Symposium, Sandefjord, Norway, May 1978.

L-1011 ACTIVE CONTROLS, DESIGN PHILOSOPHY AND EXPERIENCE

by
David M. Urie
Lockheed-California Company
Burbank, California
USA

SUMMARY

Aircraft active controls can be defined as control effectors activated by sensors through computers without pilot commands. They can be applied to provide any combination of weight savings, reduced fuel consumption, or expanded operating envelope. A certificated commercial transport airplane, the Lockheed L-1011, currently employs several highly sophisticated systems satisfying this definition. Significant among these are the yaw stability augmentation system (yawSAS) and the Lockheed Autoland automatic landing system. The yawSAS allowed a 20 percent reduction in design load on the fin. The Autoland system performs precision landings under visibility conditions which preclude a conventional instrument approach. The acceptability of both systems was established using probabilistic techniques to demonstrate equivalent safety.

Similar techniques are being used to certify wing load alleviation active controls. In addition to the familiar gust probability approach, maneuver load spectra are combined with systems reliability and active controls performance to provide design loads less than those required for unalleviated wing structure. The availability reliability level used for this design is higher than that assumed in the yawSAS fin analysis because years of experience with current systems have shown failure rates orders of magnitude less than originally assumed. Active controls performance in wing load alleviation applications has been demonstrated in L-1011 baseline and extended-span flight tests sponsored by the NASA Aircraft Energy Efficiency (ACEE) program. These tests have verified the mathematical models and tools used to derive control laws by showing generally good correlation between predictive analysis and experiment. Flight data show the predicted 3-percent fuel efficiency improvement from the 6-percent span increase.

Flight simulation of relaxed static stability (RSS) and stability augmentation has also been conducted under NASA-ACEE auspices. The subject configurations, a current L-1011 and an L-1011 derivative having a horizontal tail 60 percent as big as the baseline, were evaluated by test pilots. Static margin and air turbulence were independent variables. The handling qualities of the aircraft with each of several candidate augmentation systems operating and inoperative were studied in varied flight conditions. These simulator flying-qualities data provide the basis for a proposed criterion for assessing the acceptability of pitch stability augmentation system (pitch SAS) performance and availability. Application of the proposed criterion is demonstrated for the landing approach segment of a typical mission profile. This example suggests that a lagged pitch damper with availability no greater than currently being obtained from the operational L-1011 yawSAS is an acceptable augmentation concept for a neutrally stable transport-type aircraft.

Flight test data from stall demonstrations have been employed to define a pitch control power criterion for use in preliminary design balance and tail (or canard) sizing. A survey of nearly 400 stall histories from three aircraft provided data on pitch acceleration demanded during stall recovery. A statistical interpretation of these data permits their use for assuring nose-down acceleration equivalent to that required from current aircraft. This criterion replaces static margin in setting an aft cg limit for a given tail size for RSS designs.

Lockheed experience with flight and simulator testing of active control derivatives of the L-1011 allow two general conclusions to be stated.

- New criteria for active controls do not appear to be required. Existing criteria interpreted in terms of equivalent safety are satisfactory.
- An extensive data base is invaluable to the successful application of active controls.

INTRODUCTION

Although it is not a combat aircraft, the Lockheed L-1011 TriStar is representative of a class of large aircraft designed for optimal cruise or loiter performance which might see service in transport, patrol, warning, and control or missile carrier mission roles. The original model of the L-1011 was equipped with systems now described as active controls. Currently, a new model – the L-1011-500 with additional advanced active controls applications for performance improvement – is being readied for delivery in early 1980. This aircraft will have extended wing span without significant structural beef-up made possible by an active control load alleviation system. This system is based on research and development conducted under contract to NASA as part of the Energy Efficient Transport (EET) segment of their ACEE program. The experience gained through development flight testing, commercial flight operation, and flight simulation research on these and extended active controls applications are shared here with the intent of relating design philosophy and results.

PHILOSOPHY OF EQUIVALENT SAFETY

Lockheed's approach to U.S. Federal Aviation Administration (FAA) certification of active controls is to rely on the philosophy of equivalent safety as allowed in the Federal Aviation Regulations, Part 1. Some use has been made of this philosophy in certifying current wide-body transports. It will be used more extensively for the extended span wing load alleviation program. Under this philosophy, it is shown that the safety of the aircraft is equivalent to that of aircraft successfully certified within traditional deterministic

criteria envelopes. In the application of this philosophy, much of the safety analysis is conducted using quantitative combined probability techniques. Probabilistic analyses account for system reliability in conjunction with exposure to predicted load or hazard levels.

Figure 1 depicts the equivalent safety concept in terms of two load-exceedance functions. The upper line represents the frequency at which a given load quantity is exceeded with no active control system operating. At some arbitrary frequence (E_L), usually selected to be once in the design service life of the aircraft, a design load level (P_R) for the load quantity, such as bending moment at a specific wing station, is defined for the no-active-control case. This would be the design limit load for a conventionally designed structure based on statistically determined gust or maneuver load spectra. The lower load-exceedance function represents the effect of a normally operating active control system having some finite failure rate in reducing the frequency at which a given load is exceeded. At the once-per-lifetime frequency, the design load (P_D) is less with active controls reflecting the potential for weight saving compared to the conventionally designed element. The constraint on the use of the active controls design load is that the probability of exceeding the design load based on normal operation of the active control system not be greater than the probability of exceeding the design load without an active control system.

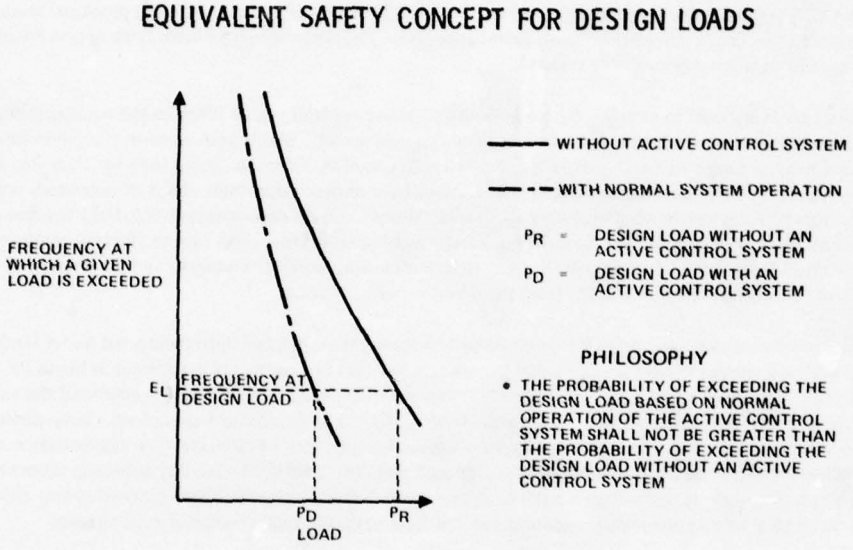

Figure 1

Figure 2 depicts the way in which the design philosophy is applied to determine a design limit load for a specific load quantity such as bending moment at a wing station. As in Figure 1, the limit load without active control (P_{R_L}) is established at the selected frequency (E_L). The exceedance function with active controls is shown as the lower (left) line. This function describes the frequency at which a given load is exceeded with an active control system operating all the time. From these two functions for no active controls and full-time active controls, the load-exceedance function for normal operation of active controls, considering system availability, can be developed. This is accomplished by adding the product of the failure rate times the exceedance frequency without active controls to the availability (1 minus the failure rate) times the exceedance with active controls always operating. The exceedance function so defined is drawn between the first two. The design limit load is the intercept of the middle curve at the selected frequency.

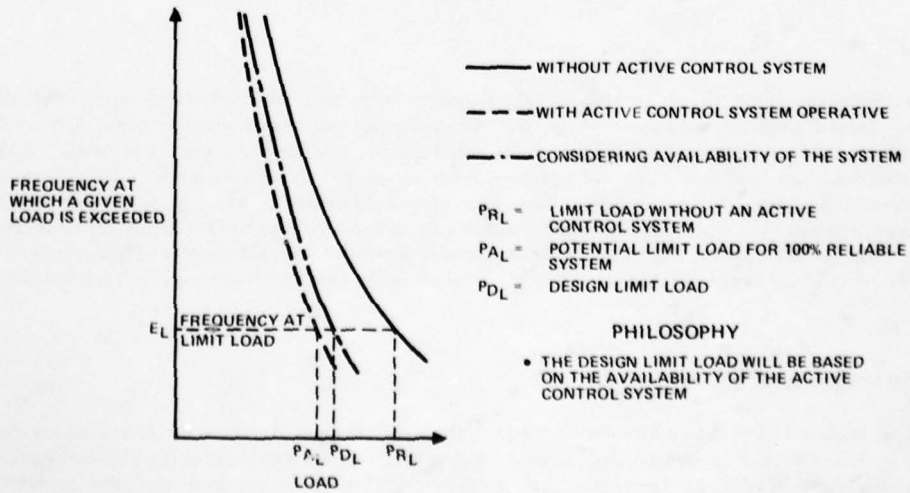

Figure 2

LOADS DESIGN

Application of this philosophy to a specific design, L-1011 vertical fin gust loads, was described thoroughly in Reference 1. The effect of the yaw damper on vertical tail shear near the fin root was presented as a typical example of the use of frequency-of-exceedance curves in design limit load selection. With the use of Figure 3, that example is repeated here.

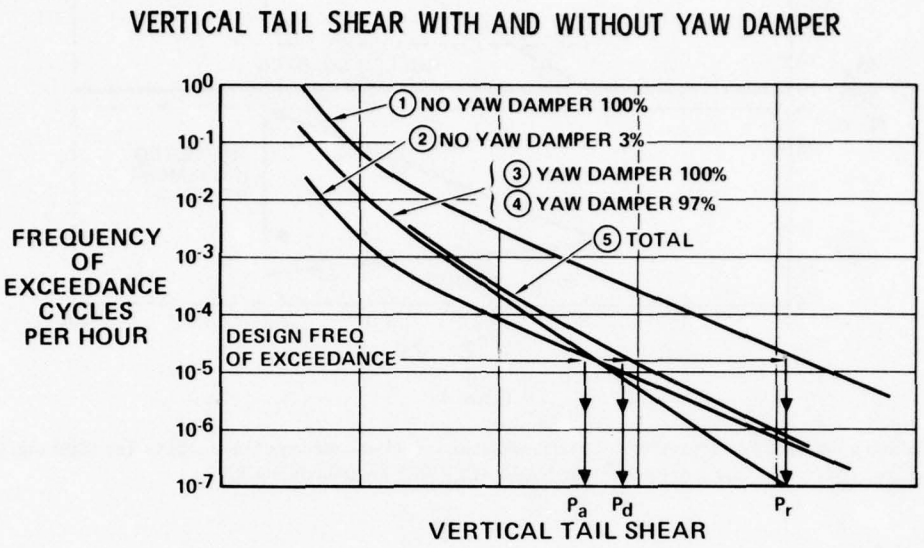

Figure 3

In the development of the L-1011, early estimates indicated that the yaw damper might be inoperative as much as 3 percent of the time. The exceedances accumulated during that portion of the total flight time during which the damper is not in operation are then given by 0.03 of Curve 1; the result is Curve 2, obtained by shifting Curve 1 down by a factor of 0.03. The exceedances accumulated during the 97 percent of flight time during which the yaw damper is operating are then given by shifting Curve 3 down in the ratio 0.97 to give Curve 4. (Curves 4 and 3 differ imperceptably and are shown by a single line.) The total exceedances are then given by the sum of Curves 2 and 4, or Curve 5. This is the curve from which the actual design load is obtained, indicated by P_d on Figure 3.

Operational experience with the L-1011 yaw damper and other sophisticated avionics equipment has shown the estimated 3 percent for time inoperative was one to two orders of magnitude too great. In the design analysis for the active controls version of the L-1011-500 with extended wing span, system inoperative time is assumed to be 0.1 percent. Exceedances accumulated during the time the system is operating (99.9 percent) are all but identical to the exceedance function with a full-time system. Applying this availability ratio to the foregoing example results in a design limit load for normal operation which is only 2 to 3 percent higher than the load with a full-time system. Load exceedance functions, considering active controls system availability, are obtained, accounting for the total mission profile gust exposure for shears, bending moments, and torsions at as many locations on the wing as considered necessary. Each curve is entered at a limit design frequency of exceedance of 2×10^{-5} cycles per hour (one exceedance in 50 000 hours) to get the limit design value of the load.

The L-1011-500 active control system incorporates maneuver load control. Calculation of design limit loads for maneuver conditions follows a procedure analogous to the one described for gusts. To use this method for maneuver loads, the probability density of maneuver load factor is totalled over a typical set of mission flight profiles. Exceedance functions for selected load quantities are computed for normal active control system performance and availability. Unpublished statistical data on maneuver load factor exceedance frequency obtained from L-1011 test and operational flight records were used to develop the mission analysis probability density. Predicted loads with active controls operating have been verified by flight test measurements (Reference 2). An example of these data are shown in Figure 4. These plots show bending moment at a wing station just inboard from the root of the outboard aileron (the active control surface) as a function of normal load factor at the airplane center of gravity. These data show that, as predicted, the incremental bending moment at this station is held to zero by the active control. This is true for symmetric and assymetric maneuvers.

FLYING QUALITIES CRITERIA

Based on flight experience with the application of probabilistic limit design criteria for loads alleviation and on simulator studies of relaxed static stability (RSS), a rule analogous to the loads criteria is suggested for determining the handling qualities acceptability of proposed stability augmented aircraft. The rule accounts for augmentation performance, unaugmented aircraft characteristics and augmentation system availability. Demonstration of compliance is based on flight simulation corroberated by flight tests. Existing atmospheric turbulence models are used in a mission analysis probabilistic method.

In this method, pilot overall opinion is substituted for structural load quantity in the equivalent safety concept to establish a frequency-of-exceedance function for flying qualities evaluation. An example demonstrating the possible application of the proposed

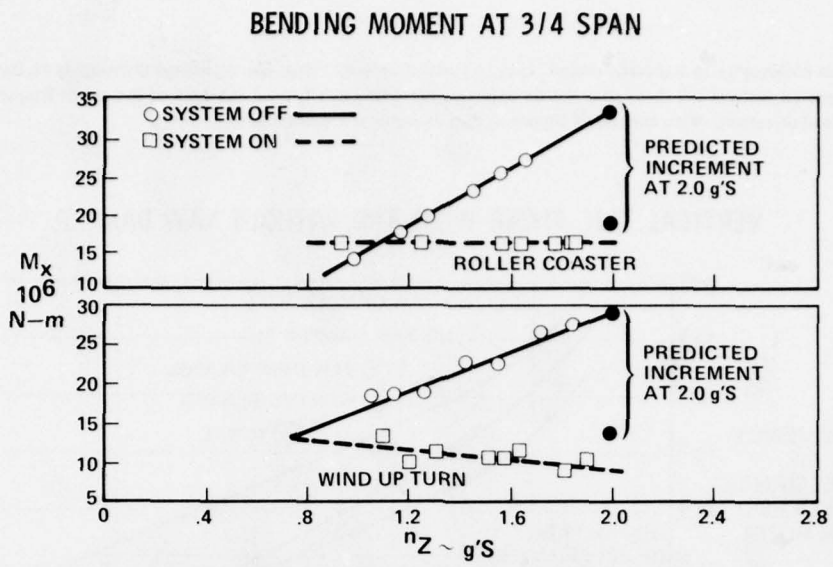

Figure 4

rule is constructed using simulation data from tests of a relaxed-stability, small-tail version of the L-1011. The flight simulation data were obtained from selected concepts studies sponsored by the NASA-ACEE/EET program during 1977.

Flight Simulator Model

Flying qualities evaluations were conducted by three test pilots on the Lockheed Rye Canyon visual flight simulator (VFS). This facility provides an L-1011 cab on a four-degrees-of-freedom motion system. The cab is a detail mock-up of the L-1011 flight station including primary controls and basic flight instruments including a flight director. Forward out-the-window visual presentation is provided by a video system. The motion system is capable of +0.8g to −1.0g vertical acceleration and ±15 degrees/sec pitch rate.

Aerodynamic data for the L-1011 with the existing production horizontal tail and with a proposed smaller tail were input into the math model. A complete nonlinear flexible model of longitudinal aerodynamics was programmed, since the evaluation was to be concentrated on longitudinal flying qualities. A simplified lateral-directional model was employed to be representative of the airplane response at the test conditions, but not containing a complete description of the airplane. The aerodynamic data representing the basic and small-tail configurations are the L-1011 flight-validated data set plus supplementary data from wind-tunnel tests of the small horizontal tail. These wind-tunnel data show an energy efficiency improvement attributable to the small tail of 3 to 3.5 percent in cruise.

An engine dynamic model was programmed with time variations of engine pressure ratio adjusted to match flight-test derived engine accelerations and decelerations. The variation of thrust with altitude and Mach number was also derived from flight data. Engine effects were combined with aerodynamic forces and moments and inertial characteristics to describe the total aircraft responses using standard six-degrees-of-freedom equations of motion.

Air turbulence was simulated by inserting random velocity inputs into the aerodynamic equations. Characteristic lengths in the Dryden turbulence model were kept at greater magnitude near the ground than described in the basic Dryden form. This resulted in peak velocity gusts simulating vertical and horizontal wind shear bursts on landing approach. The maximum air roughness used in this study was 3.7 m/sec (12 fps) root-mean-square (RMS) random turbulence velocity. This level was selected from observation of the load factor and glide-slope excursions caused by turbulence. Because of the importance of air turbulence in this evaluation, motion system gains were optimized to present the most realistic turbulence simulation possible within the limits of the actuators. The control column forces experienced by the pilot were provided by a hydraulic column-loader, which is a closed-loop servo system giving column position and rate feedback representative of the L-1011 Mach feel schedule.

Three augmentation system control laws were evaluated for the small-tail configuration. These were a lagged pitch rate damper, the lagged damper with stick quickening, and the damper with reduced control response. Coefficients of the control-law parameters were selected by analysis to satisfy classical modal characteristic objectives and recent time history criteria. Values of the short period and phugoid frequency domain characteristics and time history of control response were established for the basic statically stable L-1011. Because of the basic airplane's good handling qualities, these responses were used as target values for those of the augmented small-tail configuration. This procedure yielded augmentation control laws giving closed-loop responses approximately equivalent to those of the basic unaugmented production airplane under manual control.

Piloted Flight Simulation

Three pilots familiar with the L-1011 participated in these tests. Fidelity of the simulator model was established by agreement from all three pilots that the basic big-tail model flew like their impressions of the real airplane. Tests then proceeded using both the baseline and small-tail versions with variable center-of-gravity position and various levels of turbulence. Flying tasks concentrated on landing

approach in instrument flight conditions and on typical cruise flying tasks. No autopilot was used, with all simulation being done in the manual mode. All flying tasks were repeated for the three augmentation models and with no augmentation. Pilot subjective opinion of handling qualities was recorded in terms of the Cooper-Harper rating scale. Analytic data on airplane flight-path behavior and control motion was recorded for correlation with pilot ratings and comments. Generalized results from analysis and interpretation of the L-1011 relaxed stability simulator study data are summarized below.

- Enhanced or reduced augmentation control response show no advantage over the simple lagged pitch damper.
- Handling qualities of the augmented relaxed stability airplane are superior to those of the inherently stable baseline in heavy turbulence.
- Handling qualities of the unaugmented neutrally stable small-tail version are generally acceptable.
- Airplane motion and control activity in rough air are less for the augmented relaxed-stability version than for the baseline.

Study results are presented in more detail in References 2 and 3.

These generalizations hold for both high-speed cruise and landing-approach flight conditions. Specific data from the landing-approach simulations are used in the present example of the proposed method. A similar treatment using the cruise simulation results could be done for that flight profile segment.

Landing-approach testing was initiated at a distance of 18.5 km (10 miles) from the runway threshold in level flight at an altitude of 457m (1500 ft) above ground level. An instrument approach was flown down to 91m (300 ft), at which time the visual presentation of the airport was available for final approach and touchdown. The initial aircraft configuration was gear up and flaps at 10^{o}. The pilots flew level to glide slope intercept at which time the landing gear was extended and flaps increased to 22^{o} and finally to 33^{o} as the aircraft descended on glide slope. Appropriate power adjustments were made during descent. This procedure provided a realistic flying task with a workload typical of the flight condition. The test engineer occupied the right-hand seat and performed the normal first-officer chores. The landing approach sequence from initialization to touchdown occupied approximately four minutes. The task was performed repeatedly with center-of-gravity varied to provide static stability margins from 17%$\bar{c}$ (mean aerodynamic chord) stable to 2%$\bar{c}$ unstable in turbulence levels from calm to heavy.

The Cooper-Harper handling qualities rating scale was used by the pilots to quantify their subjective evaluation. Each case was rated for damping, control response, ease of maintaining attitude, and glide slope control. The individual ratings were summarized into an overall rating for each pilot. The Cooper-Harper scale extends from 1 to 10 with decreasing acceptability. Ratings from 1 to 3.5 are given for satisfactory qualities where no improvement is deemed necessary. Ratings from 3.5 to 6.5 are considered acceptable but reflect an increased workload. Above 6.5 the ratings indicate greatly increased workload reaching uncontrollability at 10.

A presentation of composite overall handling qualities ratings from all pilots as a function of static margin is given for the approach task without augmentation in Figure 5. These data include both large-tail and small-tail results and show that on landing approach the tail size effects were restricted to static stability differences only. The baseline configuration with the large horizontal tail was evaluated at comparable stability levels by flying at more aft centers of gravity. The somewhat greater pitch damping and control power of the large tail do not appear to improve pilot opinion at this flight condition. It can be seen that the ratings are essentially insensitive to static margin for levels greater than about 10%$\bar{c}$. Operation is degraded by decreasing stability and increasing turbulence. Acceptable approaches were flown with 2%$\bar{c}$ negative static margin in moderate turbulence. Turbulence intensity is clearly a significant factor. The effects of updrafts or downdrafts and horizontal wind shears degrade glide slope control. In heavy turbulence, unaugmented glide slope control is marginally acceptable regardless of stability margin because of rapid excursions above or below the glide slope, which could be controlled with considerable effort.

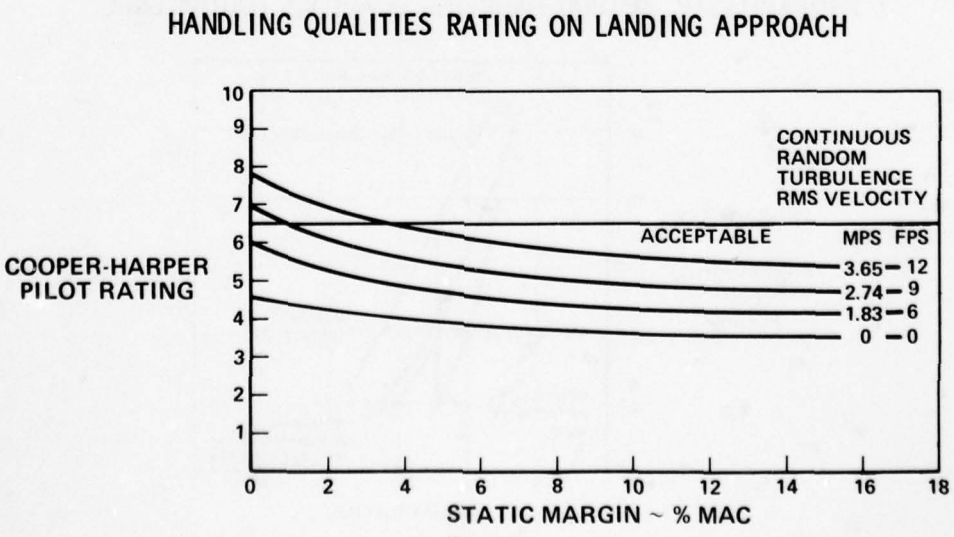

Figure 5

Handling Qualities Equivalence

A similar presentation of ratings from tests of the small-tail airplane with the lagged pitch damper shows some overall improvement in calm air handling qualities with no variation in rating level as a result of static margin and much reduced trend with turbulence. The damper-on results, combined with the unaugmented airplane data, provide a set relating handling qualities acceptability with air turbulence intensity, inherent stability, and augmented performance. To obtain a probability density for the effects of these factors on handling qualities during landing, a turbulence model of the lower atmosphere is used. One such model is shown in Figure 6. These data (Reference 4) show the probability per hour that a given root-mean-square gust velocity is exceeded in low altitude continuous random turbulence. To account for exposure time in a typical flight profile, a second line has been added reflecting the once-per-flight exceedance on a 4-minute final approach to landing.

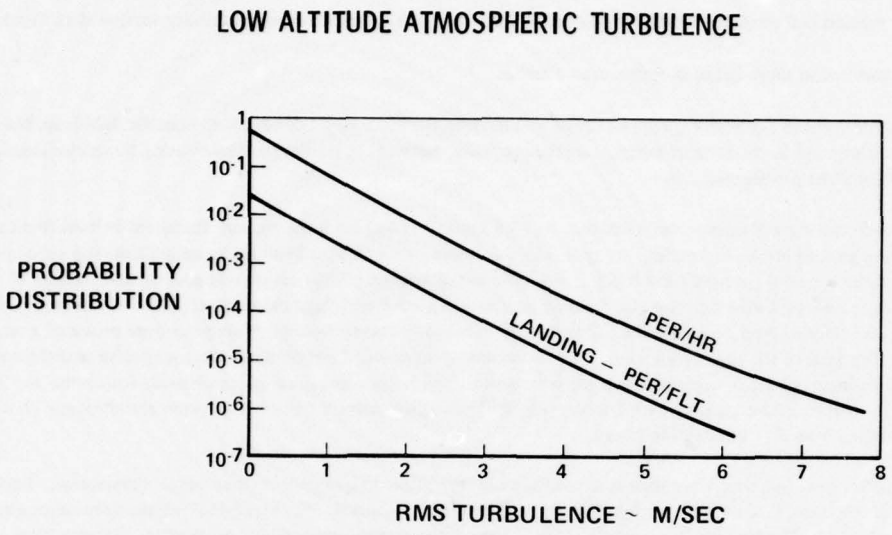

Figure 6

The proposed method for relating flying qualities *with* numerical probability is demonstrated in Figure 7. This plot presents the landing approach simulation pilot rating data in terms of the probability of exceeding a given rating level once per flight. Probability is associated with pilot rating by correlating the rating data of Figure 5 as a function of turbulence RMS velocity with the gust probability model of Figure 6. These data are plotted for the small-tail L-1011 version with the center of gravity located at the neutral point. The upper line represents the probability of handling qualities rating with no augmentation. The bottom line shows ratings probability for the same configuration with the lagged pitch damper operating 100 percent of the time.

A line representing the current unaugmented airplane with a conventional static margin of 12%$\bar{c}$ is added from the same simulation test series to provide a criterion for handling qualities equivalence. The maximum air turbulence intensity in which the test pilots say they would continue a landing to touchdown in the conventionally stable airplane is 2.7 m/sec (9 fps) RMS. This provides a limit value for pilot rating of handling qualities. The gust model indicates a probability of approximately 10^{-4} of encountering turbulence exceeding this level on one landing approach. The conventional unaugmented airplane with a static margin of 12 percent would receive

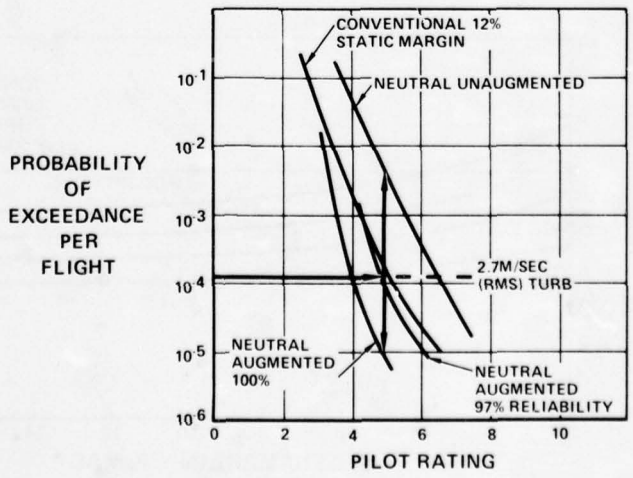

Figure 7

a pilot rating of 5 in that turbulence based on these simulation data. A rating of 5 is selected as the "design load" on the pilot in terms of handling qualities for the landing approach flight segment.

Using 5 as the allowable value of pilot rating, it can be determined from a summation of the unaugmented and 100 percent augmented probability values that an augmentation failure rate of 3 percent would provide a probability of exceedance just less than equivalent to that of the conventionally stable airplane. Working numerically from the plot:

$$0.03 \times 3 \times 10^{-3} + 0.97 \times 9 \times 10^{-6} = 9 \times 10^{-5} + 0.873 \times 10^{-5} \quad \approx 10^{-4}$$

This means that the probability of electing to discontinue a landing approach due to handling qualities difficulty would be no greater for a neutrally stable airplane with a 97 percent reliable augmentation system, whose performance equals the one tested, than for a comparable inherently stable airplane with 12%$\bar{c}$ static margin. If the availability assumed for the L-1011 load alleviation active controls system (99.9 percent) is used, the augmented small-tail airplane would be considerably less likely to encounter degraded handling qualities leading to a wave-off decision by the pilot.

The preceding example is confined to the landing approach phase of the flight profile. A similar exercise using the cruise condition data from the same simulation study is contemplated. This technique could be applied to any part of a typical mission profile that might be critical. The objective of the mission analysis is to ensure that at the most critical conditions, the CCV design is at least as safe as an equivalent configuration designed to conventional envelope criteria. This technique allows the design engineer to define augmentation system performance in conjunction with combined reliability and probability of perturbation from external sources to ensure equivalent safety on a mission performance basis.

EQUIVALENCE CONCEPT FOR CONTROL SIZING

In the design of CCVs, where inherent static stability is no longer a requirement for the airframe, the aft limit on the center-of-gravity envelope will be set by some criterion other than static margin. One requirement likely to be significant is that the airplane have satisfactory nose-down control power at aft center of gravity. A method for establishing a criterion for satisfactory design level was developed using flight-test data from the L-1011, the S-3A and the C-5A aircraft. It is assumed that for transport-type aircraft, or other cruise-designed configurations, that the peak nose-down control requirement would occur at stall speed during recovery from that condition. It is also assumed that the requirement in terms of pitch acceleration ($\ddot{\theta}$) can be established from the value of $\ddot{\theta}$ actually used by current statically stable aircraft.

Stall History Study

The magnitude of pitch acceleration was determined from a study of the stall recovery characteristics of three current jet aircraft. The objective of this study was to determine an accepted level for nose-down pitch acceleration during recovery from stalls. The data used was from development tests conducted by Lockheed pilots and from acceptance tests by FAA, British CAA, USAF, and USN pilots.

Stall-time histories from C-5A, L-1011, and S-3A flight tests were analyzed to obtain data. The maximum airplane nose down (AND) pitch acceleration was measured during recovery from stalls in all configurations. Figure 8 shows selected traces taken from an L-1011 stall flight record. The slope of the pitch rate trace is taken at its steepest point. In this case, the acceleration was relatively high, just greater than 0.1 radians/sec^2 nose down. Forward and aft cg positions and power-on as well as power-off cases are included. The total pitch acceleration results from the combined effects of inherent stick-fixed, pitch-down tendency plus incremental AND control input. The nose-down acceleration from pitch-down tendency is a function of static margin. Supplemental nose-down control was commanded by the pilot to attain satisfactory progress of recovery. Pilots have found the longitudinal characteristics of stall recovery

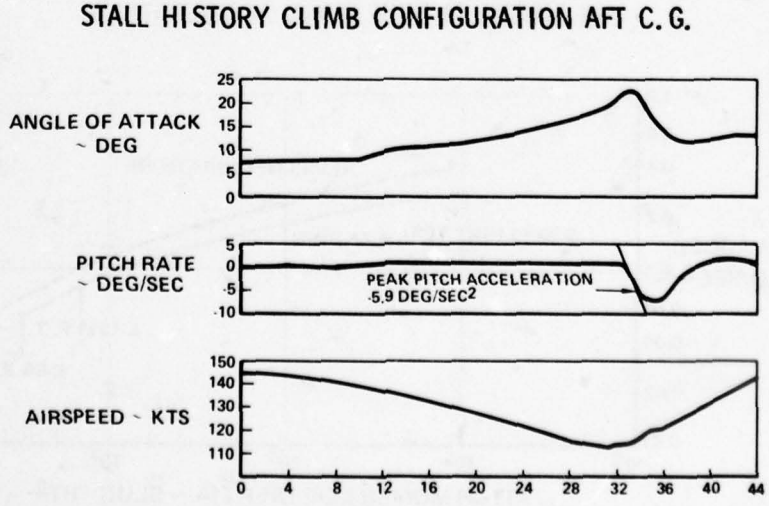

Figure 8

to be acceptable for all three airplanes. Moreover, in the recoveries of the L-1011, which has the full authority of the all-moving stabilizer and geared elevator as demand control, in no instance was the full AND control employed. Therefore, it is assumed that the measured maximum pitch-down accelerations were sufficient to satisfy the pilot that recovery from the stall was proceeding at an acceptable rate. Statistical distributions of the peak pitch accelerations for the L-1011 in landing configuration are shown in Figure 9.

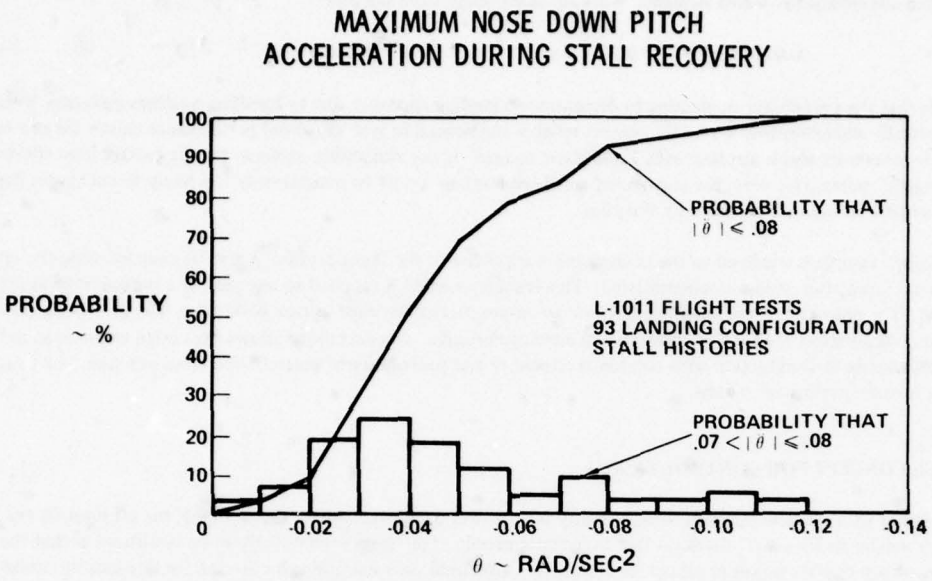

Figure 9

In all, 370 stall recoveries are included in the statistical study. They are obtained for the following aircraft configurations:

S-3A	64 stalls including 29 in the landing configuration
L-1011	265 stalls including 93 in the landing configuration
C-5A	41 stalls, all in landing configuration

Scale Effect. – The value of $\ddot{\theta}$ which equaled or exceeded the flight-demonstrated maximum in 90 percent of the cases was obtained for each of the three airplanes in the landing configuration and plotted against the mean pitch moment of inertia. When plotted on logarithmic scales, as in Figure 10, the three points fall on a curving line indicating that a power law may apply. A second line, representing the composite of all available flap settings for the S-3A and L-1011, is plotted above the first and extrapolated to higher values of Iyy based on the behavior of the landing configuration line. The upper line is closely approximated by the expression:

$$\ddot{\theta} = -3(\text{Iyy})^{-0.14+0.2} \text{ where Iyy is in slug-ft}^2.$$

Flap Effect. – The most critical configuration for nose down acceleration is apparently intermediate between clean and landing flaps. This is demonstrated by the fact that for both the S-3A and L-1011 the inclusion of flap settings other than landing increases the recovery acceleration representative of at least 90 percent of the cases. This is no doubt a function of the relative pitching moment and lift contribution of the flaps at each position. As flap angle increases, the stall speed decreases, thus reducing longitudinal control authority;

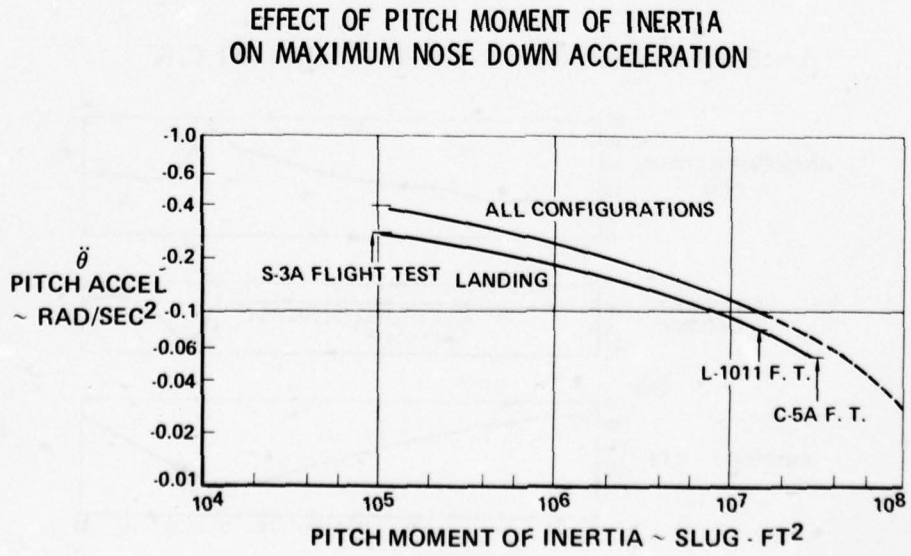

Figure 10

however, an increasing airplane nose-down moment is applied by the flap itself, thus reducing the authority required. The relative importance of this effect is a function of the specific configuration and so it is desirable to check the control size/balance limit trade for *landing flaps, clean configuration, and an intermediate flap setting.*

Preliminary Design Criterion

It is proposed that for preliminary design purposes sufficient pitch control power be reserved to perform a pushover at minimum speed in the most critical configuration. This requires that with the airplane in pitch equilibrium at the stall or minimum demonstration speed, and with the center of gravity in the most aft location, there remains enough longitudinal control authority to produce an airplane nose-down acceleration equivalent to the 10 percent exceedance level of current airplanes as represented by Figure 10. Because the aircraft upon whose data this rule is based have relatively small power effects at the stall due to thrust-to-weight ratio and thrust vector alignment, the criterion is best applied only to power-off stalls. It can also be advised that the criterion be used only for preliminary design and that time history analysis of critical maneuvers be done to assure satisfactory characteristics for an airplane in more advanced stages of development.

CONCLUSIONS

Lockheed's flight test and simulation experience in implementing active controls substantiate the philosophy that, for near-term applications, no new acceptability requirements are needed; that the intent of existing criteria can be met using the principle of equivalent safety.

It is also concluded that the success with which current active controls applications have met performance and safety objectives is due in large part to the availability of an extensive, well-substantiated data base.

REFERENCES

1. Hoblit, F. M., "Effect of Yaw Damper on Lateral Gust Loads in Design of the L-1011 Transport," presented at the 37th meeting of the AGARD structures and mechanics panel, 7-12 October 1973.

2. Johnston, J.F. and Urie, D. M., "Development and Flight Evaluation of Active Controls in the L-1011," NASA CP 2036 of conference held at Hampton, Virginia, Feb 28–March 3, 1978.

3. Urie, D.M., "Piloted Flight Simulation for Active Control Design Development," presented at the AIAA Conference on Air Transportation: Technical Perceptions and Forecasts, Los Angeles, California, 21-24 August 1978.

4. Press, H., and Meadows, M. T., " A Reevaluation of Gust-Load Statistics for Applications in Spectral Calculations," NACA TN 3540, 1955.

IN-FLIGHT HANDLING QUALITIES INVESTIGATION OF VARIOUS LONGITUDINAL SHORT TERM DYNAMICS AND DIRECT LIFT CONTROL COMBINATIONS FOR FLIGHT PATH TRACKING USING DFVLR HFB 320 VARIABLE STABILITY AIRCRAFT

by

D. Hanke
H.-H. Lange

Institut für Flugmechanik

Deutsche Forschungs- und Versuchsanstalt
für Luft- und Raumfahrt e.V. (DFVLR)
3300 Braunschweig Flughafen, West Germany

SUMMARY

The implementation of direct lift in the aircraft control system can improve pilot-vehicle performance and handling qualities for a given mission requirement. But new or revised handling qualities criteria applicable to direct lift control concepts are necessary. An in-flight investigation of DLC for wide body transport aircraft was carried out using DFVLR 320 variable stability aircraft which incorporates an advanced all digital model following system.

The capability for precise flight path control is influenced by both the longitudinal short term aircraft dynamics given by the aerodynamic heave/pitch ratio Z_α/M_α and by the control heave/pitch ratio Z_δ/M_δ which is varied by DLC application. The objective of the program is to determine the influence of various short term dynamics combined with various control derivatives on handling qualities for a flight path tracking task.

The aircraft/DLC configuration parameters are being investigated in an altitude compensatory tracking task in which the pilot has to minimize the error between commanded and actual altitude. To determine the influence of motion cues, the tracking task is carried out both on the ground and in-flight. Using the HFB 320 as a fixed base and an in-flight simulator, an ideal situation for comparing the fixed base and in-flight simulation results exists.

In addition pilot-in-the-loop analysis for flight path tracking with DLC is performed using the Neal-Smith pilot lead-lag phase compensation method. The results are given in the form of subjective pilot effort ratings and pilot-aircraft performance measures. The results are further compared with a flight path tracking criterion.

1. INTRODUCTION

Advancements in fly-by-wire technology have impacted the aircraft design cycle by allowing the optimization of both aircraft performance and handling qualities for a given mission requirement. Incorporation of direct force control into the flight control system can improve handling qualities and pilot/vehicle performance much more independent of inherent aircraft parameters. Implementation of direct force control modes however, implies the knowledge of direct force control parameters influencing handling qualities. Further a prerequisite for the design of these modes is a proper definition of mission oriented handling quality criteria. Unfortunately, there are too few direct force control related handling qualities data available which allows the definition of handling qualities criteria. Investigations that have been made have been mostly concerned with specific aircraft [1-12] and only a few experiments gave direct lift control handling qualities data [13-21]. It is known that the existing short period handling quality criteria used in the MIL-F-8785 B failed in the case of DLC or higher order control systems. New criteria or revisions are necessary and some new proposals are in discussion at present [22-24].

The flight experiment reported herein is part of a DFVLR research program to determine requirements for flight path control during landing approach for wide-bodied transport aircraft equipped with DLC. In the past DFVLR flight test programs have been concerned with coupled and decoupled flight path control DLC concepts in landing approach for a business type jet aircraft [19-21]. The results extracted from this program show that both concepts increase pilot-aircraft stability and bandwidth for flight path tracking.

The objectives of this paper are related to Coupled Flight Path Control DLC concepts (CFPC) for wide body high wing loaded transport aircraft, they include the investigation of

- the influence of DLC parameters on handling qualities
- the influence of aircraft and DLC parameter combinations on handling qualities
- the application of the Neal-Smith criterion for flight path control with DLC.

To achieve these objectives, an in-flight and ground based altitude compensatory tracking experiment was designed using the DFVLR HFB 320 variable stability aircraft.

Further, an analytical study of flight path control has been carried out to investigate the influence of aircraft/DLC parameter combinations on handling qualities using closed loop analysis method from Neal and Smith [22].

2. AIRCRAFT/DLC FACTORS INFLUENCING HANDLING QUALITIES

Using direct lift control, the two degrees of freedom of the short period longitudinal pitch and heave motion - coupled by aircraft inherent parameters Z_α and M_α - can now be independently varied by two control inputs, pitch control by the moment control surfaces (elevator or canards) and heave control by the direct lift device.

Independent of control surface interconnects the overall aircraft control sensitivities can be represented by generalized control derivatives Z_δ and M_δ which are the sum of all lift and moment control derivatives.

The influence of M_δ and Z_δ on aircraft short period response (short period approximation) and on existing short period handling qualities criteria is shown in figure 1 by plotting a new DLC parameter $n_{z(o)}/n_{z(\infty)}$ over $M_\delta/n_{z(\infty)}/\delta$. Figure 1 is a general representation of short period handling qualities parameters valid for any combination of aircraft aerodynamic and control derivatives.

$n_{z(o)}/n_{z(\infty)}$ - the initial to steady state normal acceleration ratio due to control input - gives an indication of the initial flight path response, normally negative, caused by elevator negative lift. The parameter $M_\delta/n_{z(\infty)}/\delta$ - the initial pitch acceleration to steady state normal acceleration (or pitch rate) due to control input - gives an indication of the pitch response of the aircraft. This parameter is equal to the control anticipation parameter CAP approximated by $\omega_{nsp}^2/n_z/\alpha$ for $Z_\delta = 0$. Any deviation from the shadowed area of elevator or canard control with low negative or positive $n_{z(o)}/n_{z(\infty)}$ values represents a combination of moment- and force control with the two extremes of pure moment control ($Z_\delta = 0$) and pure force control ($M_\delta = 0$). The aircraft short period response is mainly given by the Z_w/M_w-ratio. All Z_w/M_w-ratios of physical significance are located within the boundaries given by $Z_w/M_w \to \infty$ (neutral stability) and $Z_w/M_w \to 0$ (no lift curve slope).

For all lines going through point C the steady state load factor per control input $n_{z(\infty)}/\delta$ is constant and each line represents another Z_w/M_w-ratio, the main parameter influencing short period frequency. Looking at the conventional elevator controlled aircraft represented by point A, the CAP approximation is valid. Time histories of pitch rate and vertical acceleration response due to control input show poor initial vertical acceleration response compared to pitch rate. The combination of moment and direct lift control allows the ratio of $n_{z(o)}/\dot{q}_{(o)}$ to be varied. Along the line Z_w/M_w = const. (for a given aircraft) the requirement for $n_{z(\infty)}/\delta$ = constant causes M_δ to decrease as Z_δ increases. With increasing Z_δ the response of pitch rate and vertical acceleration are interchanged (point B). Point C represents the special case of steady state angle of attack response due to control input is equal zero. Summarizing, the generalized aircraft/DLC parameters influencing handling qualities parameters are

$$M_\delta/n_{z(\infty)}/\delta$$

$$n_{z(o)}/n_{z(\infty)}$$

and $$n_{z(o)}/\dot{q}_{(o)}$$

and, naturally, the basic aircraft parameters, short period frequency ω_{nsp} and damping ratio ζ_{sp}.

It should be emphasized at this point that the parameters mentioned above naturally cannot describe the complete dynamic behaviour. In reality the initial values can be computed from in-flight measured control derivatives or they must be replaced by the maximum amount of heave or pitch acceleration occured due to control inputs. But parameters shown in figure 1 represent the main influence of DLC on aircraft response.

3. PILOT-AIRCRAFT SYSTEM ANALYSIS

A theoretical parameter variation was carried out to investigate the influence of DLC on pilot-aircraft system of pitch attitude and flight path control.

The pilot-aircraft system was modeled as shown in figure 2 including moment control and direct lift control actuator dynamics. This loop structure could also be used for equivalent system approach as proposed in [24] but extended by an equivalent moment and direct lift device first order transfer function. Especially the equivalent first order time behaviour of direct lift device is necessary to avoid pitch rate and vertical acceleration response matching problems resulting from direct lift build up effects which cannot be described by a simple second order model and an equivalent time delay.

Any Z_δ/M_δ-ratio or $n_{z(o)}\dot{q}_{(o)}$-ratio can be selected by properly choosing K_M and K_{DLC} gains, according to the following relationships

$$Z_\delta = K_M \cdot Z_{\delta M} + K_{DLC} \cdot Z_{\delta DLC}$$

$$M_\delta = K_M \cdot M_{\delta M} + K_{DLC} \cdot M_{\delta DLC}$$

$$\text{with} \quad K = \frac{K_{DLC}}{K_M} \quad .$$

Then

$$Z_\delta/M_\delta = \frac{Z_{\delta M} + K \cdot Z_{\delta DLC}}{M_{\delta M} + K \cdot M_{\delta DLC}}$$

and

$$\frac{n_{z(o)}}{\dot{q}_{(o)}} = - \frac{1}{g \left(\frac{M_\delta}{Z_\delta} + M_{\dot{w}}\right)} \quad .$$

To investigate the influence of the $n_{z(o)}/\dot{q}_{(o)}$-ratio on the pilot-aircraft system for various short period frequencies the M_δ, Z_δ-derivatives were computed for given $n_{z(o)}/\dot{q}_{(o)}$-ratios holding Z_w, ζ_{sp} and $n_{z(\infty)}/\delta$ constant. The ω_{nsp} variation is then given by the M_α and M_q variations. The elevator actuator time constant was selected as T_M = 0.1 sec, the direct lift actuator time constant as T_{DLC} = 0.5 sec.

3.1 INFLUENCE OF $n_{z(o)}/\dot{q}_{(o)}$-RATIO

The influence of the initial heave/pitch acceleration parameter on the open loop pilot-aircraft system for flight path control is shown in figure 3. As can be seen increasing the $n_{z(o)}/\dot{q}_{(o)}$-ratio introduces phase lead into the system for both selected short period frequencies. For a given initial heave/pitch acceleration parameter the absolute value of direct lift characterized by the $n_{z(o)}/n_{z(\infty)}$-ratio is naturally quite different for the 'high' and 'low' short period frequencies as illustrated in figure 1.

The $n_{z(o)}/n_{z(\infty)}$-values shown in figure 3 for instance with $n_{z(o)}/\dot{q}_{(o)}$ = 200 are 0.68 (ω_{nsp} = 0.4) and 1.16 (ω_{nsp} = 1.6). That means that absolutely more direct lift is necessary for increasing short period frequency. Varying $n_{z(o)}/\dot{q}_{(o)}$ from - 1 to 200 for bandwidth frequency ω = 0.8 produces about 20 degree phase lead for ω_{nsp} = 0.4 but about 50 degree phase lead for ω_{nsp} = 1.6 rad/sec.

3.2 INFLUENCE OF DLC-ACTUATOR DYNAMICS

In addition to the amount of direct lift per elevator deflection the direct lift time constant is one of the most important parameters influencing short period vertical acceleration response. This parameter allows the pitch/vertical acceleration control harmony to be varied independently of the aircraft angle of attack response. As shown in [21] the steady state angle of attack response is given by the ratio of direct lift surface deflection to elevator deflection while the high frequency angle of attack response is given by the direct lift device time constant. With adjusted direct lift device time constant, it is possible, to drive n_z/q-response to one in both amplitude and phase over the whole frequency range.

The required direct lift device time constant for this case is

$$T_{DLC} = \frac{1}{\frac{M_{\delta DLC}}{Z_{\delta DLC}} U_o - M_q} \quad ,$$

if

$$K = K^* = \frac{M_{\delta M} U_o - Z_{\delta M} M_q}{M_{\delta DLC} U_o - Z_{\delta DLC} M_q}$$

where

$$K = K^* \text{ means } \frac{\alpha_{(\infty)}}{\delta} = 0 \quad .$$

As can be seen in figure 4 a fast acting direct lift device degrades both pitch attitude and flight path control in the short period frequency region. Fast acting DLC leads to phase lag in the pitch attitude transfer function and to extreme phase lead in the flight path transfer function for higher frequencies. By properly adapting the DLC actuator time constant to the short period frequency both the pitch and flight path responses of the aircraft can be improved. Conclusions from this are, that the direct lift device dynamic behaviour can be used as additional parameter for control system design to improve both pitch and flight path control dynamics.

3.3 INFLUENCE OF DLC ON THE NEAL-SMITH CRITERION

An exercise was performed to find out the influence of the aircraft/DLC parameters mentioned before on pilot-aircraft system using the Neal-Smith closed loop pilot-aircraft criterion. The Neal-Smith criterion as described in reference [22] was proposed for pitch tracking using a bandwidth frequency of ω_{Bw} = 1.2 rad/sec for Flight Phase Category C Class III aircraft. In addition in this investigation the Neal-Smith method was used for flight path tracking with a bandwidth frequency set to ω_{Bw} = 0.8 rad/sec.

For the pilot aircraft system shown in figure 2 the required pilot phase compensation and the closed loop resonance were computed for pitch and flight path tracking as function of short period frequency and the DLC-parameter $n_{z(o)}/\dot{q}_{(o)}$. As can be seen in figure 5 pilot compensation for pitch tracking is influenced mainly by short period frequency ω_{nsp}. Increasing ω_{nsp} requires more lag compensation and leads to higher resonance. The DLC influence on pitch tracking is minor for low ω_{nsp}-values but shows increasing influence on closed loop resonance and phase lag compensation for ω_{nsp}-values greater than 0.8 rad/sec.

As shown in figure 6 for flight path tracking both increasing ω_{nsp} and DLC show the same tendencies in lead compensation and resonance variation. The greatest influence of DLC is also seen for ω_{nsp}-values greater than 0.8 rad/sec.

The influence of aircraft and control parameters on pilot compensation required for flight path tracking using a bandwidth frequency of ω_{Bw} = 0.8 rad/sec is presented in figure 7. Lines of constant lead or lag pilot compensation indicates how DLC should be varied with short period frequency variation. In addition this figure shows that there is an optimal relationship between heave and pitch motion parameters indicating that a large amount of direct lift is necessary for short period frequency values less and higher than one.

From this, the following important questions arise:

1. What is the lowest acceptable short period frequency for flight path control?
2. Can an aircraft with unacceptable low short period frequency behaviour be improved by DLC application?
3. What corresponding DLC efficiency is necessary?

4. DESCRIPTION OF IN-FLIGHT AND GROUND BASED EXPERIMENTS

4.1 EVALUATION CONFIGURATIONS

The longitudinal dynamic characteristics selected are representative for a wide body high wing loaded transport aircraft in the landing approach phase. The short period damping ratio ζ_{sp} and the heave damping Z_w are hold fixed for all configurations.

The parameters were selected to span a wide $n_{z(o)}/\dot{q}_{(o)}$-ratio range with constant steady state load factor per stick deflection or stick force as summarized in figure 8.

4.2 VARIABLE STABILITY AIRCRAFT HFB 320

The desired longitudinal dynamic characteristics were mechanized on the In-Flight Simulator HFB 320 aircraft owned and operated by DFVLR (figure 9).

The aircraft equipment includes (figure 10)

- primary flight control system, fully fly-by-wire
- electrically controlled flaps and spoilers
- electrically controlled thrust
- on board digital computer
- artificial feel system
- electrically controlled flight instruments
- on board data acquisition system, data recording and telemetry systems
- safety equipment.

In this aircraft the evaluation pilot occupies the right seat in the cockpit, the safety pilot the left seat. The evaluation pilot's electrical inputs from conventional column, wheel and pedals are fed to a on board digital computer which incorporates the advanced model following control concept shown in figure 11. Because of the fact that the equations of motion of model actuators and the aircraft model are programmed in the on board computer full state feedforward loop structure is possible which allows reducing the state feedback gain matrix elements and allows to improve the high frequency simulation capability. The model following control system was optimized using linear optimal control theory in combination with Solheim's method of prescribed eigenvalues [26, 27], which allows shifting the poles of the closed loop system to desired locations simultaneously fulfilling the integral cost function.

The linear optimized controller was tested and adjusted on an Hybrid EAI Pacer 600 computer on which the model following concept with nonlinear HFB 320 aerodynamics nonlinearities of control surface actuators (limited rates, hysteresis) and the data acquisition system was simulated.

In addition, because of the model following concept used, the HFB 320 can be used as conventional fixed based simulator offering in-flight and ground based experiments with the identical system.

4.3 MEASUREMENT SITUATION

To obtain handling qualities data and pilot-aircraft performance measures an altitude compensatory tracking task similar to an ILS approach was selected. The pilot had to follow a commanded altitude by minimizing the indicated error between commanded and actual altitude. The altitude error was displayed to the pilot using the pitch command bar of the attitude director indicator (ADI). Full command bar scale deflection down represents 16 m too high altitude error. The effective bandwidth of the altitude forcing function used, was 0.4 rad/sec. The standard deviation of the input is 6 m, equivalent to 0.75 cm on the display instrument. In addition, the pilot had to hold speed manually within $\pm$ 5 kts and keep the wings level.

Longitudinal model response and basic aircraft's lateral response state variables were displayed to the pilot. A general view of the evaluation pilot's flight instruments is shown in figure 12. The flight tests were carried out under non turbulence conditions at flight level 170 with 145 kts speed and 30 deg reference flap position. Every tracking run was flown for at least 140 seconds measuring time in order to ensure that 125 seconds of usable test time was available for analysis. Pilot effort ratings were obtained after completition of six evaluation runs according to questions stated in a pilot questionnaire as shown in figure 13. Model and aircraft state variables were recorded on board on a digital tape for further processing. Eight-channel quicklook plots of the most important variables were available on the ground via a telemetry system.

A total of 60 compensatory tracking runs were executed in-flight and 48 on ground for eight different configurations with one pilot. The tracking runs on the ground used the HFB 320 as a fixed base simulator with controls, column forces, flight instruments and displayed variables identical to those used in-flight. These runs were carried cut to compare the results with and without motion cues.

Figure 14 presents a typical altitude tracking time history (HCM = altitude forcing function, HM = model altitude). In addition in-flight simulation quality is shown by plotting model and simulator aircraft pitch attitude and pitch rate side by side.

5. DISCUSSION OF RESULTS

Although the full planned field of configuration/pilot combinations could not be realized because of flight test time constraints, the results obtained from the eight ω_{nsp}/DLC combinations executed in-flight and on the ground with one pilot will be presented.

5.1 PILOT-AIRCRAFT PERFORMANCE

Pilot-aircraft performance is expressed in mean standard deviation (MSD) of altitude error. These data were obtained by taking the mean of the RMS-values of each run. As shown in figure 15 for ω_{nsp} = 1.6 rad/sec the altitude error decreases with increasing DLC effectiveness (increasing $n_{z(o)}/\dot{q}_{(o)}$-ratio) for both in-flight and on the ground tracking experiments. Further as can be seen in this figure the main reduction in altitude error occurs from Configuration A1 to A3 varying $n_{z(o)}/\dot{q}_{(o)}$ from - 1 to 0.5. With higher DLC effectiveness performance is not improved. For ω_{nsp} = 0.8 for all DLC configurations nearly constant pilot-aircraft performance is obtained, both in-flight and on the ground tracking. Only small altitude error reduction occurs with increasing DLC effectiveness.

5.2 PILOT EFFORT RATINGS

The effort ratings for the altitude tracking task are summarized in figure 16. For ω_{nsp} = 1.6 rad/sec increasing $n_{z(o)}/\dot{q}_{(o)}$-ratio was rated with decreased effort for both in-flight and on the ground tracking. The greatest rating difference exists between Configuration A1 to A2 ($n_{z(o)}/\dot{q}_{(o)}$ = - 1 to - 0.5). Comparing in-flight and on the ground tracking a difference in effort rating can be seen for high DLC Configuration A5 ($n_{z(o)}/\dot{q}_{(o)}$ = 20). The best rating is given for the highest DLC case (A5) in-flight.

For ω_{nsp} = 0.8 rad/sec only the DLC Configuration C4 (in-flight) ($n_{z(o)}/\dot{q}_{(o)}$ = 5) shows decreased effort ratings compared to the other configurations. Configuration C5 was repeated in-flight on another day. Results show low pilot rating variability. Rating differences between in-flight and on the ground are evident for the high DLC Configuration C5.

AD-A071 709 ADVISORY GROUP FOR AEROSPACE RESEARCH AND DEVELOPMENT--ETC F/G 1/3
STABILITY AND CONTROL.(U)
MAY 79
UNCLASSIFIED AGARD-CP-260 NL

4 OF 4
AD A071709

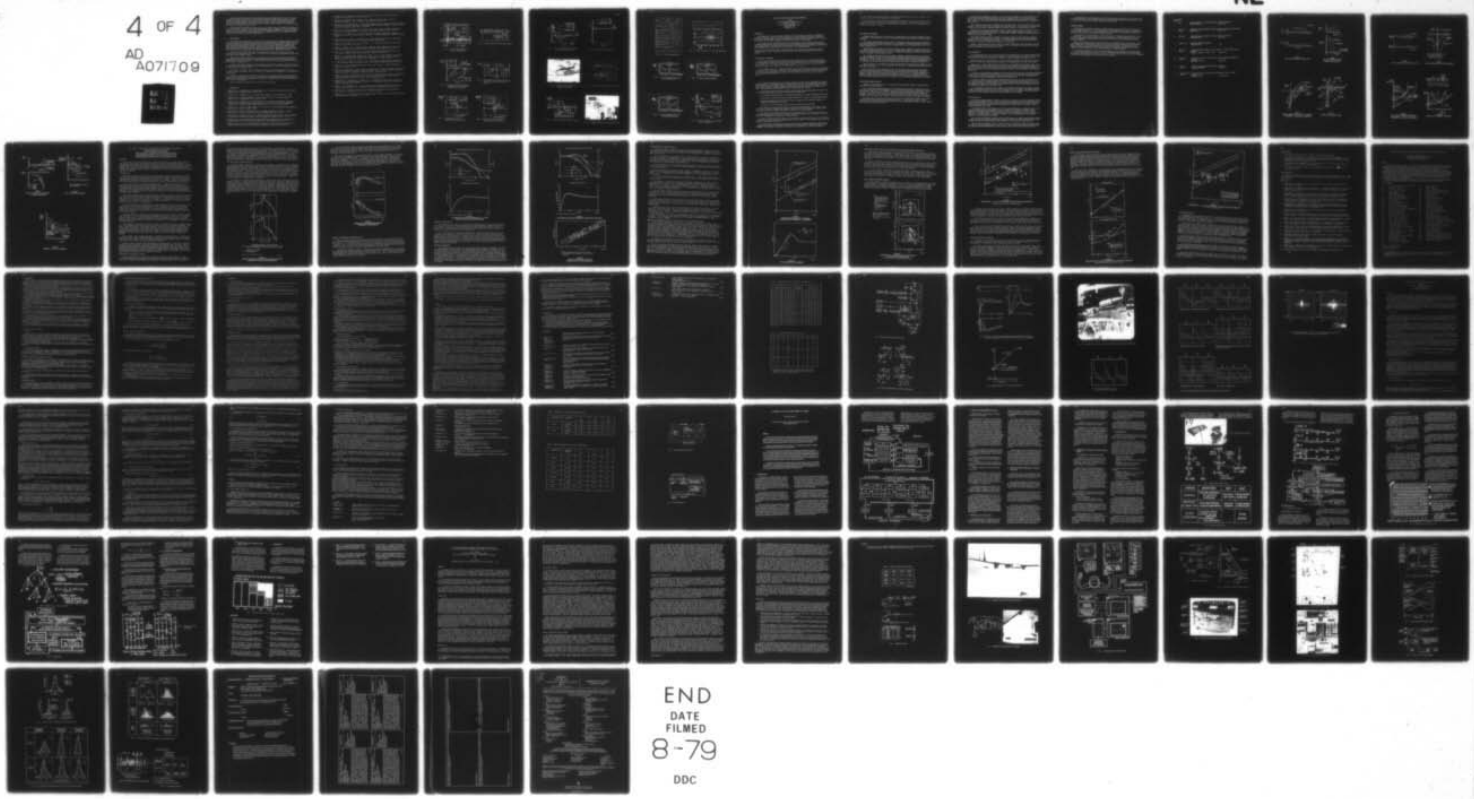

END
DATE FILMED
8-79
DDC

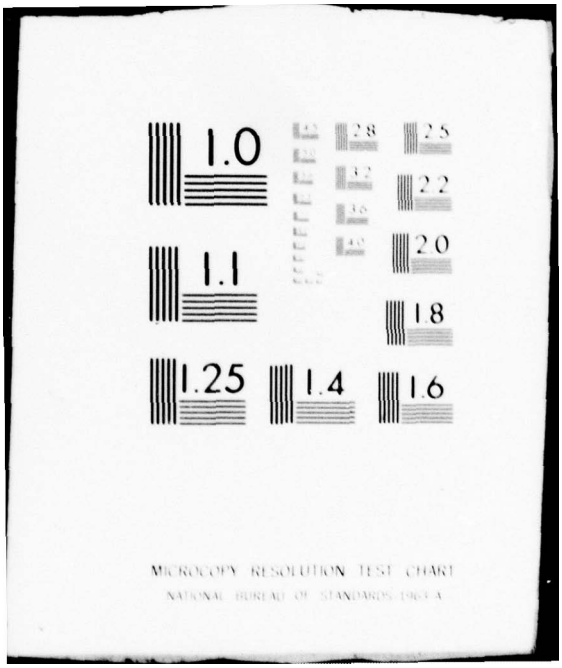
1.0
1.1
1.25
1.4
1.6
2.8
3.2
3.6
4.0
2.5
2.2
2.0
1.8
MICROCOPY RESOLUTION TEST CHART
NATIONAL BUREAU OF STANDARDS 1963 A

Mean standard deviation of column deflections are summarized in figure 17. As can be seen for both in-flight and on the ground increasing column deflections occur with higher DLC effectiveness. On the ground results with no motion cues show higher MSD-values and higher standard deviations than in-flight. Time histories show the pilot controls more agressively on the ground than in-flight and he tends to overcontrol much more due to the lack of motion cues.

Plotting the rating results in the $n_{z(Q)}/n_{z(\infty)}$ over $M_\delta/n_{z(\infty)}/\delta$-plane (see figure 18) lines of constant ratings can be drawn which show similar tendencies to the theoretical computed lines of constant pilot lead lag phase compensation shown in figure 7. Because of the few data points the relationships and the optimum region can be estimated only and must be validated by further experiments.

6. CONCLUSIONS

This paper has presented the results of a flight research program conducted to determine the influence of short period frequency/DLC combinations on handling qualities for a wide body high wing loaded aircraft for the flight path tracking task. These results have indicated the improving effects of DLC on flight path tracking as measured by pilot-aircraft performance and pilot effort rating. Further the pilot effort ratings show correlation with theoretically obtained lead-lag phase compensation of the closed loop pilot-aircraft system using the Neal-Smith method for flight path tracking.

There are some indications that the theoretical relationship between the short period aircraft eigenmotion and DLC is valid and that optimal ω_{nsp}/DLC combinations exist for flight path tracking tasks.

Comparison of data obtained from in-flight and ground based tracking experiments show similar performance results but different effort ratings for the high DLC configurations. No motion cues lead to higher standard deviation of column deflection and the pilot tends to overcontrol.

It had to be mentioned that the Neal-Smith pitch attitude control criterion cannot be used for flight path tracking as can be demonstrated for the DLC Configuration A1 with a large amount of negative lift.

The closed loop pitch control resonance and pilot phase compensation values lie within the PR 6.5 boundary. But for flight path tracking this configuration is completely unacceptable.

Therefore, especially for DLC configurations, both pitch control and flight path control had to be taken into account. To establish the handling qualities boundaries for flight path tracking more experiments with the full planned field of parameters and with more pilots are necessary.

This is planned by DFVLR for the 1979 flight test phase.

7. REFERENCES

1. Smith, L.R., Prilliman, F.W., Slingerland, R.D., "Direct Lift Control as a Landing Approach Aid", AIAA Paper No. 66-14, 1966.

2. Nelsen, G.L., Lorenzetti, R.C., "Direct Lift Control for the LAMS B-52", 1968.

3. Jansen, G.R., "Flight Evaluation of Direct Lift Control on the DC-8 Super 63", The Society of Experimental Test Pilots, 1968.

4. Chase, Th. W., Falkner, V.L., Helfinstine, R.F., "Study and Simulation Program to Investigate the Mechanization of an Aircraft Flight Control System that Employs Direct Lift", Technical Report AFFDL-TR-68-69, Vol. I, II, III, June 1968.

5. Stickle, J.W. et al., "Flight Tests of a Direct Lift Control System during Approach and Landing", NASA TN D-4854, 1968.

6. Olson, R.W., "Direct Lift Control for a Variable-Sweep-Wing Aircraft", Thesis GGC/EE/69-14, A.F. Institute of Technology, WPAFB, Ohio, Jan. 1969.

7. Quigley, H.C., Snyder, C.T. et al., "Flight and Simulation Investigation of Methods for Implementing Noise-Abatement Landing Approaches", NASA TN D-5781, 1970.

8. Gilbert, J.W., "A Theoretical and Flight Simulator Investigation of a Direct Lift Control System for a BAC One-Eleven Aircraft", ARC-Aero/8 & C/160, 1972.

9. McNeill, W.E. et al., "A Flight Study of the Use of Direct-Lift Control Flaps to Improve Station Keeping during Inflight Refueling", NASA TM X-2936, 1973.

10. Kohlman, D.L., "Evaluation of Spoilers for Light Aircraft Flight Path Control", Journal of Aircraft, Vol. 11, No. 8, 1974.

11. Weber, W.B., Mathews, R.H., Vaughn, R.E., "Model F4-J Direct Lift Control", McDonnel Company, St. Louis, Missouri, Report E 907, Sept. 1967.

12. Stumpfl, S.C., Whitmoyer, R.A., "Horizontal Canards for Two-Axis CCV Fighter Control", Air Force Flight Dyn. Laboratory, Preprint AGARD Conference "Impact of Active Control on Aircraft Design", Paris, 14.-17.10.1974.

13. Mooij, H.A., "Flight Evaluation of Direct Lift Control and its Effect on Handling Qualities in Carrier Approach", Princeton University, Report No. 811, 1967.

14. Miller, G.E., Traskos, R.L., "Flight Evaluation of Engine Response, Flight Path Stability, Tail Lift, and Direct Lift Control", Princeton University, Report No. 888, 1971.

15. Tomlinson, B.N., "Direct Lift Control in a Large Transport Aircraft - A Simulator Study of Proportional DLC", RAE Technical Report 72154, 1972.

16. Barnes, A.G., Houghton, D.E.A., Colclough, C., "A Simulator Study of Direct Lift Control", ARC CP No. 1199, 1972.

17. Hanke, D., Lange, H.-H., "Flugmechanische Probleme beim Landeanflug mit direkter Auftriebssteuerung am Beispiel der HFB 320 Hansa", DGLR Druck 73-024, 1973.

18. Mooij, H.A., "Handling Quality Criteria Development for Transport Aircraft with Fly-by-Wire Primary Flight Control Systems", NLR MP 74022 U, 1974.

19. Hamel, P.G., Wilhelm, K.K., Hanke, D.H., Lange, H.-H., "Steep Approach Flight Test Results of a Business-Type Aircraft with Direct Lift Control", DFVLR, Preprint AGARD Conference "Take-off and Landing", Edinburgh, 1.-5. April 1974.

20. v. Gool, M.F.C., Hanke, D., Lange, H.-H., "Flight Path Angle Tracking Experiments in the DFVLR HFB 320 Equipped with Direct Lift Control", DFVLR IB 154-75/32, 1975.

21. Hanke, D., "In-Flight Investigation of Direct Lift Control in Landing Approach", DFVLR IB 154-77/25, 1977.

22. Neal, T.P., Smith, R.E., "An In-Flight Investigation to Develop Control System Design Criteria for Fighter Airplanes", AFFDL-TR-70-44, Vols. I and II, Air Force Flight Dynamics Laboratory, Wright-Patterson AFB, Ohio, December 1970.

23. Chalk, C.R. et al., "Revisions to MIL-F-8785 B (ASG) Proposed by Cornell Aeronautical Laboratory under Contract F33615-71-C-1254", AFFDL-TR-72-41, Air Force Flight Dynamics Laboratory, Wright Patterson AFB, Ohio, August 1973.

24. Hodgkinson, J., LaManna, W.J., Heyde, J.L., "Handling Qualities of Aircraft with Stability and Control Augmentation Systems - A Fundamental Approach", Aeronautical Journal, Februar 1976, p.75-81.

25. Brulle, R.V., Anderson, D.C., "Design Methods for Specifying Handling Qualities for Control Configured Vehicles. Technical Discusssion", AFFDL-R-D-73-142, Vol. I.

26. Solheim, O.A., "Design of Optimal Control Systems with Prescribed Eigenvalues", Int. Journal of Control, Vol. 15, No. 1, 1972, p.143-160.

27. Henschel, F., "The Determination of Flight-Tracking Controllers Using Solheim's Pole-Shifting Method", ZFW Band 1, No. 5, 1977.

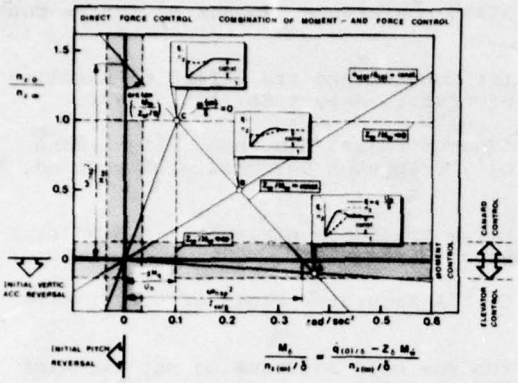

Fig. 1 Short Period Handling Quality Parameters

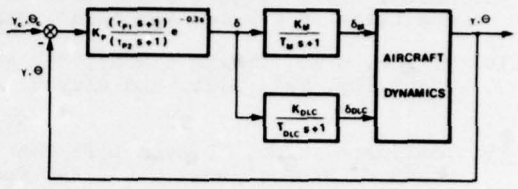

Fig. 2 Closed Loop Pilot-Aircraft System

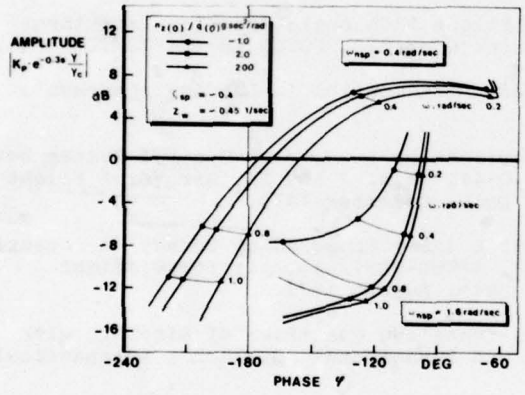

Fig. 3 Influence of Short Period Frequency/DLC Combinations on Flight Path Control

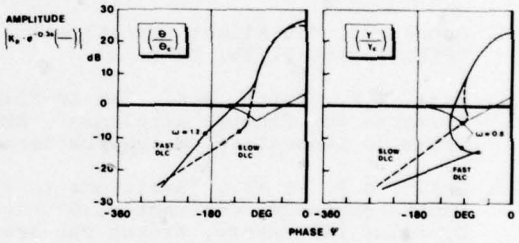

Fig. 4 Influence of DLC Actuator Rate on Pitch Attitude and Flight Path Control

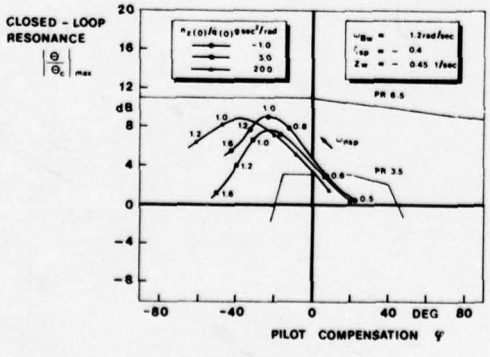

Fig. 5 Influence of DLC on Closed Loop Pitch Control

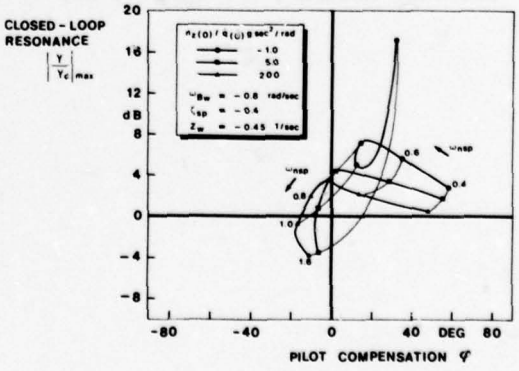

Fig. 6 Influence of DLC on Closed Loop Flight Path Control

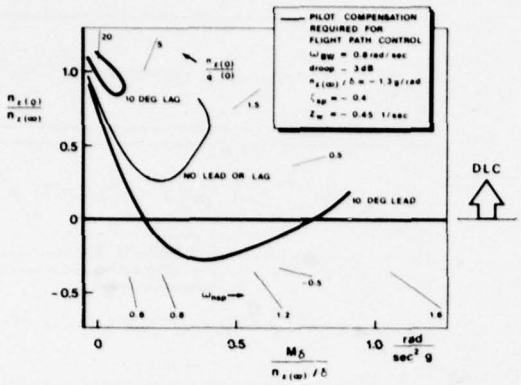

Fig. 7 Pilot Compensation Required for Flight Path Control

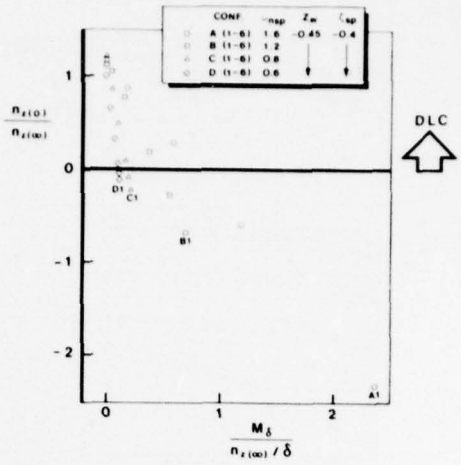

Fig. 8 Evaluation Configurations

Fig. 9 DFVLR HFB 320 Variable Stability Aircraft

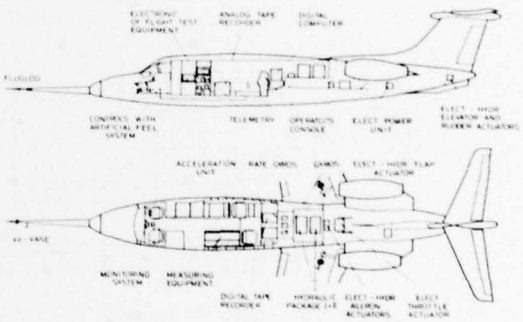

Fig. 10 Flight Test Equipment Installation

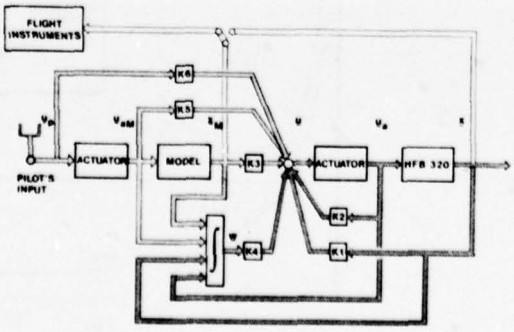

Fig. 11 Model Following Control System

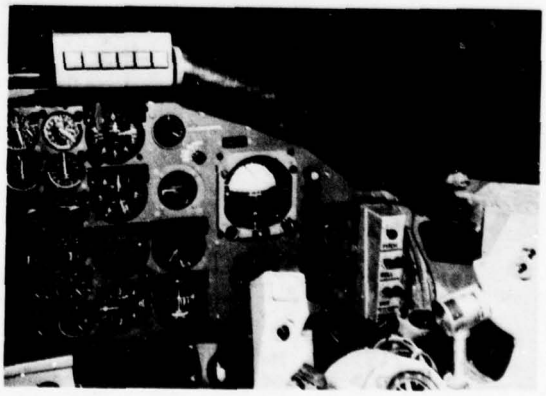

Fig. 12 Evaluation Pilot's Instrument Panel

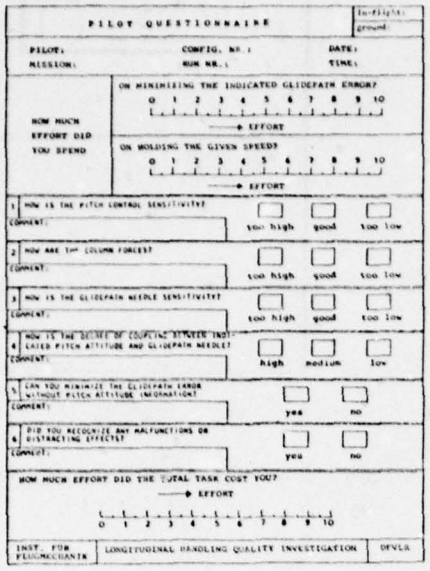

Fig. 13 Pilot Questionnaire

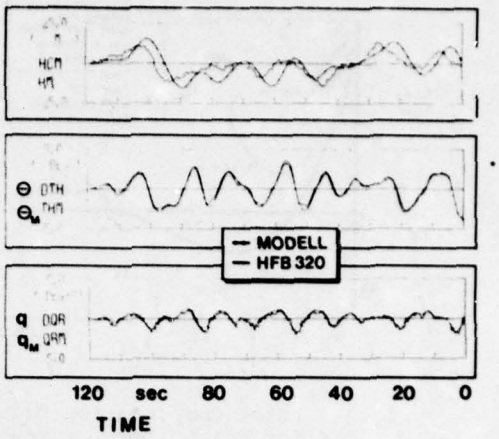

Fig. 14 Time Histories of Altitude Tracking

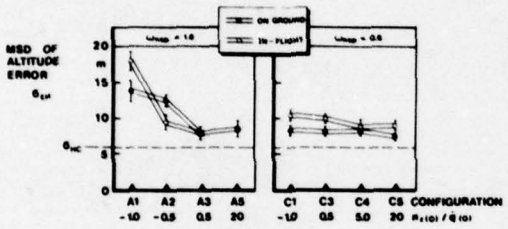

Fig. 15 Mean Standard Deviation of Altitude Error

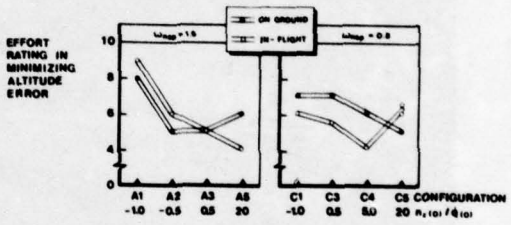

Fig. 16 Effort Rating Summary

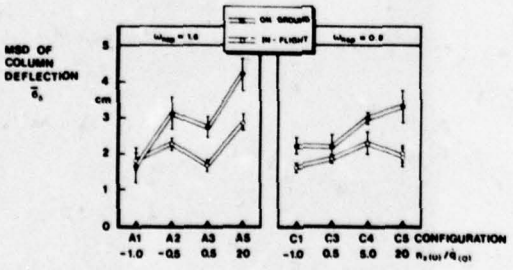

Fig. 17 Mean Standard Deviation of Column Deflection

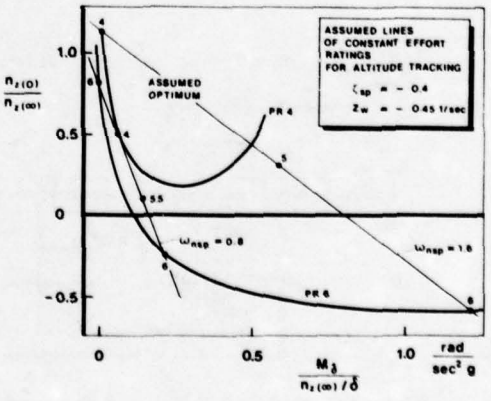

Fig. 18 Effort Ratings vs Pitch/Heave Motion Parameters

FLYING QUALITIES AND THE FLY-BY-WIRE AEROPLANE

by
J. C. Gibson
Principal Engineer - Flying Controls
British Aerospace
Aircraft Group, Warton Division
Preston PR4 1AX
Lancashire, U.K.

INTRODUCTION

The Tornado flight control system was designed to give good stability, damping, and resistance to external disturbances. This was achieved by optimisation of feedback gains and filters. Response to pilot inputs was then shaped by stick commands gains and filters. These were designed mainly to requirements based on Mil.Spec.8785B augmented by other criteria judged to be applicable.

This process resulted in generally excellent flying qualities. Pilots reported a high level of confidence inspired by the easy and precise control with extremely good circuit handling and instrument flight characteristics. However, some deficiencies were noted associated in some cases with non-aircraft-like responses and these were eliminated by modifications to the command shaping.

This experience has emphasised that a specification which will ensure entirely satisfactory flying qualities does not exist. This paper illustrates several areas where requirements are deficient or absent.

PITCH CONTROL AT TOUCHDOWN

Fig. 1 shows an incident which occurred after several hundred flights. A pilot-induced attitude oscillation developed during the last few seconds of the landing flare in which the stick was deflected to its forward limit. There was no malfunction of the control system, but when an aircraft response of this form can occur it is evident that the command shaping requires modification. Simulation and conventional analysis had not indicated the possibility of such an event.

With no handling deficiency in away-from-ground flight to explain the PIO, attention was concentrated on flying qualities in the flare. Landing with pitch augmentation off was easy and precise, but was less so with it on, with rather light stick forces. The main reasons were believed to lie in differences in the stick pumping characteristics. Stick pumping occurs in the last seconds of the flare of many aircraft.

Fig. 2 shows the calculated pitch acceleration frequency responses for the unaugmented and augmented approach mode case. Stick pumping occurs at frequencies near zero lag. The augmented case has a much higher amplitude and a much smaller range of suitable frequencies which also lie much closer to the short period natural frequency than the unaugmented case. Naturally, when acceleration is in phase with the stick, pitch attitude is 180 degrees out of phase, the basic situation in a PIO.

It was concluded that the solution would lie in modifying the stick pumping dynamics to ensure that it would remain a subconscious activity, the contributory factors being:

- a low pumping frequency results in a large attitude response at a constant acceleration amplitude,
- tight control of the pumping frequency becomes necessary if the range for low phase lags is small,,
- a pumping frequency too close to the short period frequency does not adequately separate the conscious and subconscious activities,
- a low stick force can too easily permit an excessive inadvertent gain increase.

Fig. 3 shows four calculated open loop pitch attitude frequency responses to stick input. It has been found to be useful to assess stick pumping in this Nichols plot form because attitude PIO margins can be seen directly and the basic acceleration information can be derived easily.

The unaugmented and augmented responses are from the previous slide. Here can be seen the much higher gain when augmented, the narrower spread of suitable frequencies, and the closeness of the pumping and control frequencies, in contrast to the unaugmented case.

An interim standard had similar dynamics to the original, but a gain much closer to the satisfactory unaugmented case. Flare control was greatly improved but was judged not to be completely free of the possibility of inadvertent overcontrol.

The final standard further decreased the gain and altered the dynamics considerably. The range of frequencies was widened and increased to higher values while leaving the low frequency behaviour nearly unchanged. Flare control is completely satisfactory and no possibility of a PIO is now foreseen.

Fig. 4 shows a more complete picture of the response characteristics of the final standard, and how proposals for flying qualities requirements can be derived.

Investigation of acceptable limits by flight trials or simulation is desirable but difficult because of the risks in flight or the absence of stick pumping in simulation. These criteria are expected to be valid for the general class of combat aircraft typified by Tornado, but it is not known how far they extend to larger types, for example.

ROLL CONTROL AT TOUCHDOWN

Although lateral handling in the circuit was very satisfactory, an occasional overcontrol tendency was observed in the form of about two cycles of pilot-induced bank angle oscillation immediately before touchdown.

Fig. 5 shows typical records of such an event. Although quite large stick inputs were sometimes used the bank angles reached were usually only one or two degrees. The cause was clearly the very high bank angle gain used by the pilot, equivalent on occasion to the use of full lateral stick for a five degree bank angle error.

Although records of landings on many aircraft typically show a considerable lateral stick activity at a relatively high frequency having little effect on bank angle, there is no consistent evidence of an ordered stick pumping such as in the pitch axis. A somewhat similar approach was used to derive modifications to eliminate this PIO tendency, however.

Fig. 6 shows the open loop bank attitude frequency response in Nichols plot form for the original and modified systems. Although no attempt was made to optimise the pilot-bank attitude closed loop tracking, quite clearly the modified system provides larger phase margins and hence permits better closed loop damping. The PIO frequency has been shifted to a value well above 1.0 Hz and the amplitude is so low that even the very high pilot gain seen occasionally will not result in closed loop instability.

These curves show how the effects of actuation rate saturation can reduce the gain margins if large stick inputs are used, but it is very unlikely that this will occur if good margins are maintained up to about 50% of full stick.

The only specific criterion suggested is that the pilot-bank attitude closed loop should remain stable with a pure pilot gain of full lateral stick for five degrees bank angle error. Even with excellent control characteristics, such a high gain may occur as a result of an adverse combination of weather, visibility and other distractions at the point of touchdown. It is probably advisable in addition to ensure that the roll acceleration response at the PIO frequency is approximately constant, that the frequency spread around this is not too small, and that this basic frequency is at least 1.0Hz.

PITCH ATTITUDE DYNAMIC RESPONSE

Experience has shown deficiencies in the Calspan Corporation dynamic response criterion based on simple open loop characteristics.

Fig. 7 shows the proposed requirement based on the Neal and Smith criterion. This shows that the pitch tracking qualities of four standards at a typical flight condition did not correlate very well with this criterion. The first, D, in the Level 1 region, was good but resulted in slight overshoot. The second, E, is only just into Level 2 but gave unacceptable overcontrolling when tight tracking was attempted. The third, F, still further into Level 2, was in fact much better than E but gave a small sustained oscillation when tracking tightly. The final version, G, just back into Level 1 was excellent.

The method used to derive the final version went back to the original Neal and Smith work on pitch attitude tracking using a simple pilot model as shown in Fig. 8. This permits a droop of 3 dB at frequencies below the bandwidth at 90 degrees phase lag and some unspecified resonance at higher frequency with a pilot time delay of 0.3 seconds.

These values were modified as follows. It was not obvious that a droop of 3 dB was acceptable at all frequencies below the bandwidth and a design aim of zero droop was selected. The resonance was to be kept to less than 2 dB. A high bandwidth was difficult to achieve with a pilot delay of 0.3 seconds, and a value of 0.15 seconds was used instead, which was believed to be more appropriate to represent very tight tracking.

These curves show the closed loop response with this reduced delay, and a gain selected to give zero resonance. Versions E and F show low frequency droop, Version G none. A gain increase to eliminate droop in Versions E and F clearly introduces resonance, shown more obviously in the Bode curves in Fig. 9.

Here zero droop at 0.25Hz was arbitrarily chosen. Version E shows an extreme resonance - in flight this appeared as an unacceptable overcontrol. Version F shows a smaller resonance - in flight this appeared as a small continuous oscillation in tight tracking. Version G achieves zero droop and resonance, giving excellent tracking in flight.

This design approach has not only resulted in the correct result but also gives good correlation with pilot opinion for unsatisfactory tracking. No suggestion is made here for acceptable droop and resonance limits or an optimum pilot time delay, but a criterion based on these modified values seems to be desirable to replace or supplement the simpler open loop version.

Finally, it seems obvious that there should be a range of satisfactory stick force gains to be used in tracking, similar to stick force per g. Values of 15 to 25 N per degree of attitude error have been found to be acceptable but the limits are not known.

ROLL ACCELERATION

Roll acceleration limits are not explicitly defined in Mil.Spec.8785B. For a rolling response which can be described closely by a roll mode time constant, the specification of this constant and of the time to bank implicitly defines the maximum roll acceleration. Such a relationship is shown in Fig. 10.

This was taken from a 1959 NASA report. Lines of constant bank angle in one second and of constant steady roll rate show this unique relationship between roll acceleration and roll mode time constant.

However, this no longer need apply when a high gain roll rate command control system is used. The two cases shown are the same flight condition and have the same steady roll rate and time to bank, but the peak roll acceleration in one case is twice as high as the other. The first response was described as harsh or jerky, and control system modifications were made to produce the second result. This was highly satisfactory.

It seems that pilot opinion may depend not only upon the maximum value of the initial roll acceleration but also upon its relationship to the subsequent roll rate history. The complaints of harshness applied to small inputs as well as to large ones. Another factor may be the jerk or first time derivative of roll acceleration, which was approximately halved by this modification.

Another good reason for minimising the peak acceleration is the fact that full mass balance of the stick against lateral acceleration is usually difficult, especially with the added mass of the pilot's arm. The consequences of the high lateral g at the stick resulting from the roll acceleration can range from inadvertent nuisance force commands to the introduction of an oscillatory mode coupling the stick feel dynamics and some other control system mode.

It is suggested that there is a need to specify roll acceleration limits for such high gain control systems. The boundaries given here are too wide as has been shown. This shaded area probably represents satisfactory values for Class IV Category A roll performance. It is not possible to define the limits of this area on this experience alone, and further investigation may be needed.

STICK FORCE PER 'g'

Aircraft with unpowered controls exhibit a stick force per g which is virtually independent of speed, neglecting compressibility effects. If the stick force per g is satisfactory for structural protection at high speed, then during the final approach the stick force required to stall the aircraft may be low. This is usually acceptable because the stick displacement per g becomes large at low speed, forming a substitute feedback to the pilot.

With powered controls, the variations in stick force and displacement per g depend also on the feel and control system and it becomes possible for both to remain at low values at low speed. This is permitted by Mil.Spec.8785B but it does not seem very likely to be satisfactory. Prior to formal publication, an earlier version of this Mil.Spec. actually required greatly excessive stick forces at low speed, well above values known to be optimum. Because of this, an investigation of the literature referred to in these publications was made.

Fig. 11 shows the boundaries resulting from this investigation, for typical high and medium g limits. At high speed they have the same values as Mil.Spec.8785B. As speed decreases the required stick forces increase until they effectively become lines of constant stick force per unit angle of attack.

This shaded area represents a number of combat aircraft in the approach configuration which ranged from upper to lower satisfactory limits of stick force. Another criterion was given in a Northrop paper some years ago and when transformed into these axes also confirms these boundaries extremely well.

It is suggested that such boundaries can be taken as an optimum design aim for combat aircraft with a conventional centre stick, and possibly also for a sidestick where conventional force levels are used. For other controllers a similar form of boundaries can be expected.

CONCLUDING REMARKS

Many promising new handling criteria of the past have eventually failed the test of applicability to a wide range of aircraft. It is believed that the criteria suggested in this paper will be generally valid for combat aircraft. With the increasing number of high order control systems such experiences will become more frequent in the absence of improved criteria.

The introduction of sidesticks adds a further dimension to such problems, particularly as it does not seem obvious that the optimum layout has yet been established. The main effect may simply be to alter the optimum stick command shaping to maintain the same overall input processing into the same controlled elements.

Still further problems may arise with the introduction of selectable control mode concepts. While investigations into the usefulness of these are still far from complete, certain obvious requirements exist. There should be the least possible number of new modes to learn; the pilot should not be expected to have to command them in a way which conflicts with basic instincts learned in his early training; and he must not have to switch them individually in a combat situation.

It is probably unrealistic to expect that comprehensive new flying qualities criteria will emerge before the new generation of aircraft is in service. Nevertheless the potential for the introduction of undesirable flying qualities by the use of ever more complex fly-by-wire control laws must be constantly reviewed to avoid experiences of the kind described in this paper.

BIBLIOGRAPHY

1. Anon — Miltary Specification 'Flying qualities of piloted airplanes' MIL-F-8785B(ASG), August 1969

2. Chalk, C.R. et al — Revisions to MIL-F-8785B(ASG) Proposed by Cornell Aeronautical Laboratory. AFFDL-TR-72-41 April 1973

3. Bihrle, W. — A Handling qualities theory for precise flight path control. AFFDL-TR-65-198. June 1966

4. O'Gara, J.F. — Aircraft crosswind performance AGARD Report 492 1964

5. Neal, T.P. et al — A flying qualities criterion for the design of fighter flight control systems. Journal of Aircraft. Vol.8, No.10. October 1971

6. Creer, B.Y. et al — A pilot opinion study of lateral control requirements for fighter-type aircraft. NASA Memo 1-29-59A March 1959

7. Chalk, C.R. et al — Airplane flying qualities specification revision. AIAA Paper No.68-245 March 1968

8. Gallagher, J.T. et al — Use of simulators in the design and development of flight control systems. SAE Paper 730933. October 1973

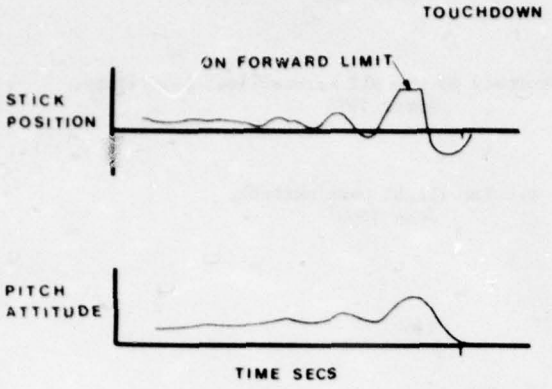

FIGURE 1
PITCH ATTITUDE OSCILLATION DURING FLARE

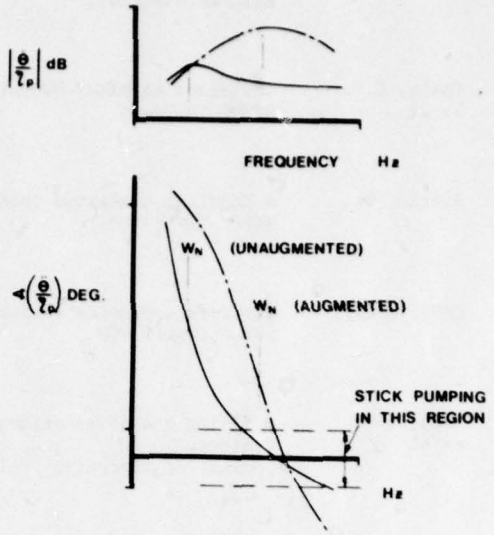

FIGURE 2
PITCH ACCELERATION RESPONSE
APPROACH CONFIGURATION

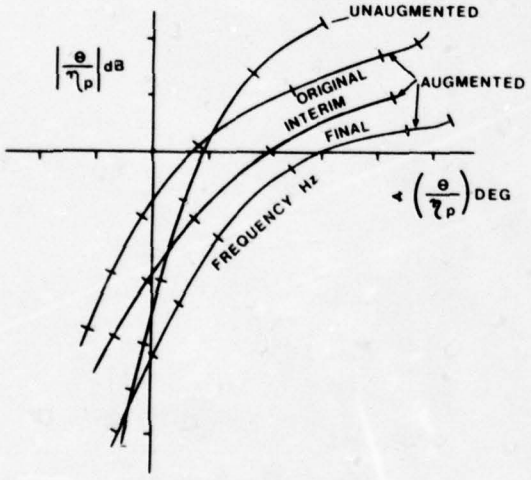

FIGURE 3
LANDING APPROACH OPEN LOOP PITCH RESPONSES
COMPARISON OF DEVELOPMENT STANDARDS

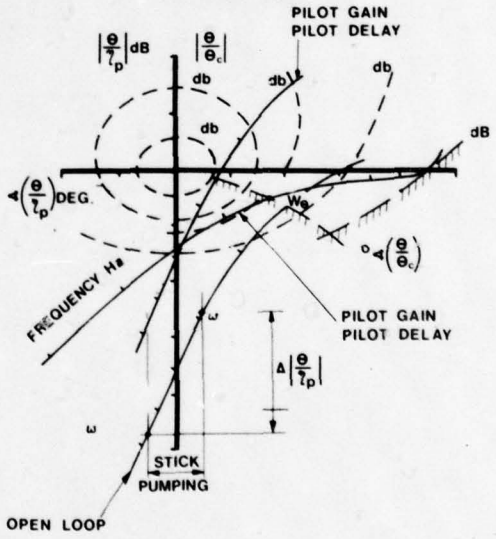

FIGURE 4
PROPOSED STICK PUMPING CRITERIA

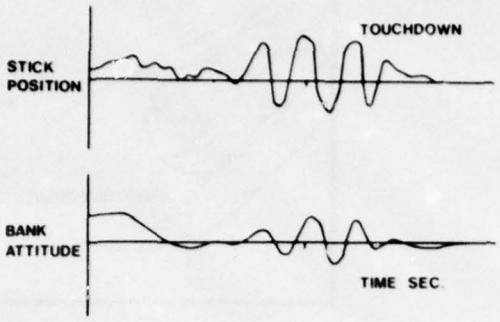

FIGURE 5
ROLL ATTITUDE OSCILLATION DURING FLARE

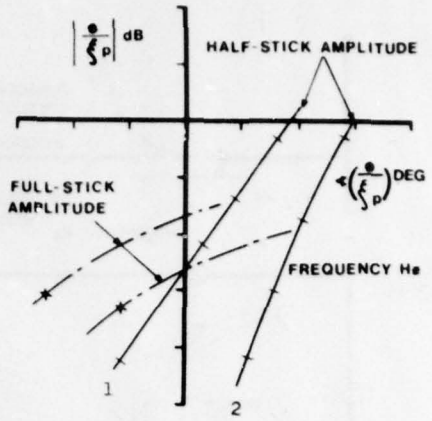

OPEN LOOP RESPONSE TO STICK :
1 PROTOTYPE STANDARD
2 PRODUCTION STANDARD

FIGURE 6
LANDING APPROACH BANK ATTITUDE RESPONSES

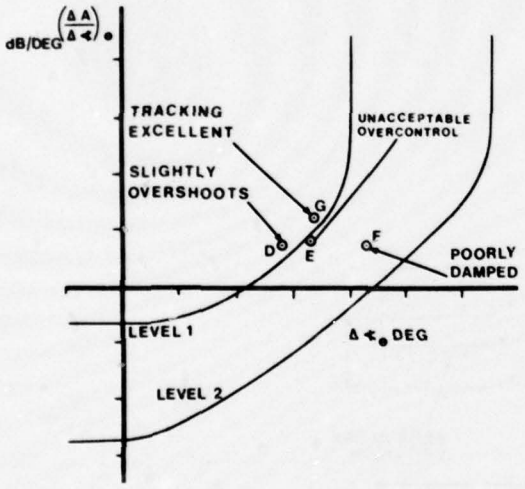

FIGURE 7
PITCH DYNAMIC RESPONSE CRITERION-REF. 2
COMPARISON WITH TORNADO DEVELOPMENT

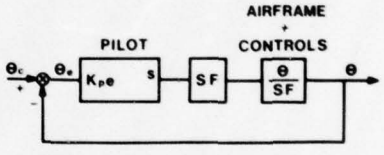

MODEL OF PITCH ATTITUDE TRACKING

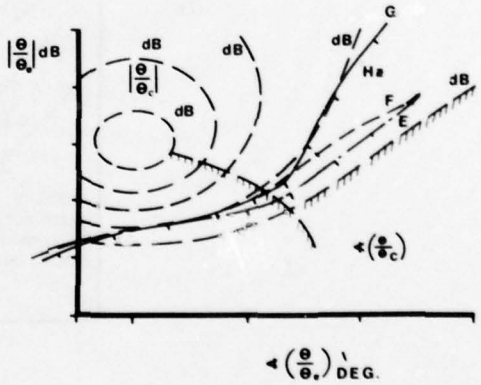

FIGURE 8
MODIFIED PITCH RESPONSE ASSESSMENT

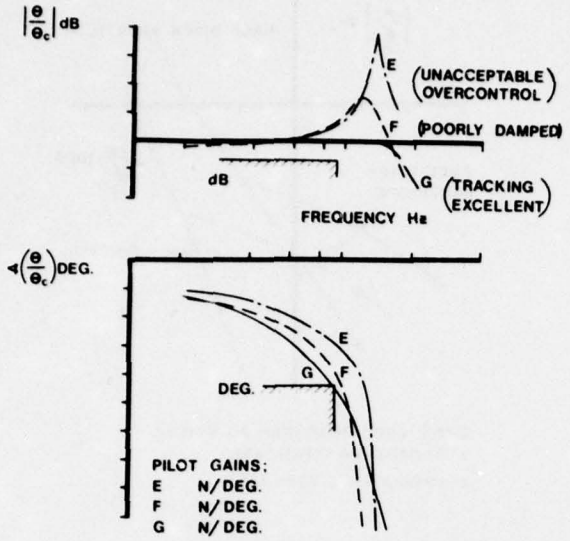

FIGURE 9
EFFECT ON CLOSED LOOP RESONANCE
OF DROOP MINIMISATION

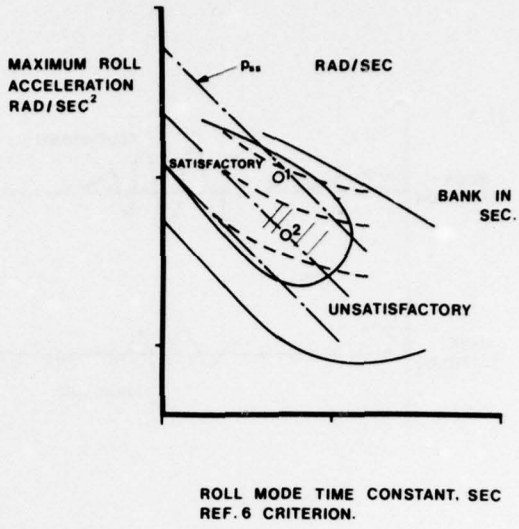

FIGURE 10
ROLL ACCELERATION CRITERION

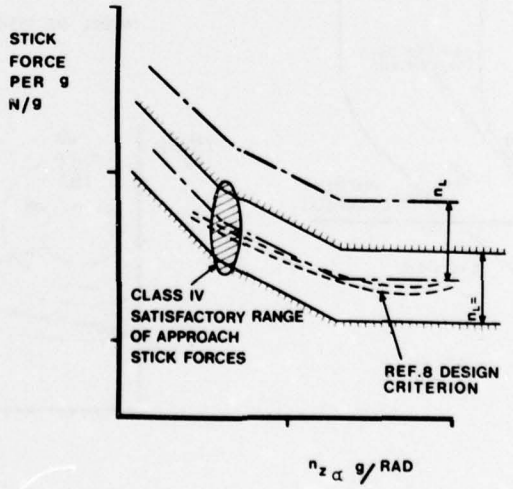

FIGURE 11
PROPOSED STICK FORCE BOUNDARIES

ARE TODAY'S SPECIFICATIONS APPROPRIATE FOR TOMORROW'S AIRPLANES?

Mr R.C.A'Harrah, Naval Air Systems Cmd Hq,
Air 53011, Washington, D.C. 20361, USA
Mr W.J.Lamanna, Dept. 241, Bldg. 33, Level 3, McDonnell Aircraft Company
McDonnell Douglas Corporation, P.O. Box 516, St. Louis, MO 63166, USA
Mr J.Hodgkinson, Dept. 241, Bldg. 32, Level 2, McDonnell Aircraft Company
McDonnell Douglas Corporation, P.O. Box 516, St. Louis, MO 63166, USA

ABSTRACT

This paper presents an approach for taking any system of a higher order than is addressed in the current Specifications, and producing an "equivalent" system of an appropriate order, which is directly relatable to the Specification parameters. Example applications of the equivalent systems approach to various higher order systems are presented; the insights of this approach to the newest fighter aircraft design are discussed; and very preliminary results are presented on a flight program which investigates equivalent systems.

INTRODUCTION

The current Flying Qualities Specifications were derived from aircraft that were only modestly influenced by any stability augmentation systems. The motions of these aircraft were adequately represented by the relatively simple equations derived in the stability and control texts over the past thirty or so years; logically, the Specifications deal only with the fundamental parameters in these classic equations of motion.

In marked contrast, the flight characteristics of tomorrow's aircraft tend to be dominated by the stability and control augmentation systems, and only modestly influenced by the bare airframe characteristics. Thus, the motions of tomorrow's aircraft are represented by significantly more complex equations, with the level of complexity and order of the system established at the discretion of the control system designer. Therefore, the interpretation, and indeed the relevancy, of the existing specification is currently being debated.

Are today's specifications appropriate for tomorrow's airplane? From the U.S. Navy, the answer is YES with respect to the current Military Specification for Flying Qualities of Piloted Aircraft, MIL-F-8785B, (Reference 1). Today's specification is just as appropriate for tomorrow's aircraft as for today's or yesterday's aircraft. The specification is not perfect, all inclusive or beyond improvement; but is rationally interpretable, effective and understandable.

From the viewpoint of the McDonnell Aircraft Company, the answer is also yes. The experience of the aircraft manufacturers is that the specification, though imperfect, logically ties their hard-won experience on six operational fighters to the current Navy fighter and their future designs. The advent of the digitally implemented high authority "fly-by-wire" stability and control augmentation system has not eclipsed the current specification.

The high authority "fly-by-wire" technology has given the aircraft designer tremendous potential for (1) tailoring the flying qualities to the flight phase; (2) minimizing the impact of stability requirements on flight performance; and (3) solving aerodynamic shortcomings. But with the increase in the positive contribution of flight controls comes a corresponding increase in the potential for catastrophic results caused by design mistakes.

High authority augmentation has the ability to overwhelm the basic aerodynamics and provide responses to the pilot's control in whatever manner the designer chooses. However, instead of having a system described by a second or third order numerator with a fourth order denominator, as suitably treated in the specification, the fly-by-wire system might involve 23rd over 25th, and is thus not at first glance suitably treated by today's specification. The fly-by-wire system will also be highly damped and not amenable to flight demonstration with the classical techniques used on yesterday's designs.

While higher order systems do appear to challenge the specification, aircraft have always had higher order systems than those addressed in the specification. The inclusion of structural modes, actuator dynamics, and cross mode coupling imposed a modeling complexity that is equal to current fly-by-wire systems.

However, modern systems which deliberately introduce modes in the flying qualities frequency range do present a significant challenge to specification validity. Specifications must be properly written and properly interpreted so they will encourage the beneficial application of fly-by-wire technology while questioning, challenging, and eliminating the potential negative aspects of misapplication. This paper will show that MIL-F-8785B gives proper guidance by using low order "equivalent systems" for the high order dynamics characteristic of tomorrow's aircraft.

BACKGROUND ON EQUIVALENT SYSTEMS

Early applications of a frequency response equivalent systems approach to the longitudinal short period dynamics of the variable stability NT-33 appear in Reference 2, and are extended to the higher order dynamics of the fly-by-wire F-4 in Reference 3.

Lateral-directional dynamics are covered in Reference 4, and Reference 5 discusses longitudinal landing approach dynamics, including the phugoid and flight path decoupling effects of automatic approach power compensation. An application of equivalent systems to the flight simulation results obtained during control system development of the F-15 is presented in Reference 6. Example applications of the equivalent systems approach using generic higher order systems are covered in References 7, 8 and 9. All these applications show that equivalent systems give valuable insight into aircraft responses and response coupling. The purpose of this paper is to discuss the use of the equivalents to demonstrate compliance with MIL-F-8785B(ASG) and also for other applications.

THE EQUIVALENT SYSTEMS APPROACH

Current control system designs dominate every facet of flying qualities parameters. Augmentation systems, by intent, primarily alter denominator characteristics. Compensation networks, filters, feel systems, washouts, digital delays, etc., alter the numerator characteristics and the time delay characteristics, as well as the denominator characteristics also. The impact of active control technology on the denominator characteristics has been the focus of innumerable papers in the past, and will not be addressed here. However, specific numerator characteristics and time delays have not been a major focus in the specification compliance of past and current aircraft. The effects of a new parameter introduced by "equivalent" systems are also important -- namely mismatch of the low order and high order systems.

An example of a higher order system and an "equivalent" lower order system is presented in Figure 1. The frequency and damping values of the equivalent system provide a Bode match of the normalized amplitude over the frequency range of interest, while the equivalent time delay coupled with the equivalent frequency and damping provides a match of the phase angle. The equivalent time delay is needed to approximate the phase lag introduced by the high frequency system components such as actuator dynamics, structural filters, digital delays, pre-filters, sensor dynamics, etc. The single most distinguishing characteristic of the new breed of flight control is the significant increase in this apparent (to the pilot) time delay or the "equivalent" time delay as discussed here.

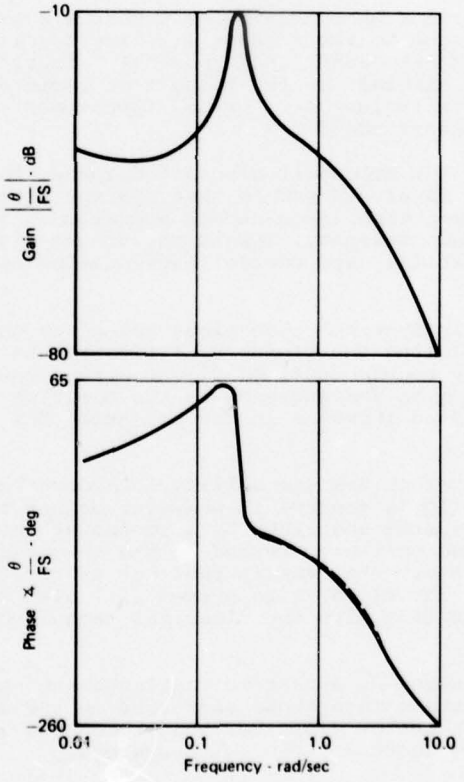

$$\text{——} \quad \frac{0.028(0.0015)(0.095)(0.52)[1;1](2.5)(5)(10)(14)(20)}{[0.13;0.14](0.75)[0.90;0.91][0.73;4.4](3.3)(4.0)(11.4)(13.3)(15.1)[0.80;64]}$$

$$\text{— —} \quad \frac{0.031(0.077)(12)e^{-0.085S}}{[0.16;0.14][0.6;3.9]}$$

Notation: $S + a \rightarrow (a)$, $S^2 + 2\zeta\omega S + \omega^2 \rightarrow [\zeta;\omega]$

GP78 0873 3

FIGURE 1
EXAMPLE EQUIVALENT SYSTEM FOR LONGITUDINAL PITCH ANGLE RESPONSE TO PILOT STICK FORCE COMMANDS

With the equivalent systems approach, the essential characteristics of the higher order system are represented by a lower order system which is addressed by the Flying Qualities Specification. The equivalent time delay, the equivalent denominator characteristics (frequency and damping) and the numerator characteristics are explicitly addressed by the specification.

The equivalent systems are obtained by using a direct search procedure to minimize the difference, or mismatch, between the high and low order frequency responses over an arbitrarily established bandwith. For example, for longitudinal short period flying qualities a bandwidth of .1 to 10 radians per second is usually used. The mismatch, illustrated in Figure 2, is the sum of the squared gain and phase errors between the high and low order systems, using an empirically established number of evaluation frequencies and amplitude-phase weighting. Incidentally, the equivalent parameters obtained have been generally insensitive to the procedural parameters.

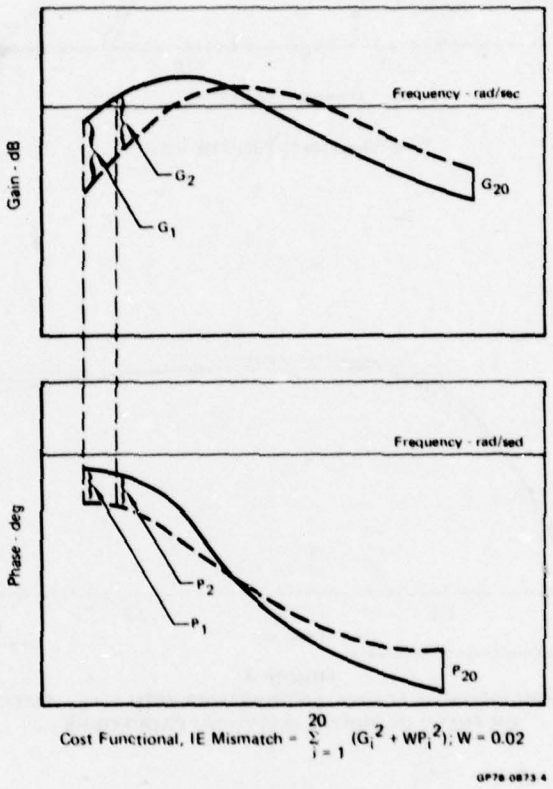

FIGURE 2
MINIMIZATION COST FUNCTIONAL IN DIGITAL EQUIVALENT SYSTEM PROGRAM

Changes in Numerator Characteristics

The early equivalent systems investigations (Reference 2) indicated that short period pitch dynamics sometimes could not be adequately matched by retaining the numerator root, $1/\tau_{\theta_2}$, reasonably close to the L_α of the airplane. The accepted practice is to assume $1/\tau_{\theta_2} = L_\alpha$. By allowing the equivalent system match routine to freely select a value of $1/\tau_{\theta_2}$ for best fit, the program sometimes selected values that were radically (10 to 20 times) larger than the L_α value derived in the wind tunnel.

An example is shown on Figure 3. This extreme value of equivalent $1/\tau_{\theta_2}$ indicates that the short period pitch dynamics resemble a pure second order response rather than the characteristic first order lead over second order lag. Or, in other words, that the pitch dynamics of tomorrow's aircraft will be similar at low speed to the characteristics of today's aircraft at high speed.

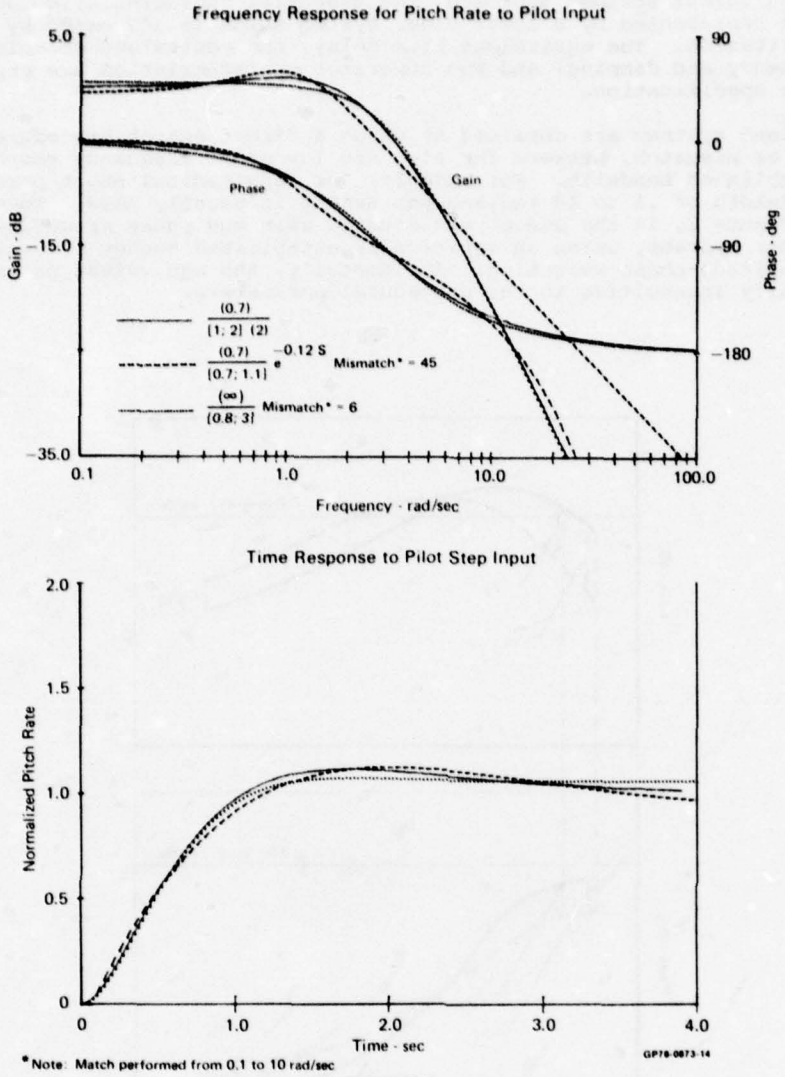

FIGURE 3
COMPARISON OF EQUIVALENT SYSTEMS WITH $1/\tau_{\theta_2}$ FIXED OR FREED IN DIGITAL MATCHING PROCEDURE

Changes in Time Delay

The equivalent time delay is convenient for representing the initially sluggish response of the aircraft resulting from the many high frequency components of the control system. Comparisons of Bode matches with and without time delay are shown in Figure 4 with the corresponding time histories. Both responses clearly indicate the need for a delay-like term to obtain a good match.

While the equivalent time delay improves the response matches, there is also the question of equivalence as perceived by the pilot. That question was specifically addressed by a joint Navy-Air Force, McDonnell Aircraft flight research program on the CALSPAN variable stability NT-33 aircraft. That program is still in progress as this paper is being written. However, the preliminary results indicate that pilots do perceive the equivalent system to be essentially identical to the higher order system, and consequently verify that the equivalent delay is an appropriate approximation of the higher frequency components.

Effects of Mismatch

The question of what constitutes an acceptable match remains unanswered. To date, all systems exhibiting high levels of mismatch have been evaluated as having level 3 flying qualities by the pilots, indicating possibly that mismatch is unimportant, since the pilot ratings are consistent with the specification level. However, by using the regression equations derived from Reference 2, mismatch can be translated into changes in pilot opinion rating. For example, an aircraft with zero time delay can be degraded one Cooper-Harper point by adding about .05 seconds time delay, according to the regression equation in Figure 5. The corresponding mismatch value between the original and delayed configurations is around 40. This directly determines the sensitivity of rating to mismatch. The sensitivity would be different for other flying qualities parameters, of course.

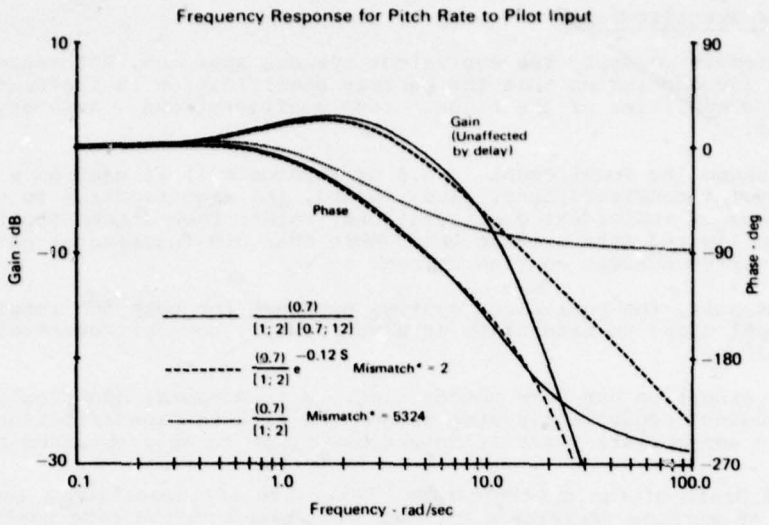

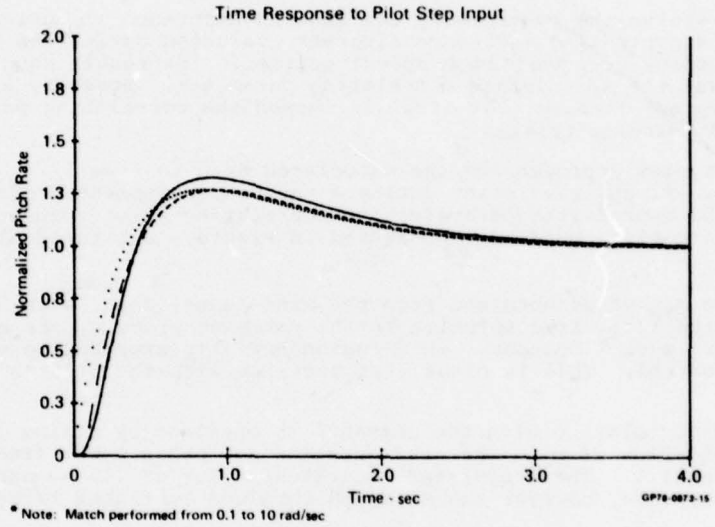

* Note: Match performed from 0.1 to 10 rad/sec

FIGURE 4
COMPARISON OF EQUIVALENT SYSTEMS WITH AND WITHOUT TIME DELAY

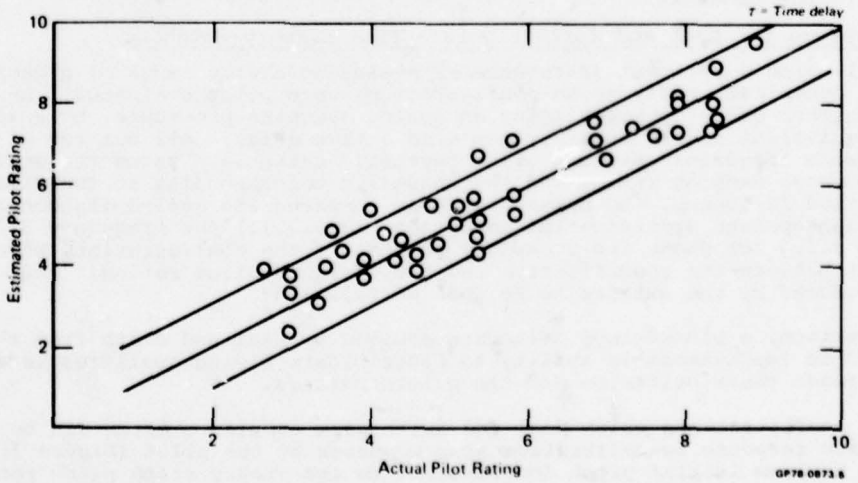

Note:
Equation developed by regression from Neal and Smith's data, Ref 8
Pilot rating = 5.16 + 18.50 τ + 0.56 (L_{α_e}/2 $\zeta_{sp}\omega_{sp}$) − 0.61 ($\zeta_{sp}\omega_{sp}$) + 0.02 (ω_{sp}^2)
(Cooper-Harper)

FIGURE 5
EXAMPLE OF PILOT RATING PREDICTION
USING EQUIVALENT SYSTEM PARAMETERS

Interpretation of Specification

Previous attempts to apply the equivalent systems approach, References 2 and 8, have resulted in the conclusion that the current specification is ineffective in predicting the flying qualities of the higher order configurations. However, the approach here is different.

First, the phase lag requirement (3.5.3 of Reference 1) is used as a screening criterion for level 1 configurations. And, second, the specification is used to "sort out" the acceptance of individual configurations, rather than attempting to generate correlations from limited data sets in which more than one fundamental parameter was unintentionally varied between configurations.

For the most part, the equivalent systems approach for both the longitudinal and lateral-directional cases to date allow straightforward, non-controversial application of the specification.

One primary exception has been noted; namely a fundamental question arises when comparing longitudinal equivalent system parameters with the specification. Is equivalent $(1/\tau_{\theta_2})$ the appropriate correlating parameter, or is n_{Z_α}, obtained from wind tunnel data?

The July 68 Draft of the specification (Reference 12) specified a lower limit on $1/\tau_{\theta_2}$. The Oct 68 version (Reference 1) used n_{Z_α}, based on the same background data as the July Draft.

An attempt to resolve the controversy was made in Reference 11, using a ground based simulation of a controlled incidence aircraft evaluated during the landing approach to a supersonic (i.e. very high speed) carrier. The result conclusively indicated that $1/\tau_{\theta_2}$ was the appropriate correlating parameter. However, since $(1/\tau_{\theta_2}) \times (U/g) = n_{Z_\alpha}$ was accepted, finding that $1/\tau_{\theta_2}$ is indeed the correlating parameter, fell into the category of academic trivia.

The equivalent system approach and the associated need to free $1/\tau_{\theta_2}$ elevates the issue and the answer. Flight simulation during a recent development program clearly confirmed $1/\tau_{\theta_2}$ as the appropriate parameter for correlating pilot opinion. Superimposed on the specification boundaries presented in Figure 6 are three alternative approaches.

First, using the n_{Z_α} value obtained from the wind tunnel data, with an equivalent frequency obtained with $1/\tau_{\theta_2}$ free to shift in the matching process, the configuration falls above the upper level 1 boundary, in a region normally expected to exhibit rapid, abrupt response to control. This is clearly at variance with the pilot's comments on sluggishness.

Somewhat better correlation with the comments is obtained by fixing $1/\tau_{\theta_2}$, again using the wind tunnel value of n_{Z_α}; the configuration now has a lower frequency, though well within level 1. The associated equivalent delay of .15 seconds is an indication of slow response, however the mismatch obtained by fixing $1/\tau_{\theta_2}$ is qualitatively rather large at 32.

By far the best correlation is obtained by freeing $1/\tau_{\theta_2}$ and using it to calculate a higher, equivalent n_{Z_α}. The equivalent delay is now .085 seconds, and the match (8) is excellent. The configuration clearly has low frequency characteristics, in good agreement with the comments.

Equivalent Systems for Neal and Smith's Data - Time History Matching

The Neal-Smith experiment (Reference 8) evaluated a wide range of higher order longitudinal dynamics. Fifty-seven configurations were pilot evaluated. Neal and Smith matched the higher order dynamics using an analog matching procedure, by a specification-compatible equivalent second order system with a time delay. All but two of the configurations were adequately matched using "eyeball" criteria. Using the equivalent systems frequency, damping ratio, and the phase lag corresponding to the time delay at the short period frequency, the present authors compared the Neal-Smith configurations against the appropriate specification paragraphs (3.2.2.1.1 for frequency 3.2.2.1.2 for damping, and 3.5.3 for phase lag). Eighty percent of the configurations were found to be consistent between the specification and the assigned pilot rating. And, eighty percent is considered by the authors to be good correlation.

By comparison, a closed-loop criterion evolved by Neal and Smith from the same data provided no improvement in ability to discriminate flying qualities level; i.e. 80% agreement between their criterion and the pilots ratings.

The two configurations which Neal and Smith were unable to match can be evaluated from pitch rate response to calibration step commands by the pilot (Figure 7). The ratio of the maximum initial pitch acceleration to the steady state pitch rate resulting from the step command is readily translated to the control anticipation parameter (CAP = $\ddot{\theta}_{max}/n_{Z_{ss}}$), which is the same as the constant $\omega_{n_{sp}}^2/n_{Z_\alpha}$ boundaries of the specification. Both configurations were level 3 by the specification, and received pilot ratings worse than 6.5, providing complete agreement between pilot rating and the specification.

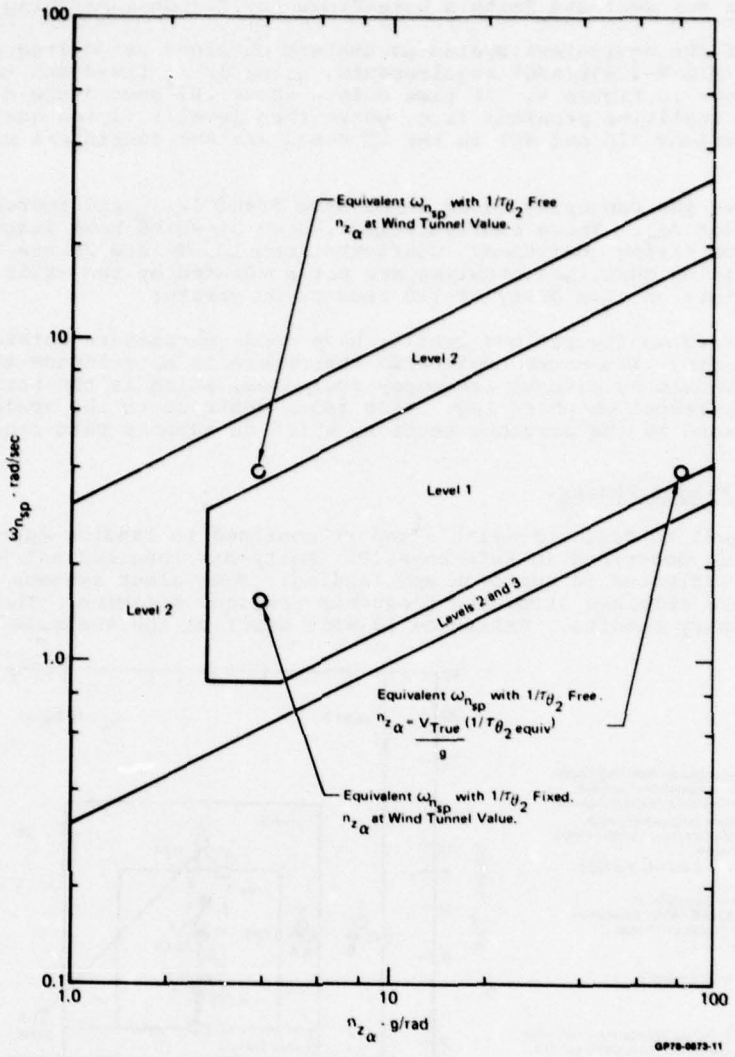

FIGURE 6
ALTERNATIVE CORRELATIONS OF "SLUGGISH" DYNAMICS WITH MIL-F-8785B CAT. C REQUIREMENT

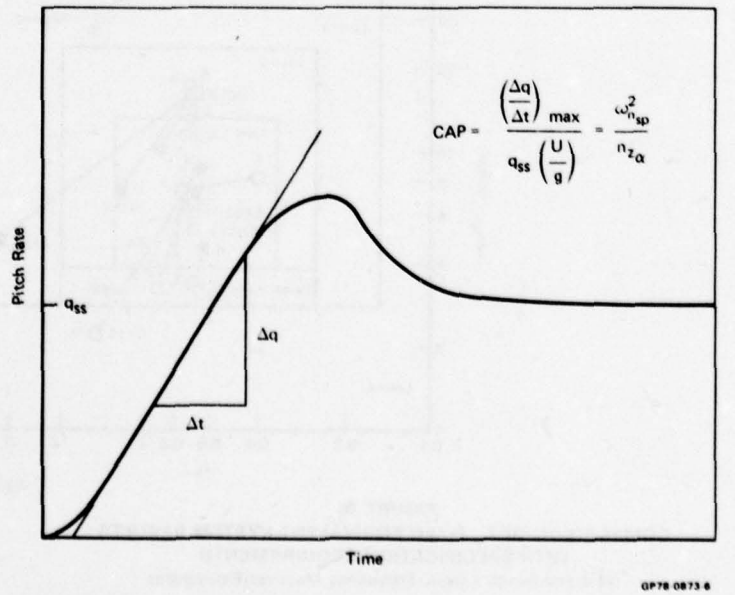

FIGURE 7
PITCH RESPONSE TO STEP COMMAND

Equivalent Systems For Neal and Smith's Data-Frequency Response Matching

Comparison of the equivalent system parameters obtained using frequency response matching, against MIL-F-8785B(ASG) requirements, using $1/\tau_{\theta_2}$ fixed and the wind tunnel n_{z_α} value, are shown in Figure 8. If time delays above .07 second are disallowed, prediction of flying qualities problems (i.e. worse than level 1 flying qualities) is good. Only two configurations (7D and 8E) in the 27 cases are not consistent with the specification.

Figure 9 shows the remaining cases which have freed $1/\tau_{\theta_2}$ and therefore have widely differing values for n_{z_α}. These configurations, some of which have large mismatches, generally have poor flying qualities. Configurations 1A, 2B and 2F are the sole cases of 22 for which flying qualities problems are not predicted by the -8785 requirements, together with a limit on time delay of .10 seconds or greater.

Note that unsafe configurations usually have modal parameters outside level 1, with a delay exceeding .10 second. Note also that there is no evidence that delays become more objectionable as natural frequency increases, which is the basis of the current specification requirement on phase lag. This is in contrast to the analog-matched equivalents discussed in the previous section, which do support that requirement.

Landing Approach Flight Phases

A recent sequel to Neal and Smith's report confined to landing approach high order systems (LAHOS), is described in Reference 10. Forty-six longitudinal high order configurations were evaluated in approach and landing. Equivalent systems for these configurations were obtained using the frequency response matching. The following describes preliminary results. Reference 13 will describe the analysis in detail.

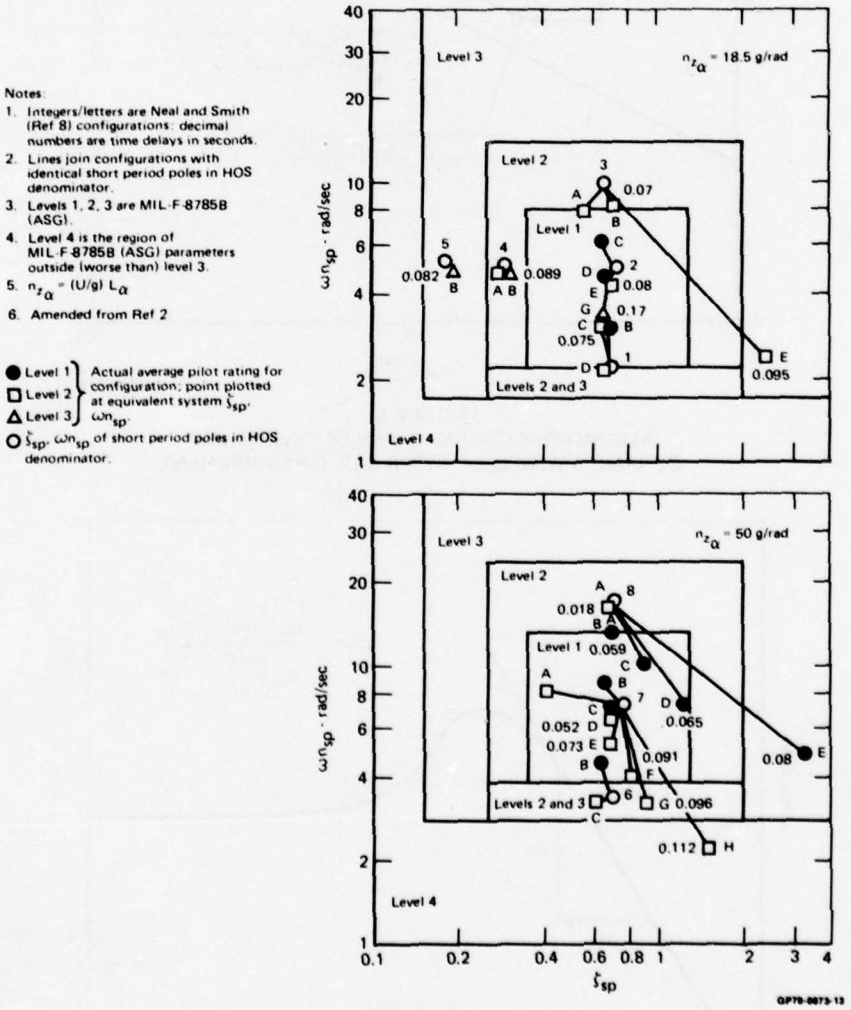

FIGURE 8
COMPARISON OF L_α FIXED EQUIVALENT SYSTEM RESULTS WITH SPECIFICATION REQUIREMENTS
Neal and Smith's Data, Frequency Matched Equivalents

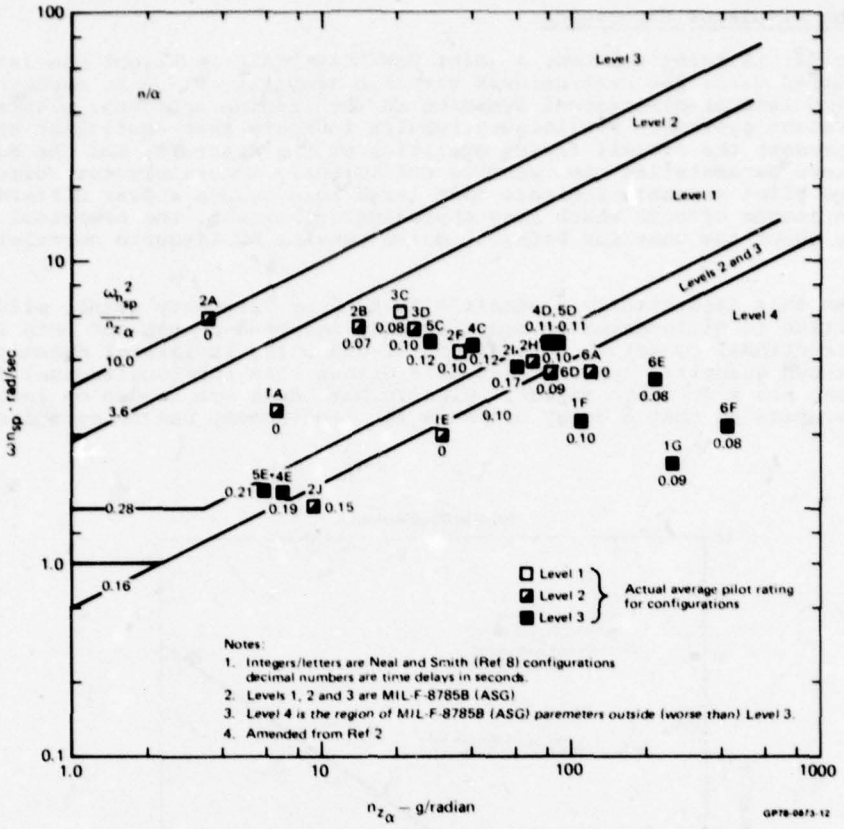

FIGURE 9
COMPARISON OF $1/\tau_{\theta_2}$ FREED CASES WITH MIL-F-8785B CATEGORY A REQUIREMENTS
Neal and Smith's Data, Frequency Matched Equivalents

The LAHOS pilot ratings for the flare maneuver appear to be broadly consistent with the up and away ratings of Neal and Smith. Most pilot comments relate to short period, rather than phugoid or flight path effects. Regression using this data set with the same functional parameters used for Neal and Smith's data produced similar values and correlation coefficients. In other words, the LAHOS pilot ratings for the flare maneuver could have been predicted using Neal and Smith's results for up-and-away flight.

The configurations with $1/\tau_{\theta_2}$ fixed can conveniently be presented by showing the variation of pilot rating with time delay (Figure 10). The baseline flying qualities of the configurations shown are adequately predicted by MIL-F-8785, and the subsequent degradation due to delay is covered by a limit on delays greater than about .12 seconds.

Figure 11 shows the MIL-F-8785B(ASG) requirement on CAP with the configurations for which $1/\tau_{\theta_2}$ had to be freed to obtain a match. This shows that the Category A requirement, together with a level 1 delay requirement around .12 seconds, adequately screen out flying qualities problems for the flare maneuver. Unsafe configurations are again those which violate the modal MIL-F-8785B(ASG) requirements and also have substantial delays. Again the phase lag requirement of MIL-F-8785B is not supported by the data.

Lateral-Directional Dynamics

Surprisingly, no systematic set of data on lateral-directional augmented dynamics are available. Successful order reduction of dynamics of modern fighters has been demonstrated in References 4 and 12 but more data are needed.

The general conclusions are that equivalent systems can be obtained readily for lateral-directional systems, provided that coupling is taken into account. Specifically, the directional response to rudder will determine the dutch roll frequency and damping, and the roll response will establish the roll damping and ω_ϕ. This is entirely natural to the flying qualities engineer who is familiar with using rudder doublets to identify the dutch roll and lateral control steps to identify the roll mode. The modest amount of lateral-directional data to date indicates the same level of correlation with MIL-F-8785B(ASG) as exhibited by past aircraft experience.

Recent Inflight Simulator Experience

As this paper is being written, a joint USN/USAF MCAIR in-flight simulator study is being conducted using the USAF/CALSPAN variable stability NT-33 to explore high order longitudinal and lateral-directional dynamics in the landing approach, with specific focus on equivalent systems. Preliminary results indicate that equivalent systems do adequately represent the overall flying qualities of the aircraft, and the equivalent system parameters parameterize the dynamics sufficiently accurately for correlation purposes. Some pilot comments indicate that large pure delays appear different to the high order continuous effects which they approximate; however, the numerical rating degradation is about the same for both, so delay remains an adequate correlating parameter.

Apart from this (essentially a sensitivity to high frequency gain), pilots appeared rather insensitive to differences in mid-frequency response shapes for both longitudinal and lateral-directional dynamics. The effect of added lag in lateral dynamics, previously an unknown quantity, appears less deleterious than for longitudinal dynamics, but nevertheless has a dramatic effect. Clearly more data are needed on lateral and directional dynamics so that a delay or phase lag requirement can be established for the specification.

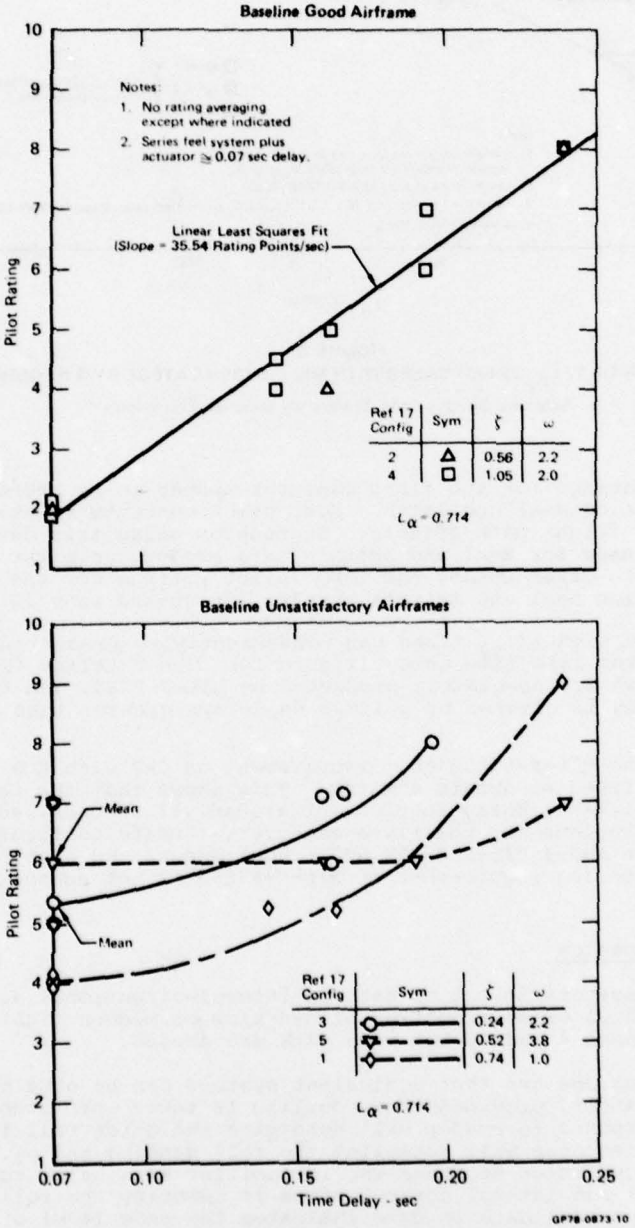

FIGURE 10
DEGRADATION OF PILOT OPINION RATING DUE TO EQUIVALENT TIME DELAY
LAHOS Data, MCAIR Equivalent Systems, $1/\tau_{\theta_2}$ Fixed

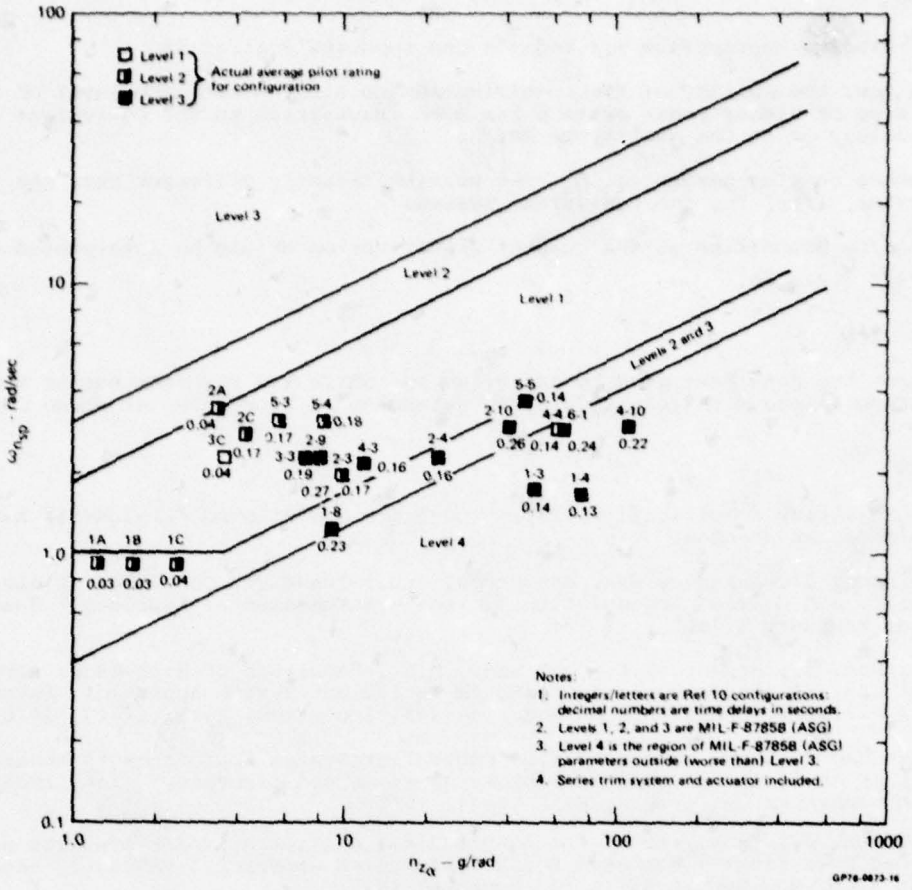

FIGURE 11
COMPARISON OF $1/\tau_{\theta_2}$ FREED CASES WITH MIL-F-8785B CATEGORY A REQUIREMENTS
Smith's Flare Maneuver Data

Future Applications

Parameterization of dynamic response is the primary purpose of equivalent systems. If the parameters are familiar to us, or if we choose familiar equivalent forms, then the parameterization is of immediate use. If the forms are unfamiliar, then the equivalents at least reduce the dynamic dimensions of the problem and we have a starting point for correlation, analysis, and design.

These general statements can be specialized to flying qualities specification for future aircraft types. For example, control configured aircraft are very amenable to order reduction; although the flight control systems commonly produce high order dynamics, and the authority over the various mechanical degrees of freedom is high, the eventual apparent order of the responses is low and decoupling is almost complete. For blended responses in which natural coupling is augmented by the controls, equivalent systems identify, for example, modified L_β values. Examples appear for blended longitudinal dynamics and direct sideforce in References 3 and 14 respectively.

Another potential application for equivalent systems is in reducing the high order flight control systems of the contemporary V/STOL designs for evaluation against the V/STOL Flying Qualities Specification. The equivalent system approach is inherently flexible, allowing for example, a first order rate command model in hover and a second order system during transition.

The equivalent systems approach should benefit significantly from the extensive parameter identification work (Reference 15) done over the past few years. Fundamental to the parameter identification work is the ability to select the plant dynamics considered appropriate, for which the coefficients will be determined, as will a fit function.

The focus of these many parameter identification programs, to identify specification-compatible models as well as to calibrate the level of match achieved, will provide a sound data base for evaluating whether the specifications are too simple, too complicated, or just right.

CONCLUSIONS

1. MIL-F-8785 is appropriate for today's and tomorrow's aircraft.

2. Up to now, the ability of the specification to discriminate the level of flying qualities of higher order systems has been insensitive to the equivalent system methodology or to the quality of match.

3. The heave damping parameter, $L_{\dot{\alpha}}$, can be significantly different than the pitch numerator, $1/\tau_{\theta_2}$ for the equivalent system.

4. The ω_n^2/n_{z_α} boundaries of the current specification should be interpreted as $\omega_n^2 e/(\frac{U}{g})\ (1/\tau_{\theta_2})e$.

RECOMMENDATION

Examine the data base used to establish the phase lag requirements of the current specification, along with recent data, to determine if time delay or phase lag is the better index.

REFERENCES

1. Anon, "Military Specification, Flying Qualities of Piloted Airplanes," MIL-F-8785B(ASG), as amended.

2. Hodgkinson, J., LaManna, W.J. and Heyde, J.L.; "Handling Qualities of Aircraft with Stability and Control Augmentation Systems - A Fundamental Approach," Journal R.Ae.s, February 1976.

3. Hodgkinson, J., Berger, R.L., and Bear, R.L.; "Analysis of High Order Aircraft/Flight Control System Dynamics Using an Equivalent System Approach," Seventh Annual Pittsburg Conference on Modeling and Simulation, April 26-27, 1976.

4. Hodgkinson, J., and LaManna, W.J., "Equivalent System Approaches to Handling Qualities Analysis and Design Problems of Augmented Aircraft," AIAA Atmospheric Flight Mechanics Conference, 8-10 August 1977.

5. Hodgkinson, J., "Analysis of the Longitudinal Carrier Approach Dynamics of an Advanced Navy Fighter Using an Equivalent System Approach," McDonnell Douglas Corporation, MDC Report A5114, 23 December 1977.

6. Brulle, R.V., and Moran, W.A., "Dynamic Flying Qualities Criteria Evaluation," AFFDL-TR-74-142, January 1975.

7. Difranco, D.A.; "In-Flight Investigation of the Effects of Higher-Order Control System Dynamics on Longitudinal Handling Qualities," AFFDL-TR-68-90, August 1968.

8. Neal, T.P., and Smith, R.E.; "An In-Flight Investigation to Develop Control System Design Criteria for Fighter Airplanes" AFFDL-TR-70-74, December 1970.

9. Craig, S.J., Ringland, R.F., and Ashkenas, I.L.; "An Analysis of Navy Approach Power Compensator Problems and Requirements," STI TR-197-1, March 1971.

10. Smith, R.E., "Effects of Control System Dynamics on Fighter Approach and Landing Longitudinal Flying Qualities," CALSPAN Report AK-5280-F-12, March 1978.

11. A'Harrah, R.C., and Lockenour, J.L., "Approach Flying Qualities - Another Chapter," Journal of Aircraft, Vol. 8, No. 5, May 1971.

12. Anonymous "Military Specification-Flying Qualities of Piloted Airplanes," MIL-F-8785A, July Draft, 1968.

13. Johnston, K.A., and Hodgkinson, J., "Flying Qualities Analysis of an In-Flight Simulation of High Order Longitudinal Control Systems Effects on Fighter Aircraft Approach and Landing", McDonnell Douglas Corporation Report MDC A5596, to be published.

14. Brulle, R.V., Moran, W.A., and Marsh, R.G.; "Direct Side Force Control Criteria for Dive Bombing," AFFDL-TR-76-78, September 1976.

15. "Methods for Aircraft State and Parameter Identification," AGARD CP-172.

A SIMULATOR INVESTIGATION OF HANDLING QUALITY CRITERIA FOR CCV TRANSPORT AIRCRAFT[1)]

by
H.A. Mooij, W.P. de Boer and M.F.C. van Gool
National Aerospace Laboratory NLR
Amsterdam, The Netherlands

SUMMARY

The introduction of CCV-concepts in the design of certain categories of future transport aircraft requires definition of handling quality criteria for such aircraft. These criteria should be applicable to guidance in flight control system design as well as in airworthiness certification.

In an attempt to contribute new insight in this matter, approach and landing flight simulation investigations have been performed at the NLR, using a moving base flight simulator. The conceptual aircraft was a jet transport aircraft developed around the relaxed static stability concept and equipped with a primary flight control system of the rate-command/attitude-hold type for pitch and roll control.

The short term pitch response dynamics and the effectiveness of a direct-lift-control system for manoeuvre enhancement (for a configuration with reduced normal acceleration sensitivity) were the characteristics varied in the experiment.

Based on measured pilot/aircraft performance, pilot ratings and pilot commentary, boundary values for satisfactory handling qualities for three parameters investigated have been established.

LIST OF SYMBOLS

a_{z_p}	normal acceleration at the pilot seat
F_{s_a}	stick force (lateral)
F_{s_e}	stick force (longitudinal)
i	input variable
j	imaginary number $\sqrt{-1}$
K_a	gain of roll rate command
K_{BC}	gain of bank compensation loop
K_{CF}	crossfeed gain
K_{DCL}	spoiler feedforward gain
K_{DR}	gain used in the r to δ_r loop
K_e	gain of pitch rate command
K_n	gain used in E.S.*) (normal accelleration)
K_p	roll rate feedback gain
K_q	pitch rate feedback gain
K_q	gain used in E.S. (pitch rate)
K_r	gain of rudder deflection
K_Θ	pitch attitude feedback gain
K_Φ	roll attitude feedback gain
n_z	normal load factor at c.g.
n_α	load factor change per unit α
p	rolling velocity about the X-axis**)
p_c	roll rate command
q	pitching velocity about the Y-axis**)
q_c	pitch rate command
r	yawing velocity about the Z-axis**)
s	Laplace operator $= \sigma + j\omega$
s_a	stick deflection (lateral)
s_e	stick deflection (longitudinal)
s_r	rudder deflection
s_{th}	throttle deflection
T_q	equivalent time delay used in E.S.
T_n	equivalent time delay used in E.S.
α	angle of attack
δ_a	aileron deflection
δ_e	horizontal tail deflection
δ_r	rudder deflection
δ_{sp}	spoiler deflection
δ_T	commanded engine thrust
ζ_q	damping ratio used in E.S.
ζ_{sp}	short period damping ratio
Θ	inclination angle; Euler angle
θ	pitch attitude
θ_c	pitch attitude command
σ	standard deviation; real part of s
τ_a	time constant of lateral stick filter
τ_e	time constant of longitudinal stick filter
τ_{DR}	wash-out time constant
τ_m	time constant used in the prefilter
τ_q	time constant used in E.S.
τ_{wo}	wash-out time constant
Φ	bank angle; Euler angle
ω_{n_n}	undamped natural frequency used in E.S.
ω_{n_n}	undamped natural frequency used in E.S.
ω_{n_q}	short period undamped natural frequency
$\omega_{n_{sp}}$	pitch attitude frequency

*) E.S. is Equivalent System

**) Stability axes system

---

1) This investigation has been carried out partly under contract for the Netherlands Agency for Aerospace Programs (NIVR nr. 1745) and partly under contract for the Department of Civil Aviation of the Netherlands (RB-RLD-1977: 1.1)

1 INTRODUCTION

Current trends in aircraft research and development indicate that future aircraft will rely more heavily on flight control systems providing improved performance and more economical flight operations. Automatic control systems will take over roles hitherto performed by the pilot and will be employed in the emerging active control technology (ACT) concepts. These systems will be critical for flight safety in part of or in the whole aircraft flight envelope.

Fly-by-wire (FBW) and active control technologies have progressed to the point that they are applied in production type military fighter aircraft to obtain improved performance. Analytical studies and flight demonstrations have also proven the advantages of fly-by-wire and active control systems in terms of more economical flight operation for transport aircraft.

An airplane designed for maximum utilization of active control concepts will most likely use FBW in the system implementation because of the design flexibility available to the designer.

At the National Aerospace Laboratory (NLR) performance aspects as well as flying qualities of subsonic transport aircraft designed according to the "relaxed static stability" concept, one of the ACT concepts, are under study for some time.

Adequate stability for such aircraft can be provided by a stability augmentation system forming an integral part of the flight control system.

Because contemporary criteria for good flying qualities are to a great extent not applicable to aircraft fitted with high-authority command and stability augmentation systems, new criteria should be established.

A recently concluded simulator experiment using the NLR research flight simulator (four degrees of freedom motion simulation and TV-model visual scene simulation) was aimed at the establishment of such criteria.

In particular the longitudinal handling qualities during final approach and landing of aircraft equipped with a rate-command/attitude-hold (RC/AH) system for pitch and roll control have been considered. As the pilots controller a side-stick was used.

The characteristics of the basic aircraft used in the simulation were those of a medium-size jet transport aircraft developed around the relaxed static stability concept.

The short term pitch response dynamics (frequency of the equivalent short period mode and the pitch rate overshoot parameter) and the effectiveness of a direct lift control (DLC) system for manoeuvre enhancement (for a configuration with reduced normal acceleration sensitivity) were the characteristics varied in the experiment.

During the program, 150 evaluation approaches and landings (and the same number for "learning" purposes) have been performed by three pilots according to a thoroughly designed experimental plan.

2 HANDLING QUALITIES CRITERIA

2.1 General

The performance of the pilot-aircraft system while flying precision tasks, such as a specified approach path with a prescribed airspeed is dependent upon the aircraft's inherent turbulence response characteristics and the ability of the pilot to close the appropriate control loops.

Rate-command/attitude-hold is the form of the flight control system considered here. Due to the high quality of attitude stabilization which is relatively easy to obtain, the emphasis in this study was put on the aircraft response to command inputs.

Manoeuvre enhancement through washed-out direct lift control is considered in this program in relation to the trend towards lower values of the normal acceleration sensitivity (due to increasing wing loading).

2.2 Contemporary criteria

A few remarks are made with respect to contemporary criteria for satisfactory longitudinal characteristics. Due to its comprehensive background documentation, the (US) Military Specification "Flying Qualities of Piloted Airplanes" is used as prime reference for this discussion (Refs. 1 and 2). Attention is mainly paid to the requirements for satisfactory (Level 1) handling qualities:

Longitudinal stability with respect to speed

With respect to "longitudinal static stability" a RC/AH system in pitch shows no tendency for the airspeed to diverge aperiodically when the airplane is disturbed from trim in case of "front-side" operation. However, it violates the requirement for a stable pitch (elevator) control force versus airspeed relationship, also called Positive Stick Force Stability (PSFS).
A flight test program with a jet transport with a RC/AH system in pitch, reference 3, has shown that Neutral Stick Force Stability (NSFS) as compared to (artificially generated) PSFS has no negative aspects on the execution of the landing approach.

An "oscillatory phugoid" is normally absent in aircraft with a RC/AH flight control system for pitch control.

The requirement regarding "flight path stability" should probably be changed in the sense that no flight-path instability ("back-side" operation) should be allowed unless an autothrottle of high integrity is available.

Longitudinal control

Requirements related to maximum allowable pull forces are kept outside the scope of the investigation. Due to the envisaged application of side-sticks in advanced flight control systems, new stick force criteria should be generated. Experience obtained in several programs, references 3, 4, 5 and 6, indicate that this area in itself is not considered "critical". (The proper combination of the force-displacement relationship, command shaping and stick filtering is however of great importance).

Longitudinal manoeuvring characteristics

The contemporary criterion on short-period response related to abrupt pitch control inputs will be discussed in the following section on "new" criteria. Further requirements related to linearity, maximum and minimum stick force per g gradients, control power limits and so-called transient control forces will not be dealt with.

2.3 New criteria

The conventional short period response criterion (Military Specification, Ref. 1) requires that the short period undamped natural frequency ($\omega_{n_{sp}}$) is located within prescribed boundaries depending on the normal acceleration sensitivity (n_a); in addition the damping ratio of the short period mode (ζ_{sp}) shall be within prescribed limits. This criterion is in particular applicable to conventionally (open-loop) controlled aircraft.

Although many new criteria have been proposed, only two criteria, proposed as a replacement for the contemporary (Military Specification) short period response criterion have been selected for further discussion in this paper.

The pilot-in-the-loop criterion

In reference 7 a proposed new requirement on "pitch dynamic response in manoeuvring flight" based on pilot-aircraft system analysis is presented. The basis for this requirement is formed by the following conditions:

1) The closed-loop pilot-aircraft system should have a reasonable bandwidth for control of pitch attitude. The bandwidth is here defined as the frequencies at which the closed-loop phase angle $\sphericalangle \frac{\theta}{\theta_c}$ does not exceed -90 degrees.
2) Maximum "droop" in closed-loop amplitude ratio $\left|\frac{\theta}{\theta_c}\right|$ should not exceed a certain value (magnitude of 3 dB).
3) Good high-frequency stability is essential; closed-loop resonance $\left|\frac{\theta}{\theta_c}\right|_{max}$ should be limited.
4) The so-called "pilot compensation" (equalization) in the system has to be limited as well.

Plotting the quantities 3) and 4) against each other in a rectangular axes system reveals an area in which favourable pilot ratings appear. This plot can probably be the basis for numerical criteria to be met.

The equivalent systems approach

The concept of equivalent system is based on replacing the high-order mathematical model, describing the output-input relation of the aircraft-flight control system combination, by a simple low-order model. The equivalent system approach is described in references 8, 9, 10 and 11.

For pitch rate response to stick inputs the following low-order system is used

$$\frac{q}{F_{s_e}} = \frac{K_q(s + 1/\tau_q)e^{-T_q s}}{s^2 + 2\zeta_q\omega_{n_q} s + \omega_{n_q}^2} \qquad (2.1)$$

and for normal acceleration to stick inputs

$$\frac{n_z}{F_{s_e}} = \frac{K_n e^{-T_n s}}{s^2 + 2\zeta_n\omega_{n_n} s + \omega_{n_n}^2} \qquad (2.2)$$

The matching is performed in the frequency domain. The aim of the equivalent system technique is the reduction of a great number of parameters to a small number which can be used in the contemporary criteria e.g. Military Specification for short period response.

The technique as it stands now is to fit separately the q/F_{s_e} and n_z/F_{s_e} transfer functions and to compare independently the results obtained with contemporary short period response requirements. It is claimed that when ζ_q, ω_{n_q} and $1/\tau_q$ (translated in an n_a-value) as well as ω_{n_n} and ζ_n meet the contemporary requirements, a system with satisfactory flying qualities exists.

Requirements concerning T_q and T_n as well as the required quality of the "match" are areas for further investigation.

At present, work concerning the relationship of pilot-in-the-loop criteria and equivalent system parameters is performed at the National Aerospace Laboratory, reference 12.

3 EXPERIMENT

3.1 Simulated airplane

The transport airplane programmed for the flight simulator experiment was a modified F-28/Mk 6000 airplane. The following hypothetic modifications have been applied:

- a 40 percent reduction of the horizontal tail surface; substitution of the stabilizer/elevator combination by an all-flying tail configuration
- the standard flight control system, including the yaw damper system, has been replaced by a fly-by-wire flight control system especially designed for the experiment as will be described below; spoilers are added for the generation of direct lift control
- a 40 percent increment of airplane gross weight, inertial moments and product and maximum thrust (only for four configurations).

3.2 Simulated flight control system

Longitudinal control

A functional block diagram of the flight control system is shown in figure 1. Longitudinal control is performed by means of a pitch rate-command/attitude-hold system. A side stick controller is used with a two-gradient force-pitch rate command function as indicated in figure 2. A low-pass filter has been incorporated in the command path to block high-frequency inputs. Washed-out direct lift control can be selected for the purpose of manoeuvre enhancement. A bank compensation loop is included in order to assist the pilot in maintaining vertical equilibrium when performing banking manoeuvres. Thrust variation with throttle is accomplished in the conventional way.

Lateral-directional control

The concept of roll rate command has been used for lateral control (Fig. 1). When there is no roll command and the bank angle is greater than 3 degrees a bank angle hold mode is activated. When the bank-angle is less than 3 degrees and no roll command is given, a "wing leveler" function is switched on which drives the bank angle to zero degrees. For lateral control a three-gradient force-roll rate command function as shown in figure 2 has been used in combination with the side stick controller. A low-pass filter has been applied also in this command path. A yaw damper, consisting of washed-out yaw rate feed-back to the rudder, has been included. A second-order crossfeed of aileron to rudder has been incorporated for good turn-coordination characteristics. A direct link was used between the rudder pedals and the rudder.

3.3 Choice of flight control system parameters and characteristics

Longitudinal control

The flight simulator program was aimed at the formulation of handling quality criteria for longitudinal manoeuvring. Therefore airplane/flight control system configurations with various longitudinal manoeuvring characteristics, as obtained by a systematic variation of parameters which determine these characteristics, have been programmed. These parameters which are discussed below are indicated by ω_{Θ}, τ_m and K_{DLC}.

The selected definition of ω_{Θ} is the frequency at which $\not\prec \frac{\Theta}{i}$ of the aircraft including its pitch attitude and pitch rate feedbacks equals -90°. This parameter is one possible measure of the quasi short period mode frequency. By taking ω_{Θ} as configuration parameter instead of the natural frequency of the dominant mode in the $\frac{\Theta}{i}$ transfer function, the phase effect of the non-equalized poles and zeros in the $\frac{\Theta}{i}$ transfer function has been accounted for. The parameter ω_{Θ} has been varied for a constant value of the damping ratio of the dominant mode being equal to 0.7. This variation has been accomplished by taking selected values for the feedback gains K_{Θ} and K_q (Fig. 1). As shown in table 1 five configurations E-1 through E-5 have been programmed for the ω_{Θ}-variation. The values of ω_{Θ} have been selected on the basis of results presented in reference 4 and pilot opinion results obtained from test runs on the flight simulator.

It is mentioned that for these configurations the value of the basic airplane parameter n_{α} has been fixed at 4.71 g/rad. Values of the prefilter time constant τ_m have been taken according to the relationship $1/\tau_m = 0.7\ \omega_{\Theta}$ which was based on the experience gained during previous experiments. Resulting values of τ_m have been presented in table 1 as well.

The value of the pre-filter time constant τ_m in relation to the parameter ω_{Θ} determines the amount of pitch rate overshoot for step-type command inputs. This important characteristic is directly observable to the pilot as the amount of "nod-back" in pitch attitude after termination of a block-type command input. Therefore a systematic variation of the relation between τ_m and ω_{Θ} has been investigated in this experiment. This variation has been performed for a constant value of ω_{Θ} for which the "good" value of 1.24 rad/s was taken. Four configurations have been programmed for this part of the investigation: F-1, F-2, F-3 and F-4 (equal to E-5). The values of τ_m have been summarized in table 1 and have been chosen on the basis of results of a pilot-in-the-loop system analysis and pilot opinion obtained from test runs on the flight simulator.

The effectiveness of washed-out direct lift control as a means for manoeuvre enhancement has been investigated. This has been done for the airplane with a reduced n_{α}-value (3.41 g/rad as compared to 4.71 g/rad) which has been obtained by means of a 40 percent increment of airplane gross weight. Inertial moments and product and maximum thrust capability have been increased also by 40 percent. This value for n_{α} was selected because it is of the magnitude of the estimated Level 1 boundary value without manoeuvre enhancement for aircraft with satisfactory characteristics for pitch control. This has been established in the investigation described in reference 4. The amount of direct lift control has been varied at the constant, "good" , value of ω_{Θ} (1.20 rad/s) and τ_m (1.19 s based on $1/\tau_m = 0.7\ \omega_{\Theta}$); a wash-out time constant τ_{wo} of 5 s was selected.

Four configurations have been programmed for the investigation of direct lift control effectiveness: G-1 through G-4, see table 1. The maximum amount of direct lift control simulated $(K_{DLC})_{max}$ for configuration G-4 has been chosen such that the maximum DLC-generated normal acceleration response at the pilots seat to a step-type command input is at the same level as the maximum response generated by the pitch rate command function for $K_{DLC} = 0$. For the other configurations the value of K_{DLC} has been related to this maximum value as shown in table 1.

In figure 3 time histories of pitch rate, normal acceleration at the pilot seat after a step-input (E- and G-configurations) and pitch attitude after a block-input (F-configurations) are presented.

It is remarked that for the presentation of results, use has been made of the equivalent systems approach as described in section 2.3. Consequently, the low-order system parameters ω_n and $1/\tau_q$ have been used for the definition of pitch rate response characteristics instead of ω_Q and $1/\tau_{m_q}$. Values of these equivalent systems parameters have been summarized in table 1.

The two-gradient force-pitch rate command function as shown in figure 2 has been optimized during test runs on the flight simulator. For the low-pass filter time constant τ_e a value of 0.1 s was taken which appeared to be satisfactory. The value of the gain K_e was taken such that the sensitivity of long-term pitch rate response to command inputs was constant over all configurations simulated.

For the bank compensation loop gain K_{BC} values have been taken that resulted in vertical equilibrium during banking for a true airspeed of 82.31 m/s (160 knots).

Lateral-directional control

The parameters and characteristics of the lateral-directional part of the flight control system have been taken such that satisfactory lateral-directional handling qualities could be assured for all configurations simulated.

Roll rate response approached the response of a first-order system with a time constant of about 0.35 s. This response is realized by the selected value for the roll rate feed-back gain K_p. The three-gradient force-roll rate command function as shown in figure 2 has been optimized during test runs on the flight simulator. The low-pass filter time constant τ_a was 0.05 s. The value of the gain K_a has been taken such that the sensitivity of roll rate response to command inputs was constant over all configurations simulated.

Satisfactory values of the parameters defining the characteristics of the bank angle hold mode and "wing leveler" function have been determined on the basis of bank angle response to block-type roll rate command inputs and on pilot opinion obtained during test runs on the simulator.

The yaw damper was designed to provide for an effective Dutch roll damping ratio of about 0.4. The aileron-to-rudder crossfeed designed, appeared to be very effective, leading to satisfactory turn-coordination. During a block-type roll command input, resulting in a bank angle of 30 degrees, the sideslip angle did not exceed 1.5 degree.

3.4 Experimental design

The following parameters have been varied

1. Quasi short period mode frequency ω_Q : Configurations E1-E5
2. Overshoot parameter τ_m : Configurations F1-F4
3. Direct-lift-control effectiveness K_{DLC} : Configurations G1-G4

The total number of configurations evaluated was twelve*).
In addition, a reference aircraft (F-28/Mk 6000 controlled with the conventional control system) was used in the evaluation process. To eliminate possible influence of the order in which the configurations were evaluated, a pseudo randomization of this order has been applied.

Evaluating a configuration consisted of the following:

1 One approach and landing was carried out with the reference aircraft without turbulence and one with turbulence to set a reference frame for the evaluation of the configuration of that session and to refresh the pilots' knowledge of the simulation, the approach procedures etc.
2 Two approaches and landings were carried out with the configuration to be evaluated without turbulence, to be able to evaluate the configuration characteristics uninfluenced by turbulence.
3 Four approaches and landings were carried out with that configuration with turbulence. These last four runs were the important measurement runs which have been used in the subsequent data analysis.

Three experienced pilots, current in medium to heavy jet transports, participated in the flight simulator program.

3.5 Data acquisition and reduction

The important quantities have been recorded on magnetic tape; a sampling rate of 10 times per second was used from glideslope intercept to touchdown. Mean values and standard deviations have been computed (on-line) for relevant quantities from glide slope intercept to flare altitude.

A second important source of information was formed by the recorded subjective pilot ratings and commentary.

So-called "effort ratings" on a 10 point non-adjectival rating scale concerning effort required for specific items were given by the pilot after each run. Two Cooper-Harper ratings, one for longitudinal and one for lateral handling qualities were assigned to each configuration after completion of the full session. Furthermore the pilots commented on a number of items listed on a comment card.

3.6 Flight procedure

Each approach was initiated at a distance of 20372 m (11 NM) before runway threshold, 1852 m (1 NM) to the right-hand side of the extended centre line of a runway with direction 240° at an altitude of 609.60 m (2000 ft).

---

*) Configuration F-4 is equal to configuration E-5.

The aircraft was stabilized and trimmed in a horizontal flight condition, heading 215°, indicated airspeed 82.36 m/s (160 knots), flaps 6° and landing gear retracted.
During the approach the following actions were taken:
The pilot intercepted the localizer. At 2 dots below glide path he extended the landing gear. At glide path intercept he selected full flaps (42°) and reduced to a final approach speed of 64.35 m/s (125 knots). At 8728 m (4.7 NM) before runway threshold, approximately at the Outer Marker, an ILS glide slope offset of 54.86 m (180 ft) on the low side, being equal to one dot on the ILS indicator, was removed so that the pilot had to make a (second) glide slope capture.
Cloud break occurred at 121.9 m (400 ft) altitude and cloud base was at 91.44 m (300 ft) altitude. At the latter point, 1744 m (0.94 NM) from runway threshold an ILS-localizer offset of 83.5 m (274 ft), being equal to 1 dot on the ILS indicator to the left was removed, so that the pilot had to make a side-step manoeuvre before landing. The situation in a vertical and in a horizontal projection is presented in figure 4.

The pilot was instructed to execute approach, flare and touchdown according to airline operational practice.

In figure 5 the flight simulator motion system, cockpit and collimating display system are shown.

4 RESULTS

The preliminary results derived from the experiments can be summarized as follows:

In table 2 the Cooper-Harper ratings as assigned by the three pilots to the twelve configurations tested are presented. The participating pilots appeared to use the Cooper-Harper system in a consistent manner.
In figure 6 the mean of and the spread in the ratings per configuration are given.
In figure 7 a survey is given of a number of derived quantities averaged over the twelve measuring runs (with turbulence).

- Comparing the configurations E-5 through E-1 (decreasing equivalent short period ω_{n_q}) shows increasing standard deviations of the stick deflection in pitch, the pitch rate and the vertical acceleration at the pilots seat. These increases, although small, proved to be statistically significant.
  Furthermore a significant increase in the vertical speed at touchdown and in the pilot effort ratings for most of the control tasks was observed.
  From the Cooper-Harper ratings a lower (Level 1) boundary for the equivalent short period frequency of about 1 rad/s was estimated for the cases considered (equivalent short period damping ratio of 0.6 and $1/\tau_q = 0.8\ \omega_{n_q}$).
- Comparing the configurations F-4 through F-1 (increasing pitch rate overshoot parameter) showed a small but significant decrease in the standard deviation of stick deflection in pitch combined with significant increases of the standard deviation of the pitch rate and the vertical acceleration at the pilot seat. Moreover, the vertical speed at touchdown and the pilot effort ratings for most of the control tasks increased significantly. These phenomena indicate an increasing tendency towards PIO (pilot-induced oscillations), which tendency was confirmed by the pilots' comments.
  From the Cooper-Harper ratings a minimum (Level 1) boundary of 0.5 was estimated for the ratio of $1/\tau_q$ (inverse of the time constant in formula (2.1)) and ω_{n_q}.
- Comparing the configurations G-4 through G-1 (decreasing the amount of direct lift control) did not show firm trends in the derived quantities presented in figure 7. The pilots' comments, however, indicated a decreasing precision in controlling the rate of descent and increasing problems to maintain altitude or glide slope.
  From the Cooper-Harper ratings a minimum required (Level 1) amount of direct lift control that leads to an initial (DLC-generated) normal acceleration response at the pilot seat to a step-type command input that equals 70 percent of the longer term (α-generated) response (see figure 3) has been derived. This minimum amount of direct lift control has been established for an airplane with a satisfactory equivalent short period frequency but a relatively low value of the normal acceleration sensitivity parameter (n_α = 3.41 g/rad).
  The form used above to describe the required direct lift control is considered tentative; an improved format for use in an appropriate criterion should be developed.
  (For all G-configurations control of airspeed formed a problem especially when compared to the E- and F-configurations. It is remarked here that a pronounced difference existed in the flight path stability for the G- respectively E- and F-configurations. For the G-configurations the local gradient of flight path angle versus true airspeed at the approach speed was slightly positive (just "backside") while for the E-, and F-configurations a negative local gradient existed).

It is mentioned here that although various opinions concerning DLC do exist in the engineering community, manoeuvre enhancement through direct lift control activated by the pitch controller can be very beneficial as shown for the simulated configuration with a low value of normal acceleration sensitivity.

Side-stick control was readily accepted for the approach and landing task performed by the three participating pilots (all current in contemporary medium to heavy jet transports). Some interesting features of the usage of the side-stick as part of this particular flight control system are illustrated in figure 8. In this figure two two-dimensional histograms are presented indicating the percentage of the time the side-stick has been deflected towards certain angles. The plot shows the average values overall measurement runs over the three pilots. Segment 1 covers the time period between glide slope capture and cloud base, Segment 2 covers the time period between cloud base and the moment of touchdown. The pronounced increase of stick activity during Segment 2 as compared to Segment 1 is evident: distinct roll inputs for the side step manoeuvre and pitch inputs related to the flare and touchdown regulation are shown. It can be observed that during the-low activity-ILS flight phase, the pilots apparently alternated their corrective pitch and roll inputs while during Segment 2, combined deflections occurred more frequently.
(Flight tests of the relaxed static stability concept in the Concorde supersonic aircraft have been reported in another paper presented at this conference, reference 13. A side-stick comparable to the one

used in the present experiment was used. Very favourable comments concerning the use of this controller in approach and landing as well as in cruising flight have been obtained).

The (attitude) stabilization feature of the simulated configurations was highly appreciated. For nearly all configurations a dramatic reduction in workload was observed as compared to the workload during the same task performed in a conventional jet transport also simulated as part of the program.

(Flying qualities evaluations of a baseline Lockheed L-1011 and a L-1011 derivative relaxed static stability version with 40 % reduction of the horizontal tail surface and three stability augmentation control laws have been reported at this conference, reference 14. Two important conclusions from the evaluation are repeated here:

- handling qualities of the augmented relaxed static stability airplane are superior to those of the inherently stable baseline in heavy turbulence
- airplane motion and control activity in rough air are less for the augmented relaxed static stability version than for the baseline).

Finally it can be remarked that most of the complaints about the "bad" configurations were in particular related to the visual segment of the approach and the flare plus touchdown. Should only instrument flight have been considered, certain (bad) features would not have emerged.

A more detailed presentation of the results will be presented in the formal report on the investigation which will be published shortly (Ref. 15).

5 CONCLUSIONS

The simulation of a conceptual jet transport aircraft developed around the relaxed static stability concept and equipped with a primary flight control system of the rate-command/attitude-hold type for pitch and roll control resulted in estimated numerical boundary values for three important parameters describing longitudinal manoeuvring characteristics.

Side-stick control was readily accepted for the approach and landing task. Alternating pitch and roll control activity was apparent during a large part of the approach.

The (attitude) stabilization feature of the simulated configurations was highly appreciated.

As expected the experiment has shown that the landing manoeuvre is the most demanding part of the approach/landing task, which therefore affects the pilots opinion to a considerable extent.

In the near future the obtained information will be used to refine the pilot-in-the-loop criterion.

6 REFERENCES

1		Military specification-flying qualities of Piloted Airplanes. MIL-F-8785 B (ASG), Aug. 7,	1969.
2	Chalk, C.R. Neal, T.P. Harris, T.M. Pritchard, F.E. Woodcock, R.J.	Background information and user guide for MIL-F-8785 (ASG), "Military Specification - Flying Qualities of Piloted Airplanes", AFFDL-TR-69-72,	1969.
3	Mooij, H.A. Gool, M.F.C. van	Flight test of stick force stability in attitude-stabilized aircraft. Journal of Aircraft, Vol. 15, No. 9	1978.
4	Mooij, H.A.	Handling quality criteria development for transport aircraft with fly-by-wire primary flight control systems. NLR TR 74141 U	1976.
5	Gool, M.F.C. van	The influence of simulator motion wash-out filters on the performance of pilots when stabilizing aircraft attitude in turbulence. NLR TR 78022 U	1978.
6	Gool, M.F.C. van Mooij, H.A.	Human pilot describing function, remnant and associated information for pitch attitude control: results from in-flight and ground-based tracking experiments. NLR TR 75062 C	1975.
7	Chalk, C.R. DiFranco, D.A. Lebacqz, J.V. Neal, T.P.	Revision to MIL-F-8785 B (ASG) proposed by Cornell Aeronautical Laboratory under contract F 33615-71-C-1254. AFFDL-TR-72-41	1973.
8	Hodgkinson, J. LaManna, W.J. Heyde, J.L.	Handling qualities of aircraft with stability and control augmentation systems - a fundamental approach. Aeronautical Journal, Feb. 1976,	1976.
9	Hodgkinson, J. Berger, R.L. Bear, R.L.	Analysis of high order aircraft/flight control system dynamics using an equivalent system approach. McDonnell Aircraft Company MCAIR76-009	1976.
10	Hodgkinson, J. LaManna, W.J.	Equivalent system approaches to handling qualities analysis and design problems of augmented aircraft. AIAA paper 77-1122	1977.
11	A'Harrah, R.C. Hodgkinson, J. LaManna, W.J.	Are today's specifications appropriate for tomorrow's airplanes? AGARD Flight Mechanics Panel Symposium on Stability and Control Ottawa, Canada	1978.

12 Gool, M.F.C.van — A pilot-in-the-loop criterium and its application to "equivalent system" dynamics. NLR Memorandum VS-78-023 L 1978.

13 Cazenave, A.; Irvoas, J. — Resultats relatifs a l'experimentation sur simulateur et en vol d'un système de commandes de vol electriques généralisables. AGARD Flight Mechanics Panel Symposium on Stability and Control Ottawa, Canada 1978.

14 Urie, D.M. — L-1011 active controls design philosophy and experience. AGARD Flight Mechanics Panel Symposium on Stability and Control Ottawa, Canada 1978.

15 Mooij, H.A.; Boer, W.P.de; Gool, M.F.C.van — Determination of low-speed manoeuvring criteria for transport aircraft with advanced flight control systems. NLR TR 78 (to be published) 1978.

Table 1: Characteristics of the simulated configurations

Conf.	n_α (g/rad)	ω_θ (rad/s)	τ_m (s)	$\frac{K_{DLC}}{(K_{DLC})_{MAX}}$	ζ_q	ω_{n_q} (rad/s)	τ_q (s)
E-1	4.71	.56	2.55	0	.78	.68	1.72
E-2	4.71	.66	2.16	0	.74	.75	1.67
E-3	4.71	.88	1.62	0	.66	.94	1.37
E-4	4.71	1.05	1.36	0	.63	1.12	1.15
E-5	4.71	1.24	1.15	0	.62	1.31	.96
F-1	4.71	1.24	5.38	0	.63	1.23	5.26
F-2	4.71	1.24	2.69	0	.62	1.24	2.56
F-3	4.71	1.24	1.61	0	.61	1.27	1.45
G-1	3.41	1.20	1.19	0	.62	1.30	.93
G-2	3.41	1.20	1.19	.32	.62	1.31	.93
G-3	3.41	1.20	1.19	.68	.62	1.32	.92
G-4	3.41	1.20	1.19	1.0	.62	1.33	.92

F-4 = E-5

Table 2: Cooper-Harper handling qualities ratings.

Conf.	Pilot A	Pilot B	Pilot C	Mean
E-1	10	9	5	8
E-2	6*	6	4	5.3*
E-3	5	3	4	4.0
E-4	2	3	4	3.0
E-5	2	2	3	2.3
F-1	8	6	5	6.3
F-2	6	4	3	4.3
F-3	4	3	3	3.3
F-4	2	2	3	2.3
G-1	4	8	5	5.7
G-2	3-4	5	4	4.2
G-3	2	4	5	3.7
G-4	2	3	4	3.0

*) Rating of Pilot A for Conf. E-2 is estimated on the basis of commentary; the pilot indicated problems to select the proper rating; the original rating given was 2.

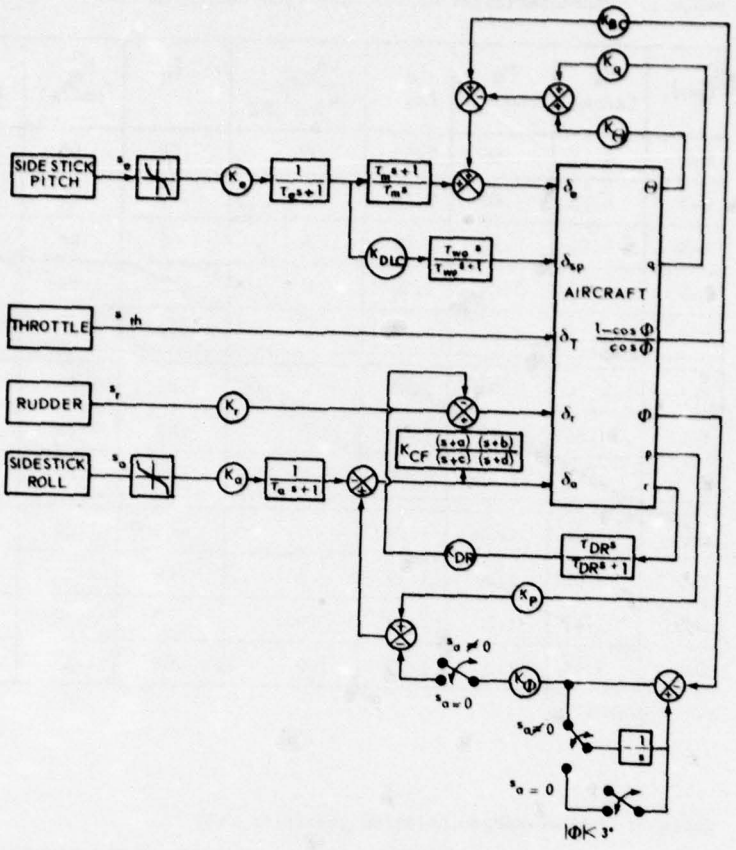

Fig. 1 Flight control system functional block diagram

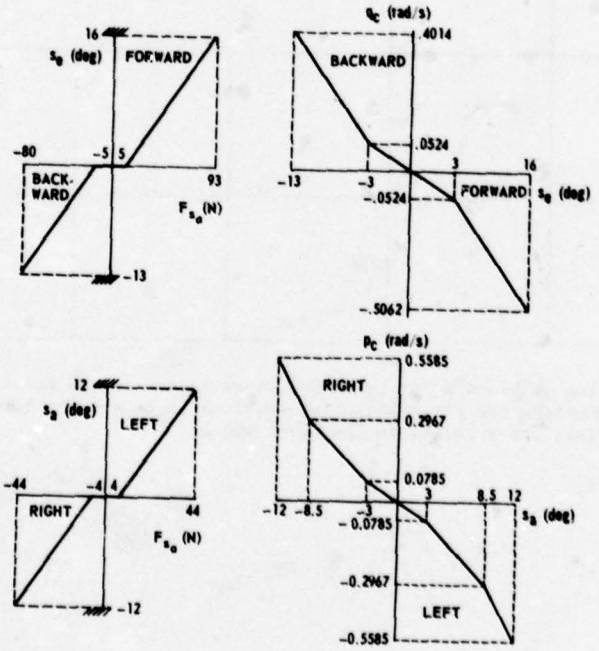

Fig. 2 Side-stick controller characteristics and command gradients

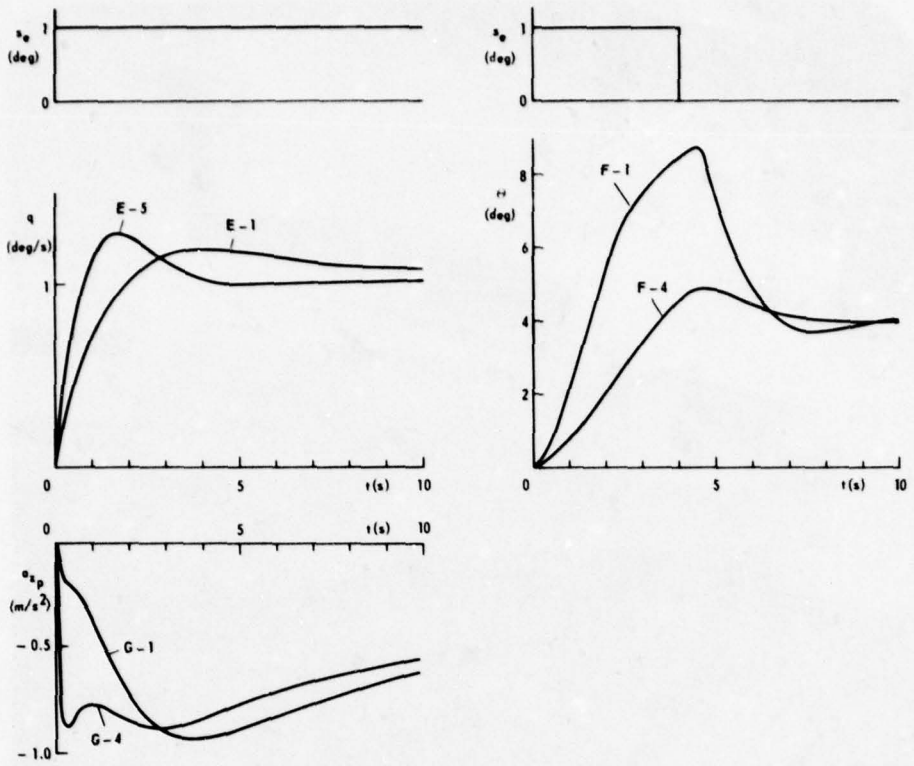

Fig. 3 Time histories of pitch rate, normal acceleration at the pilot seat after a step-input s_e (E–, and G– configurations) and of pitch attitude after a block-input s_e (F– configurations)

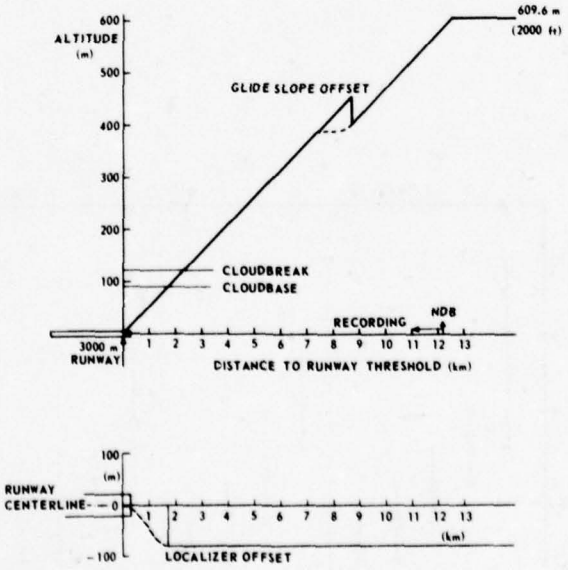

Fig. 4 Approach situation in a vertical and horizontal projection

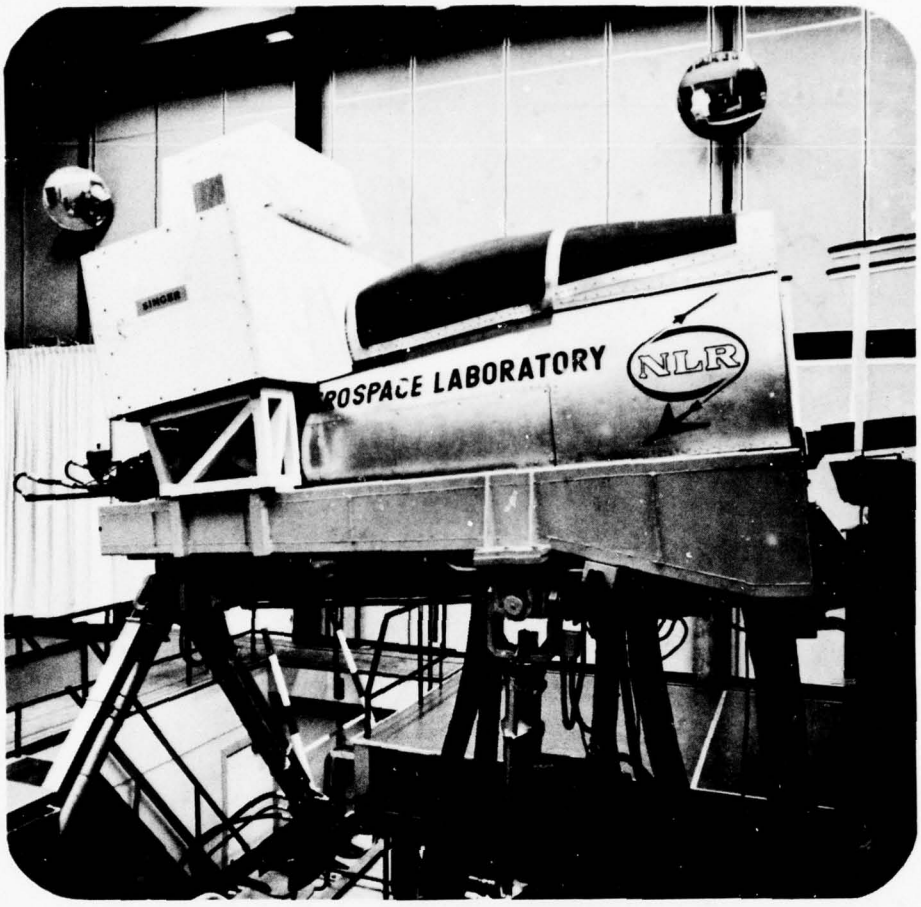

Fig. 5 The four degrees-of-freedom motion system with single seat cockpit and collimating display system

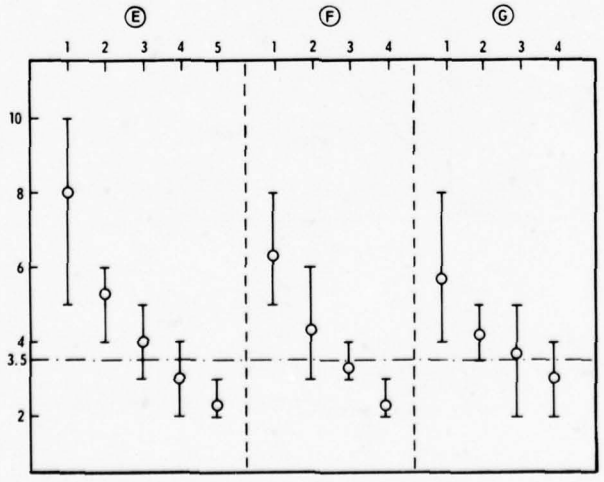

Fig. 6 Cooper-Harper handling quality rating
Bars indicate the range of ratings given

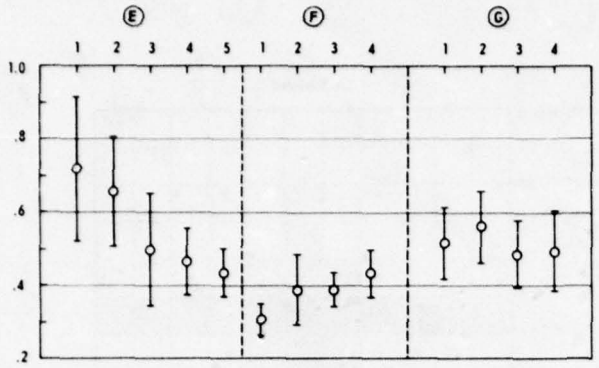

Standard deviation of longitudinal stick deflection (deg)

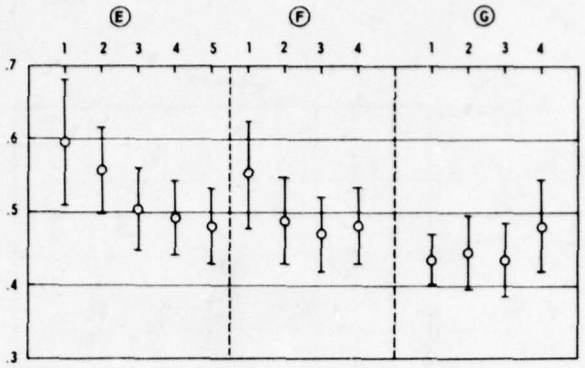

Standard deviation of normal acceleration at the pilot seat (m/s^2)

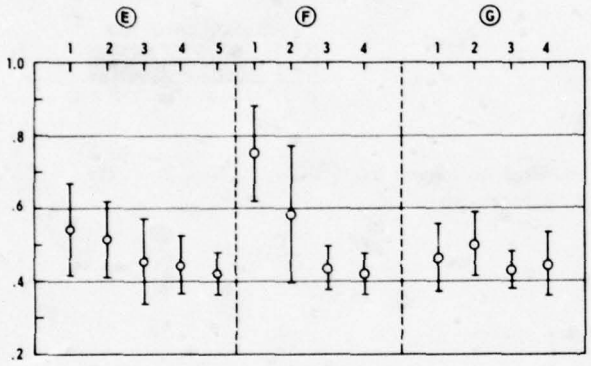

Standard deviation of pitching velocity (deg/s)

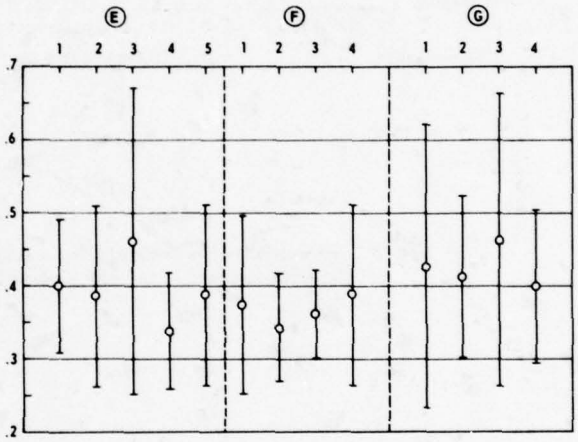

Standard deviation of the angular deviation from the ILS glide path (dots on the ILS indicator)

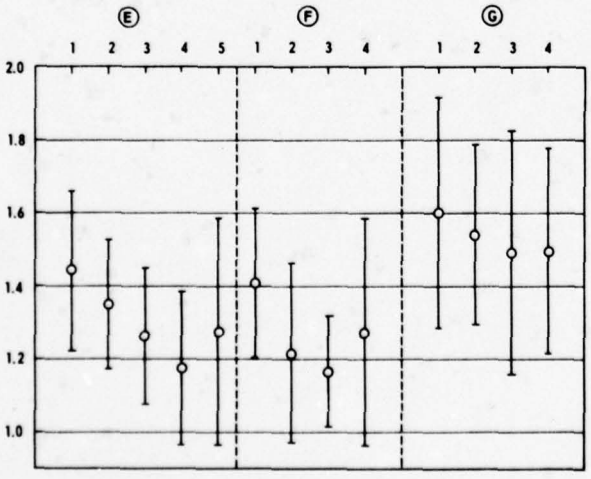

Standard deviation of inclination angle (deg)

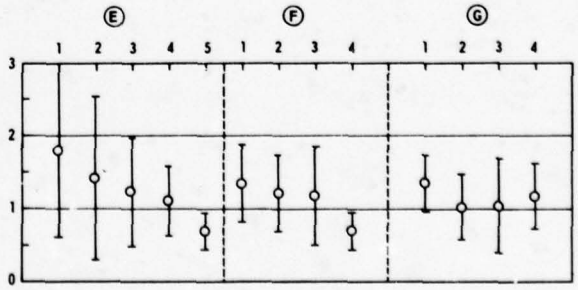

Rate of descent at touchdown (m/s)

Fig. 7 Derived quantities averaged over the pilots. Bars indicate plus and minus one sigma

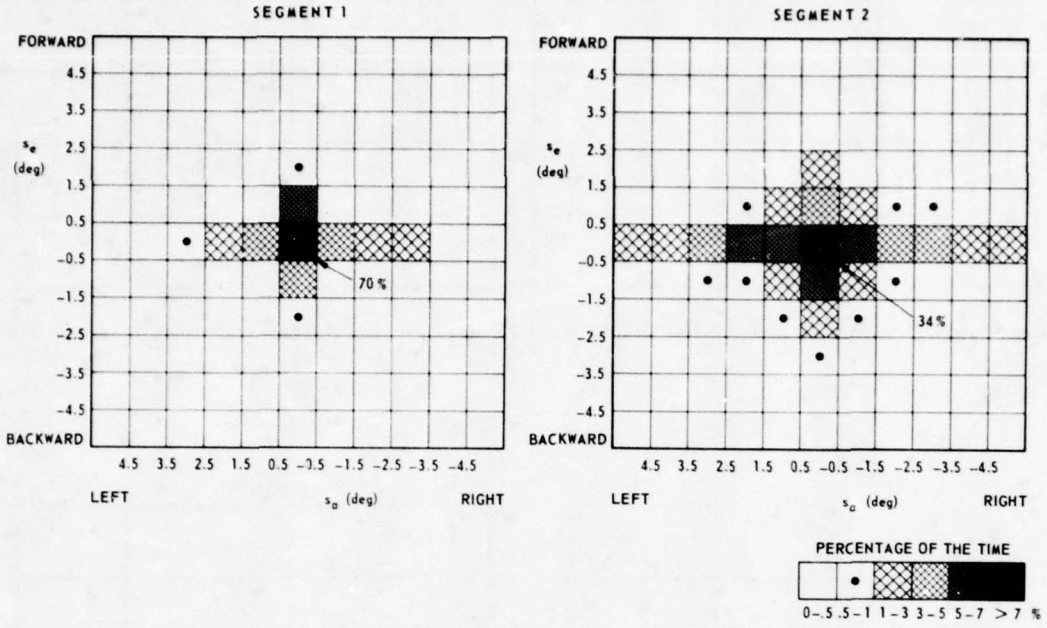

Fig. 8 Two-dimensional histograms of side-stick control on the segment from glidepath intercept to cloudbase (Segment 1) and from cloudbase to touchdown (Segment 2)

MATHEMATICAL MODELS OF MANNED AEROSPACE SYSTEMS

by
P.H.Wewerinke
National Aerospace Laboratory NLR
Anthony Fokkerweg 2
Amsterdam, The Netherlands

SUMMARY

Mathematical models of human operator's participation in manned aerospace systems are reviewed. Herewith pilot's functioning is described in terms commensurate with those used for other system elements. This is desirable in order to deal with the complex interaction between pilot-related and task-related characteristics. The result is an integrated model of the man-machine system serving as a diagnostic tool (for existing systems) and allowing the extrapolation to new situations.

The theoretical framework deals with manned aerospace systems involving the human operator performing continuous control and/or decision making tasks. In the paper it will be illustrated that the pilot-aircraft model provides a powerful task analysis tool. The example given concerns a visual manual aircraft approach. The straightforward investigation includes the effect of outside world visibility conditions, Direct Lift Control and a simple Head-Up display.

1 INTRODUCTION

Many piloted aircraft problems can successfully be solved utilizing engineering models of manned aerospace systems. This concerns not only design problems by which these models allow a systematic investigation of the effect of design alternatives on mission success but also operational research questions can be answered on the basis of a profound insight in the complex interaction among mission- and pilot-related variables rendered by the model.

Just because overall system reliability primarily pertains to this complex interaction between pilot functioning and his task environment it is desirable to describe human behavior in terms commensurate with those used for other system elements. The more so as human behavior primarily reflects (adapts to) his task environment it seems a reasonable approach to describe man and machine in similar terms. Of course, this makes only sense to the extent model results are in agreement with the corresponding measures of human behavior. In other words, the substantial success of engineering models has to be related to the limited domains that they address.

In order to treat realistic, complex task situations, the model structure must be multivariable and formulated in the time domain. This theoretical framework is provided by the state space optimization and estimation theory which is sufficiently general to allow the description of meaningful (i.e., relevant with respect to overall system reliability) pilot functional characteristics.

Up till now, this involved primarily continuous human information processing (resulting in an internal representation of the task) and control behavior as described by the optimal control model (Refs. 1, 2 and 6). However, preliminary attempts have been made to address human monitoring and decision making as well (Refs. 14 and 15). A block diagram of these human functions in the man-machine system is given in figure 1. However, the general structure of the model allows an evolutionary development in order to deal with many relevant piloted aircraft characteristics.

In the next chapter the afore-mentioned pilot-aircraft model will be reviewed. Analogously to the previous discussion, pilot functioning will be described according to the various stages of information processing and functional aspects.
Chapter 3 contains an illustrative application of the model demonstrating its capability to analyze realistic pilot-aircraft situations.
Concluding remarks are made in chapter 4.

2 PILOT-AIRCRAFT MODEL

The present pilot-aircraft model is based on the fundamental hypothesis that the well-motivated, well-trained human operator behaves in a near optimal manner subject to his inherent constraints and the extent to which he understands the objectives of the task. This implies that the description of human operator behavior is concentrated on two aspects: (subjective) criteria for optimality, and the human limitations. In addition, it is assumed that the human operator is dealing with a linear system. Although, strictly speaking, such a system does not exist, the behavior of many systems can be described by linear differential equations, often after some linearization scheme (assuming small perturbations around a trim condition, describing function techniques, etc.).

Once these assumptions are made, linear optimization and estimation theory can be used to formulate the foregoing notions. This is described in the following sections.

2.1 System description

The controlled process is mathematically represented by a vector linear differential equation

$$\dot{x} = Ax + Bu + Ew \qquad (1)$$

where x is the vector of the system states, u is the vector of human control inputs and w is the vector of linear independent, Gaussian, white noises (system disturbance).
This linear(ized) process comprises the controlled system, any dynamics associated with measurement, control

and display systems as well as the environmental disturbances. In case the human operator is not actively engaged in the control loop and only monitors the dynamics process, B = 0 in eq. (1).

It is assumed that the display variables y are linear combinations of the state and control variables (the word display refers to visual cues both from instruments and from the outside world; in general, also aural and vestibular cues can be included)

$$y = Cx + Du \tag{2}$$

The matrices A, B, C, D and E of eqs (1) and (2) may be constant corresponding with a given flight condition and display situation. On the other hand, also time variations in system dynamics, disturbance and display characteristics can be treated on a piece-wise constant basis over a given interval. The controlled system and display is shown in the block diagram of figure 2.

For a stationary process system performance can be expressed in variances and probability measures of system variables of interest. Also frequency domain measures can be obtained such as describing functions, remnant and power spectra (Ref.2).

In case of deterministic inputs and time-varying characteristics of the task environment, such as gust disturbance variations, windshears, variations in displayed information, vehicle dynamics and task instructions (different mission segments, approaching the runway, etc.) the time-average measures are not applicable. Now, performance is conveniently described by means of covariance propagation methods. Statistically, this implies ensemble-averaging.

2.2 Human operator model

Human operator functioning in the afore-mentioned dynamic process will be described in paragraph 2.2.1 according to the various stages of information processing. The first stage concerns the perception of displayed information. Basically, this amounts to a relationship between the display variables y and the perceived variables y_p.
In paragraph 2.2.2 it is described how this perceived information is (optimally) utilized to update the present knowledge about the dynamic process. This knowledge is based on all past data and the (learned) dynamics of the process. The result is an internal representation (internal model) of the task (environment). This internal model describes how well aware the human operator is of the various system states which directly pertains to human monitoring.
Furthermore, also pilot's control responses (if applicable) are based on this information. The optimal response selection and response execution is described in paragraph 2.2.3 by the control response model. In this combination the foregoing (sub)models are known in the literature as the optimal control model (e.g. Ref. 2).
The aspect of human controller's workload, indispensable for a complete description and prediction of human control behavior and its impact on mission success, is taken into account by the workload model discussed in paragraph 2.2.4. Because of the adaptive human capabilities workload is often the most sensitive to task characteristics under consideration. Also human monitoring and decision making can be crucial functions to fulfil (apart from controlling), especially in view of increasing complexity and automation of aerospace vehicles. Decision making which is also based on the information provided by the internal model of the dynamic process, is described by the model discussed in paragraph 2.2.5. The various stages of information processing are shown in the block diagram of figure 2. This figure pertains also to the following paragraphs.

2.2.1 Perceptual model

The perceptual model indicates how the "displayed" variables y, are related to the perceived variables, y_p according to

$$y_p(t) = y(t-\tau) + v_y(t-\tau) \tag{3}$$

where τ is a lumped equivalent time delay, representing the various internal time delays associated with visual (or aural, vestibular, etc.), central processing and neuromotor pathways. The various sources of human randomness (unpredictable in other than a statistical sense) are represented by errors in observing and processing information. This lumped noise v_y is assumed to be an independent, zero-mean, Gaussian, "white" (wide-band) noise process. Each element of v_y is, therefore, specified by its autocovariance V_{y_i}.

This autocovariance is a crucial part of the human operator model. It has been found (Ref.3) that this autocovariance scales with the signal variance $\sigma^2_{y_i}$ (in accordance with the Weber-Fechner law). In addition, it can be related to the fraction of attention f_i, dedicated to variable y_i (Ref.4): the autocovariance appears to be inversely proportional to f_i. Instead of assuming a parallel information processing mechanism (capacity model), one could interpret the same mathematical relationship also as a time-sharing mechanism (Ref.5). In that case f_i represents the fraction of time attended to variable y_i. The same reference shows that f_i can also be interpreted as the probability that the human operator will be attending to y_i.

The autocovariance is given by

$$V_{y_i} = \frac{P_o \sigma^2_{y_i}}{f_i K_i^2} \tag{4}$$

where P_o is the "noise-signal" ratio and has units of normalized power per rad/sec (over positive frequencies) A typical numerical value for P_o of 0.01π has been found for well-designed displays. This relative constant value suggests a basic, primarily human operator-related characteristic. It reflects a given amount of attention (or fraction of time, etc.) dedicated to the task and is an essential part of the workload model discussed in paragraph 2.2.4. The quantity K_i is the describing function gain associated with a threshold. This can represent a perceptual threshold, but also "indifference" thresholds (within certain bounds the

human operator disregards the displayed information) can be accounted for. Furthermore, the threshold can be related to other viewing phenomena such as signal reference characteristics.

2.2.2 Information processing model

Based on the perceived data y_p up to time t and the learned dynamics of the system, the best (least-squares) estimate ($\hat{x}$) of the system state (x) is made. This concerns the situation at the time t-τ (due to the perceptual delay). A predictor provides the best estimate at time t. Leaving, for the sake of discussion, the delay out of consideration the resulting internal representation (estimate $\hat{x}$) of the task (state x) is given by

$$\dot{\hat{x}} = A_c\hat{x} + K(y_p - C\hat{x}) \tag{5a}$$

where A_c represents the closed-loop system dynamics (in the case of control; otherwise A_c=A) and K is the Kalman filter gain which is optimally adjusted, i.e. the best use is made of new information y_p. This can be illustrated by an alternative expression for equation (5a) by combining equations (2), (3) and (5a)

$$\dot{\hat{x}} = A_c\hat{x} + K(Ce + v_y) \tag{5b}$$

with

$$K = \sum C'V_y^{-1} \tag{5c}$$

where $e = x-\hat{x}$ is the estimation error and $\sum$ is the variance of e. Equation (5b) indicates that the present knowledge of the system ($\hat{x}$) is updated on the basis of new, noisy (v_y) information (e). Equation (5c) shows that more emphasis is placed on new information when the uncertainty about the system is large and the new information is reliable. In other words, K is large when $\sum$ is large and V_y is small.

In equation (5) it is assumed that the human operator "knows" ("has learned") the dynamics of the system (A_c). Although this assumption is questionable for large-scale processes this model has worked well in many applications.

2.2.3 Control response model

Human control response selection is assumed to be generated by a control command process which is represented by a set of optimal gains, L, operating on the estimated state, $\hat{x}$, according to

$$u_c = -L\hat{x} \tag{6}$$

These gains, L, are optimal in the sense that they minimize (in the steady-state) the performance index

$$J(u) = E\left\{ y'Q_y y + u'Q_u u + \dot{u}'Q_{\dot{u}}\dot{u} \right\} \tag{7}$$

where the quadratic cost functional J(u) reflects the objectives of the task and Q_y, etc. are the cost functional weightings which can depend on objective and subjective factors.

Human control response is executed according to

$$T_N\dot{u} + u = u_c + v_u \tag{8}$$

indicating how the commanded control, u_c, results in the actual control input, u. Herein, T_N is the "neuro-motor" lag matrix resulting from the weightings on control rate. It can be identified with neuro-motor bandwidth limitations and/or pilot reluctancy to make rapid control movements. v_u is an "equivalent" motor noise vector representing imperfect knowledge of generating control inputs. For well-designed manipulators the autocovariance V_{u_i} appears to scale with the control variance $\sigma^2_{u_i}$ approximately according to $V_{u_i} \approx \approx 0.01\,\sigma^2_{u_i}$.

The optimal control model has been validated against experimental data for a variety of both stationary and non-stationary control tasks (see e.g., Refs. 1, 2, 3, 4, 6, 7 and 11).

2.2.4 Workload model

Performing the continuous information processing and control task described in the foregoing paragraphs is accompanied by a certain "cost". This "side of the coin" is often the most sensitive (variable) because of the adaptive capabilities of the human operator and therefore an essential aspect of the (reliability of the) man-machine system.

Several psychological notions can be associated with this concept, e.g., attention, effort and workload. One way to deal with such a global, intervening (not directly measurable) psychological concept, is to resort to a specific definition providing a meaningful representation of the pertinent concept.

In this context, human operator "workload" is defined in terms of the foregoing pilot-aircraft model. Specifically, the workload model involves two psychological notions: "attention" and "arousal".

In accordance with the usual definitions of workload, attention, as defined before, reflects the fraction of information processing capacity or fraction of time available. This level of attention, P_c, is partly voluntary devoted to the task and partly dictated by the properties of the task (often referred to as "the demand of the task").

Not only this quantitative information processing aspect determines the load imposed on the human operator. Some information is more "arousing" than other. Arousal can be associated with the activity of the central nervous system and is widely assumed to be an important component of human operator workload. This aspect of arousal (or unvoluntary attention in reference 9) is included in the workload model in

terms of the sensitivity of task performance (cost functional, J) to the momentary attention paid by the subject.

The workload model represents the components attention (following reference 8) and arousal according to the expression

$$W = S/P_o \text{ (dB)} \tag{9}$$

with

$$S = \partial J/\partial P_o \text{ (dB)}$$

where the partial derivative indicates that the other model parameters are kept constant. This model has been shown to correlate excellently with subjective ratings and physiological measurements both in laboratory experiments and in-flight (Refs. 6, 7, 10 and 11).

2.2.5 Monitor and decision making model

The perceptual model combined with the information processing model describes the manner in which the human operator will process the data available to him, y_p, to generate an estimate of the system state, $\hat{x}$, with certain accuracy (indicated by the error covariance $\sum$). The pair $(\hat{x}, \sum)$ constitutes a sufficient statistic for testing hypotheses about x based on the data y_p.

This can be described by the subjective expected utility model (Refs. 12-15) which is based on the assumption that the human operator decides (selects between possible hypotheses) to obtain the maximum (expected) profit. The decision process is characterized by the following stages

- formulate N possible hypotheses, H_j
- asses (posterior) probabilities of all hypotheses based on the available information, y_p, $P(H_j/y_p)$
- determine M possible decisions, D_i
- assign the utilities to each hypothesis/decision combination, U_{ij}
- determine the maximum utility-decision $D_i = D^*$ yielding $E = E_{max}$, where

$$E\left\{U/D_i\right\} = \sum_{j=1}^{N} U_{ij}\, P(H_j/y_p) \tag{10}$$

Many decisions involve the choice between two hypotheses (e.g., a successful landing or a go-around). In that case the binary decision strategy is given by

$$\begin{aligned} &D = D_1 \quad \text{if } U_1 P(H_1/y_p) > U_o P(H_o/y_p) \\ &D = D_o \quad \text{otherwise} \end{aligned} \tag{11}$$

where $U_1 \equiv U_{11} - U_{01}$ and $U_0 \equiv U_{00} - U_{10}$

For given utilities the model can be used to compute the various measures of decision performance (the probability of wrongly deciding D_0 and D_1, etc.). The model is validated for single variable tasks (Ref.14) as well as for tasks involving multivariable hypotheses (Ref.15).

3 EXAMPLE

In this chapter a typical example is presented in order to illustrate how the foregoing theoretical framework can be utilized to study manned aerospace systems.

The task considered is a visual manual approach. The task is described into some detail in the following section as well as the various variables investigated in the analysis.

3.1 Visual manual approach task

A manual approach task on the basis of outside world information is analyzed. Two visibility conditions are considered: a good visibility condition (VC1) implying that the complete runway and horizon can be perceived and a restricted visibility condition (VC2): at a nominal height of 200 ft in front of the runway no runway end or horizon can be discerned so that vertical control has to be based on the inclination angle (ω) of the runway sides.

Furthermore, the effect of Direct Lift Control (DLC) on the manual approach performance is investigated by comparing a basic configuration (typified by an approximated relationship between flight path angle and pitch attitude $\gamma \doteq \Theta - \dot{\gamma}/Z_w$) and a configuration with DLC implemented such that the vertical damping represented by Z_w is large and therefore $\gamma \doteq \Theta$. Details concerning gust disturbance characteristics, aircraft dynamics, etc. are given in references 11 and 16.

Finally, the potential use of a simple Head-up display (HUD) is demonstrated. The HUD consists of a displayed pitch bar which has to coincide with the touch-down "point" (by nulling $\tilde{\Theta} = \Theta - \alpha$). Pilot model parameters are given in reference 16. In the case of the HUD perceptual thresholds are assumed corresponding with the pitch bar position of 0.1^o visual angle and with the pitch bar velocity of 0.1^o/sec.

3.2 Results and discussion

Only the vertical approach performance is considered in terms of the glidepath deviation (α) at 200 ft in front of the runway, and the variances of the pitch angle (θ) and the elevator (δ_e).

The DLC-configurations have been investigated also in the theoretical and experimental program (fixed-based simulation) described in reference 11. The agreement between model performance sores and experimental results which is shown in table 1 indicates that the model accurately describes the visual approach tasks. The corresponding, rather unique set of pilot model parameters (primarily the perceptual thresholds involved and the attention dedicated to the tasks) can be used to reliably predict the effect of the afore-mentioned variables: visibility, DLC and HUD.

In table 2 the resulting approach performance of all selected configurations is summarized. Also the computed (optimal) fractions of attention paid to the available visual cues are given.

The main effect of DLC is a considerable reduction of pitch angle and control activity for both visibility conditions. The actual approach angle is only slightly reduced (5 % to 10 %). The model analysis reveals that this is due to the fact that both visibility conditions are to poor (relatively large perceptual thresholds) to take advantage of the improved aircraft dynamics.

Interestingly enough, the effect of a HUD providing the difference ($\tilde{\theta}$) between the pitch angle and the approach angle is exactly complementary. Now, considerably superior approach angle information is available. The model predicts that 20 % to 26 % of the time this information will be attended to, and the remaining time will be devoted to the approach angle variations ($\dot{\alpha}$). The resulting approach angle performance is improved with 50 % for both visibility conditions.

Combining the improved aircraft dynamics and the superior viewing condition yields the expected substantial improvement in overall approach performance. This is only conducted for the good visibility condition (VC1). Now, the improved aircraft dynamics result in an additional approach angle performance improvement of 50 % because, in this case, the viewing conditions allow to take advantage of the superior aircraft handling qualities. The final improvement in the approach angle performance is a factor of 4 ('). Control activity is reduced with about the same factor. Pitch angle deviations are even reduced with a factor of 10.

In summary, the foregoing model analysis illustrates that the study of manned aerospace systems involves the complex interaction of various task-related and pilot-related variables. The pilot-aircraft model has been shown to provide a useful tool to assess quantitatively the effect of pertinent mission characteristics.

Specifically, the example shows the effect of the visibility condition on the manual approach performance. Furthermore, the model analysis leads to the favourable combination of DLC and a simple HUD resulting in a dramatic improvement of overall approach performance.

4 CONCLUDING REMARKS

The foregoing pilot-aircraft model is based on the fundamental assumption that the well-motivated, well-trained human operator behaves in a near optimal manner subject to his inherent constraints and the extent to which he understands the objectives of the task.

Operationalizing this hypothesis amounts to a specification of criteria for optimality and human limitations by modeling (describing) human operator functioning according to the various stages of information processing.

In linear optimization and estimation theoretical terms it is described how the pilot perceives (senses) and processes information resulting in an internal representation of the task. This process directly pertains to human monitor behavior.

Based on the information provided by this internal model the pilot controls the aircraft according to an optimal control strategy (yielding a minimal cost functional). This optimal control model has been extensively validated and shown to represent meaningfully continuous information processing and control behavior even of complex in-flight control tasks (Ref. 6).

Also pilot decision making is modelled. Based on the information of the same internal model the pilot is assumed to decide (select between possible hypotheses) to obtain the maximum profit. Although this model has been successful in describing stationary, multivariable, binary decision tasks, it will have to be tested for rare events in order to enhance the fidelity of the model and its predictive capability.

Finally, the previous example shows that the pilot-aircraft model provides a powerful task analysis tool. It represents a rational and systematic structure of the complex manned aerospace system allowing a straightforward investigation of a variety of highly interacting task-related and pilot-related characteristics.

5 REFERENCES

1 Baron, S. and Levison, W.H. — Display analysis with the optimal control model of the human operator. Human Factors, 1977, 19(5).

2 Kleinman, D.L. and Baron, S. — Manned Vehicle system analysis by means of modern control theory. NASA CR-1753, June 1971.

3 Levison, W.H. — The effect of display gain and signal bandwidth on human controller remnant. AMRL-TR-70-93, March 1971.

4 Levison, W.H. et al — Studies of multivariable manual control systems. A model for task interference. NASA CR-1746, May 1971.

5 Kleinman, D.L. and Curry, R.E.	An equivalence between two representations for human attention sharing. IEEE Trans. on systems, man and cybernetics, September 1976.
6 Wewerinke, P.H.	Performance and workload analysis of in-flight helicopter missions. NLR MP 77013 U, April 1977.
7 Wewerinke, P.H.	Effort involved in single- and two-axis manual control systems. NLR TR 75060 U, November 1974.
8 Levison, W.H.	A model for mental workload in tasks requiring continuous information processing. Nato Symposium on mental workload, Mati, Greece, September 1977.
9 Kahneman, D.	Attention and effort. Prentice-Hall Inc. 1973.
10 Smit, J. and Wewerinke, P.H.	An analysis of helicopter pilot control behavior and workload during instrument flying tasks. NLR MP 78003 U, February 1978.
11 Wewerinke, P.H.	Visual scene perception process involved in the manual approach. NLR TR 78 (forthcoming).
12 Edwards, W. et al.	"Emerging Technologies for Making Decisions" in New Directions in Psychology II. Holt Rinehart and Winston, New York, 1965.
13 Edwards, W. and Tversky, A. (editors)	Decision Making. Penguin Modern Psychology Readings. UPS 8, 1967.
14 Levison, W.H. and Tanner, R.B.	A control theory model for human decision making. NASA CR-1953, December 1971.
15 Wewerinke, P.H.	Human control and monitoring - models and experiments. NASA TM X-73, 170, May 1976.
16 Wewerinke, P.H.	A theoretical and experimental analysis of the outside world perception process. Paper presented at the 14th Annual Conference on Manual Control, Los Angeles, USA, April 1978 (also NLR MP 78020 U).

Table 1 Comparison of model and experimental results

CONFIGURATION	PERFORMANCE	σ_{α}^2 (deg^2)	σ_{θ}^2 (deg^2)	$\sigma_{\delta_e}^2$ (N^2)
VC1/DLC	measured	0.077	0.054	23.0
	model	0.084	0.062	23.5
VC2/DLC	measured	0.193	0.098	26.4
	model	0.189	0.095	26.7

Table 2 Approach performance of all model configurations

CONFIGURATION	ATTENTION ALLOCATION f_i	σ_{α}^2 (deg^2)	σ_{θ}^2 (deg^2)	$\sigma_{\delta_e}^2$ (N^2)
VC1/BASIC	α : 0.6 $\dot{\alpha}$: 0.4	0.095	0.471	74.8
VC1/DLC	α : 0.6 $\dot{\alpha}$: 0.4	0.084	0.062	23.5
VC1/HUD	$\dot{\alpha}$: 0.74 $\dot{\theta}$: 0.26	0.049	0.423	68.8
VC1/DLC/HUD	$\dot{\alpha}$: 0.85 $\dot{\theta}$: 0.15	0.022	0.045	21.7
VC2/BASIC	ω : 0.55 $\dot{\alpha}$: 0.45	0.198	0.535	84.6
VC2/DLC	ω : 0.55 $\dot{\alpha}$: 0.45	0.189	0.095	26.7
VC2/HUD	$\dot{\alpha}$: 0.8 $\dot{\theta}$: 0.2	0.094	0.517	81.7

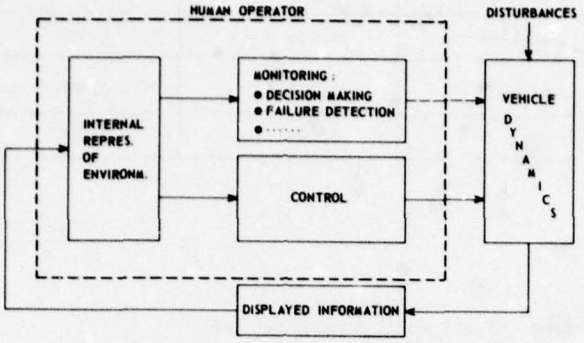

Fig. 1 Block diagram man – machine system

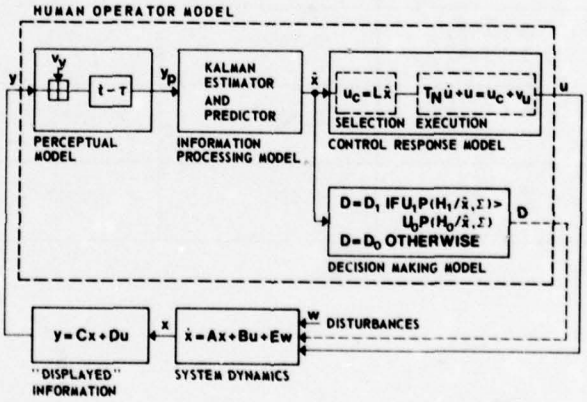

Fig. 2 Pilot – aircraft model

LE MODELE DE PILOTE EN TEMPS DISCRET DE L'ONERA

par Daniel CAVALLI

Office National d'Etudes et de Recherches Aérospatiales (ONERA)
92320 Châtillon (France)

♦

RÉSUMÉ

Un programme numérique simulant le comportement du pilote humain peut fournir aux bureaux d'études un outil permettant d'évaluer l'efficacité du système "pilote-avion". Cette évaluation présente le grand intérêt de pouvoir se placer bien avant l'utilisation du simulateur de vol, au niveau de l'avant-projet, favorisant ainsi l'étude de la pilotabilité d'avions nouveaux dès le stade de la conception.

L'objectif de ce papier est de montrer l'originalité de notre approche par rapport aux modèles de pilote déjà existants et de présenter les résultats obtenus.

Le comportement du pilote est considéré comme un processus en temps discret où la prise de décision a un caractère séquentiel. Ce modèle contraste très nettement des approches précédentes, c'est-à-dire le modèle quasi-linéaire issu de la théorie classique de la commande et le modèle de commande optimale qui considère l'opérateur humain comme un estimateur-prédicteur de Kalman. L'objectif que se fixe le pilote ne peut pas se formuler sous la forme d'un critère à minimiser, c'est une mesure plus floue de la réalité qui consiste à faire suivre à l'avion une trajectoire de référence.

Les paramètres du modèle, dans le programme simulant le comportement du pilote, ont été comparés avec succès, en termes d'écarts-types et de performances, avec ceux de pilotes professionnels en configuration IFR. La première application pratique du modèle de pilote a été l'étude de la dégradation de ses performances quand la marge statique du modèle d'avion simulé décroît.

1 – INTRODUCTION

Les recherches sur les modèles d'opérateurs humains et plus particulièrement sur ceux d'engins spatiaux, d'avions ou d'hélicoptères ont souvent été fortement influencées par les connaissances du moment. L'opérateur humain est, vue de l'extérieur, hautement adaptatif, variable, complexe et suffisamment riche pour que l'on retrouve dans la multiplicité des stratégies qu'il peut utiliser celle que l'on connait bien et que l'on veut y retrouver.

La première approche a été celle de l'automaticien des années 1950 tendant, à l'époque des servo-mécanismes, à introduire son outil de base : la fonction de transfert linéaire du type régulateur-avance de phase [1]. Ces études ont fait fortement appel aux techniques de simulation sur calculateur analogique.

Une des représentations les plus communément acceptées est le modèle quasi-linéaire de MacRuer [2, 3, 4], ainsi appelé parce qu'il représente l'opérateur humain par une fonction de transfert linéaire plus un résidu (remnant) qui décrit la partie de la réponse humaine qui n'a pas été traduite par l'approximation linéaire. La fonction de transfert est essentiellement le résultat d'une approximation du premier harmonique, quant au résidu il tient compte des non-linéarités d'ordre supérieur et surtout des erreurs de caractérisation. La meilleure conclusion de ce type d'étude est sans doute le "cross-over model" qui est basé sur le fait que l'opérateur humain ajuste les paramètres de sa propre fonction de transfert de telle sorte que la réponse en boucle ouverte satisfasse les conditions de stabilité en boucle fermée avec une erreur raisonnable.

En même temps apparaissent des modèles échantillonnés ainsi que le prélèvement de l'information sous forme discrète [5]. Ce type de recherche se prête bien au calcul numérique sur ordinateur cependant, l'hypothèse d'échantillonnage à cadence fixe semble être le point faible de cette représentation.

Une alternative au modèle quasi-linéaire a été développée par Kleinman, Baron et Levison (1971) [6, 7, 8]. Cette approche est basée sur la commande optimale moderne et la théorie de l'estimation et repose sur l'hypothèse que l'opérateur humain bien entraîné se comporte d'une manière optimale compte tenu de ses limitations inhérentes, ses contraintes et les exigences de sa tâche. Mais peut-on dire que l'être humain n'est qu'un estimateur de Kalman dont l'objectif se formule sous la forme d'un critère à minimiser ?

Ces études font un pas décisif lorsqu'elles deviennent interdisciplinaires par l'introduction de psychologues dans les équipes de recherche. Ceux-ci sont sans doute à l'origine de l'apparition de la notion d'image opératoire [9 à 12] qui est un modèle intériorisé de la machine permettant à l'opérateur humain de prévoir les réactions de celle-ci à court terme. On assiste maintenant à une fusion entre l'approche classique et l'approche purement psychologique [13]. Sans renier ce qui a été fait précédemment, notre approche cherche à en faire une synthèse tout en concevant le modèle de l'opérateur humain sur de nouvelles bases fondées sur une analyse précise du comportement du pilote d'avion [14 à 18].

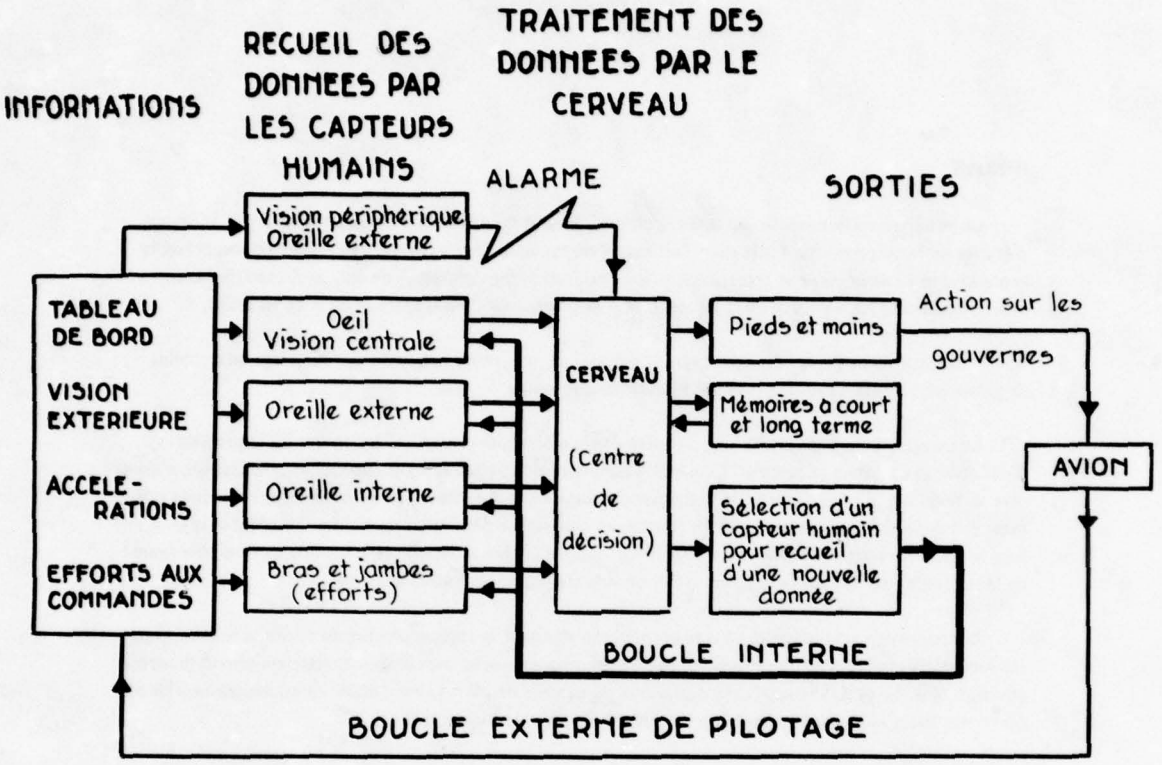

Fig. 1

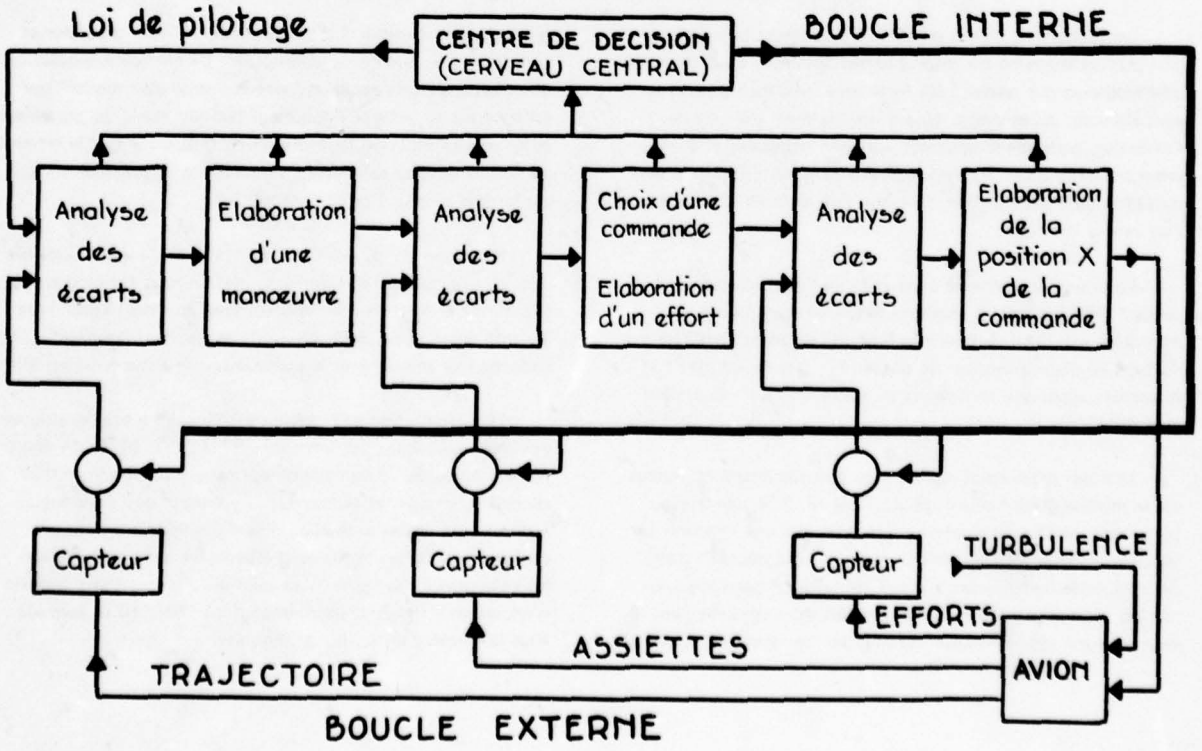

Fig. 2

2 – ANALYSE DU COMPORTEMENT DU PILOTE

Essayons d'analyser le comportement de l'opérateur humain dans le cas du pilotage.

La position de l'avion, fournie au pilote par la lecture des instruments ou par la vue extérieure, est comparée avec la position requise pour le respect de la trajectoire nominale. Par exemple, la barre horizontale de l'ILS est au-dessus du point central, cet écart est analysé par le pilote qui choisit la manœuvre correcte à exécuter de façon à le corriger. Cette manœuvre une fois choisie, le cerveau (centre de décision), par l'intermédiaire d'une boucle interne (fig. 1), demande aux yeux de prélever les informations concernant l'assiette longitudinale. La différence entre l'assiette réelle et l'assiette désirée est analysée et le pilote choisit la bonne commande à déplacer et détermine l'effort à y appliquer. Dans l'exemple précédent, le pilote tire sur le manche avec une force qu'il estime être correcte en demandant à son bras, par l'intermédiaire d'une autre boucle interne, de transmettre les sensations d'efforts. Le mouvement du manche est arrêté lorsque le pilote sent la force prévue.

Ainsi, le centre de décision met successivement en service différentes boucles en demandant des informations nouvelles par l'intermédiaire des capteurs humains. Il y a trois types de boucles (fig. 2) :

– les plus grandes qui concernent les paramètres intéressant la sécurité à court terme, c'est-à-dire la trajectoire, la position, la vitesse,

– les intermédiaires qui concernent les paramètres intéressant la sécurité immédiate, c'est-à-dire les angles d'assiette, l'incidence, etc.

– enfin, les plus petites qui sont des boucles d'effort aux commandes.

On note qu'à chaque instant *il y a une boucle et une seule* en service et ceci constitue l'une des plus fondamentales différences entre un pilote et un pilote automatique. Le choix de la boucle en service est fait par le centre de décision (cerveau central) qui donne l'ordre au capteur choisi de prélever et de transmettre l'information nécessaire par l'intermédiaire d'une boucle interne.

La conséquence immédiate de cette analyse est que l'on ne peut déterminer directement la charge de travail : il semble pratiquement impossible pour l'instant de suivre en détail le traitement de l'information dans le cerveau.

Une autre conséquence de cette analyse est qu'il est sans espoir de bâtir expérimentalement une fonction de transfert représentant le pilote puisqu'il n'y a pas une seule fonction de transfert même très complexe, mais une série de fonctions de transfert utilisées successivement dans un ordre déterminé par le balayage des divers capteurs ; ce balayage dépend lui-même des données, de l'environnement, de l'entraînement du pilote, etc..., c'est-à-dire en partie de phénomènes aléatoires. Ce caractère aléatoire devra nécessairement être traduit dans une partie du modèle de comportement du pilote.

3 – TENUE DE LA LOI DE PILOTAGE

La loi de pilotage, qui est le respect d'écarts corrects sur les paramètres par rapport à la trajectoire nominale, permet le respect de la sécurité immédiate comme de la sécurité à court terme. Le pilote utilise cette loi comme guide, celle-ci dépend de l'objectif que se fixe le pilote et de l'adaptabilité de celui-ci aux conditions d'exécution de la phase de vol.

Tout d'abord, l'objectif que se fixe le pilote ne peut se formuler sous la forme d'un critère à minimiser (comme le propose Kleinman, Baron et Levison [6 à 8], le pilote n'est ni un être parfait ni un singe savant bien entraîné qui, comme chacun le sait, exécute un meilleur travail qu'un pilote humain, quand ce travail est un travail de pur robot. Le cerveau humain est capable de rassembler un grand nombre de données quantitatives et qualitatives, certaines n'étant que des sensations, il est capable de bâtir un modèle de la situation, de la comparer avec des situations types qu'il a en mémoire et de prendre alors une décision d'action même lorsque le cas n'a pas été prévu au préalable. Son objectif est donc beaucoup plus flou, celui-ci consiste à faire suivre à l'avion une trajectoire de référence aussi proche que possible de la trajectoire nominale, cette référence correspond à son apprentissage du pilotage et à sa connaissance de l'avion.

Le pilote possède des qualités d'adaptabilité assez remarquables qui se traduisent dans la nature des commandes qu'il émet. Une interprétation de cette adaptabilité est la notion d'image opératoire ou modèle interne. Le pilote possède en mémoire un modèle qui est sans aucun doute très simplifié de l'avion mais qui lui permet de prévoir les réactions à court terme de son engin compte tenu des actions passées. Cette notion de modèle interne, c'est-à-dire le caractère prédictif de l'opérateur, s'oppose au pilote automatique classique.

4 – CHOIX D'UN MODELE SÉQUENTIEL A BOUCLES MULTIPLES

Compte tenu de ce qui a été vu précédemment, pour être aussi proche que possible du pilote humain, un modèle mathématique doit remplir les conditions suivantes [15] :

a) Les opérations élémentaires de perception des données, l'élaboration des procédures de correction, les actions sur les commandes sont faites en séquence, et non pas simultanément comme c'est le cas dans les modèles continus.

b) Les différentes boucles de contrôle doivent être identifiées compte tenu du type d'engin, de la nature et du nombre des paramètres observés. Le type de chaque boucle doit être précisé : boucle de trajectoire relative à la sécurité à court terme, boucle d'attitude relative à la sécurité immédiate, boucle sur les commandes (voir fig. 2).

c) Les instants où les différentes boucles entrent en action ne sont pas définies d'une manière déterministe mais sont purement aléatoires (processus de Poisson). *Une boucle et une seule* peut être en service à un instant donné, le pilote utilise des règles basées sur son entraînement et sur son expérience personnelle pour commuter d'une boucle à une autre ou pour surveiller le tableau de bord. Ces règles ne sont pas strictes et dépendent du libre arbitre du pilote. Le modèle précis du processus de choix entre ces différentes boucles est un des problèmes les plus difficiles, celui-ci est complètement ignoré dans les modèles à simple boucle.

d) Le modèle doit être conçu de façon à ce que ses différents paramètres caractéristiques soient ajustable lorsque l'on change d'avion tout en restant dans le même type d'avion, en effet le modèle pour un chasseur à Mach 2 est nécessairement différent de celui d'un avion subsonique conventionnel.

e) Le modèle doit être enfin conçu pour donner une bonne évaluation de la charge de travail du pilote.

Des recherches sur un tel modèle multiboucles, qui est appelé modèle en temps discret à cause de son caractère séquentiel, ont été entreprises depuis 1973 à l'ONERA. Ces études [16 à 18] ont débouché sur l'obtention d'un programme numérique simulant le comportement d'un pilote d'avion de transport lourd (du type Airbus A300B) capable d'effectuer une sous-phase de vol (descente finale de l'approche ILS). Le modèle est en voie d'être modifié pour devenir ajustable à différents avions du même type (cette version est actuellement testée avec un modèle du Falcon 20 de Dassault).

5 – DESCRIPTION DU MODELE DE PILOTE EN TEMPS DISCRET

5,1. Hypothèses sur le comportement du pilote

Le comportement du pilote a été étudié dans le cas de la descente finale d'une approche ILS sur un poste de pilotage fixe. On a pu utiliser un équipement électro-oculographique (EOG) permettant de connaître à chaque instant la direction du regard du pilote.

Compte tenu de ces conditions expérimentales, le pilotage n'est considéré ici que comme une tâche de surveillance et de contrôle des paramètres indiqués sur le tableau de bord. Les "tâches secondaires", telles que rapport avec le contrôle aérien ou le reste de l'équipage, n'ont pas été prise en compte. De plus, on a négligé toute prise d'information "involontaire" de la part du pilote : vision périphérique du tableau de bord et de l'environnement extérieur, effets des accélérations sur l'oreille interne, bruits, etc. On peut noter qu'en vol sans visibilité, une partie importante de l'entraînement du pilote consiste à ne pas tenir compte de ces informations prises involontairement (en particulier les accélérations).

On considère qu'à un instant donné le pilote peut soit prendre une décision, soit exécuter une des trois actions élémentaires suivantes :

- agir sur une commande,
- lire une information sur le tableau de bord,
- surveiller un paramètre donné lu sur un cadran.

On considère que la stratégie du pilote, c'est-à-dire le processus de choix entre les différentes procédures de correction sur les paramètres a un caractère séquentiel et est une fonction du cas de vol défini par le type et l'état de l'avion, la phase de vol et l'état de l'atmosphère.

On suppose l'existence dans la mémoire du pilote :

– *d'une bibliothèque d'actions.* Le pilote choisit une des actions en bibliothèque en fonction des différences entre l'image de la situation réelle qu'il a en mémoire et l'image de la situation type où l'exécution de chacune des actions est indiquée ;

– *d'une image opératoire ;* c'est-à-dire d'un modèle intériorisé de l'avion qui lui permet de prévoir les réactions à court terme de celui-ci, donc d'estimer la situation compte tenu d'actions passées, cette estimation est bien entendu réactualisée après chaque lecture.

Le modèle de pilote muni de cette estimation de la situation réelle, appelée situation mémorisée, peut calculer en utilisant son image opératoire les situations prévues et choisir l'action à effectuer en fonction d'une évaluation de ces situations prévues ainsi que de leur gravité évaluée subjectivement.

5,2. Expérimentation

Les équations de la mécanique du vol de l'avion de transport lourd cité au Chap. IV ont été câblées sur un calculateur hybride relié à un poste de pilotage fixe.

La nécessité de savoir quelle information est lue à un instant donné par le pilote à imposé la réalisation d'un tableau de bord particulier. Plusieurs informations généralement intégrées dans un même instrument ont été séparées afin de n'associer qu'une seule information à une direction du regard (par exemple l'ILS dont les deux informations ont été découplées). Pour la descente finale considérée dans cette étude, on dispose des neuf instruments suivants :

- indicateur d'écart localizer ε_{loc}
- indicateur d'écart glide ε_{glide}
- indicateurs d'assiette longitudinale θ, d'angle de gite Θ, d'azimut ψ,
- indicateurs de vitesse verticale $\dot{z}$, d'altitude z,
- indicateur de poussée F, de vitesse V.

Le poste de pilotage est aussi composé de cinq commandes :

- commande en latéral $D\delta l$
- commande en longitudinal $D\delta m$ } sur le manche
- commande de direction au palonnier $D\delta n$
- manette des gaz $D\delta z$
- et un trim de profondeur.

Les fixations de l'œil du sujet sur les différents cadrans peuvent être repérées par l'intermédiaire d'un équipement électro-oculographique (EOG) (fig. 3). Des différences de potentiel, fonction de la position relative des yeux par rapport à la boîte cranienne, sont recueillies par des électrodes posées sur le visage du sujet. En faisant l' hypothèse que la tête du sujet reste fixe, on peut déduire des signaux amplifiés, puis filtrés, quel est le cadran fixé par le sujet à chaque instant.

Dans une première phase expérimentale, le véhicule simulé a été piloté par cinq pilotes professionnels. Lorsque l'on demande aux pilotes quelle idée ils se font de l'avion simulé et de sa dynamique, ils expriment leur image opératoire en termes de relations différentielles entre les divers paramètres et entre les paramètres et les commandes. Cette image est conforme aux équations linéarisées de la dynamique de l'avion en ce qui concerne le pilotage en latéral mais paraît beaucoup plus complexe en ce qui concerne le pilotage en longitudinal (couplage écart glide-vitesse) (fig. 4).

Le modèle de pilote est muni de cette image opératoire représentée par un vecteur d'état qui résume la situation mémorisée de l'avion et par un système d'équations conforme à la dynamique qu'utilise le pilote pour effectuer ses prévisions.

Dans une deuxième phase, on analyse les résultats des phases de vol simulées par les sujets humains en distinguant trois niveaux d'activité dans le mode opératoire du pilote (fig. 5). Cette classification est seulement une hypothèse de travail mais semble proche de la réalité observée et correspond aux trois différents types de boucles vus précédemment.

Fig. 3 – Photo montrant l'oculomètre.

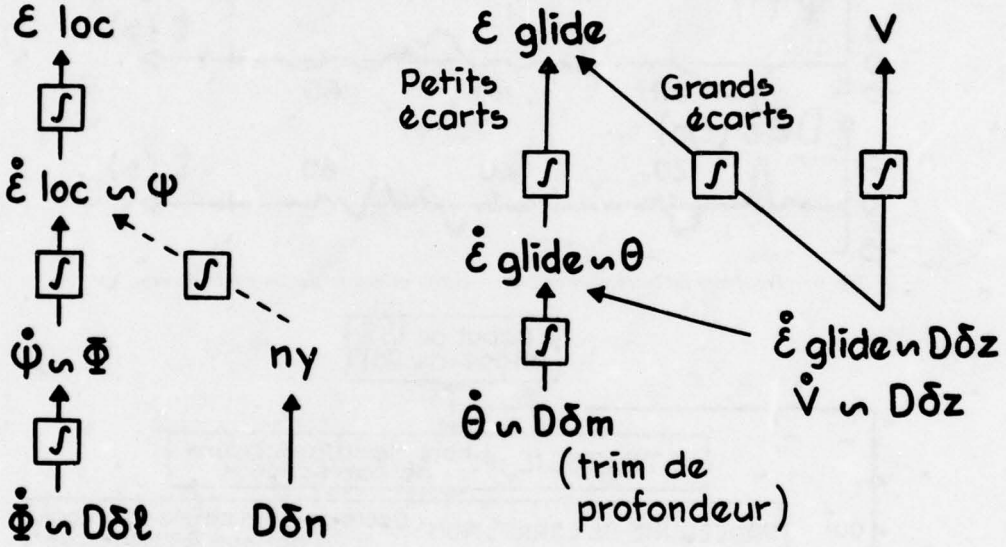

Fig. 4 – Image opératoire (modèle interne).

NIVEAU	DEFINITION	BUT	COUT
STRATEGIE	Choix des procedures de correction à effectuer	Sécurité à court terme	Charge mentale de décision
PROCEDURE DE CORRECTION	Suite algorithmique d'actions élémentaires	Sécurité immediate	Charge mentale de memorisation
ACTION ELEMENTAIRE	* Lecture cadran. * Action sur une commande. * Surveillance d'un paramètre.		Charge physique

Fig. 5 – Niveaux du mode opératoire.

Le respect de la sécurité à court terme est le but de la stratégie ; la sécurité immédiate est une contrainte qui peut être respectée en n'envisageant que des procédures de correction maintenant la trajectoire réelle proche de la trajectoire nominale.

Les phases enregistrées sont découpées en procédures de correction ou en lectures de surveillance des différents paramètres. On peut alors mesurer différentes valeurs telles que temps moyen de fixation sur chaque cadran, fréquence de surveillance de chaque paramètre, lois d'action sur les commandes, succession des cadrans fixés, etc .. Un exemple de procédure de correction en écart localizer est donné figure 6

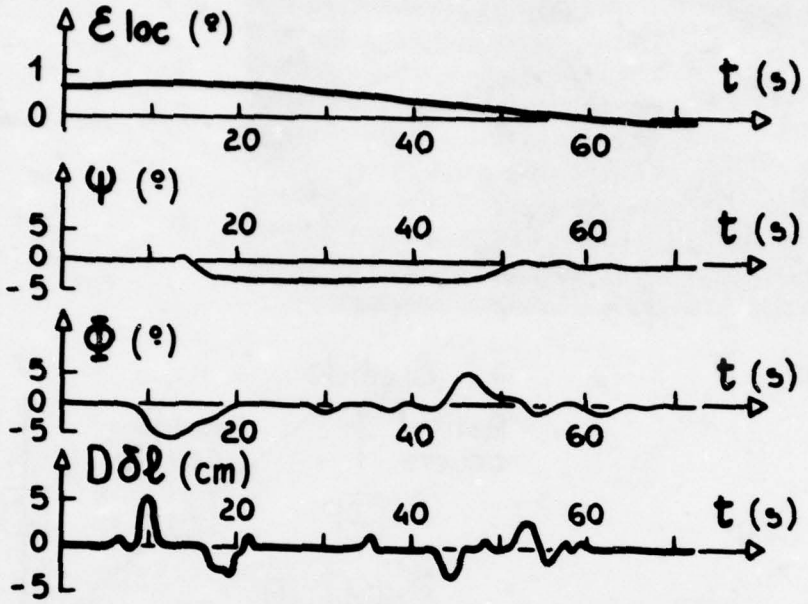

Fig. 6 – Procédure de correction en écart localizer effectuée par un pilote humain.

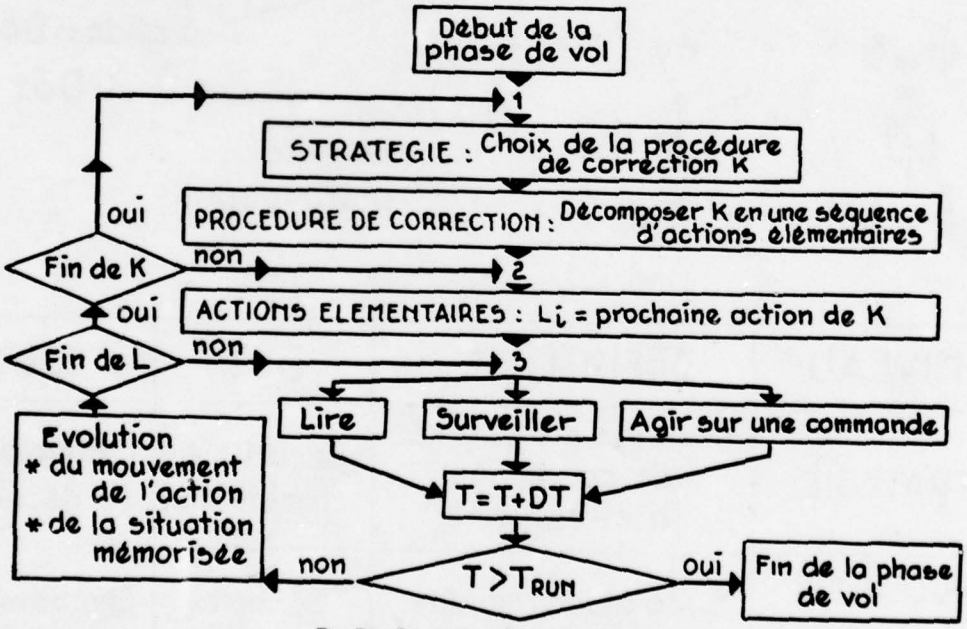

Fig. 7 – Description du programme.

5,3. Modèle numérique

5,3.1. Description du programme

L'organigramme est donné figure 7.

Après les initialisations, le modèle de pilote choisit, suivant la stratégie utilisée, la procédure de correction qui doit être effectuée. Cette procédure de correction est alors décomposée en une suite d'actions élémentaires (lecture d'un instrument, attente sur un paramètre, action sur une commande) qui sont successivement exécutées.

En fait, pendant une période d'attente, le modèle peut choisir et commencer l'exécution d'une autre procédure de correction qui vient se ranger devant la pile des actions à exécuter.

L'incérment DT du temps, au cours d'une action élémentaire, commande d'une part l'intégration de la trajectoire suivant les équations du mouvement, d'autre part l'intégration des équations conformes à l'image opératoire de la situation mémorisée par le modèle.

5,3.2. Modèle de stratégie utilisé

La stratégie est le niveau le plus élaboré du comportement du pilote. Dans le programme numérique, la stratégie permet au modèle de pilote, à un instant donné, de choisir quelle procédure de correction ou quelle lecture de surveillance il va effectuer. Ce choix se fait en cherchant à respecter la sécurité à court terme.

Dans la stratégie utilisée, on a cherché à distinguer le choix de la surveillance des cadrans (on utilise alors une stratégie à lectures markoviennes qui a un caractère aléatoire) du choix des procédures de correction de paramètres (utilisation d'une stratégie par évaluation à court terme). La différenciation entre ces deux stratégies est basée sur la notion de gravité de la situation instantanée perçue par le modèle de pilote qui est définie par :

$$G(O) = \underset{\substack{\text{sur les paramètres} \\ \text{principaux}}}{Max.} \left| \frac{\text{écarts estimés}}{\text{écarts tolérés}} \right|$$

C'est le rapport maximum sur l'ensemble des paramètres principaux de la phase de vol entre l'écart estimé (mémorisé ou prévu par l'image opératoire) et l'écart toléré sur un paramètre. Les écarts tolérés sont déterminés expérimentalement, ce sont les écarts moyens corrigés. Si $G(O)$ est en-dessous d'un certain seuil de gravité minimum, la situation est considérée comme calme et le modèle de pilote adopte la stratégie de surveillance des cadrans. Si $G(O)$ est au-dessus du seuil, la situation est considérée comme grave et le modèle adopte la stratégie de procédures de correction des paramètres.

Pour la stratégie de surveillance des cadrans, la lecture des instruments obéit dans le programme numérique à un double phénomène aléatoire : la séquence des instruments consultés est considérée comme une chaîne de Markov, la séquence des instants de lecture comme un processus de Poisson.

La succession des appareils consultés est régie par une matrice de probabilités conditionnelles de lire un instrument après en avoir lu un autre. Cette matrice est appellée matrice de commutation. Après chaque lecture d'instrument, la valeur d'une variable aléatoire détermine, compte tenu de la matrice de commutation quel est le prochain cadran qui doit être lu.

La lecture des instruments se fait à un rythme variable, le temps moyen de lecture est noté MTBS (Mean Time Between Switches). Cet intervalle correspond au temps de la lecture nécessaire à l'acquisition d'une donnée par le modèle de pilote.

Le caractère aléatoire de la succession des appareils consultés est supprimé si un ou plusieurs paramètres ont franchi ou franchissent à l'instant t de lecture un certain seuil fixé à l'avance pour chaque paramètre. Le processus devient alors déterministe.

Si un seul paramètre dépasse son seuil, c'est l'instrument correspondant à ce paramètre qui est lu. Si plusieurs paramètres ont franchi à l'instant de lecture les seuils qui leur sont fixés, c'est l'instrument correspondant au paramètre ayant la plus forte probabilité d'après la matrice de commutation qui sera lu.

Le phénomène peut être observé expérimentalement : si un paramètre diverge, le regard du pilote se dirige généralement vers l'instrument correspondant à ce paramètre car sa vision périphérique lui permet de détecter une déviation importante sur l'un des cadrans. Si plusieurs paramètres divergent, le pilote s'occupe du paramètre qui lui semble prioritaire et laisse provisoirement les autres qui continuent d'évoluer.

Une matrice de commutation déterminée expérimentalement en utilisant le poste de pilotage et l'équipement électro-oculographique (EOG) est donné figure 8 dans le cas de la descente finale d'une approche ILS. On constate que l'on retrouve dans cette matrice la trace des lois de surveillance élémentaires de pilotage aux instruments, par exemple la consultation très fréquente de l'horizon artificiel.

	ε_{glide}	ε_{loc}	$\dot{z}$	$\ddot{\Phi}$	θ	ψ	F	z	V
$\varepsilon_{gl.}$	0,03	0,10	0,11	0,04	0,15	0,03	0,06	0,21	0,20
ε_{loc}	0,28	0,15	0,05	0,21	0,06	0,23	0,05	0,05	0,08
$\dot{z}$	0	0,03	0,06	0,07	0,10	0,05	0,06	0,11	0
Φ	0,10	0,39	0,12	0,29	0,18	0,28	0,17	0,09	0,10
θ	0,40	0,14	0,20	0,16	0,29	0,13	0,19	0,21	0,18
ψ	0,08	0,12	0,16	0,13	0,13	0,10	0	0,16	0,07
F	0	0,01	0,10	0,01	0	0,05	0,11	0	0,09
z	0,03	0,04	0,13	0,07	0,07	0,11	0,12	0,12	0,08
V	0,08	0,02	0,07	0,02	0,02	0,02	0,24	0,05	0,20

$\Sigma = 1 \quad =1 \quad =1 \quad =1 \quad =1 \quad =1 \quad =1 \quad =1 \quad =1$

Matrice obtenue avec un équipement EOG (pour le cas de la descente finale)

* Tous les paramètres $x_i < L_i$
➡ Les lectures d'instruments sont gouvernées par la matrice de commutation.

* Un paramètre $x_i \geq L_i$
➡ Lecture de x_i.

* Plusieurs paramètres $x_i \geq L_i$
➡ Lecture du x_i qui a la plus grande probabilité dans la matrice de commutation.

L_i : Seuil donné à l'avance pour chaque paramètre x_i.

Fig. 8 – Stratégie pour la surveillance des cadrans.

La stratégie de procédures de correction est basée sur le fait que le pilote prend des décisions dépendant de l'évolution prédite à court terme de la situation, compte tenu des actions passées.

Le modèle n'a pas accès aux équations régissant la dynamique du véhicule mais est capable, grâce à son image opératoire, de prédire approximativement la situation à court terme. Cette possibilité de prédiction est utilisée par le modèle pour choisir, à chaque fois que cela lui est nécessaire, la meilleure procédure de correction à exécuter. Ce choix se fait en déployant une arborescence (fig. 9) pour laquelle :

– la racine est la situation mémorisée So

– les branches sont des procédures de corrections dont l'exécution est envisagée.

– les sommets autres que la racine sont des situations prévues à partir de la racine à l'aide de l'image opératoire et compter tenu des procédures de correction envisagées.

La gravité instantanée $G(K)$ est calculée en chaque sommet K. En considérant qu'elle reste constante durant le temps Δt_I écoulé jusqu'au sommet I depuis son prédécesseur, le modèle calcule une gravité moyenne à court terme $\mathcal{G}(I)$ sur chaque chemin menant à un sommet terminal. Pour celà, la gravité instantanée est pondérée par le temps écoulé sur chaque branche et

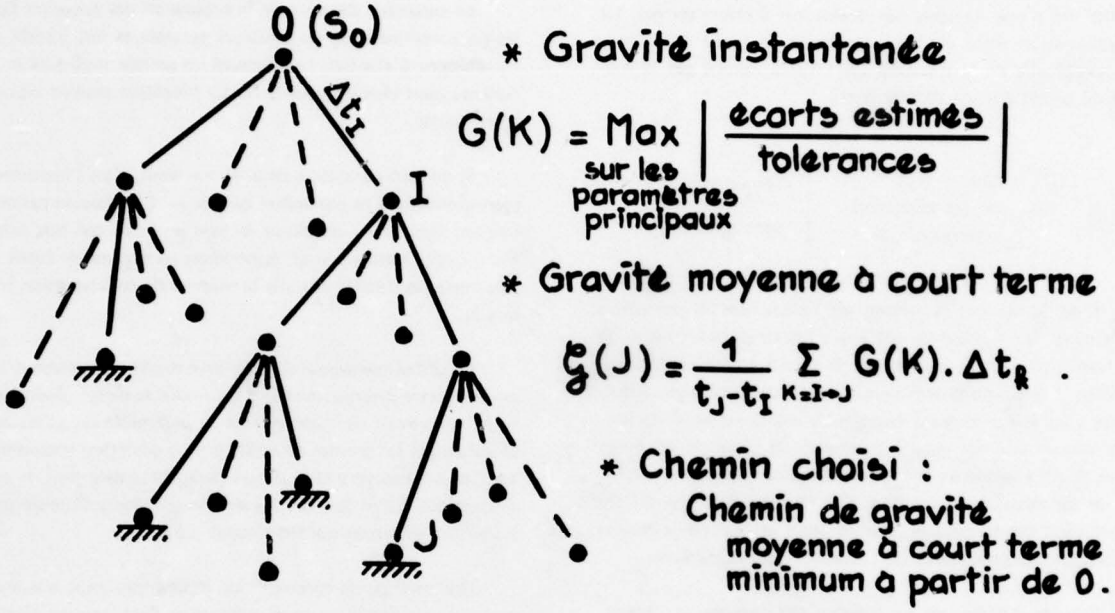

Fig. 9 – Stratégie pour la correction des paramètres.

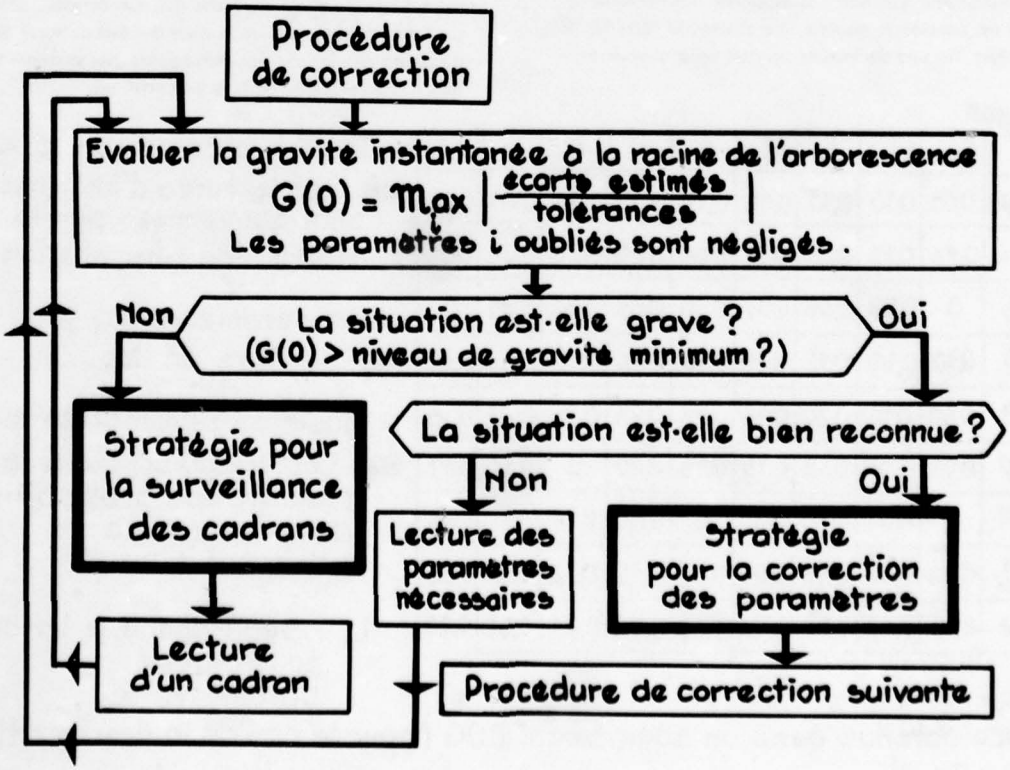

Fig. 10 – Stratégie globale.

le résultat est divisé par le temps total écoulé sur le chemin. La gravité moyenne à court terme d'un chemin (I, J) est donc notée par :

$$\mathcal{G}([I, J]) = \frac{1}{t_J - t_I} \sum_{K=I \to J} G(K) \cdot \Delta t_K$$

On note $\mathcal{G}(I)$ la gravité moyenne du meilleur chemin $\mathcal{G}([I, J])$ choisit en I. Ce choix est fait tout simplement en prenant parmi tous les chemins possibles à partir de I celui ayant la gravité moyenne minimum.

Le chemin issu de la racine ayant la gravité moyenne minimum est alors choisi et l'exécution de la procédure de correction correspondant à sa première branche peut être commencée.

Une stratégie globale, incluant la stratégie de surveillance des cadrans et la stratégie de procédures de correction, est alors utilisée (fig. 10).

Le modèle commence par l'évaluation de la gravité instantanée $G(O)$ à la racine de l'arborescence. Cette évaluation est limitée aux paramètres principaux présents en mémoire, ceux qui ont été lus depuis trop longtemps sont volontairement oubliés (ce phénomène d'oubli modifie la gravité de la situation ressentie par le pilote et rend son comportement plus réaliste).

Après l'évaluation de $G(O)$, le modèle de pilote se pose la question : la situation est-elle grave ? ($G(O)$ est-il au-dessus d'un certain seuil de gravité minimum).

– Si la réponse est non, le modèle effectue des lectures de surveillance en utilisant la stratégie à lectures markoviennes et recommence ensuite l'évaluation de la gravité instantanée $G(O)$.

– Si la réponse est oui, le modèle se demande si la situation est bien reconnue.

. Si la situation ne l'est pas, le modèle effectue de façon déterministe toutes les lectures permettant la connaissance complète de la situation.

. Si la situation est grave et bien reconnue, le modèle développe l'arborescence des corrections prévues et fait un choix parmi celles-ci en évaluant la situation à court terme.

6 – UTILISATIONS DU PROGRAMME

Deux applications ont été faites pour valider le programme. Toutes deux ont été effectuées dans le cas de la descente finale d'une approche ILS pour un avion de transport lourd du type Airbus A300B. Tout d'abord on a réalisé une comparaison statistique entre les performances du modèle et celles de pilotes professionnels. Ensuite, on a étudié la dégradation des performances du modèle de pilote lorsque la marge statique de l'avion simulé décroît.

6,1. Comparaison entre le modèle numérique et des pilotes professionnels

Il est illusoire de vouloir faire une comparaison portant sur les tracés du modèle et du pilote humain, la coïncidence des deux sortes de courbes, pour bonne qu'elle soit, ne peut jamais être parfaite. Il vaut donc mieux s'orienter vers une comparaison de type statistique. On a choisi la comparaison entre les écarts-types et les performances sur les divers paramètres du vol.

On définit l'écart-type et la performance sur un paramètre x par :

Ecart type $\quad \sigma x = \sqrt{\frac{\int_0^t x^2 dt}{t}}$

Performance $\quad Px = \frac{t}{\int_0^t |x| dt}$

t représentant ici la durée de la descente finale de l'approche ILS.

Les résultats du modèle ont été comparés avec ceux de cinq pilotes professionnels effectuant, en configuration IFR, des descentes finales sur simulateur sur lequel était affiché l'avion de transport lourd choisit pour cette étude. La comparaison est donnée figure 11, le modèle a un comportement voisin de celui des pilotes en ce qui concerne les écarts-types et les performances.

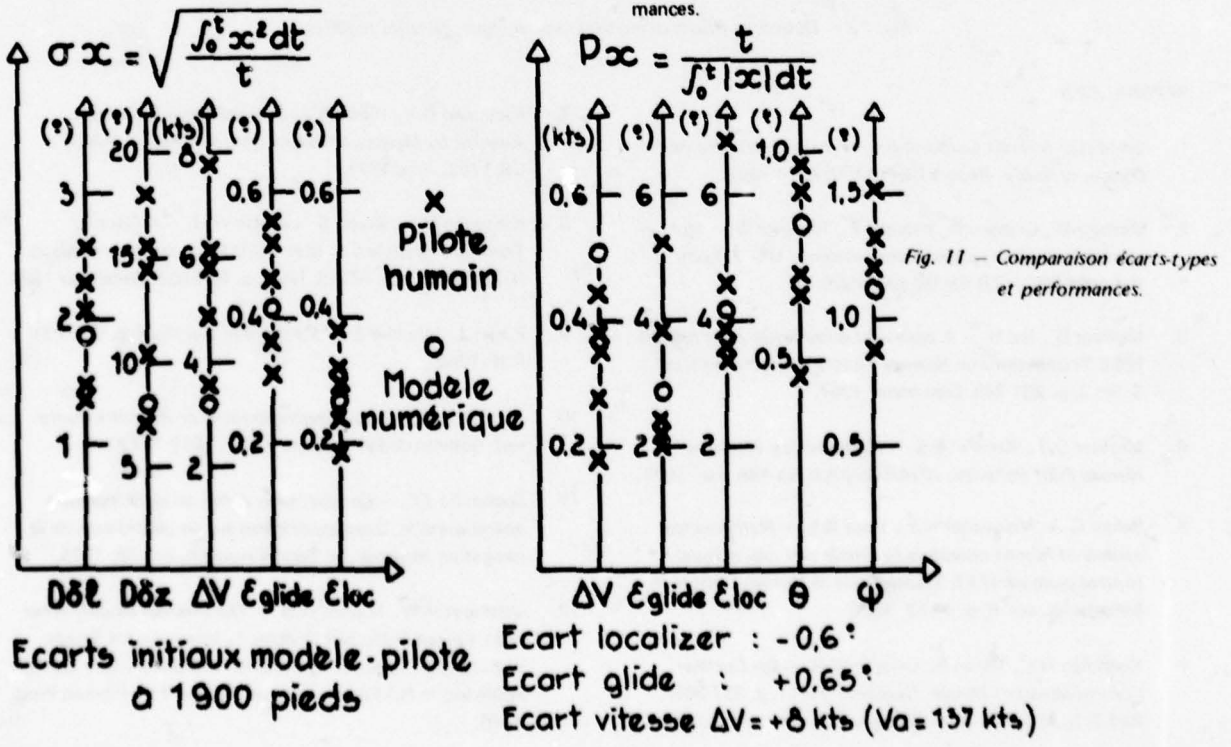

Fig. 11 – Comparaison écarts-types et performances.

6,2. Application du modèle au pilotage avec marge statique réduite

Une première application pratique du modèle de pilote a été l'étude de la détérioration de ses performances quand la marge statique du modèle d'avion décroît (c'est-à-dire quand le centre de gravité recule, déstabilisant progressivement l'avion).

On constate que les performances du modèle de pilote se dégradent lorsque la marge statique diminue, ce qui semble réaliste. La perte de contrôle survient brusquement (fig. 12) lorsque la charge de travail, consécutive à une diminution de marge statique, devient excessive. Mais le résultat le plus intéressant de cette étude est que lorsque les difficultés de pilotage surgissent sur l'axe de tangage, c'est bien l'ensemble du contrôle de l'avion qui se dégrade, car la plupart des pertes de contrôle surviennent sur l'axe transversal.

7 – CONCLUSION

Le modèle qui est décrit dans ce papier se veut plus conforme au comportement du pilote que les recherches précédentes. Il cherche à faire la synthèse entre l'approche classique et l'approche psychologique représentée par l'introduction du modèle interne du véhicule.

Un programme numérique simulant le comportement d'un pilote d'avion de transport (du type Airbus A300B) est actuellement capable d'effectuer une sous-phase de vol (descente finale de l'approche ILS).

Les recherches futures viseront à introduire la notion d'adaptabilité du pilote à chaque type d'avion nouveau, ainsi que la notion d'apprentissage qui permet de rendre compte du degré d'évolution professionnelle de chaque pilote.

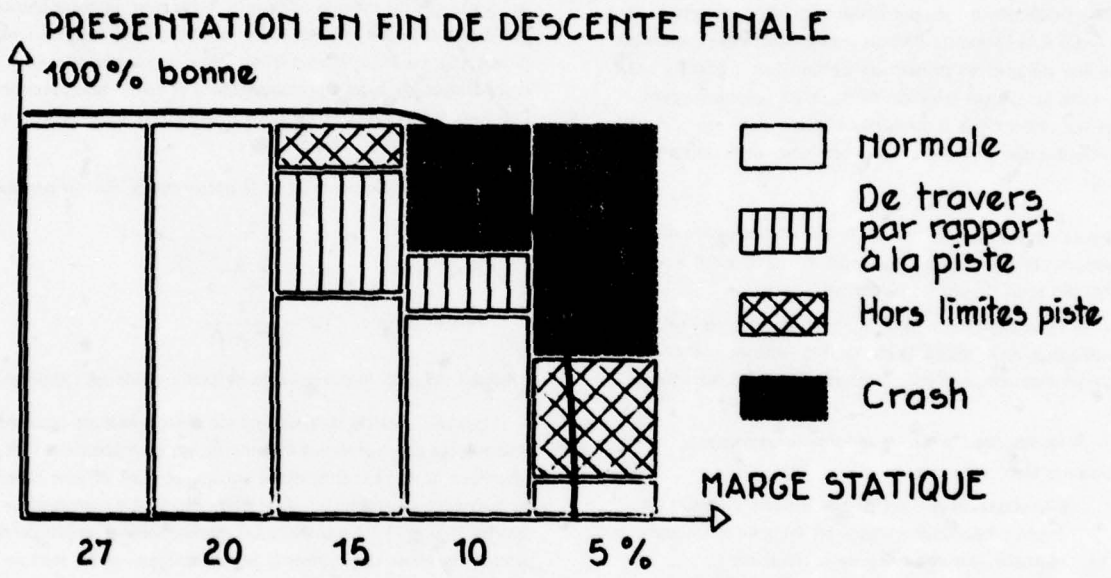

Fig. 12 – Descentes finales effectuées avec marges statiques réduites.

RÉFÉRENCES

1. Goodyear Aircraft Corporation – *Final Report : Human Dynamics Study.* Report GER-4750, APril 1952.

2. McRuer D., Graham D., Krendel E., Reisener W. – *Human pilot dynamics in compensatory systems.* USAF Tech. Report AFFDL TR-65-15, July 1965.

3. McRuer D., Jex H. – *A review of quasi linear pilot models.* IEEE Transactions on Human Factors in Electronics, vol. 8, No 3, p. 231-249, September 1967.

4. McRuer D.T., Krendel E.S. – *Mathematical Models of Human Pilot Behavior.* AGARDograph No 188, Jan. 1974.

5. Bekey G.A., Meissinger H.F., Rose R.E. – *Mathematical models of human operators in simple two-axis manual control systems.* IEEE Transactions of Human Factors in Electronics, vol. 6, p. 42-52, 1965.

6. Kleinman D.L., Baron S., Levison W.H. – *An Optimal Control Model of Human Response.* Part I, p. 357-369, Part 2, p. 370-383, Automatica, vol. 6, No 3, May 1970.

7. Kleinman D.L., Baron S. – *Manned Vehicle Systems Analysis by Means of Modern Control Theory.* NASA CR-1753, June 1971.

8. Kleinman D.L., Baron S., Levison W.H. – *A Control Theoretic Approach to Manned-Vehicle Systems Analysis.* IEEE Trans., vol. AC-16, No 6, p. 824-832, December 1971.

9. Piaget J., Inhelder B. – *Mémoire et Intelligence.* Col. BSI-PUF-1968.

10. Bisseret A. – *Mémoire opérationnelle et structure du travail.* Bulletin de Psychologie XXVI, 1972-1973.

11. Sperandio J.C. – *Compléments à l'étude de la mémoire opérationnelle. Deux expériences sur les contrôleurs de la navigation aérienne.* Le Travail Humain, vol. 38, 1975.

12. Veldhuyzen W., Stassen H.G. – *The Internal Model - What does it mean in Human Control ?* . International Symposium NATO "Monitoring Behavior and Supervisory Control", Published in NATO Conf. Series III, vol. 1 by Plenum Press, 1976.

13. Phatak A V. – *Formulation and Validation of Optimal Control Theoretic Model for Human Operator.* IEEE Systems Man and Cybernetics Newsletters, vol. 2, June 1976.

14. Wanner J.C. – *General guideline for the design of manned aerospace vehicles - Automation on manned aerospace system.* AGARD Conf. Proc. No 114 (1973).

15. Wanner J.C. – *The multiloop concept of the pilot work-load as a basis of future experiments and studies.* TP ONERA No 1978-10, à paraître dans un AGARDograph.

16. Cavalli D., Soulatges D. – *Discrete-time modelization of human pilot behavior.* Proceedings of the 11th Annual Conference on Manual Control. NASA Ames Research Center, Ca. May 1975, NASA TM X-62, 464, p. 119-129.

17. Cavalli D. – *Discrete-time modeling of heavy transport plane pilot behavior.* Proceedings of the 13th Annual Conference on Manual Control, MIT, Cambridge, Mass., June 1977, p. 321-328.

18. Cavalli D. – *Discret-time pilot model.* Proceedings of the 14th Annual Conference on Manual Control, University of Southern California, Los Angeles, Ca., April 1978.

FLIGHT EXPERIENCE WITH ADVANCED CONTROLS AND DISPLAYS DURING PILOTED CURVED DECELERATING APPROACHES IN A POWERED-LIFT STOL AIRCRAFT

W. S. Hindson
National Aeronautical Establishment
National Research Council of Canada, Ottawa, Ontario, Canada

and

G. H. Hardy
NASA-Ames Research Center, Moffett Field, California 94035, U.S.A.

SUMMARY

A program to assess the feasibility of piloted STOL approaches along predefined, steep, curved, and decelerating approach profiles was carried out with a powered-lift STOL aircraft. To reduce the pilot workload associated with the basic control requirements of a powered-lift aircraft equipped with redundant controls and operating on the backside of the power curve, separate stability augmentation systems for attitude and speed were provided, as well as a supporting flight director and special electronic cockpit displays.

It was found to be particularly important to assist the pilot through use of the flight director computing capability with the lower frequency control-related tasks, such as those associated with (1) monitoring and adjusting configuration trim as influenced by atmospheric effects, and (2) preventing the system from exceeding powerplant and SAS authority limitations.

This paper briefly describes the control, display, and procedural features of the flight experiment that have led to the conclusion that, given an adequate navigation environment, such constrained approaches may be feasible from a pilot acceptance point of view. Many of the technical and pilot related issues identified in the course of this flight investigation are representative of similarly demanding operational tasks that are thought to be possible only through the use of sophisticated control and display systems.

INTRODUCTION

A capability to perform steep, turning, and decelerating approaches under manual control and in instrument meteorological conditions has been developed and flight tested in the Augmentor Wing Jet STOL Research Aircraft. This powered-lift STOL aircraft is operated by the NASA-Ames Research Center as part of a comprehensive investigative program in terminal-area STOL operating systems, and is partially supported by funding and personnel from the Canadian Government. The general objective of this program is to assess the potential for enhancing the operational efficiency of STOL aircraft by reducing terminal-area arrival times, selectively locating the final approach route for reasons of noise curtailment, obstruction clearance, conflicting CTOL operations, or military tactical constraints. The emphasis of this experiment was on the manual control and flight director considerations for powered-lift STOL terminal-area operations, with the objective of evaluating the extent to which significant operational utility can be achieved without requiring the extensive use of automatic systems, with their attendant reliability and cost considerations.

That powered-lift aircraft require special attention arises from the peculiar lift, drag, and pitching aerodynamics and perhaps their undesirable couplings that are associated with thrust turning. Accompanying this thrust turning feature is the requirement for use of an additional longitudinal control to adjust lift-drag trim states during steep approach operations. In addition, low aerodynamic dampings associated with low speed flight, and the details associated with lift sharing between the more conventional wing aerodynamics and the propulsive lift forces generally result in dynamics with a more sluggish and less stable response relative to CTOL aircraft. The result of these factors is an increase in complexity of the pilot's control task, or alternatively, the need to incorporate an appropriately designed automatic control or stability augmentation system.

Recognizing the comprehensive nature of the STOL instrument approach task, the major objective of this work was to integrate the navigation, guidance, control and handling qualities, cockpit display, and procedural factors into a potentially feasible operational framework. The curved approach task was carried out in a real navigation environment and furnishes new operationally oriented data for this class of aircraft. Features contributing to the feasibility of the task were a multi-function, three-cue flight director along with integrated electronic cockpit displays. A variety of STOL control concepts were also evaluated for their effect on the task. This paper discusses the essential elements of the approach task, briefly describes the test aircraft and associated avionics, and presents representative data from the flight experiments. A more detailed description of the flight test effort is to be found in a prospective NASA report,[1] which also substantiates the general conclusions summarized in this paper.

APPROACH TASK

Approach profiles similar to that shown in figure 1 were used for the evaluation. Included were some minor variations in turn radius and final approach roll-out altitude optional to the pilot. Choice of the 180° descending turn ensured that methods be developed to deal with (1) the discontinuity in the terminal-

[1]W. S. Hindson and D. W. Smith: Flight Evaluation of Several STOL Control and Flight Director Concepts for a Powered-Lift Aircraft Flying Steep Curved and Decelerating Approaches. Prospective NASA Technical Publication.

area navigation environment (during transition from VORTAC to precision Microwave Landing System (MLS) coverage), and (2) the effects of the changing relative direction of significant ambient winds on lateral and longitudinal control requirements. Conversion from the conventional terminal area arrival configuration to an intermediate powered-lift flap setting (50°) was accomplished during the level downwind leg before capturing the 7° descent path. The major deceleration from the terminal area arrival speed was also carried out in this segment. The final deceleration to landing speed was generally accomplished immediately prior to roll-out at 150 m (500 ft) from the descending turn. A simulated decision height of 30.54 m (100 ft) was used for the hooded approach, where the glidepath performance objectives were chosen for purposes of initial evaluation to be those currently used for CTOL Category II operations. Landing transitions were carried out to a 30.5-m-wide STOL runway, where touchdown dispersions were measured. Provision was also made for adapting the landing configuration and associated approach airspeed to the wind conditions of the day and the runway length available for landing, hence recognizing an additional variable believed necessary for economical operation of powered-lift STOL or V/STOL aircraft. The configuration-speed schedule used for the test aircraft is shown in figure 1.

THE RESEARCH AIRCRAFT

The research aircraft used for these tests was a modified DeHavilland of Canada DHC-5 Buffalo shown in figure 2. The aircraft is equipped with an augmentor flap arrangement, shown in figure 3, which is blown internally by the cold bypass flow from two Rolls Royce Spey 801-SF engines. This cold flow is crossducted to minimize lateral and directional transients in the event of an engine failure. The residual hot thrust from each engine is exhausted through rotatable nozzles, which when vectored to a downward position, conveniently provides ample reduction in longitudinal force for steep approaches. These nozzles are capable of high rotation rates, and when also modulated about their deployed position, furnish significant control of longitudinal force without any major disruption in lift.

The aircraft is equipped with a rate-command, attitude-hold Stability Augmentation System (SAS) for pitch and roll, and has turn coordination and rate-damping augmentation in yaw.

A flexible digital avionics system known as STOLAND, pictured in figure 4, is installed in the aircraft. A 32K/18bit word minicomputer serves navigational, guidance and control requirements through interfaces with the cockpit displays, electronic servos, and the pilot's mode selection panel. A rho-theta area navigation system is incorporated, providing a flexible capability for multi-segment and curvilinear profiles in a VOR, TACAN, or MLS navigation environment.

The variable stability capability of this system was also used to incorporate an autospeed control augmentation system for use in the powered-lift descent configuration. This system, shown in figure 5 modulates the vectored thrust nozzles to maintain a specified speed reference while maneuvering with other longitudinal controls, or in the presence of atmospheric disturbances such as shears. This system is conceptually similar to one evaluated during the previous research reported in reference 1, where it had yielded encouraging pilot ratings. However, in this work, considerably more attention was given to some of the many factors involved in the design of such a system for operational use, such as engagement procedures, trim control, and authority limits. Use was also made of electrohydraulically actuated surfaces located within the augmentor flaps. These "chokes" can be modulated symmetrically about an intermediate deployed position to provide direct lift control, and are used for heave damping augmentation and to offset small lift losses that occur as the hot thrust nozzles are rotated aft when controlling to the reference speed. The speed reference in the system is indirectly controlled by flap angle as shown in figure 6, so that as the pilot progressively configures the aircraft towards the final landing flap setting, the speed reference automatically reduces to programmed values appropriate to configuration and weight. This provides a convenient way to control a decelerating approach without any additional cockpit actions.

Finally, the authority of the autospeed control system is sufficient to deal with the secondary control coupling generated when throttle is used for path control, commonly referred to as the Backside Control Technique, as well as the primary control coupling associated with using pitch attitude to control glidepath, as in the conventional Frontside Control Technique. With the Backside Control Technique, pitch attitude is maintained constant at an appropriate trim position, while with the Frontside Technique throttle is maintained at an appropriate trim position, effectively determining the optimum proportion of powered-lift needed for the approach. Consequently, three differing STOL control concepts, summarized in Table I, were available for evaluation during the flight tests reported here, since the Basic Aircraft, without speed control augmentation, was also tested.

COCKPIT DISPLAYS AND FLIGHT DIRECTOR

Two electronically generated cockpit displays provide an integrated display format, which contributed greatly to the reduced workload necessary to permit the curved approach. As shown in figure 7, the electronic attitude director indicator (EADI) embodies a three-cue director format for pitch, throttle, and roll angle. Other symbology includes an inertially referenced flight path angle bar, a speed error thermometer scale, a raw-data tracking box of increasing sensitivity towards decision height, and three digital display windows as shown in figure 7. Also included is a perspective runway presentation, calculated from MLS position data for use with the flight path angle bar.

The multifunction display (MFD), shown in figure 8, fills a requirement conventionally met by a horizontal situation indicator (HSI), furnishing a pictorial plan position presentation particularly suitable for constrained multisegment, curvilinear, terminal-area navigation. Also shown in figure 8 are main symbology elements, and the several options for map orientation, scale sensitivity, map content, and route selection available to the pilot. The location of these displays in the cockpit is illustrated in figure 9.

The functional design of the flight director that evolved to support the curved decelerating approach task is shown in figure 10. Four distinct requirements are involved in contrast to the usual situation for

CTOL aircraft where, in addition to mode switching, the flight director consists simply of guidance laws combining path error and path error rate in suitable proportions. The basic guidance laws used here remain basically conventional, except that they include control-feedback limiting, such as maximum and minimum power settings, to ensure that control parameters remain within prescribed bounds, thus reducing the need for additional pilot monitoring. Also incorporated are control configuration blending constants, which meet the requirement to smoothly blend the pilot's control technique from frontside to backside as the aircraft's configuration is changed toward powered-lift settings. The configuration-dependent form of these parameters is shown in figure 11; they begin to come into play during the initial level deceleration on the downwind leg, typically to a flap setting of 50°. The trim management function of the flight director assists the pilot in establishing appropriate lift-drag trim settings during the turning approach through trim data stored over a range of aerodynamic flight path angles. This trim management requirement is an important consideration for all powered-lift aircraft, including V/STOL aircraft, which are especially sensitive in terms of operating economics and safety margins to the larger variations in aerodynamic flight path angle encountered during steep approach operations in moderate wind fields. The computed trim setting is displayed to the pilot on the EADI either through the throttle director bar for the Frontside autospeed mode, the pitch bar for the Backside autospeed mode, or through the center window as a fourth director cue for the manual nozzle positioning necessary for the Basic Aircraft mode. Finally, the decelerating approach reference speed, mentioned earlier in connection with the autospeed control system, is incorporated in the flight director. Errors from this reference are either input to the autospeed control system (if engaged) or drive the pitch director bar for the Basic Aircraft mode.

SELECTED FLIGHT TEST RESULTS

Data from approximately 60 approaches were analyzed from the viewpoint of achieved outer loop navigation and guidance performance, inner loop flight director tracking performance, pilot control inputs, and aircraft control utilization measures. These results constitute an initial body of data that can contribute to the development of navigation and airspace requirements, pilot workload factors, control authority design requirements, and pilot and passenger acceptance factors for this class of aircraft. Among others, these factors, will determine the mission capability of powered-lift STOL aircraft. Representative flight test data selected from the experiment are provided here.

The net profile performance achieved during thirteen approaches flown on one of the experimental approach profiles is shown in figure 12. The width of the lateral performance envelope in the earlier stages of the approach represents profile capture peculiarities, as well as day-to-day variations in the enroute VORTAC navigation signal accuracies, particularly bias errors in range measurement. These data were analyzed in greater detail for all approaches during the sequential approach segments defined by the downwind leg, the descending turn, and the final approach, and are summarized in the prospective report[2] in the form of tabulated dispersions of lateral and vertical navigation and guidance errors.

Although the emphasis of this work was on longitudinal performance and control, some lateral parameters of significance were also studied. Lateral control data during the descending turn are illustrated in figure 13 for approximately 50 approaches. These probability density functions represent the relative amount of time during all turn segments that the parameters shown fall within the intervals defined along the abscissa. Despite the moderately strong winds which prevailed during some of the evaluation flights, the nominal bank angle during the turn was maintained near the desired 15° by appropriate choice of turn radius and initial approach airspeed. Recognizing the importance of winds during the approach on both lateral and longitudinal kinematics and hence control requirements, the wind profile to be anticipated on descent was available to the pilot from a wind estimate calculated on board and displayed, and from a wind forecast briefing derived from balloon and surface wind data. Figure 13 also shows the statistics for roll flight director tracking during the descending turn, along with the amplitude characteristics of the pilot's roll control input.

Differences in the three STOL concepts evaluated are most evident in terms of the speed control achieved. Figure 14 illustrates how speed errors from the reference are substantially reduced for either version of the autospeed control system described previously, relative to the Basic Aircraft mode where larger speed dispersions and a mean velocity error on the slow side are evident. This speed bias for the Basic Aircraft arises from the high degree of thrust turning that is characteristic of the Augmentor Wing concept. This feature results in a reduction in forward speed when power is added, unless pitch attitude is decreased. The data suggest that the pilot, although continuously reminded by the flight director to use this abnormal control technique, remains reluctant to pitch down when adding power to make an up correction to path. The glidepath performance statistics, shown in figure 14, are similar for all three STOL concepts. However, somewhat poorer performance is shown for the Basic Aircraft mode, where the bias toward persisting errors below path correlates with the slow speed bias just discussed. Despite the improved performance and safety margin that inherently accrue from good speed control, these tests did not encounter the atmospheric conditions of turbulence and shear in which these benefits of automatic speed control are likely to be important.

The utilization of the longitudinal controls during the final straight approach segment is illustrated in figure 15 for the Basic Aircraft mode and the Frontside autospeed control mode. In the Basic Aircraft mode, power is used to control glidepath, while pitch attitude is used for speed control. Nozzle angle is used for trim with the objective of maintaining power and pitch close to their optimum settings for the wind conditions of the day. The range of power settings encountered during the final 30 sec of 24 approaches is shown in figure 15, together with the range of pitch excursions and an associated typical use of nozzle trim as adjusted by the pilot. A separation of the data according to mean wind condition illustrates the effect of wind on the operation of powered-lift aircraft equipped with both thrust and thrust vector controls. For the Frontside autospeed control mode, power is used for lift-drag trim, while pitch attitude is used for glidepath control. The nozzle is driven by the autospeed control system to maintain

---

[2]See footnote 1

speed at the predetermined value. The data demonstrate that one disadvantage of this type of STOL control concept is a noticeably greater activity in pitch control. However, the advantages of (1) maintaining a nearly constant power setting on the approach, (2) preserving a fixed reserve of propulsive lift for go-around or engine failure, and (3) reducing the pilot's longitudinal control task to manipulation of a single control may present significant considerations for aircraft operation and design. Some of these considerations may be in the form of (1) requirements for preserving aerodynamic safety margins, (2) ensuring consistency of pilot control technique over the entire flight envelope, (3) specifying installed thrust-to-weight, (4) defining control authority and bandwidth of the speed control device, or (5) limiting the effects of power modulation transients on engine life.

Vertical and lateral performance achieved at the 30.54 m decision height for the three control modes combined is shown in figure 16. There were no discernible differences in glidepath performance with control mode in the atmospheric conditions of these tests. The vertical guidance errors are shown in relation to the ± 3.7 m performance criterion currently established for CTOL operations. It was not an objective of these tests to relate the lateral performance objectives to currently established CTOL criteria. Rather, moderate lateral offsets were intentionally induced to provide the pilot with a more demanding landing task. The width of the shaded area in figure 16 encompasses the lateral guidance errors that were experienced. Despite the dispersions recorded at decision height, satisfactory landings were accomplished from all approaches. Nevertheless, some reservations were expressed about acceptable combinations of vertical position error and instantaneous flight path angle occurring at breakout.

Shown in figure 17 is the range of pilot opinion ratings assigned to the three STOL control concepts during the descending turn, final approach, and landing task segments. Three pilots provided the data from 14 evaluation flights. Atmospheric conditions consisted of both light and moderately strong winds; however, turbulence conditions were generally negligible to light. Under these conditions, little preference among the three STOL control concepts is evident, the assigned ratings reflecting a relatively uniform level of pilot effort involved in executing this moderately complex precision approach task. This level was considered comparable to that encountered in a conventional ILS approach task performed without the aid of a flight director in a CTOL jet aircraft.

Of greater significance was the totally new capability, provided chiefly by the area navigation system and the flight director, to perform tight, turning, and decelerating approaches to the STOLport with repeatable precision. Despite extensive flight experience with this aircraft, represented by more than 1600 landing approaches, the pilots felt that this capability substantially exceeded that formerly possible, even during visual approaches, hence providing a measure of the improvement in mission capability that can be achieved. The single control feature contributing most to this capability is the trim management function of the flight director, relieving the pilot of the otherwise burdensome task of determining lift-drag trim strategy.

CONCLUSIONS

A flight test program was carried out using electronic cockpit displays and a specially designed flight director concept, which permitted curved decelerating STOL approaches to be flown in simulated instrument conditions. Also evaluated were three STOL control concepts representative of those applicable to powered-lift STOL and V/STOL aircraft. Two of these control concepts used a speed control augmentation system modulating lift and drag forces, which was additional to a three-axis rotational stability augmentation system normally used in the aircraft. Although complete supporting data has not been included in this paper, based on a more detailed study to be published, the following general conclusions have been drawn.

- Curved decelerating approaches in instrument meteorological conditions do appear feasible in powered-lift STOL aircraft from a pilot acceptance point of view.
- By providing suitable guidance and display information, a notable improvement in approach profile efficiency appears possible for visual approaches.
- Differences in pilot acceptance, workload, and performance are not widely separated for the various STOL control concepts evaluated, at least in atmospheric conditions of light turbulence and gentle shears.
- It was found important to provide the pilot with a computed position for the longitudinal control used for trim, primarily to relieve the mental workload associated with evaluating and determining satisfactory longitudinal lift-drag trim states.
- Changing the pilot's control technique from frontside on the initial approach to backside on the turn and final approach, which was accomplished by blending in a multiloop flight director, was well received by the pilots and resulted in no control difficulties.
- The equivalent of Category II decision heights and performance criteria for manual powered-lift STOL operations may differ from those now used for CTOL aircraft. In addition, they are likely to be strongly influenced by both the nominal descent rate on approach and excursions about this nominal rate that may exist at decision height, created in the course of attempting to follow the flight director control laws.

The control and flight director features developed for the aircraft of this study may differ in detail when applied to other powered-lift configurations, but nevertheless represent general design considerations. Assuming the existence of an adequate navigation environment, most of these considerations for powered-lift aircraft are control related, and if dealt with satisfactorily, offer potential for operational acceptance. On the other hand, it is considered that operations on these approach profiles with low wing loading STOL aircraft, or RTOL aircraft, present substantially fewer control considerations, and principally require an adequate navigation, profile computation, control authority, and cockpit display environment for their implementation.

REFERENCE

1. Franklin, J.A. et al. "Flight Evaluation of Advanced Flight Control Systems and Cockpit Displays for Powered-Lift STOL Aircraft." NASA SP-416, Oct. 1976, pp. 43-62.

Table 1. Summary of STOL control concepts.

CONTROL CONCEPT	BASIC AIRCRAFT	BACKSIDE SAS	FRONTSIDE SAS
PRIMARY CONTROL (PATH)	THROTTLE	THROTTLE	PITCH ATTITUDE
SEC'Y CONTROL (SPEED)	PITCH ATTITUDE	NOZZLE*	NOZZLE*
TRIM CONTROL	NOZZLE	PITCH ATTITUDE	THROTTLE

*SAS MANAGED

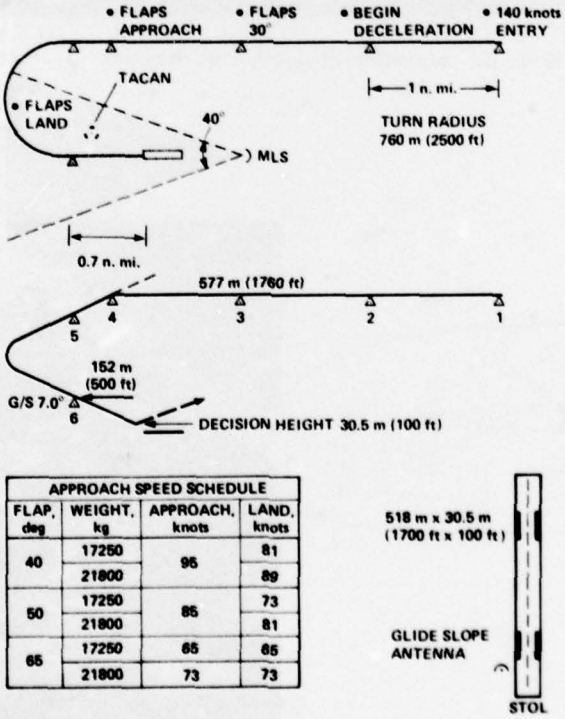

APPROACH SPEED SCHEDULE			
FLAP, deg	WEIGHT, kg	APPROACH, knots	LAND, knots
40	17250	95	81
	21800		89
50	17250	85	73
	21800		81
65	17250	65	65
	21800	73	73

Fig. 1. Approach profile.

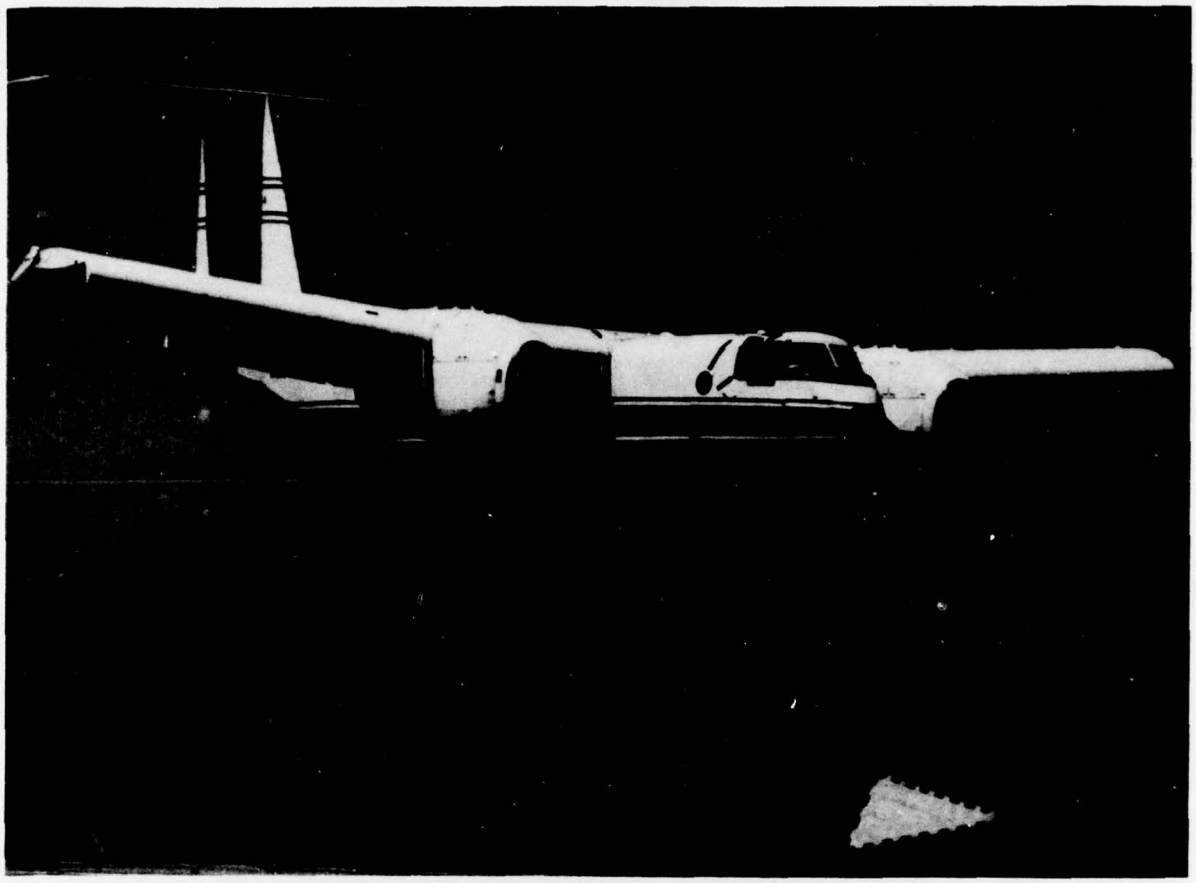

Fig. 2. Augmentor Wing Jet STOL Research Aircraft.

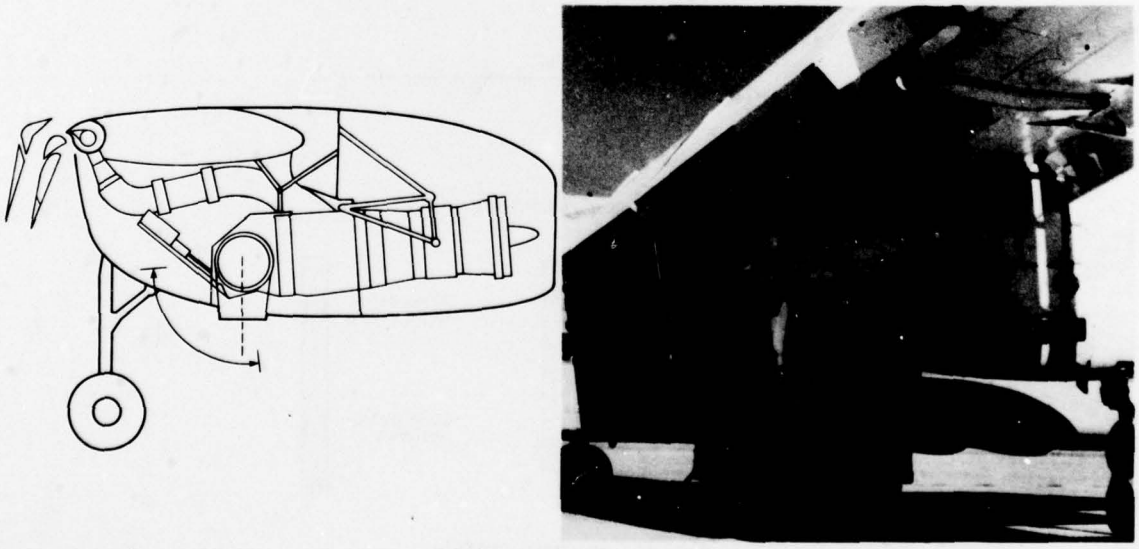

Fig. 3. Augmentor wing propulsive lift system.

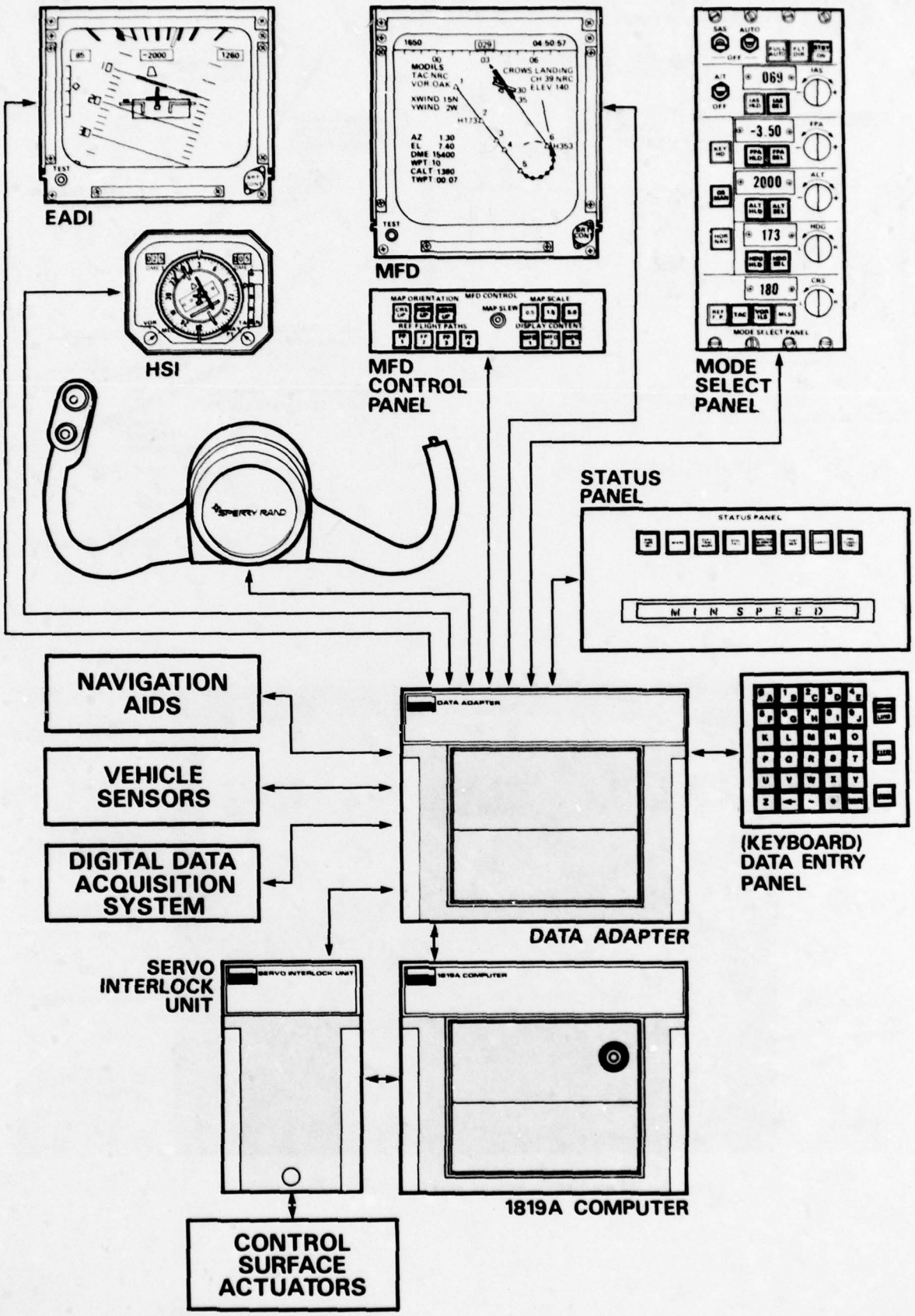

Fig. 4. STOLAND Research AVIONICS System.

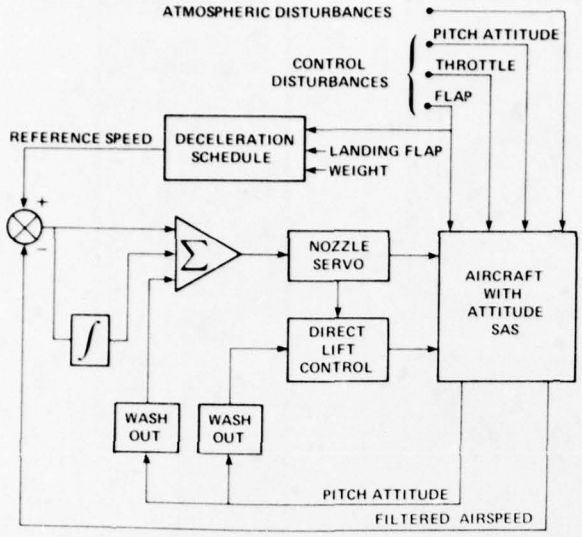

Fig. 5. Autospeed control system.

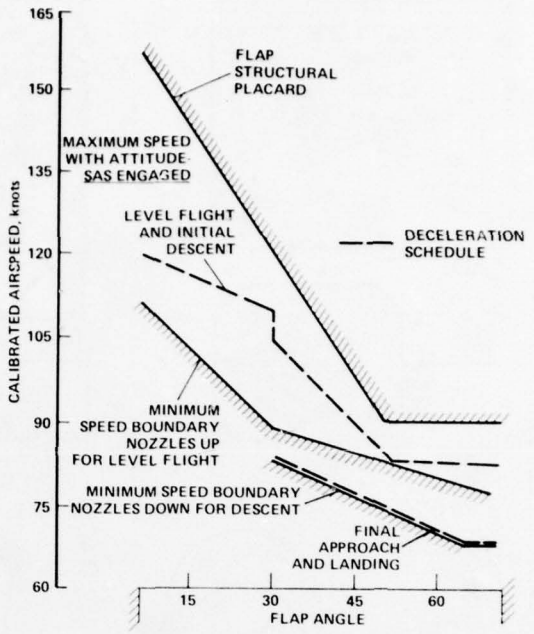

Fig. 6. Decelerating Reference Speed Scheduling.

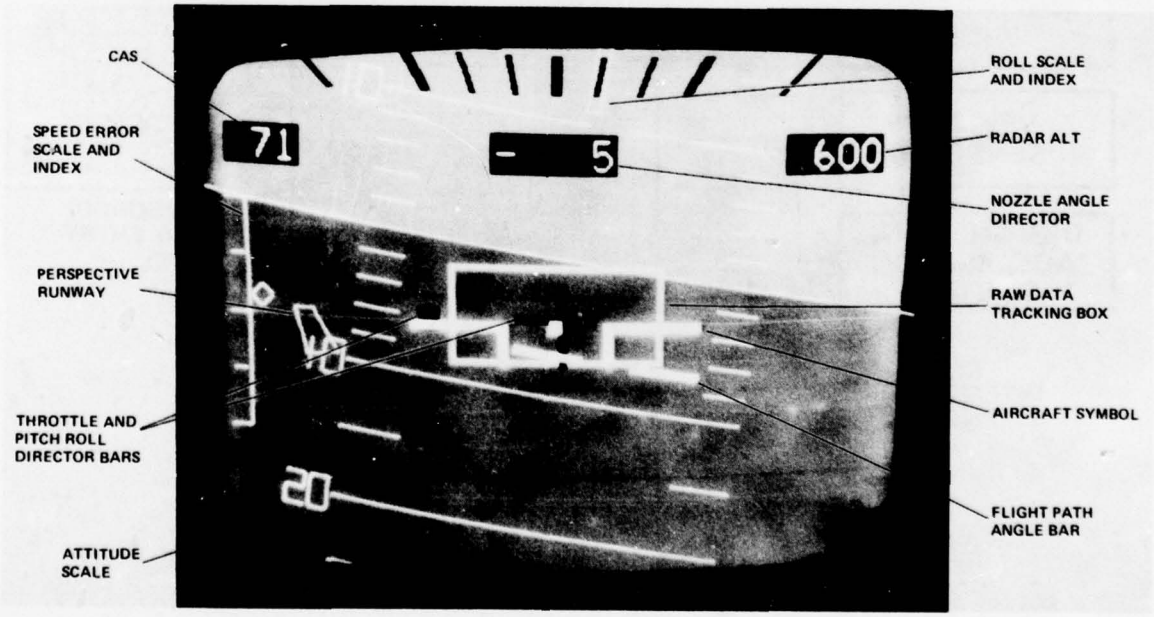

Fig. 7. Electronic attitude director indicator (EADI).

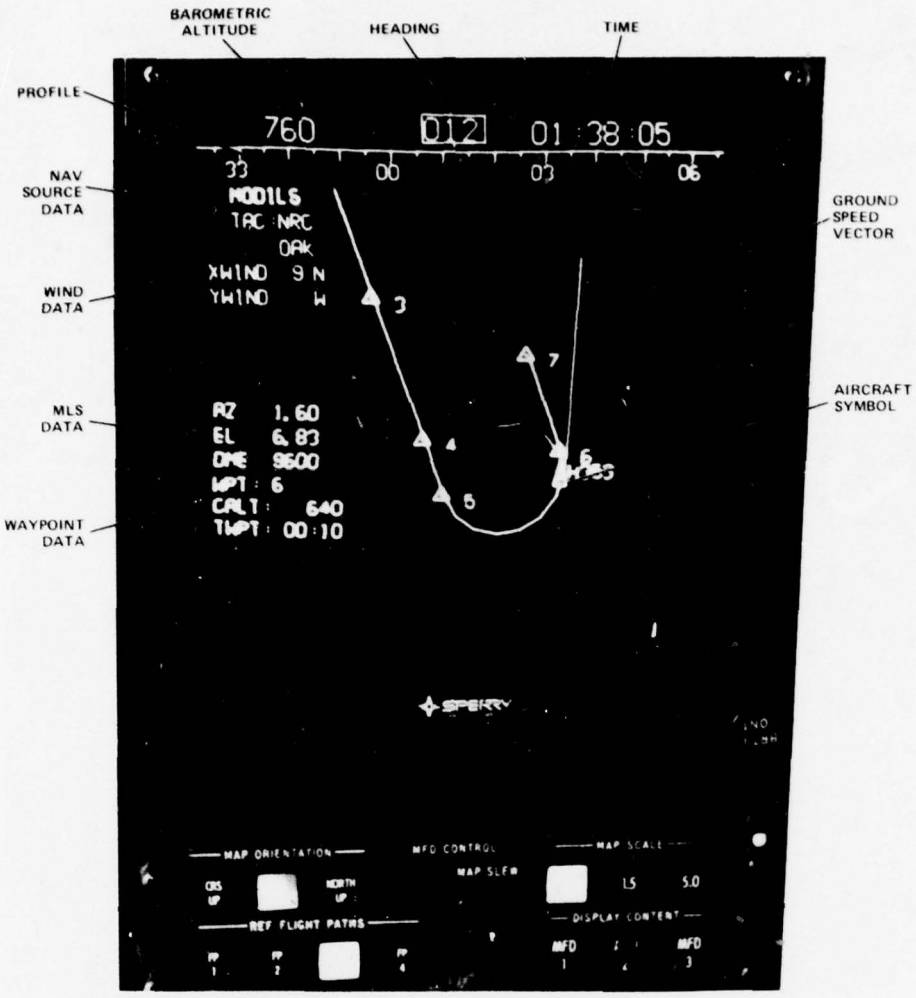

Fig. 8. Multifunction display (MFD).

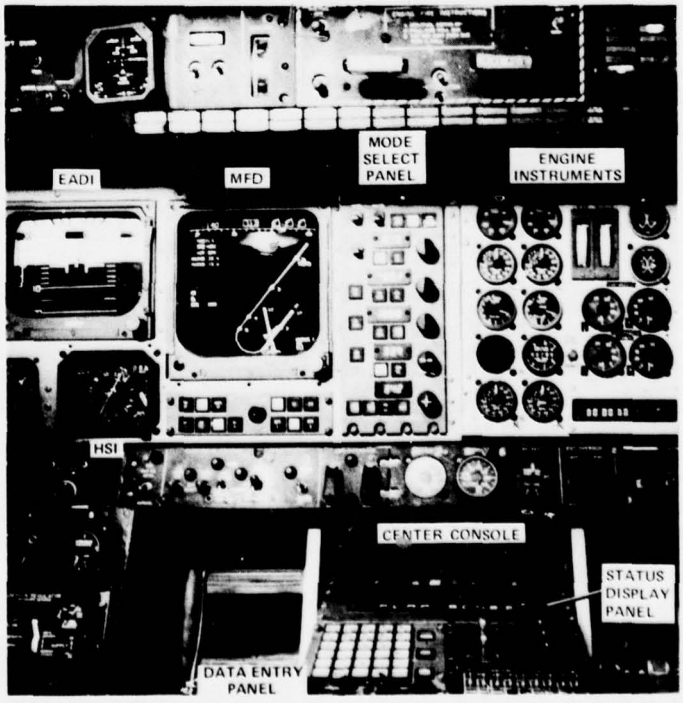

Fig. 9. Cockpit display installation.

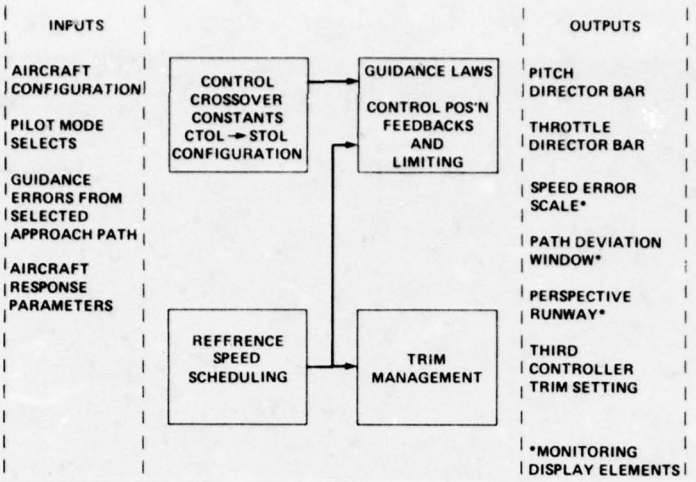

Fig. 10. Flight director functional design.

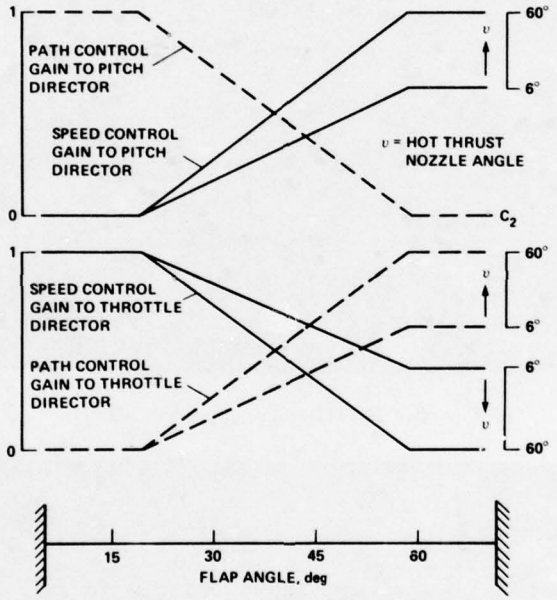

Fig. 11. Normalized control blending gains.

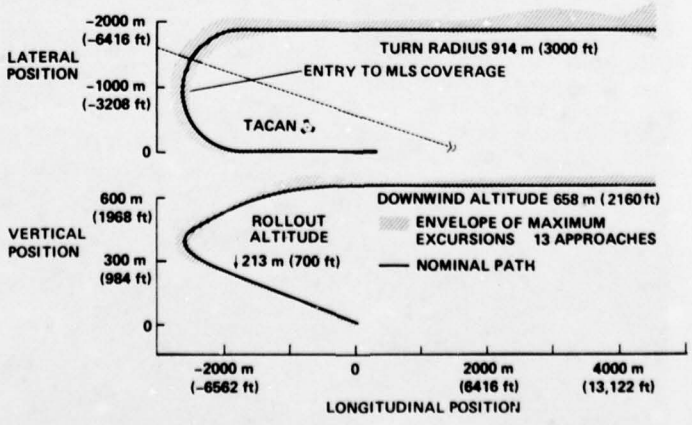

Fig. 12. Typical profile performance.

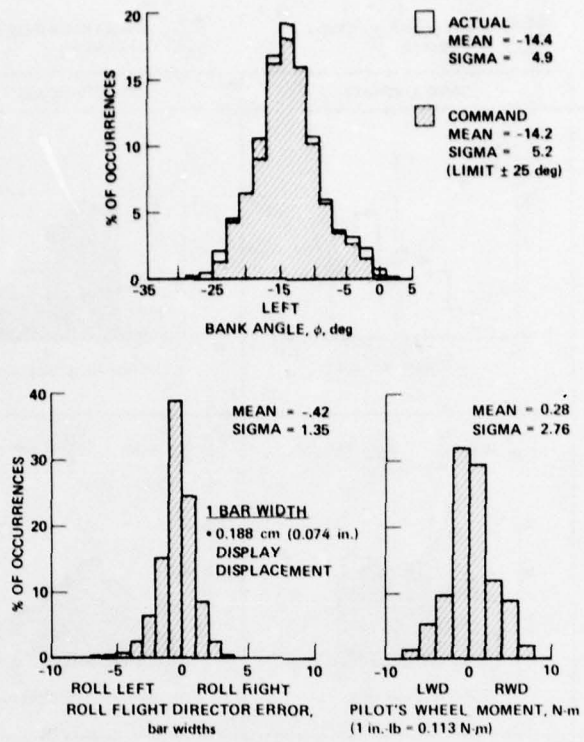

Fig. 13. Lateral control parameters during descending turn.

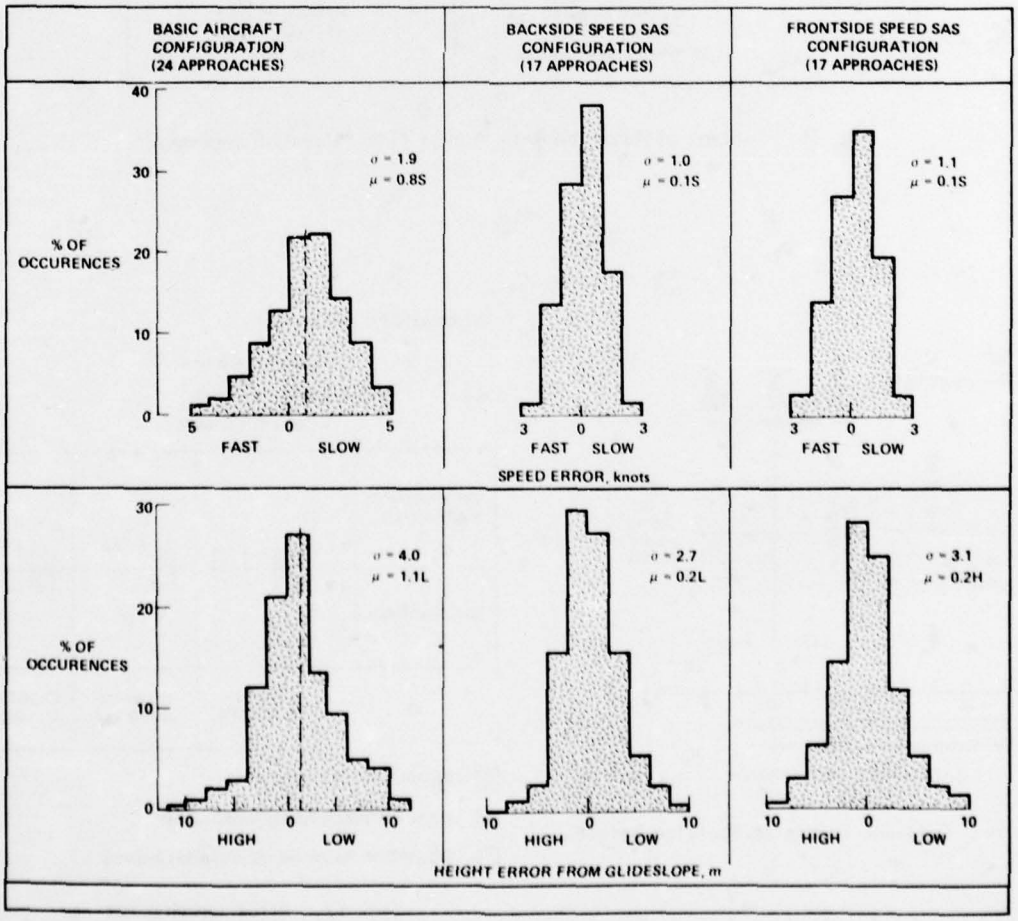

Fig. 14. Longitudinal performance measures during final straight segment.

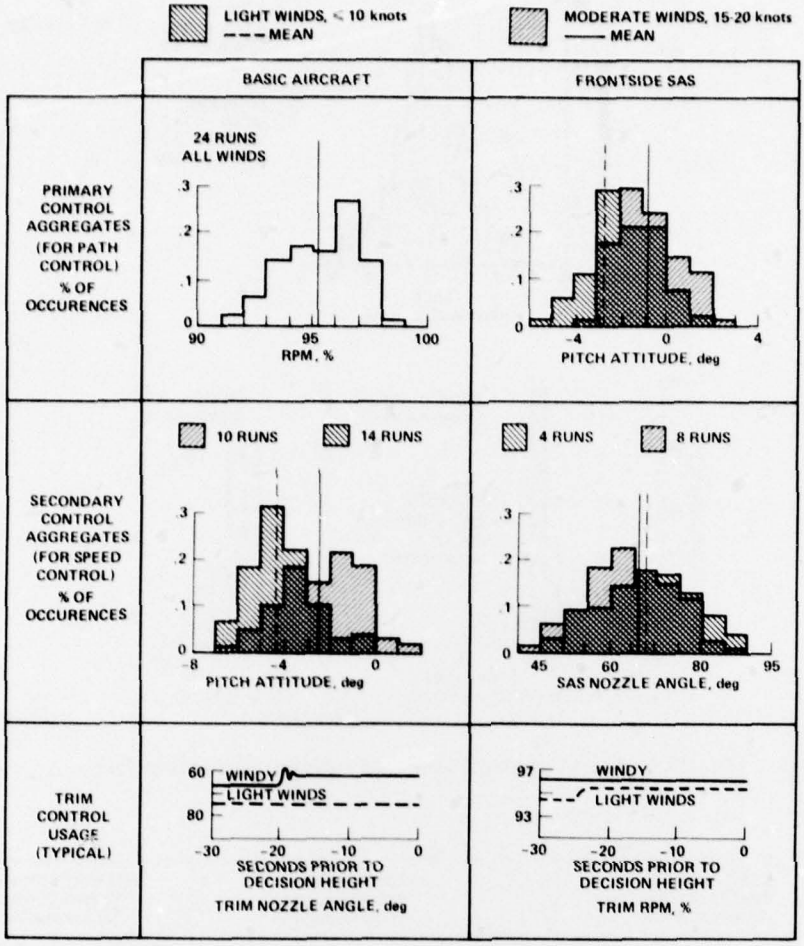

Fig. 15. Control utilization data during final straight segment.

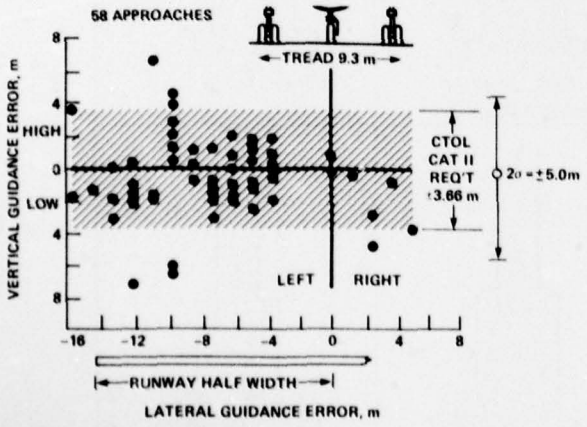

Fig. 16. Guidance errors at decision height.

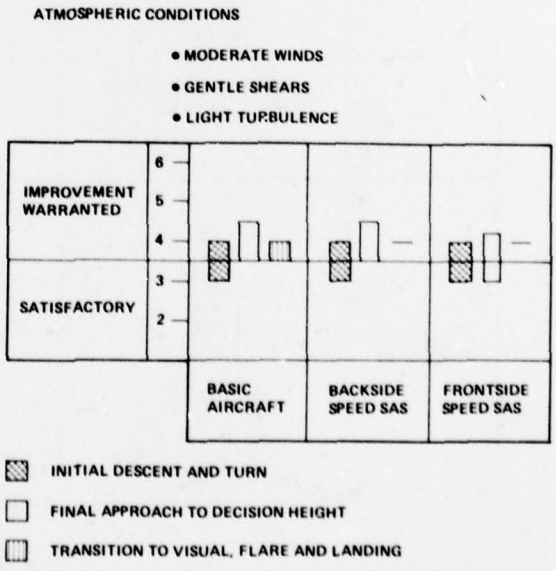

Fig. 17. Pilot opinion ratings.

REPORT DOCUMENTATION PAGE

1. Recipient's Reference	2. Originator's Reference	3. Further Reference	4. Security Classification of Document
	AGARD-CP-260	ISBN 92-835-0239-6	UNCLASSIFIED

5. Originator Advisory Group for Aerospace Research and Development
North Atlantic Treaty Organization
7 rue Ancelle, 92200 Neuilly sur Seine, France

6. Title

STABILTY AND CONTROL

AD" 665205, 665329, 754524

7. Presented at the Flight Mechanics Panel Symposium on Stability and Control held in Ottawa, Canada, 25–28 September 1978.

8. Author(s)/Editor(s)	9. Date
Various	May 1979
10. Author's/Editor's Address	**11. Pages**
Various	370 pages

12. Distribution Statement This document is distributed in accordance with AGARD policies and regulations, which are outlined on the Outside Back Covers of all AGARD publications.

13. Keywords/Descriptors

Stability	Control configured vehicles
Aerodynamic stability	Mathematical models
Flight control	Pilots (personnel)

14. Abstract

These proceedings consist of the papers presented at the FMP Symposium on Stability and Control. The papers cover: recent experiences in stability and control; the application of active control and the general problems concerning its use, including those of mathematical models; results obtained with CCVs; criteria for satisfactory behaviour of aircraft with advanced stability and control systems; and the participation of the pilot. A comprehensive Technical Evaluation of the meeting appears in AGARD Advisory Report No. 134.

AGARD Conference Proceedings No.260 Advisory Group for Aerospace Research and Development, NATO STABILITY AND CONTROL Published May 1979 370 pages These proceedings consist of the papers presented at the FMP Symposium on Stability and Control. The papers cover: recent experiences in stability and control; the application of active control and the general problems concerning its use, including those of mathematical models; results obtained with CCVs; criteria for satisfactory behaviour of aircraft with advanced stability and control systems, and the participation of the pilot. A comprehensive Technical Evaluation of the meeting appears in AGARD Advisory Report No. 134. P.T.O.	AGARD-CP-260 Stability Aerodynamic stability Flight control Control configured vehicles Mathematical models Pilots (personnel)	AGARD Conference Proceedings No.260 Advisory Group for Aerospace Research and Development, NATO STABILITY AND CONTROL Published May 1979 370 pages These proceedings consist of the papers presented at the FMP Symposium on Stability and Control. The papers cover: recent experiences in stability and control; the application of active control and the general problems concerning its use, including those of mathematical models; results obtained with CCVs; criteria for satisfactory behaviour of aircraft with advanced stability and control systems, and the participation of the pilot. A comprehensive Technical Evaluation of the meeting appears in AGARD Advisory Report No. 134. P.T.O.	AGARD-CP-260 Stability Aerodynamic stability Flight control Control configured vehicles Mathematical models Pilots (personnel)
AGARD Conference Proceedings No.260 Advisory Group for Aerospace Research and Development, NATO STABILITY AND CONTROL Published May 1979 370 pages These proceedings consist of the papers presented at the FMP Symposium on Stability and Control. The papers cover: recent experiences in stability and control; the application of active control and the general problems concerning its use, including those of mathematical models; results obtained with CCVs; criteria for satisfactory behaviour of aircraft with advanced stability and control systems, and the participation of the pilot. A comprehensive Technical Evaluation of the meeting appears in AGARD Advisory Report No. 134. P.T.O.	AGARD-CP-260 Stability Aerodynamic stability Flight control Control configured vehicles Mathematical models Pilots (personnel)	AGARD Conference Proceedings No.260 Advisory Group for Aerospace Research and Development, NATO STABILITY AND CONTROL Published May 1979 370 pages These proceedings consist of the papers presented at the FMP Symposium on Stability and Control. The papers cover: recent experiences in stability and control; the application of active control and the general problems concerning its use, including those of mathematical models; results obtained with CCVs; criteria for satisfactory behaviour of aircraft with advanced stability and control systems, and the participation of the pilot. A comprehensive Technical Evaluation of the meeting appears in AGARD Advisory Report No. 134. P.T.O.	AGARD-CP-260 Stability Aerodynamic stability Flight control Control configured vehicles Mathematical models Pilots (personnel)

Papers presented at the Flight Mechanics Panel Symposium on Stability and Control held in Ottawa, Canada, 25–28 September 1978.

ISBN 92-835-0239-6

Papers presented at the Flight Mechanics Panel Symposium on Stability and Control held in Ottawa, Canada, 25–28 September 1978.

ISBN 92-835-0239-6

Papers presented at the Flight Mechanics Panel Symposium on Stability and Control held in Ottawa, Canada, 25–28 September 1978.

ISBN 92-835-0239-6

Papers presented at the Flight Mechanics Panel Symposium on Stability and Control held in Ottawa, Canada, 25–28 September 1978.

ISBN 92-835-0239-6

6130/3

AGARD
NATO OTAN
7 RUE ANCELLE · 92200 NEUILLY-SUR-SEINE
FRANCE
Telephone 745.08.10 · Telex 610176

DISTRIBUTION OF UNCLASSIFIED AGARD PUBLICATIONS

AGARD does NOT hold stocks of AGARD publications at the above address for general distribution. Initial distribution of AGARD publications is made to AGARD Member Nations through the following National Distribution Centres. Further copies are sometimes available from these Centres, but if not may be purchased in Microfiche or Photocopy form from the Purchase Agencies listed below.

NATIONAL DISTRIBUTION CENTRES •

BELGIUM
Coordonnateur AGARD – VSL
Etat-Major de la Force Aérienne
Quartier Reine Elisabeth
Rue d'Evere, 1140 Bruxelles

CANADA
Defence Scientific Information Service
Department of National Defence
Ottawa, Ontario K1A OZ2

DENMARK
Danish Defence Research Board
Østerbrogades Kaserne
Copenhagen Ø

FRANCE
O.N.E.R.A. (Direction)
29 Avenue de la Division Leclerc
92 Châtillon sous Bagneux

GERMANY
Zentralstelle für Luft- und Raumfahrt-
dokumentation und -information
c/o Fachinformationszentrum Energie,
Physik, Mathematik GmbH
Kernforschungszentrum
7514 Eggenstein-Leopoldshafen 2

GREECE
Hellenic Air Force General Staff
Research and Development Directorate
Holargos, Athens, Greece

ICELAND
Director of Aviation
c/o Flugrad
Reykjavik

ITALY
Aeronautica Militare
Ufficio del Delegato Nazionale all'AGARD
3, Piazzale Adenauer
Roma/EUR

LUXEMBOURG
See Belgium

NETHERLANDS
Netherlands Delegation to AGARD
National Aerospace Laboratory, NLR
P.O. Box 126
Delft

NORWAY
Norwegian Defence Research Establishment
Main Library
P.O. Box 25
N-2007 Kjeller

PORTUGAL
Direcção do Serviço de Material
da Forca Aerea
Rua da Escola Politecnica 42
Lisboa
Attn: AGARD National Delegate

TURKEY
Department of Research and Development (ARGE)
Ministry of National Defence, Ankara

UNITED KINGDOM
Defence Research Information Centre
Station Square House
St. Mary Cray
Orpington, Kent BR5 3RE

UNITED STATES
National Aeronautics and Space Administration (NASA)
Langley Field, Virginia 23365
Attn: Report Distribution and Storage Unit

THE UNITED STATES NATIONAL DISTRIBUTION CENTRE (NASA) DOES NOT HOLD STOCKS OF AGARD PUBLICATIONS, AND APPLICATIONS FOR COPIES SHOULD BE MADE DIRECT TO THE NATIONAL TECHNICAL INFORMATION SERVICE (NTIS) AT THE ADDRESS BELOW.

PURCHASE AGENCIES

Microfiche or Photocopy
National Technical
Information Service (NTIS)
5285 Port Royal Road
Springfield
Virginia 22161, USA

Microfiche
Space Documentation Service
European Space Agency
10, rue Mario Nikis
75015 Paris, France

Microfiche
Technology Reports
Centre (DTI)
Station Square House
St. Mary Cray
Orpington, Kent BR5 3RF
England

Requests for microfiche or photocopies of AGARD documents should include the AGARD serial number, title, author or editor, and publication date. Requests to NTIS should include the NASA accession report number. Full bibliographical references and abstracts of AGARD publications are given in the following journals:

Scientific and Technical Aerospace Reports (STAR)
published by NASA Scientific and Technical
Information Facility
Post Office Box 8757
Baltimore/Washington International Airport
Maryland 21240, USA

Government Reports Announcements (GRA)
published by the National Technical
Information Services, Springfield
Virginia 22161, USA

Printed by Technical Editing and Reproduction Ltd
Harford House, 7–9 Charlotte St, London W1P 1HD

ISBN 92-835-0239-6